TRANSPORTATION RESEARCH
RECORD

No. 1278

Soils, Geology, and Foundations

Dynamic Testing of Aggregates and Soils and Lateral Stress Measurements 1990

A peer-reviewed publication of the Transportation Research Board

TRANSPORTATION RESEARCH BOARD
NATIONAL RESEARCH COUNCIL
WASHINGTON, D.C. 1990

Transportation Research Record 1278
Price: $34.00

Subscriber Category:
IIIA soils, geology, and foundations

Mode
1 highway transportation

Subject Areas
24 pavement design and performance
32 cement and concrete
35 mineral aggregates
61 soil exploration and classification
62 soil foundations
63 soil and rock mechanics

TRB Publications Staff
Director of Publications: Nancy A. Ackerman
Senior Editor: Naomi C. Kassabian
Associate Editor: Alison G. Tobias
Assistant Editors: Luanne Crayton, Kathleen Solomon, Norman Solomon
Graphics Coordinator: Diane L. Ross
Office Manager: Phyllis D. Barber
Production Assistant: Betty L. Hawkins

Printed in the United States of America

ISBN 0-309-05055-3
Library of Congress Catalog Card No. 91-60418

Sponsorship of Transportation Research Record 1278

GROUP 2—DESIGN AND CONSTRUCTION OF TRANSPORTATION FACILITIES
Chairman: Raymond A. Forsyth, Sacramento, California

Evaluations, Systems, and Procedures Section
Chairman: Terry M. Mitchell, Federal Highway Administration, U.S. Department of Transportation

Committee on Mineral Aggregates
Chairman: Vernon J. Marks, Iowa Department of Transportation
Bernard D. Alkire, David A. Anderson, John S. Baldwin, George M. Banino, Steven Chrismer, Robert J. Collins, Warren B. Diederich, Stephen W. Forster, James G. Gehler, Robert F. Hinshaw, Richard C. Ingberg, Ian L. Jamieson, George J. Kassal, Rita B. Leahy, Dah-Yinn Lee, Peter Malphurs, Charles R. Marek, W. R. Meier, Jr., Richard C. Meininger, John T. Paxton, Charles A. Pryor, Jr., William J. Quinn, Barbara J. Smith, Mary Stroup-Gardiner, Lennard J. Wylde

Geology and Properties of Earth Materials Section
Chairman: William Lovell, Purdue University

Committee on Soil and Rock Properties
Chairman: Mehmet T. Tumay, Louisiana State University
Robert C. Bachus, S. S. Bandy, Roy H. Borden, Timothy D. Bowen, William H. Highter, Robert D. Holtz, Richard H. Howe, An-Bin Huang, Steven L. Kramer, Rodney W. Lentz, C. William Lovell, Kenneth L. McManis, Priscilla P. Nelson, Norman I. Norrish, Sibel Pamukcu, Gerald P. Raymond, James J. Schnabel, Kaare Senneset, Allan Tice, Recep Yilmaz

G. P. Jayaprakash, Transportation Research Board staff

Sponsorship is indicated by a footnote at the end of each paper. The organizational units, officers, and members are as of December 31, 1989.

Transportation Research Record 1278

Contents

Foreword

The 26 papers in this Record cover material and soil testing and concerns related to pavement design and foundation design for transportation facilities. The papers should interest highway, geotechnical, and foundation engineers.

Aggregates constitute 95 percent of all construction materials used in pavements. Therefore, the quality of the aggregate is important in ensuring longevity of the product. Past testing and evaluation of aggregate or aggregate layers has been of a static nature. In most highway applications aggregate layers are subjected to repeated dynamic loadings. Six researchers discuss dynamic testing of aggregates and determination of the shape of aggregate particles. Qedan et al. evaluate a sample preparation method that uses dynamic testing equipment for compaction. Their evaluation included consideration of number of layers, compaction time, vibration frequency, and fines and moisture content of material that contained aggregate with a maximum size of 1½ in. and 4 to 12 percent fines. The authors conclude that materials with low fines content are less sensitive to moisture and generally provide improved granular base performance. Drnevich et al. use deflection-basin measurement and surface wave propagation methods to determine the resilient modulus of pavement layers. They indicate that the surface wave method gives better results than the deflection basin method. Woolstrum presents the results of resilient modulus testing of field samples from Nebraska and compares them with other parameters. He concludes that the Nebraska Group Index Soil Classification could be used to estimate the resilient modulus. Bathurst and Raymond investigate aggregates of varying resistance to fracture and abrasion. They found that good-quality aggregate endures 1,000 times as many loadings as poor-quality aggregate for the same magnitude of permanent deformation. Carr et al. use fractal dimensions to express the surface roughness of aggregate particles. In general, rough, irregular aggregate particles yield greater fractal dimensions.

Nine authors address concerns that are related to pavement design criteria, subgrade behavior under repeated loads analysis and design of deep foundations, in situ soil testing and evaluation, shear strength of peat soils, and soil reinforcement interaction. Claros et al., and Stokoe et al. describe modifications to the AASHTO resilient modulus testing procedure and the use of synthetic samples for equipment evaluation and calibration. Raad and Zeid report on the development of a model and its application to investigate the effects of load repetition on subgrade modulus and shear strength. Zachary and Lohnes describe a new confined compression tester that measures wall friction along with vertical and horizontal stresses. Stark and Delashaw use triaxial and cone penetration test (CPT) results to develop correlations between undrained shear strength and CPT results in soft to medium alluvial clays. Thompson and Smith report the results of an evaluation of the effect of a decrease in fines content on the pertinent engineering properties of typical well-graded granular base materials. Kramer et al. describe the use of an instrumented pile lateral load test for evaluation of strength and stiffness characteristics of a peat deposit. Wilson et al. describe a unique low-pressure multiaxial device that they used to test resilient behavior of subgrade soils. Yuan and Chua focus on the soil-reinforcement interaction. They show that the nonlinear interface shear parameters obtained from direct shear tests can accurately predict pullout resistance.

The economic design of foundations for transportation facilities is dependent on the accuracy of the assessment of the horizontal stress throughout the soil profile. Insertion of the devices used to measure the horizontal stress alters these very stresses. The remaining papers describe a broad spectrum of field and laboratory investigations conducted in five countries to understand better the relationship between measured parameters and existing stresses. Handy et al. present a review of the K_o stepped blade and how to use the predicted lateral stresses to make inferences on consolidation state, inadequate compaction, and potential slope instability. Lawter and Borden examine the amplification factor (K_D/K_o) as a function of both relative density and state parameter on the basis of the results of dilatometer tests in sand in a calibration chamber. They present test data on three normally consolidated sands. Mayne and Kulhawy, using self-boring pressuremeter test results, demonstrate that stress

history is a predominant factor affecting the magnitude of the lateral stress. They propose a simplified cavity expansion approach for obtaining indirect assessments of K_o from cone, piezocone, and dilatometer tests. Benoit et al. compare lateral stress results from self-boring pressuremeter and dilatometer tests in soft sensitive clays. They found dilatometer dissipation test results to be in close agreement with the maximum values measured with the self-boring pressuremeter. Huang and Haefele describe self-boring pressuremeter, self-boring lateral stress cell, and dilatometer tests in marine clays. They discuss the influence of soil stiffness, disturbance, and strain path on the measured lateral stress. Sully and Campanella describe use of full displacement probes for estimation of lateral stress in cohesive soils. They evaluate test data from total stress cells, dilatometer, lateral stress piezocone, and seismic cone pressuremeter. Rankka presents data on a study of the lateral stress distribution in slopes in soft clay. She compares in situ measurements with pressure cells and dilatometer tests with those obtained by Janbu's generalized method of slices and found them to be in reasonably good agreement. Lunne et al. propose a new correlation between the dilatometer parameter K_D and K_o for young clays based on a data base containing information from research sites in Norway and the United Kingdom. Lutenegger presents a comparison of dilatometer, full-displacement pressuremeter, hydraulic fracture, and prebored pressuremeter techniques used to determine in situ lateral stress in a dense, glacial till. Juran and Mahmoodzadegan discuss the use of a hollow cylinder cell for the measurement of lateral stress and excess pore water pressure induced by cavity expansion in both clayey and granular soils. The application of these test data to the interpretation of pressuremeter test results is discussed. Campanella et al. describe a lateral stress piezocone developed at the University of British Columbia. On the basis of laboratory and field investigations, they indicate that the lateral stresses measured with this device are dependent on, inter alia, the existing horizontal stress, the in situ state of sand, and its grain characteristics.

Preparation of Aggregate Samples for Dynamic Testing

BASHAR A. QEDAN, ROBERT P. ELLIOTT, SAM I. THORNTON, AND MARK KUSS

A compaction device was developed that permits aggregate samples to be compacted by using the dynamic test equipment. Use of the device eliminates the need to move the specimen after it has been prepared. Tests were conducted to establish compaction procedures and to determine whether specimens compacted with the device experienced moisture or fines migration. The tests demonstrated that the method can be used to compact dense-graded aggregate materials to the modified Proctor (AASHTO T 180) maximum density without creating segregation or moisture migration. However, fines and moisture migration were observed when dry material and material significantly wetter than optimum were used. Recommendations are presented for preparing samples for dynamic testing using the device developed. Also included is an engineering drawing of the compaction device.

Aggregate samples for dynamic testing (i.e., resilient modulus and rapid shear strength) are normally compacted by vibratory methods. Typically, this involves the use of a small vibratory hammer equipped with a flat, cylindrical compaction head that fits within the compaction mold. The sample is compacted with the mold assembled on the triaxial cell base plate (Figure 1). After the sample is compacted, it is necessary to move the sample and base plate to the test machine.

DEVELOPMENT OF METHOD

The University of Arkansas, Department of Civil Engineering, developed an alternate method of sample preparation. The development was instigated because the department did not have the type of vibratory compaction equipment normally used. Also, the researchers wished to eliminate the need to move the sample after it was compacted. Therefore, this alternate method involves compacting the specimen by using dynamic test equipment.

Dynamic test equipment is a closed loop, hydraulic cyclic loading machine manufactured by MTS Systems Corporation, Minneapolis, Minnesota. The initial development attempt involved mounting a flat, cylindrical compaction head on the MTS load piston and then applying a vibratory force in essentially the same manner as was normally used with the vibratory hammer. However, several attempts with this approach by using various vibration frequencies failed to produce the target sample density. The target sample density was the maximum density determined by the modified Proctor test, AASHTO T 180 (*1*).

Subsequently, a modified compaction head (Figure 2) was developed that is able to produce the target density. The modification consists of attaching a ⅝-in. square bar across the diameter of the compaction head and then inserting a spring in the loading shaft. During compaction, the head is manually rotated. The square bar provides a concentration of the compactive effort and, during rotation, causes a reorientation of the aggregate particles. Although the bar protrudes into the top of the material during compaction, a uniform top surface is achieved by gradually raising and rotating the compaction head at the conclusion of compaction so that the bar "finishes" the surface during the final rotations.

The compaction head is mounted on the MTS loading shaft (Figure 3) in place of the load cell. The system is operated in strain control with the applied load limited by the maximum shaft movement and the spring in the compaction head. By using the strain control setting the maximum shaft movement is limited to 0.7 in. (18 mm). The head position is adjusted during compaction so that it lifts slightly above the aggregate at the top of each stroke to permit the manual rotation. As a result, the load spring is typically compressed between 0.4 and 0.5 in. (10 to 13 mm) during each compaction stroke.

It was determined through trial and error that the target density in a layer could be achieved by the MTS system being operated at a loading frequency of 10 Hz for 2 min. Five compaction layers were used for the 6-in. (152 mm) diameter by 12-in. (305 mm) high samples of crushed stone. Some adjustment in the time and frequency of loading may be necessary for other aggregates.

TESTING PROGRAM

Once a method had been established that produced the desired density, questions remained regarding the efficiency of the method and the uniformity of the resulting sample. Operational concerns involved the number of compaction layers, the vibrational frequency, and the compaction time. The uniformity concerns centered around potential problems of moisture and fines migration during compaction. A testing program was conducted to answer those concerns (*2*).

The measures of effectiveness used in the testing program were the achieved dry density and the migration of fines and moisture. The compacted samples were divided into top and bottom halves to check for fines and moisture migration. Each half was dried for moisture content and sieved for fines con-

B. A. Qedan, Arkansas State Highway and Transportation Department, P.O. Box 2261, Little Rock, Ark. 72203. R. P. Elliott, S. I. Thornton, and M. Kuss, University of Arkansas, Fayetteville, Ark. 72701.

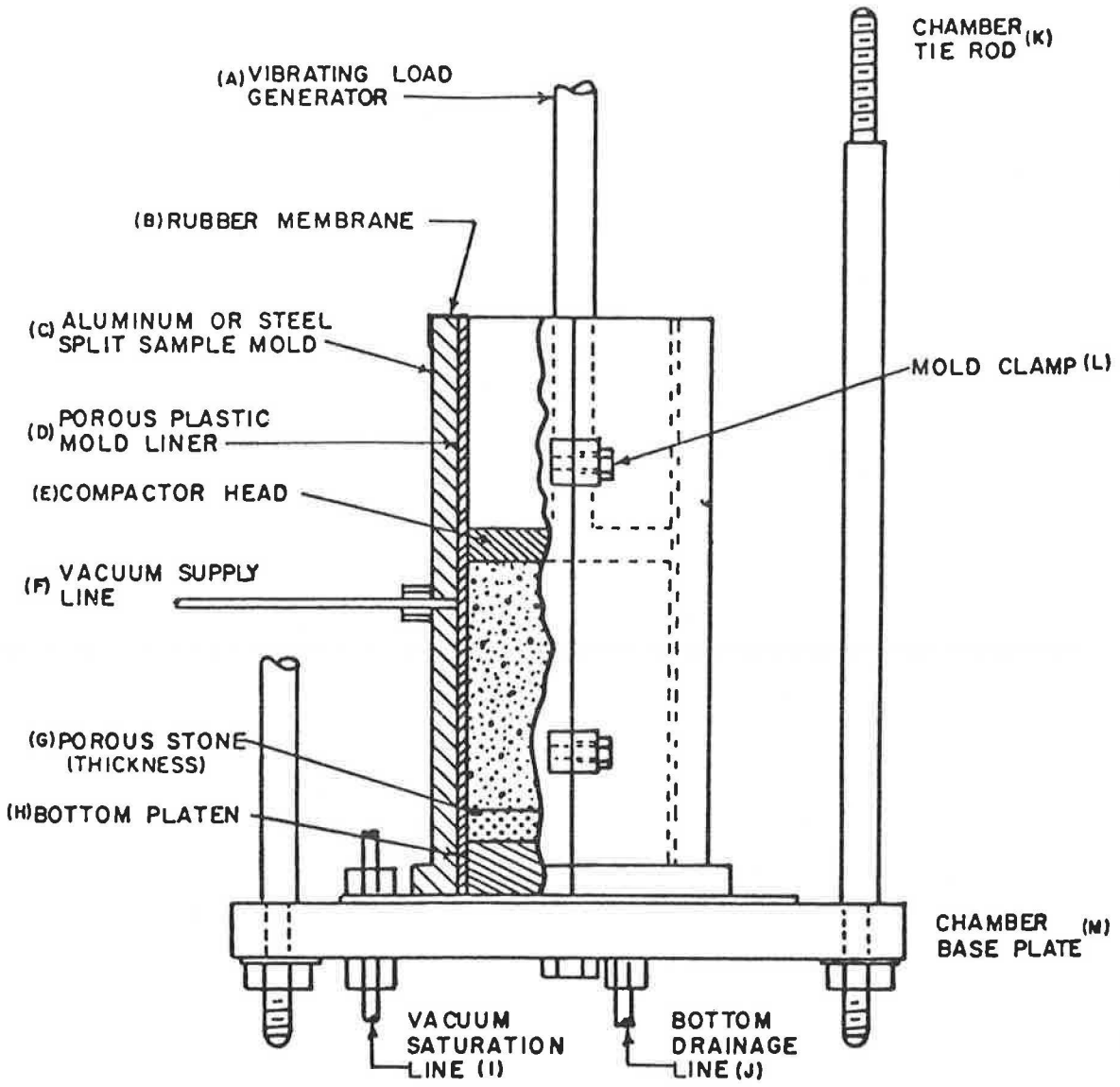

FIGURE 1 Vibratory compaction configuration from AASHTO T 180 (*1*).

tent. The ratios of top to bottom half contents provided a measure of migration.

The material used in the testing program was a dense-graded crushed limestone base material with the fraction larger than 0.75 in. (19 mm) replaced by material smaller than 0.75 in. (19 mm) but larger than the No. 4 (4.75 mm) sieve. Figure 4 presents a grain size curve of the gradation used in the testing. The laboratory maximum density and optimum moisture content for this material was 133 pcf (2130 kg/m^3) and 7.5 percent, respectively. The aggregate was sieved into five size fractions and recombined for each layer to the proper gradation and moisture content to ensure uniformity of the material for each compaction layer.

Number of Layers

To examine the possibility of using fewer compaction layers samples were prepared by using one, three, and five layers. The material for each layer was prepared to the proper gradation and the optimum moisture content.

The density of each layer was monitored by checking the compacted thickness. For the one- and three-layer samples, the compaction time per lift was increased to more than 2 min in an effort to achieve the target density. Nevertheless, the target density was not achieved for those specimens. The dry densities achieved were 121.9 pcf (1953 kg/m^3) for one layer, 123.5 pcf (1978 kg/m^3) for three layers, and 133.9 pcf (2145 kg/m^3) for five layers.

In addition to low density, the one-layer sample also showed serious moisture and fines migration (Figures 5 and 6). There was no evidence of significant migration for the three- and five-layer samples.

Compaction Time

Samples were prepared by using total compaction times of 6 min. per layer to investigate the significance of compaction time. The layer and sample thicknesses were checked periodically during compaction. There was no significant decrease in layer and sample thickness (i.e., increase in density) after

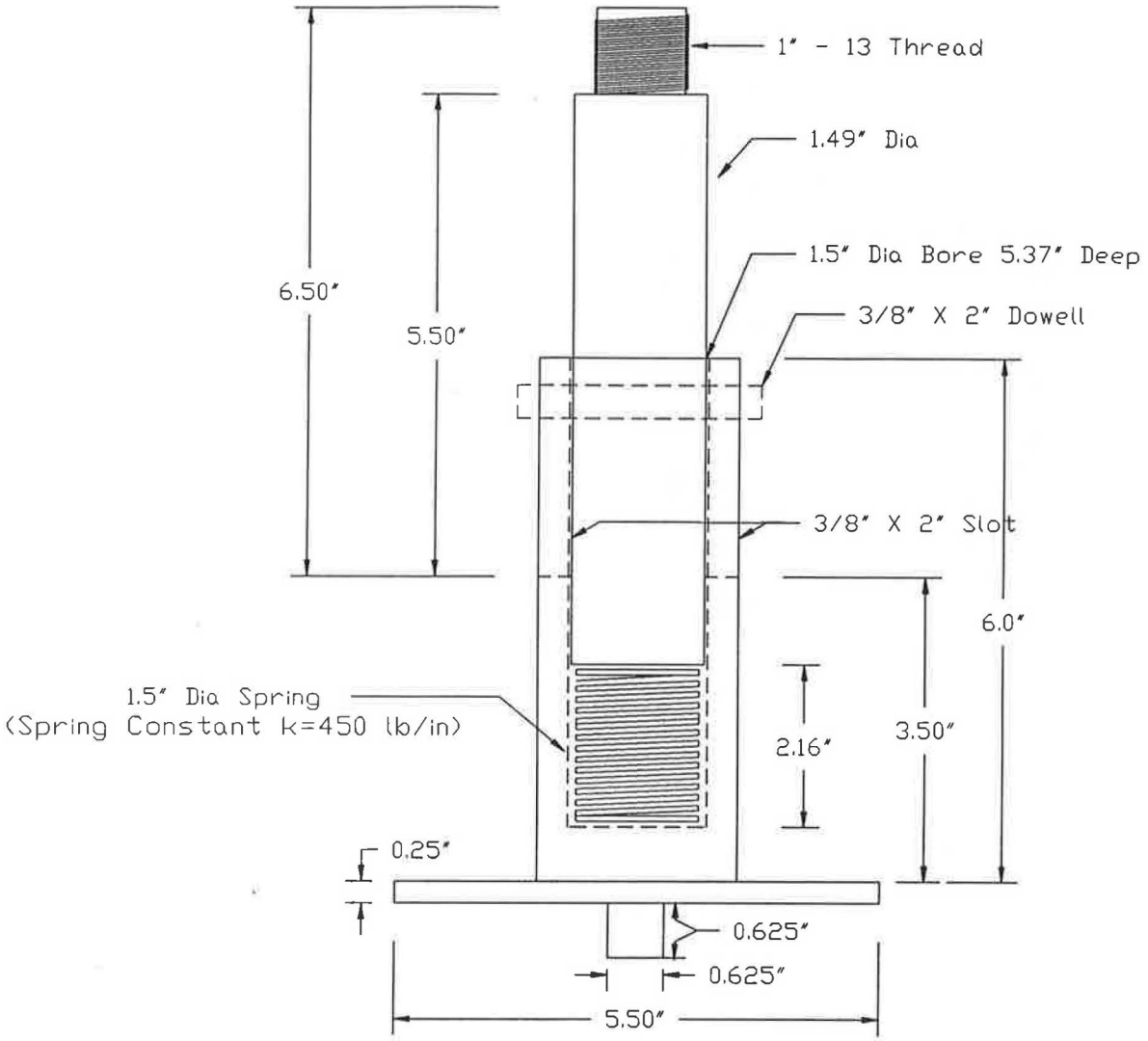

FIGURE 2 Engineering drawing of compaction device.

the first 2 min. Therefore, sample density for the aggregate tested is not significantly increased by using compaction times greater than 2 min per layer.

Vibration Frequency

The 10-Hz vibration frequency was selected through trial and error. To check whether other frequencies might be used, samples were prepared by using 5, 10, and 30 Hz. The target density could not be achieved except at the 10-Hz frequency.

Fines Content

Tests were also conducted to determine the effect of varying the fines and moisture content. The effect on fines and moisture migration was the primary interest in those tests.

To investigate the effect of fines content, samples were prepared with fines contents (percent passing the No. 200 sieve) of 3, 6, and 10 percent. The other gradation percentages were unchanged, and the moisture content was held at 7.5 percent. The samples were prepared by using five layers, 2 min of compaction per layer, and a 10-Hz vibration frequency.

The densities achieved were 122.0 pcf (1954 kg/m^3) at 3 percent fines, 133.9 pcf (2145 kg/m^3) at 6 percent fines, and 134.8 pcf (2159 kg/m^3) at 10 percent fines. None of the samples showed evidence of significant moisture or fines migration (Figures 7 and 8).

Moisture Content

Similar tests were conducted to examine the effect of moisture content. Three samples were prepared by using the normal gradation (Figure 4) and moisture contents of 0, 5, 7.5, and 10 percent. The samples were prepared by using five layers, 2 min of compaction per layer, and a 10-Hz vibration frequency.

The sample densities were found to increase when moisture content increased. The dry densities achieved were 124.5 pcf at 0 percent moisture, 128.1 pcf (2052 kg/m^3) at 5 percent moisture, 133.9 pcf (2145 kg/m^3) at 7.5 percent moisture, and 136.4 pcf (2185 kg/m^3) at 10 percent moisture. Fines migration was found in both the 0 and the 10 percent moisture content

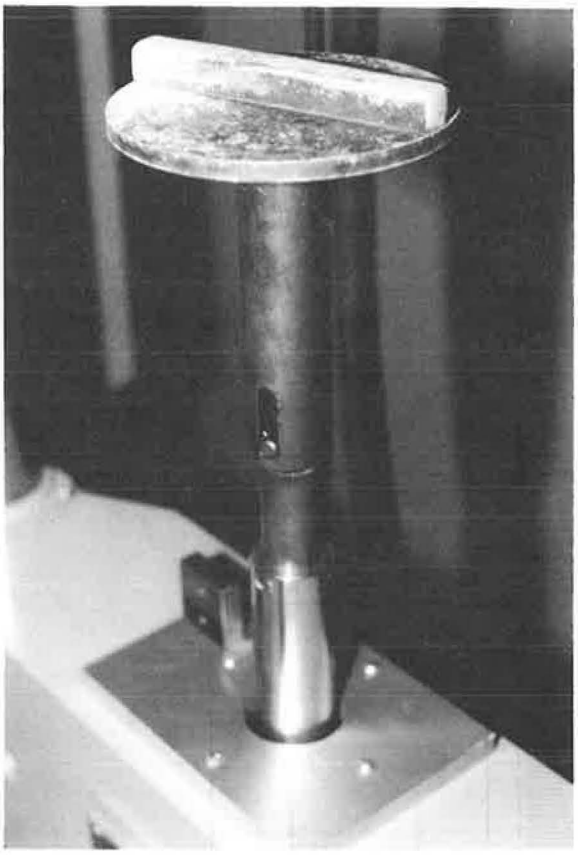

FIGURE 3 Compaction device mounted on MTS.

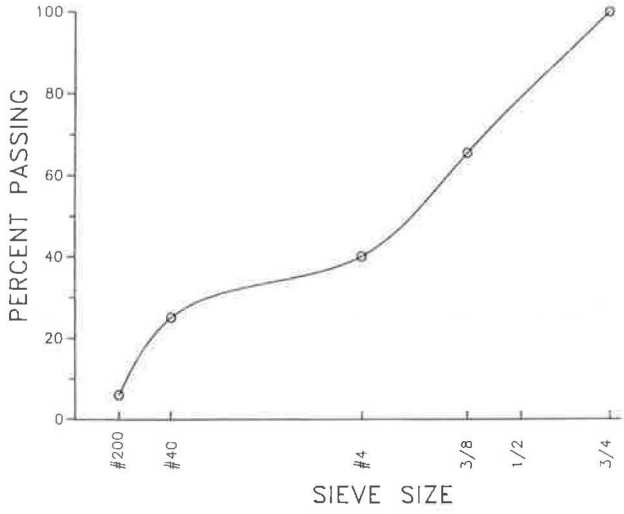

FIGURE 4 Gradation of aggregate used in test program.

samples (Figure 9). The fines migrated to the bottom in the 0 percent sample and to the top in the 10 percent sample. The 10 percent fines sample showed a corresponding migration of moisture (Figure 10). There was no evidence of fines or moisture migration for the 5 and 7.5 percent moisture content samples.

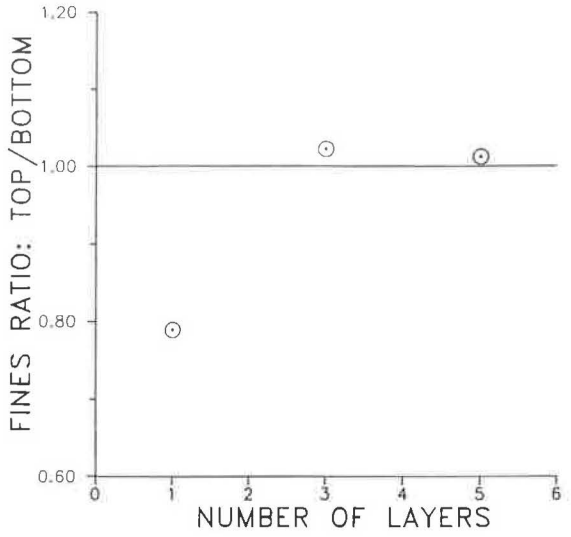

FIGURE 5 Fines migration results for 1, 3, and 5 layers.

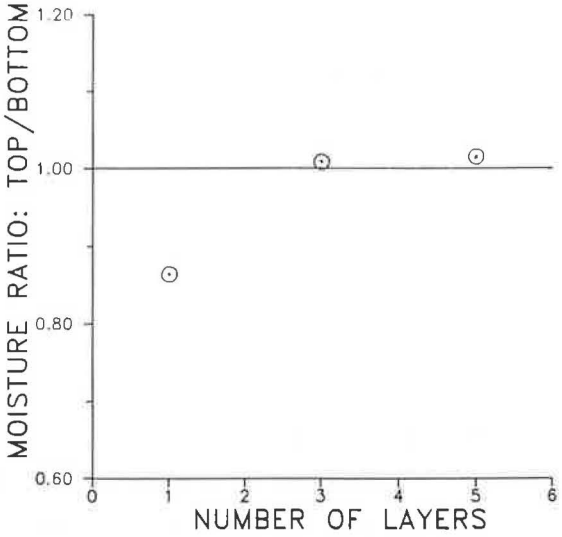

FIGURE 6 Moisture migration results for 1, 3, and 5 layers.

One additional sample was prepared to examine the combined effect of low fines content (3 percent) and high moisture (10 percent). This sample also experienced fines and moisture migration (Figures 9 and 10). Interestingly, however, the fines and moisture migrated to the bottom in the low fines sample, opposite to the direction in the normal gradation sample (6 percent fines).

CONCLUSIONS

An alternate method for preparation of aggregate samples for dynamic testing has been developed. The method allows the sample to be prepared by using the dynamic test equipment, thus eliminating the need to move the sample after it is prepared. Visual examination of samples prepared by using the method showed the samples to be uniform.

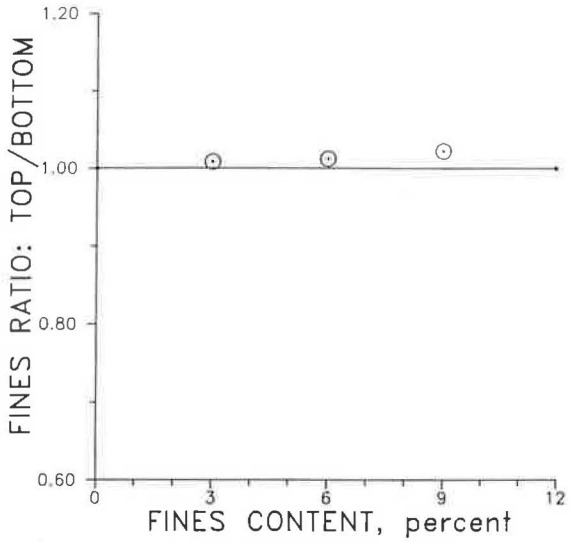

FIGURE 7 Fines migration for samples with varying fines content.

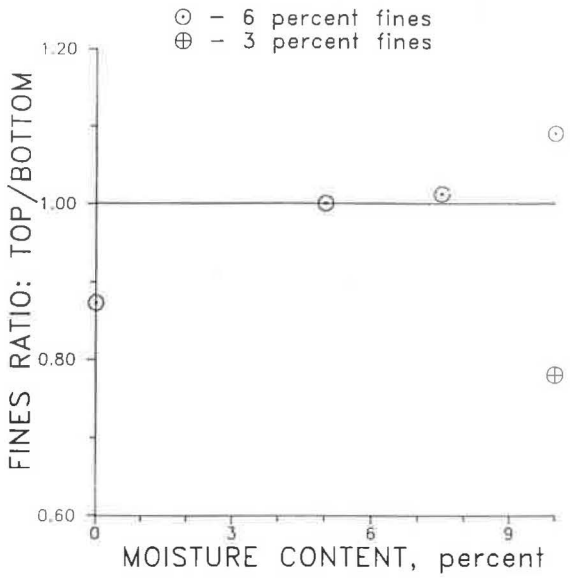

FIGURE 9 Fines migration at various moisture contents.

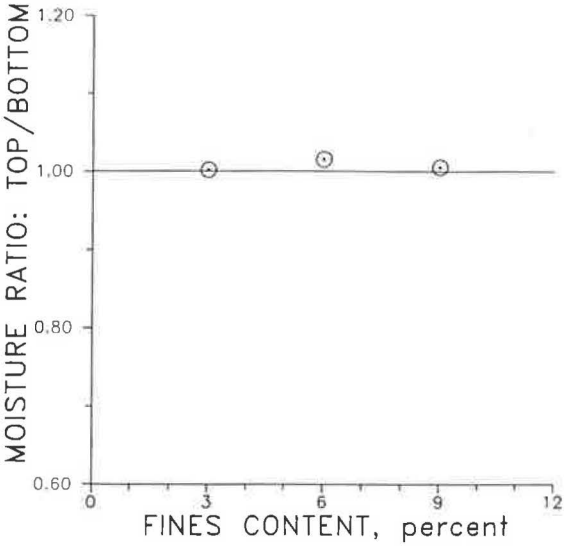

FIGURE 8 Moisture migration for samples with varying fines content.

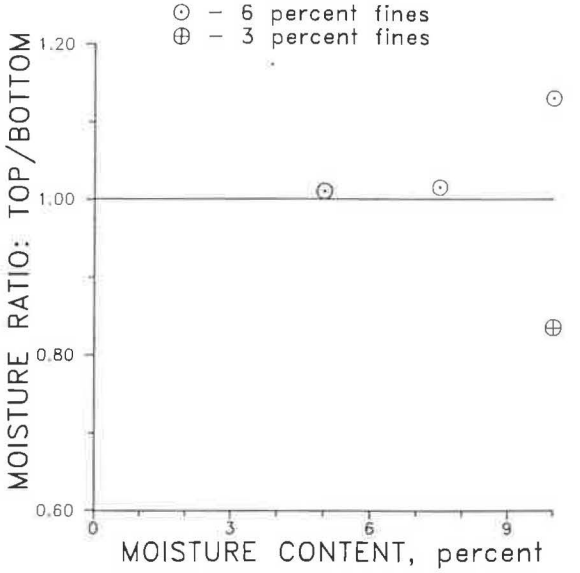

FIGURE 10 Moisture migration at various moisture contents.

A small test program confirmed that the method can compact dense-graded aggregate materials to densities equivalent to the AASHTO T 180 maximum density without creating segregation or moisture migration. However, when dry materials were used, problems were experienced in achieving the target density and fines migration was observed. Fines and moisture migration were also observed when the method was used with materials significantly wetter (10 percent versus 7.5 percent) than the optimum moisture content.

RECOMMENDED COMPACTION METHOD

What follows is the recommended method for preparing 6-in.-diameter by 12-in. high aggregate samples by using the compaction head developed at the University of Arkansas (Figures 2 and 3).

1. Determine the total amount of material needed on the basis of target density.
2. Weigh out and mix the proper amount of aggregate and water. To prevent fines and moisture migration, the moisture content should be from 2 percent below to 1 percent above optimum.
3. Compact the sample in five layers of equal thickness (2.4 in., 61 mm). The amount of material placed in the mold should be one-fifth the total amount needed for the sample on the basis of target density.
4. Mount the compaction head on the loading shaft of the dynamic test device.

5. Set the test device strain controls such that the maximum shaft movement is 0.7 in. (18 mm).

6. Set the operational frequency at 10 Hz. (Note: The test program used to develop the procedure was tried with frequencies of 5, 10, and 30 Hz. The target density could not be achieved except at 10 Hz. In some subsequent work, frequencies of 11 and 12 Hz were found to improve the compaction of some aggregates.)

7. For each sample layer, place the material in the mold and lower the compaction head so that the bar just touches the material.

8. During compaction, maintain the compaction head so that the head lifts slightly above the aggregate at the top of each vibrational stroke while manually rotating the load shaft (approximately 6 rpm) so as to rotate the compaction head.

9. Compact each layer for 2 min or until the appropriate layer height has been achieved. (Note: The test program used to develop the procedure was tried with only one aggregate. Although other aggregates have been compacted successfully in 2 min, some adjustment of the 2-min time may be necessary for other aggregates.)

10. To achieve a finished top surface, slowly raise the compaction head at the conclusion of the compaction time while continuing to operate and rotate the head. This should be done for the final layer and for any other layer for which the sample height is to be measured.

11. Measure the sample height by using the top of the mold as a point of reference to check the density achieved.

REFERENCES

1. *Standard Specifications for Transportation Materials and Methods of Sampling and Testing*, Part II: *Methods of Sampling and Testing*. American Association of State Highway and Transportation Officials, Washington, D.C., 1986.
2. B. A. Qedan, *Resilient Modulus Sample Preparation for Granular Materials*. M.S. thesis. University of Arkansas, Fayetteville, 1987.

Publication of this paper sponsored by Committee on Mineral Aggregates.

Repeated Triaxial Characterization of Granular Bases

M. R. THOMPSON AND K. L. SMITH

Granular bases are utilized extensively in Illinois flexible pavement construction. Typically, the granular materials are dense graded with a maximum size of 1.5 in. and 4 to 12 percent passing the No. 200 sieve (fines). The Illinois specification gradation designation is CA-6. More "open-graded" granular materials with reduced fines content are less moisture sensitive and generally provide improved granular base performance. In recognition of those factors, an additional granular base course gradation (CM-06) has been proposed. The current CA-6 and the proposed CM-06 gradation limits only differ in the permissible amount passing the No. 200 sieve. The CM-06 limits are 2 percent ± 2 percent, and the CA-6 limits are 8 percent ± 4 percent. As part of an overall evaluation of the proposed gradation modification, a comprehensive triaxial testing program (repeated loading and rapid shear strength tests) was conducted to establish the pertinent properties [resilient modulus, permanent deformation accumulation with loading repetitions, and shear strength characteristics (cohesion and friction angle)] of typical crushed stones, crushed gravels, and gravels meeting CA-6 and CM-06 gradation requirements. Seven materials were included in the program. Results of the testing program indicated the following: (a) For near maximum dry density and optimum moisture content conditions, friction angles show little variability and cohesion values ranged from 9.6 to 24.4 psi. (b) The resilient modulus parameters K and n fell within expected ranges, and only limited differences were noted among the various granular materials. Resilient modulus is not a good property for ranking granular base performance potential. (c) The rapid shear strength of "conditioned" (previously loaded) specimens was always greater than the "unconditioned" strength (increases from 34 to 217 percent). This is a very significant finding. (d) Permanent deformation under repeated loading varied considerably. In fact, four of the materials (all gravel products) did not survive the standard conditioning loading (45 psi deviator stress/15 psi confining pressure). It is apparent that permanent deformation under repeated loading provides a more definitive evaluation of granular base materials than does shear strength or resilient modulus.

Granular bases are utilized extensively in Illinois flexible pavement construction. Typically, the granular materials are dense graded with a maximum size of 1.5 in. and 4 to 12 percent passing the No. 200 sieve (fines). In Illinois, the dominant gradation is CA-6 (see Table 1 for gradation limits).

Poor granular base performance generally is linked to the use of "near to" or "out of" specification (with respect to fines) granular materials and in situ moisture contents in excess of optimum moisture (AASHTO T-99). Frequently, the high fines content aggregates are also near to or above the PI requirements [<6 for gravel; <4 for crushed stone and crushed gravel in Illinois Department of Transportation (DOT) specifications].

M. R. Thompson, Department of Civil Engineering, 205 North Mathews, Urbana, Ill. 61801. K. L. Smith, ERES Consultants, Inc., 1401 Regency Drive East, Savoy, Ill. 61874.

More "open-graded" granular materials with reduced fines content are less moisture sensitive and generally provide improved granular base performance. In recognition of those factors, and as a result of cooperative deliberations by the Illinois DOT with Illinois aggregate producers, an additional granular base course gradation (CM-06) has been proposed. The current CA-6 and the proposed CM-06 gradation limits are listed in Table 1. The only difference in the two specifications is the permissible amount passing the No. 200 sieve. The CM-06 limits are 2 percent ± 2 percent, and the CA-6 limits are 8 percent ± 4 percent.

Repeated loading properties (i.e., resilient modulus and permanent deformation accumulation with loading repetitions) and shear strength characteristics are major factors that influence the structural responses (stresses, strains, displacements) and performance of conventional flexible pavements. As part of an overall evaluation effort, a comprehensive triaxial testing program (i.e., repeated loading and rapid shear strength tests) was conducted to establish the pertinent properties of typical crushed stones, crushed gravels, and gravels that meet CA-6 and CM-06 gradation requirements. The various materials were also used to construct field test sections (3-in. asphalt concrete surface plus 12-in. granular base) on a Livingston County, Illinois, highway. Only the triaxial testing component of the evaluation program is presented here.

MATERIALS

Granular materials indigenous to the Livingston County, Illinois, area were used in the program. All of the crushed stone products were produced at a local limestone quarry. The gravel products were provided by two locally operated pits. Crushed gravel was produced by crushing gravel particles equal to or larger than the maximum nominal size in the target gradation. The partially crushed gravel (Material No. 8A) was produced by crushing and returning the oversized particles in a gravel (the percent crushed particles was about 30 to 35 percent). A total of seven materials were included in the triaxial testing program. They are listed in Table 2. Gradation and AASHTO T-99 (Method C) compaction data for the materials are summarized in Table 3.

TESTING PROGRAM

The triaxial testing program included three types of tests.

1. Type A: Rapid shear strength testing at near T-99 maximum dry density and optimum moisture content conditions and confining pressures of 5, 15, and 30 psi;

TABLE 1 CA-6 AND CM-06 GRADATION LISTS

CA-6 and CM-06 Gradation Limits

Sieve	% Passing	
	CA-6	CM-06
1.5 inches	100	100
1.0 inches	95±5	95±5
1/2 inch	75±15	75±15
#4	43±13	43±13
#16	25±15	25±15
#200	8±4	2±2

TABLE 2 GRANULAR MATERIALS LISTING

Material	Type	Gradation
#1	Crushed Stone	CA-6
#2	Crushed Stone	CM-06
#5	Crushed Gravel	CA-6
#6	Crushed Gravel	CM-06
#7	Gravel	CA-6
#8	Gravel	CM-06
#8A	Partially Crushed (30-35%) Gravel	CA-6

2. Type B: Rapid shear strength testing (15 psi confining pressure) at "maximum achievable" dry density and "wet of optimum" (i.e., target value was 1.5 percent wet of AASHTO T-99 optimum) conditions; and
3. Type C: Repeated load triaxial testing (i.e., nonfailure stress state conditions) at near maximum dry density and optimum moisture content followed by rapid shear strength testing (15 psi confining pressure).

The general descriptions of the testing procedures and operations are presented next.

Triaxial Specimen Preparation

Test specimens were prepared in the same manner for all types of testing. Test specimen dimensions were 6-in. diameter and 12-in. nominal height.

The granular material was batch-mixed at the target moisture content. A vertically segmented steel mold lined with a 31-mil neoprene membrane was assembled on the triaxial cell base plate. A full-faced vibratory compaction hammer was used to densify five successive lifts to achieve the target density level. Following compaction, the loading cap was placed on the specimen, and the compaction membrane was sealed to the load cap. An internal vacuum was then pulled on the specimen. When the segmented steel mold was removed, the specimen was supported by the internal vacuum. Because the neoprene compaction membrane was frequently punctured, a second 25-mil latex membrane was placed on the specimen. Finally, the triaxial cell and top plate was placed on the base plate. The specimen was then placed in the loading frame.

TABLE 3 GRADATION, COMPACTION, AND PI DATA

	Percent Passing						
	Material						
Sieve	#1	#2	#5	#6	#7	#8	#8A
(Gradation)	CA-6	CM-06	CA-6	CM-06	CA-6	CM-06	CA-6
1-inch	100	100	100	100	95.1	100	99.1
3/4-inch	97.5	85.2	93.1	95.8	89.5	92.4	92.0
1/2-inch	90.2	67.9	72.3	77.0	81.8	78.4	78.1
#4	53.1	42.0	32.1	33.1	46.9	42.8	55.2
#16	25.4	12.7	15.8	14.1	20.3	15.7	23.8
#200	10.5	3.4	7.8	3.1	5.0	4.8	8.5
AASHTO T-99							
Max. Dry Density, pcf	143.6	122.5	134.1	128.4	134.4	135.0	133.4
Optimum Moisture, %	6.6	4.0	7.7	6.9	7.6	8.0	9.0
AASHTO T-90							
Plasticity Index	4	NP	NP	NP	4	NP	3

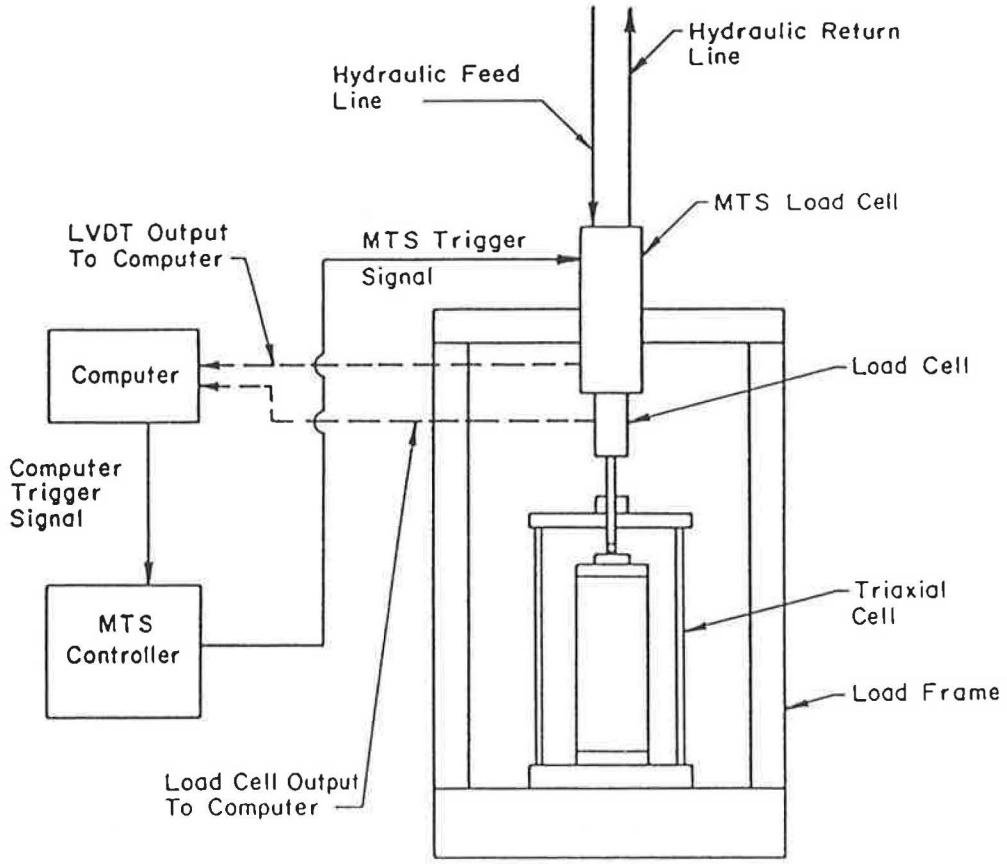

FIGURE 1 Triaxial testing apparatus.

Triaxial Testing

A computer-interfaced closed-loop hydraulic loading apparatus was used in all of the testing (refer to Figure 1). The computer was programmed to conduct the various tests automatically and collect and store the test data (deviator loads and total axial deformations as a function of load repetitions and time or both) for subsequent processing. Air was used as the confining pressure, and the tests were conducted with the sample being vented to the atmosphere (open or drained condition).

Rapid Shear Test

The specimen was rapidly loaded (1.5 in./sec) to failure. The 1.5 in./sec deformation rate corresponds to achieving a 5 percent failure strain (12-in. specimen length) in 400 msec. This load duration is considered a realistic simulation of a relatively slow-moving vehicle.

Repeated Load Testing

The repeated load triaxial test was executed in three steps:

1. Step 1: 5,000 stress repetitions (15 psi confining pressure and repeated deviator stress of 45 psi) were applied, and permanent deformations were recorded throughout the loading sequence. Materials No. 5, No. 7, No. 8, and No. 8A suffered extensive permanent deformation under the listed stress state and were evaluated at a reduced stress state (15 psi confining pressure and 30 psi deviator stress).
2. Step 2: A series of repeated stress states was then applied to the specimen, and the "resilient deformations" (total axial deformations) were monitored. The stress state application sequence is indicated in Table 4. Those data were used to calculate resilient moduli, which is defined as the repeated deviator stress divided by the resilient strain.
3. Step 3: The specimen was subjected to rapid triaxial testing at a confining pressure of 15 psi following the completion of the repeated loading sequence.

TEST DATA

Rapid Shear Strength Tests

Specimen properties and rapid shear strength results for Type A and Type B tests are presented in Table 5. The C and ϕ values presented in Table 6 were calculated by establishing a linear regression relation of the form

$$\sigma_1 = a + b\,\sigma_3$$

where

$C = a/(2 \times b^{0.5})$ and
$\phi = \sin^{-1}$ of $[(b - 1)/(b + 1)]$.

TABLE 4 REPEATED LOADING SEQUENCE

Loading	Number of loads	σ_1, psi(1)	σ_3, psi(2)	Deviator stress, psi(3)	θ, psi(4)	Stress ratio(5)
Condition	5000	60	15	45	90	4
1	500	60	15	45	90	4
2	500	45	15	30	75	3
3	500	50	10	40	70	5
4	500	30	10	20	50	3
5	500	25	5	20	35	5
6	500	20	5	15	30	4
7	500	15	5	10	25	3
8	500	90	15	75	120	6

1 - σ_1 is major principal stress

2 - σ_3 is the minor principal stress (equal to the cell pressure)

3 - Deviator stress is $\sigma_1 - \sigma_3$

4 - θ is bulk stress = $\sigma_1 + \sigma_2 + \sigma_3$. For the triaxial test, θ is equal to $\sigma_1 + 2\sigma_3$.

5 - σ_1/σ_3

TABLE 5 RAPID SHEAR STRENGTH DATA

Material	% Compaction*	Moisture Content, %	Confining Pressure, psi	Maximum Deviator Stress, psi
#1	98.8	6.8	5	147
	99.0	6.7	15	194
	99.0	6.8	30	274
	97.0	8.1	15	173
#2	99.8	4.1	5	97
	100.	4.1	15	171
	100.	4.0	30	217
	97.7	5.6	15	136
#5	99.3	7.8	5	78
	99.4	7.8	15	164
	99.6	7.7	30	209
	96.8	9.1	15	110
#6	99.9	6.9	5	92
	99.9	7.1	15	175
	99.6	6.6	30	226
	96.6	8.1	15	111
#7	99.9	7.5	5	76
	99.9	7.4	15	127
	99.6	7.6	30	189
	98.0	9.0	15	108
#8	99.3	8.4	5	64
	99.1	7.9	15	109
	99.3	8.1	30	170
	95.9	9.5	15	74
#8A	99.9	9.1	5	75
	99.9	8.9	15	116
	99.9	8.7	30	185
	97.8	10.3	15	109

* Relative to AASHTO T-99

TABLE 6 RAPID SHEAR STRENGTH AND RESILIENT MODULI DATA

			Resilient Testing			
Material	Cohesion (psi)	Friction Angle (Degrees)	K* (psi)	n	R**	Modulus*** (ksi)
#1	24.4	45.9	15,310	0.28	0.93	35.4
#2	17.7	44.4	11,590	0.33	0.93	31.1
#5	13.4	45.8	10,270	0.35	0.91	29.3
#6	15.1	46.4	10,240	0.35	1.0	29.2
#7	11.9	43.8	12,230	0.31	0.96	31.0
#8	9.6	42.7	9,440	0.37	0.97	28.6
#8A	11.1	43.5	9,720	0.23	0.61	19.4

* Antilog of "a" in Log $E_R = a + n \log \theta$

** Correlation coefficient in above $E_R - \theta$ relation

*** Resilient Modulus for $\theta = 20$ psi

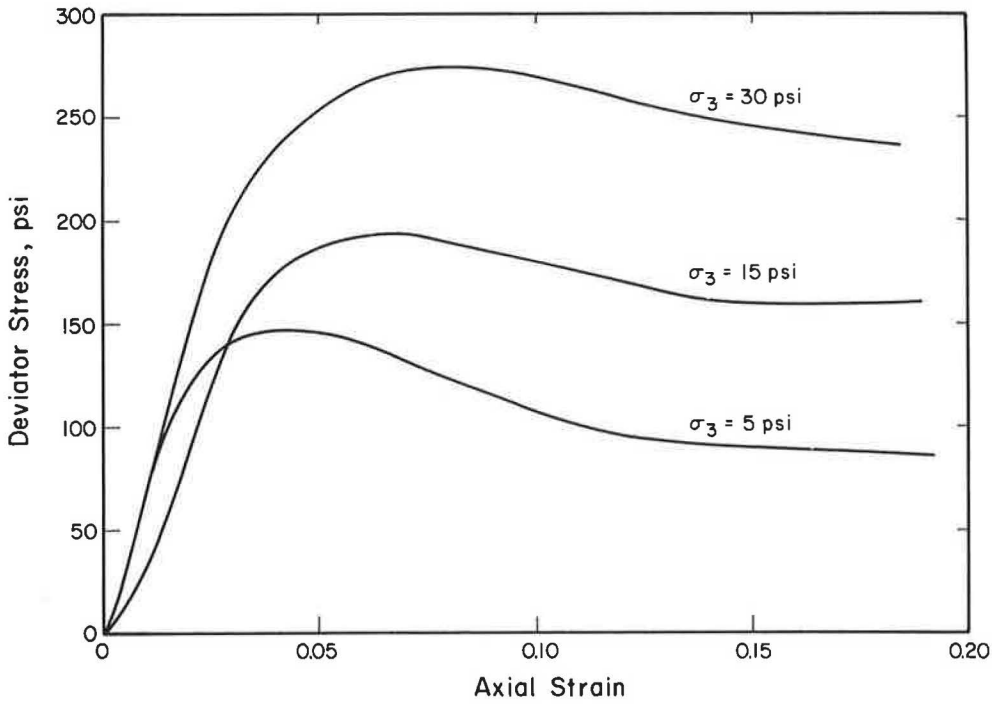

FIGURE 2 Rapid shear strength stress-strain relations for material No. 1 (type A test).

Typical stress-strain plots for Type A rapid shear strength tests at various confining pressures are indicated in Figure 2. Illustrative comparative stress-strain plots (15 psi confining pressure) for Type A, Type B, and Type C tests are presented in Figure 3. In some of the "conditioned" tests, the deviator stress peaked at 354 psi, which is the limit of the 10-kip ram in the testing frame.

Repeated Load Testing

Resilient moduli data are presented in Table 6 in terms of K and n, the constant and exponent in the stress-dependent modulus relation:

$$E_R = K\,\theta^n$$

where

E_R = resilient modulus (repeated deviator stress/ resilient strain),

θ = bulk stress ($\sigma_1 + \sigma_2 + \sigma_3$) or $\sigma_1 + 2\sigma_3$ in the triaxial test, and

K and n = experimentally established parameters.

Permanent deformation data in the form of log permanent strain and log number of load repetitions are presented in Figure 4 for the various materials and stress-state test conditions.

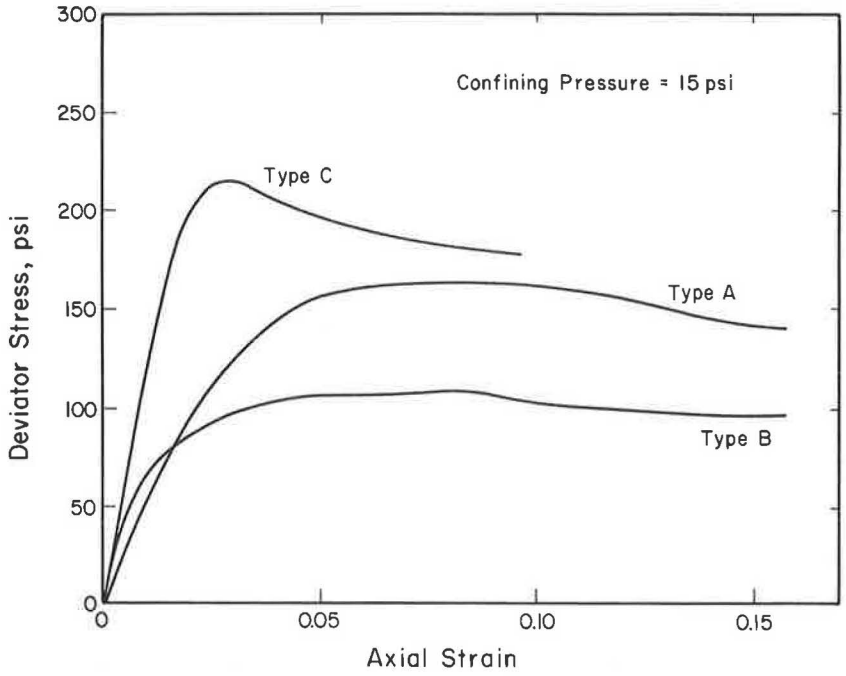

FIGURE 3 Typical stress-strain relations for types A, B, and C testing (material No. 5).

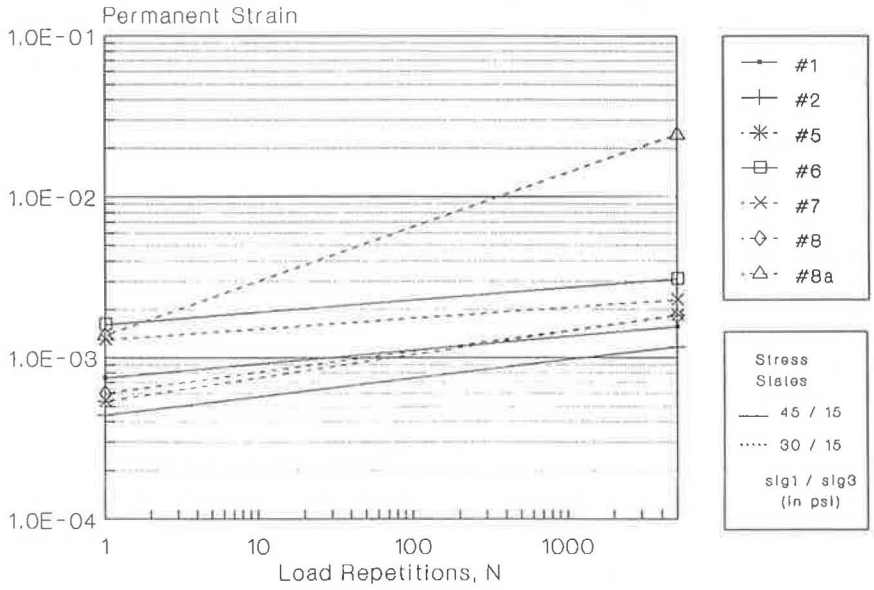

FIGURE 4 Permanent strain-log *N* relations for all materials (type C testing).

DATA ANALYSIS AND DISCUSSION

General

The data in Tables 5 and 6 are for material "pairs" with differing gradations (CA-6 or CM-06). No. 1 and No. 2 are crushed stones, No. 5 and No. 6 are crushed gravels, and No. 7 and No. 8 are gravels. The fines contents for No. 7 and No. 8 are practically the same. Material No. 8A (CA-6 gradation/partially crushed gravel) was included in the testing program because the original material initially selected for the program (No. 8/CM-06 gradation/gravel) could not be satisfactorily compacted under field construction conditions. It is important to note that all of the materials are within the CA-6 and CM-

06 specification ranges. The maximum fines content is 10.5 percent (Material No. 1), which is less than the maximum permissible value of 12 percent for CA-6.

Rapid Shear Strength

The rapid shear strength data for optimum moisture content and near maximum dry density are presented in Table 6. The data are reasonable and are expected values for those materials. The friction angles only vary from 42.7 degrees for No. 8A to 46.4 degrees for No. 6. The cohesion varies over a larger range, from a low of 9.6 psi for No. 8 to a high of 24.4 psi for No. 1. The CA-6 gradations provide slightly larger (relative to the CM-06 gradations) cohesion and friction values for the crushed stone (No. 1 and No. 2) and gravel (No. 7 and No. 8) pairs, but, for the crushed gravel pair (No. 5 and No. 6), the CM-06 gradation displayed a slightly larger cohesion and friction angle.

Moisture Sensitivity

The maximum deviator stress (i.e., confining pressure of 15 psi) data (see Table 7) for "optimum" and "wet" of optimum moisture contents are indicative of the moisture sensitivity of the various materials. The Retained Strength Index (RSI), defined as "wet" strength/strength at optimum moisture content, ranged from a high of 0.94 for No. 8 to a low of 0.63 for No. 6, with an average of 0.78 (standard deviation of 0.12). An RSI of 1.0 is "complete" strength retention. Thompson (*1*) has reported similar data for the AASHO Road Test crushed stone base, which indicated considerably lower RSI values (around ± 0.4) for moisture content differences (wet minus dry) of 1.4 to 2.6 percent and confining pressures ranging from 6 to 20 psi. The RSI value may prove to be a simple procedure for characterizing moisture sensitivity. Additional data are needed to develop the concept further.

Repeated Load Testing

The repeated loading data from the Type C testing procedure can be used to establish stress-dependent modulus effects (i.e., modulus increases with stress state) and to characterize permanent deformation behavior. The rapid shear strength test (15 psi confining pressure) conducted on the sample, following application of the conditioning (5,000 load repetitions) and resilient moduli stress state sequences, is useful in establishing stress history effects on shear strength.

Resilient Modulus

The K and n parameters presented in Table 6 are realistic and compare favorably with the comprehensive data base developed by Rada and Witczak (*2*). Figure 5 presents the typical K-n relations for various granular materials developed by Rada and Witczak. ILLI-PAVE analyses for the Livingston County pavement section (3-in. AC surface and 12-in. granular base) indicated that 20 psi is a representative θ value for mid-depth in the granular base. Resilient modulus values (θ = 20 psi) for the various materials are presented in Table 6. If Material No. 8A is excluded, then the resilient modulus ranges from 28.6 to 35.4 ksi. It is apparent that the resilient modulus properties of the various aggregates are similar. Elliot and Thompson (*3–5*) have demonstrated that the type of aggregate base material (crushed stone/gravel) has a limited effect (± 10%) on ILLI-PAVE calculated structural responses (AC strain, surface deflection, subgrade deflection, subgrade strain, subgrade deviator stress). In the same studies, analyses of Loop 4 AASHO Road Test surface deflection data also indicated that the "type" of granular material had little effect on surface deflection response. It is apparent that the "resilient responses" of a conventional flexible pavement section are not the sole determinant of pavement performance.

Permanent Deformation

The permanent deformation response parameters A and b for the log permanent strain/log N relation are summarized in Table 8. A is indicative of the permanent strain experienced under the first load application, and b represents the "rate" of permanent strain accumulation.

It is important to note that Materials No. 5, No. 7, No. 8, and No. 8A, which were all gravel products, did not survive the standard conditioning of 5,000 repetitions of a stress state of 45 psi/15 psi (repeated deviator stress/confining pressure). The specimen suffered extensive permanent stain accumulation. The three materials that survived the standard conditioning stress state (Materials No. 1, No. 2, and No. 6) were

TABLE 7 MOISTURE CONTENT AND SHEAR STRENGTH DATA

	Maximum Deviator Stress,* psi		
Material	"Optimum" Moisture	"Wet" of Optimum	Retained Strength***
#1	194 (+0.1)**	173 (+1.5)**	0.89
#2	171 (+0.1)	136 (+1.6)	0.80
#5	164 (+0.1)	110 (+1.4)	0.67
#6	175 (+0.2)	111 (+1.2)	0.63
#7	127 (-0.2)	108 (+1.4)	0.85
#8	109 (-0.1)	74 (+1.5)	0.68
#8A	116 (-0.1)	109 (+1.3)	0.94

* 15 psi confining pressure
** ( ) moisture content -%- relative to AASHTO T-99 optimum
*** RSI = Retained Strength Index = "Wet" strength/"Optimum" strength

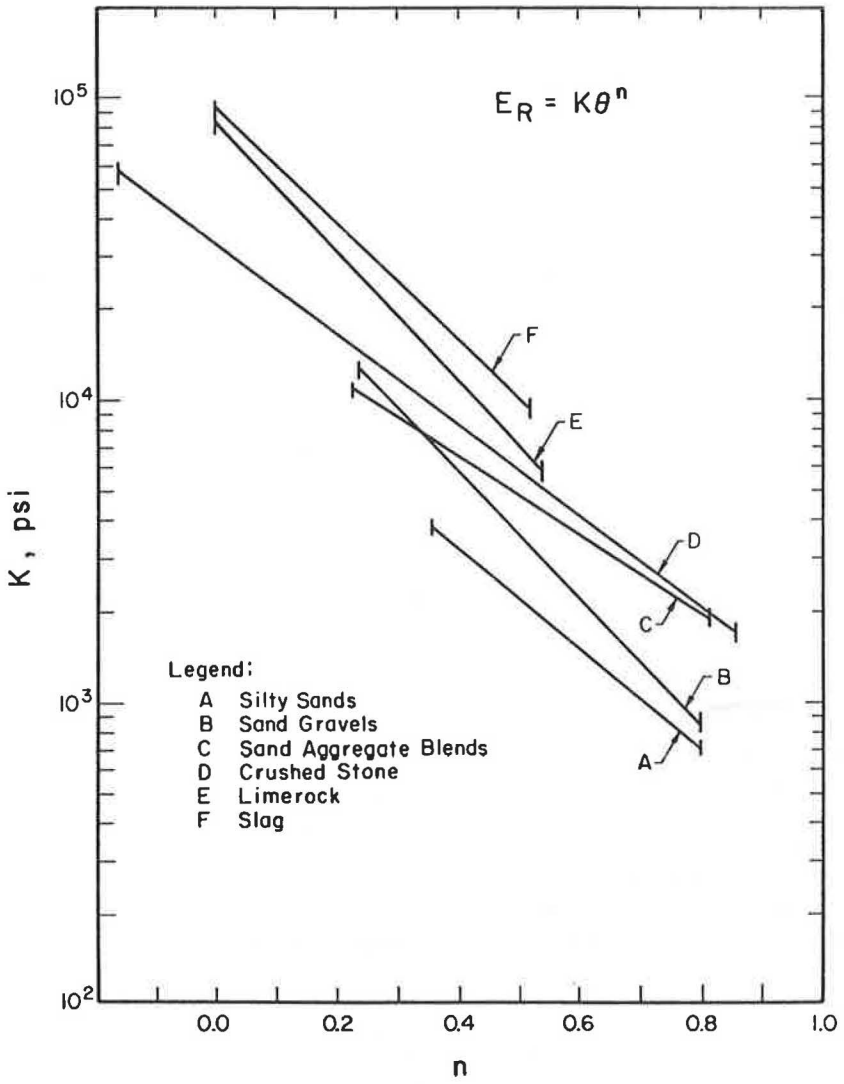

FIGURE 5 ***K*** **and** ***n*** **relationships for various types of granular materials identified by Rada and Witczak (*2*).**

TABLE 8 PERMANENT STRAIN DATA

Material	% Compaction*	Moisture Content, %	Stress State, psi (σ_D/σ_3)	A**	b**	R***
#1	99	6.5	45/15	7.4×10^{-4}	0.087	0.94
#2	100	4.0	45/15	4.4×10^{-4}	0.114	0.99
#5	99	7.6	30/15	5.3×10^{-4}	0.145	0.98
#6	100	6.9	45/15	16.1×10^{-4}	0.076	0.97
#7	100	7.5	30/15	12.9×10^{-4}	0.067	0.98
#8	99	8.0	30/15	6.0×10^{-4}	0.130	0.99
#8A	100	8.9	30/15	13.8×10^{-4}	0.337	0.99

* - Relative to AASHTO T-99
** - Log Permanent Strain = a + b Log N
A = antilog of "a"
Permanent Strain = AN^b
*** - Correlation coefficient

the materials with the higher shear strengths as quantified by the maximum deviator stress at a 15 psi confining pressure. The range of shear strengths for the "survivors" was from 171 to 194 psi.

The shear strengths (at 15 psi confining pressure) for the "nonsurvivors" ranged from a low of 109 psi to a high of 164 psi. Stress ratios (45 psi repeated deviator stress divided by maximum deviator stress at 15 psi confining pressure) for the "nonsurvivors" were all greater than 0.27 (Material No. 5) with a high of 0.41 (Material No. 8).

The data for Material No. 5 (shown in Figure 6 as a permanent strain/number of load repetitions plot) illustrate the "unstable" behavior of the 45 psi/15 psi stress state (deviator stress/confining pressure) condition and the more typical "stable" data of the 30 psi/15 psi stress state. The Table 8 data are either for the standard conditioning stress state or for the reduced stress state of 30 psi/15 psi.

When compared with values referenced in NCHRP 1-26 (*6*), the *b* values are typical and realistic except for Material No. 8A, which is very high. The permanent strain/log *N* plot for Material No. 8A (see Figure 7) indicates "unstable" behavior (i.e., an increasing rate of deformation accumulation with increased load repetitions) even at the reduced conditioning stress state of 30 psi/15 psi. Thus, the *A* and *b* data are misleading for Material No. 8A.

Other than the general shear strength relations noted, the *A* and *b* factors for the two stress state conditions (45 psi/15 psi and 30 psi/15 psi) do not appear to be functionally related to such factors as deviator stress ratio or shear strength. It is apparent that it is difficult to predict permanent strain accumulation accurately even under carefully controlled laboratory conditions.

Stress History/Rapid Shear Strength

In Type C testing, a rapid shear strength test (15 psi confining pressure) is conducted following the application of the conditioning and resilient testing stress repetitions (see Table 4). In contrast, Type A tests are conducted on specimen that have not experienced any stress history. Typical comparative stress/strain data (15 psi confining pressure) for Type A and Type C tests on Material No. 5 are indicated in Figure 3. The maximum deviator stress data for comparable Type A and Type C tests are summarized in Table 9.

In all cases, the conditioned (Type C tests) strengths and initial tangent moduli are larger and the failure strains (strain corresponding to maximum deviator stress) are smaller. The 354 psi maximum deviator stress limit (loading ram limit) was achieved for Materials No. 1, No. 2, No. 6, and No. 7. Thus, the Type C/Type A strength ratios for those materials are actually greater than the values shown in Table 9.

The lowest Type C shear strength (211 psi for Material No. 8A) exceeds the largest Type A shear strength (194 psi for Material No. 1). For those materials that did not reach the 354 psi limit, the strength ratios varied from a low of 1.34 to a high of 3.17. Note that the largest ratios (3.17 for Material No. 8 and 2.79 for Material No. 7) are for "gravels" and are for lower-shear-strength (Type A test) materials.

It is apparent that stress repetitions have a significant strengthening and stiffening effect. It is not possible from the data developed in this study (no-load repetition strength and the stress history outlined in Table 4) to establish accurately the trend of "strength gain" with loading repetitions, but it probably is related to the position on the plot of permanent deformation to number of load repetitions (see Figure 6) where

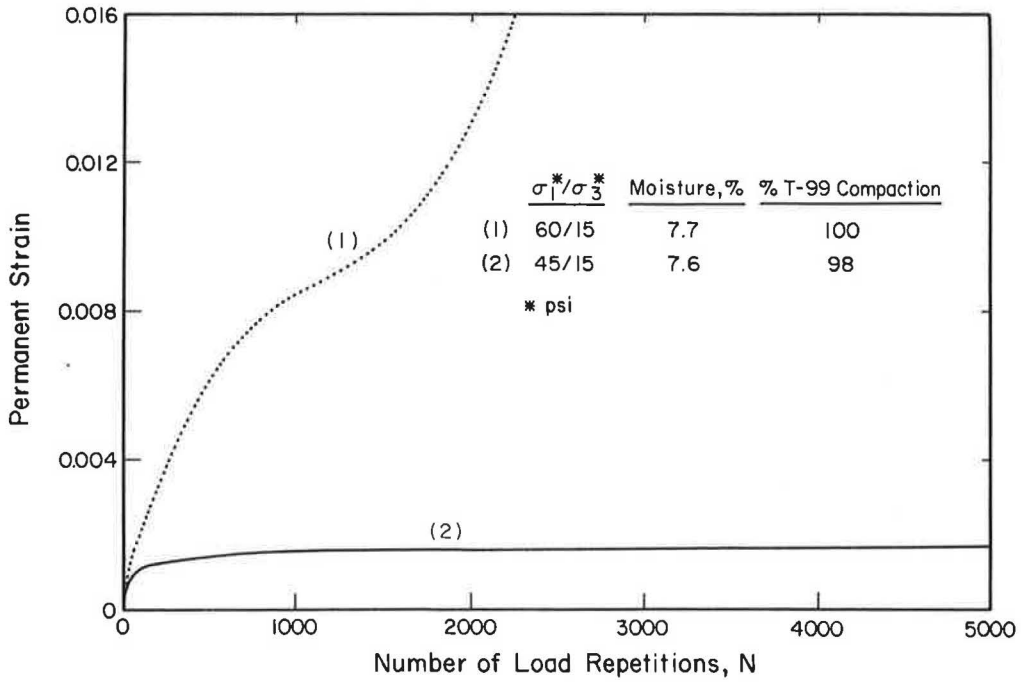

FIGURE 6 Stress state effect on permanent strain-load repetitions relations (material No. 5).

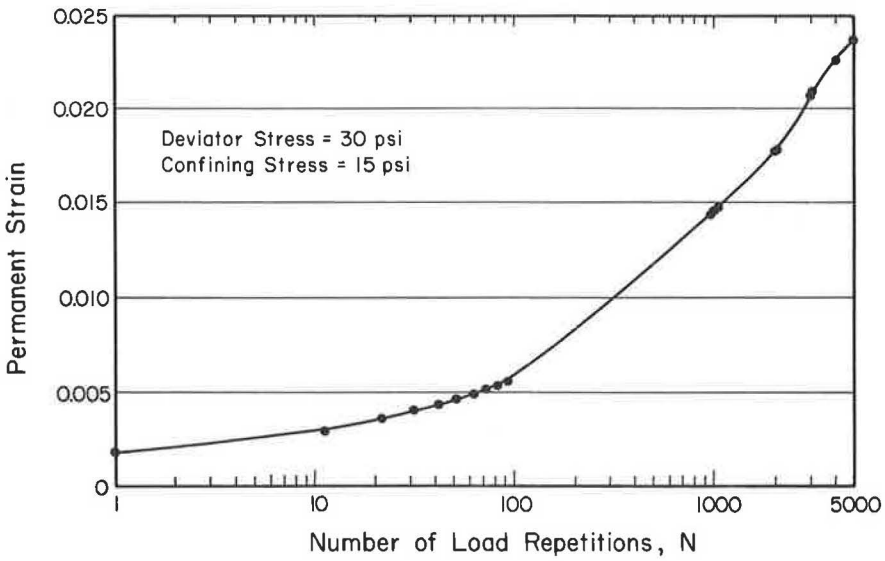

FIGURE 7 Permanent strain-load repetitions relation for material No. 8A.

TABLE 9 STRESS HISTORY AND RAPID SHEAR STRENGTH DATA

Material	Type A Test			Type C Test			Ratio
	% Compaction	% Moisture	Maximum Stress, psi*	% T-99 Compaction	% Moisture	Maximum Stress psi*	C/A***
#1	99.0	6.7	194	99.0	6.5	354**	1.82
#2	100.0	4.1	171	100.0	4.0	354**	2.07
#5	99.4	7.8	164	99.0	7.6	220	1.34
#6	99.9	7.1	175	100.0	6.9	354**	2.02
#7	99.9	7.4	127	100.0	7.5	354**	2.79
#8	99.1	7.9	109	99.0	8.0	346	3.17
#8A	99.9	8.9	116	100.0	8.9	211	1.82

* 15 psi confining pressure
** Maximum capacity of test ram
*** Type C Strength/Type A Strength

a rather sudden change, or decrease, in permanent deformation accumulation rate is typically noted. This point is generally around 100 to 1,000 load repetitions for a material that will ultimately achieve a "stable" permanent deformation and number of load repetitions performance trend.

Those data support the "stage construction" philosophy. A conditioned granular base (i.e., granular material that has experienced at least a few thousand load repetitions prior to placement of the final AC surface course) should exhibit superior shear strength and "rutting resistance."

SUMMARY

As part of an overall evaluation effort to establish the effect of a small decrease in fines content (No. 200 material) on the pertinent engineering properties of typical well-graded granular base materials, a comprehensive triaxial testing program (i.e., repeated loading and rapid shear strength tests) was conducted. Typical crushed stones, crushed gravels, and gravels meeting CA-6 and CM-06 gradation requirements (see Table 1) were included in the program.

The results of the testing program indicated the following conclusions:

1. Friction angles show little variability and ranged from 42.7 to 46.4 degrees for near maximum dry density and optimum moisture content conditions.
2. Cohesion values indicated compaction conditions ranged from 9.6 to 24.4 psi.
3. Moisture sensitivity, as measured by the RSI (see Table 7), were relatively high and varied from 0.63 to 0.94. It is important to note that the highest fines content was only 10.5 percent.

4. The resilient modulus parameters K and n fell within expected ranges. Limited differences were noted among the various granular materials. For a representative bulk stress of 20 psi, resilient moduli (with the exception of Material No. 8A) were in the narrow range of 28.6 to 35.4 ksi. Resilient modulus is not a good property for ranking granular base performance potential.

5. The rapid shear strength of "conditioned" specimens (Type C testing) was always greater than the "unconditioned" strength. Strength increases from 34 to 217 percent were produced by conditioning. This is a very significant finding. It is apparent that the shear strength of an "unconditioned" specimen does not represent the strength of an in-service compacted and trafficked granular base material.

6. Permanent deformation under repeated loading varied considerably. In fact, four of the materials (all gravel products) did not survive the standard conditioning loading (45 psi deviator stress/15 psi confining pressure). A reduced stress state (30 psi deviator/15 psi confining pressure) was used to characterize the permanent deformation behavior of those four materials. It is apparent that permanent deformation under repeated loading provides a more definitive evaluation of granular base materials.

The Livingston County Test Road project was completed in June 1987. Field performance (rutting and cracking) and FWD responses are being monitored on a continuing basis. A future report summarizing the field information and considering the relation between field performance and laboratory testing data and findings will be prepared by the Illinois DOT and The University of Illinois.

ACKNOWLEDGMENTS

This paper is based on the results of project IHR-524, Mechanistic Design Implementation and Monitoring. IHR-524 is sponsored by the Illinois Department of Transportation (Division of Highways). The excellent cooperation and support of the Illinois DOT Bureau of Materials and Physical Research and the Livingston County Highway Department are gratefully acknowledged.

REFERENCES

1. M. R. Thompson. Important Properties of Base and Subgrade Materials. *Proc., Conference on Crushed Stone for Road and Street Construction and Reconstruction*, National Crushed Stone Association, 1984.
2. G. Rada and M. W. Witczak. Comprehensive Evaluation of Laboratory Resilient Moduli Results for Granular Material. In *Transportation Research Record 810*, TRB, National Research Council, Washington, D.C., 1981.
3. R. P. Elliott and M. R. Thompson. *Mechanistic Design Concepts for Conventional Flexible Pavements*. Transportation Engineering Series 42, University of Illinois, Urbana-Champaign, 1985.
4. R. P. Elliott and M. R. Thompson. ILLI-PAVE Mechanistic Analysis of AASHO Road Test Flexible Pavements. In *Transportation Research Record 1043* TRB, National Research Council, Washington, D.C., 1985.
5. M. R. Thompson and R. P. Elliott. ILLI-PAVE-Based Response Algorithms for Design of Conventional Flexible Pavements. In *Transportation Research Record 1043*, TRB, National Research Council, Washington, D.C., 1985.
6. NCHRP Project 1-26: Calibrated Mechanistic Structural Analysis Procedures for Pavements, National Cooperative Highway Research Program, TRB, March 1990.

Publication of this paper sponsored by Committee on Mineral Aggregates.

Determination of Layer Moduli in Pavement Systems by Nondestructive Testing

VINCENT P. DRNEVICH, M. MAKBUL HOSSAIN, JIANREN WANG, AND RONNIE C. GRAVES

Two methods of nondestructive testing of pavements (deflection basin measurement and surface wave propagation measurement) are compared. The assumptions associated with each are examined. Ideally, both methods should provide the same values of modulus for each layer in the pavement system if appropriate mathematical models are used and accurate field data are obtained. Falling Weight Deflectometer and Spectral Analysis of Surface Wave (SASW) tests were performed at five sites on a variety of different pavement systems. Results are compared and discussed. Because of the high contrast in modulus (or wave propagation velocity) between the pavement and the base, accurate values of modulus for granular base materials were difficult to obtain for both methods. Moduli for base materials obtained by the SASW method appeared to be more reasonable.

Nondestructive tests on pavements are having a significant impact on structural design and evaluation of pavement systems and on pavement management. To determine the modulus profile of the pavement system is the principal objective of those tests. Two types of nondestructive tests are studied in this paper: deflection basin measurement and surface wave propagation measurement.

The deflection basin measurements may be made by static loading (Benkelmann Beam), by steady state vibratory loading, or by impact loading. For this study, a Falling Weight Deflectometer (FWD) was used. The FWD is a device that applies an impact loading to the surface of the pavement. Sensors at the location of loading and at fixed radii are used to measure the resulting deflection (i.e., the deflection basin). Much background information on this method has been given in the literature (*1–3*). Special computer programs are used to calculate a modulus profile for the pavement system from the peak values of measured input force and resulting deflection basin.

The surface wave propagation measurements also rely on an impact to the surface. Waves are propagated, and the phase velocity of the surface wave is measured for a range of frequencies that span the audio range. The method was developed for geophysics in the 1950s by Haskell (*4*) and Thompson (*5*), Knopoff (*6*), and Jones and Thrower (*7*). Nazarian and Stokoe (*8*) pioneered the use of those techniques for pavement systems in the early 1980s, and it was they who named the technique Spectral Analysis of Surface Waves (SASW). Additional development of the method has occurred since then, and summaries are available (*9–11*).

University of Kentucky, Lexington, Ky. 40506.

Rather than having an input force and deflection basin, SASW produces values of surface wave phase velocities versus wavelength (i.e., a dispersion curve). A computer program is used to establish a velocity profile with depth from the dispersion curve. From this velocity profile, moduli and thicknesses of layers are determined.

This paper describes a real pavement system and then outlines the basic assumptions associated with the models typically used by both the deflection basin method and the surface wave propagation velocity method. Some modifications to the SASW method for acquiring data in the field are given. Procedures used for converting acquired data to the final result also are discussed for both methods.

Field data were obtained at five Kentucky sites. Each site had a different pavement system, ranging from simple Portland cement concrete (PCC) over crushed stone to an asphaltic concrete overlay of a broken and seated Portland cement concrete pavement. Data are reduced and compared. Differences between the two methods (FWD and SASW) are discussed with consideration given to the nature of the test and assumptions made in the mathematical models.

PAVEMENT MODELS

Real Pavement System

A real pavement system is indicated schematically in the left side of Figure 1. The pavement itself is likely to have imperfections, such as cracks, ruts, and worn areas. The base, whether it be stabilized or unstabilized, may differ from one location to another in, for instance, thickness, density, and moisture content. The subgrade, especially in cut and nonengineered fill areas, may be extremely variable in composition, and its properties will vary with, for instance, location, depth, and moisture content. Finally, bedrock may be at shallow depths. When there is bedrock, the depth may vary significantly from one location to another, and its presence will significantly affect the performance of the pavement system.

Idealized Model for the Deflection Basin Method

Most deflection basin data currently are obtained by use of an FWD, which applies an impact to the pavement surface. The peak load is measured, and, by use of velocity-measuring

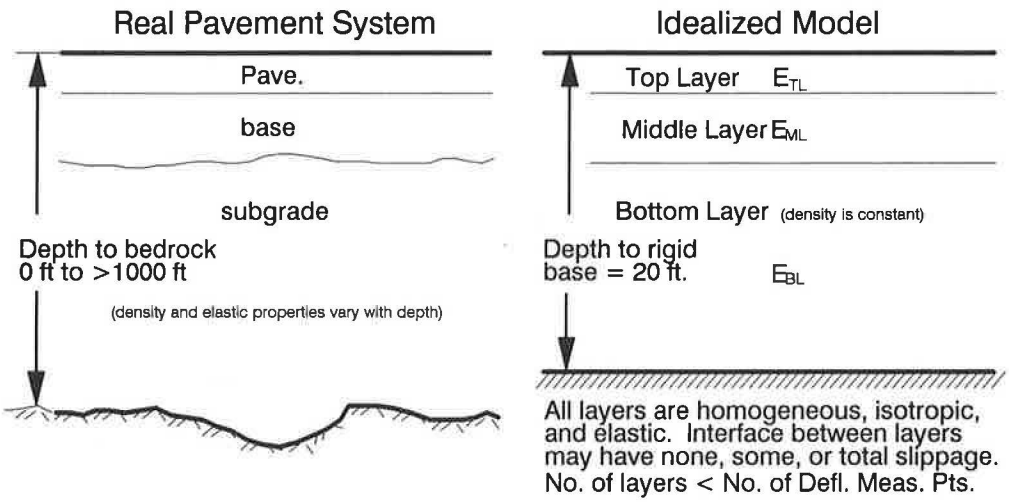

FIGURE 1 Real pavement system and idealized model for deflection basin measurement method.

transducers, the peak deflections are determined at various radii from the center of load application. A deflection basin composed of peak deflections never really occurs during the test because there is a phase lag between transducers. Anderson and Drnevich (*12*) have shown that phase lag effects are significant, even for "rigid" pavements, where the phase lag should be smaller than for flexible pavements. Nearly all models used for deflection basin analysis are placed on a static deflection basin and completely ignore wave propagation effects. Besides phase lag, wave propagation could significantly influence the measured peak deflections when bedrock or very stiff layers exist at shallow depths. Other assumptions associated with typical models used for deflection basin analyses are indicated on the right side of Figure 1. Usually, only three to five layers and their thicknesses are assumed. Because the depth to bedrock is not known, it is frequently assumed the depth is about 20 ft. Each layer is assumed to be continuous and of uniform thickness in all horizontal directions and homogeneous, elastic, and isotropic. Values of density and Poisson's ratio also must be assumed. Even in the layer representing the subgrade, the engineering properties of the layer are assumed to be constant. In the real pavement system, the engineering properties are likely to be highly variable in this layer.

Back Calculation of Moduli from Deflection Basin Measurements

The procedure followed by most computer programs is to start with some "seed" values of moduli for each of the assumed system of layers. The peak applied dynamic load is represented by a static load on the surface, and a static deflection basin is calculated for the model. A comparison is made of the calculated deflection basin with the measured deflection basin. Differences are used to guide adjustment of moduli in the various layers, and another set of deflections is calculated for the model. The comparison-adjustment-recalculation procedure is carried out until the calculated static deflections are within an acceptable tolerance of the measured peak dynamic deflections. The result is a set of moduli for the layers of the model that gives a calculated static deflection basin close to the measured dynamic deflection basin. Many users of this method mistakenly identify those moduli as inherent properties of the real pavement system. They are not. They are the properties of the model used to simulate the real pavement system.

Idealized Model for Surface Wave Propagation Velocity Method

Similar to the model for the deflection basin method, the model for this method assumes each layer to be continuous and of uniform thickness in all horizontal directions and homogeneous, elastic, and isotropic as indicated on the right side of Figure 2. Values of density and Poisson's ratio also must be assumed for a given layer. However, there may be many layers, and the thicknesses of each do not need to be known. The model is a dynamic one in that inertia of the materials and wave propagation (phase lags, reflections, and refractions) are accounted for.

Back Calculation for the Surface Wave Propagation Velocity Method

Like the deflection basin method, an impact is applied to the surface. However, its magnitude is much smaller. Vibration transducers are placed at fixed radii from the point of impact, and the phase lag of the surface wave is measured as a function of frequency by use of a spectrum analyzer, as indicated in Figure 3. With the horizontal distance between transducers and the phase lag, it is possible to calculate the phase velocity for each frequency by use of Equation 1.

$$C = \frac{2\pi f x}{\theta} \tag{1}$$

where

C = phase velocity,
f = frequency,
x = horizontal distance between transducers, and
θ = phase lag.

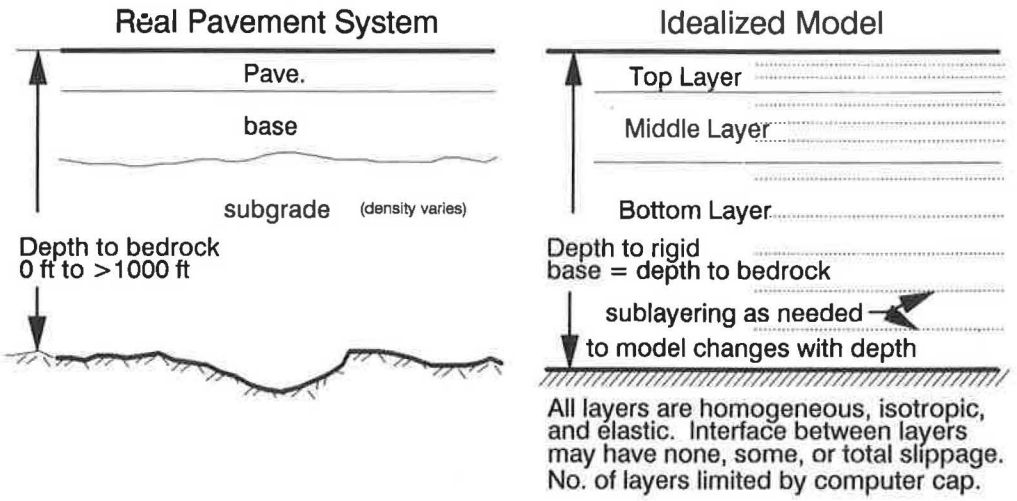

FIGURE 2 Real pavement system and idealized model for spectral analysis of surface waves method.

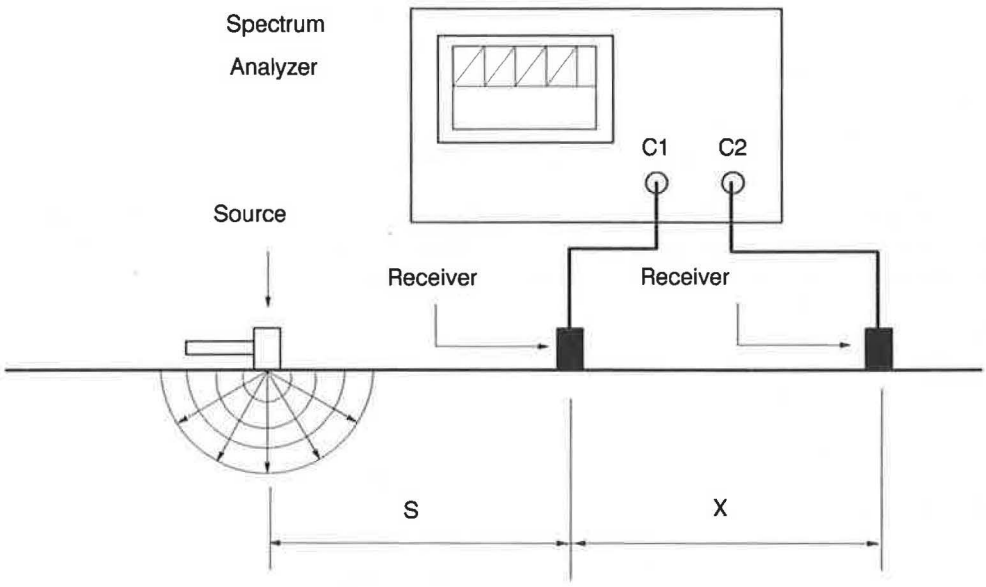

FIGURE 3 Typical configuration of SASW tests.

For each frequency, wavelength also is calculated from Equation two.

$$\lambda = C/f \quad (2)$$

where λ equals wavelength.

A plot of phase velocity versus wavelength is called a dispersion curve, and it can be thought of as being analogous to the deflection basin. The back-calculation process for this method requires, for the dynamic model, a selection of layering and moduli such that the calculated dispersion curve is within tolerable limits of the measured dispersion curve. The process can be simple for dispersion curves that have well-defined and simple shapes (*13,14*) but usually requires an extensive computer program (*8,11*). Similar to the deflection basin method, the result of this method is a set of moduli for the layers of the model that gives a calculated dispersion curve close to the curve calculated from measured phase lags.

TESTING PROGRAM

Description of Test Sites

Five sites have been tested in this study, and they include one rigid and four flexible pavements. Pavement type and thickness for each test area are indicated in Table 1.

The rigid pavement of Site 1 exhibited some cracks. However, all tests were performed in the area of intact PCC.

TABLE 1 PAVEMENT TYPE, THICKNESS, AND MODULUS

Test Site	Location	Pavement Thickness and Material	Modulus of Elasticity (psi)	
			SASW	FWD
1	KTRB* Garage	6" PCC	5,070,000	4,000,000
		4" Crushed Stone	35,200	10,000
		36" Compacted Subgrade	55,000	16,000
		Limestone Subgrade	740,000	35,000
2	KTRB Compound	2.5" AC	690,000	650,000
		6" Crushed Stone	30,300	10,000
		36" Compacted Subgrade	51,900	75,000
		Limestone Subgrade	901,000	175,000
3	Louisa Bypass, Kentucky	13" AC	655,000	250,000
		4" Crushed Stone	24,200	18,000
		4" DGA	16,600	25,000
		12" Crushed Shale	42,600	57,000
		Shale Subgrade	103,500	130,000
4	I-64, Near Grayson Exit 172	12" AC	764,000	750,000
		18" DGA	14,550	35,000
		Shale Subgrade	66,250	65,000
5	Mountain Parkway, Kentucky	8" AC	890,000	650,000
		8" PCC (Broken)	1,980,000	200,000
		5" DGA	25,900	6,000
		Stiff Clay	45,700	45,000

* Kentucky Transportation Research Building

Asphalt in Site 2 was very thin when compared with that in other sites. The rest of the sites were in good performance conditions. In fact, Site 3 was a newly constructed bypass, and Site 5 consisted of new asphalt overlaying broken and seated concrete.

Description of Test Equipment and Configurations

Falling Weight Deflectometer Tests

The device used for deflection basin measurements was a JILS 20 Falling Weight Deflectometer, manufactured by Foundation Mechanics, Inc., El Segundo, Calif. The device has a capability of applying a peak dynamic load to pavements of up to 24,000 lb with a nominal duration of 25 msec and simultaneously measures the force applied to the pavement and the velocities at seven locations from the applied load (as indicated in Figure 4). The results of the peak force applied to the pavement and the peak displacements at each of the seven sensor locations were measured and stored by using a microcomputer-based data acquisition system. The seven sensors were located at distances of 2.95, 12, 24, 36, 48, 60, and 72 in. from the center of load application.

SASW Tests

The major components of the SASW testing system are a source, receivers, and a recording device. Several impact sources were used, such as hammers (4-oz, 8-oz ball peen, 16-oz claw, and 8-lb sledge hammers). Two types of vertical transducers (accelerometers and geophones) were used as receivers. The recording device was a Fourier spectrum analyzer, a digital oscilloscope that has a microcomputer built into it so it can perform operations directly in either time or frequency domains.

Mostly, two types of source-to-receiver geometries are used in the SASW method: Common Receiver Midpoint (CRMP) and Common Source (CS). To reduce the testing time, a third type of geometry, the Common Near Receiver (CNR), can be used, and it was used for this study.

Common Receiver Midpoint Geometry Proposed by Nazarian (*9*), an imaginary center line is selected between the receivers (Figure 5a). Two receivers are moved away from the imaginary center line at equal distances, and the source is also moved such that the distance between the source and near receiver (S) is equal to the distance between the two receivers (X) (i.e., $S/X = 1$).

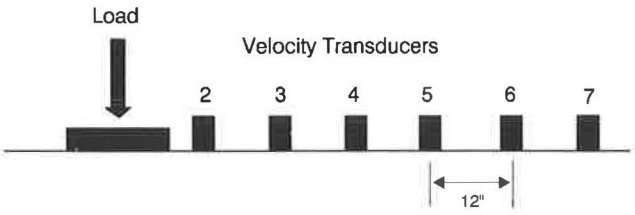

FIGURE 4 Typical FWD configuration.

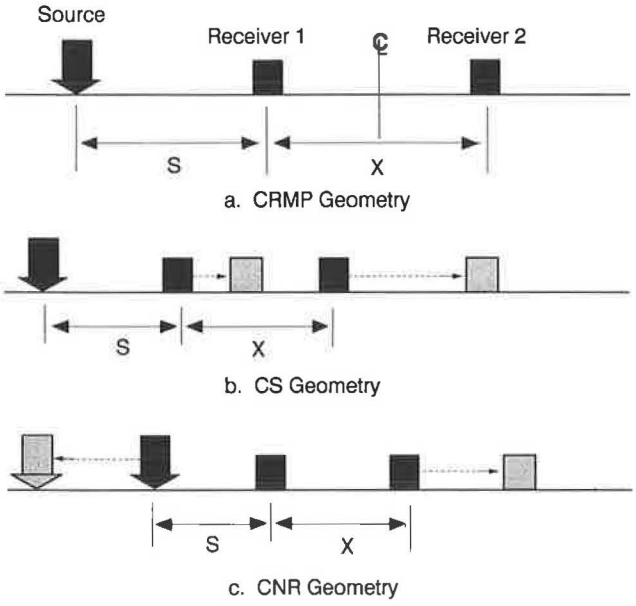

FIGURE 5 Source to receiver geometry for SASW.

Common Source Geometry The source is fixed at one location, and two receivers are moved during testing such that $S/X = 1$ (Figure 5b). It was observed from a series of SASW tests conducted at asphalt concrete (AC) pavement sites (*10*) that the scatter within all collected data was similar for each geometry. CS geometry is preferable to the CRMP geometry with regard to the testing time.

Common Near Receiver Geometry In both CS and CRMP geometries, considerable time is spent fixing receivers on the pavement surface. To save testing time, the receivers were fixed to the surface, and the source and the other receiver were moved (Figure 5c). A test was conducted at a concrete pavement site to study the effect of the three geometries on experimental dispersion curves. All the geometries gave almost identical average dispersion curves. Because CNR geometry reduces testing time considerably, this geometry was used in this study. The spacings between the receivers for all tests reported were 0.5, 1, 2, 4, and 8 ft while maintaining $S/X = 1$.

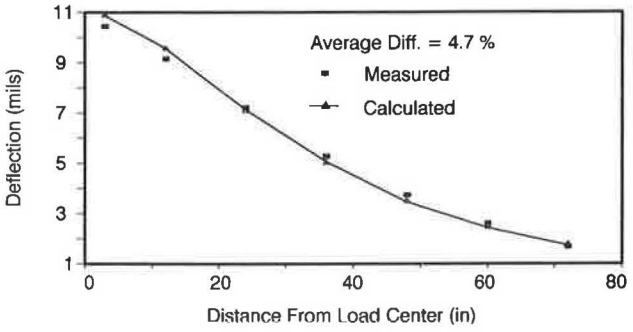

FIGURE 6 Deflection basins, Site 1.

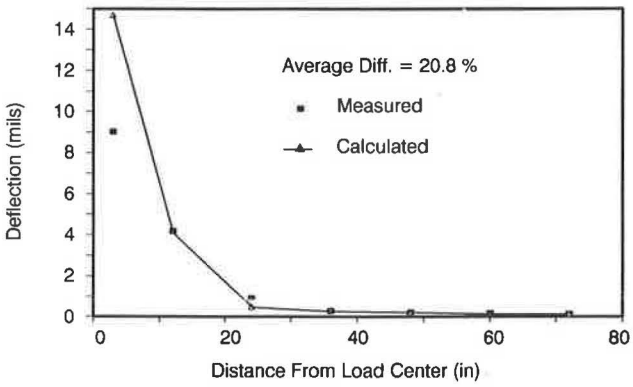

FIGURE 7 Deflection basins, Site 2.

TEST RESULTS

Falling Weight Deflectometer Tests

Back calculation of layer moduli was performed and was based on an iterative procedure that used a layered-theory program, ELSYM5 (*15*). Deflections were calculated from the initial input values of moduli obtained from SASW tests. At first, iterations were made to evaluate the subgrade modulus by matching the deflections corresponding to sensor locations 6 and 7. The modulus was accepted if the difference between measured and calculated deflections was around 5 percent. The next step was to adjust the modulus of the surface layer. The moduli of intermediate layers were determined by subsequent iterations. The calculated deflection basins for each site are presented with those measured in Figures 6–10. Average percent difference also is shown in those figures. The values are within 5 percent in almost all cases except Site 2. The reason for the 20.8 percent difference for Site 2 can be attributed to the behavior of the very thin asphalt layer, which was only 2.5 in. thick, and because of some fine cracks. Moduli calculated from FWD deflection basins are given in Table 1.

In performing the FWD data reduction, a new back-calculation program, WESDEF (*16*), was tried, even though the conditions at the sites were not well suited for those kinds of programs. In general, WESDEF gave values of moduli for pavement and subgrade similar to those obtained by ELSYM5,

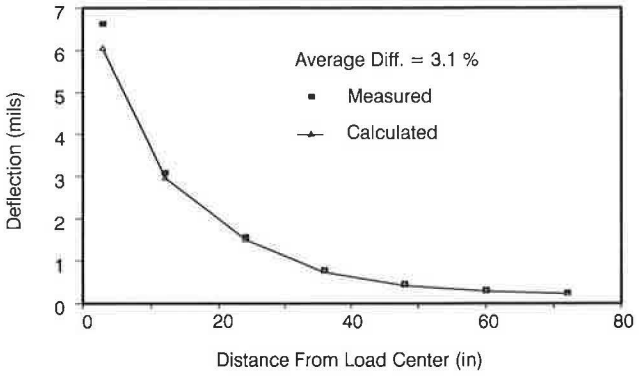

FIGURE 8 Deflection basins, Site 3.

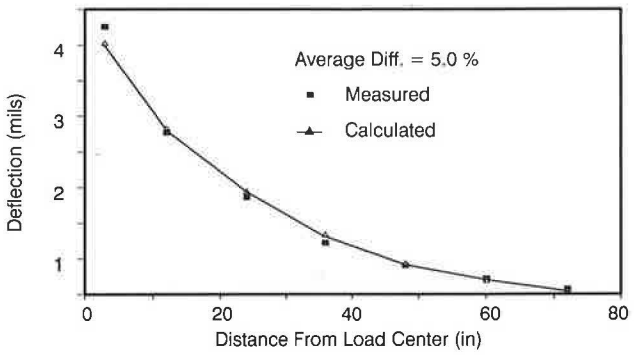

FIGURE 9 Deflection basins, Site 4.

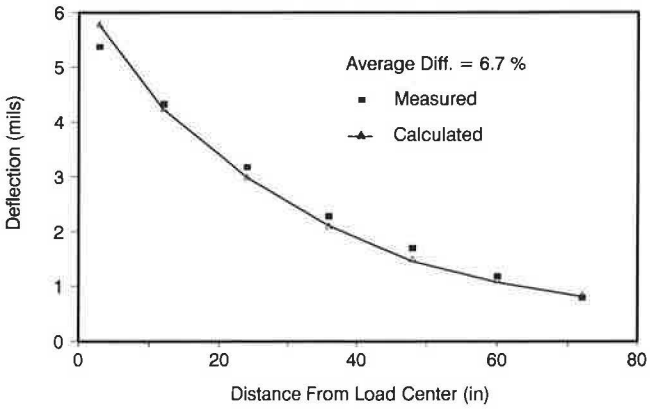

FIGURE 10 Deflection basins, Site 5.

which used manual iterations. However, WESDEF generally gave the built-in lower bound value for the base layers at all sites except for Site 4. The difficulty arose from having a low modulus layer (base) or layers (base and sub-base) between high modulus layers (pavement and stiff subgrade). The deflection basin and the procedures used by the program generally provide inaccurate values for the low modulus material, especially in the base because of the large modulus contrast.

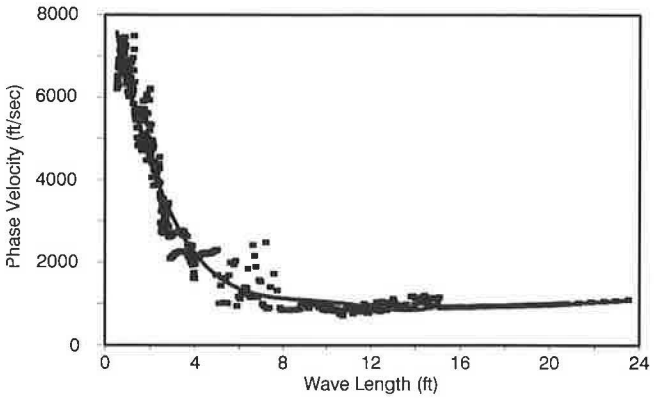

FIGURE 11 Experimental dispersion curve, Site 1.

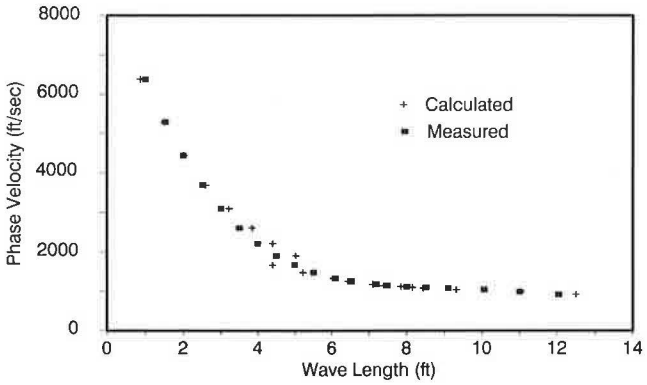

FIGURE 12 Dispersion curves, Site 1.

Automatic back-calculation programs should be used with caution for sites not well suited.

SASW Tests

SASW tests were performed at the same sites. After field testing, data were transferred from the Dynamic Signal Analyzer to a personal computer. The average experimental dispersion curve was obtained for each site by using the program SASWOPR (*17*). A typical experimentally determined dispersion curve is presented in Figure 11. There are 300 to 500 data points on this curve. For small and for large wavelengths the curve is relatively well defined, but, for intermediate wavelengths, the data show more scatter. This scatter is due to the mixing of various modes caused by the high-velocity contrast between the pavement and the base.

For back calculation, the program KENSALPS was then used to determine shear wave velocity profile. To execute the program, suitable data points were selected from the average dispersion curve (such as those in Figure 11) to provide a simplified measured dispersion curve. Those were used in the back-calculation process and are presented, along with the calculated dispersion curves, in Figures 12–16.

Thicknesses of individual layers for each pavement site were known from coring. Constant values of Poisson's ratio (0.33)

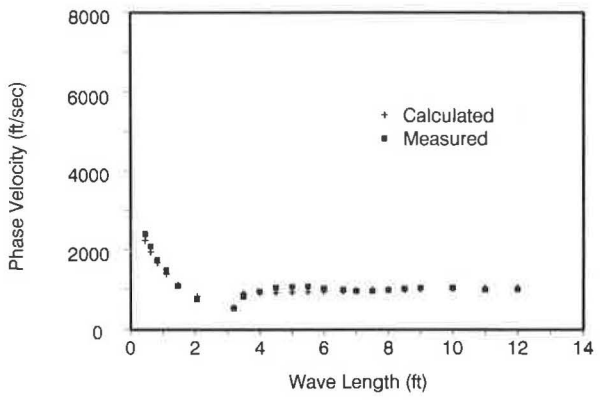

FIGURE 13 Dispersion curves, Site 2.

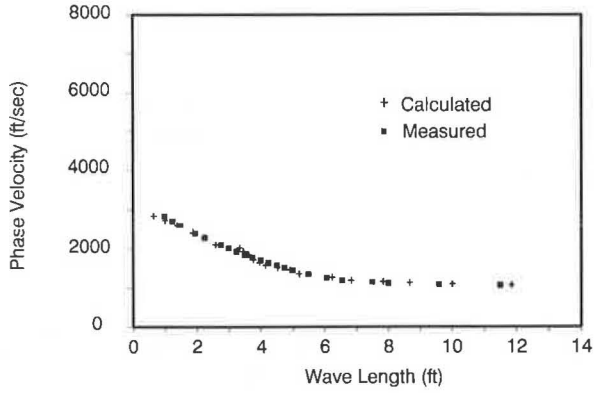

FIGURE 14 Dispersion curves, Site 3.

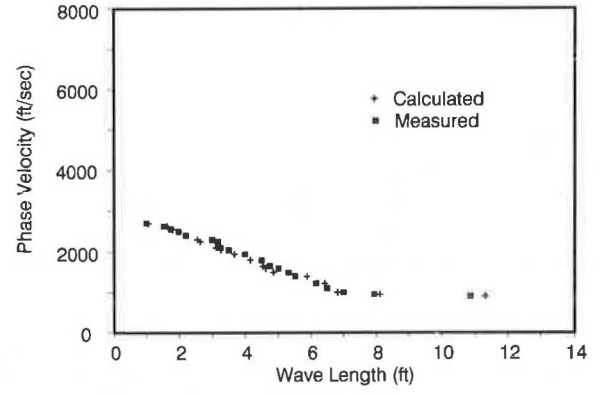

FIGURE 15 Dispersion curves, Site 4.

and unit weight (125 pcf) were assumed for crushed stone, dense-graded aggregate (DGA), and subgrade materials. For PCC and AC, corresponding values of those parameters were 0.15, 145 pcf and 0.25, 135 pcf, respectively. The initial shear wave velocities for surface layer and the half-space were determined by using the procedure developed by Vidale (*14*). Layer velocities were assumed for base and sub-base materials for initializing the optimization process. The calculated dispersion

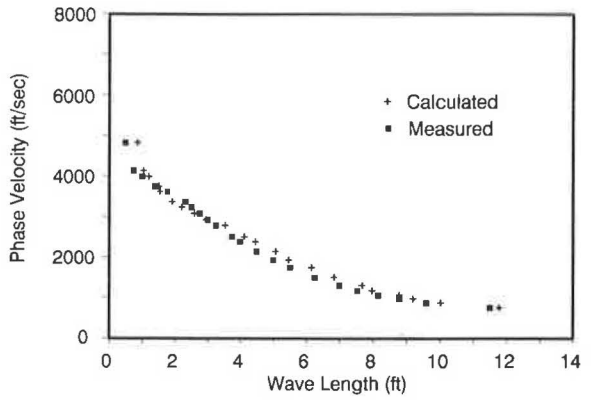

FIGURE 16 Dispersion curves, Site 5.

TABLE 2 SHEAR WAVE VELOCITIES FROM SASW TESTS

Material	Shear Wave Velocity (ft/s)				
	Site 1	Site 2	Site 3	Site 4	Site 5
PCC	8400	—	—	—	—
AC	—	3080	3000	4340	3500
CS	700	650	580	—	—
DGA	—	—	480	420	600
Broken Shale	—	—	770	—	—
Subgrade	875	850	1200	960	850

— Data not applicable

curves also are shown in Figures 12–16. From those figures it can be gathered that the agreement between theoretical and experimental curves is quite good for all wavelengths. The thickness of the surface layer was only 2.5 in. in the case of Site 2. This thin layer produced vibration similar to that of a flexural-type of a plate, as indicated by Jones (*13*). A plate vibration solution was used in this case to match the dispersion curve for wavelengths between 0 and 3 ft. However, a layered solution was used for wavelengths greater than 3 ft. The back-calculated shear wave velocity profiles for the five sites are given in Table 2.

COMPARISON AND DISCUSSION OF RESULTS

Sites 1 and 2 were very close to each other, and the depth to limestone bedrock was on the order of 4 ft. The SASW results for the crushed stone, compacted subgrade, and limestone compared well between the two sites, whereas the results for the FWD test did not. At Site 1, the stiff concrete pavement layer appeared to mask the stiffness of the underlying bedrock. At Site 2, where a thin AC pavement existed, the values of modulus for bedrock were much higher. Recall that the average error in the back calculation for the FWD was large (20.8 percent) and that this error was primarily due to the two data points near the source. For the SASW test, a dif-

ferent dynamic model had to be used to fit the dispersion curve for the close-in data. Thus, at least two separate modes of deformation existed for this site (one for near-source behavior and one for far-field behavior) and that a single model for the back calculation by the FWD method was not adequate. At both sites, the values of moduli for the crushed stone base by the SASW method were much higher than those obtained by the FWD method. Values of moduli for the compacted subgrade by FWD at those two sites differed significantly.

Site 3 is similar to Sites 1 and 2 in that a bedrock subgrade is at shallow depths. However, at Site 3, the AC pavement is much thicker than at Site 2, 13 in. versus 2.5 in. This site also proved difficult for the FWD test because the moduli for the pavement and crushed stone base layers are significantly smaller than expected for a newly constructed pavement.

At Site 4 the base consists of an 18-in.-thick layer of DGA. Values of modulus for this layer by the SASW were similar to the values for DGA at Site 3, but corresponding values from FWD were significantly higher.

Site 5 is an interesting one in that a PCC pavement had been broken and seated prior to being overlain by an 8-in. thick AC pavement. The sizes of the broken pieces were on the order of 12 to 24 in. Data in the SASW test for the overlay and broken concrete pavement require close transducer spacings (typically 6 in. to 24 in.) and are obtained by using accelerometers that have good response at high frequencies. The likelihood of having the wave propagation measured on an intact piece of broken pavement is great, and, hence, a large value of modulus is obtained. The FWD test takes the overall action into account by measuring the deflections and, hence, gave a much smaller value for the moduli for the broken pavement. It is important to recall the assumptions associated with both methods, that is, that each layer is uniform and continuous in all directions. Clearly, this assumption is invalid when broken and seated pavements are tested. (Obviously, this assumption also is invalid when badly cracked pavements of any kind are tested.)

Besides Table 1, moduli obtained by both methods are compared in Figure 17, where the FWD values are plotted versus the SASW values. The diagonal curve represents equal values by both methods. Many of the data points lie on or near the curve. In general, the SASW method gives the larger values.

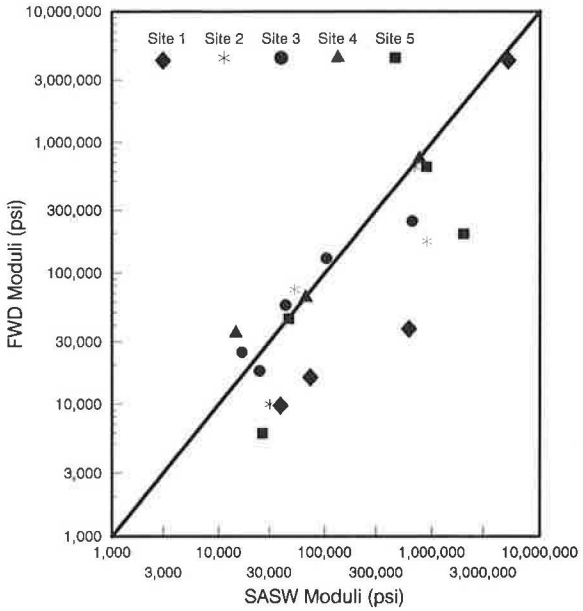

FIGURE 17 Comparison of moduli from FWD and SASW tests.

CONCLUSIONS

The assumptions associated with the models used for back calculation of layer moduli need to be kept in mind as the data for pavement systems are analyzed. Both the deflection basin method and the surface wave propagation velocity method give similar values of layer moduli when the assumptions associated with the models are satisfied. The model associated with the surface wave propagation velocity method is more flexible in that many more layers may be handled and the existence of a very stiff subgrade (bedrock) at shallow depths does not pose any problem. The back-calculation schemes associated with the deflection basin method for well-conditioned sites generally are strong in calculating subgrade moduli and pavement moduli but are weak in calculating base moduli because of the high modulus contrast that typically exists. Finally, the moduli calculated are for the layers in the idealized model used in the back-calculation scheme and are not inherent engineering properties for the layers in the real pavement system.

ACKNOWLEDGMENTS

The authors wish to acknowledge the National Stone Association, the Kentucky Crushed Stone Association, and the Department of Civil Engineering for their support of this research. The authors also are indebted to David Allen of the Kentucky Transportation Center at the University of Kentucky and to the Federal Highway Administration, U.S. Department of Transportation, for their assistance and in providing the deflection basin data. The authors appreciate the assistance of Albert J. Bush III of the U.S. Army Corps of Engineers, Waterways Experiment Station, for WESDEF. Finally, the authors wish to acknowledge the services of the University of Kentucky Computing Center.

REFERENCES

1. W. Uddin, A. H. Meyer, W. R. Hudson, and K. H. Stokoe II. Project-Level Structural Evaluation for Pavements Based on Dynamic Deflections. In *Transportation Research Record 1007*, TRB, National Research Council, Washington, D.C., 1985, pp. 37–45.
2. A. J. Bush III and R. D. Alexander. Pavement Evaluation Using Defection Basin Measurements and Layered Theory. In *Transportation Research Record 1022*, TRB, National Research Council, Washington, D.C., 1985, pp. 16–29.
3. B. E. Sebaaly, M. S. Mamlouk, and T. G. Davies. Dynamic Analysis of Falling Weight Deflectometer Data. In *Transportation Research Record 1070*, TRB, National Research Council, Washington, D.C., 1986, pp. 63–68.
4. N. A. Haskell. The Dispersion of Surface Waves on Multilayered Media. *Bulletin of the Seismological Society of America*, Vol. 43, No. 1, 1953, pp. 17–34.

5. W. T. Thomson. Transmission of Elastic Waves through a Stratified Solid Medium. *Journal of Applied Physics*, Vol. 21, No. 2, 1950, pp. 89–93.
6. L. Knopoff. A Matrix Method for Elastic Wave Problems. *Bulletin of the Seismological Society of America*, Vol. 54, No. 1, 1964, pp. 431–438.
7. R. Jones and E. N. Thrower. An Analysis of Waves in a Two-layer Composite Plate and its Application to Surface Wave Propagation Experiments on Roads. *Journal of Sound and Vibration*, Vol. 2, No. 3, 1965, pp. 328–335.
8. S. Nazarian and K. H. Stokoe II. *Evaluation of Moduli and Thicknesses of Pavement Systems by Spectral-Analysis-of-Surface-Waves Method*. Research Report 256-4. Center for Transportation Research, The University of Texas at Austin, 1984.
9. S. Nazarian. *In Situ Determination of Elastic Moduli of Soil Deposits and Pavement Systems by Spectral-Analysis-of-Surface-Waves Method*. Ph.D. dissertation, The University of Texas at Austin, 453 pp.
10. D. R. Hiltunen and R. D. Woods. Influence of Source and Receiver Geometry on the Testing of Pavements by the Surface Wave Method. In *Nondestructive Testing of Pavements and Backcalculation of Moduli*, ASTM STP 1026, (A.J. Bush III and G.Y. Baladi, eds.), American Society for Testing and Materials, Pa., 1989.
11. M. M. Hossain and V. P. Drnevich. Numerical and Optimization Techniques Applied to Surface Waves for Backcalculation of Layer Moduli. In *Nondestructive Testing of Pavements and Backcalculation of Moduli*, ASTM STP 1026 (A. J. Bush III and G.Y. Baladi, eds.), American Society for Testing and Materials, Pa., 1989.
12. M. Anderson and V. P. Drnevich. A True Dynamic Method for Nondestructive Testing of Pavements with Overlays. Presented at 4th International Conference on Concrete Pavement Design and Rehabilitation. Purdue University, April 18–20, 1989.
13. R. Jones. Surface Wave Techniques for Measuring the Elastic Properties and Thickness of Roads: Theoretical Development. *British Journal of Applied Physics*, Vol. 13, 1962, pp. 21–29.
14. R. F. Vidale. *The Dispersion of Stress Waves in Layered Media Overlying Half-Space of Lesser Acoustic Rigidity*. Ph.D. dissertation, University of Wisconsin, 1964.
15. S. Kopperman, G. Tiller, and M. Tseng. *ELSYM5 Interactive Microcomputer Version, User's Manual*. IBM-PC Compatible Version. Report No. FHWA-TS-87-206, 1986.
16. A. J. Bush III. Nondestructive Testing of Light Aircraft Pavements, Phase II. In *Development of the Nondestructive Evaluation Methodology*. Report no. FAA-RD-80-9-II, Federal Aviation Administration, 1988.
17. M. Sayyedsadr and V. P. Drnevich. SASWOPR: A Program to Operate on Spectral Analysis of Surface Wave Data. In *Nondestructive Testing of Pavements and Backcalculation of Moduli*. ASTM STP 1026 (A. J. Bush III and G. Y. Baladi, eds.), American Society for Testing and Materials, Pa., 1989.

Publication of this paper sponsored by Committee on Mineral Aggregates.

Dynamic Testing of Nebraska Soils and Aggregates

GEORGE WOOLSTRUM

The results of a study to develop an indirect test for the resilient modulus of Nebraska's aggregates and soils is summarized. Aggregate and soil samples were collected at 14 locations and tested for several engineering properties. The modulus of resilience was measured by the University of Nebraska soil mechanics laboratory, and other chemical and physical tests were performed by the Nebraska Department of Roads. Statistical comparisons were made between the resilient modulus and the other test results. It is concluded that it is possible to reliably determine the resilient moduli of subgrade materials by an indirect method.

The 1986 AASHTO *Guide for Design of Pavement Structures* uses the resilient modulus of soils in pavement determination equations. The purpose of our research was to find a reliable indirect, or proxy, method of determining the resilient modulus without elaborate triaxial testing equipment.

STUDY DESIGN

The study was structured in four stages. The first stage was to collect material samples and to conduct field tests. The next two stages were to be done concurrently, with the University of Nebraska at Lincoln, Civil Engineering Department, conducting the resilient modulus testing, while the Nebraska Department of Roads Materials and Tests (MAT) laboratory conducted the other tests. The last stage was the statistical analysis to find which of the laboratory data had the best relationship to the resilient modulus.

MATERIAL SAMPLING

The first stage of the study was to collect soil samples from various locations around the state. The intention was to select samples that would be representative of the state's major soil groups. Fourteen locations, presented in Figure 1, were selected, and the soils ranged from granular to fine-grained cohesive. At each location two bag samples of the parent soil were collected from the right-of-way, and thin-walled tube samples of the subgrade were taken through holes bored through the pavement.

Along with the soil sampling, deflection tests with a Dynaflect machine were conducted at the sites of the tube samples. No other field testing was necessary for the purpose of this study.

Table 1 presents the soil descriptions and characteristics. One bag sample from each site was delivered to the University of Nebraska, Civil Engineering Department, for the resilient modulus tests. All other tests were performed by the MAT laboratory.

Nebraska Department of Roads, P.O. Box 94759, Lincoln, Neb. 68509-4759.

TRIAXIAL TESTS

The resilient modulus measurements were made by using confined triaxial tests according to the provisions of AASHTO test T274-82. Deformations were measured with internally mounted linear variable differential transformers. The samples were prepared, using the procedures outlined in T274-82, with the cohesive soils compacted by kneading and the noncohesive soils compacted by impact (*1*). Much of the equipment and computer software used for the tests were developed by the University of Nebraska.

The testing was done in two phases. In phase 1, 15 to 25 tests were performed on six different soils. The tests were conducted at optimum moisture content, as was determined by AASHTO T99, and at several dynamic stress and cell pressure combinations (*1*). The purpose of phase 1 was to determine if the testing variability were within an acceptable range. Phase 2 was to be implemented only if the results of phase 1 were satisfactory.

The testing was totally automated, with the test results read directly by a computer. Each specimen was conditioned with 15,000 cycles of haversine loading prior to testing. The rate of loading was two cycles per second, with each cycle consisting of a 0.1-sec load application and a 0.4-sec recovery period.

Table 2 presents the result of the phase 1 testing. The coefficient of variation was found to be $\leq$10 percent for 71 percent of the tests and $\leq$12 percent for 84 percent of the tests. Those results were considered adequate to proceed with the phase 2 testing.

In phase 2, the triaxial tests were performed on samples from all 14 locations. The cohesive soils tests were conducted by using various combinations of three different cell pressures, five different dynamic stresses, and three different moisture contents. The nonplastic soils were tested according to the T274 procedure for granular soils, using combinations of five different cell pressures, up to 6 different dynamic stresses, and three different moisture contents (*1*).

Each sample was tested at optimum moisture content and at approximately optimum $+1$ percent and -1 percent. No attempt was made to test at saturation, because it was felt that it represented realistic field conditions. The aggregates and soils and the moisture contents where they were tested are presented in Table 3.

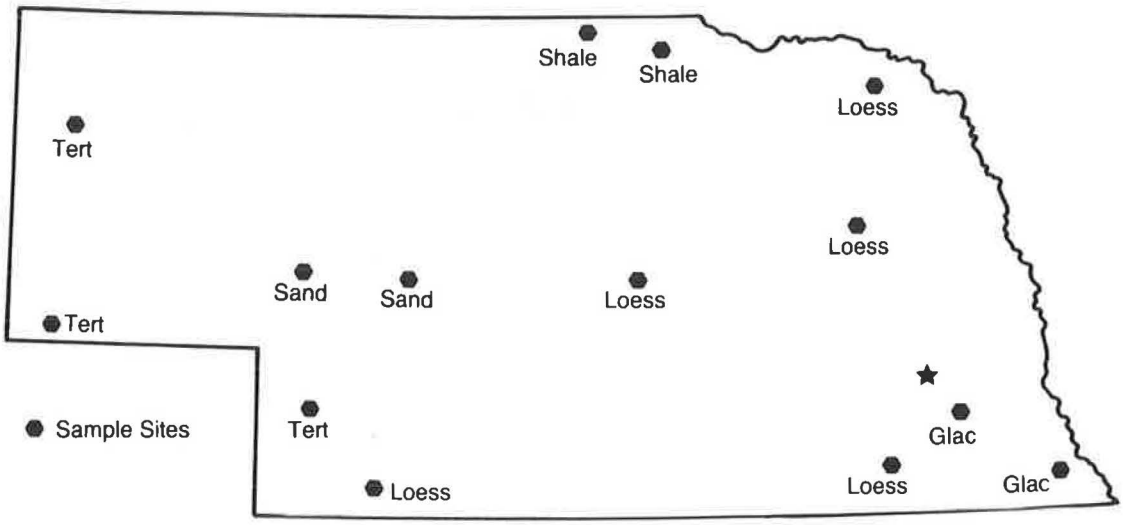

FIGURE 1 Sample locations.

TABLE 1 CHARACTERISTICS OF SOILS AND AGGREGATES

Smpl. No.	Soil Type	% Ret. on #4	% Ret. on #200	Sieve w/0 % Ret.	LL*	PI**	AASHO Class	Nebr. Group Index
171	Fine Sand	0	88	10	--	NP	A-2-4 (0)	-2.0
176	Fine Sand	0	88	10	--	NP	A-2-4 (0)	-2.0
174	Tertiary	0	44	10	--	NP	A-4(3.8)	4.2
223	Tertiary	11	65	1	24	2	A-2-4 (0)	-1.0
335	Tertiary	0	46	4	20	NP	A-4(4.2)	3.8
246	Loess	0	2	10	36	15	A-6(10)	10.0
172	Loess	0	1	100	31	8	A-4(8)	8.0
336	Loess	0	4	100	26	3	A-4(8)	8.0
184	Loess	0	1	100	43	22	A-7-6(13.8)	13.4
297	Loess	0	3	40	45	26	A-7-6(15.3)	15.4
278	Glacial	0	23	4	34	15	A-6(8.4)	10.0
313	Glacial	0	21	4	51	32	A-7-6(18.2)	19.0
247	Shale	0	4	4	68	46	A-7-6(20)	28.0
249	Shale	0	3	10	66	43	A-7-6(20)	26.4

*LL Liquid Limit
**PI Plastic Limit

TABLE 2 PHASE 1 OF VARIABILITY (*1*)

Soil Type	No. of Test	% with Coef. of Variation ≤10%	% with Coef. of Variation ≤12%
Fine Sand	25	80	84
Tertiary	15	67	80
Glacial	15	73	87
Medium Loess	15	47	80
High Loess	15	73	87
Pierre Shale	15	80	87

TABLE 3 MOISTURE CONTENT FOR RESILIENT MODULUS TESTING (*1*)

Sample No.	Soil Type	Avg. Dry Wt. pcf	Percentage Moisture Optimum	Wet	Dry
171	Fine Sand	112.0	11.3	12.3	10.2
176	Fine Sand	109.9	12.7	13.5	11.4
174	Tertiary	101.9	15.8	16.5	14.8
223	Tertiary	111.0	14.0	15.7	13.4
335	Tertiary	111.0	14.0	14.7	12.6
246	Loess	106.4	17.8	18.8	16.9
172	Loess	105.0	17.8	18.8	16.7
336	Loess	105.9	17.1	17.9	15.8
184	Loess	102.1	20.8	21.6	19.6
297	Loess	100.8	20.4	21.4	19.3
278	Glacial	116.2	15.5	16.5	14.5
313	Glacial	109.2	17.4	18.4	16.9
247	Shale	94.7	26.4	27.1	25.1
249	Shale	98.6	24.0	25.0	23.0

The test cell pressures for the cohesive soils were 0, 3, and 6 psi and for the granular soils 1, 5, 10, 15, and 20 psi. Statistical analysis was performed with all of the resilient modulus test results. However, the tests that used a confining pressure of 0 psi were considered the most important. For that reason, the 0 psi cell pressure test results are given the most attention.

Figures 2–8 show some of the results of resilient modulus tests. The results of some of the tests, such as Figure 5, appear to be contrary to conventional wisdom. Those atypical results were observed with some of the low plasticity soils, and additional tests were conducted to verify the first tests. The curve inversion may be caused by negative pore water pressure, which develops during the load impulse and does not have time to equalize during the 0.1-sec load cycle. The following explanation was suggested by the University of Nebraska: "During the haversine load pulse, rapid shearing strains are

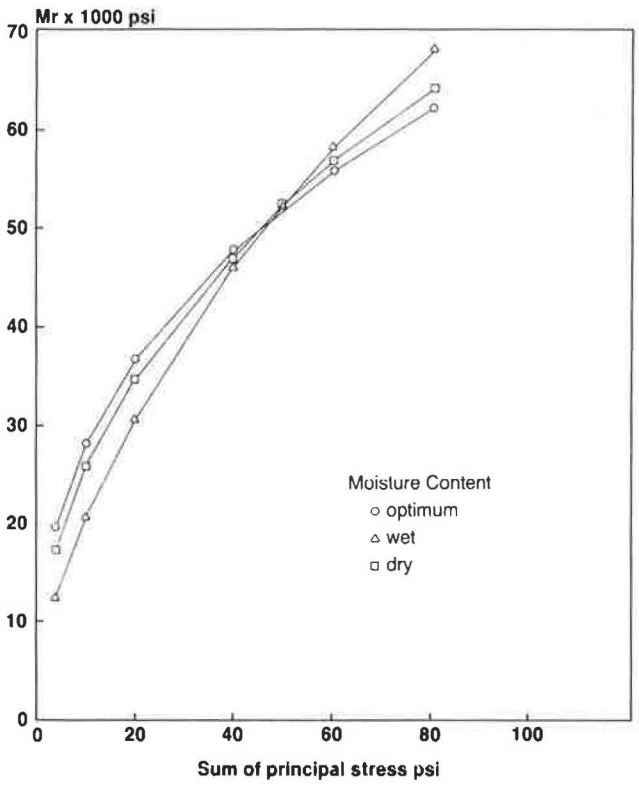

FIGURE 2 Resilient modulus, fine sand (*I*).

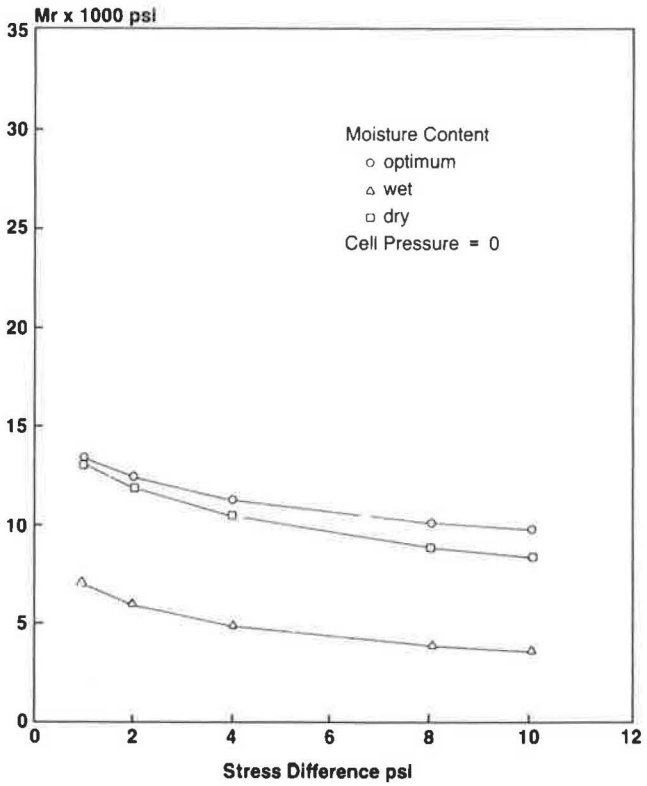

FIGURE 4 Resilient modulus, Peorian loess, medium plasticity (*I*).

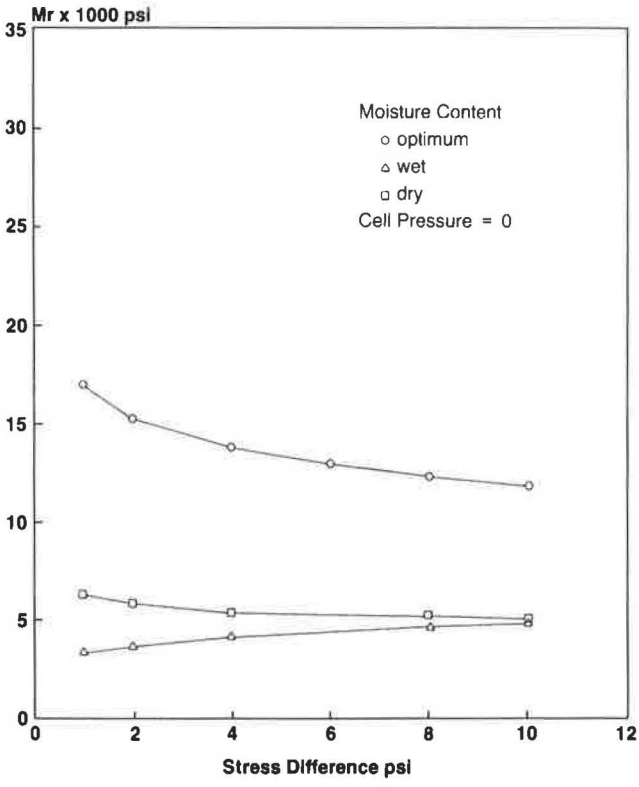

FIGURE 3 Resilient modulus, tertiary (*I*).

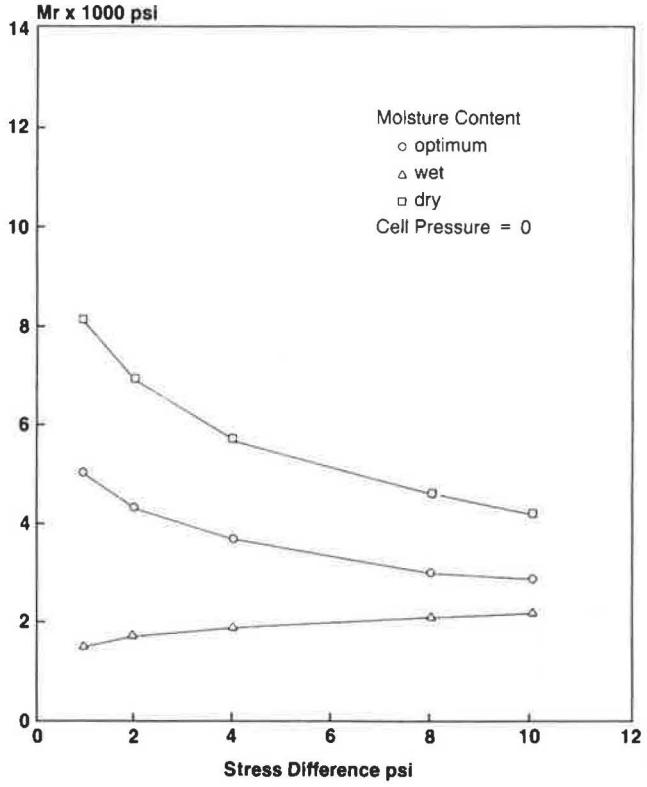

FIGURE 5 Resilient modulus, Peorian loess, low plasticity (*I*).

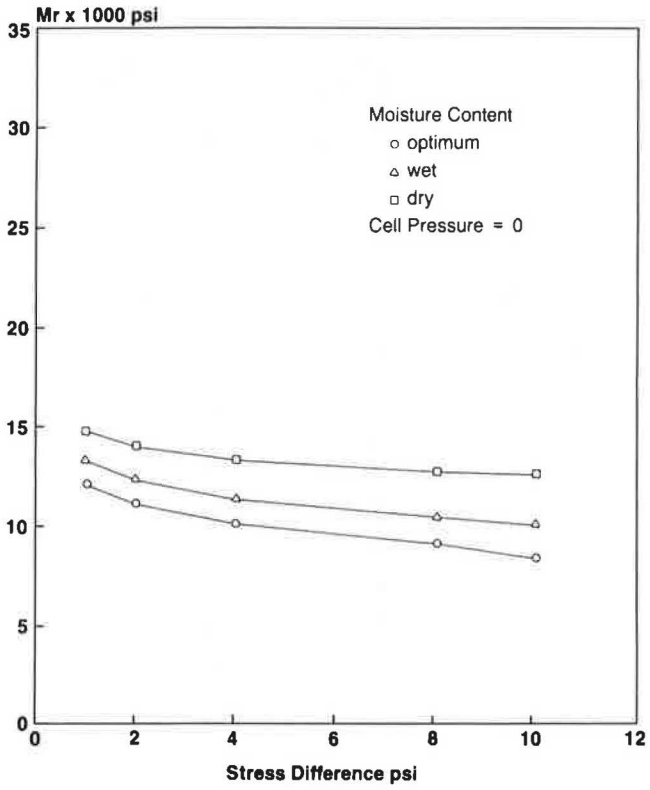

FIGURE 6 Resilient modulus, Peorian loess, high plasticity (*I*).

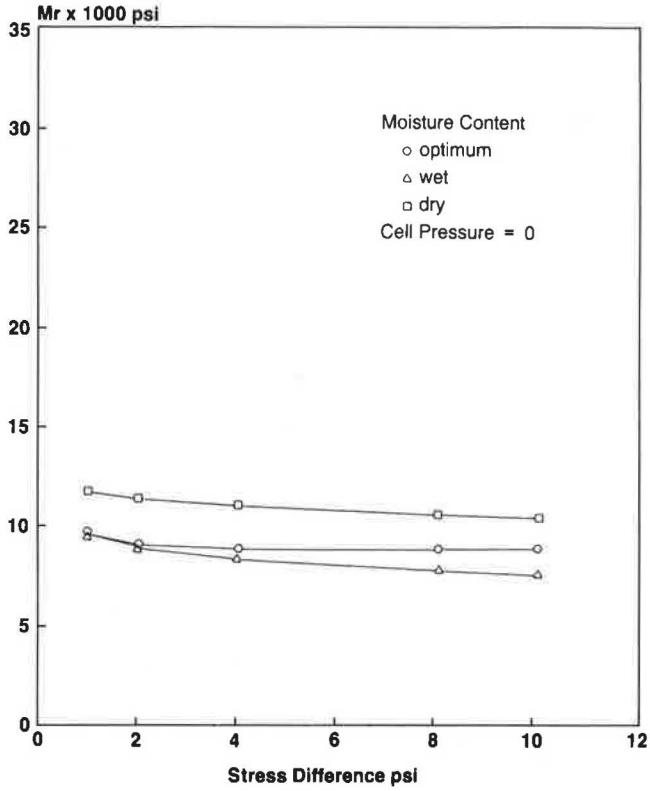

FIGURE 8 Resilient modulus, Pierre shale (*I*).

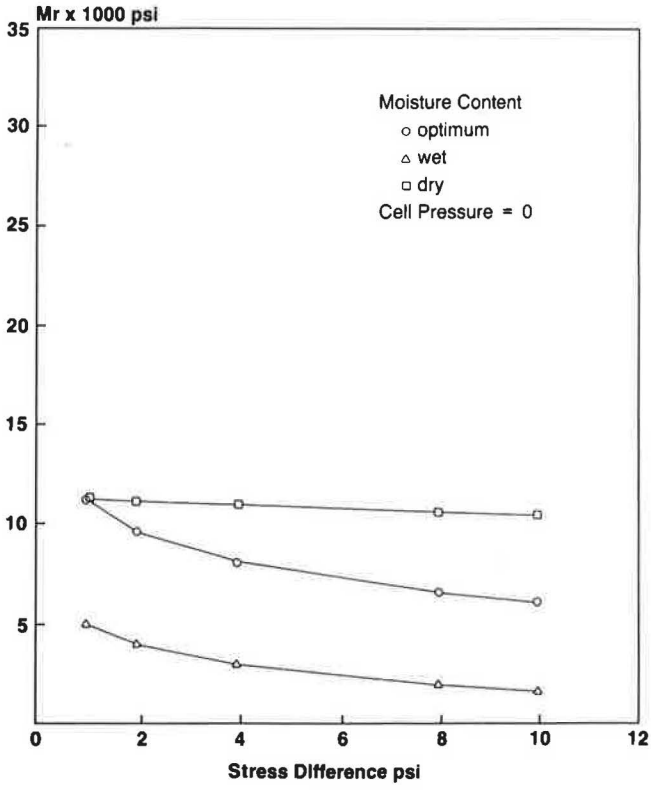

FIGURE 7 Resilient modulus, glacial (*I*).

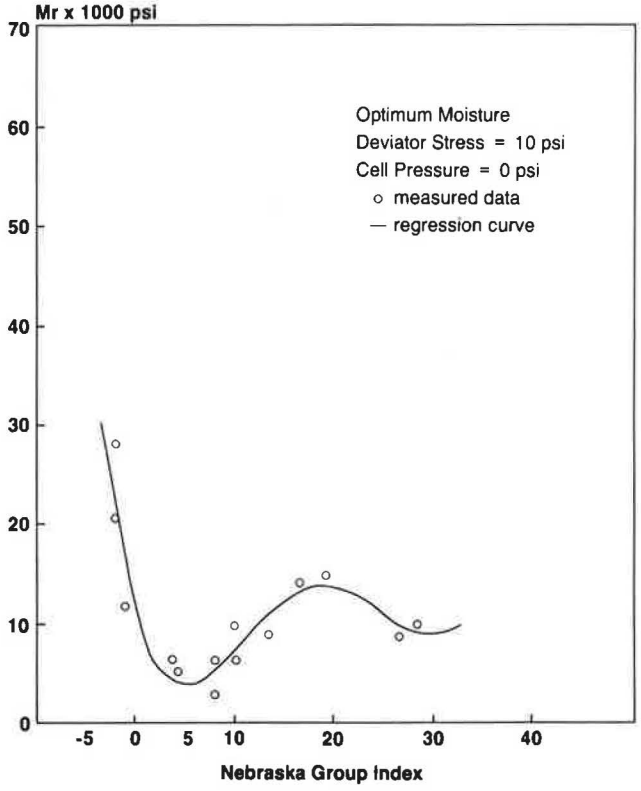

FIGURE 9 Resilient modulus versus Nebraska Group Index.

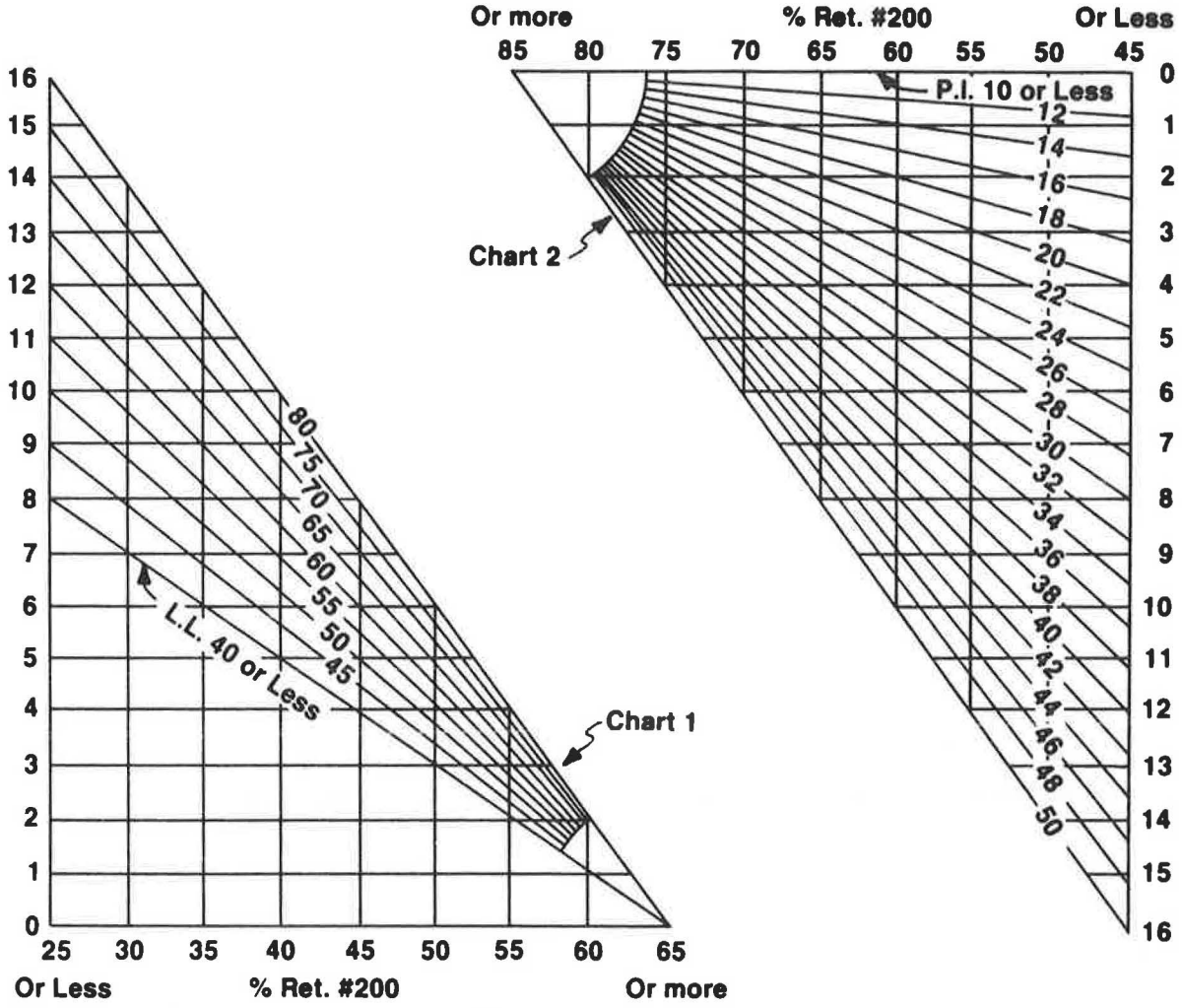

Group Index { Positive Values - Sum of Readings on Vertical Scale of Charts 1 & 2.
Negative Values - Use Chart 3.

	Well Graded Gravel Base	Clean Coarse Sand	Clean Fine Sand	Loamy Coarse Sand	Loamy Fine Sand	Loamy Very Fine Sand
Group Index	- 4	- 3	- 2		- 1	0
% Ret. #10	40 Min.					
% Ret. #40	60 Min.	35 Min.	34 Max.	35 Min.	34 Max. 10 Min.	9 Max.
% Ret. #200	85 Min.	85 Min.	85 Min.	84 Max. 65 Min.	84 Max. 65 Min.	84 Max. 65 Min.
P.I.	4 Max.	4 Max.	4 Max.	10 Max.	10 Max.	10 Max.

The first group from the left into which the test data will fit is the correct classification.

FIGURE 10 Nebraska Group Index charts.

induced. At low confining pressures and high degrees of saturation, a drop in pore water pressure is produced, caused by dilation of the well-compacted granular material. Since the load pulse is only 0.1 sec in duration, there is not sufficient time for pore water migration as the sample dilates; thus the pore water pressure must drop. The drop in pore water pressure increases the effective stress and the sample appears more stiff" (*1*). This effect was most apparent under wet conditions and low confining pressures.

No tests have been conducted to try to prove the theory.

OTHER LABORATORY TESTS

The following tests were performed by the MAT laboratory: soil gradations, liquid limit, plastic limit, X ray diffraction, optimum moisture content, and in situ moisture content from the tube samples. The data from the laboratory tests and the deflection tests were used for the statistical analysis.

STATISTICAL ANALYSIS

Regression equations were derived both individually and in combinations for the resilient moduli and for the other measurements. The initial results were not encouraging. Most of the comparisons yielded little more than scatter-gun graph patterns. However, certain characteristics yielded better results than others did: the percent retained on the No. 200 sieve, the liquid limit, and the plasticity index. Because those are the characteristics used to determine the soil group index, regression equations were developed by using group indices as the known variables. This procedure yielded a very close fit to the measured data, as indicated by Figure 9.

The group index used in the regression analysis is the Nebraska Group Index (NGI). The NGI, as determined from Figure 10, is similar to that developed by AASHTO, but it is somewhat more sensitive and permits negative values for granular materials.

Regression analyses were performed for resilient moduli produced by a cell pressure of 0 psi with a deviator stress of 10 psi and a cell pressure of 6 psi with a deviator stress of 10 psi. Although a cubic equation seemed to give the best fit for the low plasticity soils, the best overall fit, under all three moisture levels, turned out to be the fourth-order equations given in Equations (1) and (2).

$$Mr = 100[B_0 + B_1(G) + B_2(G^2) + B_3(G^3) + B_4(G^4)] \quad (1)$$

where Mr is the resilient modulus (psi) and G is the Nebraska Group Index.

	Optimum	*Wet*	*Dry*
B_0 =	123.69	92.15	99.51
B_1 =	−38.81	−32.66	−36.39
B_2 =	5.52	4.33	6.42
B_3 =	−0.25	−0.17	−0.33
B_4 =	0.004	0.002	0.005
[R square	0.96	0.92	0.93]

The deviator stress is 10 psi, and the cell pressure is 0 psi.

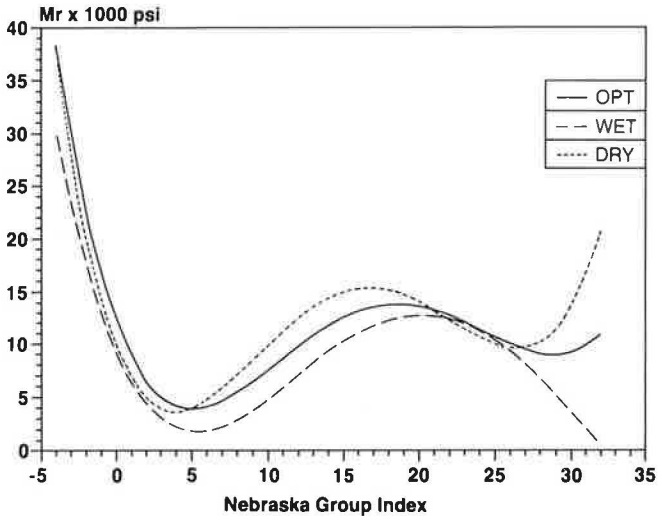

FIGURE 11 Resilient modulus versus Nebraska Group Index, deviator stress = 10, confining pressure = 0.

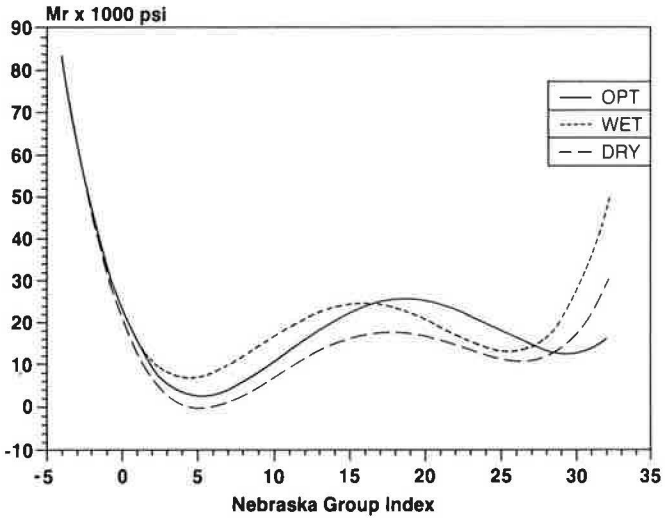

FIGURE 12 Resilient modulus versus Nebraska Group Index, deviator stress = 10, confining pressure = 6.

$$Mr = 100[B_0 + B_1(G) + B_2(G^2) + B_3(G^3) + B_4(G^4)] \quad (2)$$

	Optimum	*Wet*	*Dry*
B_0 =	249.44	226.31	241.26
B_1 =	−98.38	−105.03	−95.17
B_2 =	13.51	14.93	15.63
B_3 =	−0.60	−0.71	−0.82
B_4 =	0.008	0.011	0.013
[R square	0.92	0.88	0.88]

The deviator stress is 10 psi, and the cell pressure is 6 psi.

The equations, as indicated by Figures 11 and 12, conform fairly well to the observed data. Within an NGI range of approximately −3 to +28, the equations are fairly well behaved. However, the equations should not be used for aggregates and soils outside of this range, because the fourth-

order term begins to dominate and the results are no longer reliable. The effective range, however, covers most soil-aggregate mixtures used for Nebraska road construction.

SUMMARY

The purpose of the study was to determine if there was a reliable, easily performed test for the resilient moduli of subgrade soils and aggregates. While there was some initial concern, the small sample and the variability within soils and aggregates of the same classification were not fatal problems.

The regression analysis demonstrated that it is possible to reliably determine the resilient modulus of soils through indirect methods. The results of the study did raise some questions about using resilient modulus, as measured by AASHTO test T274-82 for pavement design. The main problems are the apparent increase in strength with increasing load of some low plasticity soils.

CONCLUSIONS

From the results of the various tests and the statistical regression analysis it has been determined that

1. The resilient moduli of soils can be reliably determined by indirect methods.
2. Some high plasticity soils show very high strengths under dynamic loading.
3. Pavement deflection results, as measured with a Dynaflect, did not show enough relationship to the resilient modulus to be used as an indicator.
4. The Nebraska Group Index is a reliable indicator of the resilient moduli of soils within an NGI of -3 to $+28$.

ACKNOWLEDGMENTS

The author acknowledges the contributions of Roy V. Sneddon in the resilient modulus testing and Ronald E. Bohling in the statistical analysis.

REFERENCE

1. R. V. Sneddon. *Resilient Modulus Testing of 14 Nebraska Soils.* University of Nebraska, Lincoln, Nov. 1988.

The opinions and conclusions expressed in this paper are those of the author and do not necessarily represent the official position of the Nebraska Department of Roads.

Publication of this paper sponsored by Committee on Mineral Aggregates.

Dynamic Response of Open-Graded Highway Aggregates

RICHARD J. BATHURST AND GERALD P. RAYMOND

The results are presented of a laboratory study that was carried out to investigate the stability of thin layers of coarse single-sized (open-graded) highway aggregates under dynamic plate loading. The investigation considered a range of aggregates having variable quality as defined by the Aggregate Index Number. The Aggregate Index Number is a quantitative measure of the combined durability of an aggregate that is based on the aggregate's resistance to fracture and abrasion as measured in the Los Angeles Abrasion and Mill Abrasion Tests. Other variables between tests were gradation size and support compressibility. The test results showed that for the coarsest gradation investigated, the semi-logarithmic permanent deformation rate could be reduced significantly by increasing aggregate quality and/or increasing underlying support stiffness. The sensitivity of deformation rate to aggregate quality and underlying support compressibility decreased for parallel but finer gradations. Finally, implications to selection criteria for aggregate used in unbound open-graded drainage layers below highway and airfield pavements are identified.

Infiltration of surface water into pavement cracks and joints is a major source of pavement deterioration in highway and airfield pavements. A strategy becoming increasingly more common in North America to reduce or eliminate this problem is to construct an open-graded drainage layer (OGDL) directly below the surface course that can direct infiltrated water to pavement shoulders or drains (*1–4*). An example of a pavement structure that incorporates an OGDL is given in Figure 1.

The aggregate must have high permeability because of the high volume/short duration flows that may be required of an OGDL layer. A successful OGDL must be capable of removing water at a rate greater than the infiltration rate. For this reason, relatively coarse-grained single-sized (open-graded) aggregates are recommended. The aggregate layer must be protected, using suitable bases or filters, and be provided with outlet drains that ensure positive drainage. Owing to the proximity of any OGDL to the pavement-bearing surface the OGDL must possess adequate stability against traffic-induced shearing stresses. Those shearing stresses may be further amplified near pavement cracks or, in the case of reinforced concrete pavements, joints. Under those conditions traffic wheel loads may not be attenuated through the surface course, and the OGDL may experience overstressing.

The necessity of providing both adequate drainage capacity and adequate stability can lead to conflicting requirements in the specification of the aggregate source because the stability of granular material generally increases if a material has a well-graded particle size distribution (i.e., strength increases with decreasing void ratio). In many instances, a 1.5 to 2 percent asphaltic cement (AC) binder is added to the aggregate to stabilize the layer during construction activities. The AC content is just great enough to coat the aggregate and does not significantly reduce permeability of the material. Nevertheless, unbound open-graded drainage layers have also been successfully constructed (*2,3*). The influence of grain size distribution on aggregate permeability in pavement structures has been the topic of investigation by many researchers [e.g., (*2,5–8*)]. Less well understood is the influence of properties such as fracture resistance (toughness), abrasion resistance (hardness), and grain-size distribution of open-graded aggregates on the stability of materials under repetitive loading [e.g., (*9*)]. Related works (*10*) (*11*) concerned with predicting longevity of ballast aggregates in railway tracks offer guidance to experimental programs for open-graded aggregates in highway and airfield pavements. For example, Canadian Pacific Rail (CP Rail) has adopted a track model that relates longevity of ballast to aggregate fracture resistance, aggregate hardness, and cumulative tonnage on track (*12*). A work by Raymond and others (*13*), concerning the CP Rail track model has, in part, inspired the experimental approach adopted in the current investigation.

SCOPE OF CURRENT INVESTIGATION

A preliminary laboratory investigation that examines, under simulated traffic loading, the influence of aggregate properties on the stability of unbound open-graded drainage layer models is described in this paper. The properties of the aggregates investigated were fracture resistance, hardness, and grain size distribution.

TEST PROGRAM

Three different aggregates from eastern Ontario were examined. The properties used to characterize the aggregates follow:

1. Aggregate gradation (i.e., ranging from a gradation with a top size of 37.5 mm to parallel finer grain size distributions with a top size of 19 and 9.5 mm) and
2. The combination of hardness and resistance to fracturing of the aggregate samples as defined by the Mill Abrasion (MA) value, Los Angeles Abrasion (LAA) value, and the Aggregate Index Number.

R. J. Bathurst, Civil Engineering Department, Royal Military College of Canada, Kingston, Ont. K7K 5L0. G. P. Raymond, Civil Engineering Department, Queen's University at Kingston, Kingston, Ont. K7L 3N6.

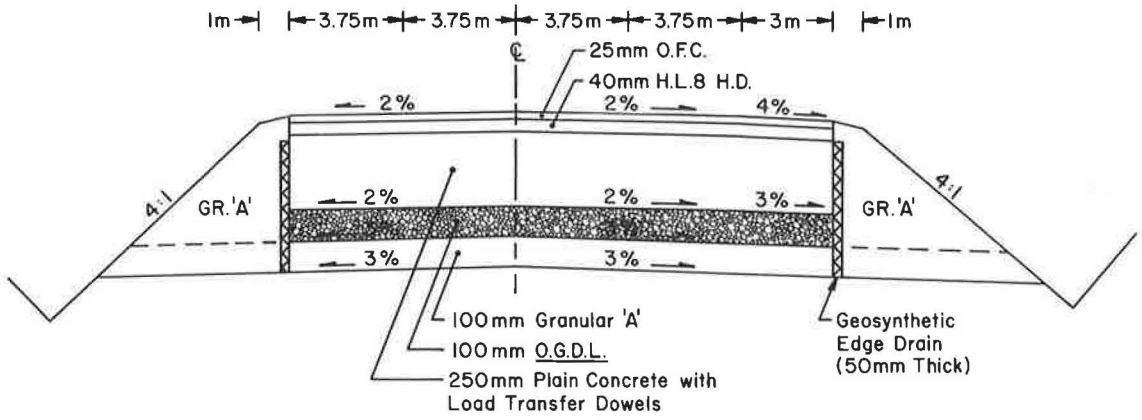

FIGURE 1 Example of highway pavement with open-graded drainage layer.

The relative stability of the aggregate materials was determined by comparing the cumulative load-deformation response of thin layers of aggregate during repeated loading in a laboratory plate-loading apparatus. The principal variable between model configurations with respect to the plate-bearing test was the use of either a rigid or flexible support to model a range of compressibility in the underlying road structure. Experience from similar test programs on the stability of railway ballast has shown that the compressibility of the underlying structure has a very important influence on the cumulative load-deformation response of aggregate materials (*14*). A total of 22 plate-bearing tests were carried out, of which four were replicate tests to examine test repeatability.

Aggregate Sources

The aggregate sources used in this investigation comprised 100 percent crushed rock. The properties are summarized in Table 1. The meaning and significance of the characteristic properties of the aggregates are given in the following sections. The Elginburg limestone and Jasper dolomite have been used as base materials in roadworks by the Ministry of Transportation of Ontario (MTO) in eastern Ontario and the Marmora Trap as ballast in branchline track by CP Rail.

TABLE 1 SUMMARY OF AGGREGATE PROPERTIES

Aggregate Type	Specific Gravity	Mill Abrasion (MA) (%)	Los Angeles Abrasion (LAA) (%)	I_a*	C_u**	C_c***
Elginburg Limestone	2.68	9.1	28.9	74	3.6–4.3	1.0–1.3
Jasper Dolomite	2.76	6.6	20.9	54	3.9	1.1
Marmora Trap	2.98	5.1	14.1	40	4.0–4.4	1.0–1.3

* Aggregate Index Number $I_a = 5 \times MA + LAA$
** Coefficient of Uniformity D_{60}/D_{10}
*** Coefficient of Curvature $D^2_{30}/D_{60}D_{10}$

Gradation

The standard grain-size curves investigated are given in Figure 2. Gradation 1 represents the coarsest material considered and is close to the current OGDL specification presently adopted by MTO (Figure 2a). Gradation 2 (medium) and 3 (fine) have similar slopes and shape to gradation 1 (i.e., similar coefficient of uniformity (C_u) and coefficient of curvature (C_c)) but are shifted to essentially parallel gradations with finer particle sizes. For comparison purposes, the hatched regions in Figures 2b and 2c correspond to gradation specifications that have been used for OGDL construction in the United States. Gradation 1 is close to the AASHTO 57 specification for coarse aggregate (*1*), and gradations 1 and 2 fall within specifications for OGDLs recently adopted by the Pennsylvania Department of Transport (PennDOT) (*2*). The target gradations were achieved by blending presieved aggregate size ranges taken from laboratory stock piles.

Los Angeles Abrasion Test

LAA tests were carried out on aggregate samples as given in ASTM Designations C535-81 and C131-81 to give a relative measure of particle resistance to fracturing.

The LAA test simulates the effect of high contact forces on aggregate particles, including those generated by impact loading. High impact forces on OGDL aggregates will occur in the vicinity of transverse cracks in asphaltic pavements and below joints in concrete pavements. The ability of an aggregate to survive high contact forces is dependent on the toughness of the aggregate (i.e., particle resistance to fracturing). A low LAA value indicates a material with a high resistance to fracturing under high contact forces.

Because the samples tested covered a range of aggregate sizes, the Standard Test Method ASTM C535-81 was used for materials having a particle size greater than 19 mm, and the test method given in ASTM C131-81 was used for materials with a particle size less than 19 mm.

Mill Abrasion Test

The MA test is a nonstandard test that simulates autogenous grinding and measures the relative resistance to abrasion or

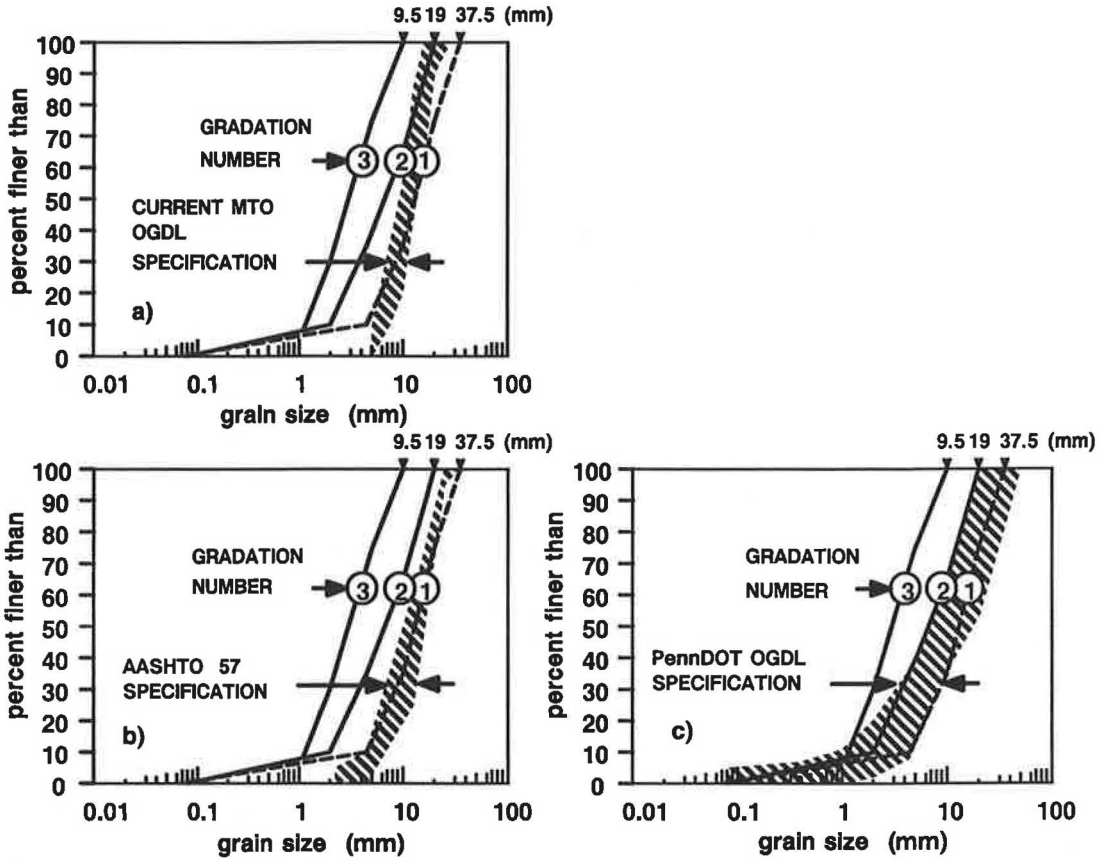

FIGURE 2 Examples of grain size distributions for open-graded drainage layers.

hardness of aggregate materials as a result of the autogenous grinding of the aggregate particles. Abrasion of aggregate particles in an OGDL will result from the constant movement of aggregate particles against each other, particularly near pavement cracks and joints.

The specifications for the MA test follow and are reproduced from the current CP Rail specification (*12*). In the current investigation, the CP Rail method of test was modified for samples having a smaller top-size than that designated in the original specification.

The Mill Abrasion Test (from CP Rail Specification for Ballast 1984):

A representative sample is obtained and sized by using current ASTM Methods of Test. From the coarse aggregate, split a representative portion into a sample consisting of 1.5 kg passing the 38.1-mm sieve and retained on the 25.4-mm sieve plus 1.5 kg passing the 25.4-mm sieve and retained on the 19-mm sieve. The sample shall be washed and oven dried in accordance with the Los Angeles Abrasion procedure. The sample will then be placed in a 4.546-l, 230-mm external diameter porcelain ball mill pot, along with 3 kg of distilled water. The mill pot shall be sealed and rotated at 33 rpm for a total of 10,000 revolutions (5 hours). The sample shall then be wash-sieved through a No. 200 sieve and oven dried before weighing. Mill Abrasion shall be calculated as a percentage loss in weight, using the following formula:

$$\text{mill abrasion} = \frac{\text{loss in weight}}{\text{original weight}} \times 100$$

The Modified Mill Abrasion Test for small-size aggregate:

The procedure just described was modified for samples of aggregate having particle sizes less than 19 mm. For those samples, a single 3-kg charge was used composed of particle sizes passing 19 mm and retained on the No. 4 sieve.

Hardness-Toughness Trade Offs and Aggregate Index Number

Experience with railway ballasts (*10,11*) has shown that aggregates that are tough with respect to fracture resistance are not necessarily highly abrasion resistant. Rather, the same longevity of ballast under cumulative tonnage can be obtained by aggregates having different combinations of MA (hardness) and LAA (toughness) values. A parameter that reflects the contribution of both mechanisms to aggregate durability in track is the Aggregate Index Number (I_a) where

$$I_a = 5 \times \text{MA} + \text{LAA}$$

CP Rail has adopted limits on the Aggregate Index Number as a ballast criterion and have correlated the I_a value and aggregate gradation with ballast life (i.e., cumulative tonnage to aggregate fouling). In the CP Rail specification, the Aggregate Index Number is called the Abrasion Number.

The work by Raymond and CP Rail has inspired the current experimental approach and has led to an investigation of the Aggregate Index Number as an indicator of relative stability of coarse single-sized highway aggregates.

The aggregates tested in the current investigation were selected to give a range of hardness and fracture resistance and Aggregate Index Number. The Elginburg limestone was the poorest quality aggregate investigated (i.e., greatest I_a value) and in qualitative terms represents an aggregate with low hardness/low toughness (soft/weak). The Marmora Trap is a metamorphic rock and was the highest quality aggregate (i.e., lowest I_a value) investigated. It has medium hardness/high toughness. Finally, the Jasper dolomite is an intermediate quality aggregate and is defined by medium hardness/medium toughness.

Plate-Bearing Test Procedure

The general arrangement for the plate-bearing test is given in Figure 3; the test system is shown in Figure 4. The OGDL was modeled as a layer of aggregate 100 mm thick and was supported by a rigid or flexible base. The 100 mm thickness is typical of OGDL installations in Ontario (Ministry of Transportation, Personal Communication) and in the United States (*1*). Nevertheless, 100 mm is likely the minimum thickness that would be considered in actual installations to facilitate construction and to ensure adequate flow capacity. The OGDL samples were 1 m by 1 m in plan area and were confined within a rigid thick-walled aluminum tray, which permitted unbound aggregate samples to be placed and compacted away from the loading system. The flexible support condition was created by using a closed-cell gum-rubber mat (12 mm thick). The equivalent subgrade modulus (k_s) of the mat material was determined to be 370 MN/m^3, using a rigid 457-mm diameter steel plate and a static load of 40 kN (i.e., maximum bearing pressure = 244 kPa). The measured mat flexibility is considered to be representative of the compliance because of the combined effect of a good granular subbase overlying a competent cohesive subgrade. In a previous investigation (*14*), the CBR of this artificial "subgrade" was estimated to be equivalent to a granular material with a CBR of 40.

A sinusoidal loading pulse with an amplitude of 2 to 40 kN was applied to the surface of each sample by using the same rigid steel plate. The maximum 40 kN load represents a standard half-axle load. The 457-mm diameter plate (as opposed to, say, a 300-mm diameter plate) was selected to simulate the increased bearing area that would exist in the pavement structure at the elevation of the OGDL as a result of the vertical load that spread through the overlying surface course. The minimum load level of 2 kN was selected to ensure a good contact between the aggregate and the loading plate. The load was delivered to the plate by using an MTS closed-loop electrohydraulic actuator controlled by a DEC PDP11/34 computer. A load cell and linear variable displacement transducer (LVDT) located above the actuator base was used to monitor footing loads and vertical displacements. The load-deformation response of the footing during a loading cycle was recorded and stored by the computer at programmed intervals. The load was applied at a rate of 5 Hz for 1 to 2 million load applications. The plate was maintained in a horizontal position throughout the test by passing the actuator piston through a rigidly supported Teflon® bushing.

A concrete plinth was used to support the aluminum tray that confined the aggregate sample. The purpose of this structure was to provide a catchment system for in-situ permeability tests as part of a related research program.

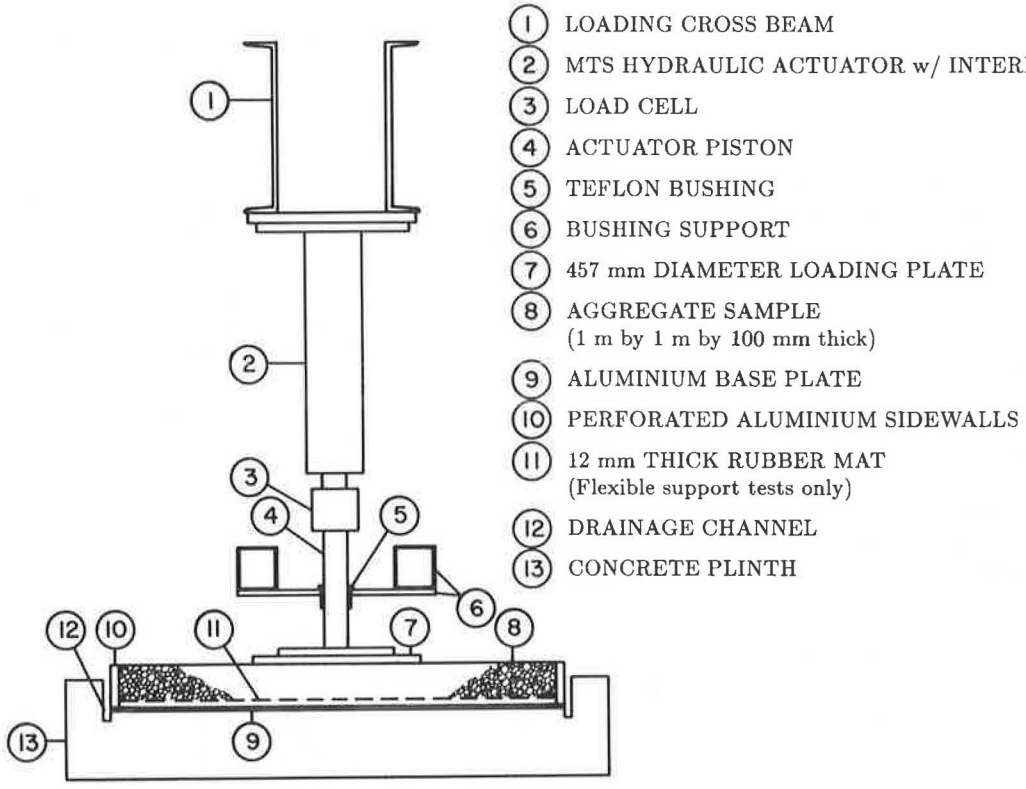

FIGURE 3 Plate-bearing test apparatus.

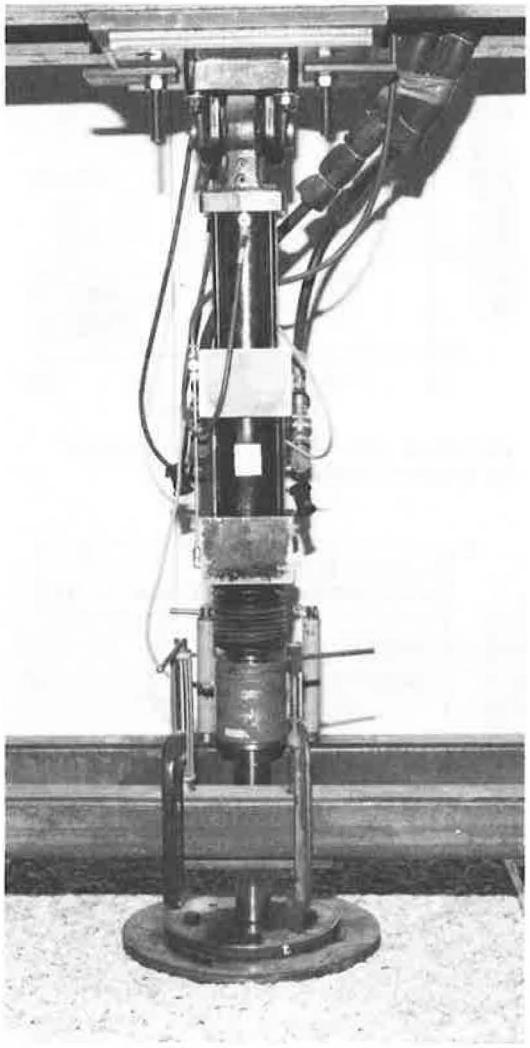

FIGURE 4 Testing system.

The aggregate samples were compacted by using a hand-held tamping plate that weighed 10.4 kg and had a tamping area 250 mm by 250 mm. The same number of passes from the same height were used in the preparation of each specimen.

TEST RESULTS

The results of density measurements showed that void ratios varied from about 0.42 to 0.61 for samples of the Elginburg limestone, Jasper dolomite, and Marmora Trap. Void ratio data were plotted in Figure 5. There was no systematic variation in void ratio between samples constructed with a rigid support. The void ratios for the flexible-support models with the finest gradation were somewhat lower than for the comparable rigid-support configurations. Nevertheless, the mean value of void ratio at a particular gradation was reasonably constant at about 0.49 for both rigid and flexible models. The independence of void ratio from aggregate type was a consequence of similar particle shape for the 100 percent crushed materials and the light compaction effort applied to the samples to prevent particle crushing during construction.

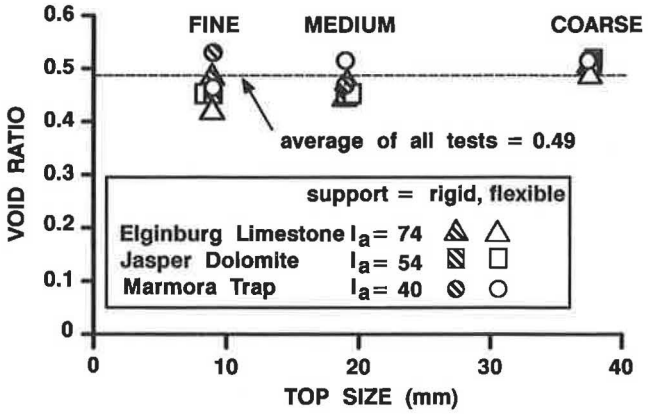

FIGURE 5 Void ratio versus top size.

The results of the plate-bearing tests with the coarsest aggregate (gradation 1) are shown in Figures 6 and 7. The cumulative (permanent) displacement with the number of load repetitions was highly nonlinear, with most of the deformation occurring early in the loading program. The same data were replotted with semi-logarithmic axes. In general, the data show that over a wide range of load repetitions the permanent displacements varied linearly with the log number of load applications. The data from those tests indicate that the magnitude of permanent displacement increases with the value of Aggregate Index Number I_a and with the compressibility of the underlying support.

Permanent deformation as a relative measure of aggregate stability under load can be misleading, because the magnitude

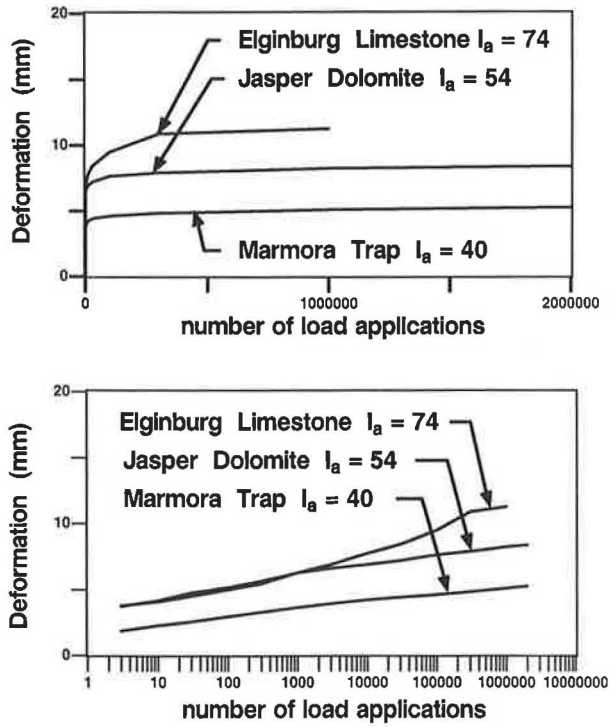

FIGURE 6 Load deformation response of aggregates over rigid support (gradation 1): linear scale (*top*), semi-logarithmic scale (*bottom*).

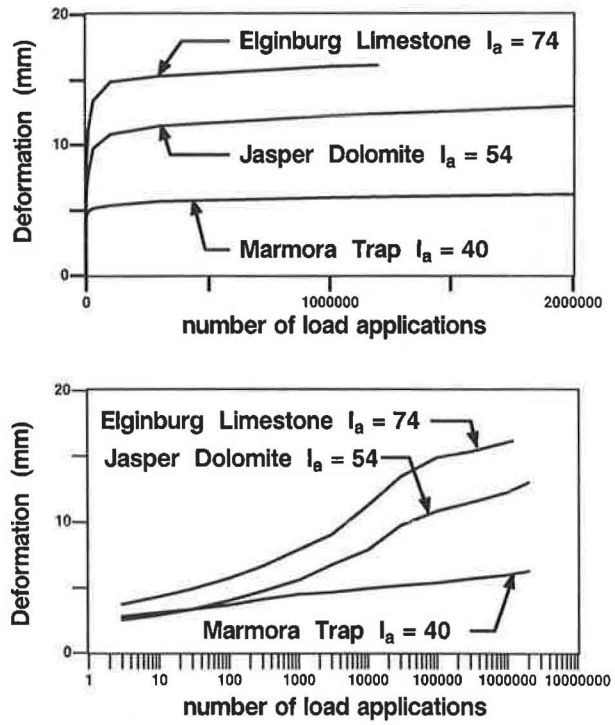

FIGURE 7 Load deformation response of aggregates over flexible support (gradation 1): linear scale (*top*), semi-logarithmic scale (*bottom*).

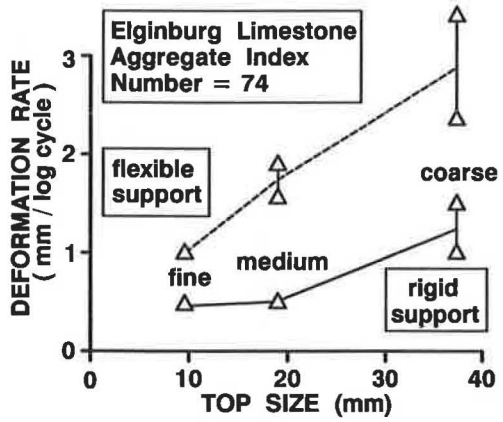

FIGURE 8 Deformation rate versus top size for Elginburg limestone.

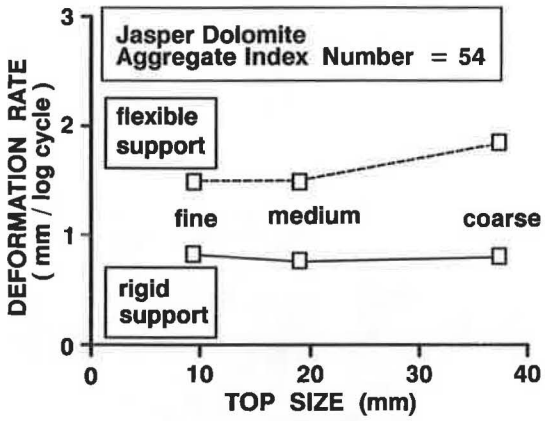

FIGURE 9 Deformation rate versus top size for Jasper dolomite.

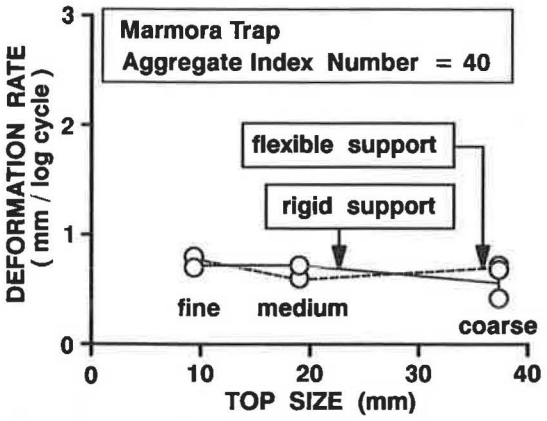

FIGURE 10 Deformation rate versus top size for Marmora Trap.

of permanent deformation after a given number of load applications is sensitive to the effects of initial plate seating. In this investigation the most reliable measure of relative stability between tests was found to be the rate at which permanent deformation had accumulated with respect to the log number of load repetitions (i.e., mm/log cycle) taken over 10 to 10^6 load applications. For brevity, this quantity is referred to as deformation rate.

Deformation rates versus aggregate size for all test configurations are summarized in Figures 8–10 and are based on the three aggregates investigated. For the poorest aggregate (Elginburg limestone in Figure 8), the test results show that deformation rates diminished with finer aggregate size and greater support stiffness. Figure 9 shows that for the intermediate quality aggregate (Jasper dolomite) the deformation rates were essentially insensitive to aggregate size but decreased with lower support compressibility. The same data for the highest quality aggregate (Marmora Trap) show that deformation rates were essentially independent of aggregate size and support condition (Figure 10).

The influence of test parameters on model stiffness can be described by rebound values measured over the course of each test. The rebound values have been calculated as the difference between permanent and peak plate deformations during a load cycle. An average rebound value was calculated for 10 to 10^6 load applications in each test, and those values are plotted in Figure 11, which illustrates that rebound values were essentially insensitive to grain size but (as expected) were dependent on the support stiffness. For the flexible support condition, the rebound values showed a tendency to increase with decreasing aggregate quality. Nevertheless the magnitude of the values recorded are close to the limit of the instrumentation accuracy, and it is therefore difficult to confidently isolate the influence of aggregate quality on system rebound values.

The deformation rate values from all tests can be replotted against the Aggregate Index Number (I_a), as shown in Fig-

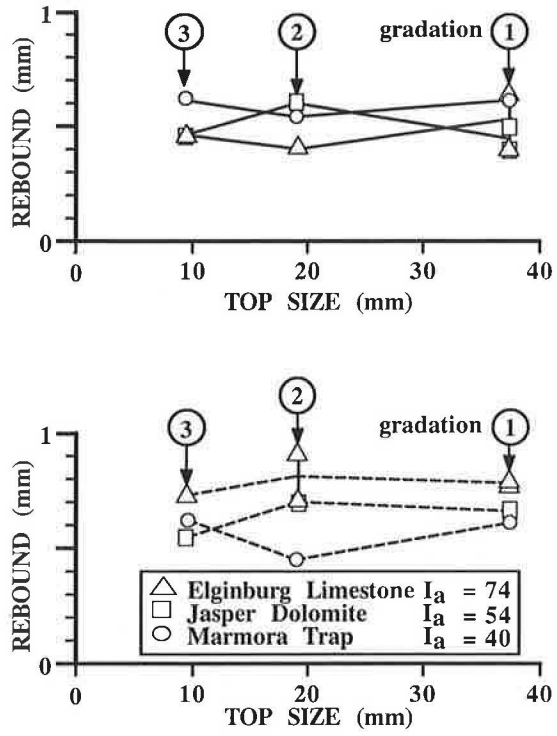

FIGURE 11 Rebound versus top size: rigid support (*top*), flexible support (*bottom*).

ures 12–14 for gradations 1 (coarse), 2 (medium), and 3 (fine). The figures illustrate that the stability of OGDLs meeting the coarsest size specification could be improved by selecting a higher quality aggregate as defined by its Aggregate Index Number. This is particularly true for open-graded aggregates over compressible bases. For example, reducing the Aggregate Index Number from 74 to 40 corresponds to a reduction in the (log) cumulative deformation rate by a factor of three. On a linear scale, this improvement corresponds to a thousand-fold increase in the number of load applications to achieve the same deformation level as for the poorest aggregate. Figure 13 illustrates that the performance of OGDLs having a size distribution corresponding to a medium gradation (gradation 2) could only be improved by selecting a higher quality aggregate if the layer were over a compressible base. Finally, for the finest gradations investigated, Figure 14 shows that the quality of the aggregate did not systematically influence the stability of those systems on the basis of deformation rate.

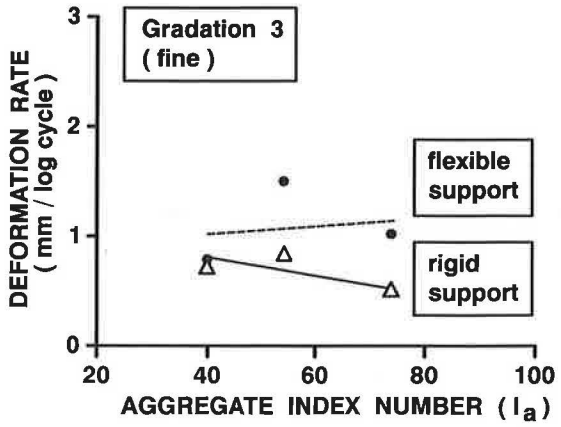

FIGURE 12 Deformation rate versus Aggregate Index Number (I_a) for gradation 1.

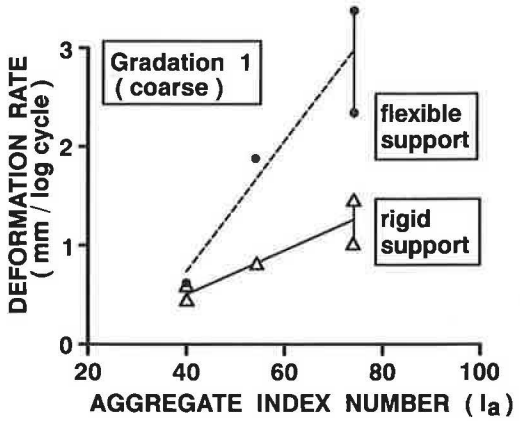

FIGURE 13 Deformation rate versus Aggregate Index Number for gradation 2.

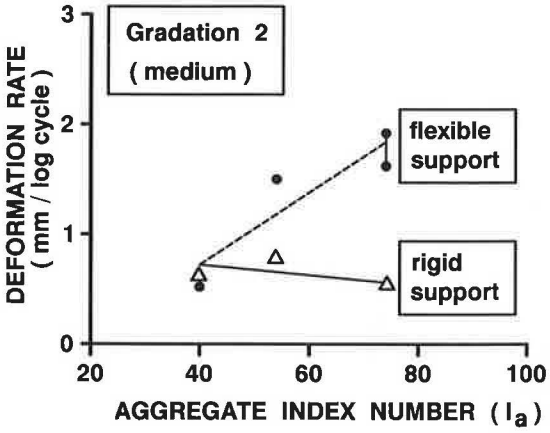

FIGURE 14 Deformation rate versus Aggregate Index Number for gradation 3.

CONCLUDING REMARKS

The results of the current laboratory investigation have shown preliminary qualitative relationships between aggregate stability under dynamic loading and the quality of the aggregate and the stiffness of the underlying support. The coarse and medium-sized open-graded aggregates investigated cover a range that would be considered in OGDL construction on the basis of a number of current specifications that ensure adequate flow capacity for those aggregates when used as drainage layers below pavement. The tests show that the ability of the unbound aggregate to resist cumulative permanent deformation generally diminishes as the quality of the aggregate decreases (i.e., increasing Aggregate Index Number) and as

the compressibility of the underlying support increases. For example, if a coarse aggregation gradation (say, gradation 1) were desirable based on drainage criteria, then an aggregate with a low Aggregate Index Number would be needed to ensure adequate resistance to fracturing and resistance. This is particularly true of OGDLs placed over compliant road support. Under those conditions, the results of the current investigation have shown that a thousand-fold increase in the number of load applications is required for the highest quality aggregate to achieve the same level of permanent deformation as does the poorest aggregate. Highway pavement performance is evaluated in part by the magnitude of surface rut depth. If the number of load applications to achieve an unacceptable level of deformation in the OGDL were to be increased by a factor of a thousand, then pavement repair cycle times would be dramatically reduced. An alternative strategy to selecting a better quality material is to use a finer gradation (say, gradation 2) to improve the stability of the aggregate.

It is current practice in many jurisdictions to use a 1.5 to 2 percent AC binder to stabilize the open-graded drainage layer during construction. The influence of parameters such as grain size distribution, aggregate quality, support compressibility, AC content, and compaction density on those bound systems warrant investigation. Nevertheless, it has been observed in some prototype-scale test sections by the authors that stripping of the OGDL aggregate can occur because of water infiltration, and, therefore, it can be argued that ultimately the stability of the OGDL is dependent on the unbound condition of the aggregate.

In practice, the Aggregate Index Number should not be considered a substitute for petrographic evaluation of highway aggregates. Petrographic analysis is a primary tool in aggregate evaluation particularly with respect to mineral composition (e.g., minerals may be susceptible to weathering), consistency, particle shape, and structure (e.g., foliation, cleavage, and bedding planes). A thorough petrographic evaluation should be carried out to eliminate aggregates unsuitable regardless of their Aggregate Index Number. Nevertheless, as this investigation has shown, the interrelation between Aggregate Index Number, gradation size, and support compressibility does reveal important trends that can assist the engineer to choose between aggregates that are potential candidates for OGDL construction.

ACKNOWLEDGMENTS

The authors would like to express their appreciation to R. Lee and J. Bell, who carried out the physical tests, and to the Ministry of Transportation of Ontario, which provided the research funds. The authors are also indebted to Jerry Hajek at MTO for his valuable advice over the course of this investigation.

REFERENCES

1. J. S. Baldwin and D. C. Long. Design, Construction, and Evaluation of West Virginia's First Free-Draining Pavement System. *Transportation Research Record 1159*, TRB, National Research Council, Washington, D.C., 1988.
2. K. L. Highlands and G. L. Hoffman. Subbase Permeability and Pavement Performance, *Transportation Research Record 1159*, TRB, National Research Council, Washington, D.C., 1988.
3. Open-Graded Base Course Placed at Portland Airport. *Engineering News-Record*, July 5, 1979.
4. H. R. Cedergren. Why All Pavements Should be Well Drained. Presented at 67th Annual Meeting, TRB, Washington D.C., Jan. 1988.
5. H. R. Cedergren, J. A. Arman, and K. H. O'Brien. *Development of Guidelines for the Design of Subsurface Drainage Systems for Highway Pavement Structural Sections*. Final Report, Office of Research, FHWA, U.S. Department of Transportation, 1973.
6. T. J. Moynahan and Y. M. Sternberg. Effects on Highway Subdrainage of Gradation and Direction of Flow Within a Densely Graded Base Course Material. *Transportation Research Record 497*, TRB, National Research Council, Washington, D.C., 1977.
7. T. W. Smith, H. R. Cedergen, and C. A. Reyner. Permeable Materials for Highway Drainage. *Highway Research Board 68*, HRB, National Research Council, Washington, D.C., 1965.
8. W. E. Strohm, E. H. Nettles, and C. C. Calhoun. Study of Drainage Characteristics of Base Course Materials. *Highway Research Board 203*, HRB, National Research Council, Washington, D.C., 1967.
9. H. F. Winterkorn. Application of Granular Principles for Optimization of Strength and Permeability of Granular Drainage Structures. *Highway Research Board 203*, HRB, National Research Council, Washington, D.C., 1967.
10. G. P. Raymond. Ballast Properties That Affect Ballast Performance. *American Railway Engineering Association Bulletin 673*, Vol. 80, June–July 1979.
11. G. P. Raymond, C. J. Boon, and R. W. Lake. *Ballast Selection and Grading*. Report 79-4. Canadian Institute of Guided Ground Transport, 1979.
12. *CP Rail Specification for Ballast*, 1984.
13. R. J. Bathurst and G. P. Raymond. *Stability of Unbound Open-Graded Aggregate Layers*. Report PAV-90-01. Ministry of Transportation of Ontario, March 1990.
14. G. P. Raymond and R. J. Bathurst. Performance of Large-Scale Model Single Tie-Ballast Systems. *Transportation Research Record 1131*, TRB, National Research Council, Washington, D.C., 1987.

Publication of this paper sponsored by Committee on Mineral Aggregates.

Characterization of Aggregate Shape Using Fractal Dimension

JAMES R. CARR, GARY M. NORRIS, AND DAVID E. NEWCOMB

A fractal is a term used in geometry to describe an object the shape of which is intermediate between topological ideals. A fractal object is described by a fractal dimension. Such a parameter describes the deviation that a line, surface, or volume has from a topological ideal. For example, an ideal topological line has a dimension equal to 1, and an ideal plane has a topological dimension equal to 2. A fractal line, though, has a fractal dimension greater than 1, but less than 2, and a fractal surface has a fractal dimension greater than 2 but less than 3. As an experiment, the distance can be measured between two arbitrarily located points on a coastline. By using different rulers of progressively smaller sizes, the measured length will be found to increase as ruler size decreases. This epitomizes fractals. If the number of rulers required to travel between two points is called N and the ruler length is called y, then length L is equal to Ny. For a fractal, the plot of log (N) versus log (y) yields a straight line; moreover, fractal dimension is equal to the absolute value of the slope of this line. Initial experiments show that circumferential traces of aggregate are fractal lines, with dimensions between 1 and 1.3. In general, greater fractal dimensions are found for rough, irregular aggregate. Fractal dimensions approach 1 for circumferential tracks of smooth, rounded pieces and for flat, elongated pieces. Lower fractal dimension are also found for aggregate where shapes approach ideal, angular shapes, such as squares or triangles. The fractal dimension, therefore, appears promising for the characterization of aggregate.

Mineral aggregates are critical components of construction materials and are used by themselves as low-traffic-volume road surfaces and base layers for higher trafficked pavements. Aggregates make up approximately 95 percent of the weight in asphalt concrete. Thus, the characteristics of mineral aggregates can dictate the performance of the structures in which they are used.

As important as aggregates are to the performance of construction materials, there are relatively few methods to quantify their contribution to performance. This is particularly true with respect to the surface characteristics such as particle shape, roughness, and surface charge. Those attributes are important to the interaction between the grains and to the interaction between the aggregate and whatever binder may be present in the material. Most tests that provide information on aggregate surface quality are subjective or are based on arbitrarily defined parameters.

In asphalt concrete, particle shape has been related to the optimum binder content, the quantity of air voids, the workability, the shear resistance, and the tensile strength of the mixture (*1–3*). Generally, it is desirable to have a somewhat angular shape in asphalt mixtures. Flat or elongated particle shapes are undesirable.

The surface texture or roughness is dependent on the degree to which the aggregate is polished or dull. It is usually described in terms of being very rough, rough, smooth, or polished. The texture can affect the fatigue resistance, air voids, binder content, tensile strength, and stability of asphalt mixtures (*4,5*).

Experiments are subsequently presented that attempt to quantify aggregate surface shape by using the concept of fractal dimension. In describing the geometry of aggregate by using the concept of fractals, it is hoped that a quantitative method is developed for the characterization of concrete aggregate shape that is more easily applied than existing methods.

SUMMARY OF EXISTING METHODS

Aggregate shape can be defined by methods such as those developed by Krumbein (*6*) or Rittenhouse (*7*). The Krumbein roundness number of a particle is expressed as

$$\text{roundness} = r/R$$

where r is the average radius of the corners of the projected image of the particle and R is the radius of the maximum inscribed circle of the projected image.

The Krumbein number can range from 0 to 1, though the typical range is from 0.1 (angular) to 0.8 (well rounded). Rittenhouse defined sphericity as the ratio of the diameter of a circle with an area equal to that of the projected area of the particle to the diameter of the smallest circumscribing circle of the particle. The range for sphericity is from 0 to 1, though the practical range is from 0.45 (elongated) to 0.97 (very spherical). Charts have been developed for visual comparison of both these methods.

Mather (*8*) proposed that the roughness of aggregate particles could be described in terms of the arithmetic average deviation of the actual surface from the surface mean. As was discussed earlier, surface texture is usually subjectively rated as being very rough to polished.

ASTM has a test method (D 3398) in which the particle index of an aggregate may be determined as an indication of the overall particle shape and texture. This method relies on the calculation of voids in the aggregate system at defined levels of compaction. These void quantities are then used in an equation that gives the particle index. The levels of com-

J. R. Carr, Department of Geological Sciences, Geological Engineering Division, University of Nevada, Reno, Nev. 89557. G. M. Norris, Department of Civil Engineering, University of Nevada, Reno, Nev. 89557. D. E. Newcomb, Department of Civil and Mineral Engineering, University of Minnesota, Minneapolis, Minn. 55455.

paction used in this test were arbitrarily chosen, and there is no actual measurement of the aggregate surface geometry.

A NEW APPROACH: FRACTAL CHARACTERIZATION

Concept of Fractals

Mandelbrot (*9*) illustrated the use of fractals in determining the length between two points (*A* and *B*) on the west coast of Great Britain, which is very irregular and complex (see Figure 1). The length of the coastline between *A* and *B* may be measured with a ruler of arbitrary length *y*. Beginning at point *A*, the ruler is placed end to end until point *B* is reached (see Figure 2). A segment smaller than *y* remains at the end and is designated *f* (see Figure 3). The length between *A* and

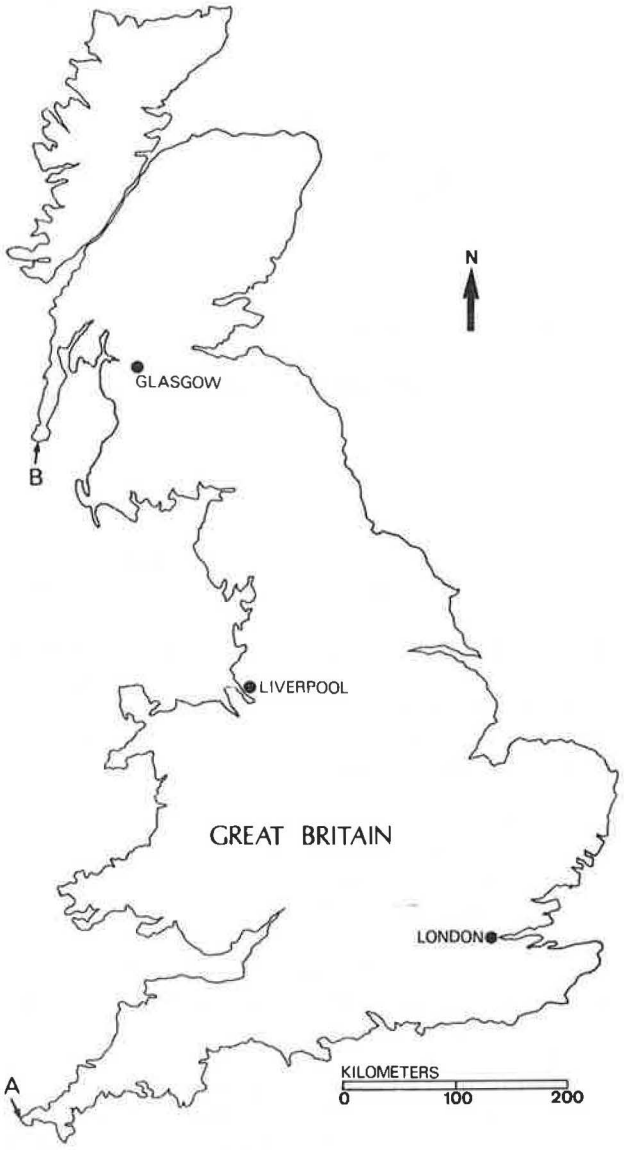

FIGURE 1 Outline of the coast of Great Britain. Two arbitrarily located points, *A* and *B*, are shown.

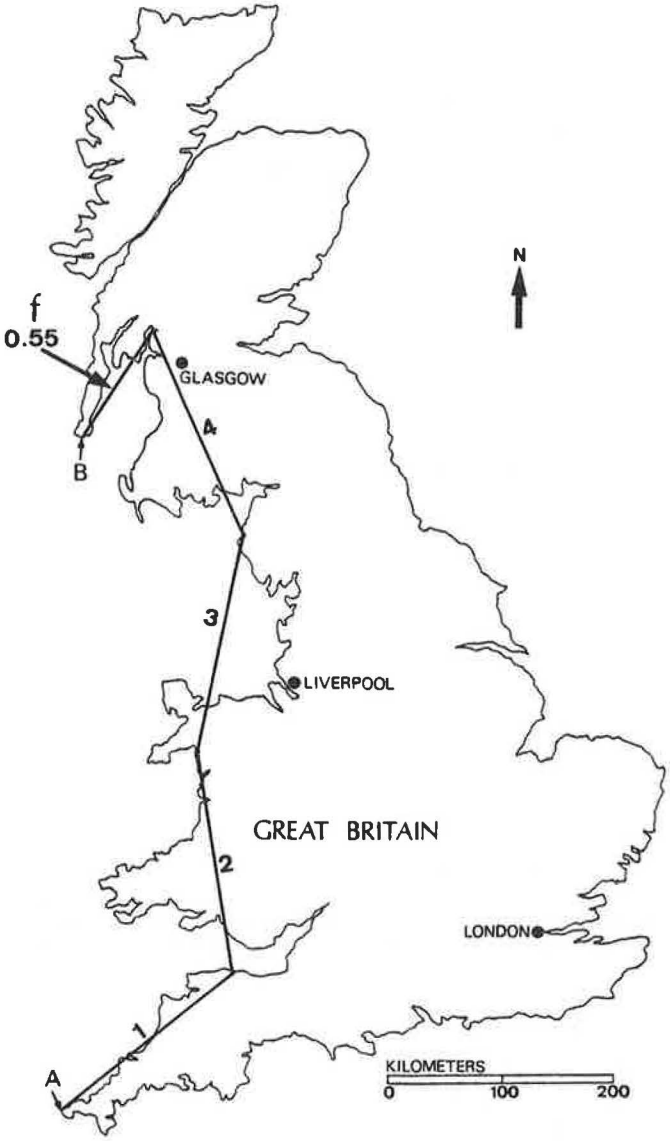

FIGURE 2 Attempt to measure the length between points *A* and *B* by using a 200-km ruler.

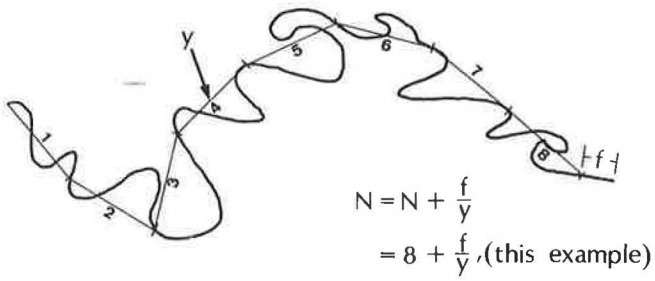

FIGURE 3 Demonstration of the concept of the remainder, *f*, left over when measuring the length by using a fixed-ruler length.

B can be calculated as

$$L = Ny + f \tag{1}$$

where y is the ruler length and N is the number of rulers placed end to end between the two points. Expressed another way,

$$L = \left[N + (f/y)\right]y \tag{2}$$

If a shorter ruler were used to repeat the measurement of length between A and B, the total length measured with the shorter ruler would exceed that measured with the longer one. The shorter ruler would sample bays and inlets that were bridged with the longer ruler. Thus, the scale of the ruler is important.

The relationship between total length and ruler length can be expressed as

$$L = \left[N + (f/y)\right]y^D \tag{3}$$

where D is the fractal dimension (*10*). This parameter is also known as the Hausdorff-Besicovitch dimension as defined by Equation 3. It is also referred to as the divider, or compass, method fractal dimension, to acknowledge its calculation procedure.

For a straight line, D has a value of 1. The topological dimension of a straight line is also unity. Therefore, the topological and fractal dimensions are equal. A fractal line, however, is where the fractal dimension is greater than unity.

Equation 3 can be rewritten to become

$$Ly^{-D} = N + f/y \tag{4}$$

Normalizing Equation 4 so that $L = 1$,

$$y^{-D} = N + f/y \tag{5}$$

Taking the log of Equation 5 yields

$$-D \log(y) = \log (N + f/y) \tag{6}$$

The value of D may be obtained as the negative slope of the plot of log $(N + f/y)$ versus log (y) for several different ruler lengths y (see Figure 4). Even where L of Equation 3 is not equal to 1, its value would not affect the slope of the plot.

In the example of the British coastline, suppose that three different rulers were used to measure the length between points A and B in Figure 1. Those rulers, along with the resultant $N + f/y$ values, are presented in Table 1. Figure 4 is the log-log plot of those results indicating that the slope is -1.3 and, thus, D is 1.3. Therefore, the western coast of Great Britain is a fractal with a fractal dimension of 1.3.

The coastal segment is an example of a deterministic fractal in that the fractal dimension is calculated deterministically. The western coast of Great Britain is also a self-similar fractal, where appearance (bays, spits, etc.) is similar regardless of the scale at which the coast is examined.

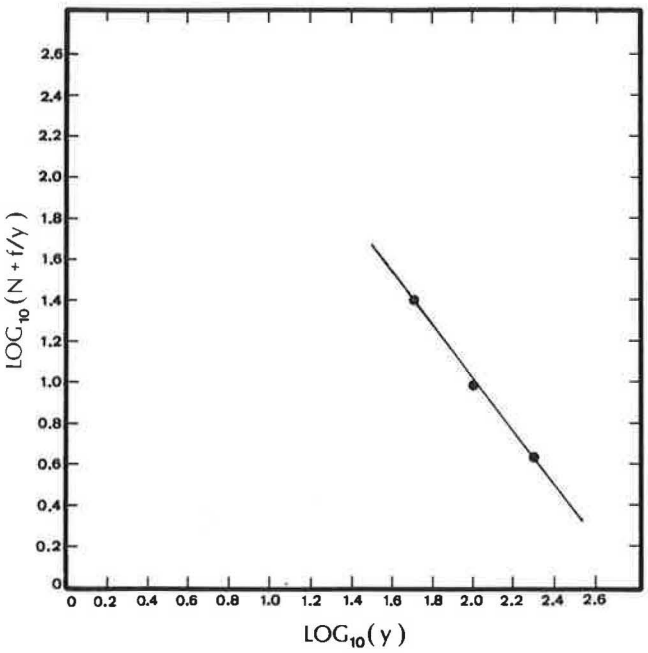

FIGURE 4 Log-log plot of results in Table 1. Slope of plot is −1.3. Thus, fractal dimension is 1.3.

TABLE 1 ATTEMPTS TO MEASURE LENGTH *A* AND *B* (FIGURE 1) BY USING THREE DIFFERENT RULERS

y	N + f/y	L: (N + f/y)y
200 km	4.55	910 km
100 km	10.75	1075 km
50 km	28.25	1412.5 km

Note: y values, in km, refer to the scale shown in Figure 1.

Fractal Characterization of Aggregate

Peleg and Normand (*11*) apply the concept of the fractal dimension to the characterization of instant coffee particles. A fractal dimension is calculated for the silhouette of each particle following the procedure presented in Figure 5. The objective is simply the characterization of particle irregularity that has relevancy for the dissolution of the particle. The current study seeks to characterize aggregate shape by using fractal dimension. Because aggregates are particles similar in shape and profile to instant coffee particles, the Peleg and Normand study is a model for the application of fractals to the characterization of aggregate.

Four example aggregates are presented in Figures 6–9. Those aggregates were photographed against contrasting backgrounds to obtain silhouettes. Dividers opened to different ruler sizes and walked around the perimeter of each silhouette yielded the results indicated in Table 2. This procedure follows Figure 5. It is noted in Table 2 that flat and elongated pieces have the lowest fractal dimension (i.e., the fractal dimension is 1.0). In contrast, water-rounded limestone and crushed pieces have greater fractal dimensions.

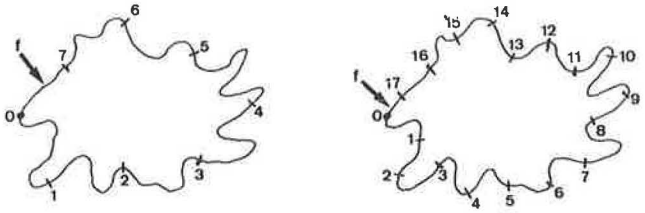

FIGURE 5 Richardson profiles. Two profiles show circumference measured with two different ruler lengths y [from Peleg and Normand (*11*)].

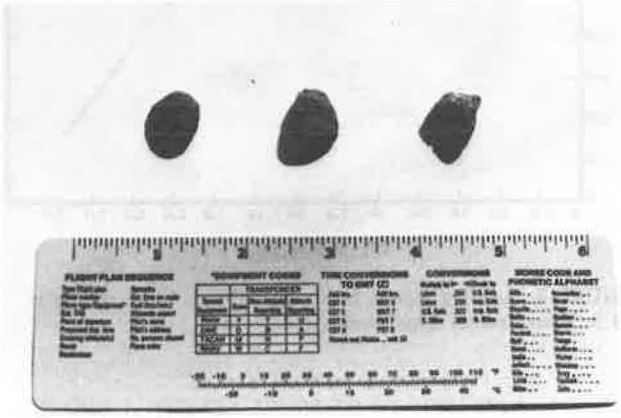

FIGURE 6 Rounded aggregate pieces.

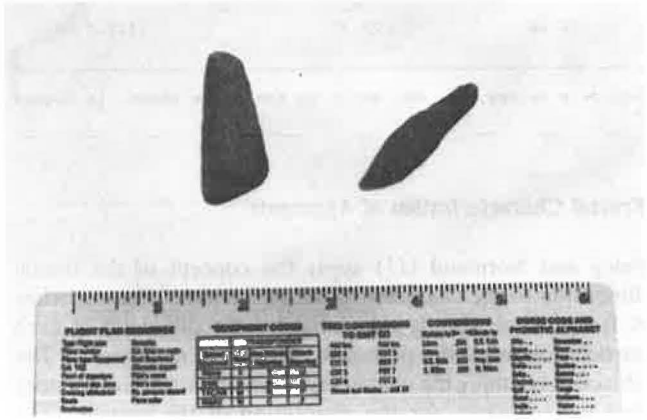

FIGURE 7 Flat and elongated aggregate pieces.

Using photographs of silhouettes poses a problem. The silhouette of a flat, circular object is identical to that of a marble. Each silhouette will yield a fractal dimension of 1.0. On edge, the flat, circular object is rectangular (which may or may not yield a fractal dimension of 1.0). Therefore, it is perhaps desirable to photograph aggregate pieces from several perspectives to examine the fractal dimension for the entire piece.

The fractal dimension of each aggregate is determined in Table 2 by using only three ruler lengths y. This small sample size was chosen because dividers were used to walk the perim-

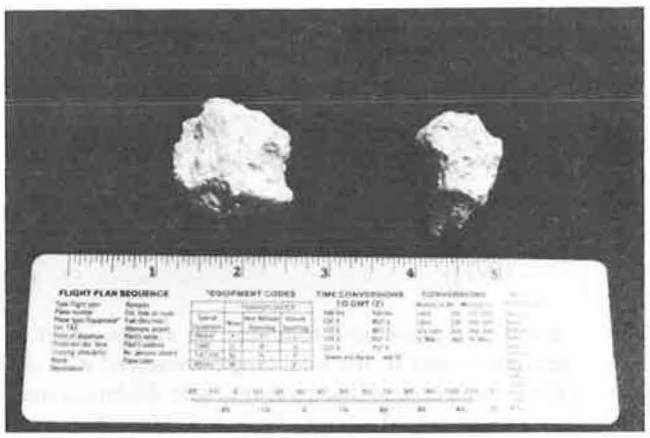

FIGURE 8 Crushed aggregate pieces.

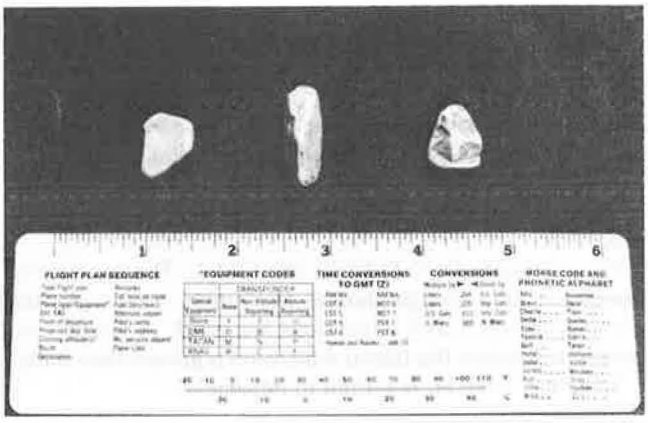

FIGURE 9 Water-rounded limestone pieces.

eter of each silhouette (Figures 6–9). The fractal dimension will vary somewhat for such a small sample size, but, provided ruler lengths are selected greater than the minimum resolution of the photograph, this variability will be small.

Application of the fractal technique in the manner proposed here requires the use of a camera. This is a practical method, nevertheless. Photographs are simply obtained of aggregate silhouettes (by photographing an aggregate piece against a contrasting background). Dividers are then used to measure the circumference of the silhouette. Finally, a fractal dimension is calculated on the basis of the results described previously. This is the total number of steps involved in this method.

To demonstrate further the usefulness of the fractal dimension for aggregate characterization, two photographs are chosen from Krynine and Judd [(*12*), Figures 8.16, 8.17, pp. 323–324]. Those figures contrast rounded aggregate (Figure 8.16) with harsh (crushed, angular) aggregate (Figure 8.17). Each figure is a photograph of nine samples. Figures 10 and 11 here indicate outlines for those pieces of aggregate.

Those figures also show the fractal dimension calculated for the outline of each sample. Table 3 presents the summary of measurements used to calibrate each fractal dimension. The mean fractal dimension for the nine samples in Figure

TABLE 2 FRACTAL DIMENSION FOR EXAMPLE AGGREGATES

y in.	$N + f/y$
Rounded Pieces (Figure 6)	
½	4.45
¼	9.00
⅛	18.00
$D = 1.017$	
Flat and Elongated Pieces (Figure 7)	
½	7.8
¼	16.0
⅛	30.0
$D = 0.983$	
Crushed Aggregate (Figure 8)	
½	8.7
¼	17.4
⅛	39.0
$D = 1.083$	
Water-Rounded Limestone (Figure 9)	
½	3.6
¼	7.8
⅛	16.0
$D = 1.067$	

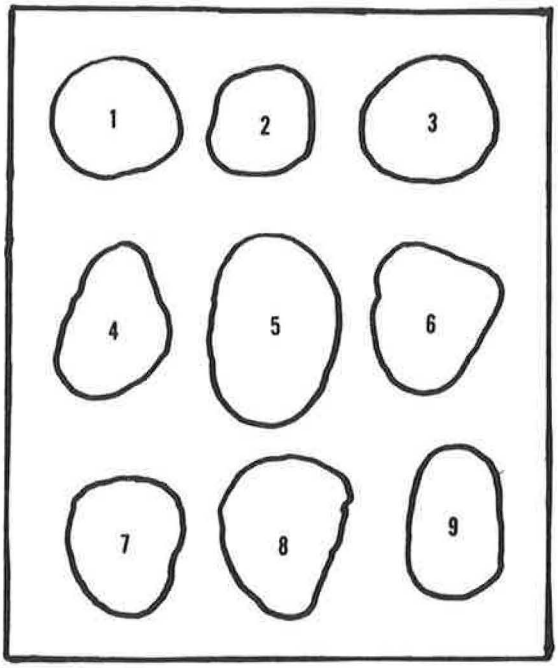

FIGURE 10 Traces (outlines) of nine samples of rounded aggregate [from Krynine and Judd (*12*) Figure 8.16, p. 323]. Numbers inside the outlines are sample numbers used in Table 3.

10 is 1.056, and the mean fractal dimension for the samples in Figure 11 is 1.077.

It may be useful to determine whether the fractal dimensions for Figures 10 and 11 are significantly different. If the null hypothesis is posed that 1.056 is equal to 1.077 (i.e., that the mean fractal dimensions are equal), and a t-statistic is

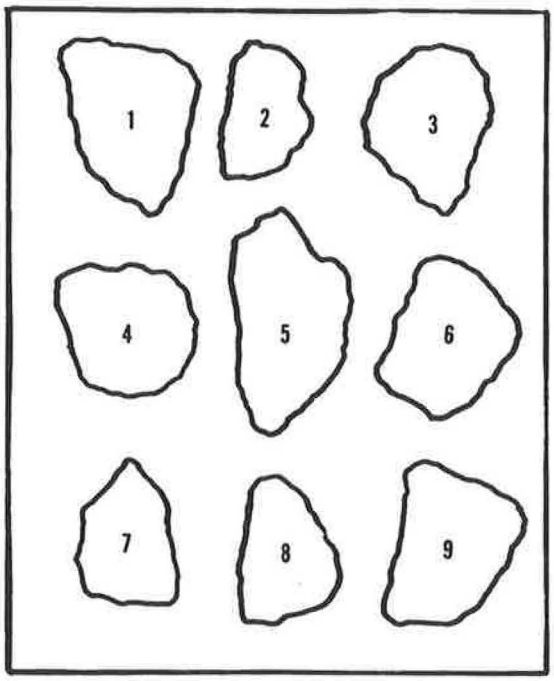

FIGURE 11 Traces (outlines) of nine samples of aggregate displaying various degrees of angularity [from Krynine and Judd (*12*), Figure 8.17, p. 324]. Numbers inside the outlines are sample numbers used in Table 3.

used to test this hypothesis, the t-statistic for the two samples is -1.70. If further the alternative hypothesis is posed that 1.056 is less than 1.077, then by using table values for the t-statistic for a one-tailed test, the null hypothesis is not rejected at the 5 percent significance level (the table t value is -1.75) but the null hypothesis is rejected and the alternative hypothesis is accepted at the 10 percent significance level (the table t value is -1.34). Further, by using a nonparametric Wilcoxon rank sum test, the sum of ranks for fractal dimensions in Figure 10 is 68, and for Figure 11 the rank sum is 103. For a one-tailed test at the 5 percent significance level, the table values for the lower sum and upper sum are 66 and 105, respectively. The sum for Figure 10 is 68, just inside this interval, so the null hypothesis that both samples are equal is not quite rejected. The t-test and the Wilcoxon rank sum test show that the difference between the fractal dimensions for the two aggregate groups, rounded and harsh, is almost significant for the 5 percent level and certainly significant at the 10 percent level. It does appear that the fractal dimension characterizes aggregate shape: the more angular (harsh) the aggregate is, the greater is its fractal dimension.

DETAILED APPLICATION OF FRACTAL DIMENSION TO CHARACTERIZATION OF AGGREGATE

A broader experiment is now complete where the concept of fractal dimension was applied to 30 different samples of aggregate. A fractal dimension for each aggregate sample is calculated as follows:

TABLE 3 FRACTAL DIMENSION RESULTS FOR FIGURES 10 AND 11

Sample	y(cm)	N + f/y	Sample	y(cm)	N + f/y
1	1.0	6.30	1	1.0	7.70
	0.7	9.29		0.7	11.43
	0.3	21.30		0.3	29.00
	D = 1.006			D = 1.101	
2	1.0	5.20	2	1.0	5.70
	0.7	8.00		0.7	8.79
	0.3	18.67		0.3	22.00
	D = 1.050			D = 1.115	
3	1.0	6.60	3	1.0	7.40
	0.7	9.71		0.7	10.64
	0.3	22.50		0.3	26.50
	D = 1.014			D = 1.063	
4	1.0	6.70	4	1.0	6.90
	0.7	9.70		0.7	10.29
	0.3	24.00		0.3	25.50
	D = 1.061			D = 1.083	
5	1.0	8.3	5	1.0	8.60
	0.7	12.20		0.7	13.00
	0.3	29.80		0.3	31.67
	D = 1.060			D = 1.077	
6	1.0	6.90	6	1.0	7.40
	0.7	10.29		0.7	10.86
	0.3	25.30		0.3	26.00
	D = 1.076			D = 1.041	
7	1.0	6.40	7	1.0	6.15
	0.7	9.57		0.7	9.36
	0.3	23.70		0.3	22.67
	D = 1.084			D = 1.076	
8	1.0	7.10	8	1.0	6.20
	0.7	10.64		0.7	9.57
	0.3	26.00		0.3	23.30
	D = 1.074			D = 1.091	
9	1.0	6.40	9	1.0	7.80
	0.7	9.64		0.7	11.50
	0.3	23.70		0.3	27.70
	D = 1.083			D = 1.050	
	Mean D = 1.056			Mean D = 1.077	
	Variance = 0.00082			Variance = 0.00056	

1. The aggregate sample is photographed along with a ruler scale against a contrasting background (such as in Figures 6–9).
2. Calipers (dividers), set at different ruler lengths, are walked around the perimeter of the sample silhouette. The ruler length is determined from the scale shown in the photograph.
3. A fractal dimension is calculated on the basis of the results from the second step (as is done in Tables 2 and 3). The three steps follow what is illustrated in Figure 5.

Results for those 30 samples are presented in Table 4. A summary of the results for this table is as follows:

Sample	*No. of Samples*	*Avg Fractal Dimension*
Rounded aggregate	10 (5, 6, 7, 9, 12, 13, 16, 17, 18, 25)	1.052
Rectangular prof	12 (2, 8, 10, 11, 14, 15, 20, 21, 26, 27, 29, 30)	1.120
Square profiles	2 (3, 4)	1.068
Triangular prof	5 (1, 22, 23, 24, 28)	1.110
Elongated pieces	1 (19)	1.00

This summary shows that the fractal dimension is a useful technique for characterizing aggregate shape. Angular pieces, such as rectangular, square, or triangular pieces, on average, have larger fractal dimensions than do rounded pieces.

CONCLUSIONS

Existing methods for characterizing aggregate shape determine the deviation of a particle from an ideal sphere. A fractal is any line, surface, or object that differs from a topological ideal, such as a sphere. The fractal dimension contributes to existing methods for concrete aggregate characterization. The greater the fractal dimension of a concrete aggregate silhouette, the more different this particle is from a topological ideal, which may be a square, rectangle, triangle, or sphere. Hence, the fractal dimension is sensitive to concrete aggregate shape deviation from any ideal shape and not just a sphere. In this manner, the fractal dimension contributes to existing shape characterization methods.

This fractal technique is not proposed as a replacement for existing techniques. The Rittenhouse ratio describes roundness: the closer the ratio is to 1, the more like a sphere the particle is. The Krumbein ratio describes angularity. A square particle, for example, has a low ratio because the four angular corners have minute radii.

A square, though, is a good object to use in describing the difference between the fractal dimension and the Krumbein ratio. A perfect square has a fractal dimension of 1 (i.e., its perimeter has this fractal dimension) but has a Krumbein ratio less than 0.1. Suppose that on each of the four sides of the

TABLE 4 FRACTAL DIMENSION RESULTS FOR 30 AGGREGATE SAMPLES

Sample ID #	Fractal Dimension	Description
1	1.03	triangular profile
2	1.07	rectang profile
3	1.06	square profile
4	1.075	square profile
5	1.00	rounded profile
6	1.00	round elong prof
7	1.00	rounded profile
8	1.00	rectang profile
9	1.10	round profile; one broken edge
10	1.14	rounded rectangle
11	1.17	rectang profile
12	1.00	round elong prof
13	1.08	rounded profile
14	1.15	rectang profile
15	1.00	rectang profile
16	1.175	round elong prof
17	1.155	rounded profile
18	1.00	rounded profile
19	1.00	elong rectangle
20	1.275	rectang profile
21	1.15	rectang profile
22	1.22	triangle with one rounded edge
23	1.00	triangular prof
24	1.07	triangular prof
25	1.00	rounded profile
26	1.07	rectang profile
27	1.09	rectang profile
28	1.22	triangular prof
29	1.24	rectang profile
30	1.11	rectang profile

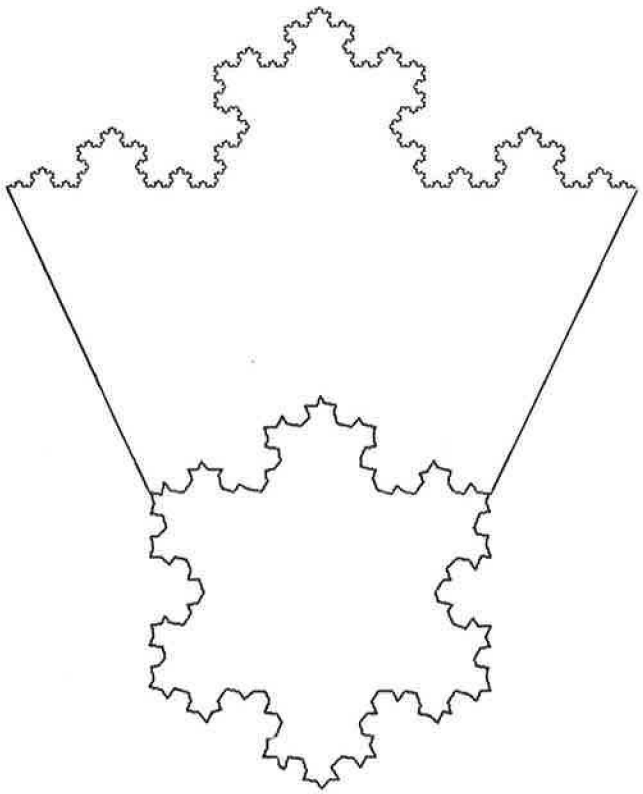

FIGURE 12 Artificial Koch curve constructed by using different sizes of isoceles triangles. The partial curve on the top represents an enlarged section. The Krumbein ratio would describe the global shape of this object. The fractal dimension describes not only the shape but also the finer detail, such as is shown in the top, more detailed portion of the curve. This finer detail relates to particle roughness.

square a triangle is affixed where the apex points outward. Moreover, let the apex of the triangle have the same angularity as each of the four original corners of the square. This object will have the same or similar Krumbein ratio, but the fractal dimension will increase (i.e., it will be greater than 1.0).

The fractal dimension, therefore, is sensitive to the number of asperities present on the circumference of a particle. Likewise, it can account for the presence/distribution of particle features as they grow smaller in size (i.e., transitioning from shape size features to surface roughness features). By contrast, the Krumbein and Rittenhouse ratios are established only when the particle(s) are viewed as a whole and therefore are limited to the "shape size" features. This is best seen in Figure 12, a figure of an artificial Koch curve constructed by using multiple scales of triangles. Its fractal dimension is 1.26 (*10*). The Krumbein ratio for Figure 12, though, would be low because of the high angularity of this object.

In summary, where the Rittenhouse ratio described form, the Krumbein ratio describes angularity and the fractal dimension describes the presence or absence of multiple scales of asperities on the circumference of a particle. This relates to the roughness and texture of the particle surface.

REFERENCES

1. E. R. Hargett. Effects of Size, Surface Texture, and Slope of Aggregate Particles on the Properties of Bituminous Mixtures. *Special Report 109*, HRB, National Research Council, Washington, D.C., 1970, p. 25.
2. F. J. Benson. Effects of Aggregate Size, Shape, and Surface Texture on the Properties of Bituminous Mixtures: A Literature Survey. *Special Report 109*, HRB, National Research Council, Washington, D.C., 1970, pp. 12–21.
3. M. Livneh and J. Greenstein. Influence of Aggregate Shape on Engineering Properties of Asphaltic Paving Mixtures. In *Highway Research Record 404*, HRB, National Research Council, Washington, D.C., 1972, pp. 42–56.
4. C. L. Monismith. Influence of Shape, Size, and Surface Texture on the Stiffness and Fatigue Response of Asphalt Mixtures. *Special Report 109*, HRB, Washington, D.C., 1970, pp. 4–11.
5. J. M. Griffith and B. F. Kallas. Influence of Fine Aggregates on Asphaltic Concrete Paving Mixtures. *HRB Proc.*, Vol. 37, 1958, pp. 219–255.
6. W. C. Krumbein. Measurement and Geological Significance of Shape and Roundness of Sedimentary Particles. *Journal of Sedimentary Petrology*, Vol. 13, No. 2, Aug. 1941, pp. 64–72.
7. G. Rittenhouse. A Visual Method of Estimating Two Dimensional Sphericity. *Journal of Sedimentary Petrology*, Vol. 13, No. 2, Aug. 1941, pp. 79–81.
8. B. Mather. *Shape, Surface Texture, and Coatings of Aggregates*. Misc. Paper No. 6-710. U.S. Army Corps of Engineers, Waterways Experiment Station, Vicksburg, Miss., Feb. 1965.
9. B. B. Mandelbrot. How Long Is the Coast of Great Britain? Statistical Self-Similarity and Fraction Dimension. *Science*, Vol. 155, 1967, pp. 636–638.
10. B. B. Mandelbrot. *The Fractal Geometry of Nature*. W. H. Freeman, San Francisco, Calif., 1982.
11. M. Peleg and M. D. Normand. Characterization of the Ruggedness of Instant Coffee Particle Shape by Natural Fractals. *Journal of Food Science*, Vol. 50, 1985.
12. D. P. Krynine and W. R. Judd. *Principles of Engineering Geology and Geotechnics*, McGraw-Hill, New York, 1957.

Publication of this paper sponsored by Committee on Mineral Aggregates.

Modifications to Resilient Modulus Testing Procedure and Use of Synthetic Samples for Equipment Calibration

GERMAN CLAROS, W. R. HUDSON, AND KENNETH H. STOKOE II

Modifications to the resilient modulus testing procedure (AASHTO T-274) and the use of synthetic samples for equipment evaluation and calibration are described. The modifications to the AASHTO T-274 were carried out to produce a testing protocol for use in the testing program of the Strategic Highway Research Program. The modifications were aimed at producing a more repeatable and less complicated test procedure. The main changes are the use of external linear variable differential transformers (LVDTs) for deformation measurements of all soil types and complete modification of the loading sequence and eliminating low deviator stresses, which produce high variability and high deviator stresses, which produce sample failure. The use of synthetic samples (polyurethane) with well-known properties to calibrate and evaluate resilient modulus equipment is also described. Synthetic samples could be an excellent choice in the development of a standard procedure for calibration of resilient modulus equipment.

The resilient modulus test for soils was orginally developed by Seed et al. (*1*) and was initially formulated for highway applications. Later, the test was applied to earthquake research.

The resilient modulus is a measure of the "elastic" behavior (load-unload response) of the soil layer that may be in the nonlinear range. The resilient modulus can be used directly for the design of flexible pavements but must be converted to a modulus of subgrade reaction (k-value) for the design of rigid or composite pavements.

Traditionally, this test measures the elastic properties of the unbound soils and requires specialized, and expensive, equipment. The test is also fairly difficult to perform. While the test is considered the state of the art, it is not widely accepted for routine application by state transportation departments. It was not until 1986 that the resilient modulus was formally accepted and included in the AASHTO *Guide for Design of Pavement Structures* (1986).

The resilient modulus was selected to replace the soil support value used in previous editions of the AASHTO design guide for the following reasons:

1. It indicates a basic material property, which can be used in mechanistic analysis of multilayered systems for predicting pavement distresses such as cracking, roughness, rutting, and faulting.
2. It has been internationally recognized as a method for characterizing materials for use in pavement design and evaluation.
3. Techniques are available for estimating the resilient modulus of various in-place materials from nondestructive tests.

Center for Transportation Research, University of Texas at Austin, Austin, Tex. 78712.

The resilient modulus of cohesive subgrade materials or unbound base materials is determined in a repeated load triaxial compression test, such as the one in Figure 1. The load is applied with any device capable of providing a variable load of fixed cycle and load duration. The test is conducted by placing a specimen in the triaxial cell. The specimen is subject to all-around confining pressure (σ_3), and a repeated axial stress, $\sigma_d(\sigma_d = \sigma_1 - \sigma_3)$, is applied to the sample. During the test the recoverable axial strain ε_a is determined by measuring the recoverable deformation across a known gauge length or the total sample height. The resilient modulus is calculated by using the following expression:

$$M_R = \frac{\sigma_d}{\varepsilon_r}$$

where σ_d is cyclic deviation stress and ε_r is resilient strain.

The test procedure for estimating the resilient modulus of a particular material depends on the material type. Materials with relatively low stiffnesses, such as natural soils, unbound granular layers, and even slightly stabilized layers, should be tested by using the resilient modulus test method (AASHTO T-274). Alternatively, the stiff materials, such as stabilized bases and asphalt concrete, may be tested by using the repeated-load indirect tensile test (ASTM D4123).

The focus of this paper is the analysis of changes made to the testing procedure (AASHTO T-274) for determining the resilient modulus (M_R) of soils and unbound granular layers for use in the Strategic Highway Research Program (SHRP). The use of synthetic samples with known moduli to test and calibrate M_R equipment is also included. A calibration procedure for M_R equipment may be very important in SHRP, because several laboratories perform the resilient modulus testing. Uniformity of equipment and testing techniques is essential to obtain comparable data.

CHANGES IN THE AASHTO T-274 TEST PROCEDURE

The resilient modulus of soils and unbound granular materials is commonly measured by using the AASHTO T-274 procedure (*2*), although, unfortunately, some researchers have

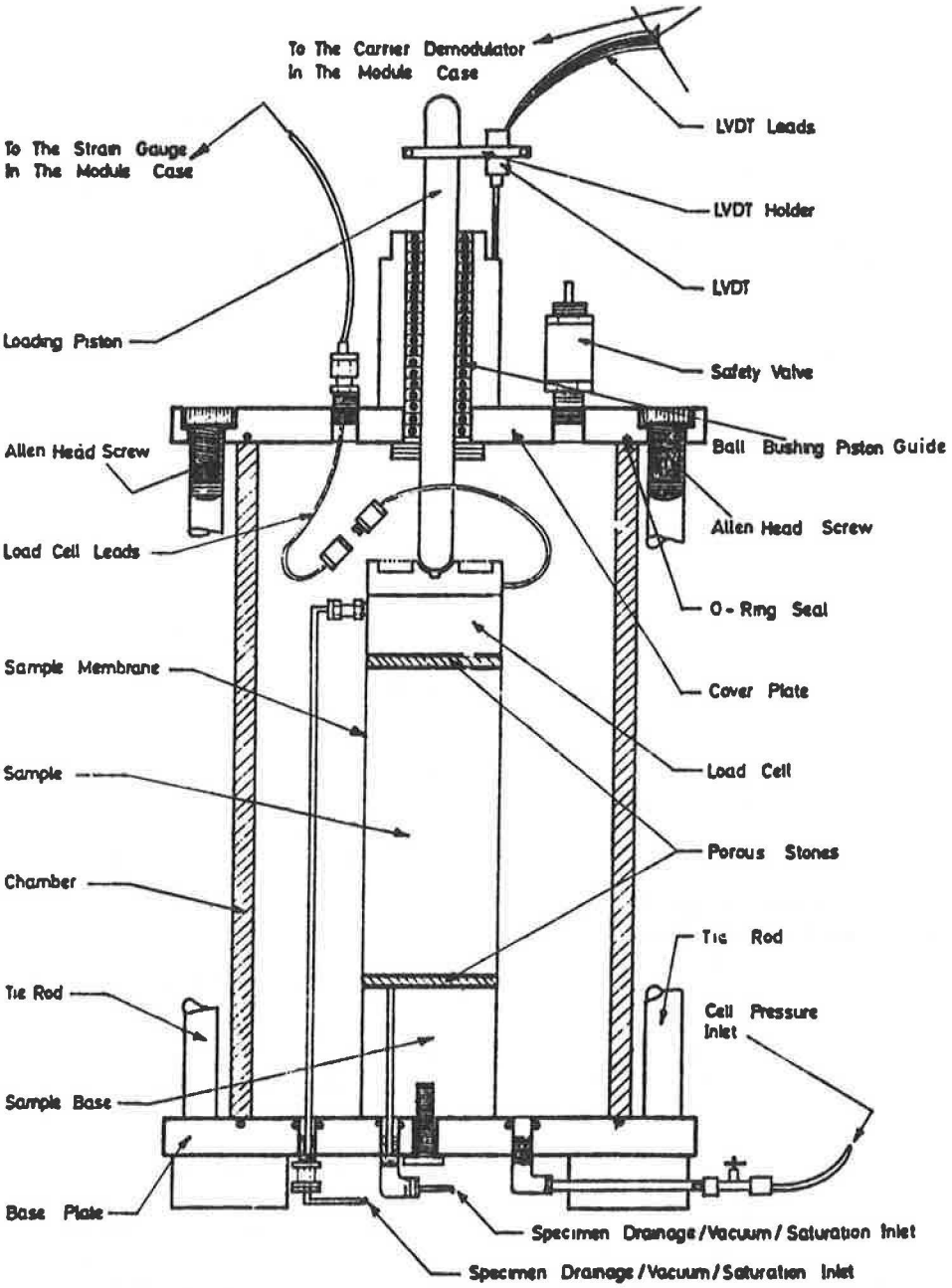

FIGURE 1 Triaxial test cell with test specimen in place.

used variations of this test procedure, which has led to nonuniform results. Even if this test procedure were to be followed, different results could occur, given the very open nature of this test, which would allow the researcher to choose from various options in the procedure. Some experts in this area have pointed out that the T-274 procedure is not a "mature" test. Few state highway agencies or commercial testing laboratories routinely conduct resilient modulus testing. Therefore, most of the available data on the resilient modulus of soils and granular materials have been developed from research-oriented activities. Unfortunately, there are no widely used and accepted test procedures, and many agencies have expressed considerable dissatisfaction with the AASHTO T-274 procedure.

To fulfill the testing needs of SHRP, experts were assembled in Austin, Texas in early April 1989. The AASHTO T-274 procedure and the draft version of the ASTM (Committee D18.09) procedures were used as the base documents for SHRP protocol P-46, which was the most important modification to AASHTO T-274 made by the Austin group.

Equipment

The triaxial pressure chamber for AASHTO T-274 has two different layouts that allow the measurement of the resilient deformation using internal or externally mounted linear variable differential transformers (LVDTs). The use of internal

LVDTs on stiff samples increases the variability of results because it is very difficult to secure the clamps on the specimen to ensure that there is no movement. The sample also has an outer membrane, which can slip, inducing small clamp movements. A movement of 0.05×10^{-3} in. in the clamps can change by 50 percent the resilient modulus of a sample with a 40,000 psi modulus when tested under a 2-psi deviator stress. On the other hand, fine plastic soils have much permanent deformation, which make the internal LVDTs slip out of range, forcing the test to be stopped, the triaxial chamber to be opened, and the LVDTs to be readjusted. The use of voltage suppressor knobs is not recommended because the core position in the LVDTs is physically out of the range of calibration. On the basis of this fact, the SHRP protocol uses an externally mounted LVDT, which measures the resilient deformation of the total sample height for all soil types and granular unbounded materials. The layout of the triaxial chamber for the SHRP protocol, presented in Figure 1, includes an internal load cell to eliminate the piston friction.

The external loading source for the P-46 protocol is a closed-loop electrohydraulic system. Other systems, such as open-loop air or static weights, are not acceptable. The load duration is 0.1 sec, and the cycle duration is 1 sec. This short load duration can not be achieved with an open-loop air system or static weights. The recently developed closed-loop air system has the capability to apply a 0.1-sec load duration if the resilient deformation is not very large. This type of system can be an alternative to the more complex electrohydraulic systems.

A haversine stress pulse was chosen for protocol P-46 because it better represents the shape of a truck load on pavement (*3*) and is also similar to the load pulse applied by a nondestructive testing device, such as the Falling Weight Deflectometer. The triaxial chamber fluid for the protocol is air, and the chamber pressure should be monitored with pressure gauges, manometers, or pressure transducers with an accuracy of 0.1 psi. The load cell and LVDTs to be used in this test are specified and depend on the sample diameter. This may ensure uniform accuracy of the load and deformation measuring devices. Recommended load cells and LVDTs are included in Table 1. The use of suitable recording devices, which allow simultaneous recording of axial load and deformation, is recommended. The signal for the transducer should be free of noise. If filters are used, they should have a frequency that cannot attenuate the transducer signal.

TABLE 1 RECOMMENDED LOAD CELLS AND LVDTS FOR M_r TESTING

Sample Diameter (inches)	Load Cell Capacity (lb)	LVDT Range (inches)
2.8	100	±0.05
4.0	600	±0.10
6.0	1,400	±0.25

Preparation of Test Specimens

Specimen length should not be less than two times the diameter. The miminum specimen diameter is 2.8 in., or five times the nominal size. The compaction of fine plastic soils uses the AASHTO T-99 method. A partial face hammer (with 30 percent of the specimen area) is recommended. The number of blows per layer should be adjusted to reproduce the field dry density. Granular soils are compacted by using AASHTO T-180. Manually operated vibrators (electric or air-driven) are an option for this type of soil. For fine nonplastic soils, a full face plate with a vibrating system can be used to obtain the desired dry density.

Testing Procedure

The load sequence during the test procedure depends on the type of soil to be tested. Two criteria were used for soil Types 1 and 2:

1. Soil Type 1 is all unbound granular base and subbase materials. Unbound subgrade soil has the following criteria: (a) less than 70 percent passing the No. 10 sieve and (b) a maximum of 20 percent passing the No. 200 sieve.
2. Soil Type 2 is all unbound subgrade soil not meeting criterion 1.

Because it is important to test soils at the levels of stress to which they will be subjected in a pavement structure, these soil definitions are different from those in AASHTO T-274. Subgrade soils, whether granular or fine cohesive, will be subjected to much lower stresses than the subbase and base materials. Therefore, the soils should be tested at lower stress levels.

The loading sequence for soil Type 1 is presented in Table 2. The σ_1/σ_3 ratio has a maximum value of 3 to prevent the

TABLE 2 SOIL TYPE 1 TESTING SEQUENCE

Sequence Number	Confining Pressure σ_3 (psi)	Deviator Stress σ_d (psi)	Number of Load Applications
1	3	3	100
2	3	6	100
3	3	9	100
4	5	5	100
5	5	10	100
6	5	15	100
7	10	10	100
8	10	20	100
9	10	30	100
10	15	10	100
11	15	15	100
12	15	30	100
13	20	15	100
14	20	20	100
15	20	40	100

sample from failing. This condition was never followed in AASHTO T-274, and samples failed many times before the test was completed. The number of load applications after conditioning was reduced to 100 repetitions per each sequence. There is no change in the size of the deformation after the conditioning, and it is not necessary to wait for 200 load repetitions before recording deformations as is recommended in AASHTO T-274.

The loading sequence for soil Type 2 (subgrade soils) is presented in Table 3. It can be seen that the test at zero confining pressure ($\sigma_3 = 0$) was eliminated because there is no realistic state of stress for a subgrade in a pavement structure. The deviator stresses applied to the sample are 2, 4, 6, 8, and 10 psi. The deviator stress of 1 psi was eliminated because experience has shown that the major dispersion of results is at this stress level. The high dispersion is the product of the small resilient deformation, which cannot be measured accurately and sometimes is not bigger than the noise of the signal.

The number of load repetitions was reduced to 100 for each load sequence, as for soil Type 1. This also allows the testing to be shortened. A failure criterion was included in the test to eliminate samples with large permanent deformations. A specimen is considered failed if the permanent deformation (vertical strain) exceeds 10 percent.

The deviator stress and the resilient deformation are recorded for the calculation of the resilient modulus during the last five loading cycles for soil Types 1 and 2. The forms in Figures 2 and 3 are recommended for this purpose.

Calculations of the Test

Calculations are performed by using the tabular arrangement forms in Figures 2 and 3. The mean and standard deviation of the applied load and the recoverable deformation are calculated. The mean values are used to compute the deviator stress and the resilient strain.

TABLE 3 SOIL TYPE 2 TESTING SEQUENCE

Sequence Number	Confining Pressure σ_3 (psi)	Deviator Stress σ_d (psi)	Number of Load Applications
1	6	2	100
2	6	4	100
3	6	6	100
4	6	8	100
5	6	10	100
6	4	2	100
7	4	4	100
8	4	6	100
9	4	8	100
10	4	10	100
11	2	2	100
12	2	4	100
13	2	6	100
14	2	8	100
15	2	10	100

Test Report

A report of the resilient modulus test should include the data forms (Figures 2 and 3) and a simple linear regression predicting M_R as a function of bulk stresses ($\theta = \sigma_1 + 2\sigma_3$). For soil Type 1, the regression equation has the following form:

$$M_R = K_2 \theta^{n2}$$

or

$$\log M_R = \log K_2 + n_2 \log \theta$$

For soil Type 2, the regression equation of M_R should be expressed as a function of deviator stress ($\sigma_d = \sigma_1 - \sigma_3$) in the following form:

$$M_R = K_1 \sigma_d^{n2}$$

or

$$\log M_R = \log K_1 + n_1 \log \sigma_d$$

The coefficient of determination (R^2) is reported, and this value can be used to judge the quality of the test. Outlier points could be eliminated by using a statistical test for outliers.

Limitation of the New Testing Procedure

The modifications made to AASHTO T-274 to produce protocol P-46 make this test more repeatable, but there are some problems still to be resolved. A summary of those problems follows.

1. The measurement of the resilient deformation, using the external LVDT, assumes that the strain distribution in the sample is uniform, which is not correct as some researchers have found (*4*). Unfortunately, the measurements of strains in the middle portion of the sample are not reliable owing to the slight movement of the clamps, as was previously mentioned. The only possibility is to use some type of noncontact transducer to make those measurements. Researchers at The University of Texas at Austin are experimenting with an electro-optical biaxial tracking system that will allow the measurement of deformation in the sample without contact. Because the strain distribution depends on the sample stiffness, a series of correction factors can be obtained by using an optical-tracking device to correct the resilient modulus obtained with external LVDTs. This correction is also dependent on sample stiffness.
2. The test procedure has two loading sequences. The criterion for use is the type of soil to be tested. This criterion is incorrect because the most important factor should be the position of the soil in the pavement (subgrade, subbase, or

Soil Sample _____

Location _____

Sample No. _____

Specific Gravity _____

Soil Specimen Measurements:

Diameter
- Top _____
- Middle _____
- Botttom _____
- Average _____

Membrane Thickness _____

Net Diameter _____

Ht Specimen + Cap + Base _____

Ht Cap + Base _____

Initial Length, Lo _____

Inside Diameter of Mold _____

Soil Specimen Weight:

Initial Weight of Container

* Wet Soil gms _____

Final Weight of Container

* Wet Soil gms _____

Weight Wet Soil Used _____

Soil Specimen Volume:

Initial Area, Ao

in2 (cm2) _____

Initial Volume, Ao Lo

in3 (cm3) _____

Wet Density.pcf (kN/m3) _____

Compaction Water Content, Wc % _____

% Saturation _____

Dry Density.pcf (kn/m3) _____

Date _____

Compaction Method _____

Constants

Vertical LVDT _____

Load Cell _____

Water Content After
Resilience Testing % _____

Comments _____

Pressure Chamber	Nominal Deviator Stress (in PSI)	Load Cell Reading	Deviator Load (lb)	Mean Deviator Load (lb)	Standard Deviation of Load (lb)	Applied Deviator Stress (in psi)	Recoverable Deformation LVDT Reading	Recoverable Deformation (inches)	Mean Recoverable Deformation (inches)	Std. Dev. of Recoverable Deformation (inches)	Resilient Strain	MR	Bulk Stress
3	3												
3	6												
3	9												
5	5												
5	10												
5	15												
10	10												
10	20												
10	30												
15	10												
15	15												
15	30												
20	15												
20	20												
20	40												

FIGURE 2 Form for resilient modulus test on soil Type 1.

Soil Sample _____
Location _____
Sample No. _____
Specific Gravity _____
Soil Specimen Measurements:
Diameter Top _____
Middle _____
Botttom _____
Average _____
Membrane Thickness _____
Net Diameter _____
Ht Specimen + Cap + Base _____
Ht Cap + Base _____
Initial Length, Lo _____
Inside Diameter of Mold _____

Soil Specimen Weight:
Initial Weight of Container
* Wet Soil gms _____
Final Weight of Container
* Wet Soil gms _____
Weight Wet Soil Used _____

Soil Specimen Volume:
Initial Area, Ao
in2 (cm2) _____
Initial Volume, Ao Lo
in3 (cm3) _____
Wet Density.pcf (kN/m3) _____
Compaction Water Content, Wc % _____
% Saturation _____
Dry Density.pcf (kn/m3) _____

Date _____
Compaction Method _____

Constants
Vertical LVDT _____
Load Cell _____

Water Content After
Resilience Testing % _____
Comments _____

Pressure Chamber	Nominal Deviator Stress (in PSI)	Load Cell Reading	Deviator Load (lb)	Mean Deviator Load (lb)	Standard Deviation of Load (lb)	Applied Deviator Stress (in psi)	Recoverable Deformation LVDT Reading	Recoverable Deformation (inches)	Mean Recoverable Deformation (inches)	Std. Dev. of Recoverable Deformation (inches)	Resilient Strain	Resilient Modulus MR=
6	2											
6	4											
6	6											
6	8											
6	10											
4	2											
4	4											
4	6											
4	8											
4	10											
2	2											
2	4											
2	6											
2	8											
2	10											

FIGURE 3 Form for resilient modulus test on soil Type 2.

base) and not the type. A more rational approach would be to have loading sequences for testing subgrades, subbases, and bases based on average pavement structures.

3. The stress levels of the loading sequences were reduced to reflect a more realistic state of stresses in pavement layers, but they are still fairly large. Those stresses applied to soils produce a wide range of strains, as is indicated in Figure 4. For example, soil A-2-6 can have strains going from 3×10^{-3} to 3×10^{-2} percent when tested as soil Type 2. The wide variation on the slope of the relationship E versus strain observed in Figure 4 makes the characterization of this soil more imprecise if the secant slope is calculated. If the testing stress levels were reduced to comparable stresses in the pavement structure, then the strain range will be smaller and the characterization will be more accurate. The same analysis is true for soil A-7-5.

4. The linear regression models used to predict the resilient modulus have deviator stress (σ_d) and bulk stresses (θ) as independent variables for soil Types 1 and 2, respectively. Those independent variables are not the best predictors of the resilient modulus. Other variables, such as resilient strain (ε_r) and confining pressure (σ_3), have coefficients with a higher correlation with M_R. As an example, the following regression models were tested for the same set of data (A-2-6 soil):

Model 1:

$$M_R = K_1 \sigma_d^{n1}$$

$$M_R = 65629\ \sigma_d^{-0.552} \qquad R^2 = 0.61$$

Model 2:

$$M_R = K_2 \varepsilon_r^{n2}$$

$$M_R = 882\ \varepsilon_r^{-0.3990} \qquad R^2 = 0.85$$

Model 3:

$$M_R = K_3 \sigma_3^{n3} \varepsilon_r^{n4}$$

$$M_R = 906.6\ \sigma_3^{0.1252}/\varepsilon_r^{0.3756} \qquad R^2 = 0.87$$

Models 2 and 3 give the highest coefficient of correlation (R^2) for the same set of data, and therefore, those independent variables are better predictors of M_R.

CALIBRATION OF RESILIENT MODULUS EQUIPMENT USING SYNTHETIC SAMPLES

If accurate results are desired, the resilient modulus test requires very good calibrations of each one of the transducers and the complete device. Calibrations of the load cell and the LVDTs are standard procedures, but those calibrations do not test the complete equipment. A multilaboratory calibration will be necessary for SHRP if comparable data results are expected. To test the complete M_R equipment and to be able to compare results between laboratories, some kind of standard material is required. Some researchers have used standard sands for this purpose, but the sample preparation could be another factor in the variation between laboratories.

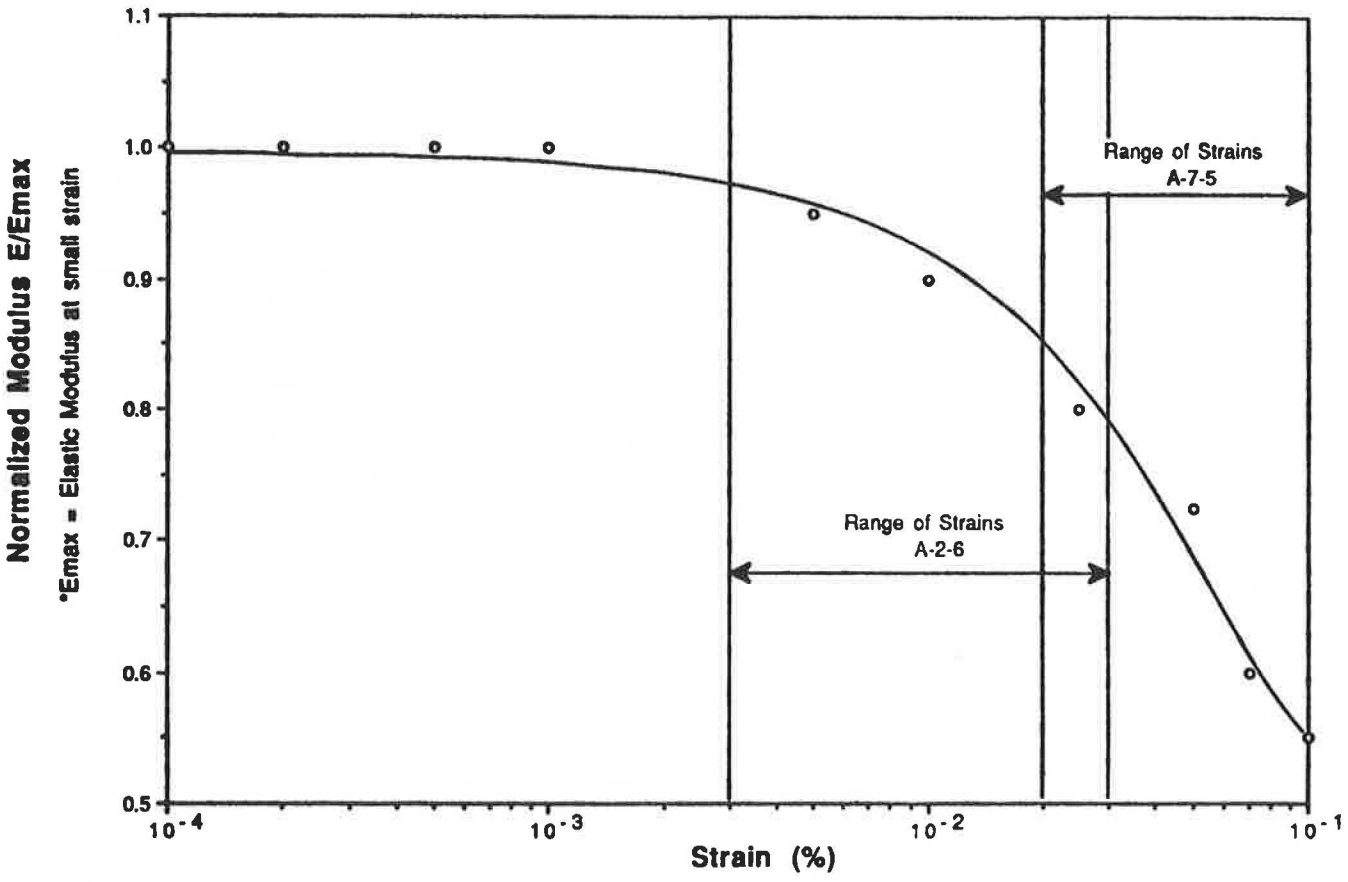

FIGURE 4 Normalized Young's modulus: vertical strain general relationship.

The authors have been developing polyurethane specimens for equipment calibration. The complete characteristics of these sample are presented in a companion paper in this Record. Typical shear-modulus versus shear-strain and shear-modulus versus confining-pressure curves for one specimen are indicated in Figures 5 and 6, respectively.

The use of those specimens for equipment calibration has the following benefits:

1. The properties can be accurately determined by independent methods, such as the resonant column test, the torsional shear test.
2. Specimens with any reasonable subgrade stiffness (from about 2,500 to 100,000 psi, Young's modulus) can be manufactured.
3. Identical specimens can be manufactured for testing by different laboratories.
4. The properties are essentially independent of stress and strain so that flaws or limitations or both in the measurement systems can be evaluated.
5. Test procedures can be developed and evaluated because the properties of the specimens are known and constant with time.

It is the fifth benefit that makes the use of those specimens so important in the evaluation and calibration of equipment. The specimens will permit a systematic evaluation of the stress and strain measurement procedures to be evaluated so the most appropriate procedures can be logically selected and their limitations determined.

Synthetic samples (polyurethane) with three levels of stiffness were cast for calibration of the resilient modulus equipment at The University of Texas at Austin and at The University of Texas at El Paso, as part of Research Study 2/3-10-8-89/0-1177, sponsored by the Texas State Department of Highways and Public Transportation. The samples were named synthetic 1 (TU960), with Young's modulus of approximately

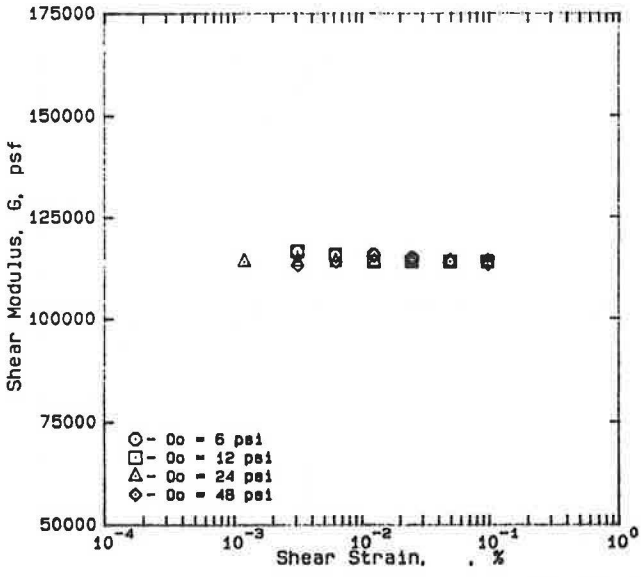

FIGURE 5 Shear modulus versus shear strain for synthetic 3 (TU700).

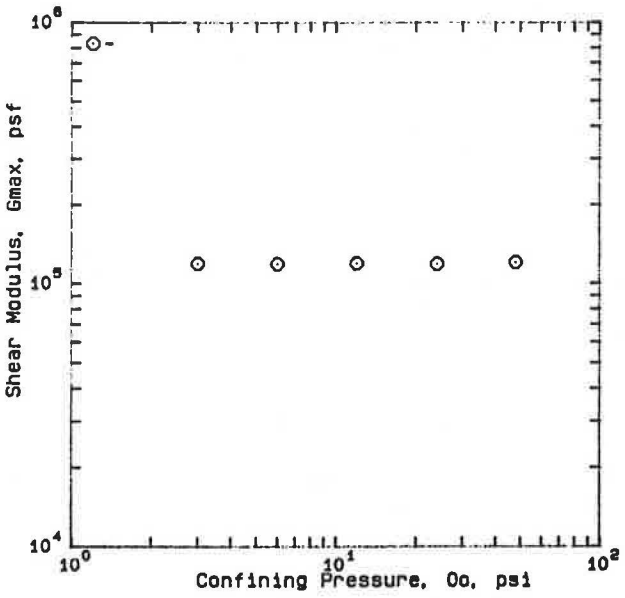

FIGURE 6 Shear strain versus confining pressure for synthetic 3 (TU700).

40,000 psi; synthetic 2 (TU900), with a modulus of 8,000 psi; and synthetic 3 (TU700), with a modulus of 2,500 psi.

Sample Testing Using Resonant Column and M_R Test

These samples were tested for preliminary comparison by using the resonant column and the M_R equipment. The moduli obtained by each of the testing devices were then compared. The resilient modulus for synthetic 1 (the stiffest) showed a much lower modulus (around 50 percent) than the one obtained in the resonant column. The resilient modulus for samples 2 and 3 were also somewhat lower (around 10 to 15 percent). Those resilient moduli were calculated without considering that the internal load cell also deflects under load. Those small deformations need to be subtracted from the deformation measured by the external LVDTs. A calibration of the load cell deflection was obtained for three seating pressures and is shown in Figure 7. By using this calibration, the resilient modulus values were corrected and plotted in Figures 8–10 for samples 1, 2, and 3. Because the resonant column measures shear modulus, those values were transformed to Young's modulus values by using the elastic relationship between E and G.

$$E = 2G(1 + \mu)$$

where

E = Young's modulus,
G = shear modulus, and
μ = Poisson's ratio.

The Poisson's ratios of the synthetic samples were measured statically (5) and their values are as follows: Sample 1, μ = 0.39, and Samples 2 and 3, μ = 0.5.

Figures 8 10 indicate that the moduli obtained with the resonant column and the M_R equipment are comparable, but

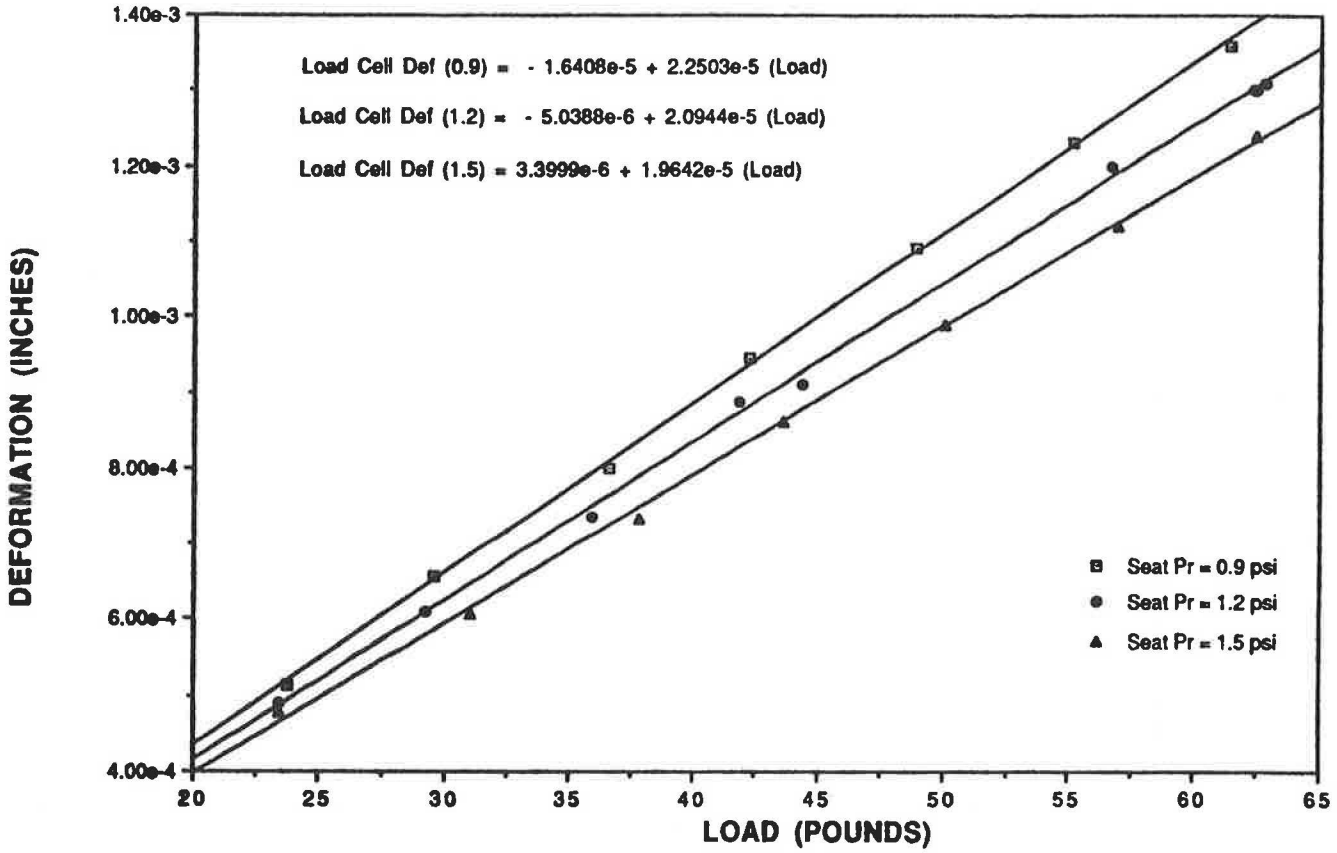

FIGURE 7 Calibration of load cell deformation.

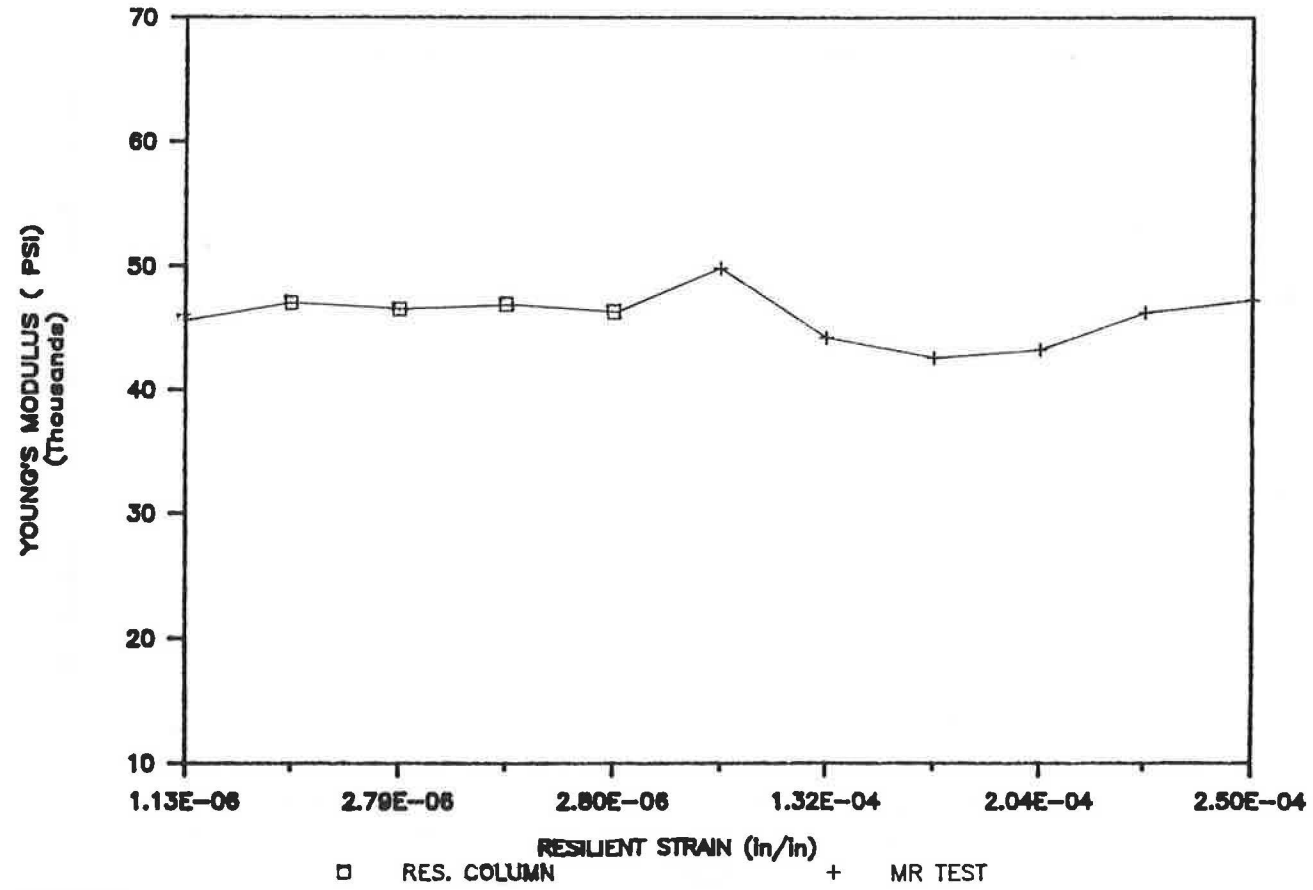

FIGURE 8 Comparison of modulus values for synthetic 1.

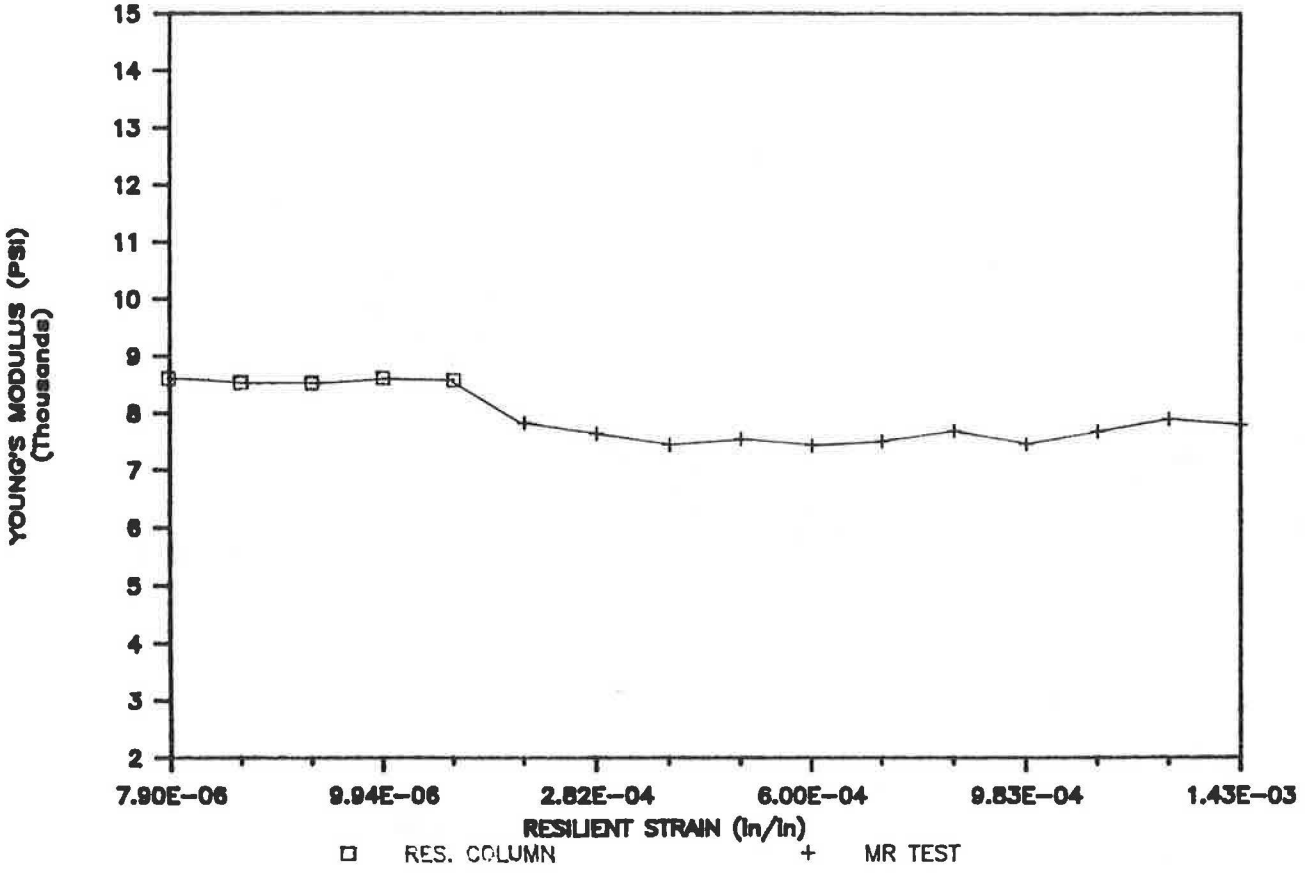

FIGURE 9 Comparison of modulus values for synthetic 2.

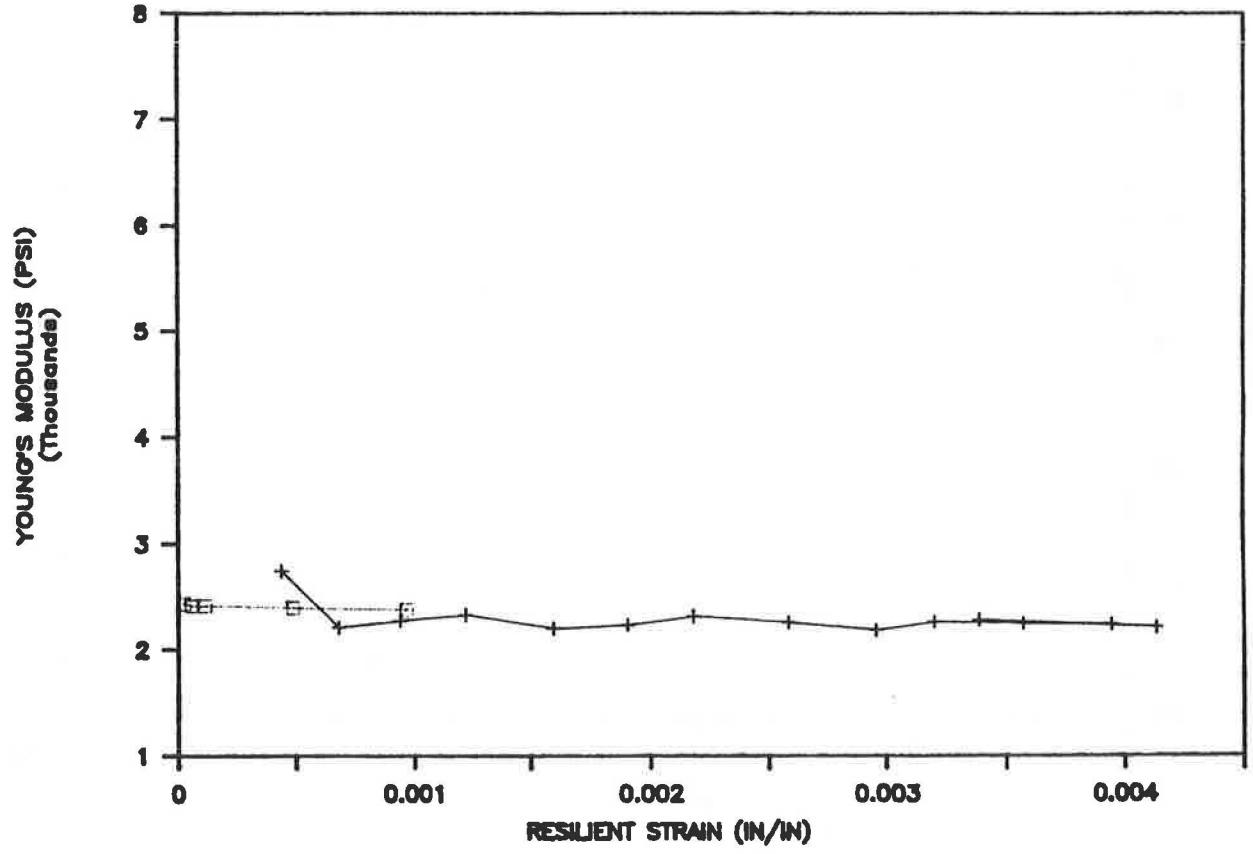

FIGURE 10 Comparison of modulus value for synthetic 3.

samples 1 and 2, when compared with those shown in sample 3, indicate a greater disparity between modulus values. The modulus variation in sample 1 obtained with the M_R equipment is also greater than the moduli in the outer two samples. This difference results because the resilient deformation in sample 1 is very small and is very difficult to measure.

Sample Testing Using Torsional Shear

To investigate further the influence of loading frequency on the synthetic samples, a series of torsional shear tests was performed (*5*).

The results of those tests show that the moduli of those samples are frequency dependent, as is shown in Figure 11 for synthetic 3. This plot shows the low frequency for the torsional shear and the high frequency for the resonant column. The resilient modulus has a load duration of 0.1 sec, which leads to a frequency of 5 Hz if half the period is considered.

The shear moduli of those samples, using the torsional shear test, depend on the frequency of loading at fixed shear strain amplitude. On the other hand, the resilient moduli depend on the deformation amplitude at loading (resilient strain), because the loading frequency for the M_R test is fixed to 5 Hz for a load duration of 0.1 sec. To compare both tests, a series of repeated modulus determinations was performed at the same deformation amplitude and frequency (5 Hz). The results of those tests and the descriptive statistics are included in Table 4. The shear strain (γ) was transformed to axial strain (ε_a) for comparison with the M_R test, using the expression

$$\varepsilon_a = \frac{\gamma}{(1 + \mu)}$$

where

ε_a = axial strain,
γ = shear strain, and
μ = Poisson's ratio.

The test results in Table 4 indicate that sample 1 (TU960) measured modulus had a 2.5 percent difference by using those tests, which in practice is very small. A statistical test (two-sample test) shows a significant difference between the means, indicating that the two sets of data are different, but for all practical purposes a 2.5 percent difference is not significant.

The moduli obtained for sample 2 (TU900) with both tests show that there is a larger discrepancy in the results (about 12 percent difference). This discrepancy may be explained by the fact that the load cell deflection calibration was done for

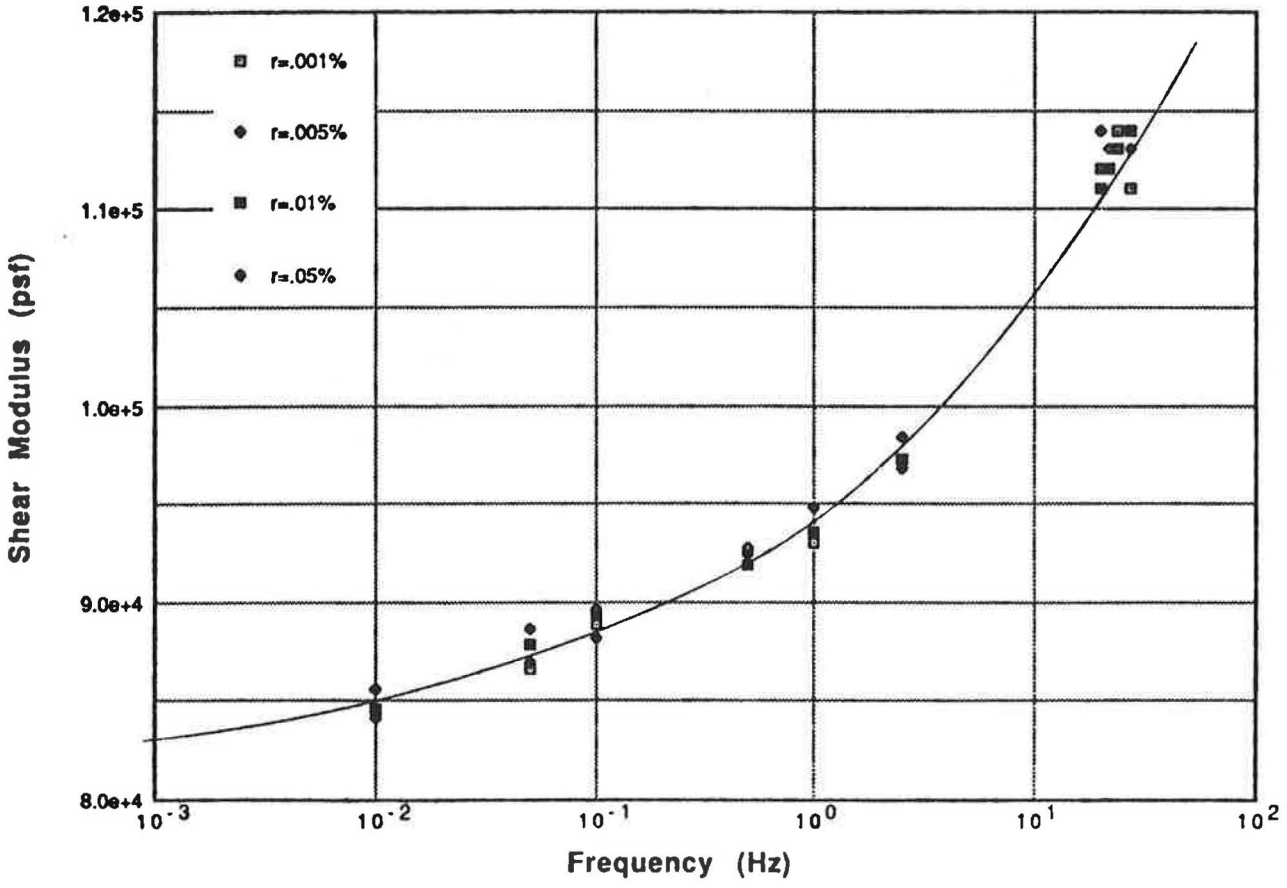

FIGURE 11 Shear modulus versus loading frequency for synthetic 3 (TU700).

TABLE 4 MULTIPLE TEST RESULTS FOR SYNTHETIC SAMPLES

	Resilient Modulus Test				Torsional Shear Test			
Sample	Number of Tests	Mean (psi)	Standard Deviation	Coefficient of Variation (percent)	Number of Tests	Mean (psi)	Standard Deviation	Coefficient of Variation (percent)
Sample 1 (TU960)	25	40,630	144.5	0.35	5	39,070	323.2	0.82
Sample 2 (TU900)	45	7,288	178.5	2.4	5	8,266	17.09	0.2
Sample 3 (TU700)	25	2,388	12.4	0.5	1	2,145	-	-

sample 1, the stiffness of which is higher than that of sample 2. Because the M_R is a dynamic test, the static solution to subtract the load cell deflection from the total deflection measured by the external LVDT may not be applicable. The authors are currently studying, through the use of accelerometers, the displacements of different parts of the M_R device during testing to locate the best reference point for measuring sample deformations that eliminate the load cell deflections.

Repeated torsional shear tests for sample 3 are not available because of limitations in the torsional shear equipment that induce large deformations in soft specimens. A shear modulus value for sample 3 can be obtained from Figure 11 at a 5-Hz frequency. This value is approximately 103,000 psf, or a Young's modulus of 2,145 psi, for a Poisson's ratio of 0.50. If this value were to be compared to the modulus value obtained by using the M_R equipment (2,388 psi), then an 11 percent difference would be observed. Again, this discrepancy is explained because the load cell deflections are not corrected properly.

There is a general tendency to make a static analysis of a dynamic test, as is the case of the M_R test. The M_R test needs to be analyzed dynamically to understand better the limitations of the test and the equipment used.

CONCLUSIONS

The following conclusions can be drawn:

1. The modifications to the AASHTO T-274 procedure are moving in the right direction, although further improvements are necessary.
2. The test procedure in protocol P-46 is repeatable and easy to perform and could be adopted as the standard procedure because it is specific. Perhaps it is still not the ideal test, but it is a base for further development.
3. Polyurethane samples with a range of stiffness are very useful in calibration and for familiarization with M_R equipment.
4. Synthetic samples have the potential to become standard in the procedure for M_R equipment calibration.

REFERENCES

1. H. B. Seed, C. K. Chan, and C. E. Lee. Resilience Characteristics of Subgrade Soils and Their Relation to Fatigue Failures in Asphalt Pavements. In. *Proc., International Conference on Structural Design of Asphalt Pavements*, University of Michigan, 1963, pp. 611–636.
2. *Resilient Modulus of Subgrade Soils*. AASHTO T274-82. American Association of State Highway and Transportation Officials, August 1986.
3. M. R. Thompson and Q. L. Robnett. *Resilient Properties of Subgrade Soils*. Final Report. Illinois Cooperative Highway and Transportation Series 160, Department of Civil Engineering, University of Illinois at Urbana-Champaign, June 1976.
4. Robert K. H. Ho. Repeated Load Tests on Untreated Soils: A Florida Experience. Presented at Florida Department of Transportation, Workshop on Resilient Modulus Testing, Oregon State University, Corvallis, Oregon, March 28–30, 1989.

Publication of this paper sponsored by Committee on Soil and Rock Properties.

Development of Synthetic Specimens for Calibration and Evaluation of M_R Equipment

KENNETH H. STOKOE II, DONG-SOO KIM, AND RONALD D. ANDRUS

Laboratory measurement of the deformational characteristics of subgrade materials can be quite difficult because of the small values of stress and strain typically involved and the need to eliminate equipment compliance. Measurement of resilient modulus (M_R) of subgrades falls into this category. Therefore, synthetic specimens with known stiffness characteristics would be beneficial in evaluating and calibrating M_R equipment as well as training personnel. Two-component urethane elastomer resins are shown to make good candidates for calibration specimens. They can be made with a wide range of stiffnesses that vary from soft subgrades to stiff uncemented bases. Urethane can be modeled as a linear, viscoelastic material with stiffness characteristics essentially independent of confining pressure, strain amplitude, and stress history for the type of cyclic loading used in M_R testing. Urethane stiffness is, however, dependent on loading frequency and temperature. Therefore, values of Young's modulus used to equate to M_R have to be selected at the appropriate frequency and temperature.

Laboratory measurement of the deformational characteristics of subgrade materials in the linear and nonlinear ranges can be performed by various cyclic and dynamic methods. Acceptance of the resilient modulus (M_R) as a measure of the deformational characteristics of subgrades (*1*) has resulted in the use of a number of different systems to perform such measurements. The strengths and weaknesses of those systems deserve further study for optimum use. Experience gained in applying the cyclic triaxial test in geotechnical earthquake engineering has shown that great care must be exercised in evaluating the deformational characteristics of geotechnical materials at small ($\varepsilon < 0.001$ percent) to intermediate (0.001 percent $< \varepsilon <$ 0.1 percent) strains or significant inaccuracies can occur (*2–4*).

One means of evaluating the performance of M_R equipment is to use the equipment to test specimens with known stiffness characteristics. (Such specimens are referred to as calibration specimens.) Values of M_R determined with the equipment can then be compared with stiffnesses of the calibration specimens that have been established by independent tests. If there are differences between the measured and calibration stiffnesses, then modifications to the equipment or procedures or both can be undertaken.

The purpose of this paper is to discuss the development of calibration specimens. Synthetic materials, rather than real soils, are used to construct such specimens. The stiffnesses are conveniently evaluated in terms of Young's modulus, E, which is taken to be equal to M_R for this material. Use of the calibration specimens with M_R equipment is discussed in a companion paper in this Record. Synthetic specimens have advantages: (a) They are easy to construct in the appropriate sizes for M_R equipment, (b) have physical characteristics that remain constant with time, and (c) have stiffness properties that can be determined by independent tests, and (d) can be repeatedly tested as desired by different personnel and laboratories or both. Specimens made from urethane elastomers have those characteristics.

Department of Civil Engineering, The University of Texas at Austin, Austin, Tex. 78712.

CALIBRATION SPECIMENS

Calibration specimens were constructed by using a two-component urethane elastomer resin system manufactured by Conap, Inc., of Olean, New York. The first component consisted of dicyclohexylmethane-4,4′-diisocyanate for all specimens. The second component consisted of diethyltoluene diamine for specimens TU-700 and TU-900 and 4,4′-methylenedianiline for specimen TU-960. One key characteristic of urethane elastomers, also called polyurethanes, is their very broad hardness range. Specimens can be formed with hardnesses (stiffnesses) ranging from that approximating a very soft subgrade to that approximating a stiff, uncemented base. Unlike other plastics, the hardness of polyurethane is governed by the molecular structure of the prepolymer (*5*) and not by the addition of plasticizers and fillers. As a result, constructing specimens of a preselected stiffness is straightforward, a task that can be difficult with other synthetic materials. Urethanes are also tough, durable, and have a high resistance to abrasion, weather, ozone, oxygen, and radiation.

Three individual mixtures were used to create synthetic specimens (Conathane® TU-700, TU-900, and TU-960) for this study. Casting procedures outlined by the manufacturer were followed. Each component was measured according to the specified accuracy and mix ratio. Disposable plastic containers were used for both weighing and mixing for ease in handling and cleanup. The two components were mixed thoroughly and then degassed for about 5 min to remove entrapped air caused by mixing. For effective degassing, the manufacturer recommended a vacuum of 28 to 29 in. of mercury (14 psi), a factor the authors found to be important. The working life of the mixture was about 20 min so that once mixing was started, construction progressed quickly.

Before pouring, a mold release (Conap® MR-5002) was applied to the inner surface of the cylindrical mold. The degassed mixture was then carefully poured into the mold in a manner

that attempted to minimize the trapping of air bubbles. Nevertheless, several tiny air bubbles would always become trapped during the pour. The trapped air bubbles would slowly move upward in the mixture and collect at the top. As the mixture cured, 1 to 1.5 percent shrinkage occurred. When a closed mold was used, even if vent holes were added at the top, the effects from the bubbles and shrinkage were unfavorable. These unfavorable effects were eliminated by (a) using a mold that was completely open at the top and (b) warming the mold and freshly poured urethane with a hair dryer, heating tape, or oven.

A curing time of 7 days was recommended by the manufacturer. However, the specimen could be removed from the mold after 1 day. As with most polyurethanes, it was necessary to wear gloves and work in a well-ventilated area when handling unmixed and uncured materials.

Both acrylic split molds and metal pipe molds were tried. The metal pipe mold was the simplest to use. However, a pipe of the proper dimensions may require special ordering, and an extruder is needed to push the cured specimens out of the pipe. Molds having diameters of 1.4, 2.0, and 2.8 in. and lengths of 2 to 3 times the diameter were used. The top inch of the cured urethane specimens was cut off, and the end was machined flat and perpendicular to the cylindrical axis by a surface grinder. Removal of the top inch of the specimen also had the beneficial effect of eliminating material with bubbles in it because bubbles tended to collect there.

The majority of the specimens used in this initial study were 2.8 in. in diameter and 5.6 in. long. Unit weights for those specimens ranged from 65 to 67 pcf.

Since completion of the initial study, the authors have constructed additional specimens not presented here. The urethane material was purchased locally in 2- to 3-ft long rods of specified hardnesses (hardness and stiffness are related in Figure 13). The rods were then cut in desired lengths, and the specimens were machined to their final dimensions. Happily, this approach eliminated the rather messy casting process used initially. The main hurdle in machining precise circular cylinders is the tendency of soft urethane to bend away from the cutting tool. This problem has been overcome through the use of a surface grinder.

TEST EQUIPMENT AND PROCEDURES

Once the calibration specimens were constructed, the deformational characteristics of each had to be measured by several independent methods to establish the stiffness characteristics of the material. The specimens became reference specimens with known stiffnesses for use in evaluation of M_R equipment and test procedures. Static compression, torsional resonant column, and slow cyclic torsional tests were used to establish the stiffness characteristics and to evaluate variables affecting them.

Static Compression Testing

Static measurements of Young's modulus and Poisson's ratio were determined by using the test setup shown in Figure 1. Axial loads were applied by placing known weights concentrically on top of each urethane specimen. A special top cap

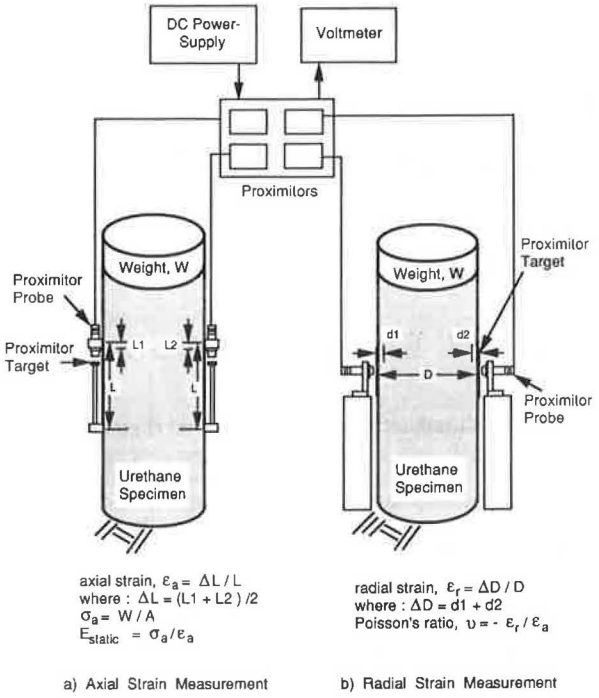

FIGURE 1 Configuration of equipment used to perform static compression measurements.

was used to align the weights concentrically. Proximitor probes and targets positioned near the middle of the specimen measured the axial and radial deformations. Those proximitors (MicroProx® Proximity Transducer System manufactured by Bently Nevada, Minden, Nevada) were capable of measuring displacements to within an accuracy of 0.000005 in. To ensure concentric loading, proximitors were located on opposite sides of the specimen, and their outputs had to exhibit deformations within 5 percent of each other for measurements to be accepted.

By using the relationships given in Figure 1, axial and radial strains were determined. Static Young's modulus or modulus of elasticity, E, was then calculated from

$$E = \sigma_a / \varepsilon_a \tag{1}$$

where σ_a is axial stress and ε_a is axial strain.

Poisson's ratio, ν, was determined from the ratio of radial strain to axial strain:

$$\nu = -\varepsilon_r / \varepsilon_a \tag{2}$$

where ε_r is radial strain.

The testing procedure was simply to add a load and then measure the resulting deformation. Measurements were made about 1 min after application of each load when the proximeter signal had stabilized.

Torsional Resonant Column Testing

Resonant column equipment of the torsional fixed-free type was used. A simplified diagram of a fixed-free resonant col-

umn is supplied in Figure 2. In this configuration, the bottom of the test specimen is fixed to the base with a hard epoxy glue. The top (free end) is connected to a drive system used to excite and monitor torsional motion. The basic operational principle is to vibrate the cylindrical specimen in first-mode torsional motion. Once first mode is established, measurements of the resonant frequency and amplitude of vibration are made. Those measurements are then combined with equipment characteristics and specimen size to calculate shear wave velocity, shear modulus, and shearing strain amplitude (*6,7*).

By using the wave equation, the basic data-reduction equation can be expressed as (*8*)

$$I/I_0 = (\omega_r L/V_s) \tan (\omega_r L/V_s) \quad (3)$$

where

I = mass moment of inertia of test specimen,
I_0 = mass moment of inertia of drive plate,
ω_r = resonant circular frequency,
L = length of the specimen, and
V_s = shear wave velocity.

Once the value of shear wave velocity is determined from Equation 3, shear modulus G and Young's modulus E are calculated from

$$G = \rho V_s^2 \quad (4)$$

$$E = 2G (1 + \nu) \quad (5)$$

where ρ is mass density of the urethane. The value of Poisson's ratio was taken from the static compression tests.

Shearing strain γ is calculated from the peak rotation of the top of the specimen at 0.67 times the radius (*6,7*). By following standard procedures in relating cyclic triaxial and resonant column results, the axial strain compatible with this shearing strain is then (*9*)

$$\varepsilon_a = \gamma/(1 + \nu) \quad (6)$$

In applying Equation 6, the material is assumed to be homogeneous and isotropic.

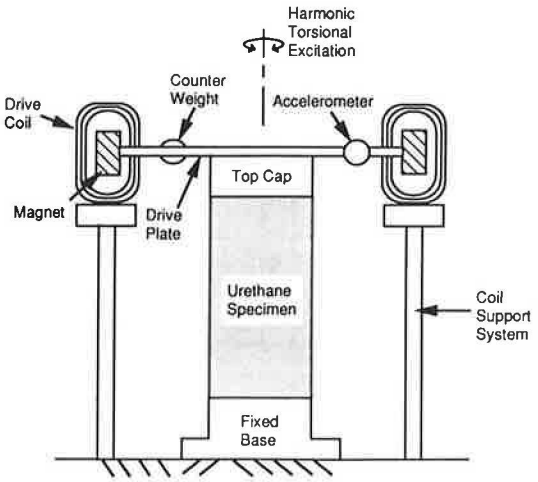

a. Synthetic Specimen in Test Apparatus

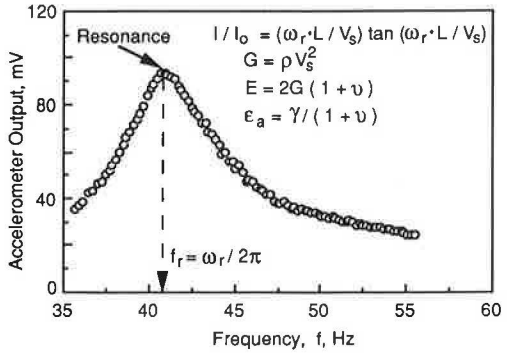

b. Typical Measurement

FIGURE 2 Configuration of fixed-free resonant column test and typical test results.

Torsional Shear Testing

The torsional shear test is another method of determining shear and Young's moduli, using the same resonant column equipment but operating it in a different manner. In this test, a cyclic torsional force with a given frequency, generally below 10 Hz, is applied at the top of the specimen. Instead of determining a resonant frequency, the stress-strain hysteresis loop is determined from measuring the torque-twist response of the specimen. Proximitors are used to measure twist, and the current applied to the coils is calibrated to yield torque. Shear modulus G corresponds to the slope of a line through the end points of the hysteresis loop as indicated in Figure 3 and is calculated from

$$G = \tau/\gamma \quad (7)$$

where τ is shearing stress and γ is shearing strain.

Values of shearing strain are presented as single-amplitude values and are calculated at 0.67 times the radius of the specimen, just as in resonant column tests. When the torsional shear test is performed at low frequencies, 0.01 to about 1 Hz, the inertial effect can be ignored. However, at higher frequencies, inertia significantly magnifies the amount of strain. The amount of strain caused by inertia can be estimated by using the dynamic magnification factor equation for a viscously damped single-degree-of-freedom system (*8*). This approach was followed in the calculations of shear modulus above 2 Hz but well below the resonant frequency.

Once G and γ were determined, Young's modulus and axial strain were calculated from Equations 5 and 6, using a value of Poisson's ratio from the static compression tests.

Torsional Testing Procedures

Before testing in either the resonant or the torsional shear mode, each specimen was glued to the base pedestal and top cap by using a hard, 5-min epoxy. The glue was allowed to cure overnight. This approach, which had worked well in testing other materials, eliminated any seating problems in

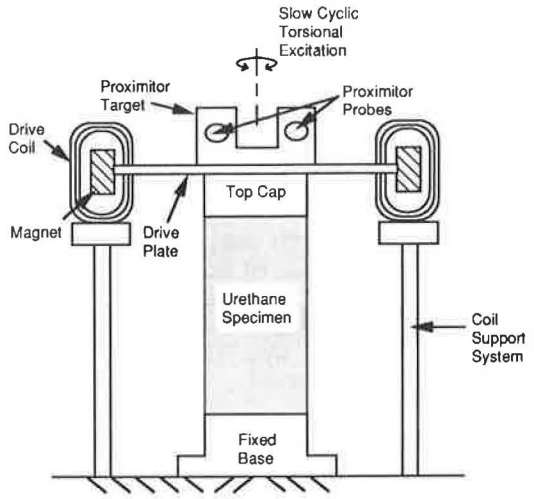

a. Synthetic Specimen in Test Apparatus

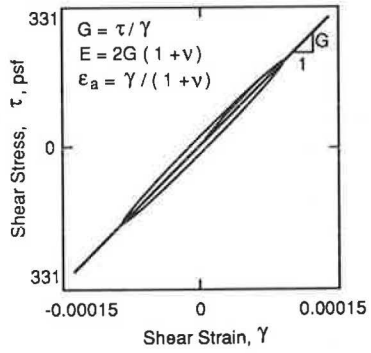

b. Typical Measurement

FIGURE 3 Configuration of torsional shear test and typical test results.

the tests. Each specimen was then tested under isotropic confining pressures of 0, 2, 4, 8, 16, 32, and 64 psi. Low-amplitude resonant column tests ($\gamma < 0.001$ percent) were performed at about 10-min time intervals at each pressure level. The tests are low-amplitude because the specimens exhibit linear behavior in this range (as well as at higher strains, as will be seen later). A series of those measurements at an isotropic confining pressure of 64 psi for each specimen stiffness is presented in Figure 4. The small-strain shear moduli reported for each specimen in subsequent figures and tables are the values calculated from measurements made 50 min after applying each confining pressure, even though the values were essentially independent of confinement time, as presented in Figure 4.

A series of torsional shear tests was performed after finishing low-amplitude resonant column tests at each confining pressure. The loading frequency and strain amplitude were varied in the torsional shear tests. Loading frequencies between 0.01 and 40 Hz were used, and shearing strain amplitudes ranging from 0.0005 to 0.05 percent (single amplitude) were generated at each frequency. High-amplitude resonant column tests were then performed at the same strain amplitudes as was the torsional shear tests. Finally, low-amplitude resonant column tests were again performed to see if any

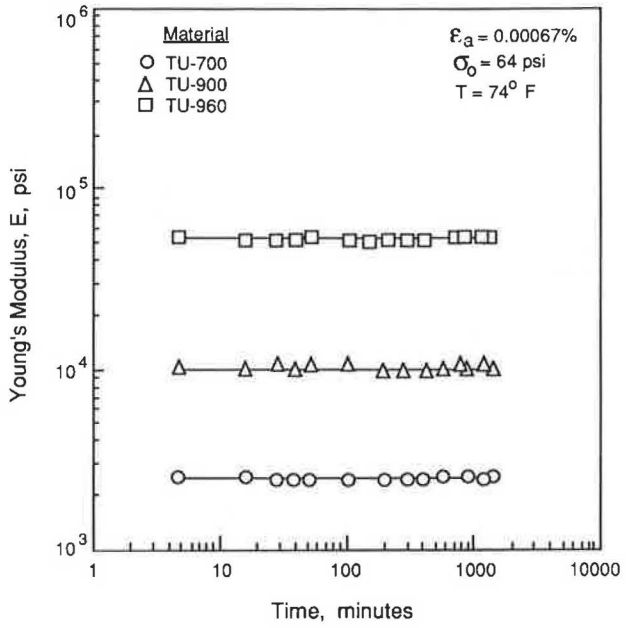

FIGURE 4 Variation in small-strain Young's modulus with time of confinement determined by resonant column tests with specimens confined at an isotropic pressure of 64 psi.

changes had occurred in the low-amplitude modulus. Variations in the low-amplitude moduli measured before and after high-amplitude testing were less than 3 percent and were considered to be within experimental scatter.

A typical series of measurements at one confining pressure is listed in Table 1. One specimen was tested at two different times to study the repeatability of the measurements. The specimen was removed from the apparatus and then reglued to the top cap and base between testing. As is indicated in the table, values of modulus for the two test series are within 3 percent, which indicates the high degree of repeatability. Smaller variations in modulus were observed if the specimen did not need to be reglued to the top cap and fixed base.

CALIBRATION TEST RESULTS

Factors involving material characteristics, specimen characteristics, and testing procedures need to be considered when developing calibration specimens. Material characteristics include the effect of the following factors: confining pressure (isotropic and anisotropic), strain amplitude, loading frequency, temperature, moisture, and time (e.g., changes with time of curing, ultraviolet radiation, as well as "creep" under load). Specimen characteristics include specimen length, diameter, uniformity, and end conditions. Test procedures include load history, seating load, rest times, equipment stiffness, and reproducibility.

This study started the initial steps in understanding the material and specimen characteristics of urethane calibration specimens. The effects of isotropic confining pressure, time under confinement, strain amplitude, loading frequency, and temperature have been evaluated. Specimen characteristics and the repeatability of the test results also have been studied. Testing procedures in terms of M_R tests are addressed in a companion paper in this Record.

TABLE 1 TYPICAL SERIES OF MEASUREMENTS ON ONE SPECIMEN* FROM COMBINED RESONANT COLUMN/ TORSIONAL SHEAR TESTS AT ONE CONFINING PRESSURE

Type of Test	Time,▽ minutes	Shearing Strain γ,%	Shear Modulus, G, ksi Trial 1			Trial 2 (reglued)△		
			@56Hz			@56Hz		
Low-Amplitude	4	1×10^{-3}	501			494		
Resonant Column	15	1×10^{-3}	496			499		
	25	1×10^{-3}	503			493		
	35	1×10^{-3}	501			497		
	45	1×10^{-3}	497			495		
	55	1×10^{-3}	503			497		
	65	1×10^{-3}	501			497		
			@0.01Hz	0.1Hz	1Hz	0.01Hz	0.1Hz	1Hz
Torsional Shear	90	5×10^{-4}	332	351	382	330	355	392
	115	1×10^{-3}	336	354	385	335	352	386
	140	5×10^{-3}	333	357	390	335	354	389
	165	1×10^{-2}	337	356	388	335	356	388
	190	5×10^{-2}	341	361	392	340	361	394
			@18Hz			@18Hz		
High-Amplitude	195	5×10^{-4}	501			501		
Resonant Column	200	1×10^{-3}	499			494		
	205	5×10^{-3}	492			497		
	210	1×10^{-2}	499			495		
	215	5×10^{-2}	498			494		

* Specimen: TU-900, Diameter = 2.8 in., Length = 5.6 in.; σ_o = 8 psi, T = 74° F

▽ Time since application of isotropic confining pressure

△ Trial 2 was performed two days after trial 1

Static Material Properties

Axial stresses ranging from 0.10 to 7.34 psi were applied to each unconfined specimen. Axial and radial deformations were measured for each load. Static Young's moduli and Poisson's ratio were determined on the basis of those measurements. The results are given in Table 2 and Figure 5. Static values of Young's modulus at small strains for the soft, medium, and hard specimens are 1,670, 6,550, and 32,300 psi, respectively. Less than a 2 percent decrease in modulus for the soft and medium specimens (TU-700 and TU-900) was found, and less than a 4 percent decrease in modulus for the hard specimen (TU-960) also was found over the time and strain ranges in the tests. The small decreases in modulus may be due to creep and nonlinear behavior or both. However, the small decrease is inconsequential for the cyclic M_R testing, as will be discussed in the next sections. Average values of Poisson's ratio for the soft, medium, and hard specimens are 0.48, 0.50, and 0.47, respectively. Only small variations exist between values of Poisson's ratio determined at the different loads. Those results show that the urethane behaves fairly linearly at small static strains (axial strains less than about 0.3 percent). Stress-strain properties of various urethanes cited in the literature (*5*) are based on large strain elongation tests. Plastic deformation in those elongation tests occurs above strains of 1 percent.

Effect of Isotropic Confining Pressure

As was outlined earlier, shear modulus was determined with resonant column and torsional shear tests at several confining pressures. Young's modulus E was then derived from Equation 5. The influence of isotropic confining pressure on small-strain Young's modulus for the three urethane specimens is shown in Figure 6. All moduli measurements were performed at an equivalent axial strain of about 6.7×10^{-4} percent after 50 min at each pressure. Moduli corresponding to zero confining pressure are not presented owing to the use of the log-log plot. However, essentially the same moduli were measured at zero confining pressure.

Average Young's moduli determined by the resonant column method for the soft, medium, and hard specimens are 2,430, 10,070, and 52,000 psi, respectively. Note that Young's moduli determined by the resonant column method are greater than those determined by static testing. This difference is due to the effect of loading frequency, which will be discussed.

Moduli measured at different confining pressures varied by less than 3 percent for each specimen. On the basis of those

TABLE 2 SUMMARY OF YOUNG'S MODULUS AND POISSON'S RATIO MEASUREMENTS PERFORMED STATICALLY

Material	Axial Stress σ_a (psi)	Axial Strain* ε_a (10^{-3}%)	Young's Modulus E (psi)	Poisson's Ratio ν
TU-700	0.10	6.1	1698	0.47
	0.22	13.1	1672	0.48
	0.33	20.1	1666	0.48
	0.84	50.2	1680	0.48
	1.35	81.0	1672	0.48
	1.86	111.0	1677	0.48
	2.37	142.0	1671	0.48
	2.88	172.0	1668	0.48
	3.39	204.0	1666	0.48
	3.90	235.0	1664	0.48
TU-900	0.23	3.5	6562	0.48
	0.74	11.3	6544	0.49
	1.25	19.1	6549	0.50
	1.76	26.9	6546	0.50
	2.27	34.7	6539	0.50
	2.78	42.6	6526	0.50
	3.29	50.6	6512	0.50
	3.80	58.5	6498	0.50
	4.31	66.5	6485	0.50
	4.82	74.5	6473	0.50
	5.45	84.5	6454	0.50
	6.08	94.2	6454	0.50
	6.71	104.0	6458	0.49
	7.34	114.0	6452	0.49
TU-960	0.51	1.6	32903	0.48
	1.02	3.1	32983	0.47
	1.53	4.6	32992	0.48
	2.04	6.2	32771	0.48
	2.55	7.8	32661	0.47
	3.06	9.4	32458	0.47
	3.57	11.1	32242	0.47
	4.08	12.7	32145	0.47
	4.59	14.3	32104	0.47
	5.22	16.3	32015	0.47
	5.85	18.3	31880	0.47
	6.48	20.3	31882	0.47
	7.11	22.4	31759	0.46

* Measurements were performed about 1 minute after applying each load
Tested at 74° F

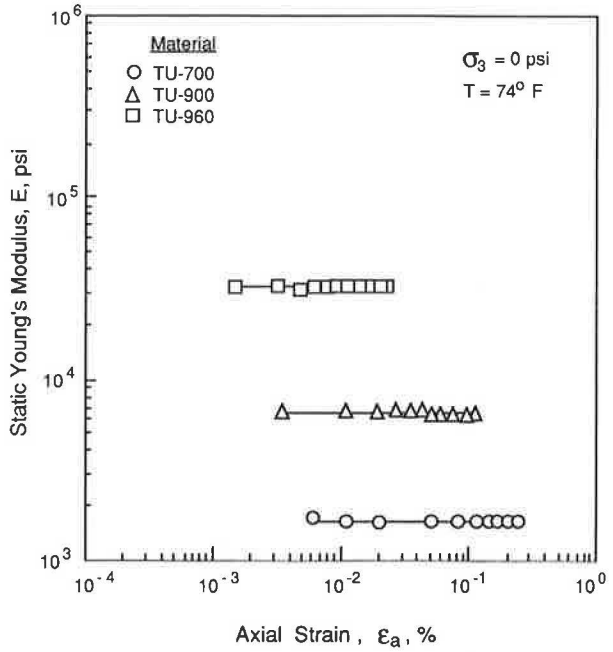

FIGURE 5 Variation in static Young's modulus with axial strain from unconfined compression tests.

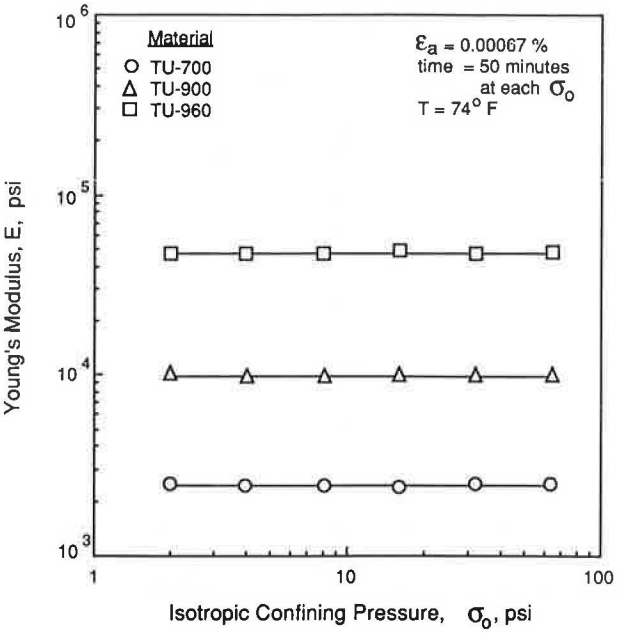

FIGURE 6 Variation in small-strain Young's modulus with isotropic confining pressure determined by resonant column tests.

results and similar results obtained with the torsional shear method, the stiffness of the urethane specimens can be assumed to be independent of confining pressure, at least for pressures between 0 and 64 psi and for measurements performed at room temperature (~ 74°F).

Effect of Strain Amplitude

Resonant column tests were performed at shearing strain amplitudes ranging from 0.0005 to 0.3 percent. Shearing strains were converted to equivalent axial strains, using Equation 6. Poisson's ratios determined from static testing were used. Figure 7 presents the resonant column test results performed at zero confining pressure with the three specimens. As is seen in the figure, the modulus is essentially constant over the range of strains tested. The small amount of creep and nonlinear behavior or both observed under static loading had no effect on the modulus measured dynamically.

To obtain a perspective on how the strains used in those tests compare with those generated in M_R testing, the range in strains in the M_R test are presented in Figure 8 for materials with stiffnesses ranging from 1,000 to 100,000 psi. In this figure, a range in cyclic axial stress of 1 to 20 psi has been used to calculate the strains. The data presented in Figure 7 for the synthetic specimens have also been included. The strains used in resonant column testing of the medium and stiff urethane specimens completely extend over the strain range generated by following the AASHTO T274-82 M_R testing procedure. The strains used in resonant column testing of the soft urethane specimen extend over about half of the strain range in M_R testing. Therefore, the specimens have been calibrated over the proper strain range.

Note that the wide range in strains generated in the M_R test as the material changes from a stiff to a soft soil, as is shown in Figure 8. Strain is a key variable in predicting soil (subgrade) behavior (*10*), and a very stiff subgrade loaded with $\Delta\sigma = 1$ psi should be expected to behave essentially linearly if $\varepsilon_a \sim 0.001$ percent. A very soft subgrade will behave very nonlinearly under the same cyclic stress because the strain will be on the order of 20 to 50 times greater.

Torsional shear tests were also performed at similar strain amplitudes to demonstrate the effect of strain amplitude at frequencies other than resonance. Those data are shown in Figure 9 for one specimen with the resonant column data also included. As is seen in the figure, Young's modulus of ure-

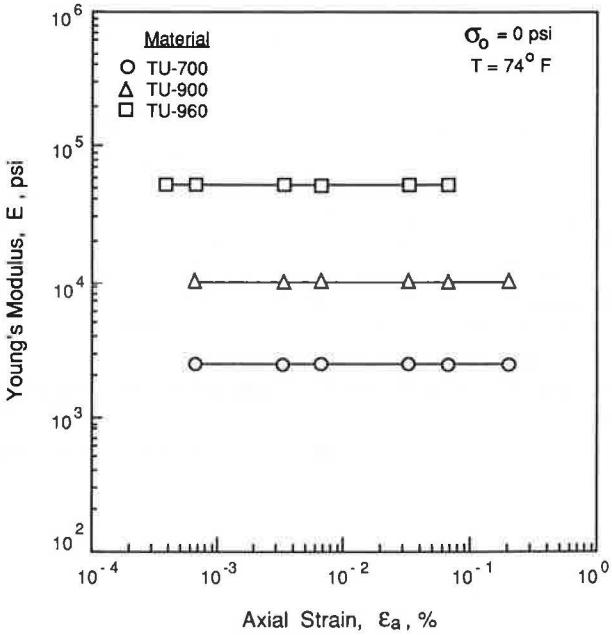

FIGURE 7 Variation in Young's modulus with axial strain as determined by resonant column testing at zero confining pressure.

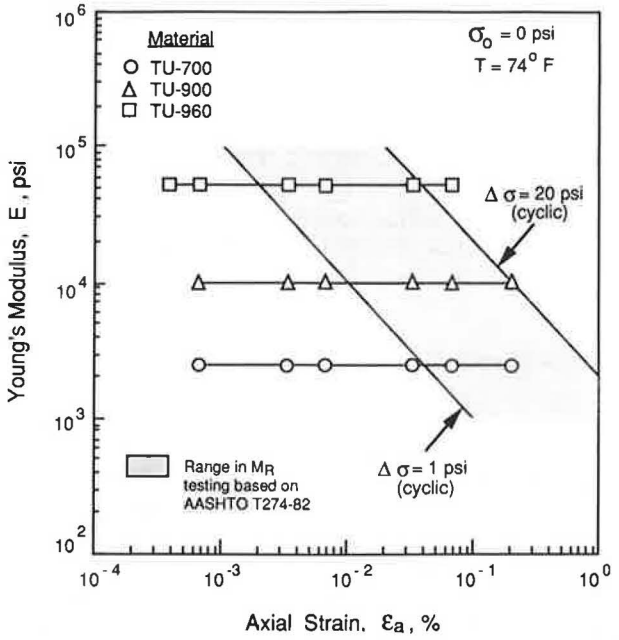

FIGURE 8 Comparison of axial strains generated in M_R testing with those generated in calibrating the synthetic specimens.

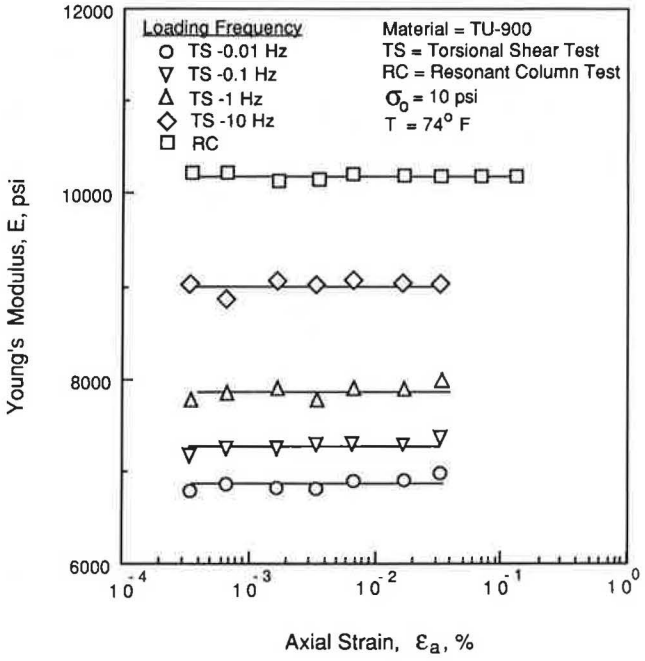

FIGURE 9 Variation in Young's modulus with axial strain for specimen TU-900 tested at various loading frequencies.

thane is independent of strain amplitude at a given excitation frequency. However, it is dependent on loading frequency.

Effect of Loading Frequency

The effect of frequency can be easily evaluated by using a combination of resonant column and torsional shear tests. Moduli determined by the resonant column test are based on first-made resonant frequency, which depends on the stiffness of the specimen and the mass moment of inertia of the drive plate. For the soft, medium, and stiff specimens, resonant frequencies were 27, 56, and 127 Hz, respectively. Loading frequency in the torsional shear test can be easily varied by changing the input frequency.

Moduli determined by the resonant column and torsional shear tests at various loading frequencies and strain amplitudes are plotted in Figure 10. Note that Young's modulus increases with increasing loading frequency but is independent of strain amplitude. Values of static Young's modulus are also shown in Figure 10. Static moduli are very close to the moduli determined at a loading frequency of 0.01 Hz. This comparison shows the consistency between Young's modulus derived from static measurements and from the torsional shear test, also suggesting that appropriate values of Poisson's ratio were measured.

All moduli shown in Figure 10 are presented in a normalized fashion in Figure 11 by using the modulus of each specimen determined at 0.01 Hz as the basis for normalization. Note that the effect of frequency on modulus is essentially the same for each specimen.

Effect of Temperature

The effect of temperature on the urethane specimens is presently under investigation. To date, only one specimen has been tested at temperatures other than room temperature, 74°F. Moduli determined for this specimen (TU-900, 2.0-in. diameter) at three temperatures, various loading frequencies, and four strain amplitudes are plotted in Figure 12. Average Young's moduli determined by the resonant column method for temperatures of 61°, 74°, and 85°F are 10,400, 9,770, and

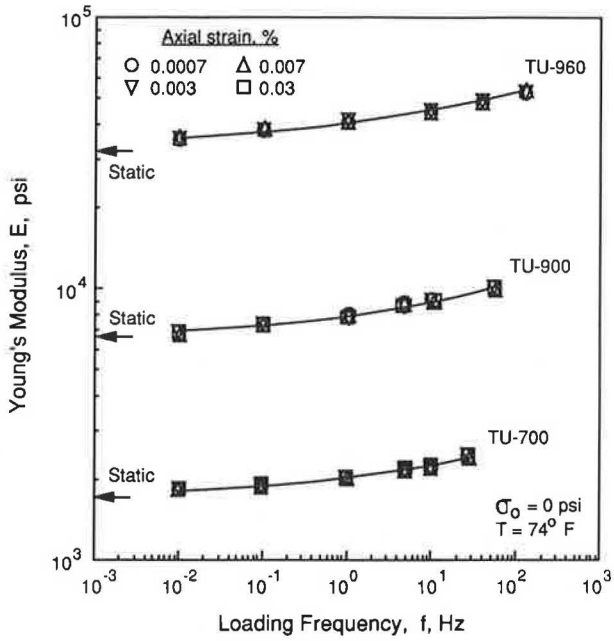

FIGURE 10 Variation in Young's modulus with axial strain amplitude and loading frequency as determined by cyclic torsional and resonant column tests at zero confining pressure.

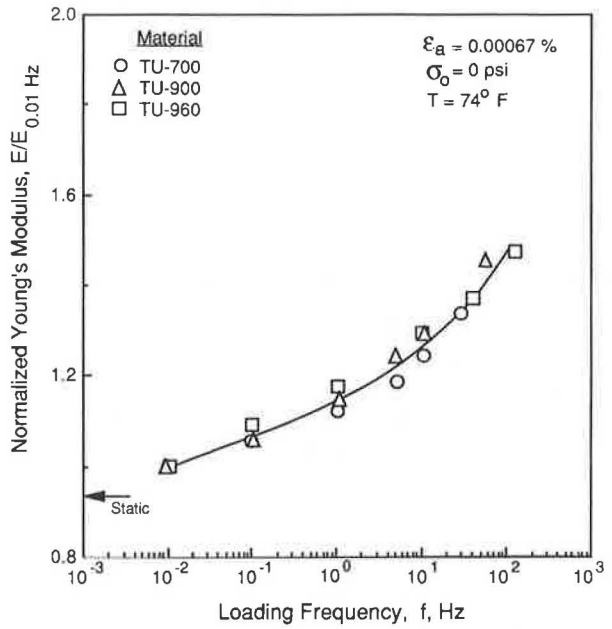

FIGURE 11 Variation in normalized Young's modulus with loading frequency as determined by cyclic torsional tests.

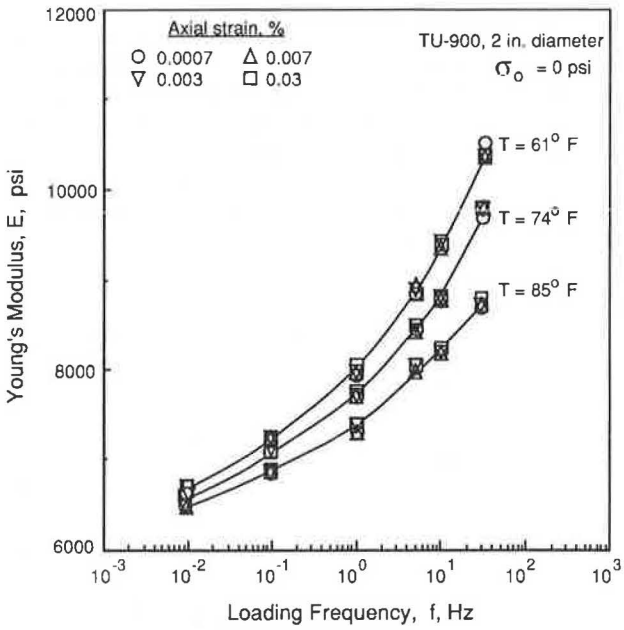

FIGURE 12 Variation in Young's modulus with temperature for specimen TU-900 tested at various loading frequencies.

8,720 psi, respectively, which reflects about an 0.8 percent change in modulus for each degree (1°F) change. The resonant frequency of the test specimen for this temperature range varied from 29.5 to 32 Hz. The effect of temperature decreased with slower loading frequencies. The change in modulus was less than 0.2 percent per degree (1°F) change at a loading frequency of 0.01 Hz. Those results provide a preliminary temperature correction factor that should be applied when using the specimens to calibrate M_R equipment at temperatures other than 74°F.

The rate at which the urethane specimens regain strength after being heated and then cooled has yet to be studied. Studies on polyurethane (5) have shown the rate at which strength is to be regained will depend on the temperature, chemistry, and molecular structure. When the synthetic specimen was heated to 85°F and then was allowed to return to room temperature, after 2 days the modulus had only returned to 96 percent of its original strength. This suggests that exposing the specimens to large temperature changes, especially after calibration, should be avoided.

Relationship Between Material Stiffness and Hardness

A common index test used when selecting synthetic elastomers is durometer hardness. The soft, medium, and hard specimens calibrated in this study have durometer hardnesses of A72.5, A90.5, and D60, respectively. Those hardness values and corresponding static Young's modulus are plotted in Figure 13. The range in moduli shown in this plot is typical for uncemented highway subgrades. Thus, the relationship shown in Figure 13 could be very useful in the selection of future elastomeric calibration materials.

CONCLUSIONS

Cylindrical urethane specimens can be constructed with stiffnesses ranging from very soft subgrade to stiff uncemented base. Three representative materials have been tested, using axial compression, torsional resonant column, and torsional shear testing techniques. On the basis of initial laboratory tests, urethane can be considered to be a linear, viscoelastic material with stiffness characteristics independent of confining pressure, strain amplitude, and stress history. Those prop-

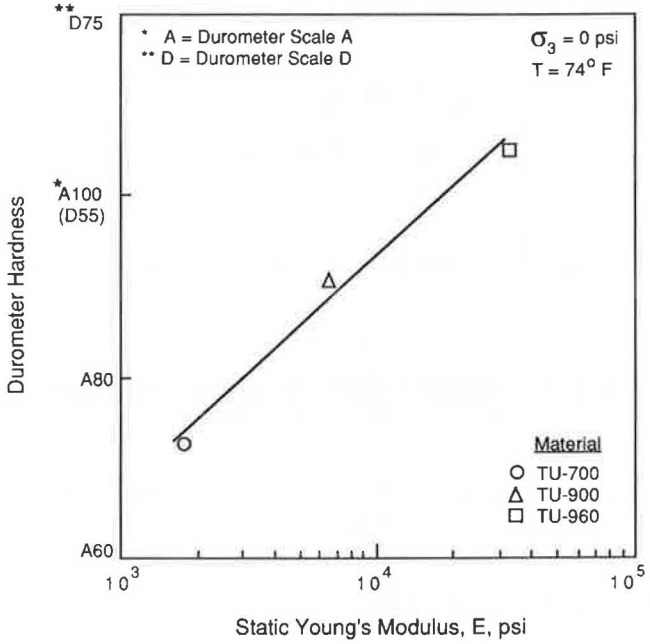

FIGURE 13 Relationship between static Young's modulus and durometer hardness.

erties make urethane a good material to construct calibration specimens that can be used in the evaluation of M_R equipment. Urethane stiffness is, however, dependent on loading frequency and temperature. Therefore, values of Young's modulus used to equate to M_R have to be selected at the appropriate frequency and temperature. Interestingly, the effect of loading frequency is similar for specimens of different stiffnesses and can be normalized to form a single curve.

Testing is presently underway that will characterize the urethane specimens further. Those investigations include the effects of large strains, long-term creep, biaxial and triaxial loading conditions, temperature, moisture, curing time, ultraviolet radiation, and specimen length and diameter. However, use of those has already been very beneficial in evaluations of M_R equipment (see paper by Claros et al. in this Record).

ACKNOWLEDGMENT

This work was supported by the Texas State Department of Highways and Public Transportation. The authors wish to express their appreciation for this support.

REFERENCES

1. *Resilient Modulus of Subgrade Soils*. AASHTO T274-82. American Association of State Highway and Transportation Officials, Aug. 1986, pp. 1157–1177.
2. R. S. Ladd, and P. Dutko. Small-Strain Measurements Using Triaxial Apparatus. *Proc., Advances in the Art of Testing Soils Under Cyclic Conditions*, ASCE, Detroit, Mich., Oct. 1985, pp. 148–165.
3. F. I. Makdisi, H. B. Seed, and I. M. Idriss. Analysis of Chabot Dam During the 1906 Earthquake. *Proc., Earthquake Engineering and Soil Dynamics*, ASCE, Geotechnical Engineering Division, Pasadena, Calif., Vol 2, June 1978, pp. 569–587.
4. T. S. Vinson. Fundamentals of Resilient Modulus Testing. Presented at the Workshop on Resilient Modulus Testing, Oregon State University, Corvallis, March 1989.
5. J. Bhattacharyya. Physical and Chemical Crosslinking of Polyurethane. In *Handbook of Polymer Science and Technology* (N.P. Cheremisinoff, ed.), Vol. 2, 1989, pp. 557–598.
6. V. P. Drnevich, B. O. Hardin, and D. J. Shippy. Modulus and Damping of Soils by the Resonant-Column Method. In *Dynamic Geotechnical Testing*, ASTM STP 654, American Society for Testing and Materials, Philadelphia, Pa., 1978, pp. 91–125.
7. Standard Test Methods for Modulus and Damping of Soils by the Resonant-Column Method. In *1987 Annual Book of Standards*, Vol. 04.08, ASTM D4015-87. American Society for Testing and Materials, pp. 507–525.
8. F. E. Richart, Jr., J. R. Hall, Jr., and R. D. Woods. *Vibrations of Soils and Foundations*, Prentice Hall, Englewood Cliffs, N.J., 1970.
9. M. L. Silver and T. K. Park. Testing Procedure Effects on Dynamic Soil Behavior. *Journal of the Geotechnical Engineering Division*, ASCE, Vol. 101, No. GT10, Oct. 1975, pp. 1061–1083.
10. B. O. Hardin and V. P. Drnevich. Shear Modulus and Damping in Soils: Measurement and Parameter Effects. *Journal of the Soil Mechanics and Foundations Division*, ASCE, Vol. 98, No. SM6, June 1972, pp. 603–624.

Publication of this paper sponsored by Committee on Soil and Rock Properties.

Repeated Load Model for Subgrade Soils: Model Development

LUTFI RAAD AND BASSAM A. ZEID

A load deformation model for subgrade soils is developed, where total cumulative axial strains are correlated with applied stresses and number of load repetitions. The model is based on the results of repeated load tests for a compacted silty clay. The concept of a constant failure strain independent of load history is presented and used in the proposed model. Results of static triaxial tests, slow cyclic tests, and repeated load tests are used to verify that the failure strain for given compaction conditions and confining pressure is essentially independent of stress history. Good agreement is obtained between predicted strains and experimental values from repeated load tests. Model predictions are within ±10 percent of experimental results.

Modern techniques for pavement design and analysis utilize limiting response criteria to control cracking and rutting in pavement structures. The behavior of the subgrade, in this case, could be of major significance to the overall performance of the pavement. The resilient behavior of subgrade soils has been defined in terms of repeated stresses and recoverable or elastic strains. Those relations have been incorporated into multilayer analyses for the purpose of predicting the resilient response of pavements under repeated traffic loads (*1–3*). Limiting values in the critical response parameters are proposed by many rational design methods as a means of achieving satisfactory pavement performance. In the case of subgrade soils, such criteria are presented in terms of strains, normal stresses, and deviator stresses on top of the subgrade layer. Those criteria have been determined in two different ways: first, through the use of structural models to analyze pavements of known performance (*4–7*) and, second, through laboratory testing of specimens under repeated stress applications (*8–10*). Other permanent deformation models, such as those proposed by Barksdale (*11*), Knutson et al. (*12*), and Monismith et al. (*13*), could be used to estimate the magnitude of subgrade strains for a different number of load applications. Some limitations of those criteria and permanent deformation models are summarized:

1. Subgrade normal strain criteria are derived through backcalculation procedures by using multilayer elastic analysis of pavements with known performance and, therefore, ignore the stress-dependent behavior of the pavement materials. Moreover, those criteria are suitable for similar pavement conditions and are not applicable, in general, to conditions of different pavement loading, materials, geometry, and environment.

L. Raad, Institute of Northern Engineering, University of Alaska, Fairbanks, Alaska 99775. B. A. Zeid, Dar Al-Handassah (Shair and Partners), Beirut, Lebanon.

2. Subgrade normal stress or strain criteria derived from laboratory tests do not explicitly account for the influence of changes in subgrade soil type, density, moisture content, and stress state on the accumulation of plastic strains under field-loading conditions. Those criteria, expressed in terms of limiting stresses or strains, are based on applicable permanent strain levels in laboratory specimens and do not provide the mechanism for predicting permanent strains in the subgrade.

3. Although available permanent strain models can be used to estimate the permanent deformations in the subgrade, the models do not provide an assessment of subgrade failure in terms of increased rate of plastic strain accumulation. Those failure conditions need to be incorporated in advanced analyses of pavements for the purpose of improving pavement response and performance predictions (*2,14*).

The development of improved stress-strain models should describe the load-deformation and strength behavior of compacted fine-grained subgrade soils under repeated loads. Those would be considered in lieu of reported findings that suggest that failure strain is generally independent of loading rate or type but depends mainly on the initial conditions of the specimen (i.e., initial stress state, density, and moisture content). Experimental work conducted by Vaid and Campanella (*15*) on undisturbed Haney clay indicates that for given testing conditions, irrespective of the creep stress level, rupture occurs approximately at the same magnitude of axial strain and that this is equal to the failure strain in conventional constant strain rate undrained shear testing. Similar observations were reported by Mitchell (*16*) on the failure strain of different types of undisturbed clays under creep loading. More recently, data provided by Ansal and Erken (*17*) on the behavior of one-dimensionally consolidated Kaolinite clay under cyclic simple shear testing show that the cyclic shear strain amplitude corresponding to the cyclic yield strength remains essentially constant for different numbers of stress cycles. Zeid (*18*) investigated the behavior of a compacted silty clay under different forms of loading that included static tests, creep tests, and repeated load tests. Results illustrate that the failure strain for a given confining pressure, dry density, and compaction moisture content remains essentially constant, independent of the type of the test performed.

Results of static triaxial tests, slow cyclic load tests, and repeated load tests for a compacted silty clay are presented here to illustrate the concept of a constant failure strain, independent of stress history. This concept is used in the development of a load-deformation model for subgrade soils, where total strains are correlated with repeated stresses and number of load repetitions. Strain predictions, using the proposed

model, are compared with experimental results from repeated load tests.

EXPERIMENTAL WORK

Testing Procedure

Strain-controlled static triaxial tests, stress-controlled slow cyclic load tests, and stress-controlled repeated (transient) load tests were conducted on a compacted silty clay in the undrained mode. The identification properties of the soil used are summarized in Table 1. The soil was compacted in a California bearing ratio (CBR) mold according to the modified AASHTO method (ASTM D1557-66T). Specimens were then extruded by using thin wall brass tube samplers and trimmed to 1.5-in diameter and 3.0-in height. Each specimen was placed between a cap and a base, encased in two rubber membranes, and cured in a water bath until ready for testing.

Two series of static triaxial tests were performed on specimens, which were cured for 24 hr and had dry densities and compaction moisture contents covering the range defined by modified AASHTO compaction. In the first series, the specimens were subjected to a confining pressure of 14.5 psi and then were loaded to failure at strain rates equal to 0.084 percent/min, 0.50 percent/min, and 1.96 percent/min. In the second series, the specimens were tested at a strain rate of 0.50 percent/min at confining pressures of zero, 14.5 psi, 29 psi, and 58 psi.

Cyclic load tests and repeated load tests were conducted on specimens cured for 2 weeks. Those specimens had a dry density of 129.5 lb/ft^3 and compaction moisture content corresponding to optimum ± 1.5 percent. The maximum dry density and optimum moisture content given by modified AASHTO compaction were 131.5 lb/ft^3 and 8.5 percent. The allowable range of variation for dry density and compaction moisture content for the tested specimens was ± 0.6 lb/ft^3 and ± 0.25 percent, respectively.

A confining pressure of 14.5 psi was used for the cyclic load tests. The specimens were then subjected to cyclic deviator stresses that had essentially a rectangular shape and a duration of 0.50 min at a frequency of 1 cpm. The specimen was immediately loaded to failure at a constant rate of strain following the applications of a specific number of load cycles. The strain rates used were 0.084 percent/min and 1.96 percent/min. The cyclic stresses corresponded to 50 percent and 80 percent of the strength associated with the applied strain rate at the end of the cyclic period. The number of stress cycles of each stress level applied were 10, 50, 100, and 150.

TABLE 1 IDENTIFICATION PROPERTIES OF SILTY CLAY USED

Parameter	Value
Liquid limit	28
Plasticity index	11
Specific gravity	2.708
Percent finer than 0.074 mm	80
Clay fraction (percent less than 0.002 mm)	18
Unified Classification	CL
AASHTO Classification	A-6(7)

In the repeated load tests, specimens were tested in the unconfined state and at a confining pressure equal to 14.5 psi. Pneumatically controlled deviator stress pulses having an approximate triangular shape and average duration of 0.2 sec were applied at a frequency of 40 cpm. Stress levels of 0.70, 0.80, 0.90, and 0.95 were used. The stress level is defined in this case as the ratio of repeated deviator stress to the strength obtained from a standard triaxial test at a strain rate of 0.5 percent per minute. For a given repeated stress level, the axial strains were monitored with number of load repetitions. A summary of testing conditions and strength properties of the silty clay used in this study is presented in Tables 2 and 3, respectively.

Results

Results of triaxial tests presented in Figures 1 and 2 indicate that the failure strain ϵ_f, defined as the axial strain at peak

TABLE 2 TESTING CONDITIONS FOR THE SILTY COMPACTED CLAY

Test Type	Confining Pressure (psi)	Stress Level	Strain Rate (% per min)	Frequency and Shape	Duration (sec)	Number of Cycles
Strain Controlled Static Triaxial Test						
- Series 1	14.5	-	0.084,0.50, 1.96	-	-	-
- Series 2	0,14.5,29,58	-	0.50	-	-	-
Stress Controlled Cyclic Test	14.5	0.50, 0.80	0.084,1.96,	1 cpm (rectangular)	30	10,50, 100, 150
Repeated Load Test	0, 14.5	0.70,0.80, 0.90,0.95	-	40 cpm (triangular)	0.20	to failure or 10^4

NOTES

- In the strain-controlled static triaxial tests, the dry density and compaction moisture content of specimens covered the range defined by modified AASHTO compaction. Specimens were cured for 24 hours prior to testing.
- In the cyclic and repeated load tests, specimens were compacted to a dry density of 129.5 lb/cu ft and moisture content of 7.0 percent and 10 percent. Specimens were cured for two weeks prior to testing.
- The maximum dry density and optimum moisture content associated with modified AASHTO compaction were 131.5 lb/cu ft and 8.5 percent respectively.

TABLE 3 SHEAR STRENGTH CHARACTERISTICS OF THE SILTY CLAY

Compaction Properties	Cohesion C (psi)	Angle of Friction ϕ(degrees)	Undrained compressive strength σ_{df} (psi)	
			$\sigma_3 = 0$	$\sigma_3 = 14.5$ psi
γ_d = 129.5 lb/cu ft m = 7 %	39.0	32	140	173
γ_d = 129.5 lb/cu ft m = 10 %	23.0	32	83	117

NOTES

- Shear strength properties were determined using strain-controlled undrained triaxial tests with rate of applied strain equal to 0.50 percent per minute.
- σ_{df} is equal to the difference of major principal stress σ_1 and minor principal stress σ_3 at failure.

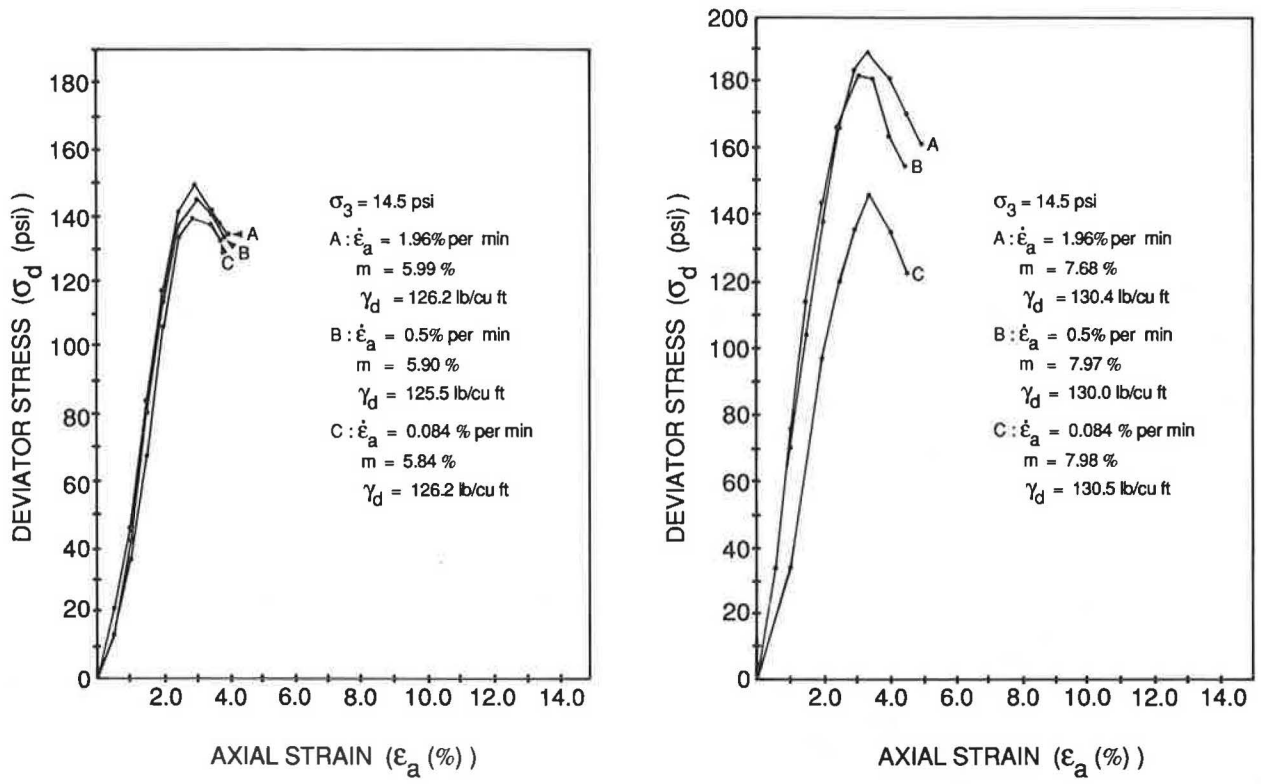

FIGURE 1 Stress-strain behavior for specimens compacted dry of optimum.

deviator stress, seems to be relatively independent of applied strain rate $d\epsilon_a/dt$ for a given confining pressure σ_3, dry density γ_d, and compaction moisture content m. Although the influence of strain rate on the strength can be significant, the variation of the strain at failure remains small. For example, the strength of specimens with average dry density of 130 lb/ft^3 and compaction moisture content of 7.88 percent exhibits a strength increase from 145 psi when subjected to a strain rate of 0.084 percent/min to 188 psi when the strain rate is 1.96 percent/min. The failure strain, however, remains in the range of 3.0 percent to 3.4 percent (Figure 1). The influence of confining pressure, compaction moisture content, and dry density on the failure strain is shown in Figure 3. An increase in confining pressure and compaction moisture content will result in higher failure strain values.

Similar observations are made in the case of the slow cyclic load tests, where cyclic deviator stress applications seem to have little effect on the failure strains as shown in Figures 4–7. The strength increases as the number of stress applications increases up to 50 cycles and then decreases with further increase in the number of cycles. The increase in strength is more significant for dry of optimum compaction conditions and lower cyclic stresses. Although the strength is influenced by cyclic stress history, the strain at failure remains virtually unaffected. In this case, the failure strain varies in the range of 2.8 percent to 3.2 percent for specimens compacted dry of optimum and 8.8 percent to 9.2 percent for specimens compacted wet of optimum.

Results of repeated load tests presented in Figures 8–11 illustrate the variation of total accumulated axial strain ϵ_a, defined as the sum of resilient strain and permanent strain, with the number of repetitions N of a given stress level q_r. The variation of the rate of accumulation of axial strain $d\epsilon_a/dN$ with the number of repetitions is also shown. The results indicate the existence of a "threshold stress level" below which the accumulation of axial strain will eventually cease and lead to a stable response and above which progressive accumulation of axial strains occurs and causes unstable response and ultimately failure. The "threshold stress level" for the repeated load tests performed lies between 0.80 and 0.90. Similar findings for a "threshold stress level" have been reported by other investigators (*19,20*). For repeated stresses larger than the "threshold value," the rate of axial strain $d\epsilon_a/dN$ decreases initially to a minimum value with the number of repetitions, after which it starts to increase. This flexure indicates a condition of incipient failure. This condition is conceived as a possible definition of failure under repeated loading, and the corresponding strains will be defined as failure strains. For example, failure strain values, obtained for a confining pressure of 14.5 psi, lie between 2.8 percent and 3.0 percent for specimens compacted dry of optimum and between 8.9 percent and 9.2 percent for specimens compacted wet of optimum. This agrees well with the failure strains obtained from cyclic load tests reported previously.

A summary of failure strain values for all the testing and compaction conditions used in this study is presented in Table

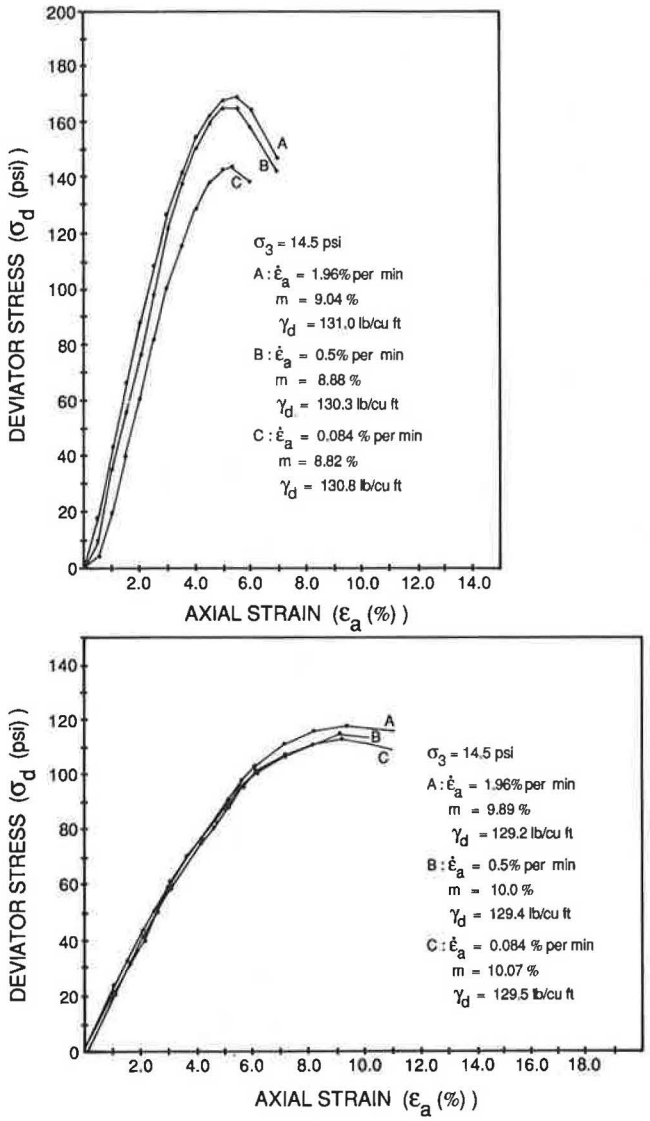

FIGURE 2 Stress-strain behavior for specimens compacted wet of optimum.

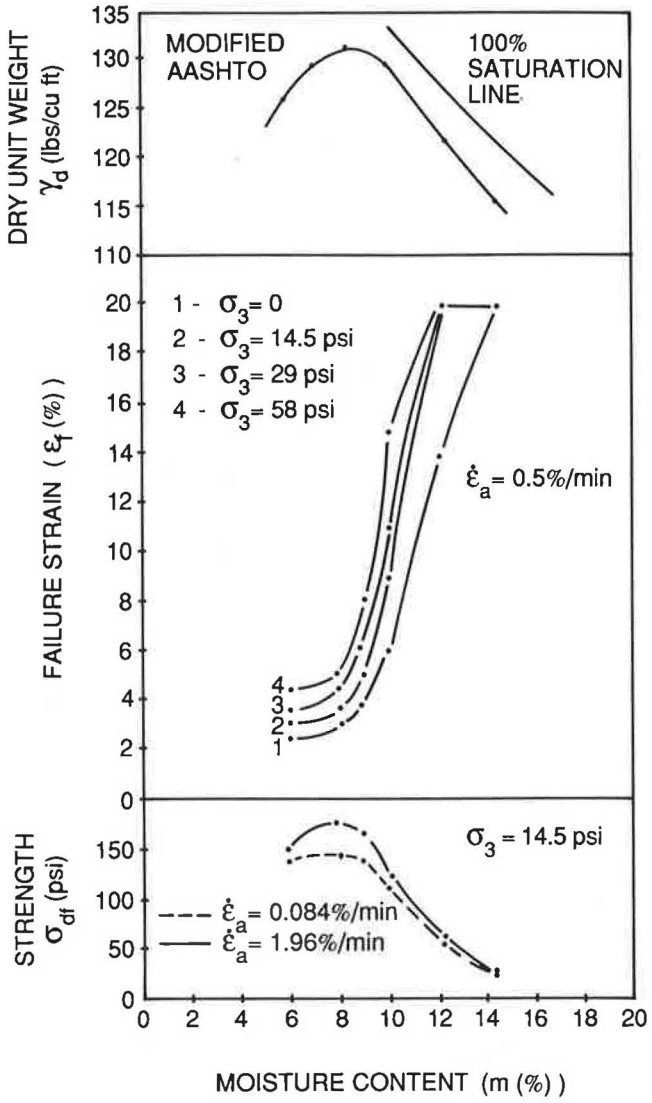

FIGURE 3 Variation of failure strain and strength for different compaction conditions.

4. Results indicate that for a given confining pressure, dry density, and compaction moisture content the failure strain is relatively independent of loading history and could, therefore, be determined from standard triaxial tests.

PROPOSED REPEATED LOAD MODEL

The behavior of the compacted silty clay in terms of axial strain ϵ_a, repeated load stress level q_r, and number of load repetitions N depends to a great extent on the magnitude of the applied stress level relative to the "threshold stress level" q_{rt}.

This behavior is schematically illustrated in Figure 12 for repeated stress level values less than q_{rt}. In this case, the variation of axial strain with the logarithm of number of repetitions can be represented by a transient state for N less than N_0, where the rate of axial strain decreases, and can be followed by a steady state where the rate of axial strain is relatively constant for N between N_0 and N_s and a stable state for N greater than N_s where no further accumulation of axial strain occurs with additional load repetitions. Repeated load test data on the compacted silty clay used in this study indicate that for q_r less than q_{rt} values of N_0 are generally less than 10, whereas N_s is less than 10^4. The range of practical interest for the variation of axial strain with number of load repetitions lies in the steady state region corresponding to N between N_0 and N_s. In this range, the experimental data seem to fit the following relation:

$$q_r = \frac{\epsilon_a}{a_L + s_L \log N} \tag{1}$$

where a_L and s_L are material parameters that can be determined from a plot of ϵ_a/q_r versus log N as shown in Figure 12.

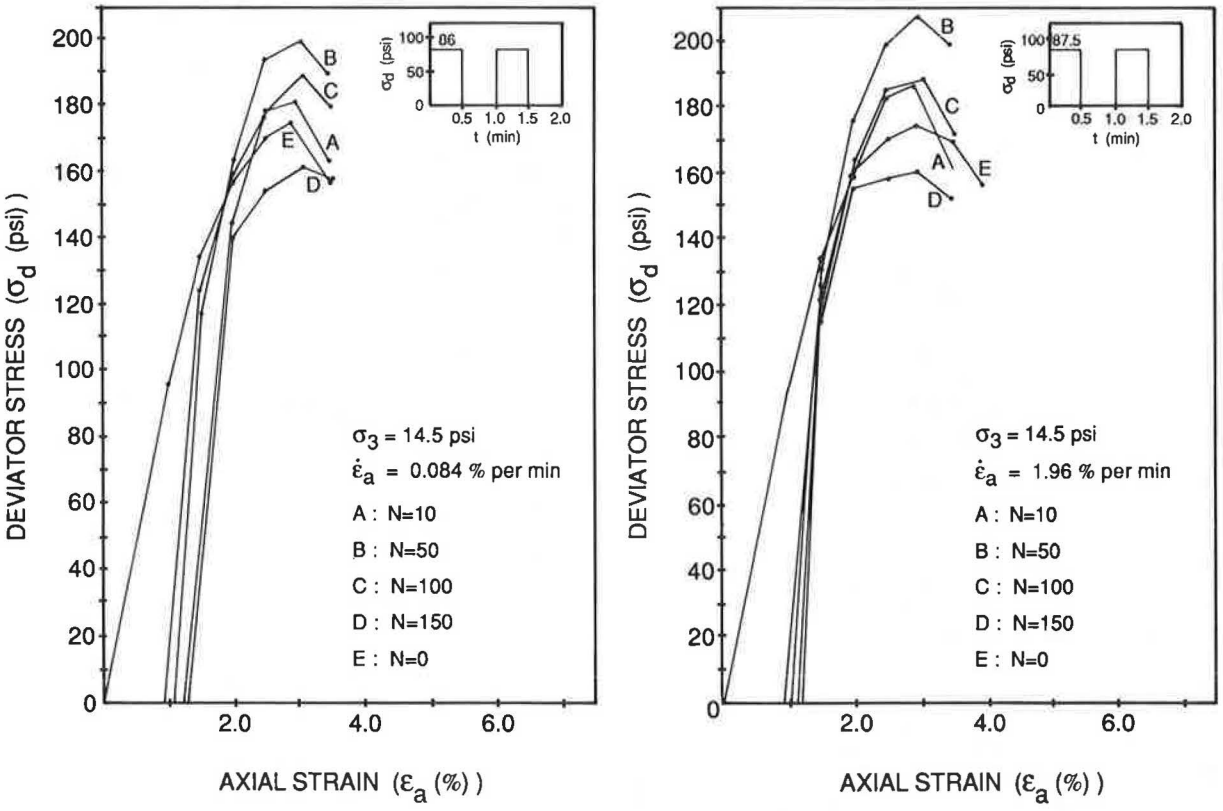

FIGURE 4 Load deformation behavior under 50 percent cyclic stress level (γ_d = 129.5 lb/ft^3, m = 7 percent).

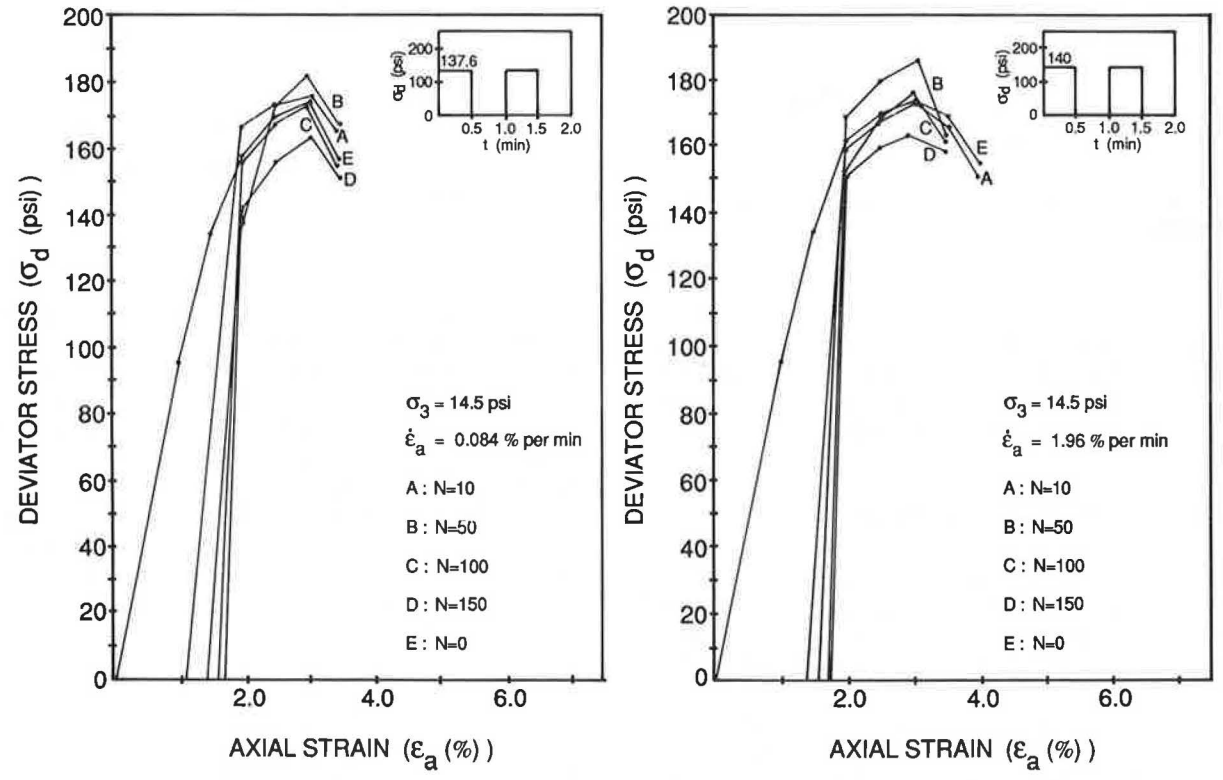

FIGURE 5 Load deformation behavior under 80 percent cyclic stress level (γ_d = 129.5 lb/ft^3, m = 7 percent).

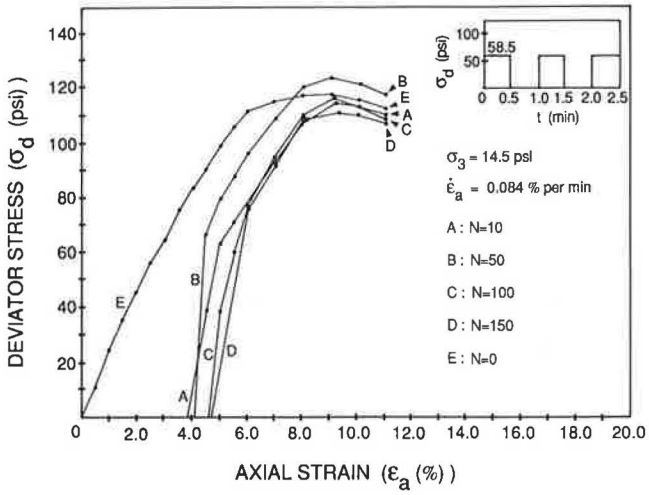

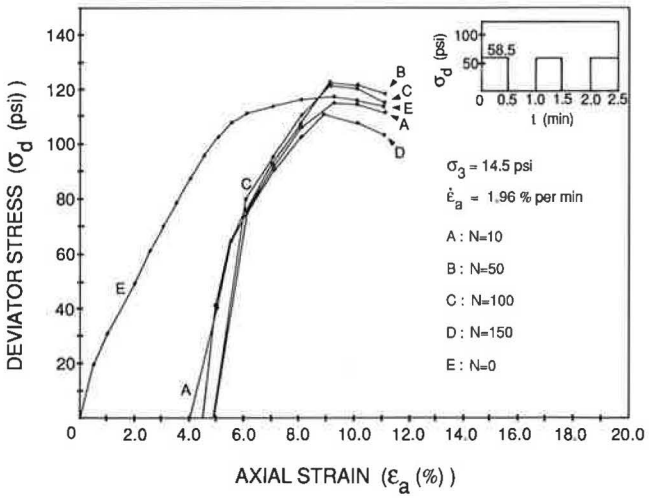

FIGURE 6 Load deformation behavior under 50 percent cyclic stress level (γ_d = 129.5 lb/ft³, m = 10 percent).

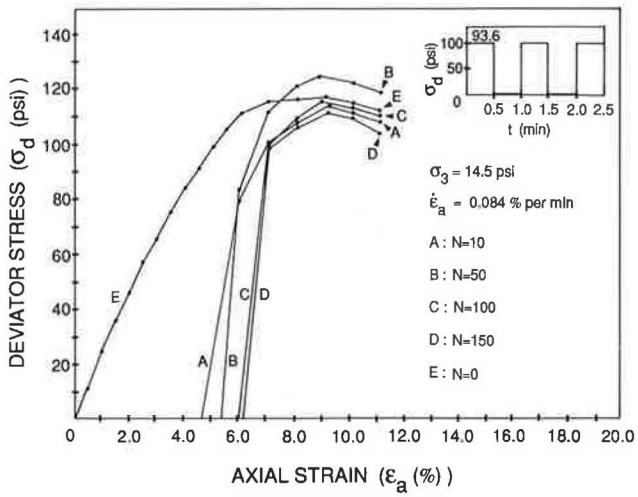

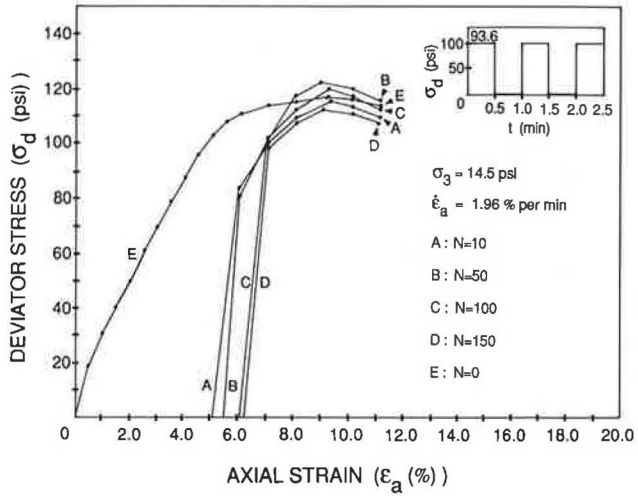

FIGURE 7 Load deformation behavior under 80 percent cyclic stress level (γ_d = 129.5 lb/ft³, m = 10 percent).

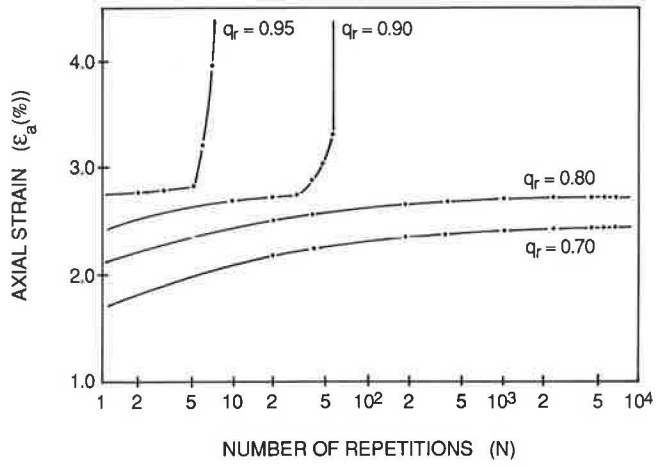

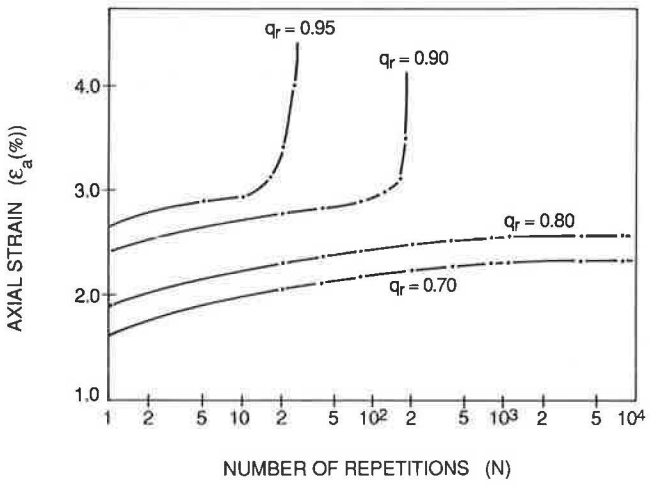

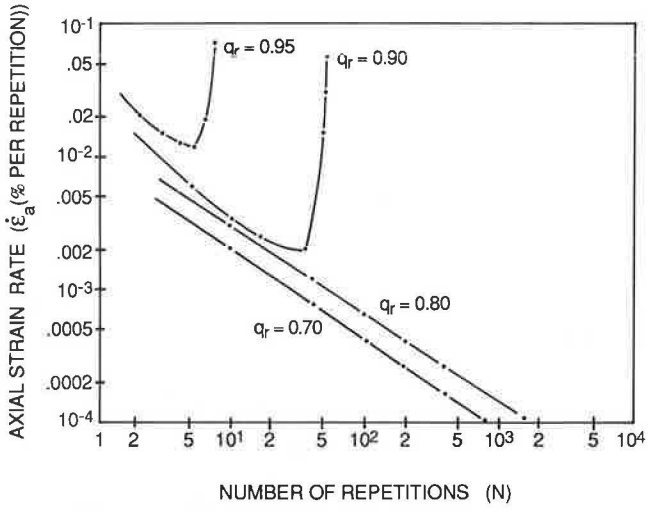

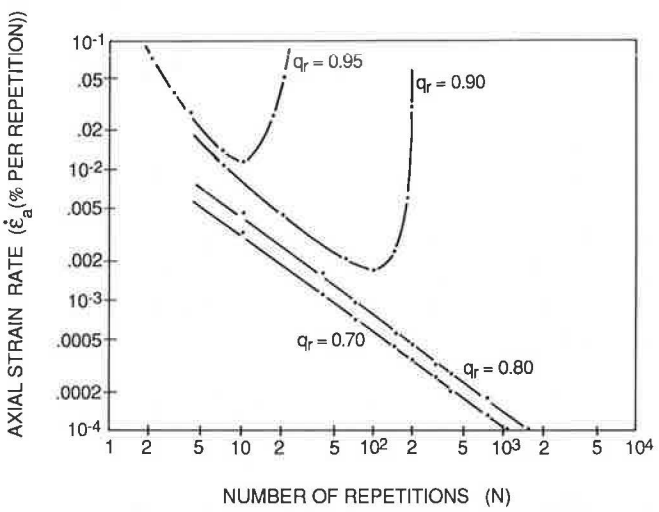

FIGURE 8 Variation of axial strain and axial strain rate with number of stress repetitions (σ_3 = 0, γ_d = 129.5 lb/cu^3, m = 7 percent).

FIGURE 9 Variation of axial strain and axial strain rate with number of stress repetitions (σ_3 = 14.5 psi, δ_d = 129.5 lb/ft^3, m = 7 percent).

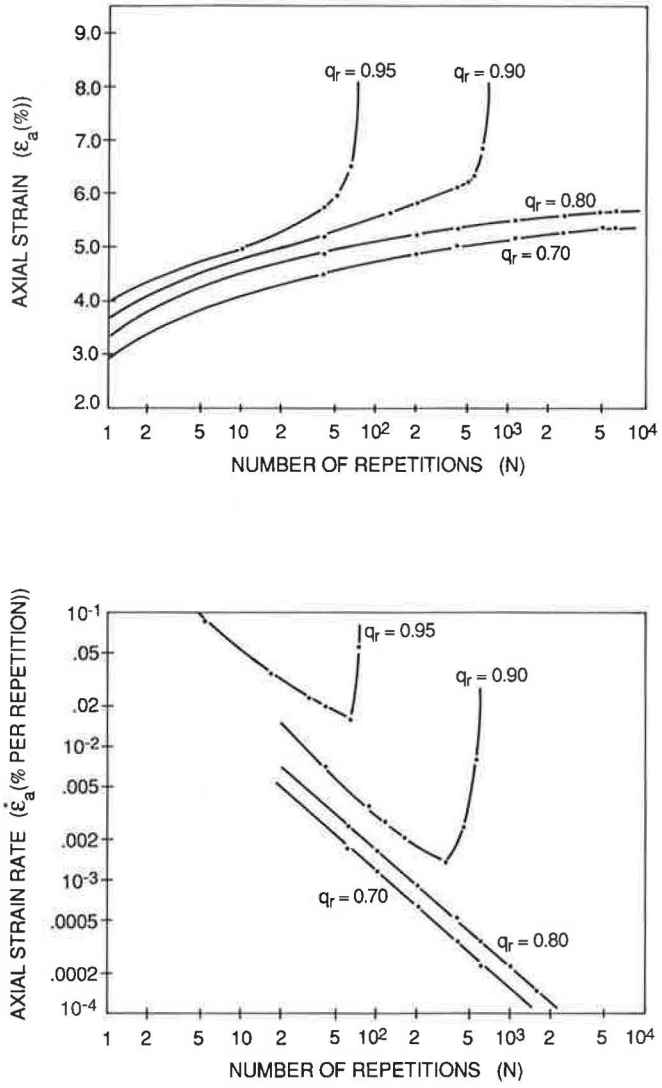

FIGURE 10 Variation of axial strain and axial strain rate with number of stress repetitions (σ_3 = 0, γ_d = 129.5 lb/ft^3, m = 10 percent).

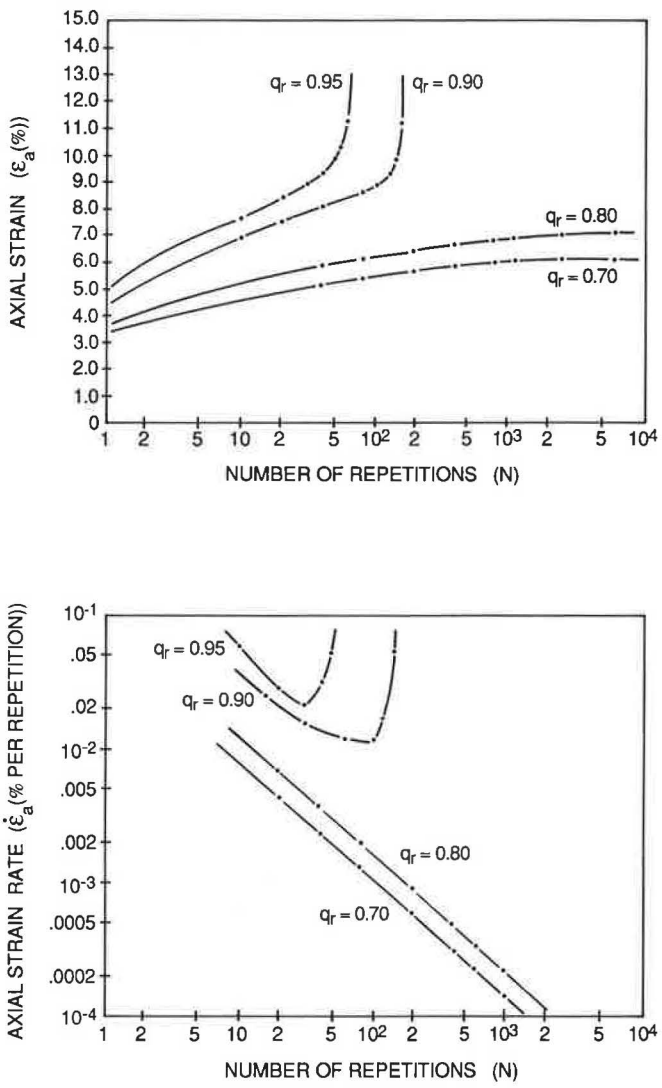

FIGURE 11 Variation of axial strain and axial strain rate with number of stress repetitions (σ_3 = 14.5 psi, γ_d = 129.5 lb/ft^3, m = 10 percent).

TABLE 4 VARIATION OF FAILURE STRAIN DETERMINED FROM TRIAXIAL, CYCLIC, AND REPEATED LOAD TESTS

Compaction Properties	Failure Strain, ϵ_f(%)	
	σ_3 = 0	σ_3 = 14.5 psi
γ_d = 129.5 lb/cu ft m = 7 %	2.70 - 2.90	2.80 - 3.20
γ_d = 129.5 lb/cu ft m = 10 %	5.90 - 6.20	8.80 - 9.40

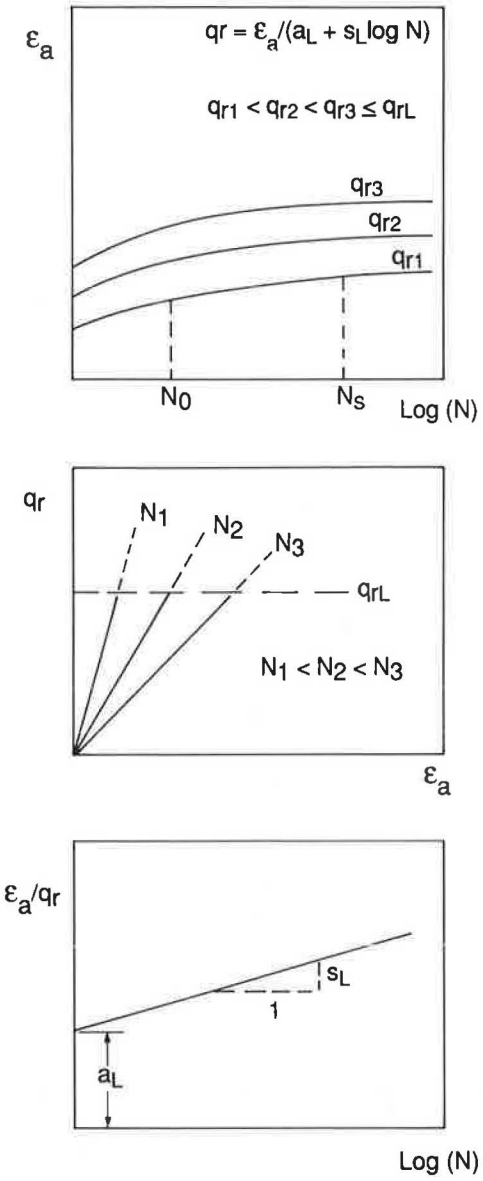

FIGURE 12 Schematic illustration of repeated load model for low stresses.

Repeated applications of stress level with a magnitude exceeding the "threshold value" lead initially to a transient variation of axial strain for N less than N_0, followed for larger N values by a steady state and then a tertiary state where the rate of axial strain will increase, leading eventually to failure when N reaches N_f. Values of N_0 were estimated to be generally less than 5. In the range where N is between N_0 and N_f, the repeated load data for axial strain, repeated stress level, and number of repetitions can be represented by the following relation:

$$q_r = \frac{\epsilon_a}{a_h + b_h \epsilon_a} \tag{2}$$

where

$$b_h = B_h + S_h \log N \tag{3}$$

and a_h, B_h, and S_h are material parameters.

Equation 2 indicates that the variation of q_r and ϵ_a for a given N is hyperbolic. For a given N, a_h and b_h can be determined from a plot of ϵ_a/q_r versus ϵ_a, as is indicated in Figure 13. Repeated load test data for the compacted silty clay were analyzed to determine material parameters in Equations 2 and 3. In this case, the variation of a_h for different values of N was found relatively insignificant, and the average a_h for

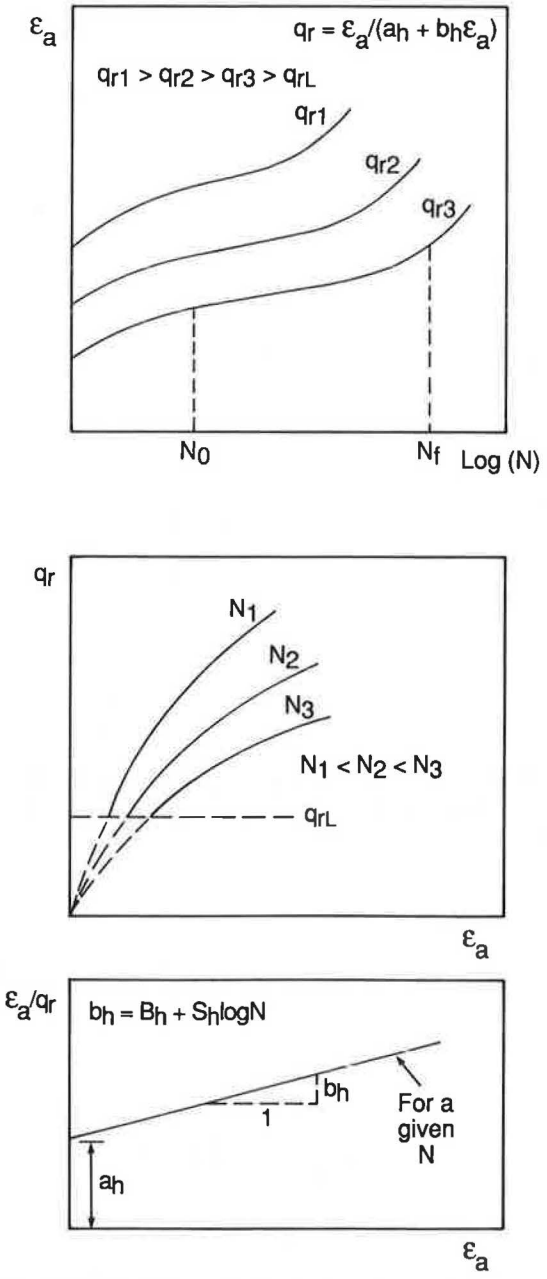

FIGURE 13 Schematic illustration of repeated load model for high stresses.

at least three selected values of N covering the range between N_0 and N_f was determined. The corresponding values of b_h were then used to find B_h and S_h in Equation 3.

The axial strain ϵ_a in Equations 1 and 2 is expressed in percent, and the corresponding material parameters are summarized in Table 5 for all testing conditions. Predictions using the proposed model are compared with experimental results in Figures 14 and 15. Model predictions of axial strains are within ±10 percent of experimental values.

SUMMARY AND CONCLUSIONS

A load-deformation model for subgrade soils is developed, where total cumulative axial strains are correlated with applied stresses and number of load repetitions and is based on the results of repeated load tests conducted on a compacted silty clay. The concept of a constant failure strain independent of load history was used in the proposed model. Results of static triaxial tests, slow cyclic tests, and repeated load tests for the compacted silty clay were used to verify that the strain at failure for given compaction conditions and confining pressure is essentially independent of stress history. Good agreement was obtained between predicted strain values by using the proposed model and experimental values from repeated load tests. Model predictions were within ±10 percent of experimental results.

ACKNOWLEDGMENTS

The experimental investigation presented in this paper was conducted at the American University of Beirut. Most of the analyses were performed at the University of Alaska, Fairbanks. The help provided by the Civil Engineering Department at both universities is greatly appreciated.

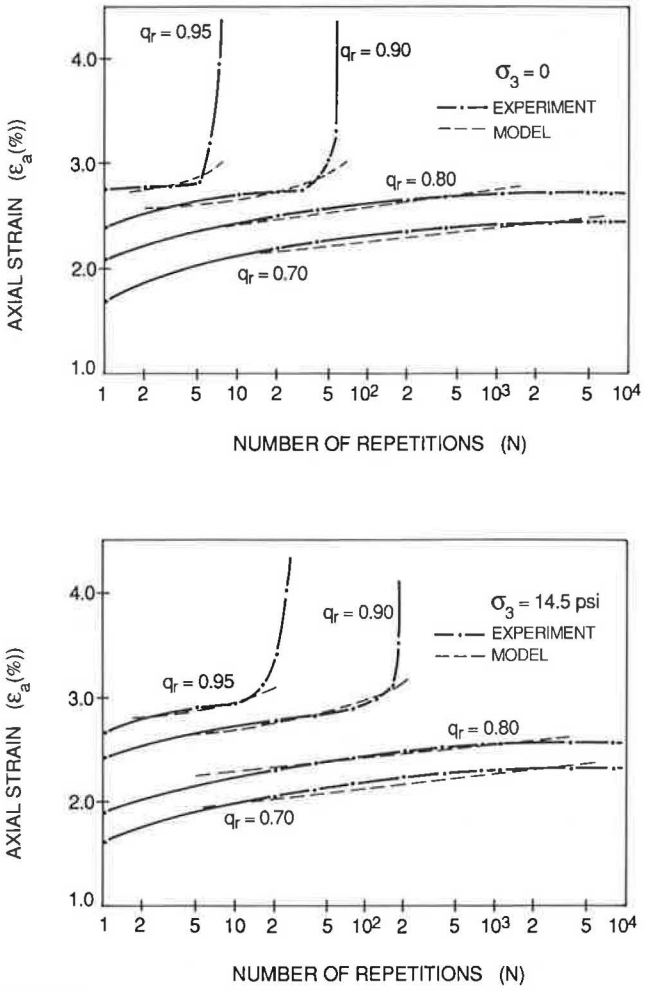

FIGURE 14 Verification of model predictions for specimens compacted dry of optimum (γ_d = 129.5 lb/ft³, m = 7 percent).

TABLE 5 PARAMETERS USED IN THE PROPOSED SUBGRADE REPEATED-LOAD MODEL

		Subgrade repeated-load model					Failure Strain
		Low Stresses ($q_r \leq 0.80$)		High Stresses ($q_r > 0.80$)			
		a_L	s_L	a_h	B_h	S_h	ϵ_f (%)
Dry of optimum compaction	γ_d = 129.5 lb/cu ft, m = 7 %, σ_3 = 0	2.78	0.231	1.96	0.322	0.0586	2.82
	γ_d = 129.5 lb/cu ft, m = 7 %, σ_3 = 14.5 psi	2.74	0.160	1.85	0.371	0.0588	2.91
Wet of optimum compaction	γ_d = 129.5 lb/cu ft, m = 10 %, σ_3 = 0	5.25	0.648	4.30	0.0253	0.170	6.00
	γ_d = 129.5 lb/cu ft, m = 10 %, σ_3 = 14.5 psi	5.71	0.950	3.90	0.380	0.163	9.02

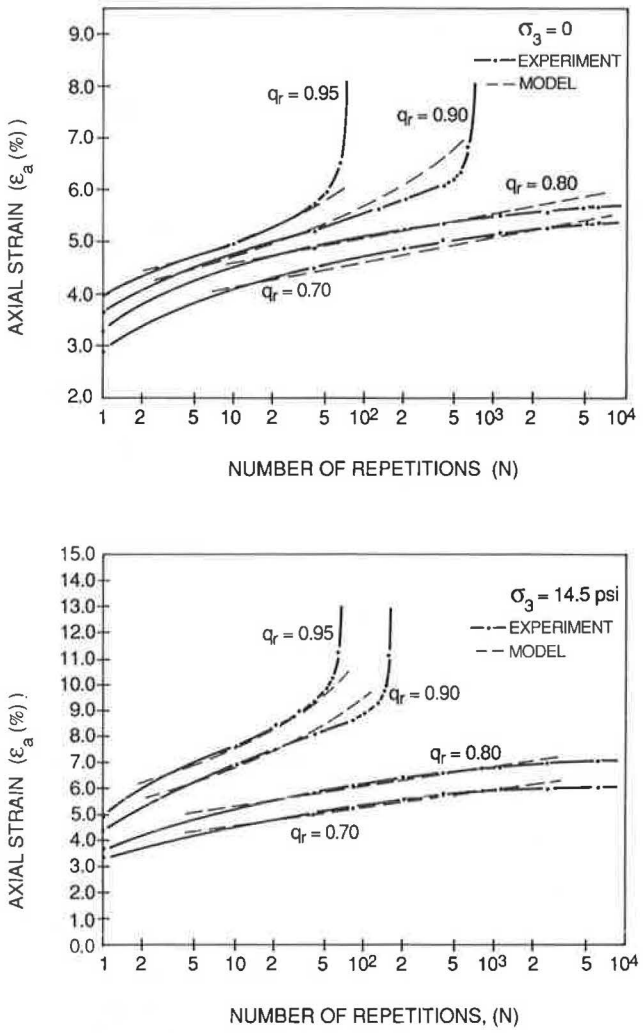

FIGURE 15 Verification of model predictions for specimens compacted wet of optimum (γ_d = 129.5 lb/ft^3, m = 10 percent).

REFERENCES

1. S. F. Brown and J. W. Pappin. Analysis of Pavements with Granular Basis. In *Transportation Research Record 810*, TRB, National Research Council, Washington, D.C., 1981, pp. 17–23.
2. L. Raad and J. L. Figueroa. Load Response of Transportation Support Systems. *Journal of the Transportation Engineering Division*, ASCE, Vol. 106, No. TE1, 1980, pp. 111–128.
3. C. L. Monismith, H. B. Seed, F. G. Mitry, and C. K. Chan. Prediction of Pavement Deflections from Laboratory Repeated Load Tests. *Proc., Second International Conference on the Structural Design of Asphalt Pavements*, 1968, pp. 109–410.
4. *Shell Pavement Design Manual: Asphalt Pavements and Overlays for Road Traffic.* Shell International Petroleum Company Limited, London, England, 1978.
5. M. I. Darter and A. J. Devos. *Structural Analysis of Asphaltic Cold Mixtures Used in Pavement Bases.* Project IHR-505, Research Report 505-4. University of Illinois, Engineering Experiment Station, Aug. 1977.
6. Y. T. Chou, R. L. Hutchinson, and H. H. Ulery, Jr. A Design Method for Flexible Airfield Pavements. In *Transportation Research Record 521*, TRB, National Research Council, Washington, D.C., 1974.
7. M. W. Witczak. Design of Full Depth Asphalt Airfield Pavements. *Proc., Third International Conference on the Structural Design of Asphalt Pavements*, London, England, 1972, pp. 550–567.
8. J. Poulsen and R. N. Stubstad. *Laboratory Testing of Intact Cohesive Subgrades: Results and Implications Relative to Structural Pavement Design and Distress Models.* Interim Report 76. National Danish Road Laboratory, November 1977.
9. W. A. Barker and W. N. Brabston. *Development of a Structural Design Procedure for Flexible Airport Pavements.* Technical Report S-75-17, Soils and Pavements Laboratory, U.S. Army Corps of Engineers Waterways Experiment Station, Vicksburg, Miss., Sept. 1975.
10. K. R. Peattie. A Fundamental Approach to the Design of Flexible Pavements. *Proc., International Conference on the Structural Design of Asphalt Pavements*, Ann Arbor, Mich., 1962, pp. 403–411.
11. R. D. Barksdale. *Repeated Load Testing Evaluation of Base Course Materials.* GHD Research Project 7002, Final Report. FHWA, U.S. Department of Transportation, 1972.
12. R. M. Knutson, M. R. Thompson, T. Mullin, and S. D. Tayabji. *Materials Evaluation Study.* Report FRA-OR and D-77-02. Ballast and Foundation Research Program, Federal Railroad Administration, Washington, D.C., 1977.
13. C. L. Monismith, K. Inkabi, C. R. Freeme, and D. B. McLean. A Subsystem to Predict Rutting in Asphalt Concrete Pavement Structures. *Proc., Fourth International Conference on the Structural Design of Asphalt Pavement*, Ann Arbor, Mich., 1977, pp. 529–539.
14. L. Raad, D. Weichert, and A. Haidar. Shakedown and Fatigue of Pavements with Granular Bases. In *Transportation Research Record 1227*, TRB, National Research Council, Washington, D.C., 1989.
15. Y. P. Vaid and R. G. Campanella. Time-Dependent Behavior of Undisturbed Clay. *Journal of the Geotechnical Engineering Division*, ASCE, Vol. 123, 1977, pp. 693–709.
16. J. K. Mitchell. *Fundamentals of Soil Behavior.* John Wiley and Sons, Inc., New York, 1976.
17. A. Ansal and A. Erken. Undrained Behavior of Clay Under Cyclic Shear Stress. *Journal of Geotechnical Engineering*, ASCE, Vol. 115, No. 7, 1989, pp. 968–983.
18. B. A. Zeid. *Load-Deformation Behavior of a Compacted Silty Clay Under Different Forms of Loading.* M.E. thesis. American University of Beirut, Beirut, Lebanon, 1988.
19. J. G. Larew and G. A. Leonards. A Strength Criterion for Repeated Loads. In *Highway Research Record 41*, HRB, National Research Council, Washington, D.C., 1962, pp. 529–556.
20. S. F. Brown, A. F. K. Lashine, and A. F. L. Hyde. Repeated Load Triaxial Testing of Silty Clay. *Geotechnique*, Vol. 25, No. 1, 1975, pp. 95–114.

Publication of this paper sponsored by Committee on Soil and Rock Properties.

Repeated Load Model for Subgrade Soils: Model Applications

LUTFI RAAD AND BASSAM A. ZEID

A load-deformation model for subgrade soils where total cumulative axial strains are correlated with applied stresses and number of repetitions is used to study the behavior of subgrade soils under repeated loads and to investigate the load repetition effects on subgrade modulus and shear strength. Predictions of allowable stresses for different limiting strains are also established, and limiting criteria in terms of applied stresses and number of repetitions to failure are compared with other subgrade criteria available in the literature. Model predictions indicate that the subgrade modulus increases for repeated stresses lower than a "threshold stress" and assumes a constant value with increased number of load repetitions. For higher stresses, the modulus decreases, indicating a strain-softening behavior and a corresponding increase in the rate of accumulation of axial strains. On the other hand, cohesion and friction associated with failure under repeated loads decrease with increase in number of repetitions to failure. The variation of repeated stress level with number of repetitions to failure determined by the proposed model is compared with subgrade criteria suggested by other investigators. Stress predictions by using those criteria are generally conservative for number of repetitions greater than about 10^3. For smaller number of repetitions, those criteria could be nonconservative. Moreover, permanent strain predictions by those criteria for number of load repetitions greater than 10^4 could range from 20 percent to 25 percent of the permanent strains at failure as determined by the proposed model.

The repeated load behavior of subgrade soils is generally considered to be of major significance on the performance of pavement structures. Present subgrade models provide correlations between repeated stresses and resilient or recoverable strains (*1–3*) and between repeated stresses and permanent or plastic strains (*4–6*). Those correlations are used to predict pavement response and assess pavement performance in terms of fatigue and rutting. However, because those conditions are limited to stresses and resilient strains or stresses and permanent strains, their incorporation in numerical algorithms such as the finite-element method will lead to solutions that do not satisfy kinematic conditions between displacements and total strains. Moreover, available subgrade models do not account for subgrade failure under repeated loads and therefore are limited in their assessment of pavement stability. Raad et al. (*7–9*) have indicated that the shear strength of pavement layers have a significant effect on whether the accumulation of strains under repeated load applications will proceed at an increasing rate or whether it will cease and thus lead to a shakedown condition and a stable response.

L. Raad, Institute of Northern Engineering, University of Alaska, Fairbanks, Alaska 99775. B. A. Zeid, Dar Al-Handassah (Shair and Partners), Beirut, Lebanon.

In a companion paper by Raad and Zeid in this Record, a load deformation model for subgrade soils is developed where total cumulative axial strains are correlated with applied stresses and number of load repetitions. The concept of constant failure strain independent of load history is presented and used in the proposed model.

In this paper, the proposed model is applied to study the behavior of subgrade soils under repeated loads. Specifically, the following points are investigated:

1. The effects of load repetitions on subgrade modulus and shear strength;
2. The relation between repeated stress state, limiting strain, and number of repetitions to failure; and
3. The variation of repeated stress level with number of load repetitions to failure as determined by the proposed model in comparison with subgrade criteria suggested by other investigators.

PROPOSED MODEL

A repeated load model for subgrade soils has been proposed and is based on results of static triaxial tests, slow cyclic tests, and repeated load tests for a compacted silty clay. Details of model development are presented elsewhere (see companion paper in this Record). According to this model, the behavior of the compacted silty clay in terms of axial strain ϵ_a, repeated load stress level q_r (defined as the ratio of repeated deviator stress to the strength obtained from a standard triaxial test at a strain rate of 0.5 percent/min), and number of load repetitions N depends on the magnitude of the applied stress level relative to the "threshold stress level" q_{rl}. The "threshold stress level" corresponds to the stress level below which the accumulation of axial strains will eventually cease and lead to a stable response and above which progressive accumulation of axial strains will occur and cause unstable response and ultimate failure. The failure strain in this case is dependent on confining pressure, dry density, and compaction moisture content but is independent of stress history. The "threshold stress level" for the repeated load tests performed lies between 0.80 and 0.90.

For repeated stress level values smaller than q_{rl},

$$q_r = \frac{\epsilon_a}{a_L + s_L \log N} \quad (1)$$

where a_L and s_L are material parameters.

For repeated stress level values greater than q_{rl},

$$q_r = \frac{\epsilon_a}{a_h + b_h \epsilon_a} \quad (2)$$

where

$$b_h = B_h + S_h \log N \quad (3)$$

and a_h, B_h, S_h are material parameters. The axial strain ϵ_a in Equations 1 and 2 is expressed in percent.

A summary of shear strength characteristics and model parameters for different dry density γ_d, compaction moisture content m, and confining pressure σ_3 is presented in Tables 1 and 2, respectively.

Incorporating the concept of a constant strain at failure into the proposed model allows assessment of upper-bound stress levels above which the subgrade will exhibit progressive increase in strains with number of load repetitions and below which the subgrade will have a stable response and the accumulation of strains will eventually cease. Those limiting stresses could be used to define failure criteria under repeated loads. The need for such criteria in advanced numerical analysis of pavement systems has been addressed by Raad and Figueroa (*3*) and more recently by Raad et al. (*7–9*). Moreover, the proposed model could be used to estimate the magnitude of total strains in the subgrade and, therefore, the permanent strains if the resilient strains are known.

MODEL APPLICATIONS

Load Repetition Effects on Subgrade Modulus and Shear Strength

The effects of repeated load applications on subgrade modulus were determined by using the proposed model defined in

TABLE 1 SHEAR STRENGTH CHARACTERISTICS OF THE SILTY CLAY

Compaction Properties	Cohesion C (psi)	Angle of Friction ϕ(degrees)	Undrained compressive strength σ_{df} (psi)	
			$\sigma_3 = 0$	$\sigma_3 = 14.5$ psi
γ_d = 129.5 lb/cu ft m = 7 %	39.0	32	140	173
γ_d = 129.5 lb/cu ft m = 10 %	23.0	32	83	117

NOTES

- Shear strength properties were determined using strain-controlled undrained triaxial tests with rate of applied strain equal to 0.50 percent per minute.
- σ_{df} is equal to the difference of major principal stress σ_1 and minor principal stress σ_3 at failure.

TABLE 2 PARAMETERS USED IN THE PROPOSED SUBGRADE REPEATED-LOAD MODEL

		Subgrade repeated-load model					Failure Strain ϵ_f (%)
		Low Stresses ($q_r \leq 0.80$)		High Stresses ($q_r > 0.80$)			
		a_L	s_L	a_h	B_h	S_h	
Dry of optimum compaction	γ_d = 129.5 lb/cu ft m = 7 % σ_3 = 0	2.78	0.231	1.96	0.322	0.0586	2.82
	γ_d = 129.5 lb/cu ft m = 7 % σ_3 = 14.5 psi	2.74	0.160	1.85	0.371	0.0588	2.91
Wet of optimum compaction	γ_d = 129.5 lb/cu ft m = 10 % σ_3 = 0	5.25	0.648	4.30	0.0253	0.170	6.00
	γ_d = 129.5 lb/cu ft m = 10 % σ_3 = 14.5 psi	5.71	0.950	3.90	0.380	0.163	9.02

Equations 1, 2, and 3. In this case, the modulus E after N repetitions was compared with an initial modulus value E_i corresponding to N_i repetitions. The subgrade modulus E after N repetitions of a given deviator stress σ_d is defined as the ratio of the repeated deviator stress to the total axial strain ϵ_t (resilient strain plus permanent strain) experienced by the subgrade during the Nth repetition. The modular ratio E/E_i could then be used as a relative measure of subgrade modulus with number of load repetitions. For a given repeated stress level, the modular ratio is expressed as

$$\frac{E}{E_i} = \frac{\epsilon_{ii}}{\epsilon_t} \tag{4}$$

where ϵ_{ii} and ϵ_t are total axial strains during repetitions N_i and N, respectively. The strain ϵ_t could be related to the total accumulated axial strain ϵ_a and resilient strain ϵ_r by the simple relation

$$\epsilon_t = \frac{d\epsilon_a}{dN}\Delta N + \epsilon_r \tag{5}$$

where ΔN is equal to 1 and ϵ_r is assumed constant for a given repeated stress level.

For stress level values less than the "threshold value" q_{rl}, it could be shown that

$$\frac{E}{E_i} = \frac{\frac{q_r s_L}{N_i} + \epsilon_r}{\frac{q_r s_L}{N} + \epsilon_r} \tag{6}$$

and for q_r greater than q_{rL}

$$\frac{E}{E_i} = \left[\frac{(a_h S_h/N_i)}{\left(\frac{1}{q_r} - B_h - S_h \log N_i\right)^2} + \epsilon_r\right] \div \left[\frac{(a_h S_h/N)}{\left(\frac{1}{q_r} - B_h - S_h \log N\right)^2} + \epsilon_r\right] \tag{7}$$

The resilient strain ϵ_r could be determined from the following relations that define resilient modulus M_R in terms of repeated deviator stress σ_d:

For dry of optimum compaction conditions (γ_d = 129.5 lb/ft^3, m = 7 percent),

$$\log M_R = 4.56 - 0.118 \log \sigma_d \tag{8}$$

For wet of optimum compaction conditions (γ_d = 129.5 lb/ft^3, m = 10 percent),

$$\log M_R = 4.36 - 0.221 \log \sigma_d \tag{9}$$

where M_R and σ_d are expressed in pounds per square inch.

The variation of modular ratio E/E_i with number of load repetitions is shown in Figures 1 and 2. It is interesting to observe that for stresses smaller than the threshold value, subgrade strain hardening will occur and thus lead to an increase in subgrade modulus with number of stress repetitions. Conversely, for stresses larger than the threshold value, initial

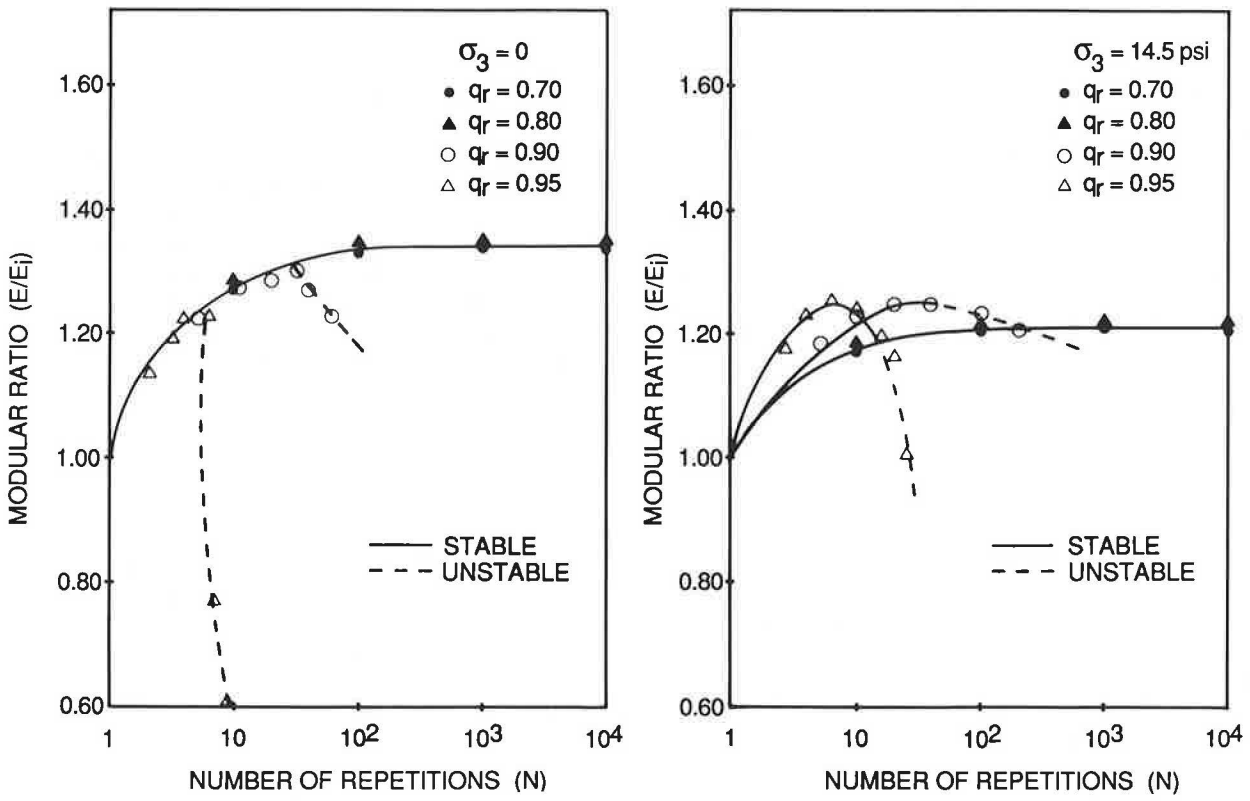

FIGURE 1 Stiffening and softening effects on subgrade under repeated loads (γ_d = 129.5 lb/ft^3, m = 7 percent).

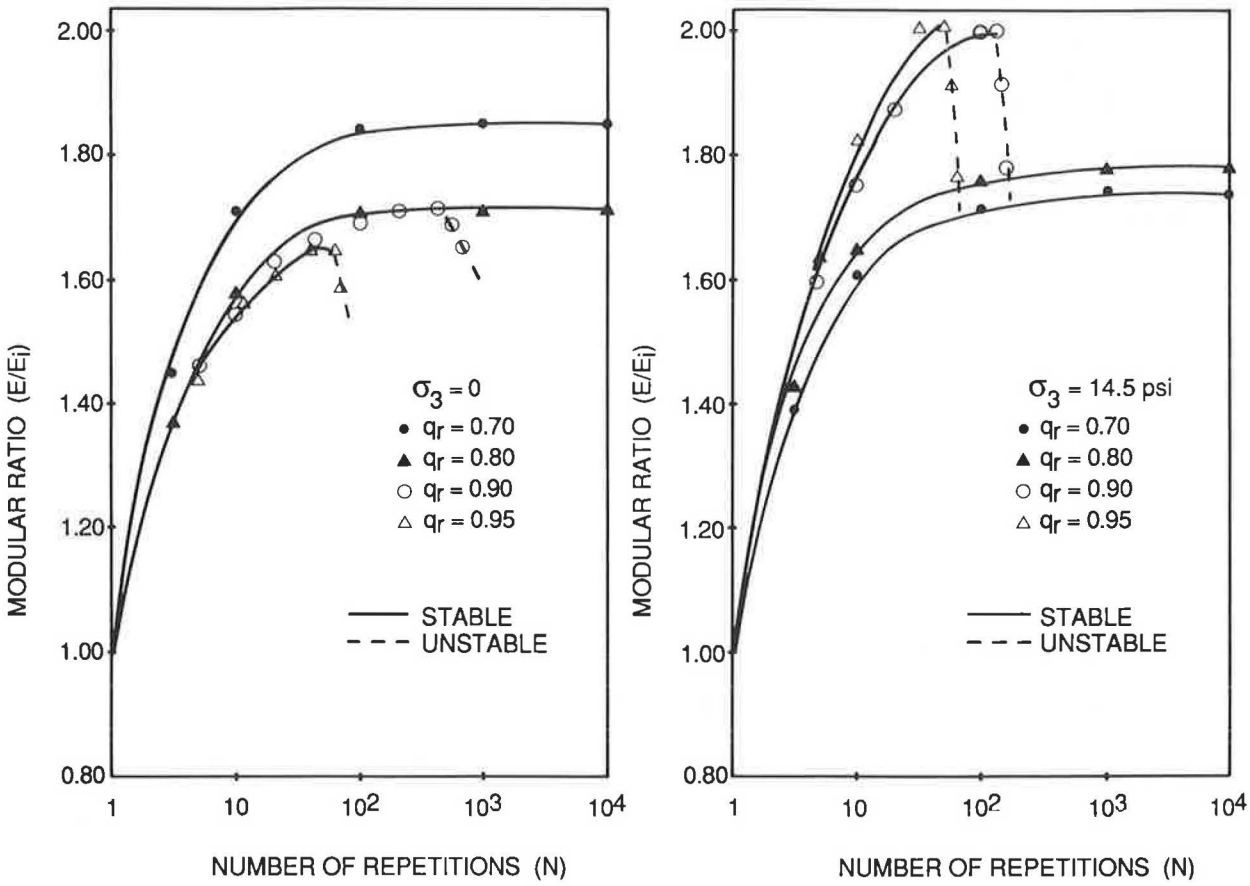

FIGURE 2 Variation of axial strain and axial strain rate with number of stress repetitions (σ_3 = 14.5 psi, γ_d = 129.5 lb/ft^3, m = 10 percent).

strain hardening is observed followed by strain softening as a result of unstable response caused by increased rate of strain accumulation. Strain-hardening effects are more pronounced for specimens with higher compaction moisture content. This could probably be attributed to local over-consolidation effects in the microstructure of the wet clay when subjected to repeated loads. However, at magnitudes of repeated loads larger than the "threshold value," the rate of accumulation of axial strains will eventually become higher and the corresponding modulus will therefore be lower.

The effect of strain hardening and strain softening on subgrade modulus and its relationship to subgrade stability can have significant practical applications. For example, if nondestructive testing equipment such as the falling weight deflectometer is used to determine the onset of subgrade softening through successive applications of loads with increasing magnitude, then a subgrade limiting load could be estimated. Progressive accumulation of strains will occur with load repetitions above this load, and below it the accumulation of strains will cease and lead to a stable subgrade response.

The proposed model was used to determine the change of shear strength parameters, the cohesion C, and angle of friction ϕ with number of load repetitions to failure. The failure strain ϵ_f is substituted in Equation 2, and the corresponding limiting principal stresses were computed for different number of repetitions to failure. Cohesion and friction associated with failure under repeated loading were compared with cohesion C_s and angle of friction ϕ_s obtained from standard strain-controlled triaxial tests at strain rate of 0.5 percent/min. Results are presented in Figure 3. A degradation effect of both cohesion and friction is observed with increase in number of repetitions to failure. The decrease appears to be more significant, particularly for cohesion, for specimens with higher compaction moisture content. This could probably be a result of higher pore-water pressure build up under repeated loading.

Limiting Criteria

Correlations between repeated stress level and number of repetitions for different limiting values of axial strain ϵ_a were derived for the compacted silty clay by using the proposed model and assuming a threshold stress level q_{rt} equal to 0.80. Those relations are presented in Figures 4 and 5. The influence of confining pressure on those limiting relations is more significant for specimens compacted wet of optimum than for dry of optimum compaction. The proposed model could also be used to determine the stress state in terms of p and q associated with a given limiting strain and a selected number

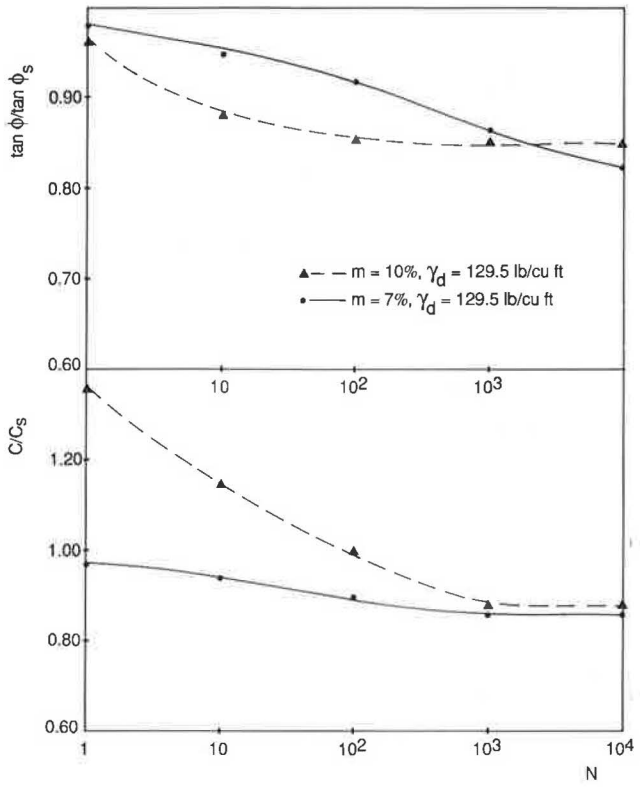

FIGURE 3 Variation of subgrade cohesion and friction with number of load repetitions.

of load repetitions. In this case,

$$p = \frac{\sigma_1 + \sigma_3}{2} \tag{10}$$

$$q = \frac{\sigma_1 - \sigma_3}{2} \tag{11}$$

where σ_1 and σ_3 are major and minor principal stresses, respectively.

The variation of p and q for different limiting strain values corresponding to number of repetitions greater than 10^4 is illustrated in Figures 6 and 7. Limiting strain criteria could be selected in this case in relation to anticipated subgrade performance under long-term repeated loading. For example, stress points higher than those defined by the p-q relationship for limiting axial strain ϵ_a equal to the failure strain ϵ_f would result in the progressive accumulation of subgrade strains with number of load repetitions and thus lead to unstable response. Conversely, for stress points located below the limiting p-q line, the response is stable and subgrade strains will eventually cease to accumulate with increased number of load repetitions. The variation of cohesion C angle of friction ϕ corresponding to number of repetitions greater than 10^4 and limiting strain ϵ_a between ϵ_f and 0.5 ϵ_f is presented in Figure 8. Values for the angle of friction, expressed as tan ϕ, lie essentially between 0.90 tan ϕ_s and 0.75 tan ϕ_s, whereas the cohesion varies in the range of $0.90C_s$ to $0.40C_s$.

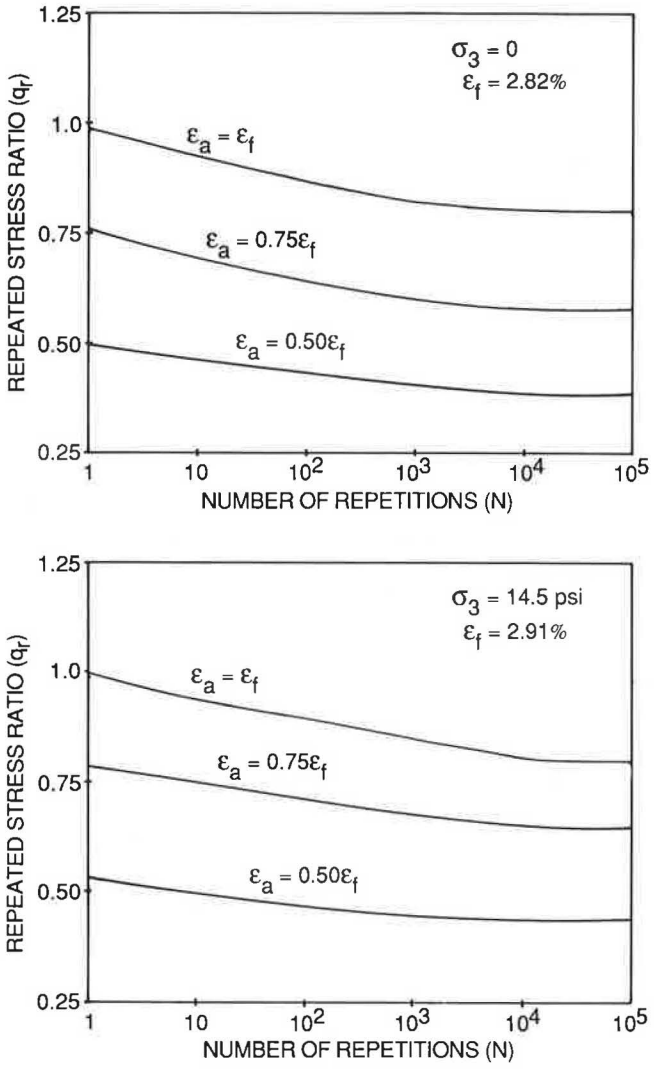

FIGURE 4 Allowable stress level for different subgrade limiting strains (γ_d = 129.5 lb/ft³, m = 7 percent).

At high moisture content and confining pressure or both, compacted clays may in some cases not exhibit a definite peak stress when tested in standard strain-controlled triaxial mode. The axial strains will progressively build up at a decreasing rate, and the test is generally stopped when the axial strain reaches 20 percent. Under repeated loading conditions, such clays may experience continuous increase in total axial strain ϵ_a and gradual decrease of the rate of strain $d\epsilon_a/dN$. In this case, a failure strain according to the definition used earlier in this paper does not exist. However, a limiting strain that corresponds to the maximum allowable value in relation to subgrade performance can be used instead. Additional research is needed to characterize the behavior of such clays and to develop improved constitutive models under repeated loads.

Comparisons with Other Models

The variation of repeated stress level with number of load repetitions to failure for the compacted silty clay as predicted

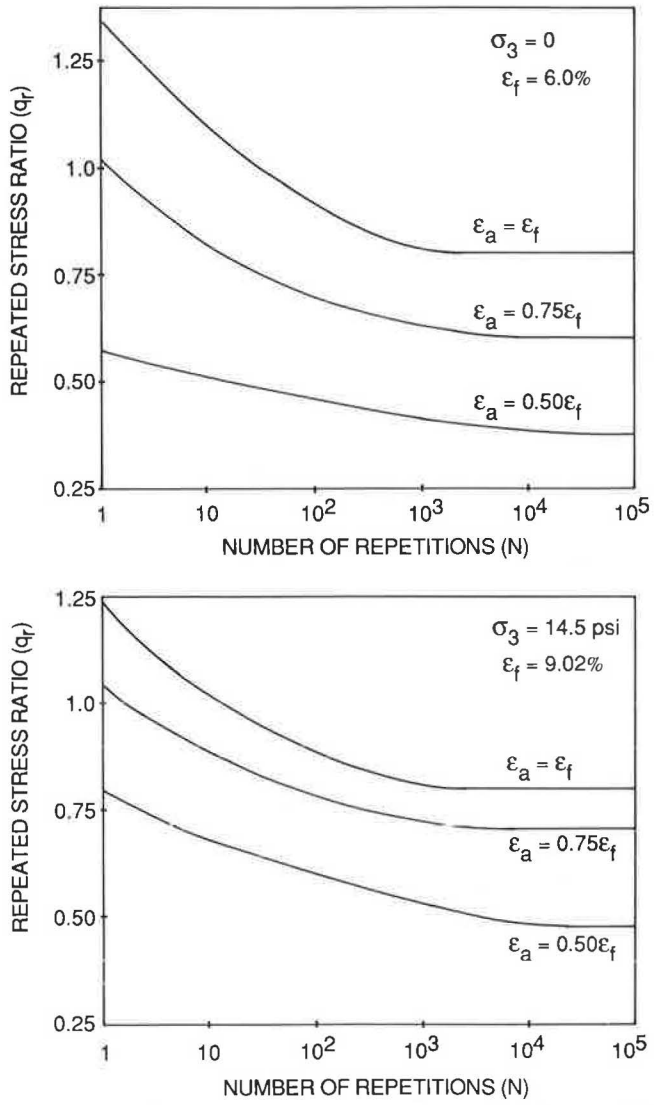

FIGURE 5 Allowable stress level for different subgrade limiting strains (γ_d = 129.5 lb/ft³, m = 10 percent).

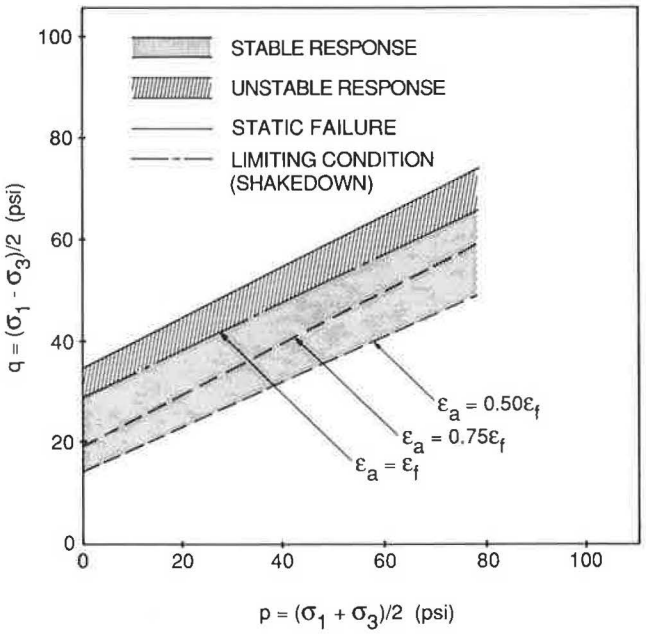

FIGURE 6 Subgrade *p-q* relations for different limiting strains (γ_d = 129.5 lb/ft³, m = 7 percent).

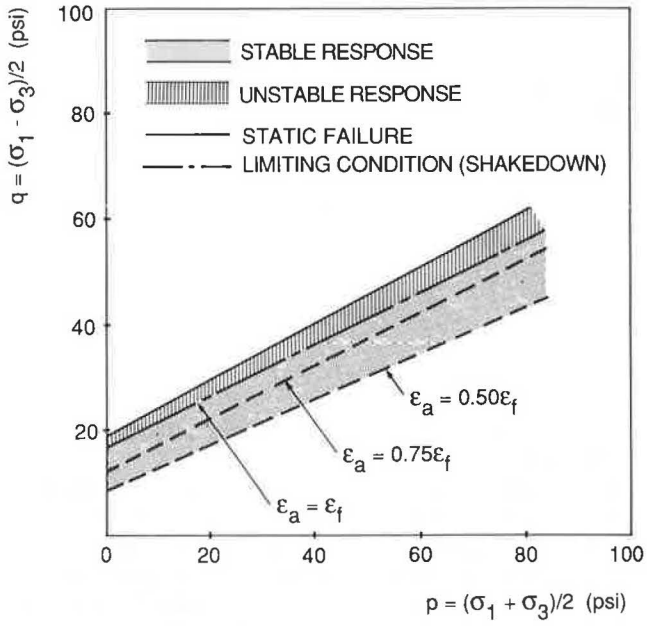

FIGURE 7 Subgrade *p-q* relations for different limiting strains (γ_d = 129.5 lb/ft³, m = 10 percent).

by the proposed model is compared with results obtained by using the Shell criterion (*10*) and other criteria developed by Darter and Devos (*11*), Poulsen and Stubstad (*12*), and Chou et al. (*13*). Comparisons presented in Figures 9 and 10 show that the Shell criterion and Darter and Devos criterion are not conservative when used for a number of load repetitions smaller than 10^2 to 10^3 and fairly conservative for a larger number of repetitions. Conversely, results obtained from criteria proposed by Poulsen and Stubstad and Chou et al. yield consistently conservative predictions. The permanent strain ϵ_p exhibited by the compacted silty clay when loaded according to those criteria is compared with values predicted by the proposed model (Table 3). Results indicate that the permanent strain is significantly higher for specimens with higher compaction moisture content. This implies that the use of existing subgrade criteria does not necessarily result in equal performance levels for different subgrade conditions. According to the criteria in Table 3, the permanent strains corresponding to load repetitions greater than 10^4 will range essentially between 0.4 percent and 2 percent in comparison with permanent strains at failure in the range of 2 percent to 8 percent as predicted by the proposed model.

SUMMARY AND CONCLUSIONS

A load-deformation model for subgrade soils where total cumulative axial strains are correlated with applied stresses

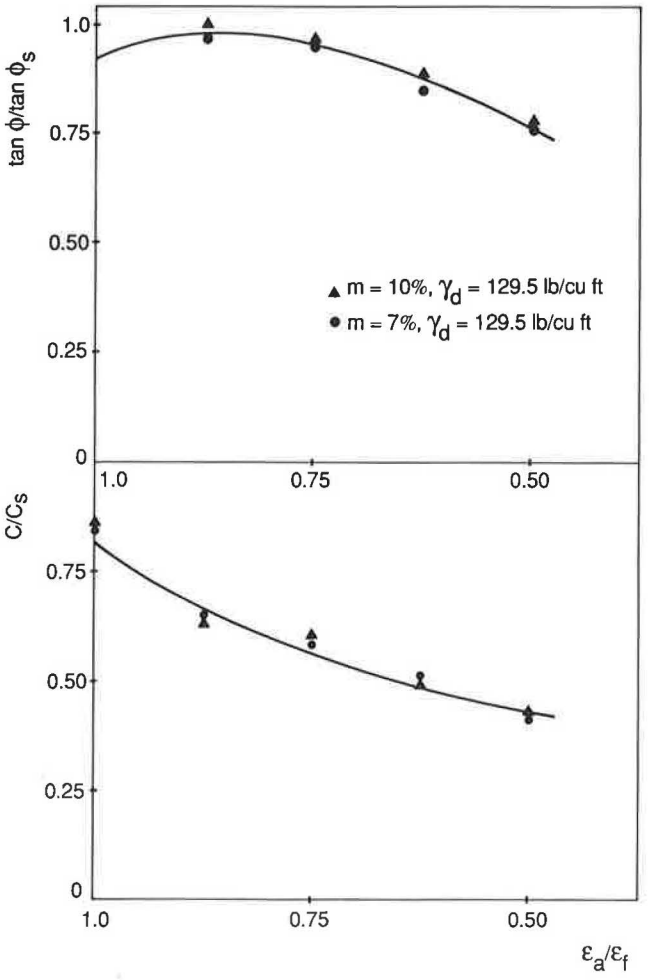

FIGURE 8 Influence of strain limits on subgrade cohesion and friction for N greater than 10^4.

and number of load repetitions was used to investigate load repetition effects on subgrade modulus and shear strength. Predictions of allowable stresses for different limiting strains were also established, and limiting criteria in terms of applied stresses and number of repetitions to failure were compared with other subgrade criteria in the literature.

Strain hardening and strain softening of the subgrade can occur, depending on the magnitude of the repeated stress relative to the "threshold stress." The subgrade modulus, defined as the ratio of repeated stress to total strain per load repetition, increases for repeated stresses lower than the "threshold stress" and maintains a constant value with increased number of load repetitions. For higher stresses, however, the modulus will eventually decrease, indicating a strain-softening behavior. If nondestructive testing equipment were to be used to determine the onset of subgrade softening through successive applications of load with increasing magnitude, then an estimate of subgrade limiting load can be determined. The accumulation of strains will cease with number of load repetitions below this value, and progressive accumulation of strains will occur above it.

Cohesion and friction associated with failure under repeated loading conditions decrease with the increase in number of

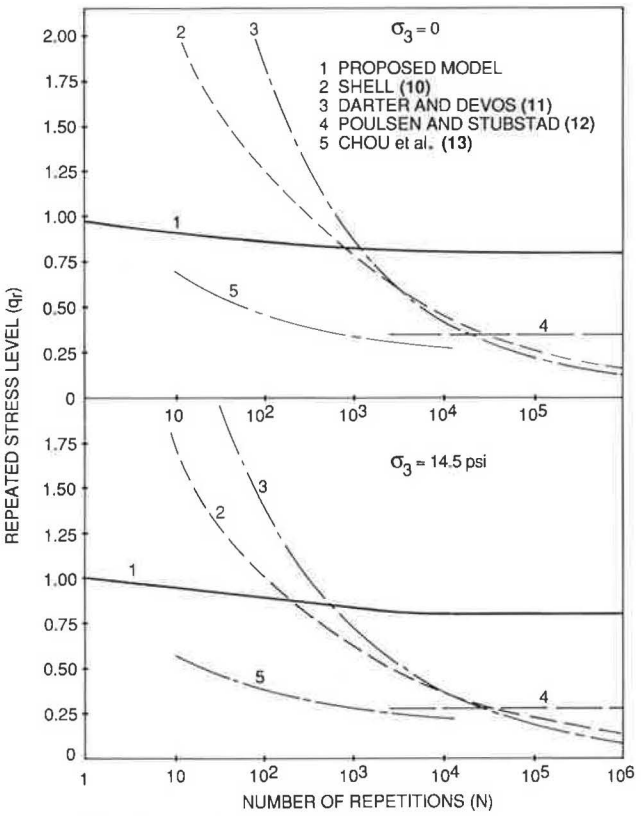

FIGURE 9 Comparisons of predicted repeated stress level at failure by using different models (γ_d = 129.5 lb/ft^3, m = 7 percent).

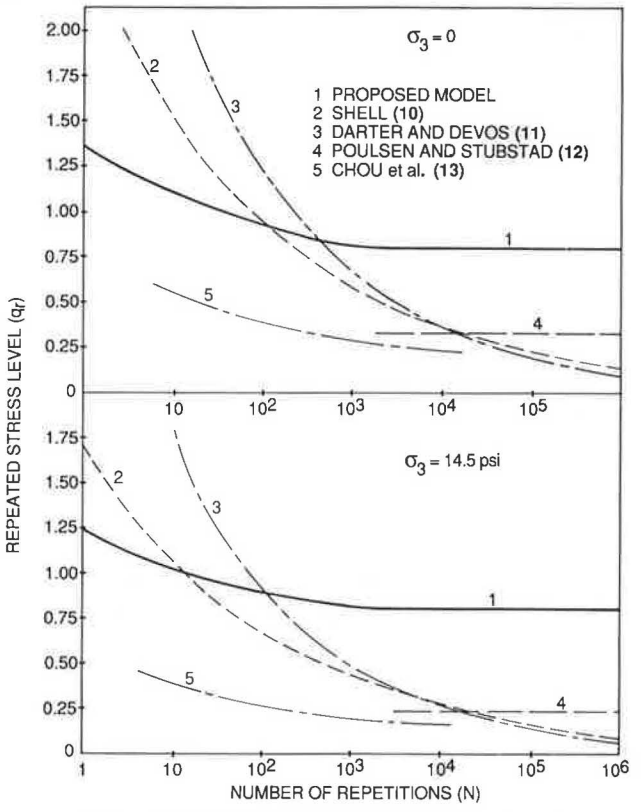

FIGURE 10 Comparisons of predicted repeated stress level at failure by using different models (γ_d = 129.5 lb/ft^3, m = 10 percent).

TABLE 3 COMPARISONS OF PERMANENT STRAIN PREDICTIONS BY DIFFERENT MODELS

	Dry of optimum (γ_d = 129.5 lb/cu ft, m = 7%)		Wet of optimum (γ_d = 129.5 lb/cu ft, m = 10%)	
	ϵ_p (%)		ϵ_p (%)	
	N = 10^4	N = 10^6	N = 10^4	N = 10^6
Proposed Model	2.23 - 2.28	2.23 - 2.28	5.27 - 7.91	5.27 - 7.91
Shell (10)	0.94 - 1.39	0.35 - 0.50	2.19 - 2.54	0.86 - 1.0
Darter & Devos (11)	0.89 - 1.29	0.18 - 0.36	2.11 - 2.39	0.70 - 0.80
Poulsen and Stubstad(12)	0.74 - 1.08	0.74 - 1.08	2.02 - 2.41	2.02 - 2.41
Chou et al. (13)	0.60 - 0.87	-	1.45 - 1.71	-

repetitions to failure. The decrease is more significant for specimens with the same dry density but higher moisture content.

Allowable repeated stress states in terms of major and minor principal stresses (i.e., *p-q* relations) were determined for different limiting strain values corresponding to number of load repetitions greater than 10^4. Similar relations can be used in advanced numerical analysis of pavement structures for the purpose of developing improved understanding of pavement behavior.

The variation of repeated stress level with number of repetitions to failure determined by the proposed model was compared with subgrade criteria suggested by other investigators. Stress predictions by those criteria are generally conservative for number of repetitions greater than about 10^3. For smaller number of repetitions, those criteria could be nonconservative. Moreover, results indicate that the permanent strains that occur in the subgrade, when loaded according to any of those criteria, is greatly influenced by compaction moisture content. In this case, the permanent strains corresponding to load repetitions greater than 10^4 will range between 0.4 percent and 2 percent in comparison with permanent strains at failure in a range of 2 percent to 8 percent as predicted by the proposed model.

ACKNOWLEDGMENTS

The analyses presented in this paper were performed at the University of Alaska, Fairbanks. The help provided by the Civil Engineering Department is greatly appreciated.

REFERENCES

1. C. L. Monismith, H. B. Seed, F. G. Mitry, and C. K. Chan. Prediction of Pavement Deflections from Laboratory Repeated Load Tests. *Proc., Second International Conference on the Structural Design of Asphalt Pavements*, 1967, pp. 109–140.
2. S. F. Brown and J. W. Pappin. Analysis of Pavements with Granular Basis. In *Transportation Research Record 810*, TRB, National Research Council, Washington, D.C., 1981, pp. 17–23.
3. L. Raad and J. L. Figueroa. Load Response of Transportation Support Systems. *Journal of the Transportation Engineering Division*, ASCE, Vol. 106, No. TE1, 1980, pp. 111–128.
4. R. D. Barksdale. *Repeated Load Testing Evaluation of Base Course Materials*. GHD Research Project 7002, Final Report. FHWA, U.S. Department of Transportation, 1972.
5. R. M. Knutson, M. R. Thompson, T. Mullin, and S. D. Tayabji. *Materials Evaluation Study*. Report FRA-OR and D-77-02. Ballast and Foundation Research Program, Federal Railroad Administration, Washington, D.C., 1977.
6. C. L. Monismith, K. Inkabi, C. R. Freeme, and D. B. McLean. A Subsystem to Predict Rutting in Asphalt Concrete Pavement Structures. *Proc., Fourth International Conference on the Structural Design of Asphalt Pavement*, Ann Arbor, Mich., 1977, pp. 529–539.
7. L. Raad, D. Weichert, and W. Najm. Stability of Multilayer Systems Under Repeated Loads. In *Transportation Research Record 1207*, TRB, National Research Council, Washington, D.C., 1988, pp. 181–186.
8. L. Raad, D. Weichert, and A. Haidar. Shakedown and Fatigue of Pavements with Granular Bases. In *Transportation Research Record 1227*, TRB, National Research Council, Washington, D.C., 1989.
9. L. Raad, D. Weichert, and A. Haidar. Analysis of Full Depth Asphalt Concrete Pavements Using Shakedown Theory. In *Transportation Research Record 1227*, TRB, National Research Council, Washington, D.C., 1989.
10. *Shell Pavement Design Manual: Asphalt Pavements and Overlays for Road Traffic*. Shell International Petroleum Company Limited, London, England, 1978.
11. M. I. Darter and A. J. Devos. *Structural Analysis of Asphaltic Cold Mixtures Used in Pavement Bases*. Project IHR-505, Research Report 505-4. University of Illinois, Engineering Experiment Station, August 1977.
12. J. Poulsen and R. N. Stubstad. *Laboratory Testing of Intact Cohesive Subgrades: Results and Implications Relative to Structural Pavement Design and Distress Models*. Interim Report 76. National Danish Road Laboratory, November 1977.
13. Y. T. Chou, R. L. Hutchinson, and H. H. Ulery, Jr. A Design Method for Flexible Airfield Pavements. In *Transportation Research Record 521*, TRB, National Research Council, Washington, D.C., 1974.

Publication of this paper sponsored by Committee on Soil and Rock Properties.

Multiaxial Testing of Subgrade

B. E. WILSON, S. M. SARGAND, G. A. HAZEN, AND ROGER GREEN

A unique testing apparatus consisting of a low-pressure multiaxial device has been applied to resilient testing of subgrade soil. Tests were conducted by applying dynamic loading under constant confining pressure. Soils from seven Ohio sites were evaluated. Laboratory results indicate that resilient behavior of the subgrade was dependent on moisture content, stress level, soil type, and density. Critical sensitivity of the resilient modulus to the moisture content was demonstrated by experiments. The testing procedure and results are discussed.

The resilient modulus is used most often in the design and rehabilitation of pavements. This parameter is given by the ratio of repeated deviator stress to the recoverable strain. The advantages of using this modulus can be seen by comparing results with data collected from a nondestructive testing apparatus, such as Dynaflect and the Falling Weight devices, where back-calculation techniques determine material moduli under dynamic loading. Nondestructive test procedures indicate that resilient modulus is a function of moisture, stress level, soil type, and density. Attempts to model the response of in situ subgrade material have been largely unsuccessful. A number of investigators have determined the resilient modulus of subgrade materials by using conventional laboratory testing devices such as unconfined compression or triaxial testing procedures (*1–3*).

This paper reports the results of a dynamic testing procedure that utilizes the multiaxial testing apparatus to obtain the resilient modulus. The low-pressure cubical system can easily be modified for dynamic testing of complex stress paths.

TESTING DEVICE

In a multiaxial device, a cubical specimen is loaded on six orthogonal faces by six flexible pressurized membranes. Any of the principal stresses can be varied independently, allowing for the simulation of complex stress histories. The three applied stresses in the direction of opposite surfaces are considered to be principal stresses. This loading will ensure that a properly prepared specimen will float between unconstrained deformations (*4–6*). A constant stress state is maintained in the horizontal planes by applying air pressure to two axes to simulate a subgrade loading. The pressure is applied with oil for the remaining axis. Here, the dynamic loading is simulated in the vertical direction by applying an alternating pressure loading. Figure 1 presents the multiaxial testing apparatus. Pressure measurements are taken in the membrane reservoir to record sample loading accurately.

Deformations were monitored along the axis of loading with six linear variable differential transformers (LVDTs). There were three LVDTs located on each face so that they were directly in line with those on the opposite face. Measurements were averaged to get the displacement of each face. Rigid body motion of the specimen could also be accounted for with this arrangement.

Pressure changes and displacements were directly measured as voltage changes. Voltages from the pressure transducer and the six LVDTs were continuously monitored with a PC-based data acquisition system. Data were recorded and stored automatically to be used in subsequent data analysis.

SAMPLE PREPARATION

Specimens were obtained from seven sites in Ohio. The location and soil classification of each site are found in Table 1.

Subgrade materials were prepared and tested in accordance with AASHTO testing procedures. The soils were sieved over a ¾-in. sieve, and coarse materials were discarded. Water was added to obtain the desired moisture content, and the sample was double bagged in plastic and stored for a minimum of 24 hr to ensure uniform moisture distribution. The specimens were compacted in a 4-in. × 4-in. × 4-in. mold to meet Ohio Department of Transportation (ODOT) field density specifications. Specimen density of each site, however, was not consistent because the varying of the moisture content made compaction of the specimens to a specific density a trial-and-error procedure. The required density was specified for a

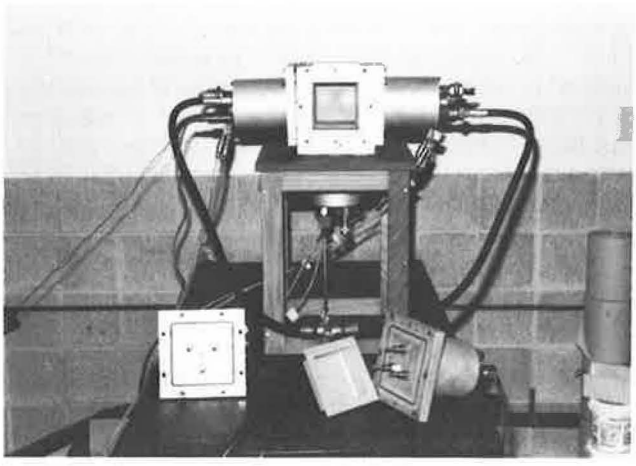

FIGURE 1 Multiaxial testing device.

B. E. Wilson, S. M. Sargand, and G. A. Hazen, Department of Civil Engineering, Ohio University, Athens, Ohio 45701. R. Green, Ohio Department of Transportation, 25 South Front St., Columbus, Ohio 43215.

TABLE 1 SITE LOCATION AND SOIL DESCRIPTION

County	Route #	Station	Description	Ohio Dept. of Transportation Classification
Jackson	32	8.68	Clay Subgrade	A-7-6
Jackson	32	20.41	Silt Clay Subgrade	A-6a
Vinton	32	1.61	Silt Clay Subgrade	A-6a
Auglaize	33	-	Clay subgrade	A-7-6
Fairfield	37	11.24	Silt Clay Subgrade	A-6a
Clark	68	-	Granular Subgrade	A-1a
Clark	675	-	Granular Subgrade	A-16

-Data Unavailable

particular soil as a percentage of the maximum dry weight that corresponded to the following specifications of ODOT.

Maximum Laboratory Dry Weight (pcf)	*Minimum Compaction Requirement (% laboratory maximum)*
90.0–104.9	102
105.0–119.9	100
120.0 and more	98

TEST PROCEDURE

Tests were performed at 5 psi confining pressure to reasonably simulate field conditions. The confining pressure was applied with air along two axes and controlled by a precision gauge and regulator. Pressure was applied with hydraulic oil to the third coordinate axis. An incompressible fluid was required because this pressure variation was used to apply dynamic loads. Pressure variation was accomplished with a simple cylinder/piston device filled with hydraulic oil and installed between loading platens of an MTS series 810 test machine. Cyclic pressure applied by the piston device was transmitted through hydraulic hoses to horizontal faces of the specimen. Loads applied were monitored with a pressure transducer.

For this application, a stress pulse with rise time of 60 to 70 msec was applied at the rate of 1 pulse/sec. Initially, a conditioning cycle consisting of 200 repetitions of five increasing increments of deviator stress was applied to minimize initial loading effects. This cycle was then repeated and the recoverable deformation recorded at or about the 200th repetition for each deviator stress level.

DISCUSSION OF RESULTS

The subgrade materials tested in this study exhibit the sensitivity of resilient modulus to percent variation of moisture content. The degree of dependence varied with soil type. As shown in Figures 2 and 3, the resilient modulus for sample JAC-32-8.68 was drastically reduced by an increase of moisture content as low as 2 percent above optimum. A similar

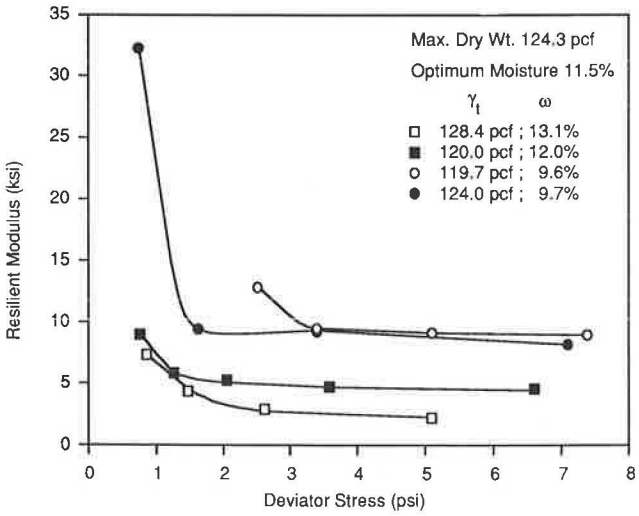

FIGURE 2 Resilient response curves for JAC-32-8.68 subgrade.

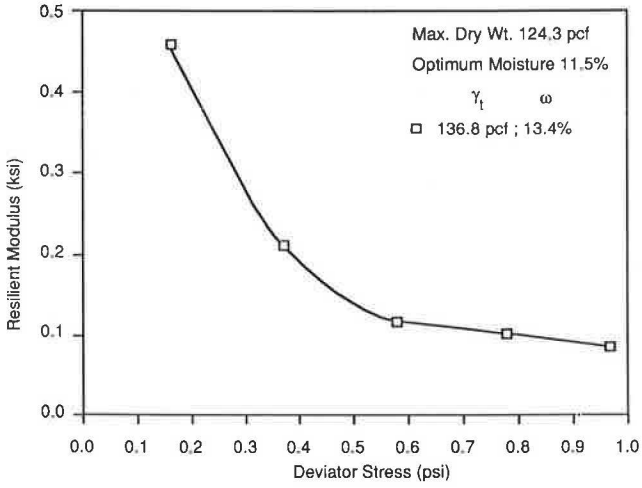

FIGURE 3 Resilient response curves for JAC-32-8.68 subgrade, γ_t, 136.8; ω, 13.4 percent.

reduction is seen in Figures 4 and 5 for the VIN-32-1.61 sample at an increase of moisture level 3 percent above optimum. The third sample from Route 32, JAC-32-20.41, does not show the sharp decrease. At 2 percent above optimum, and where the curve levels (Figure 6), a resilient modulus of approximately 5 ksi is observed. This suggests that a threshold moisture content exists that is dependent on soil type. Beyond this threshold, soil strength rapidly deteriorates. If this is true, then the threshold value was not crossed in the latter case.

The CLA-68 sample shows the least modulus variation with respect to moisture. In Figure 7 optimum moisture for CLA-68 is found to be 6.0 percent, where results are shown at moisture levels of 5.0, 5.9, and 6.3 percent. The narrow moisture range results from the sandy, granular nature of this particular soil. Increasing the moisture content further would result in drainage from the specimen during the test procedure. All tests performed on the CLA-68 soil gave slight increases in resilient modulus at higher deviator stresses.

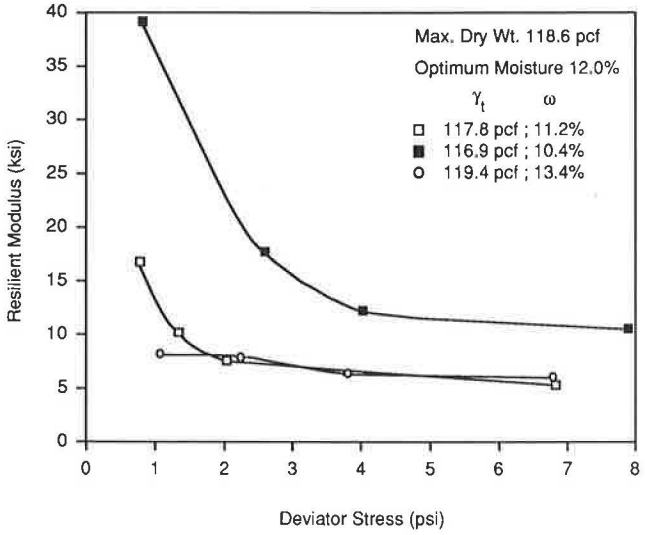

FIGURE 4 Resilient response curves for VIN-32-1.61 subgrade.

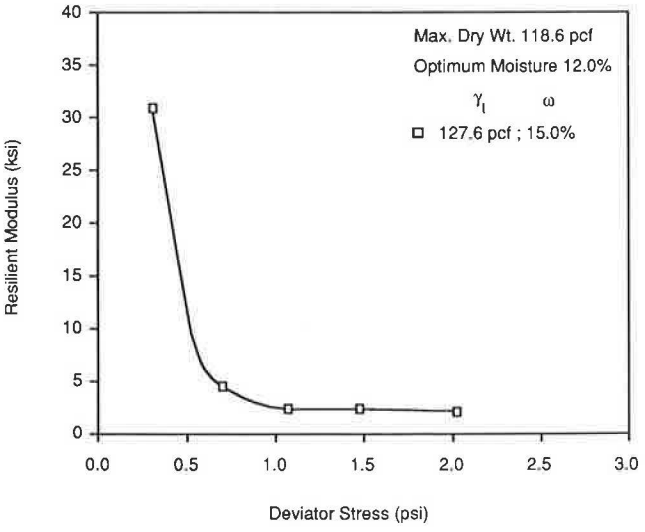

FIGURE 5 Resilient response curves for VIN-32-1.61 subgrade, γ_t, 127.6; ω, 15.0 percent.

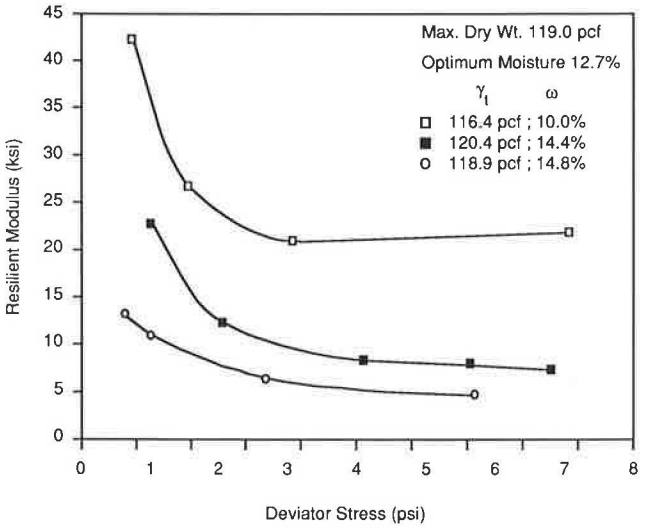

FIGURE 6 Resilient response curves for JAC-32-20.41 subgrade.

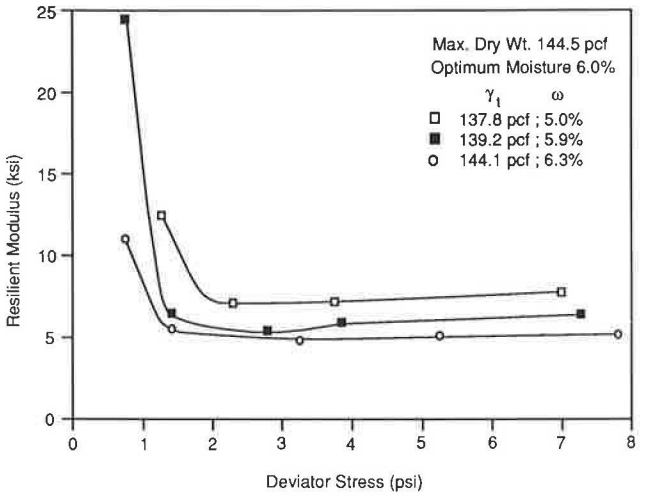

FIGURE 7 Resilient response curves for CLA-68 subgrade.

Experimental results from the remaining three sites (AUG-33, FAI-37-11.24, and CLA-675) (Figures 8–12) follow the established trend. Although the moisture content for the CLA-675 site ranged as high as 2.6 percent above optimum, it, as for the JAC-32-20.41 specimen, does not exhibit the dramatic reduction in resilient modulus common to the other samples.

All figures show higher moduli at low stress levels, followed by sharp decreases before becoming essentially constant. Also, it is important to note that although the specimen density varied in addition to the moisture content, a small variation of moisture content greatly affected the resilient moduli.

CONCLUSIONS

The multiaxial apparatus functions well when subgrade materials are tested in a dynamic environment. With this unique

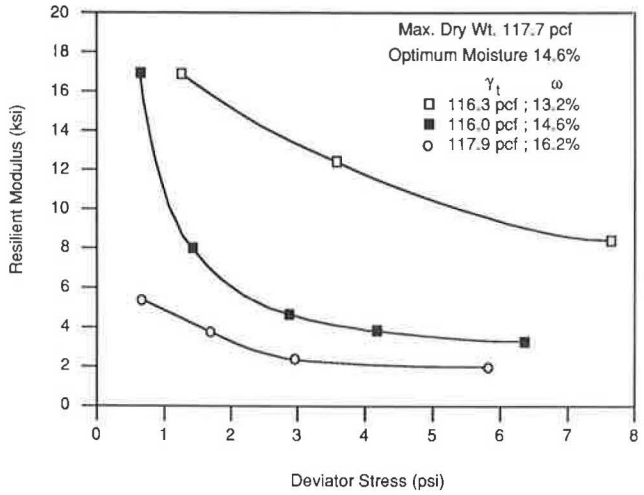

FIGURE 8 Resilient response curves for AUG-33 subgrade.

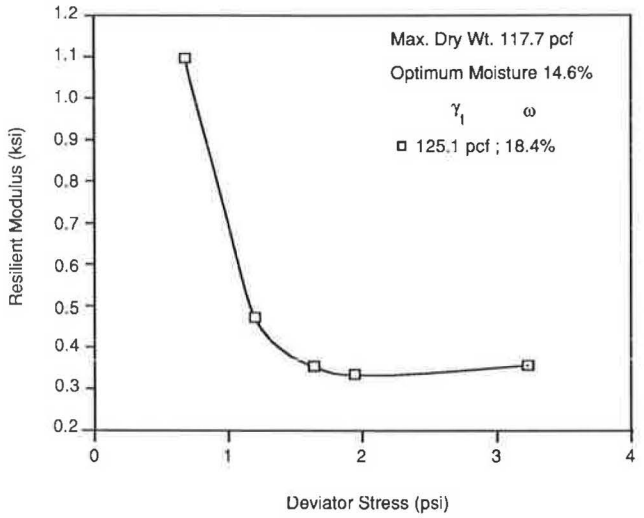

FIGURE 9 Resilient response curves for AUG-33 subgrade, γ_t, 125.1; ω, 18.4 percent.

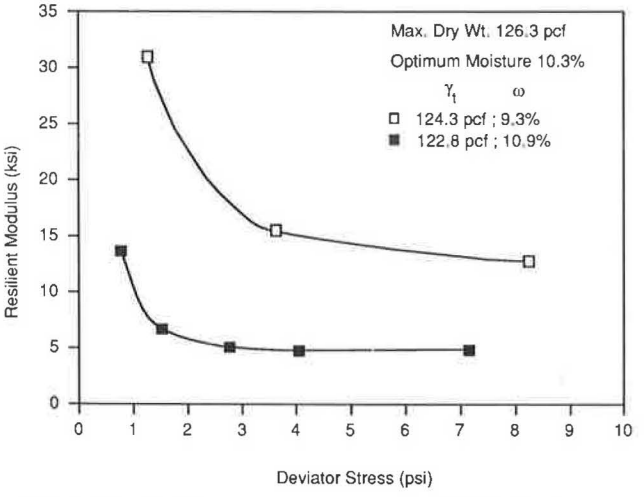

FIGURE 10 Resilient response curves for FAI-37-11.24 subgrade, part 1.

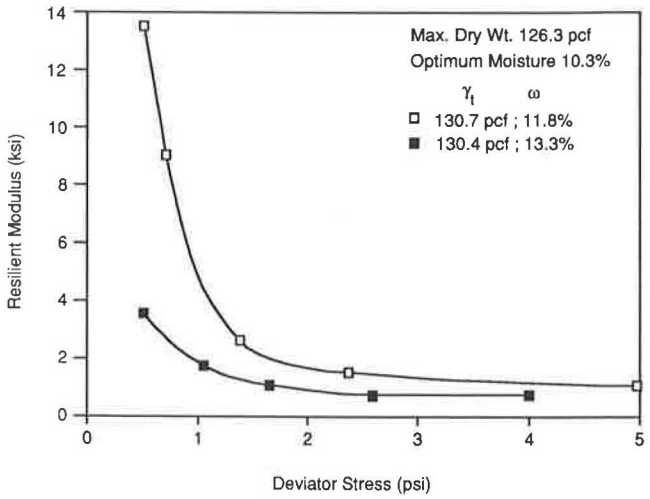

FIGURE 11 Resilient response curves for FAI-37-11.24 subgrade, part 2.

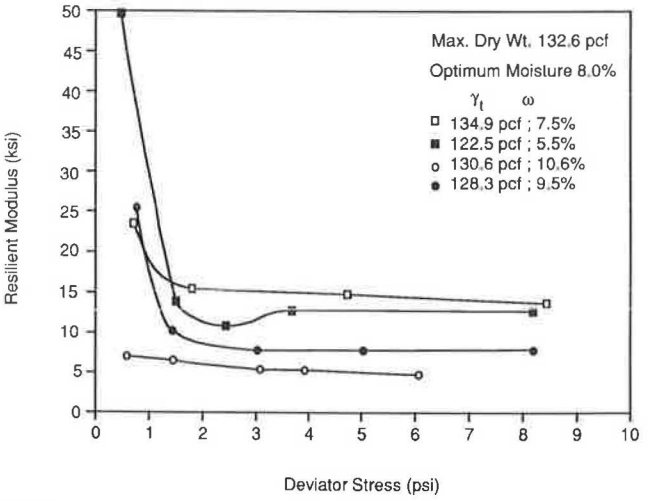

FIGURE 12 Resilient response curves for CLA-675 subgrade.

testing procedure, the following general conclusions can be drawn regarding subgrade response:

1. Resilient moduli are a function of moisture content, density, and deviator stress to varying extents depending on soil type.
2. For a particular soil at a given stress level, resilient modulus is very sensitive to the changes of moisture content.
3. The resilient modulus rapidly decreases with increasing deviator stress at low levels of stress (0 to 2 psi) and generally levels off or slightly increases at higher levels of deviator stress (2 to 8 psi). This indicates that the resilient modulus of the subgrade increases with depth beneath the pavement and cannot be adequately modeled with a single value.

REFERENCES

1. M. R. Thompson and Q. L. Robnett. Resilient Properties of Subgrade Soils. *Transportation Engineering Journal*, Jan. 1979, pp. 71–89.

2. C. Buranarom. *A Laboratory Investigation of the Dynamic Behavior of a Compacted Silty Clay.* M.S. thesis. Ohio State University, 1973.
3. T. Edil and S. Motan. *Soil-Water Potential and Resilient Behavior of Subgrade Soils.* University of Wisconsin, Madison, 1978.
4. S. M. Sargand, G. A. Hazen, and K. M. Miller. Multiaxial Testing of Compacted Shales. Presented at the International Symposium on Prediction and Performance in Geotechnical Engineering, Calgary, June 1987.
5. R. H. Atkinson. *A Cubical Test Cell for Multiaxial Testing of Material.* Ph.D. dissertation. University of Colorado, 1972.
6. S. M. Sargand and G. A. Hazen. Deformation Behavior of Shales. *International Journal of Rock Mechanics and Mining Sciences and Geomechanics Abstracts*, Vol. 24, No. 6, 1987, pp. 365–370.

Publication of this paper sponsored by Committee on Soil and Rock Properties.

Correlations of Unconsolidated-Undrained Triaxial Tests and Cone Penetration Tests

TIMOTHY D. STARK AND JOHN E. DELASHAW

Unconsolidated-undrained (UU) triaxial and cone penetration test results were used to develop correlations between undrained shear strength and cone resistance for three soft to medium alluvial clays in the San Diego area. The cone factor relating the UU triaxial strength to the cone resistance, termed N_{kuu}, had an average value and range of 11.0 ± 2.0, 11.0 ± 2.5, and 12.4 ± 0.8 for the Lopez Ridge, Creekside Estates, and Rancho Del Oro sites in San Diego, respectively. A data base of additional values of N_{kuu} was compiled from the literature for nonfissured, normally to lightly overconsolidated clays (overconsolidation ratios ranged from 1 to 5). The data base of N_{kuu} values showed considerably less scatter than that observed in previous cone factors on the basis of field vane shear tests. The reduction in scatter is believed to be due to the uncertainty in interpreting vane shear tests and the repeatability of UU triaxial tests when high-quality samples are available.

In southern California the cone penetration test (CPT) is frequently used during initial site investigations to provide information for an efficient boring and sampling program. CPT provides quick insight into soil stratigraphy and also identifies soil layers that might be problematic and require additional testing during the remainder of the investigation. Laboratory testing programs are then designed to measure the engineering properties of those soil layers by using high-quality samples obtained from soil borings located by using the CPT results. Currently in San Diego, most of the geotechnical design is based on the results of the laboratory tests. In an effort to incorporate the CPT results into the geotechnical design process, correlations between cone penetrometer resistance and undrained shear strength are being developed for soil deposits in the San Diego area.

REVIEW OF EXISTING CORRELATIONS

The undrained shear strength for clays is derived from CPT results by using theoretical solutions or empirical correlations or both. Baligh et al. (*1*) present a comprehensive overview of the different theories that can be grouped into the following three main categories: (a) bearing capacity, (b) cavity expansion, and (c) steady penetration. Those three methodologies employ a form of the traditional bearing capacity equation:

$$q_c = N_c S_u + \sigma_{vo} \quad (1)$$

where

q_c = cone resistance,
N_c = bearing capacity factor,
S_u = undrained shear strength, and
σ_{vo} = total vertical stress.

Each method incorporates a different expression for N_c and the total overburden stress, such as the horizontal or the octahedral stress, to determine the undrained shear strength.

EMPIRICAL CORRELATIONS

Owing to the difficulties in estimating the in situ horizontal stress and evaluating the various expressions for N_c, an empirical equation similar to Equation 1 is frequently used in practice to relate cone resistance to undrained shear strength. The empirical expression commonly used in practice is

$$q_c = N_k S_u + \sigma_{vo} \quad (2)$$

where N_k is the empirical cone factor.

The first empirical correlations relating q_c and S_u were developed in Europe, and, as a result, the reference undrained shear strength was usually determined from the results of field vane shear tests. Previous data collected by Lunne and Kleven (*2*) and Jamiolkowski et al. (*3*) showed that the empirical cone factor N_k decreases with plasticity index and ranges from 9 to 26 when S_u is measured by using a field vane shear test.

Bjerrum (*4*) reviewed 16 well-documented embankment failures on cohesive foundations and developed the field vane correction factor μ, as indicated in Figure 1. The correction factor reduces the measured strength to reflect the influence of anisotropy and strain rate effects on the undrained strength. Other researchers (*5–10*) have contributed additional data from other embankment failures for Figure 1. The additional data have increased the scatter about Bjerrum's recommended curve, leading some to question the use of the vane shear test for design.

If the vane shear strength values are corrected by using Bjerrum's field correction factor μ, the resulting corrected cone factor ($N_k^* = N_k/\mu$) appears to be independent of plasticity index and shows slightly less scatter than N_k. As indicated in Figure 2, the majority of the published N_k^* values are between 10 and 24, with an average of approximately 15. However, even after correcting the field vane shear strength, the values of N_k^* still show considerable scatter. The scatter shown in Figure 2 makes the determination of a design undrained shear strength very difficult.

Department of Civil Engineering, San Diego State University, San Diego, Calif. 92182.

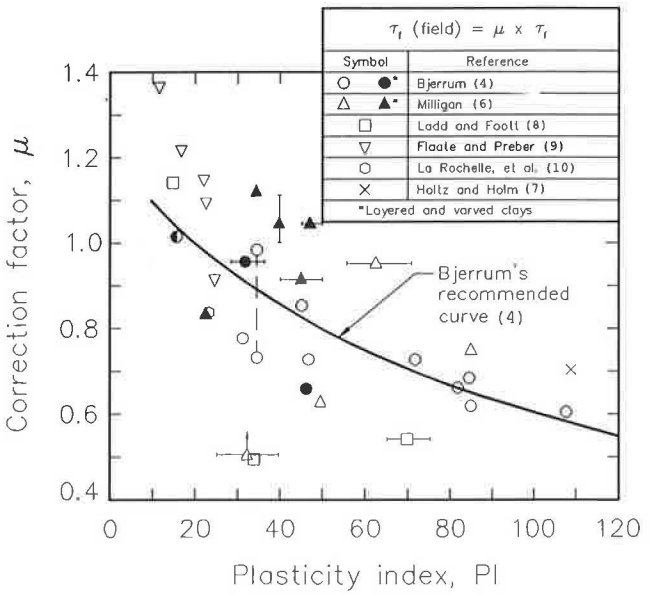

FIGURE 1 Correlation factor for the field vane test as a function of plasticity index, based on embankment failures [adapted from Holtz and Kovacs (*36*)].

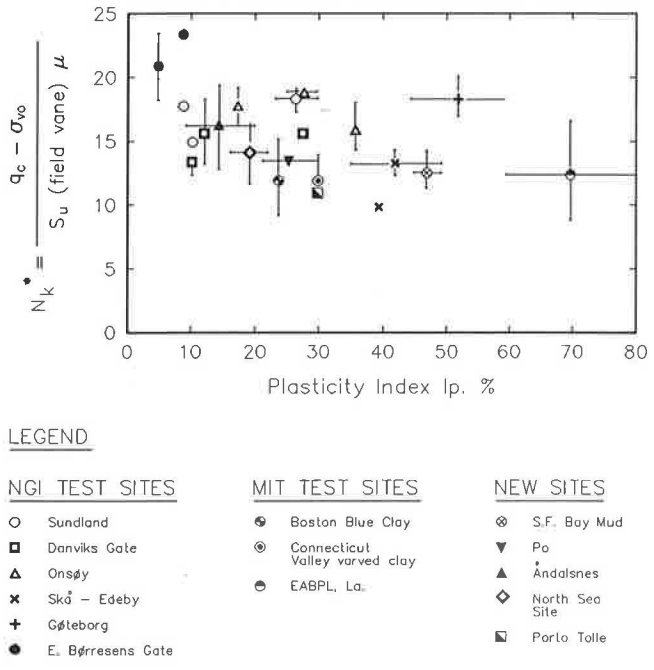

FIGURE 2 Previously published corrected cone factors [after Lunne and Kleven (*2*) and Meigh (*37*)].

NEW EMPIRICAL CONE FACTOR, N_{kuu}

The value of the empirical cone factor varies considerably depending on the type of cone, cone test procedure, the reference strength, and, most important, the soil deposit. The data bases of empirical cone factor currently available in the literature have not always been consistent because researchers have used different types of cones and different tests to measure the undrained shear strength. Researchers have also used the total horizontal stress or mean octahedral stress in Equation 2 instead of the total overburden pressure. The main objective of this research was to develop a new cone factor by using the tip resistance from standard electrical cones tested in accordance with ASTM standards, the total overburden pressure, and a consistent measurement of undrained shear strength.

A number of different techniques for measuring the undrained shear strength (field vane, isotropically consolidated-undrained triaxial, unconfined compression, anisotropically consolidated-undrained triaxial, unconsolidated-undrained triaxial, direct simple shear, and plane strain) were considered during this study. Despite the limitations of the unconsolidated-undrained (UU) triaxial test, the undrained shear strength obtained from this test is still widely used for design in the United States. The UU triaxial test provides repeatable results when high quality samples are available, does not require sophisticated laboratory equipment, and is very cost effective. Ladd et al. (*11*) also pointed out that the errors associated with UU triaxial tests are, "to some extent," self-compensating because disturbance decreases the strength while anisotropy and strain rate effects increase the strength. However, Ladd et al. warned that the effects of disturbance, anisotropy, and rate of loading are variable, and, therefore, considerable judgment should be used for cases where the factor of safety is "low."

Owing to the popularity of the UU triaxial test, the uncertainties in interpreting the vane shear test, and the difficulties in performing the other undrained strength tests mentioned, only values of S_u measured in UU triaxial tests were used in the correlations reported herein. Unconfined compression tests were not considered to be a UU triaxial test and were not used in the correlations. Therefore, the cone factors presented herein will be referred to as N_{kuu} and should be utilized to determine the undrained shear strength for use in total stress or end-of-construction stability analyses.

SAN DIEGO TEST SITES

To facilitate the use of CPTs in the San Diego area, a research program was initiated to develop cone factors for local soil deposits. To date, three sites—Lopez Ridge (*12*), Creekside Estates (*13*), and Rancho Del Oro (*14*)—have been studied. At each site a minimum of 10 cone soundings was performed by Earth Technology Corporation, using a standard electrical cone in accordance with ASTM D3441. Exploratory borings were drilled within 15 to 20 ft of selected cone penetration soundings to obtain high-quality, 3-in. diameter Shelby tube samples for laboratory testing.

All three sites are located within alluviated canyons that are proposed for development. The proposed Lopez Ridge project will necessitate the construction of a roadway embankment fill approximately 700 ft in length and varying in height from 10 to 30 ft. The proposed Creekside Estates and Rancho Del Oro projects involve the placement of compacted fills 10 and 25 ft deep, respectively. Those fills will be used to create building pads for single-family homes.

LABORATORY TEST RESULTS

Classification tests, a minimum of one consolidation test, and a minimum of three unconsolidated-undrained triaxial tests

were performed in accordance with ASTM standards on each Shelby tube sample obtained from the various sites. The measured soil properties of the canyon alluvium at the three San Diego sites are presented in Table 1. The alluvium ranges flow a low to high plasticity clay at the Lopez Ridge and Rancho Del Oro sites to a high plasticity clay or silt at the Creekside Estates site. Geologically, the alluvial deposits are young and are normally to lightly overconsolidated. As presented in Table 1, the undrained shear strength measured in UU triaxial tests ranged from 0.30 to 0.63 ton/ft^2 and was the highest at the Rancho Del Oro site. All UU triaxial tests specimens had a degree of saturation greater than 97 percent.

TABLE 1 PROPERTIES OF CANYON ALLUVIUM AT LOPEZ RIDGE CROSSING, CREEKSIDE ESTATES, AND RANCHO DEL ORO SITES

Property	Lopez Ridge	Creekside Estates	Rancho Del Oro
Alluvium thickness, ft.	10-40	30-35	40-70
Alluvium Classification	CL	CH	CH-MH
Plastic Limit	18-20	24-32	28-30
Liquid Limit	38-40	60-80	60-68
Plasticity Index	20	36-48	30-40
Natural Water Content, %	28-30	45-60	40-45
Overconsolidation Ratio	1-1.3	1-1.2	1-1.6
UU Triaxial Shear Strength, tsf	0.30-0.37	0.42-0.54	0.50-0.63
Net Cone Resistance, tsf	3.2-3.8	4.6-5.7	5.3-7.3
UU Triaxial Cone Factor, N_{kuu}	11.0 ± 2.0	11.0 ± 2.5	12.4 ± 0.8

NEW CORRELATIONS OF UU TRIAXIAL TESTS AND CONE PENETRATION TESTS

Empirical cone factors were calculated by using the undrained shear strength from UU triaxial tests, the electrical cone resistance, and the total overburden stress at the depth of the sample. At the Lopez Ridge site, the average value of N_{kuu} was 11.0 with a range of ±2.0. The Creekside Estates site also had an average value of N_{kuu} equal to 11.0 with a range of ±2.5. The Rancho Del Oro site had an average N_{kuu} value of 12.4 with a range of ±0.8. The range of net cone resistance, $q_c - \sigma_{vo}$, and UU triaxial shear strength used in the calculations of N_{kuu} at each site are presented in Table 1.

DATA BASE OF UU TRIAXIAL TESTS AND CONE PENETRATION TESTS

An extensive literature search was conducted to create a data base of sites at which values of N_{kuu} could be determined to investigate the accuracy of the N_{kuu} values calculated for the San Diego sites. A total of 18 sites was collected for the data base, and additional sites were being sought. Only sites with undrained shear strengths measured in UU triaxial tests and test specimens having a degree of saturation at or near 100 percent were selected. Unconfined compression test results were not used in the correlations. In addition, only cone soundings, using a standard electrical cone advanced at approximately 2 cm/sec (0.78 in./sec) and in accordance with ASTM D3441, were used in the correlations. The electric cones all had an apex angle of 60 degrees and a projected area of 10 cm^2 (1.55 in.^{2}). The sites, sources of the data, and the symbols used to represent the data are presented in Table 2.

VARIATION OF CONE FACTOR WITH PLASTICITY INDEX

Figure 3 indicates the variation of N_{kuu} as a function of plasticity index (PI) for the 18 data-base sites and the three San

TABLE 2 LISTING OF SITES, SYMBOLS, AND REFERENCE NUMBERS USED IN CORRELATIONS BETWEEN UU TRIAXIAL AND CONE PENETRATION TESTS

SYMBOL	SITE	(Reference)	SYMBOL	SITE	(Reference)
	AUGUSTA	(15)		PORTO TOLLE	(3)
	BEAUMONT	(17)		RANCHO DEL ORO	(14)
	BEAUMONT	(18)		SAINT ALBAN	(25)
	BOSTON BLUE	(19, 20)		S.F. BAY MUD	(26)
	CRAN	(21)		S.F. BAY MUD	(27)
	CREEKSIDE	(13)		SANTA BARBARA (SOFT)	(28)
	HAGA	(22)		SANTA BARBARA (STIFF)	(28)
	LOPEZ RIDGE	(12)		SILTY HOLOCENE	(24)
	OTTAWA SEWAGE PLANT	(23)		TEXARKANA	(29)
	PLASTIC HOLOCENE	(24)		VAL DI CHIANA	(30)

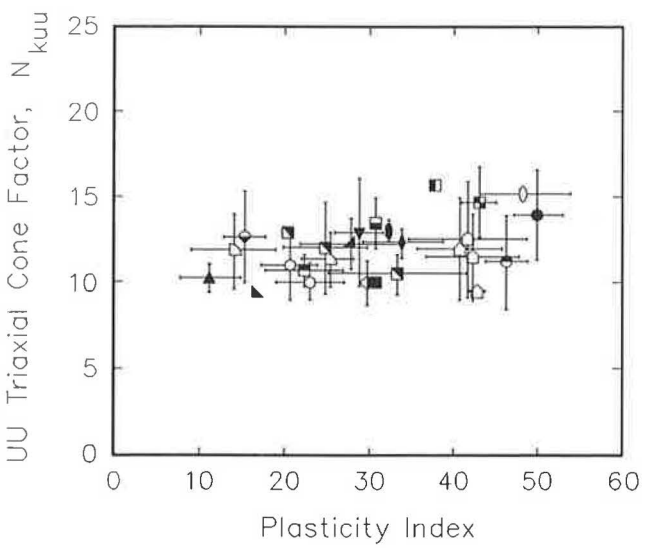

FIGURE 3 Variation of UU triaxial cone factor with plasticity index.

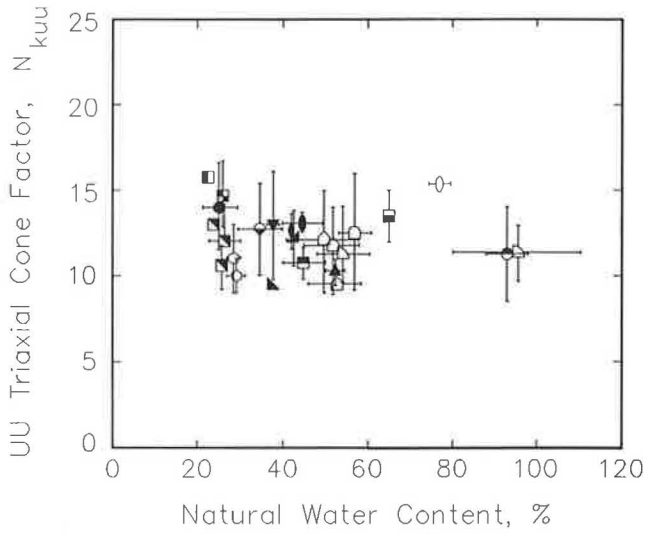

FIGURE 4 Variation of UU triaxial cone factor with natural water content.

Diego sites. It can be seen that the values of N_{kuu} range from 8.5 to 16.5, with an average value of approximately 12. Each data symbol represents the median value of PI and N_{kuu} calculated at each site, while the lines surrounding each point illustrate the range of PI and N_{kuu}. The symbols for the San Diego and San Francisco Bay Mud (*12*) sites correspond to the median value of N_{kuu} for a particular boring.

In a comparison of Figures 2 and 3, N_{kuu} shows considerably less scatter than the corrected cone factor N_k^*. The reduction in scatter is probably due to the use of tip resistance values measured by using only a standard electrical cone and the repeatability and simple interpretation of UU triaxial tests. Some of the scatter observed in N_k^* is probably due to soil anisotropy, strain rate effects, and the difficulties in interpreting and performing field vane shear tests.

VARIATION OF CONE FACTOR WITH LIQUIDITY INDEX

Figure 4 presents the variation of UU triaxial cone factor with the natural water content. The majority of the natural water contents ranges from 20 to 60. In a comparison of Figures 3 and 4, the range in natural water content for a particular site was significantly smaller than that observed in PI. In an effort to incorporate natural water content into the correlations, N_{kuu} was plotted against the liquidity index (LI).

The LI provides an index for scaling the natural water content and an insight into the engineering behavior of the deposit. It can be seen from Figure 5 that the majority of the sites had an LI ranging from 0.2 to 1.0, which indicates a plastic behavior during shear. This behavior is typical for the normally consolidated to lightly overconsolidated clays investigated during this study. Therefore, the use of the LI may provide a better index for N_{kuu} than PI because it incorporates information about water content, plasticity, and the engineering behavior of the soil. In addition, sensitivity S_t can be estimated from LI by using data presented by Eden and Kubota (*31*) and Bjerrum (*16*). Their data were used to derive the following equation for estimating sensitivity:

$$S_t = 10^{(LI - 0.20)} \tag{3}$$

To facilitate the determination of undrained shear strength, the data base was replotted in terms of net cone resistance $(q_c - \sigma_{vo})$ and undrained shear strength. It can be seen from Figure 6 that the majority of the data plots along a straight line corresponding to a value of N_{kuu} equal to approximately 12. The symbols in Figure 6 correspond to the median value of N_{kuu} for a particular site or boring. The scatter of N_{kuu} appears to increase slightly as the net cone resistance and undrained shear strength increase. This is probably due to the uncertainty of interpreting cone measurements in stiff clays.

VARIATION OF CONE FACTOR WITH UNDRAINED STRENGTH RATIO

Ladd and Foott (*8*) showed that the undrained shear strength of clays is controlled by the effective consolidation stress σ'_{vc}, or the overconsolidation ratio (OCR) or both. As a result, Mayne and Kemper (*32*) and Wroth (*33*) have suggested plotting the normalized net cone resistance $(q_c - \sigma_{vo})/\sigma'_{vc}$ versus the undrained strength ratio S_u/σ'_{vc}. The advantages of using the normalized net cone resistance are that it is dimensionless and it is directly related to the overconsolidation ratio as shown below:

$$\frac{(q_c - \sigma_{vo})}{\sigma'_{vc}} = \frac{(q_c - \sigma_{vo})}{S_u} \cdot \frac{S_u}{\sigma'_{vc}} = N_{kuu} \cdot \frac{S_u}{\sigma'_{vc}}$$

$$= N_{kuu} \cdot f(\text{OCR}) \tag{4}$$

It can be seen from Figure 7 that the normalized net cone resistance is directly related to the undrained strength ratio. Also indicated in Figure 7 is a line that corresponds to N_{kuu}

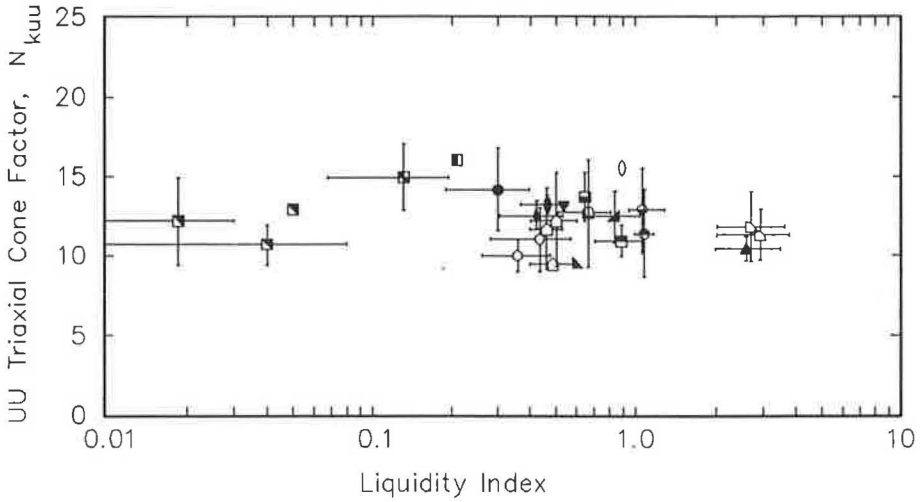

FIGURE 5 Variation of UU triaxial cone factor with liquidity index.

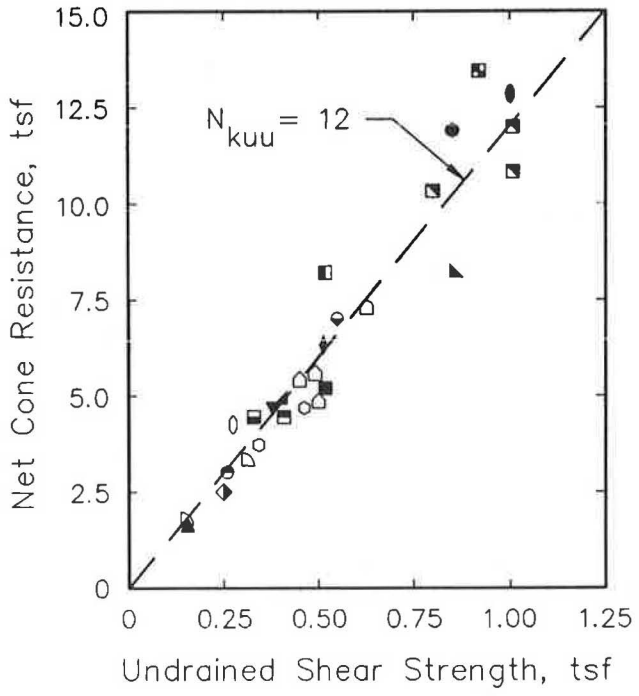

FIGURE 6 UU triaxial cone factor as a function of net cone resistance and undrained shear strength.

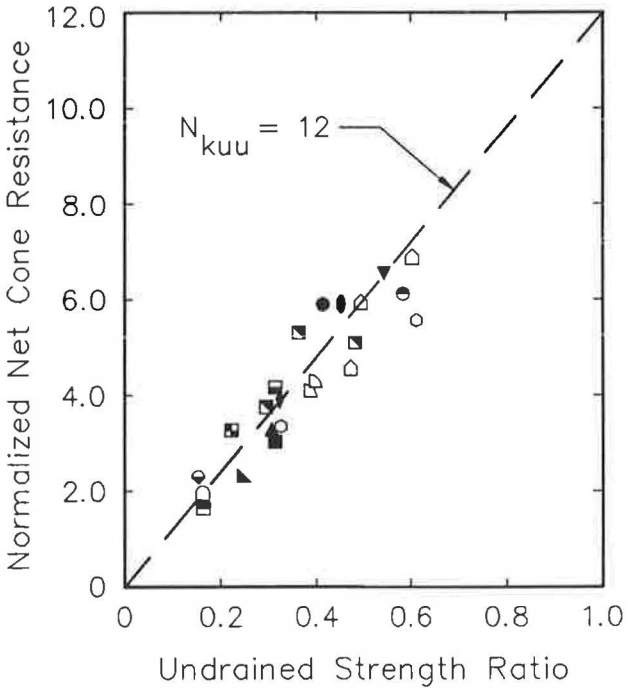

FIGURE 7 Variation of UU triaxial cone factor with normalized net cone resistance with undrained strength ratio.

equal to 12, which again is in good agreement with the data. Therefore, a reasonable estimate of undrained strength ratio for nonfissured, normally to lightly overconsolidated (overconsolidation ratios ranging from 1 to 5) clays can be obtained directly from values of normalized net cone resistance, using an N_{kuu} of approximately 12.

VERIFICATION OF UNDRAINED SHEAR STRENGTH

The undrained shear strength obtained from the design charts presented here should be verified by using previously published relationships for undrained strength ratio. One of the most widely used relationships was presented by Jamiolkowski et al. (*33*) and is shown below:

$$\frac{S_u}{\sigma'_{vc}} = (0.23 \pm 0.04) \cdot \mathrm{OCR}^{0.8} \tag{5}$$

This relationship is applicable to most soft sedimentary clays of low to medium plasticity and is frequently used to evaluate embankment stability. This relationship was developed primarily from the results of direct simple shear tests. Data presented by Ladd and Edgers (*35*) and Jamiolkowski et al. (*34*)

have shown that triaxial compression tests yield slightly higher values of undrained shear strength than direct simple shear tests. As a result, to obtain an estimate of S_u that corresponds to the UU triaxial strength, the coefficient in Equation 5 can be increased to approximately 0.3 and the equation simplified to what follows for most clays:

$$\frac{S_u}{\sigma'_{vc}} = (0.30) \cdot \mathrm{OCR}^{0.8} \tag{6}$$

SUMMARY

Values of the empirical cone factor vary considerably depending on the type of cone, cone test procedure, the reference strength, and, most important, the soil deposit. The main objective of this research was to develop a new cone factor N_{kuu} for nonfissured, normally to lightly overconsolidated clays (overconsolidation ratios ranging from 1 to 5) using the tip resistance from only electrical cones tested in accordance with ASTM Standard D3441 and values of undrained shear strength measured in UU triaxial tests. Undrained shear strengths measured by using isotropically consolidated-undrained, unconfined compression, anisotropically consolidated-undrained triaxial tests, vane shear, or other strength tests were not used in the correlations reported herein.

UU triaxial cone factors N_{kuu} were calculated for three soft to medium canyon alluviums in the San Diego area. The average value and range of N_{kuu} were calculated to be 11.0 ± 2.0, 11.0 ± 2.5, and 12.4 ± 0.8 for the Lopez Ridge Crossing, Creekside Estates, and Rancho Del Oro sites, respectively. An extensive literature search was conducted to locate 18 additional sites for which N_{kuu} could be calculated. Variations of the UU triaxial cone factor with plasticity index, natural water content, liquidity index, net cone resistance, and undrained strength ratio were developed from the data base. Those correlations show significantly less scatter than that observed in previous cone factors based on field vane shear tests. The reduction in scatter is believed to be due to the uncertainty in interpreting vane shear tests and the repeatability of UU triaxial tests when high-quality samples are available.

ACKNOWLEDGMENTS

This study was supported by a grant from Geocon Inc. of San Diego. The Shelby tube samples were provided by Geocon Inc. and F & C Drilling of San Diego. This support is gratefully acknowledged. J. E. Juhrend and G. R. Richards, research assistants at San Diego State University (SDSU), performed the laboratory tests for the Lopez Ridge Crossing and for Creekside Estates and Rancho Del Oro sites, respectively. R. S. Connely, a research assistant at SDSU, drafted the figures, using AUTOCAD 9.0.

REFERENCES

1. M. M. Baligh, A. S. Azzouz, and R. T. Martin. *Cone Penetration Tests Offshore the Venezuelan Coast.* Report R80-21. Massachusetts Institute of Technology, Cambridge, Mass., 1980.
2. T. Lunne and A. Kleven. Role of CPT in North Sea Foundation Engineering. *Proc., Symposium on Cone Penetration Engineering Division*, Oct. 1981, pp. 49–75.
3. M. Jamiolkowski, R. Lancellotta, M. L. Tordella, and M. Battaglio. Undrained Strength from CPT. *Proc., European Symposium on Penetration Testing*, Amsterdam, 1982, pp. 599–606.
4. L. Bjerrum. Embankments on Soft Ground, State-of-the-Art Report. *Proc., ASCE Specialty Conference on Performance of Earth and Earth-Supported Structures*, Lafayette, Vol. 2, 1972, pp. 1–54.
5. C. C. Ladd. *Foundation Design of Embankments Constructed on Connecticut Valley Varved Clays.* Research Report R75-7, Geotechnical Publication 343, Department of Civil Engineering, Massachusetts Institute of Technology, Cambridge, Mass., 1975.
6. V. Milligan. Discussion of "Embankments on Soft Ground." *Proc., ASCE Specialty Conference on Performance of Earth and Earth-Supported Structures*, Purdue University, Vol. 3, 1972, pp. 41–48.
7. R. D. Holtz and G. Holm. Test Embankment on an Organic Silty Clay. *Proc., Seventh European Conference on Soil Mechanics and Foundation Engineering*, Brighton, England, Vol. 3, 1979, pp. 79–86.
8. C. C. Ladd and R. Foott. New Design Procedure for Stability of Soft Clays. *Journal of the Soil Mechanics and Foundation Division*, ASCE, Vol. SM7, 1974.
9. K. Flaate and T. Preber. Stability of Road Embankments. *Canadian Geotechnical Journal*, Vol. 11, No. 1, 1974, pp. 72–88.
10. P. LaRochelle, B. Trak, F. Tavenas, and M. Roy. Failure of a Test Embankment on a Sensitive Champlain Clay Deposit. *Canadian Geotechnical Journal*, Vol. 11, No. 1, 1974, pp. 142–164.
11. C. C. Ladd, R. Foott, K. Ishihara, F. Schlosser, and H. G. Poulos. Stress-Deformation and Strength Characteristics. State-of-the-Art Report. *Proc., Ninth International Conference on Soil Mechanics and Foundation Engineering*, Tokyo, Vol. 2, 1977, pp. 421–494.
12. T. Kuper, W. Spang, and J. Juhrend. *Final Geotechnical Investigation for Sorrento Valley Boulevard Stations 128 + 50 to 136 + 80 and Staging Area Parking Lot, Calle Cristobal Assessment District, San Diego, California.* File No. D-3764-H04, Geocon Inc., San Diego, Calif., Feb. 1988.
13. J. Likins, M. Hart, and J. Juhrend. *Geotechnical Investigation and Earthwork Package for Creekside Estates, Oceanside, California.* Geocon Inc., File No. D-4061-J01 for F.D.R. Development Co., Geocon, Inc., San Diego, Calif., March 1988.
14. T. Kuper, W. Spang, and J. Juhrend. *Preliminary Engineering Investigation for Rancho Del Oro, Villages 4 through 7, Oceanside, California.* File No. D-3996-HO1 for the Fieldstone Co., Geocon Inc., San Diego, Calif., Dec. 1987.
15. R. Alperstein and S. Leifer. Site Investigation with Static Cone Penetrometer. *Journal of the Geotechnical Engineering Division*, ASCE, Vol. 102, No. GT5, May 1976, pp. 539–555.
16. L. Bjerrum. Geotechnical Properties of Norwegian Marine Clays. *Geotechnique*, Vol. 4, No. 2, 1954, pp. 49–69.
17. L. Mahar and M. O'Neill. Geotechnical Characterization of Desiccated Clay. *Journal of Geotechnical Engineering*, ASCE, Vol. 109, No. 1, Jan. 1983, pp. 56–71.
18. K. Tand, E. Funegard, and J. Briaud. Bearing Capacity of Footings on Clay CPT Method. In *Use of In Situ Tests in Geotechnical Engineering*, (S. P. Clemence, ed.), ASCE, New York, 1986, pp. 1017–1033.
19. M. Baligh, V. Vivatrat, and C. C. Ladd. Cone Penetration in Soil Profiling. *Journal of the Geotechnical Engineering Division*, ASCE, Vol. 106, No. GT4, April 1980, pp. 447–461.
20. *Performance of an Embankment on Clay: Interstate 95.* M.I.T. Soil Report No. 245, Cambridge, Mass., Oct. 1969.
21. S. Amar et al. In Situ Shear Resistance of Clays. *In Situ Measurement of Soil Properties*, ASCE, Vol. 1, 1975, pp. 22–45.
22. K. Anderson and P. Stenhamar. Static Plate Loading Tests on Overconsolidated Clay. *Journal of the Geotechnical Engineering Division*, ASCE, Vol. 109, No. GT7, July 1982, pp. 918–934.
23. J. T. Konrad and K. T. Law. Undrained Shear Strength From Piezocone Tests. *Canadian Geotechnical Journal*, Vol. 24, No. 3, July 1987, pp. 392–405.
24. D. Koutsoftas and J. Fischer. In Situ Undrained Strength of Two

Marine Clays. *Journal of the Geotechnical Engineering Division*, ASCE, Vol. 102, No. GT9, Sept. 1976, pp. 989–1005.
25. M. Roy et al. Development of a Quasi-Static Piezocone Apparatus. *Canadian Geotechnical Journal*, Vol. 19, No. 2, May 1982, pp. 180–188.
26. R. Bonapart and J. K. Mitchell. The Properties of S.F. Bay Mud at Hamilton Air Force Base, California. Geotechnical Engineering Report, University of California at Berkeley, 1979.
27. *Great American Parkway Interchange and SR237 Realignment Project, Santa Clara County, California.* CH2M Hill, Project SFO 210.11.00. Emeryville, Calif., May 1988.
28. G. Quiros and A. Young. Comparison of Field Vane, CPT, and Laboratory Strength Data at Santa Barbara Channel Site. In *Vane Shear Testing in Soils*, ASTM, Philadelphia, 1988, pp. 307–317.
29. L. D. Johnson. Correlation of Soil Parameters from In Situ and Laboratory Tests for Building 333. In *Use of In Situ Tests in Geotechnical Engineering*, (S. P. Clemence, ed.), ASCE, New York, 1986, pp. 635–648.
30. A. Cancelli and A. Cividini. An Embankment on Soft Clays with Sand Drains Numerical Characterization of the Parameters from In-Situ Measurements. *Proc., International Conference on Case Histories in Geotechnical Engineering*, Vol. 2, Rolla, Mo., May 1984, pp. 637–643.
31. W. J. Eden and J. K. Kubota. Some Observations on the Measurement of Sensitivity of Clays. *Proc., American Society for Testing and Materials*, Vol. 61, 1962, pp. 1239–1249.
32. P. W. Mayne and J. B. Kemper, Jr. Profiling OCR in Stiff Clays by CPT and SPT. *ASTM Geotechnical Testing Journal*, Vol. 11, No. 2, 1988, pp. 139–147.
33. C. P. Wroth. Penetration Testing: A More Rigorous Approach to Interpretation. *Proc., 1st International Symposium on Penetration Testing*, ISOPT-1, Orlando, Fla., 1988, pp. 303–311.
34. M. Jamiolkowski, C. C. Ladd, J. T. Germaine, and R. Lancellotta. *New Developments in Field and Laboratory Testing of Soils. Proc., 11th ICSMFE*, San Francisco, Calif., Vol. 1, 1985, pp. 57–154.
35. C. C. Ladd and L. Edgers. *Consolidated-Undrained Direct Simple Shear Tests on Saturated Clays.* Research Report R72-82, Soils Publication 284, Department of Civil Engineering, Massachusetts Institute of Technology, Cambridge, Mass., 1972.
36. R. D. Holtz and W. D. Kovacs. *An Introduction to Geotechnical Engineering.* Prentice Hall, Englewood Cliffs, N.J., 1981.
37. A. C. Meigh. *Cone Penetration Testing: Methods and Interpretation.* Butterworths, London, 1987.

Publication of this paper sponsored by Committee on Soil and Rock Properties.

Evaluation of In Situ Strength of a Peat Deposit from Laterally Loaded Pile Test Results

STEVEN L. KRAMER, RENALDI SATARI, AND ALAN P. KILIAN

Peat soils exhibit strength and stiffness characteristics that are strongly influenced by extension and interlocking of fibers within the peat. Consequently, the in situ strength and stiffness characteristics of peat cannot be measured accurately with existing small-scale laboratory or field testing instruments. The use of an instrumented pile lateral load test is described for evaluation of the strength and stiffness characteristics of a peat deposit that had been exerting lateral stresses on existing pile foundations. Pile load tests were performed on two relatively flexible piles installed in approximately 45 to 50 ft of fibrous peat. Each pile was instrumented with both strain gauges and inclinometers. The piles were loaded laterally at the ground surface until displacements increased so quickly that additional loads could not be placed. At this point, the strength of the peat had been mobilized in a relatively large volume of soil in the vicinity of the pile. Interpretation of the strain gauge and inclinometer readings allowed definition of the deflected shapes of the piles and of the unit soil resistance profiles. Those deflected shapes allowed evaluation of the *p-y* behavior of the soil from which the strength and stiffness could be obtained. Those strength and stiffness values were consistent with those obtained for other peats and with the available results of a previously performed laboratory testing program.

Measurement of the shear strength of peats has posed a difficult problem for geotechnical engineers for many years. Many peats exhibit a component of shear strength that results from extension and interlocking of fibrous, organic material within the peat (*1*,*2*). Conventional laboratory strength tests on relatively small-scale samples often do not reflect this fibrous component of shear strength. Most conventional in situ strength tests also mobilize shear strength on a relatively small surface and do not capture the fibrous component of shear strength. Landva (*2*), in a comprehensive review of in situ testing of peats, states that "cone penetration and vane testing . . . do not give meaningful results in peats and peaty organic soils" but that such results "can be obtained through large-scale or full-scale testing." In this paper, the use of a laterally loaded pile test as an in situ test to measure the strength and stiffness of peat is described. The resistance of a peat to lateral displacement of a pile requires mobilization of shear strength in a relatively large volume of soil in the vicinity of the pile. This volume of peat is large enough that the fibrous component of shear strength is reflected in the soil resistance from which an accurate estimate of the in situ shear strength can be made.

S. L. Kramer and R. Satari, Department of Civil Engineering, FX-10, University of Washington, Seattle, Wash. 98195. A. P. Kilian, Materials Laboratory, Washington State Department of Transportation, 1655 South Second Avenue, Tumwater, Wash.

In situ strength tests generally fall into two main categories: direct measurement tests, which directly measure the strength of the soil on a known and constrained failure surface, and indirect measurement tests, which mobilize the strength of the soil on an unknown failure surface where the geometry is obtained from an appropriate theory of soil mechanics. The vane shear test (*3*,*4*) and the Iowa borehole shear test (*5*,*6*) are examples of the former, and the cone penetration test (*7*,*8*), pressuremeter test (*9*,*10*), screw plate test (*11*,*12*), and plate load test (*13*,*14*) are well-established examples of the latter. The use of indirect measurement tests requires that the physical phenomena to be measured be understood and that a reasonable model relating the measured phenomena to the parameter(s) of interest be available. Modeling of the response of pile foundations to lateral loads has developed rapidly in recent years to the point where the *p-y* behavior of soft soils can be expressed in terms of their strength and stiffness characteristics (*15*,*16*).

BACKGROUND

The site, profiled in Figure 1, is located on the I-90 right-of-way immediately west of Lake Washington Boulevard near the eastern shore of Lake Washington in Bellevue, Washington. The site is traversed in the east-west direction by a pile-supported Seattle Water Department pipeline and four pile-supported I-90 elevated-bridge structures. The eastern edge of the site is bordered by the Lake Washington Boulevard embankment fill, which rises to an elevation about 15 ft above the remainder of the site. Figure 2 is a plan of the site. Subsurface soil movement in the area of the eastbound collector-distributor (EBCD) and westbound collector-distributor (WBCD) ramps of the I-90 Bellevue Transit Access project has been observed over a period of several years. This subsurface soil movement has resulted in movement of existing pile-supported structures in the area, including highway bridges and a water supply pipeline. The original purpose of the research described in this paper was to investigate the lateral load behavior of piles in the Mercer Slough peats for the design of new pile-supported structures and to estimate the forces exerted on the existing piles by lateral movement of the surrounding peat.

The site is part of Mercer Slough, which in this area has a generally flat and level surface covered with marsh grasses and small trees. The groundwater level at the site is approx-

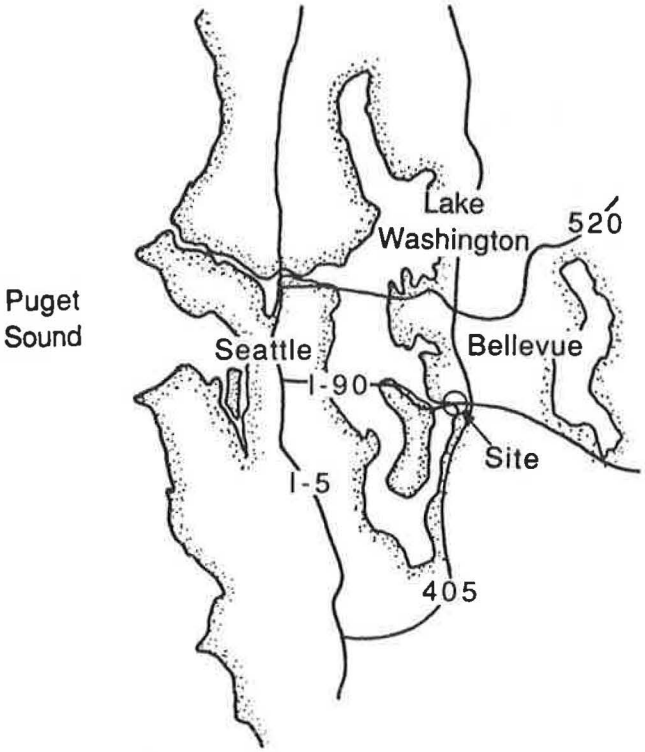

FIGURE 1 Site location.

imately at the ground surface. Subsurface investigations indicated that the site subsurface conditions are dominated by a peat deposit of variable thickness. The peat deposit generally overlies clay and silt deposits, which overlie granular materials. Artesian pressure conditions have been observed in the soils underlying the peats. The peat was described in previous subsurface investigations performed for the Washington State Department of Transportation as a "brown, fibrous, organic material, with a low dry density and shear strength and high water content and compressibility." The Lake Washington Boulevard fill rests at least partially on the Mercer Slough peat, and its weight is considered to be the driving force causing movement of the peat. A subsurface profile along the WBCD is presented in Figure 3.

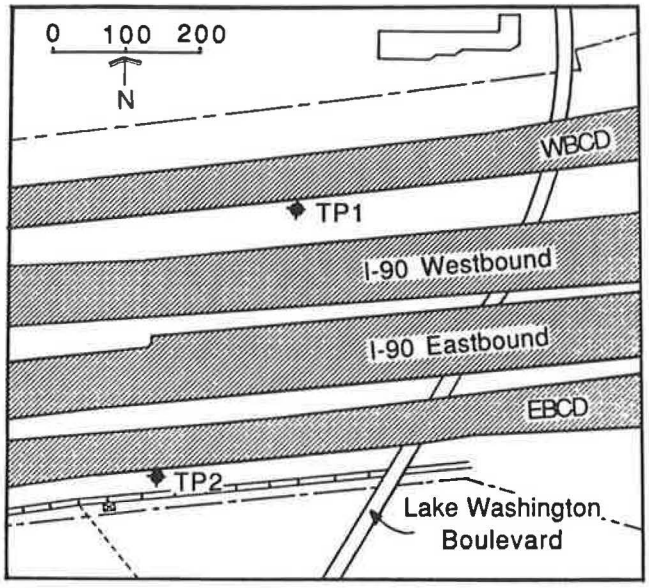

FIGURE 2 Site plan.

FIELD AND LABORATORY MEASUREMENT OF PEAT STRENGTH

Previously performed subsurface investigations in the vicinity of the pile load test sites consisted of conventional boring and sampling along with vane shear and cone penetration test

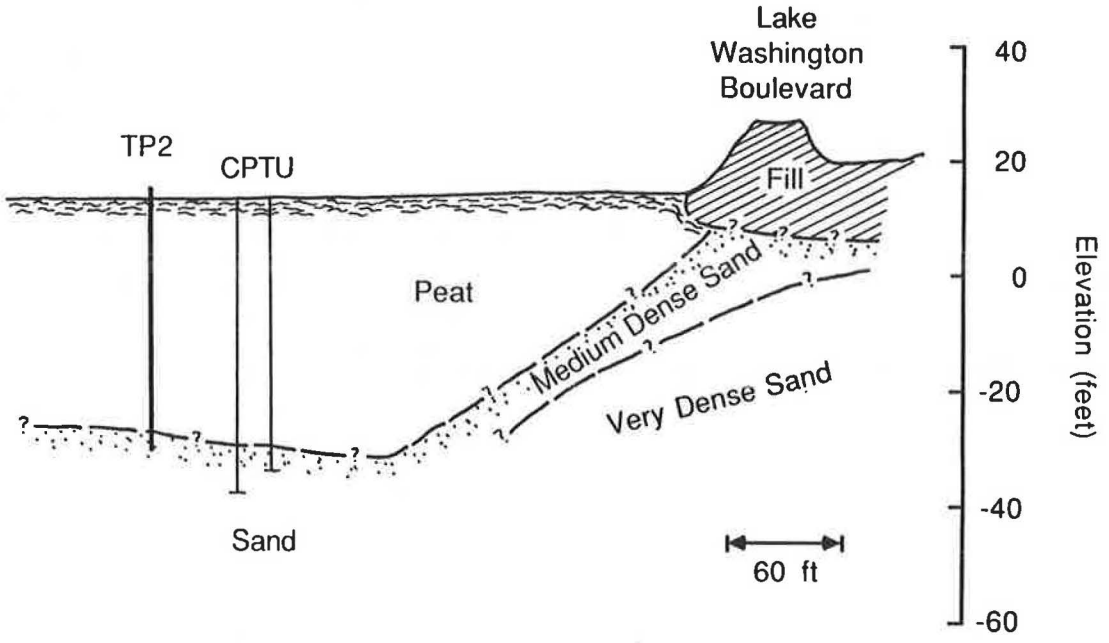

FIGURE 3 Subsurface profile.

profiling. Unconsolidated-undrained (UU) triaxial and vane shear tests indicated peak undrained shear strength ranging from values as low as 15 to 175 psf with a possible trend of modestly increasing strength with depth (see Figure 4). This large range of variability is consistent with that observed in other studies of vane shear tests in peat (*2*,*17*). Two piezocone penetration test profiles indicate a uniform tip resistance of approximately 340 psf with a friction ratio of 1.5 percent to 6 percent. Measured pore pressures were essentially hydrostatic. The cone penetration logs are as indicated in Figure 5. Interpretation of cone penetration tests in peat has been recognized as being very difficult (*2*) owing to lateral deflection of typical size penetrometers and to the mode of deformation and failure.

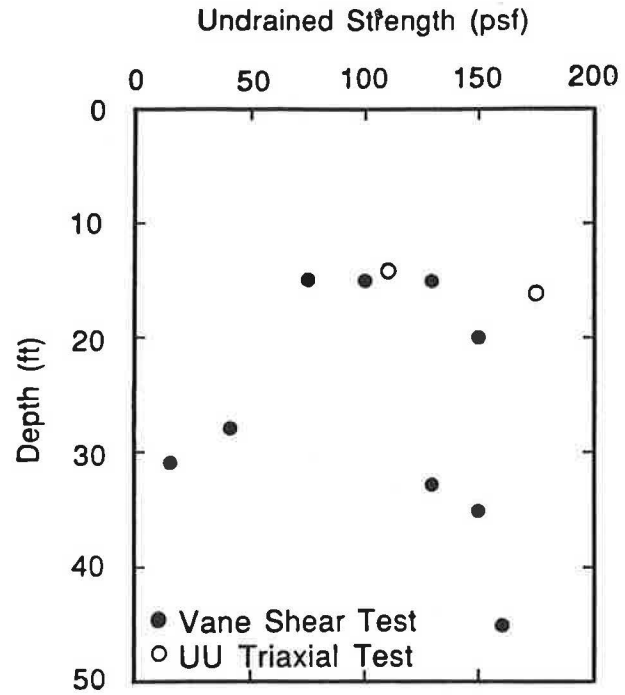

FIGURE 4 Triaxial and vane shear strength data.

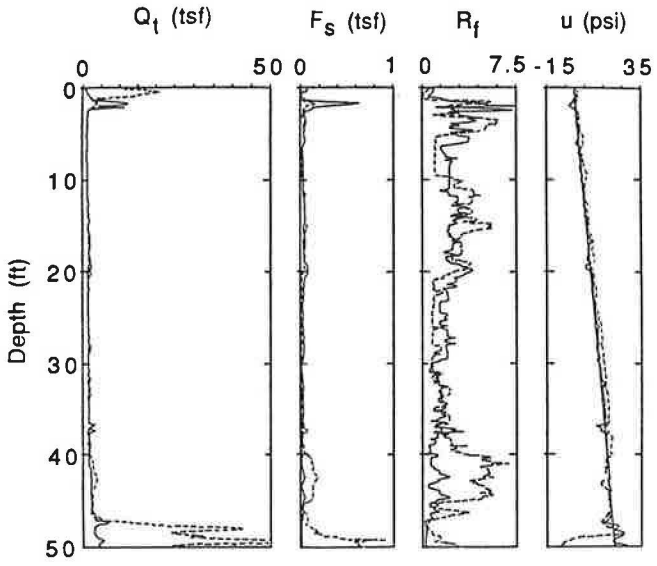

FIGURE 5 Piezocone and penetration test logs.

LATERAL LOAD BEHAVIOR

Two test piles were installed in the Mercer Slough peats and were subjected to lateral loads at the ground line. Flexible piles were required to develop the pile bending necessary for evaluation of unit soil resistance because of the very soft nature of the soil. Test pile diameters reasonably near those of the actual piles were required to model the actual piles accurately in the area with minimal scale effects. Those conflicting requirements led to the optimum selection of an intermediate size pile with relatively thin walls.

Test Materials, Instrumentation, and Procedures

The piles used in the lateral load tests were 8-in. diameter steel pipe piles with 0.25-in. wall thickness. The piles were nominally 60 ft long and were installed with open ends to allow penetration under their own weight as far as possible and then by additional static vertical load supplied by the boom of a boom truck. The piles were instrumented with 11 pairs of bonded resistance strain gauges placed diametrically opposite each other at distances of 5 ft 8 in., 6 ft 4 in., and 7, 8, 9, 11, 13, 17, 23, 29, and 37 ft from the top of the pile. The strain gauges and associated wiring were waterproofed and protected by 1½-in. steel angles welded to the outside of the piles. The steel angles were attached in 10-ft-long sections, each lightly welded at only their bottom ends, to provide the desired protection during pile installation without influencing the flexural resistance of the pile.

Test pile 1 (TP1) penetrated under its own weight to a depth of approximately 15 ft and was then pushed to refusal at a tip depth of about 51 ft. The pile, originally 59 ft long, was then removed and reinstalled nearby after cutting a 5-ft length off the bottom to allow the highest strain gauges to be located just below the ground surface. Test pile 2 (TP2) penetrated under its own weight to a depth of about 20 ft and was then pushed to refusal at a tip depth of approximately 43 ft. The pile, originally 60 ft long, was removed and reinstalled nearby after cutting a 14-ft length off the bottom. After installation, the tops of TP1 and TP2 were 5 and 3 ft above the ground surface, respectively.

Lateral loads were applied to the piles by a 100-ton capacity, 9-in. throw, hydraulic jack. The deflection and slope of the pile at the point of load application were obtained by measuring the horizontal distance between the pile and each of the three spring-tensioned horizontal wires stretched at different heights between stakes placed outside of the zone of influence of the pile. The subsurface deformation of each pile was monitored by both strain gauges and an inclinometer. The strain gauges were monitored during testing by a PC-based automatic data acquisition system that was housed at the site in a small tent and was powered by a dedicated generator. A 40-ft long slope inclinometer casing was suspended inside each of the piles and was pressed against the sides of the piles by an inflatable air bag. The air bag was constructed

of 6-mil polyethylene sheeting with an unrestrained inflated diameter of about 24 in. When installed in the 7.5-in. I.D. pile and inflated to approximately 1.5 psi by a high-volume low-pressure compressor (ShopVac), stresses in the air bag itself were very low and leakage or rupture was not observed. Slope measurements were made at 2-ft intervals along the length of the inclinometer casing.

On TP1, the loads were applied through a cabling arrangement so that the test pile was pulled toward the reacting bridge pier, located approximately 12 ft from the test pile. On TP2, the pile was jacked away from a nearby pile cap. Applied loads on TP1 were measured by a GEOKON model 3000 load cell provided by the Washington State Department of Transportation (WSDOT). The output from this load cell proved to be quite low for the load range used in the tests, and it was replaced by a load cell from the University of Washington structural engineering laboratory for TP2. The load cell used for TP2 was approximately seven times more sensitive than that used for TP1. Lateral loads were increased incrementally by an electrically controlled hydraulic pump, which operated essentially as a displacement-controlled device. The resistance of the peat to lateral loads was observed to be time dependent, with the pile head load observed to decrease with time under constant pile head deflection. The top deflection and slope, and the load cell and strain gauges, were read immediately after application of each load increment and again after a period of approximately 10 to 15 min, at which time inclinometer readings were also taken. Intermediate load cell readings were taken on a number of occasions to study the time dependent behavior of the peat.

Test Results

TP1 was installed on April 3, 1989, and was tested on April 10, 1989. Lateral loads were increased incrementally with two unload-reload loops, and a final unloading measurement was made after the pile had reached its maximum lateral displacement of approximately 8.5 in. TP2 was installed on April 21, 1989, and was tested on April 24, 1989. Lateral loads were increased incrementally with no unload-reload loop in order to simulate the type of monotonically increasing loads that would be caused by moving peat. The load-deflection response measured at the tops of TP1 and TP2 were generally similar (see Figure 6).

The survivability of the resistance strain gauges was lower than was expected. Whether owing to mechanical damage during installation or to ineffectiveness of waterproofing measures, only a few of the strain gauge pairs functioned properly. The inclinometer data, however, were consistent with independent measurements of top deflection and slope. The inclinometer (slope) and working strain gauge (curvature) data were combined for each pile and reduced by multivariate optimization with multiple constraints for conformance with the measured boundary conditions at the top of the pile and with the assumption of fixity at the bottom of the pile. This procedure allowed expression of the deflected shape of the piles in terms of 8th-order polynomials. The deflected shapes of TP2 obtained by this procedure for lateral loads of 2.4, 4.8, and 6.9 kips are presented in Figure 7.

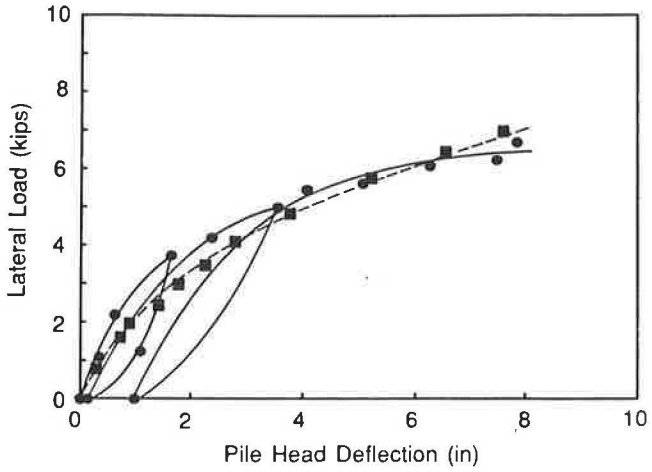

FIGURE 6 Load displacement response of TP1 and TP2.

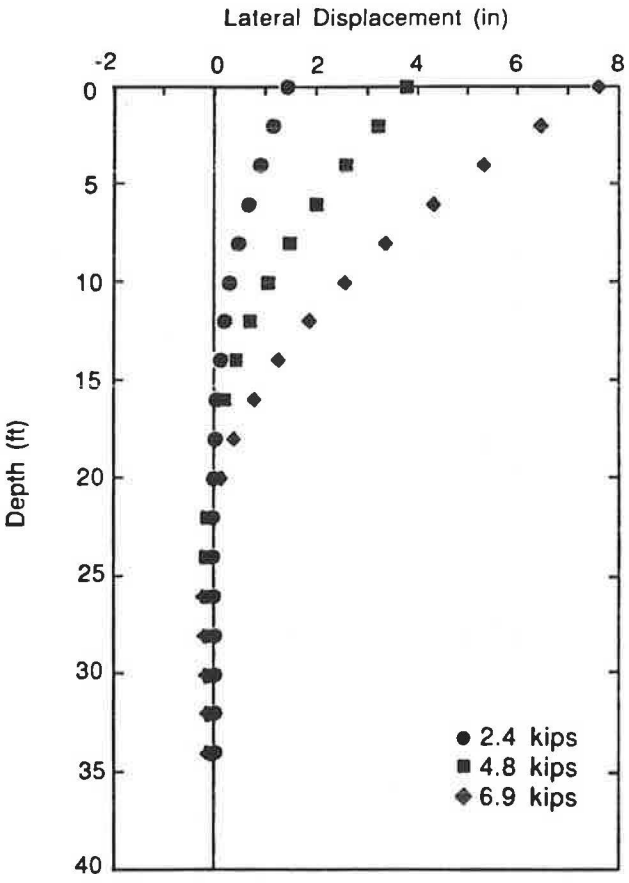

FIGURE 7 Observed deflected shapes of TP2.

INTERPRETATION OF LOAD TEST RESULTS

Evaluation of in situ shear strength from the results of an indirect in situ test requires interpretation of the test results within the framework of some applicable theory of soil mechanics. Cone penetration test interpretation, for example, often makes use of deep-bearing capacity theory, while plate

load test interpretation relies on shallow-bearing capacity theory. Interpretation of the lateral load tests described in this paper was performed within the framework of *p-y* curve analysis.

For this purpose, the data from both test piles were initially combined because no significant difference in the characteristics of the peats at the two test sites was apparent from the available information. However, because a more accurate load cell was used for TP2 and because TP2 inclinometer readings were each made at a consistent time of 15 min after the time of load application, the final interpretation of results was based solely on the TP2 data.

To correlate the results of those lateral load tests with the known behavior of laterally loaded piles in other types of soils, the test results were interpreted within the framework of an existing *p-y* curve development procedure. The procedure selected was the integrated clay criteria of O'Neill and Gazioglu (*16*). The integrated clay criteria are similar in many respects to the soft clay criteria of Matlock (*15*), but they have been shown to represent the influence of pile diameter more accurately and to be accurate over a much wider range of soil conditions than the soft clay criteria. Those features of the integrated clay criteria were considered important in the interpretation of the results of only two tests on small-diameter piles in the unusual soil conditions of Mercer Slough.

The integrated clay criteria specify a relationship between unit soil resistance p and lateral pile deflection y at depth x to be of the form

$$p = \frac{1}{2} p_{ult} \left(\frac{y}{y_c}\right)^{0.37} \leq p_{ult}$$

where

$$y_c = 0.8\, \varepsilon_c \sqrt{D} \left(\frac{EI}{E_s}\right)^{0.125}$$

$$p_{ult} = F N_p cD$$

$$N_p = \begin{cases} 3 + 6\,(x/x_{cr}) & \text{for } x \leq x_{cr} \\ 9 & \text{for } x > x_{cr}, \end{cases}$$

$$x_{cr} = 0.25 L_c$$

$$L_c = 3 \left(\frac{EI}{E_s \sqrt{D}}\right)^{0.286}$$

and

E_s = secant soil stiffness,
ε_c = critical strain [at one-half $(\sigma_d)_{max}$ in UU triaxial test],
F = soil degradability factor describing brittleness of soil,
c = cohesive strength of soil, and
D = pile diameter.

In this formulation, the unknown quantities are the soil degradability factor F, the cohesive strength of the soil c, the secant soil stiffness E_s, and the critical strain ε_c. For the ductile peat material, the soil degradability factor was assumed to be equal to 1 (*16*).

The remaining three unknowns were varied in a direct search optimization procedure to find the combination of soil properties providing the best fit with the observed results. The soil properties were assumed to be constant throughout the peat because from the information entropy standpoint (*17*) there were no compelling reasons to assume otherwise. The optimization procedure sought to minimize the weighted error between measured and predicted pile displacements along the length of the pile. To account for the fact that greater strains are induced in the soil near the ground surface, the error function gave more weight to displacement errors near the ground surface than at greater depths. For each load, the weighted error was taken as

$$\text{weighted error} = \sum_{i=1}^{n} \frac{L + 1}{x_i + 1} |y_{meas} - y_{pred}|_i$$

where n is the number of points at which measured and predicted displacements were compared, L is the length over which measured and predicted displacements were compared and y_{meas} and y_{pred} are the measured and predicted displacements, respectively, at depth x_i. To obtain parameters that predicted the observed behavior at both low loads and deflections and at high loads and deflections, the total weighted error was taken as the sum of the individual weighted errors at lateral loads of 2.4, 4.8 and 6.9 kips. The properties inferred by this procedure were c = 200 psf, E_s = 1,000 psf, and ε_c = 3.6 percent.

Integrated clay criteria *p-y* curves developed from those values predicted pile head load-displacement behavior, which agreed well with the observed behavior (see Figure 8). The predicted deflected shapes of the pile also agreed reasonably well with the observed deflected shapes (see Figure 9). As was expected, the agreement was better at shallower depths where pile deflections and soil strains were largest.

For a model to be useful in the prediction of a particular parameter value, the prediction error should be sensitive to values of that parameter. A sensitivity analysis indicated that the total weighted error was sensitive to the cohesive strength c but not to the critical strain ε_c, or to the secant soil stiffness E_s. This sensitivity is illustrated in Figure 10, where the shaded bands along each abcissa represent ±10 percent deviation from the inferred parameter value.

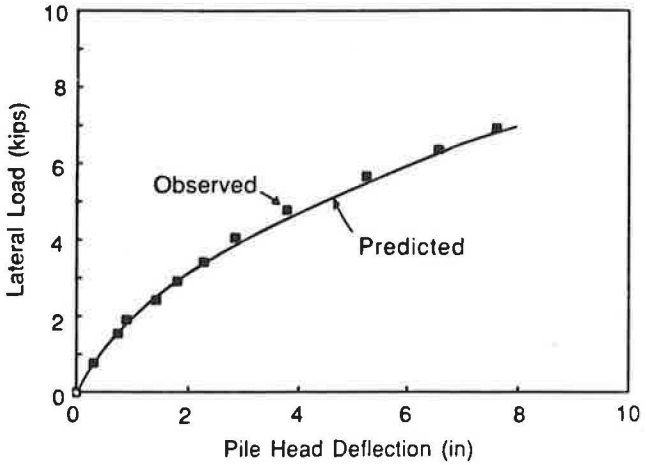

FIGURE 8 Observed and predicted load-displacement behavior.

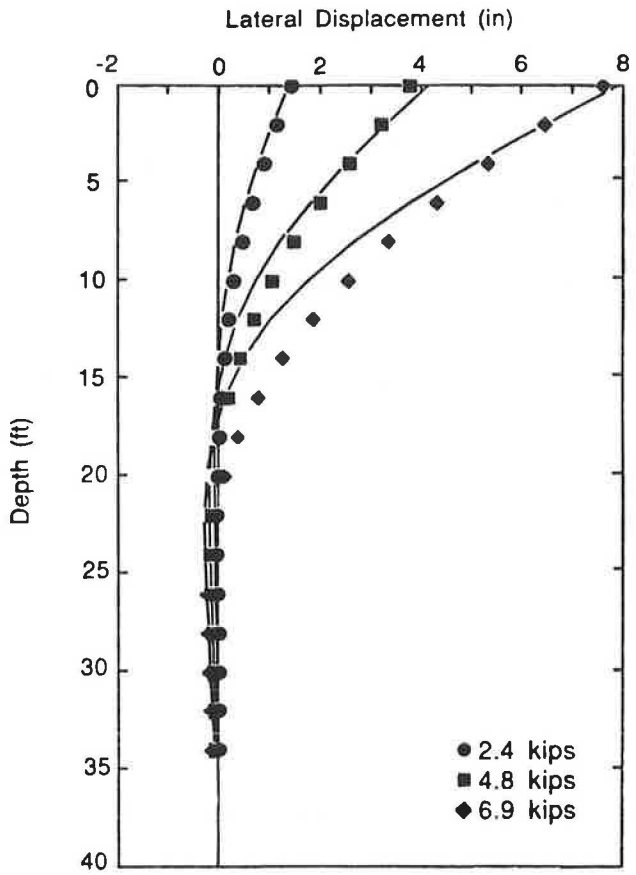

FIGURE 9 Observed and predicted deflected shapes.

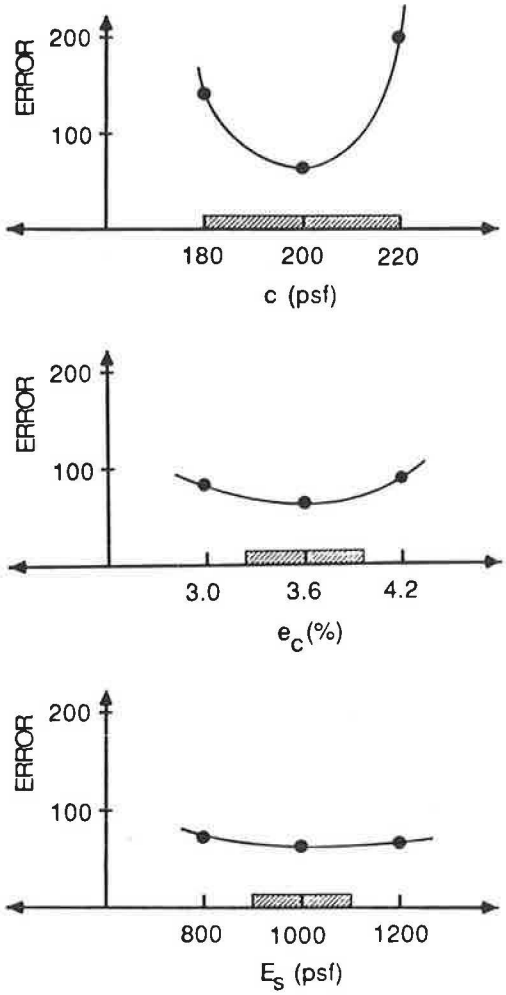

FIGURE 10 Results of sensitivity analysis.

The inferred cohesive strength of 200 psf is somewhat higher than the strengths obtained from the field and laboratory tests previously performed at the site but is within the range of shear strengths reported for other peats. The difference is likely attributable to the fibrous component of strength in the peat that is lost during sampling and not mobilized during relatively small-scale vane shear and cone-penetration testing. Poulos (*18*), on the basis of lateral load tests in cohesive soils reported by Broms (*19*), computed secant soil moduli ranging from 15 (low cohesive strength) to 95 (high cohesive strength) times the cohesive strength of the soil. The inferred secant soil modulus of 1,000 psf then appears reasonable for the Mercer Slough peat tests because the fibrous component of shear resistance provided by fiber tension in peat will require significantly more strain to be mobilized than would be required in the nonpeaty cohesive soil considered by Broms (*19*). The inferred critical strain of 3 percent is generally consistent with that observed in the UU triaxial tests on the Mercer Slough peats and for other very soft soils and is consistent with the assumption that the soil degradability factor F was equal to 1 (*16*).

SUMMARY AND CONCLUSIONS

In a case where the shear strength of a fibrous material such as peat or other soil with strong secondary structure is to be measured, an in situ test that mobilizes shear strength in a relatively large volume of soil is desirable. In a peat deposit in Washington state, a laterally loaded pile test was successfully used to measure in situ shear strength. It must be recognized, as with all in situ strength tests, that the measured strength corresponds to the failure mechanism induced in the soil by the test and should therefore be applied with care to problems involving significantly different failure mechanisms. Also, by the nature of the laterally loaded pile problem, the measured in situ strength is expected to be more representative of the strength near the ground surface than at greater depths.

The resistance to two laterally loaded test piles offered by the Mercer Slough peats was reasonably described by use of the integrated clay criteria with a cohesive soil strength of 200 psf, a soil secant modulus of 1,000 psf, and a critical strain of 3 percent. Those strength and stiffness parameters are consistent with those observed for other peats and with the results of laboratory tests of the peats at the site. Thus, they are considered to provide an indication of the strength and stiffness of the Mercer Slough peats that is improved over that obtained by small-scale field and laboratory tests.

REFERENCES

1. A. Landva and P. LaRochelle. *Compressibility and Shear Characteristics of Radforth Peats.* STP 820. ASTM, Philadelphia, Pa., 1983, pp. 141–156.
2. A. Landva. In-Situ Testing of Peat. *Proc., ASCE Conference on Use of In-Situ Tests in Geotechnical Engineering*, Blacksburg, Virginia, 1986, pp. 191–205.
3. L. Cadling and S. Odenstad. The Vane Borer. *Proceedings No. 2*, Royal Swedish Geotechnical Institute, 1950, pp. 1–88.
4. L. Bjerrum. Embankments on Soft Ground. In *Proc., ASCE Specialty Conference on Performance of Earth and Earth-Supported Structures*, Purdue University, Vol. 2, 1972, pp. 1–54.
5. J. D. Wineland. Borehole Shear Device. In *Proc., ASCE Specialty Conference on In-Situ Measurement of Soil Properties.* Raleigh, N.C., Vol. 1, 1975, pp. 511–522.
6. J. H. Schmertmann. Measurement of In-Situ Shear Strength. State-of-the Art Report. In *Proc., ASCE Specialty Conference on In-Situ Measurements of Soil Properties*, Raleigh, N.C., Vol. 2, 1975, pp. 57–138.
7. G. Sanglerat. *The Penetrometer and Soil Exploration.* Elsevier, New York, 1972.
8. *Proceedings of the European Symposium on Penetration Testing*, Stockholm, Swedish Council for Building Research, 1974.
9. L. Menard. The Menard Pressuremeter. *Les Editions Sols-Soils*, No. 26, 1975, pp. 7–43.
10. R. J. Mair and D. M. Wood. *Pressuremeter Testing: Methods and Interpretation.* Butterworths, London, 1987.
11. N. Janbu and K. Senneset. Field Compressometer: Principles and Applications, *Proc., Eighth International Conference on Soil Mechanics and Foundation Engineering*, Moscow, Vol. 1.1, 1973, pp. 191–198.
12. T. K. Mitchell and W. S. Gardner. In-Situ Measurement of Volume Change Characteristics, State-of-the-Art Report, *Proc., ASCE Specialty Conference on In-Situ Measurement of Soil Properties*, Raleigh, N.C., Vol. 2, 1975.
13. K. Terzaghi and R. B. Peck. *Soil Mechanics in Engineering Practices*, John Wiley and Sons, New York, 1948.
14. R. B. Peck, W. E. Hanson, and T. H. Thornburn. *Foundation Engineering*, John Wiley and Sons, New York, 1953.
15. H. Matlock. Correlations for Design of Laterally Loaded Piles in Soft Clays. Presented at 2nd Annual Offshore Technology Conference, 1970.
16. M. W. O'Neill and S. M. Gazioglu. *An Evaluation of p-y Relationships in Clays.* Research Report UHCE-84-3. University of Houston, April 1984.
17. M. Tribus. *Rational Descriptions, Decisions and Designs*, Pergamon, New York, 1969.
18. H. G. Poulos. Behavior of Laterally Loaded Piles: I, Single Piles. *Journal of the Soil Mechanics and Foundations Division*, ASCE, Vol. 92, No. SM5, 1971, pp. 711–751.
19. B. B. Broms. Lateral Resistance of Piles in Cohesive Soils. *Journal of the Soil Mechanics and Foundations Division*, ASCE, Vol. 91, No. SM2, 1964, pp. 3825–3863.

Publication of this paper sponsored by Committee on Soil and Rock Properties.

Confined Compression Test for Soils

L. W. ZACHARY AND R. A. LOHNES

The ratio of lateral to vertical stress at zero lateral strain (K_o) is a soil characteristic that is important in several geotechnical applications. At present, no unanimity exists as to how K_o should be calculated or how it is influenced by stress history. The uncertainty regarding this soil characteristic may be reduced through improved measurements. At present, triaxial testing and confined compression tests are used. Triaxial testing is cumbersome and limited to certain soil types. Confined compression tests ignore the presence of wall friction and thus may introduce unknown factors in the measurement. A new confined compression tester is described that measures wall shear stresses along with vertical and horizontal stresses. Confined compression tests on Ottawa sand, alluvial sand, crushed limestone, and coal and comparisons with K_o tests conducted in triaxial apparatus on replicate specimens of the two materials are included. The new test device shows promise and should lead to improved methods for evaluating K_o in soils and provide a tool for achieving an understanding of how stress history influences this important soil characteristic.

The "at rest" lateral stress ratio for soils K_o is used in retaining wall and deep foundation analyses and estimates of the loads on buried pipes, and has been shown to influence the shearing resistance of soils. K_o also affects the bearing capacity and settlement of shallow foundations, but it is seldom used. Some uncertainty exists about how to estimate or measure this soil characteristic, and the uncertainty is greatest in very loose soils, compacted fills, and overconsolidated sediments and residual soils.

Several analytical methods use the soil shear strength as the key parameter to estimate or calculate K_o and involve a measurement followed by a calculation based on assumptions. The application of K_o estimated in this manner carries with it the indeterminacy inherent with both measurement inaccuracies and analytical assumptions. The measurement of lateral stresses for zero lateral strain is accomplished by both in situ and laboratory methods. In general, interpretation of field tests is difficult because of poorly defined boundary conditions and uncertain drainage conditions. More specifically, individual in situ K_o testers are limited to a fairly narrow range of soil types. Laboratory tests suffer from sample disturbance for any measurement, and K_o tests are limited to cohesive soils and mechanical overconsolidation (*1*).

PREVIOUS STUDIES

One early application of lateral stress ratios in particulate materials is Janssen's equation (*2*) used to calculate the vertical and horizontal stresses that ensiled bulk solids exert on container bottoms and sides. This equation includes a lateral stress ratio k. Janssen explicitly stated that k should be measured for each material to be stored. Probably because of problems associated with measuring k, Rankine's (*3*) active case, K_a, was soon employed in the Janssen equation (*4*). The use of K_a has persisted into recent structural codes for silos and was employed by Marston (*6*) when he adapted Janssen's equation to calculate the loads on buried pipes. The use of K_a is inappropriate because the Janssen/Marston equations were developed on the premise that vertical loads are reduced by the shear that occurs on the vertical walls of the silo or on the sides of the ditch and that Rankine's K_a is for the ratio of minor to major principal stresses. The Rankine expression is also for failure stresses, and there is some question as to whether this is appropriate for static loads at no lateral strain.

Jaky (*7,8*) also was interested in the ratio of principal stresses for the zero lateral strain case as they applied to ensiled bulk solids and developed a theoretical equation to predict K_o from the friction angle ϕ of the material. He later showed that this equation applied to soils and retaining walls and simplified the equation to the famous form:

$$K_o = 1 - \sin\phi$$

This equation is attractive for its simplicity and is used widely for granular soils. However, the equation is flawed by a dependency on a failure parameter. Actually K_o is dependent on deformation (*9*) and not on failure.

Hendron (*10*) used a specially instrumented oedometer to measure the lateral stresses during loading and unloading of sands. His data show that for most sands during loading Jaky's equation gives reasonable estimates of K_o. During unloading the horizontal stress increased and even exceeded the vertical stress. Subsequent work with the oedometer on clays (*11*) indicated that K_o of normally consolidated clays could be estimated from an equation similar to the Jaky equation with the 1 replaced by 0.95 and that K_o of overconsolidated clays varied with overconsolidation ratio (OCR) and plasticity index of clay. Schmidt (*12*) suggested an empirical exponential relationship between K_o and OCR. This oedometer had a small height-to-diameter ratio to minimize wall friction.

A specially designed oedometer was used to establish a relationship between K_o, liquid limit, and OCR for clays (*13*). This oedometer had a height of 3.5 in. and a diameter of 7 in. to ". . . accommodate a large enough sample with minimum sidewall friction."

Mayne and Kulhawy (*14*) conducted a statistical study of 170 soils to empirically predict K_o from ϕ and OCR and concluded that the Jaky equation is valid for normally consolidated clays and "moderately valid" for normally consolidated sands. During unloading K_o is approximately dependent

L. W. Zachary, Engineering Science and Mechanics Department, Iowa State University, Ames, Iowa 50011. R. A. Lohnes, Civil and Construction Engineering Department, Iowa State University, Ames, Iowa 50011.

on ϕ, and, when reloaded, horizontal stresses can be estimated from ϕ, OCR, and the maximum OCR. All of those relationships are summarized in one equation.

Feda (*9*) used zero lateral strain triaxial tests to measure K_o of sands and concluded that the Jaky equation applied only to dense sands and that the stress-dilatancy theory (Rowe) could be used to predict K_o for normally consolidated sands. For overconsolidated sands, an exponential relationship between K_o and OCR exists up to a maximum K_o, approaching Rankine's passive stress ratio K_p.

Studies of agricultural grain in zero lateral strain triaxial tests indicated that measured values of K_o were slightly lower than those predicted by the Jaky equation (*15*). This study, intended for application to calculating static lateral stresses in silos, did not include unloading and overconsolidation effects.

The preceding brief discussion illustrates that the Jaky equation may have limited application for estimating K_o. However, recent studies use the equation for calculating stresses in compacted fills (*16*) and for evaluating the effects of anisotropic consolidation on soil shear strength (*17*). No unanimity may exist concerning how K_o should be calculated, and this, in part, may result from the various methods used to measure the lateral stresses in soils and other particulate materials. K_o is an important parameter, and an improved test method may contribute useful information.

CURRENT LABORATORY TESTS

In some K_o triaxial tests, lateral strains are monitored with a circumferential strain gauge (*9*), and it is assumed that the strains throughout the height of the test specimen are uniform. A second approach is to continuously monitor volume change and axial strain and continuously adjust confining stresses to achieve zero lateral strain, which would require computer-controlled servomechanisms for effective data collection. A third approach is to use a piston entering the cell that has the same diameter as the test specimen, and, by monitoring cell volume and by maintaining the volume at a constant value, average zero lateral strain will be maintained as the test specimen shortens (*18,15*). This last approach seems the most effective, but all triaxial tests are difficult to conduct on soft soils and are awkward for obtaining reliable data during unloading.

The oedometer test allows loading and reloading cycles but has the disadvantage of unknown shear stresses acting on the sides of the test specimen. In conventional equipment (*10,11*) or special apparatus (*13,19*), those stresses are always assumed to be zero. This is highly unlikely, even in equipment where the specimen size is thin to minimize shear. It is the opinion of the authors that thin specimens may be subjected to additional measurement errors because of end effects, and some evidence exists to support this opinion (*1*).

DESCRIPTION OF THE CONFINED COMPRESSION TESTER

The confined compression apparatus used in this work is illustrated in Figure 1. The thin-walled circular cylinder is made of acrylic and rests on an acrylic platform. Acrylic was originally chosen because of its low stiffness relative to metals and to assure that the strains in the cylinder would be large enough to measure accurately. Acrylic is clear, and the sample can be viewed during test set up and during deformation. In applications where variable lateral constraint is of interest, different cylinder diameters, wall thicknesses, and cylinder material may be used. Except for frictional considerations between the platform and cylinder, the cylinder is free to expand in the radial direction. The radial expansion is quite small, as is noted later. The vertical load is applied to the bulk solid by a piston located at the top of the cylinder.

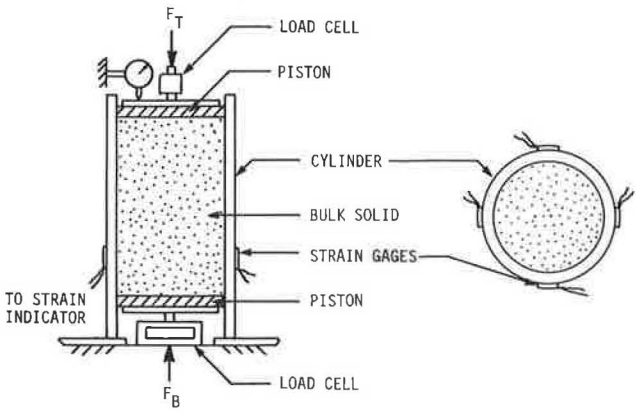

FIGURE 1 Confined compression test apparatus.

The piston is made of Delrin, which has a low coefficient of friction and also has good strength properties. The piston is backed by an aluminum stiffening plate. The piston is made slightly undersized, 2 mm on a 145-mm diameter, to keep the piston from transferring load directly to the cylinder. The load F_T at the top piston is monitored by a commercial load cell with a load capacity of 4448 N (1,000 lb). The load is supplied by a hand-operated pump and hydraulic ram. A dead load system, a lever arm and a fixed weight, could also be used in place of the hydraulic ram. The displacement of the upper piston is monitored by a dial gauge capable of measuring increments of 0.0254 mm (0.001 in.). A linear differential transformer can also be used to measure the piston movement.

At the bottom of the cylinder, another Delrin piston measures the force F_B, which is the force transferred to the soil in the axial direction. The force is monitored by a load cell of the authors' own design. The strain gauge-based load cell has a capacity of 1330 N (300 lb) and a sensitivity of 2.79 μ/N (12.42 μ/lb), where μ is in micrometers per meter of strain or microinches per inch of strain. The sensitivity is also the calibration factor of the load cell. Owing to the deflection of the load cell, the lower piston moves only very slightly when compared with the motion of the upper piston, and, it can be neglected. Again, the piston is undersized to keep the shear transmitted to the cylinder by the piston at a negligible level.

Four rectangular strain gauge rosettes are located at 90-degree increments around the cylinder at distance h_g below the top surface of the soil. Each pair of gauges measures the axial and hoop strains of the cylinder. The four axial strains are averaged to give the axial strain in the cylinder and likewise for the hoop (circumferential) strains. Because heat dissipation is a problem, 350-ohm gauges were used. Thermal

drift is insignificant for the amount of time required to take the strain readings. A switch and balance unit is used along with a constant voltage strain indicator. The bridge voltage is 2 V. The 350-ohm gauges have a gauge length of 6.35 mm (0.25 in.) and a gauge area of 46.8 mm² (0.0725 in²).

The soil vertical strain ε_v is determined by dividing the vertical movement of the upper piston by the original height h of the soil specimen. A set of tests on a granular material indicated that h/D ratios did not effect the results. This assumes that the axial strain is uniformly distributed throughout the depth of the material. The horizontal or lateral stress in the soil, σ_H, is determined by realizing that σ_H acts as an internal pressure on the thin wall cylinder. By using the thin wall pressure vessel formula to relate the internal pressure to the hoop stress σ_θ in the cylinder, plus, by incorporating the plane stress/stress-strain relationship, σ_H can be determined as follows:

$$\sigma_H = \frac{2\sigma_\theta t}{D} = \frac{2tE}{D(1 - \nu^2)}(\varepsilon_\theta + \nu\varepsilon_a) \tag{1}$$

where t, D, E, and ν are the thickness, diameter, Young's modulus, and Poisson's ratio, respectively, of the cylinder. Here, ε_θ and ε_a are the average hoop and axial strains of the cylinder as was measured by the strain gauges.

E and ν of the acrylic 145-mm (5.72-in.) diameter cylinder are needed, so a 41-mm × 300-mm longitudinal slice of material was taken from the cylinder to be used as a tensile specimen. The thickness of the cylinder wall and slice was 3.33 mm (0.131 in.). Two strain gauges were used to measure the longitudinal and lateral strains of the tensile specimen made from the longitudinal slice. The stress-strain diagram was nearly linear to 400 μ. All of the tests reported here had strains less than this value. E was found to be approximately 2.2 GPa (320 ksi). Poisson's ratio over the same range was 0.38.

A check on the σ_H values obtained from Equation (1) is desirable. However, no direct check is possible. A secondary check that involves the same strains and material properties is developed next. The axial stress in the cylinder at the gauge location is

$$\sigma_a = \frac{E}{(1 - \nu^2)}(\varepsilon_a + \nu\varepsilon_\theta) \tag{2}$$

The same axial stress will be estimated by using the forces measured by the pistons. By ignoring the weight of the bulk solid, an approach similar to Janssen's (*2*) can be used to determine the axial stress. The assumption that the weight effects are negligible is good for the apparatus illustrated in Figure 1. Referring to the free body diagram, Figure 2, that illustrates the vertical loads acting on the soil, the following equation holds:

$$dF = \pi D\tau\, dx \tag{3}$$

Then, assuming that the shearing stress is related to the horizontal stress by a constant coefficient of friction,

$$\tau = \mu\sigma_H \tag{4}$$

To relate the horizontal stress to the vertical stress σ_V, it is assumed that the stress ratio constant is

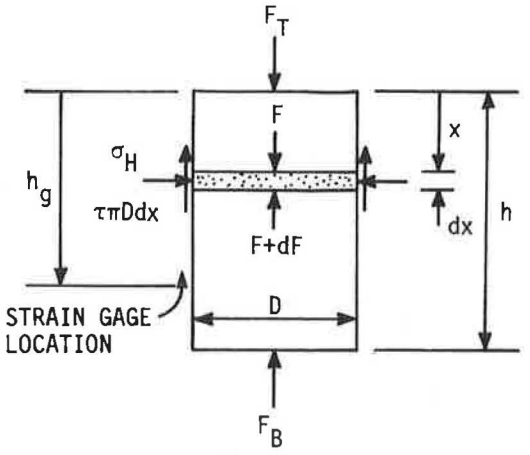

FIGURE 2 Soil free body diagram.

$$\sigma_H = k\sigma_V \tag{5}$$

Combining Equations 3, 4, and 5,

$$\frac{dF}{dx} = \mu k\pi D\sigma_V = \frac{4\mu kF(x)}{D} \tag{6}$$

where

$$\sigma_V = 4F(x)/\pi D^2 \tag{7}$$

The solution to this differential equation is of the form

$$F(x) = C_1 e^{-(\mu k/D)x} \tag{8}$$

Applying the boundary conditions

$$F(0) = F_T \tag{9}$$

$$F(h) = F_B \tag{10}$$

yields

$$F(x) = F_T(F_B/F_T)^{x/h} \tag{11}$$

and

$$\mu k = (D/4h)\ln(F_T/F_B) \tag{12}$$

The force in the wall of the cylinder at the gauge location is equal to the force at the top piston minus the force in the granular material given by Equation 11. This gives a wall stress of

$$\sigma_a = \frac{F_T}{\pi Dt}\left[1 - (F_B/F_T)^{h_g/h}\right] \tag{13}$$

Combining Equations 7 and 11 gives the average vertical stress in soil

$$\sigma_v = \frac{4}{\pi D^2}\left[F_T\left(\frac{F_B}{F_T}\right)^{x/h}\right] \tag{14}$$

PRELIMINARY TEST RESULTS

The confined compression tester was conceived to study the effects of wall roughness and stiffness on the stress distribution of ensiled particulate materials (*20,21*). Later it was recognized that the equipment has the potential to give new insights into factors that influence K_o of a wide variety of soils, especially those difficult to characterize in terms of lateral stress ratios.

Confined compression tests were conducted on Ottawa sand, an alluvial sand, crushed limestone, and coal. Hoop strains were observed to be about 0.00022 mm/mm. Because the strains were so small, the results of the confined compression tests were compared with those of K_o triaxial tests. The wall friction coefficients were compared also with direct shear tests of the Ottawa sand and coal on the same acrylic used for the confined compression tester. The wall friction coefficients agree within 0.02 and help substantiate the assumption of Equation 4. Jaky's K_o was computed from friction angles measured in triaxial tests. The confined compression tests included loading, unloading, and reloading tests. The data for those four materials are summarized in Table 1. The values for k are the ratios of horizontal-to-vertical stress as was calculated from Equations 1 and 14. The values for K_o are the ratios of minor principal stress to major principal stress calculated from the horizontal, vertical, and wall shear stresses and the equations

$$\frac{\sigma_1 + \sigma_3}{2} = \frac{\sigma_V + \sigma_H}{2}$$

$$\frac{\sigma_1 - \sigma_3}{2} = \left[\left(\frac{\sigma_V - \sigma_H}{2}\right)^2 + \tau^2\right]^{1/2} \quad (15)$$

where σ_1 and σ_3 are major and minor principal stresses, respectively; σ_V and σ_H are the vertical and horizontal stresses, respectively; and τ is the shear stress at the wall.

The wall friction μ' was calculated from Equation 12. The confined compression test results indicate that the materials tested have a wide range of K_o values and that those values roughly correlate with the K_o as measured in triaxial tests. However, confined K_o are consistently lower than triaxial K_o and, in the case of the Ottawa sand and crushed limestone approach, Rankine's active stress ratio. The behavior of the sand is consistent with Feda's (*9*) conclusion.

The variation between the triaxial and confined compression K_o values is the basis for continued study. Although it can be argued that the small lateral strains are sufficient to mobilize active case conditions, it is important to question the reliability of both the horizontal and the vertical stresses as determined in the confined compression test.

TABLE 1 RESULTS OF PRELIMINARY CONFINED COMPRESSION TESTS IN COMPARISON WITH TRIAXIAL AND DIRECT SHEAR TESTS ON THE SAME OR SIMILAR MATERIALS

	CONFINED COMPRESSION			C.C.	TRIAX	THEORY	
MATERIAL	k	K_0	μ'	K_0	K_0	K_0	K_A
OTTAWA SD	0.36	0.32	0.42	0.32	0.36	0.47	0.31
ALLUVIAL SD	0.34	0.29	0.47	0.29	0.30	0.42	0.26
CRUSHED LS	0.31	0.27	0.48	0.27	0.44	0.30	0.25
COAL	0.35	0.32	0.34	0.32	0.33	0.33	0.18

The horizontal stress is calculated from Equation 1 by using strains measured directly on the container. An internal check on the horizontal stress calculation can be found by calculating the axial wall stress from both Equations 2 and 13. Equation 2 uses the same strains used in Equation 1, whereas Equation 13 uses the forces at the top and bottom of the container. Both equations, using independent data, give the same result and verify the strain measurements and demonstrate that the horizontal stress computation is reasonable.

The main concern, then, is the computation of vertical stress. Equation 8 assumes that the vertical stress is uniform across the diameter of the specimen. Axial symmetry and the wall shear stress require that the vertical stresses vary from a maximum along the central axis of the specimen to a minimum at the wall of the container. Shear stresses acting on the vertical and horizontal planes are maximum at the wall of the container and decrease to zero at the center of the test specimen where the vertical and horizontal stresses are major and minor principal stresses, respectively. This is a fundamental limitation of the Janssen/Marston equation, and several analytical solutions have been suggested (*22–24*). All of those solutions use assumptions on the shape of the vertical stress distribution curve to solve the problem and, as such, are inadequate to validate or modify this measuring technique. The only way to determine the vertical stress distribution across the diameter of the soil specimen confidently is to measure it, and the technique for this difficult task is under development.

Figures 3, 4, and 5, illustrating Ottawa sand data, provide evidence of the potential of the confined compression tester. Similar results were obtained from other materials. Figure 3 is a plot of vertical stress versus horizontal stress for three load/unload cycles. The virgin loading cycle has a linear slope k from which K_o can be calculated. Unloading curves indicate that horizontal stresses remain high during unloading, and, as vertical stresses approach zero, horizontal stresses are higher than vertical stresses. Residual horizontal stresses occur at zero vertical stress. For reloading, k is lower, as would be expected for a densified specimen. Figure 4 is a plot of horizontal stress versus shear stress where the slope of the curve is μ'. As was expected, the loading and reloading curves are quite linear and nearly parallel. Finally, Figure 5 presents stress-strain curves with strain hardening that is typical of confined compression tests.

CONCLUSIONS

Confined compression tests with the new test device can be conducted in 20 min when compared with triaxial tests that require as much as 2 to 3 hr. The device should accommodate a wide range of soils and allows study of the effects of overconsolidation ratios and time on K_o.

Preliminary confined compression tests on sands, crushed limestone, and coal produce stress-strain curves that exhibit strain hardening, as was expected, and the measured value of k is linear throughout virgin loading. The horizontal stresses

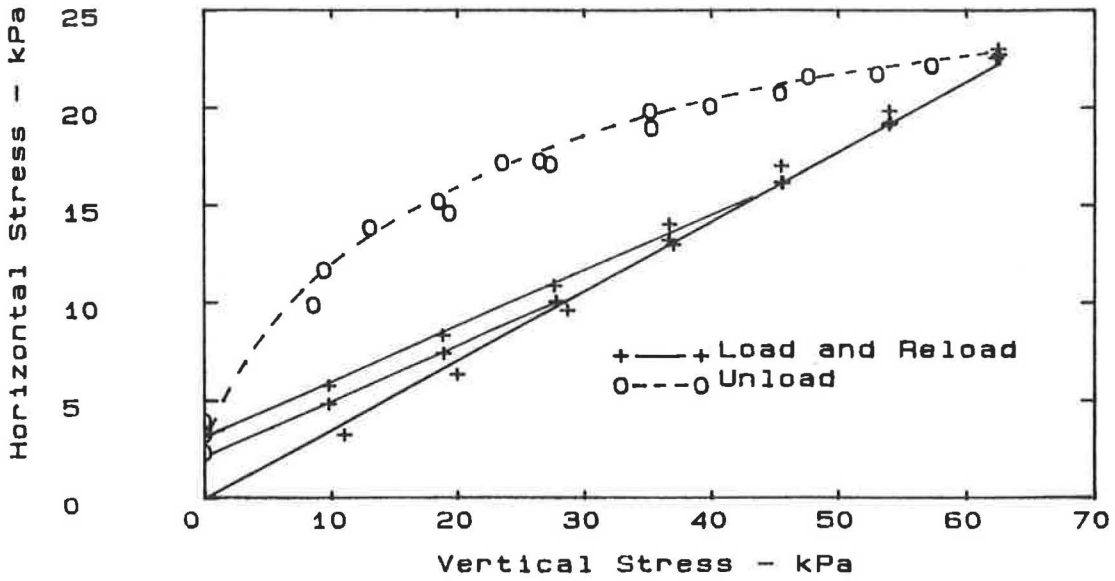

FIGURE 3 Horizontal and vertical stress curve.

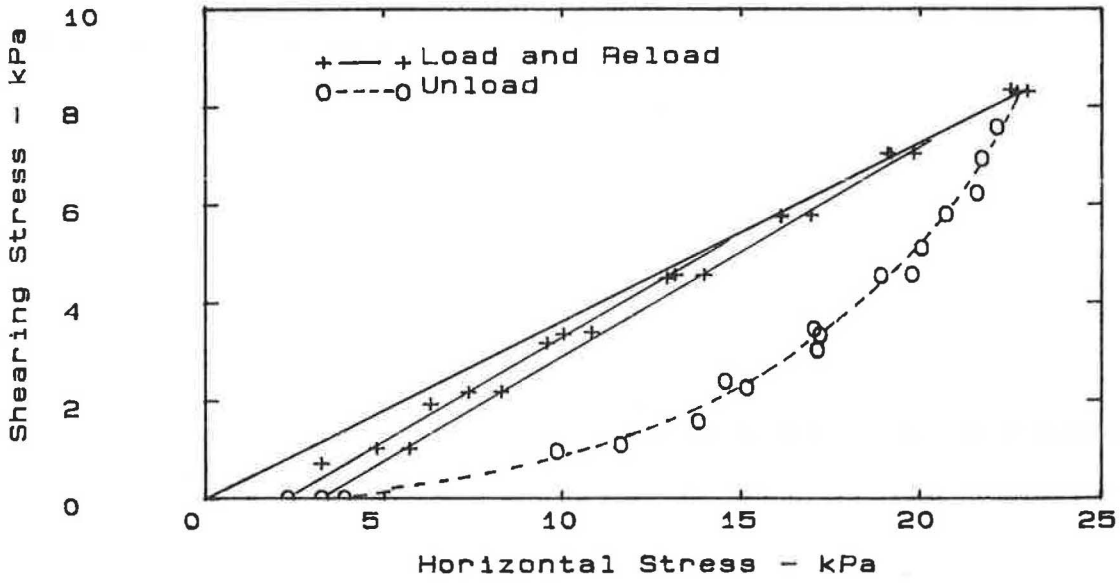

FIGURE 4 Shearing stress and horizontal stress curve.

remain higher at equivalent vertical stresses upon unloading, resulting in variable k values that approach Rankine's K_p as the vertical stresses approach zero. Residual horizontal stresses remain at zero vertical stress. The reloading curves are linear but have lower k values than the virgin loading. Wall friction coefficients determined in this confined compression test compare favorably with those measured by direct shear tests. Those data show considerable promise for the test device. However, when the contined compression results are compared with triaxial test results, the interpretation is not so straightforward.

This study illustrates the complexity of obtaining accurate K_o measurements and suggests that some previous K_o test results may have been somewhat naively interpreted and may have contributed to some of the confusion regarding accurate values of K_o. Continued development of this device appears

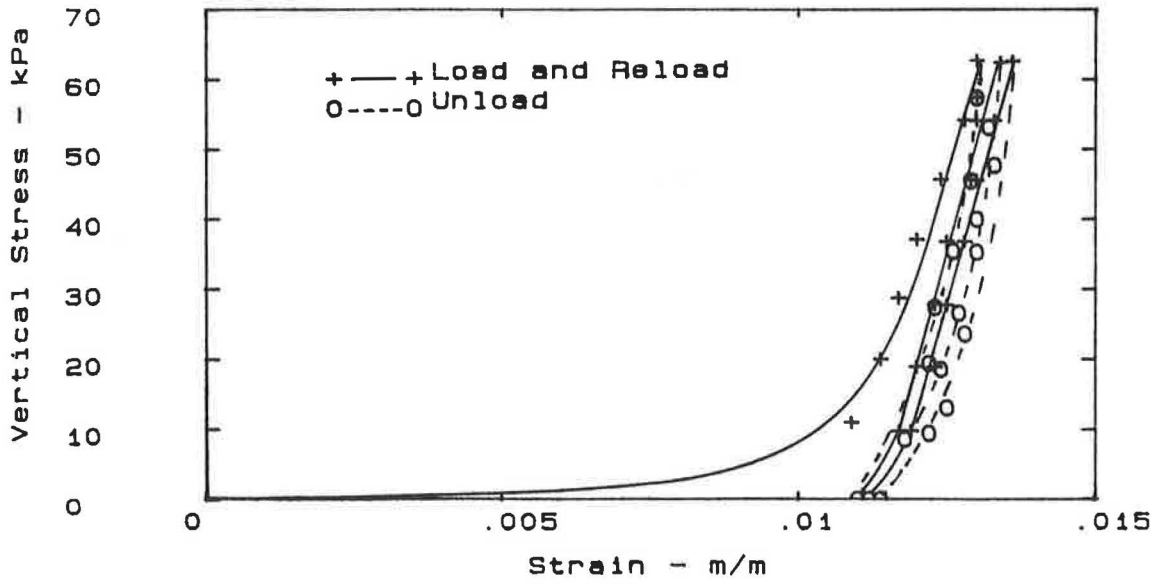

FIGURE 5 Confined stress-strain curve.

appropriate and necessary. The application of this device to saturated clays can be achieved by incorporating pore pressure transducers into the walls of the cylinder.

REFERENCES

1. M. Jamiolkowski et al. New Developments in Field and Laboratory Testing of Soils. *Proc., 11th International Conference on Soil Mechanics and Foundation Engineering*, Vol. 1, San Francisco, Calif. 1985, pp. 57–153.
2. H. A. Janssen. "Pressure in Silos." *Proceedings of the Institute of Civil Engineers*, London, 1896, p. 553.
3. W. J. M. Rankine. On the Stability of Loose Earth. *Transactions Philosophical Royal Society*, London, Vol. 147, 1857.
4. M. Koenen. Berechnung des Seiten und Bodendruckes in Silozellen. *Zentrablatt Baurerwaltung*, Vol. 5, 1896, p. 446.
5. *Recommended Practice for Design and Construction of Concrete Bins, Silos, and Bunkers for Storing Granular Materials*, American Concrete Institute, 1977.
6. A. Marston. Theory of External Loads on Closed Conduits in the Light of the Latest Experiments. *Bulletin 96 Iowa Engineering Experiment Station*, Ames, Iowa, 1930.
7. J. Jaky. A Nyugalmi Nyomas Tenyezoje. *Magyar Mern. Epitesz Egylet Kozlemenyi*, Oct. 1944, p. 355.
8. J. Jaky. Pressures in Silos. *Proc., 2nd International Conference on Soil Mechanics and Foundation Engineering*, Vol. 1, Rotterdam, 1948, pp. 103–107.
9. J. Feda. K_o Coefficient of Sand in Triaxial Apparatus. *Journal of the Geotechnical Engineering Division*, ASCE, Vol. 110, No. 1, 1984, pp. 519–524.
10. A. J. Hendron, Jr. *The Behavior of Sand in One-Dimensional Compression*. Ph.D. dissertation. University of Illinois, Urbana, 1963.
11. E. W. Brooker. and H. A. Ireland. Earth Pressures at Rest Related to Stress History. *Canadian Geotechnical Journal*, Vol. 2, No. 1, 1965, pp. 1–15.
12. B. Schmidt. Earth Pressures at Rest Related to Stress History. (discussion), *Canadian Geotechnical Journal*, Vol. 3, No. 4, 1966, pp. 239–242.
13. M. Sherif and D. E. Koch. Coefficient of Earth Pressure at Rest as Related to Soil Precompression Ratio and Liquid Limit. In *Highway Research Record 323*, HRB, National Research Council, Washington, D.C., 1970, pp. 39–48.
14. P. W. Mayne and F. H. Kulhawy. K_o-OCR Relationships in Soil. *Journal of the Geotechnical Engineering Division*, ASCE, Vol. 108, No. 6, 1982, pp. 851–872.
15. R. A. Lohnes, J. C. Liu, and W. H. Bokhoven. Experimental Determination of K_o in Grain. *Proc., 10th Powder and Bulk Solids Conference*, 1985, pp. 231–237.
16. J. M. Duncan and R. B. Seed. Compaction-Induced Earth Pressures Under K_o Conditions. *Journal of the Geotechnical Engineering Division*, ASCE, Vol. 112, No. 1, 1986, pp. 1–22.
17. N. Sivakugan, R. D. Holtz, and J. L. Chameau. CK_o UC Shear Strength of Normally Consolidated Soils from CIUC tests. *Journal of the Geotechnical Engineering Division*, ASCE, Vol. 114, No. 3, 1988, pp. 284–295.
18. R. G. Campanella and Y. P. Vaid. A Simple K_o Triaxial Cell. *Canadian Geotechnical Journal*, Vol. 9, No. 3, 1972, pp. 249–260.
19. A. G. Bishara, S. F. Ayonb, and A. S. Mahdy. Static Pressures in Concrete Circular Silos Storing Granular Materials. *American Concrete Institute Journal*, May/June 1983, pp. 210–216.
20. S. A. Masroor, L. W. Zachary, and R. A. Lohnes. A Test Apparatus for Determining Elastic Constants of Bulk Solids. *Proc., Spring Conference on Experimental Mechanics*, Society of Experimental Mechanics, Bethel, Conn., 1987, pp. 553–558.
21. L. W. Zachary and R. A. Lohnes. A Confined Compression Test for Bulk Solids. *Proc., 13th Annual Conference on Powder and Bulk Solids Handling*, Powder Advisory Centre, London, 1988, pp. 483–494.
22. D. M. Walker. An Approximate Theory for Pressures and Arching in Hoppers. *Chemical Engineering Science*, Vol. 21, 1967, pp. 975–997.
23. A. Livin. Analytical Evaluation of Pressures of Granular Materials on Silo Walls. *Powder Technology*, Vol. 4, 1970, pp. 280–285.
24. W. H. Bokhoven. *Stress-Strain Characteristics of Soybean Meal as Related to Flowability and Pressures of Bulk-Solids*. M.S. thesis. Iowa State University, Ames, 1988.

Publication of this paper sponsored by Committee on Soil and Rock Properties.

Numerical Evaluation of the Pullout Box Method for Studying Soil-Reinforcement Interaction

ZEHONG YUAN AND KOON MENG CHUA

Soil-reinforcement interaction properties are fundamental design parameters in the design of reinforced earth structures. Those properties can be determined either from direct shear or pullout tests. The pullout box test was used because it is more versatile than the direct shear test method in that it can be used to study wire meshes, strips, geogrids, geotextiles, and other types of reinforcements in different soils. The internal dimension of the pullout box is 30 in. long, 28 in. wide, and 24 in. deep. A finite-element program called GEOT2D capable of solving both the planar problem and the axisymmetric solid of revolution was developed. The soil-reinforcement system in GEOT2D is represented by isoparametric continuum elements, two-node membrane elements, and four-node interface elements. It is shown that with the nonlinear interface shear parameters obtained from the direct shear test pullout responses can be accurately predicted. Conversely, by matching numerically predicted pullout responses with measured pullout responses, it is possible to obtain nonlinear interface parameters directly from pullout tests, which can in turn be used to study performance of various types of reinforcements in earth structures. Effects of size of the apparatus, the reinforcement stiffness or extensibility, and the gap on pullout responses are discussed. The procedure presented takes into account those variables and thus yields soil-reinforcement interface properties both accurate and consistent for all applications.

In the design of reinforced earth structures, which includes reinforced earth retaining walls and reinforced slopes, the soil-reinforcement interaction properties described by the interface friction angle and cohesion are the fundamental design parameters. Those properties can be obtained either from direct shear tests or from pullout tests.

In recent years the New Mexico State Highway and Transportation Department (NMSHTD) has been considering and using different types of reinforcements in slope stabilizing and earth-retaining structures. During the past 4 years, more than 130 pullout tests have been performed for NMSHTD at the University of New Mexico (UNM). The reinforcing materials tested include wire meshes, geogrids, and geotextiles, and they were tested in concrete sands and different types of clays and silty sands. A substantial data base of pullout responses is available (*1*).

This study is presented in two parts. In the first part the soil-reinforcement interaction properties obtained from direct shear tests can be used in the numerical code to match pullout box test results. In the second part, to obtain soil-reinforcement interface properties from pullout tests accurately, those properties should be back calculated by matching numerical predictions with test results. The interface properties obtained by using this approach are thus independent of the apparatus configuration.

University of New Mexico, Albuquerque, N. Mex. 87131.

BACKGROUND

Soil Reinforcement

The concept of reinforced earth essentially involves introducing elements that can take tension into the soil mass and, as a result, increase the stability of the earth structure. This concept is an appreciable one and is shown to be reliable. However, recently and with numerous types of new soil-reinforcing elements being made available and also with more demanding design applications, there is a need to perform more accurate analysis of these reinforced earth structures.

There are two basic types of soil-reinforcing elements: metallic and synthetic. The metallic type includes galvanized steel strips, welded wire mesh, stainless steel, plain steel, and aluminum alloy. Structural plastics were introduced only in recent years. Polyester was used first in the nonwoven form. Other plastics used include polypropylene and polyethylene. These plastic materials are available in forms of geogrids and geotextiles. Geogrids are relatively stiff, netlike materials with large openings (typically ½ to 2 in.) between ribs or bars, whereas geotextiles are textiles in the traditional sense and can be found in woven and nonwoven forms.

Analysis of Reinforced Earth Structures

The conventional methods (*2*,*3*) for analyzing and designing reinforced earth structures follow the limit equilibrium approach. Basically, the methods require the assumption of the failure surface and then checking for equilibrium based on that surface. The methods are simple and easily understood by practicing engineers. However, the methods cannot be used to predict deformation behavior of reinforced earth structures and are usually very conservative. The other approach involves numerical methods, which include the finite-element method. Numerical methods can be made to predict both failure and deformation of reinforced earth structures more accurately.

The finite-element approach used in studying reinforced earth structures is divided into two methods: composite and discrete. The composite method (*4*,*5*) treats the behavior of

reinforced earth as a locally homogeneous composite material. The displacement compatibility between soil and reinforcement is inherently assumed. This approach suffers from two major drawbacks: (a) it does not allow direct assessment of the internal and local stability of reinforced earth structures and (b) the discretization of the soil-reinforcement system is somewhat arbitrary. In the discrete approach, the soil-reinforcement system is represented by continuum elements, reinforcement elements, and soil-reinforcement interface elements and can evaluate both internal stability and external stability of reinforced earth structures.

Constitutive Modeling of Soil-Reinforcement System

Modeling of Soils

The soil can be modeled as in other applications by using the hyperbolic stress-strain soil model (*6*). The tangent modulus (E_t) can be expressed as

$$E_t = \left[1 - \frac{R_f(1 - \sin\phi)(\sigma_1 - \sigma_3)}{2c\cos\phi + 2\sigma_3\sin\phi}\right]^2 KP_a\left(\frac{\sigma_3}{P_a}\right)^n \quad (1)$$

where

P_a = atmospheric pressure,
k = modulus number ,
n = modulus exponent,
R_f = failure ratio,
c, ϕ = soil cohesion and soil friction angle, respectively,
σ_1, σ_3 = maximum and minimum principal stresses, respectively, and
K, n, R_f, c, and ϕ = material parameters.

The values of those material parameters can be determined from conventional triaxial tests. The Mohr-Coulomb failure criterion is assumed, and the deviator stress is limited by

$$(\sigma_1 - \sigma_3)_f = \frac{2c\cos\phi + 2\sigma_3\sin\phi}{1 - \sin\phi} \quad (2)$$

Modeling of the Soil-Reinforcement Interface

One method of modeling soil-structure interaction behavior was suggested by Clough and Duncan (*7*). The expression for the interface shear stiffness is given by

$$k_s = K_i\gamma_w\left(\frac{\sigma_n}{P_a}\right)\left(1 - \frac{R_{fi}|\tau|}{c_i + \sigma_n\tan\delta}\right)^2 \quad (3)$$

where

K_i = interface modulus number,
γ_w = water density,
P_a = atmospheric pressure,
σ_n = normal stress,
τ = interface shear stress,
R_{fi} = failure ratio,
c_i = interface cohesion, and
δ = interface friction angle.

As can be seen, the Mohr-Coulomb failure criterion is incorporated into this hyperbolic equation.

Factors Affecting Pullout Response

A summary of the factors affecting pullout responses observed in the laboratory is given by Juran et al. (*8*), and the factors include the following:

- Density of soils: The pullout resistance is greater in a dense soil than in a loose soil.
- Confining/normal stress: The amount of dilation in dense soils decreases with increasing confining stress. As a result, the apparent friction angle also decreases.
- Particle interlocking: The degree of particle interlock is defined by the ratio between the grid opening or fiber spacing and average particle size. When this ratio approaches unity, the effective particle interlocking within reinforcement increases and the pullout resistance is also increased.
- Grid orientation: The orientation of grid reinforcements affects the total bearing area, which is the area normal to the direction of pullout.
- Stiffness of the reinforcement: The pullout resistance and thus average soil-reinforcement interface shear stresses are functions of reinforcement stiffness. For low stiffness reinforcements, the interface shear stresses are not uniformly distributed.
- Boundary effects: The effect of the rigid front face on pullout response is not well understood. Johnston (*9*) performed pullout tests with and without the front face and reported that a lower pullout resistance was generated with a rigid front face. However, the results of similar tests by Hornbeck (*10*) showed that a flexible front face produced a lower pullout resistance. This disparity suggests that it may be important to determine the appropriate gap size in the soil box to pull the reinforcement through. This issue and the effect of reinforcement stiffness are investigated in this study.

Laboratory Test Methods

As was mentioned earlier, direct shear and pullout tests are two laboratory testing methods to determine soil-reinforcement interface properties. In the direct shear test, the reinforcement is fixed on a plane face, usually onto a wooden block, with soil sliding over that. The pullout test is a more elaborate one. A reinforcement is placed at the mid-depth in a rectangular container full of soil. The reinforcement is pulled through a gap from one side of the box. For reinforcements with larger openings, such as Tensar SR2 geogrids, the shear box method may not be applicable, and a pullout box of a large dimension is more appropriate.

When comparing the results from the two different test methods, Ingold (*11*) observed that the pullout test gives higher values of the apparent friction angle for metallic and high modulus geogrid reinforcements and lower values for the more extensible geogrids and geotextiles. Also, it has been observed that the apparent friction angle obtained from pullout tests decreases with increasing normal pressure for low tensile modulus reinforcements, whereas the direct shear tests yield an

approximately constant interface friction angle (*11,12*). Thus, there appears to be a need to consider what is really being measured. In the direct shear test, because the membrane is glued to a rigid block (see Figure 1a) the tensile stress in the reinforcement is small. As a result, measurements from the direct shear test will be more a function of soil-reinforcement interface properties (i.e., interface friction angle and cohesion) and not the reinforcement stiffness. On the other hand, in the pullout test (see Figure 1b) both interface shear stress and tensile stress are mobilized owing to the pullout, and the pullout resistance depends on both interface properties and reinforcement stiffness.

COMPARING PULLOUT TEST RESULTS WITH NUMERICAL SIMULATION

Experimental Study

Pullout Box and Test Procedure

The steel pullout box at UNM was designed and built in 1985 for the NMSHTD and is described in detail by Carney (*13*). The internal dimension of the pullout box (see Figure 2) is 30 in. long × 28 in. wide × 24 in. deep. The loading system consists of three 20-ton capacity hydraulic jacks, one of which is used to apply the vertical load and the other two for the pullout. Strain-gauge–type load cells are used to measure applied loads. The applied vertical load is transmitted to the soil by a pyramid thick wooden blocks and is assumed to be uniformly distributed in the soil mass before the pullout force is applied. The maximum vertical pressure available is 6,800 psf, which is equivalent to an overburden of 60 ft of soil. The reinforcement is usually pulled at some constant rate after the vertical load is applied, and the pullout distance is measured by dial gauges at the pulling end. The dial readings are then reduced by the amount caused by extension of the exposed end of the reinforcement to obtain the accurate pullout displacement at the front face of the box.

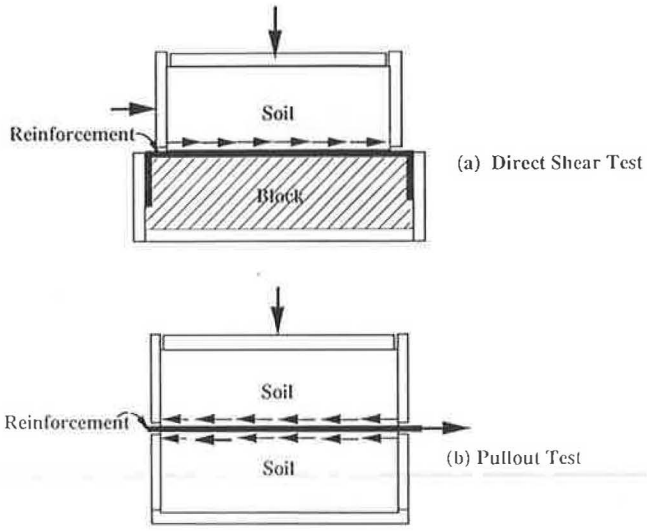

FIGURE 1 Two types of laboratory testing methods for determining soil-reinforcement interface properties.

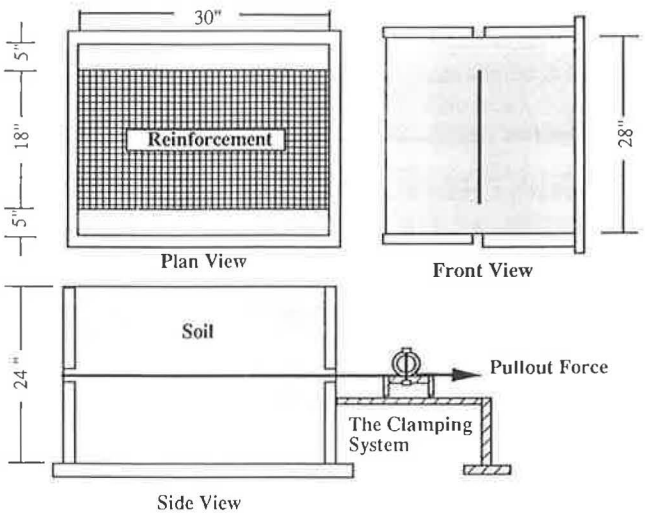

FIGURE 2 Schematic diagram of the pullout box.

Pullout Test Results

Performed pullout tests were performed with Geolon 200 and Tensar SR2 in concrete sand. The sand used was fine to medium, well graded (SW), with a coefficient of uniformity of 5.08. For all the pullout tests the sand was rained from 14-in. height to obtain a uniform dry density of about 108 pcf and a relative density of about 70 percent. Results from conventional triaxial tests indicate that the effective friction angle of the sand is 42 degrees.

Geolon 200, which is a woven geotextile, had a tensile strength of about 100 lb/in. according to uniaxial tensile tests. The stress-strain curve is given in Figure 3. For the pullout tests, the 18-in.-wide geotextile was placed at the middle horizontal section of the pullout box with 1 ft of concrete sand below and 1 ft above. The lateral clearance between the specimen and box was 5 in. on each side (see plan view, Figure 2). The geotextile was wrapped around a 3-in. diameter cylinder at the pulling end, and the cylinder was fixed to a channel beam. The channel beam moves along a track in the horizontal direction (see Figure 2). The other end of geotextile

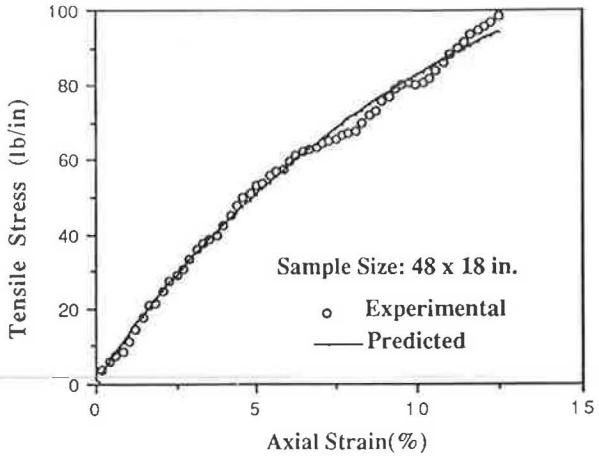

FIGURE 3 Stress-strain relationship of Geolon 200.

is free to move. The geotextile was pulled at a constant rate of about 0.3 in./min after the predetermined vertical load was applied.

The overburden pressures used were 0.71, 1.58, 4.14, and 5.03 psi, respectively. The results in terms of pullout force-displacement curves are presented in Figure 4. Figure 5 presents the average shear strength curve (τ_f-σ_n relation) of the sand-Geolon 200 interface. The average maximum shear stress is defined as the maximum pullout force from each pullout test divided by twice the embedded plan area of the reinforcement. The sand-Geolon 200 interface shear strength envelope obtained from direct shear tests is also indicated in Figure 5 for comparison.

Referring again to Figure 5, it can be seen that the maximum average shear stress τ_f obtained from pullout tests approaches a limiting value as the normal pressure σ_n is increased whereas τ_f increases linearly with increasing σ_n in direct shear tests. This is true because the maximum pullout force in any pullout tests should be less than the tensile strength of the reinforcement. The limiting value of τ_f is usually equal to the tensile strength divided by twice the embedded plan area of the reinforcement. Here, τ_f defined this way is a function of the specimen or the pullout box dimension. The limiting value of τ_f for the sand-Geolon interface with this particular pullout box (30 in. × 28 in. × 24 in.) is only about 1.67 psi, as indicated in Figure 5.

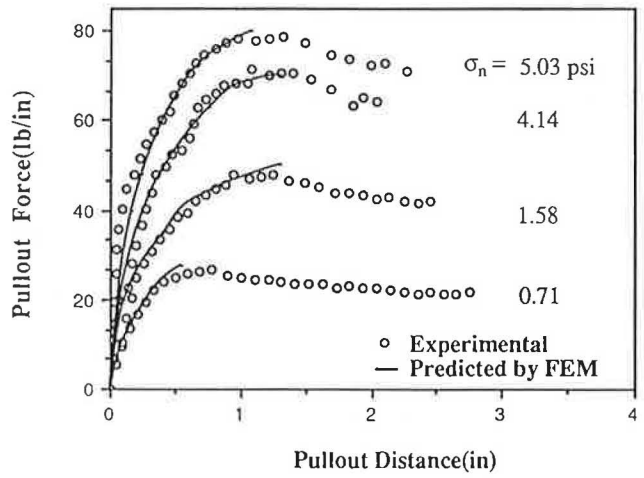

FIGURE 4 Predicted and measured pullout responses of Geolon 200 in sand.

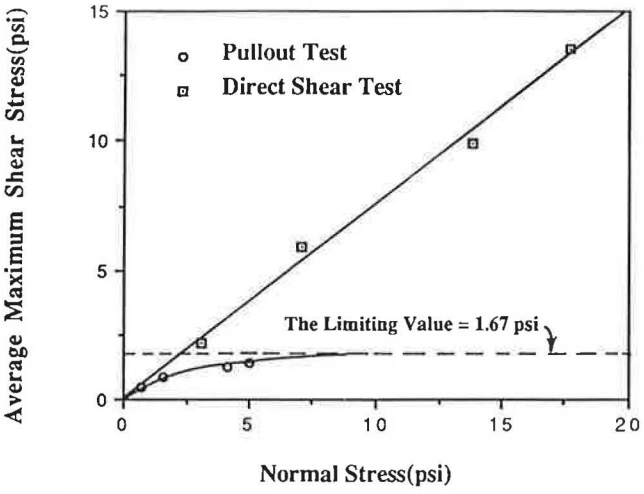

FIGURE 5 Average shear strength curves of sand-Geolon 200 interface.

Numerical Simulation

Finite-Element Code: GEOT2D

To model pullout tests and behavior of reinforced earth structures by using the discrete finite-element approach, a finite-element program GEOT2D was developed that models both the axisymmetric volume of revolution and the planner types of reinforced earth structures. This was achieved by using a combination of continuum, membrane, and interface elements. The new axisymmetric interface model and the axisymmetric membrane element model (*14*) were incorporated into the program to model accurately the axisymmetric type of reinforced earth structures. In the laboratory this feature allows the simulation of composite behavior of reinforced soil samples in conventional triaxial conditions. For modeling pullout tests, only the plane strain type of analysis will be performed.

Modeling of the Soil

The hyperbolic stress-strain relation as described in Equation 1 was used to model the sand. The values of parameters K, c, ϕ, n, and R_f were obtained from triaxial tests and are presented in Table 1.

Modeling of Reinforcement

The tensile test was performed with a 48-in. long × 18-in. wide piece of Geolon 200 geotextile. The tensile strength was found to be about 100 lb/in. width at 12.5 percent of axial strain, about 20 percent higher than that reported by the manufacturer that used a 4-in. wide specimen according to ASTM D-1682 (grab test). The larger width is more appropriate because geotextiles are normally not applied in narrow strips, and therefore the edge effects caused by the transverse reinforcement should be considered. The tensile test results of Geolon 200 show the nonlinear stress-strain behavior (see Figure 3). To take into account the nonlinearity, the following hyperbolic relationship was assumed:

$$\sigma = \frac{\varepsilon}{\alpha + \beta\varepsilon} \tag{4}$$

TABLE 1 HYPERBOLIC PARAMETERS FOR CONCRETE SAND

K	n	R_f	c	ϕ	G	F	d
200.	0.5	0.7	0	42°	0.35	0	0

where

α, β = constants,
σ = tensile stress, and
ε = tensile strain.

It can be seen from Figure 3 that the proposed model fits the test data reasonably well. The values of parameters α and β for Geolon 200 geotextile are 0.00075 in./lb and 0.0049 in./lb, respectively. The tensile modulus of Geolon 200 reduces from an initial value of 1,330 lb/in. at zero strain to about 430 lb/in. at failure (12.5 percent strain), which represents a more than three times variation. At a high strain level, the linear or linear secant tensile modulus approximation will be inaccurate.

Modeling of Soil-Reinforcement Interface

The hyperbolic interface model described by Equation 3 is obtained by incorporating the Mohr-Coulomb failure criterion into the original hyperbolic equation. In the numerical analysis, a small residual interface shear stiffness is assigned to the interface element when the mobilized interface shear stress is greater than the shear strength calculated from the failure criterion. Because the interface is actually an interaction response and not a "material," the "shear strength" and residual interface shear stiffness approach may not be appropriate. In view of this, the original hyperbolic form was followed, but without attempting to incorporate the failure criterion into the model. The interface shear stiffness k_s is directly controlled by the relative displacement between soil and reinforcement

$$k_s = \frac{\partial \tau}{\partial u_r} = \frac{a}{(a + bu_r)^2} \tag{5}$$

where

a = the inverse of the initial shear stiffness,
b = the inverse of the ultimate interface shear stress, and
u_r = the relative displacement between soil and the reinforcement.

The two fundamental hyperbolic parameters a and b are found to be dependent on the normal stress. For sheetlike reinforcements, a and b can be determined easily from the direct shear tests. Four direct shear tests were performed to determine the sand-Geolon 200 interface parameters. The shear stress-displacement curves are presented in Figure 6. The values of a and b corresponding to the different normal stresses σ_n are listed in Table 2. By correlating a and b with σ_n, we obtained the following two relationships:

$$a = 0.0036\sigma_n^{-0.5} \tag{6}$$

$$b = 1.2\sigma_n^{-1.0} \tag{7}$$

and the corresponding coefficient of correlation, R^2, is 0.97 and 0.94, respectively. The forms of expression are chosen to simplify the representation of the numerical interface model. Alternatively, the set of shear stress versus relative displacement curves can be input into the program, and interpolation

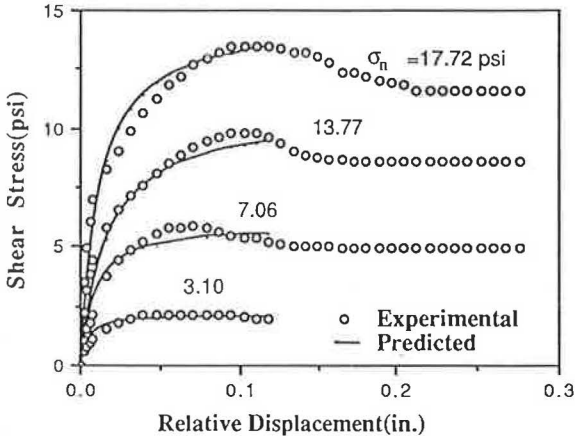

FIGURE 6 Stress-displacement curves of sand-Geolon 200 interface.

TABLE 2 VARIATION OF a and b WITH σ_n FOR SAND-GEOLON 200 INTERFACE

σ_n (psi)	3.10	7.06	13.77	17.22
a(10^{-3} in/lb)	1.98	1.37	1.02	0.76
b(10^{-3} in^2/lb)	463.40	167.62	92.61	68.01

is performed in a subroutine. This simple model can be seen to match the direct shear test results indicated in Figure 6 quite well. The data points beyond the peak shear stresses are neglected because it is inconceivable that the reinforcing material would be allowed to go beyond this level in a design. In any case, as in most laboratory tests, measurements beyond the failure threshold are affected by numerous factors not related to the soil properties.

It is possible that the a and b values are related to c_i and δ. If this is the case, then the "cohesion" will be strictly a function of the surface texture of the material and the soil. However, the "apparent friction angle" will have to include, for instance, the effects of aggregate-reinforcement interlock, grid spacing, lateral-bearing capacity, and soil dilation (and, hence, the soil properties). The aim of the subsequent phase of the study is to attempt to define a and b from the reinforcement characteristics and soil properties by using the pullout test data base at the University of New Mexico.

Simulation of the Pullout Box

The finite-element mesh used to simulate pullout tests is presented in Figure 7. Because the box is made of ½-in.-thick steel plates, it is reasonable to assume that soil particles cannot move in the direction perpendicular to the boundary. The reinforcement, however, is allowed to move freely in the longitudinal direction.

The soil-reinforcement system is represented by four-node isoparametric continuum elements, a two-mode membrane element, and four-node Goodman-type interface elements (*15*).

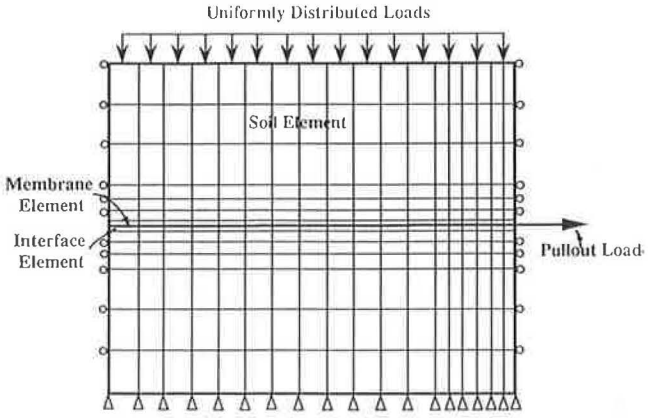

FIGURE 7 Finite-element discretization of pullout tests.

The shear stiffness of the interface element was described in an earlier section. During the pullout test, the applied vertical load is kept constant but the pullout force increases continuously until the peak value is reached. To model this process, the pullout force is applied in small increments.

Results

The x displacement fields (the lateral soil movement in the longitudinal direction) for a typical pullout test at 10, 50, and 100 percent of the maximum pullout force of 50 lb/in. width are shown in Figure 8–10. The pullout displacement corresponding to the peak pullout force is 1.28 in. A narrow high displacement band is developed around the reinforcement with the maximum occurring at some distance away from the front face owing to the rigid front face effect. Figure 11 presents the three-dimensional plot of soil movement in the x direction.

The contour of principal stress ratio (σ_1/σ_3) at maximum pullout force is presented in Figure 12. The higher stress ratios are found near the face of the pullout box and indicate the failure zone. Figure 13 presents the tensile force distributions along the reinforcement at different pullout load levels for a typical pullout test. The tensile force decreases from the pullout end to the front end in a nonlinear manner, which indicates a nonuniform distribution of shear stresses along the reinforcement.

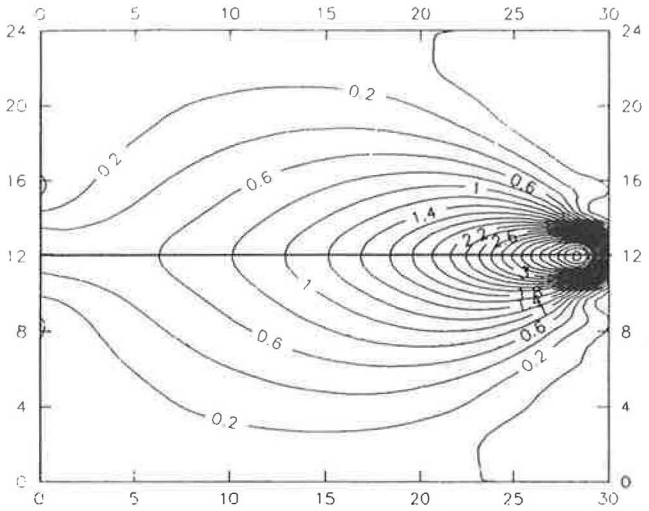

FIGURE 8 Contours of x-displacement at 10 percent of maximum pullout force (10^{-3} in.).

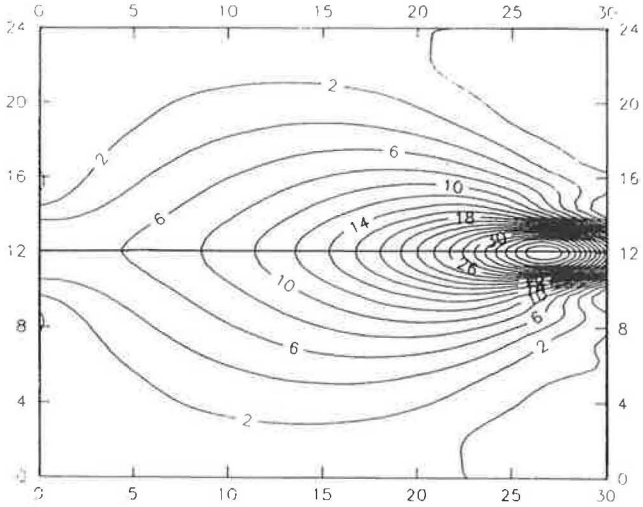

FIGURE 9 Contours of x-displacement at 50 percent of maximum pullout force (10^{-3} in.).

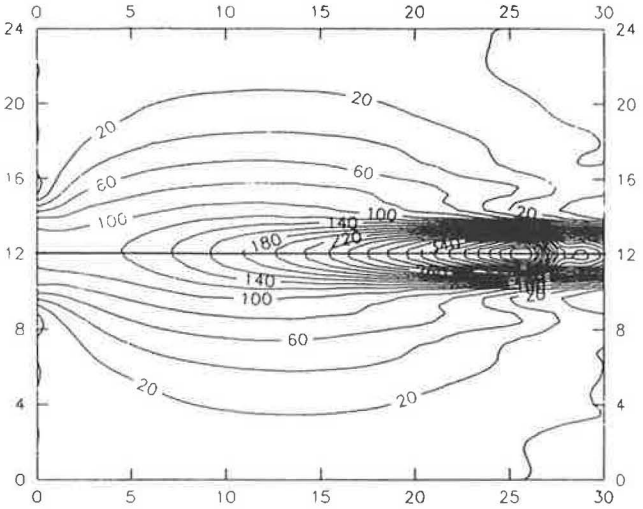

FIGURE 10 Contours of x-displacement at 100 percent of maximum pullout force (10^{-3} in.).

Referring again to Figure 4, the predicted pullout response matches the measured response of the four pullout tests quite well and suggests that the interface parameters a and b, obtained from direct shear tests as was described earlier, are essentially the same as those in the pullout tests. Thus it appears that the difference between soil-reinforcement interaction parameters obtained from direct shear and pullout tests reported by other researchers (*5–7*) may be caused by the interpretation approach rather than by testing methods. If the interface properties are obtained as shown here, then it will be possible to accurately predict responses of reinforced earth structures in the form of the pullout test as well as in the field.

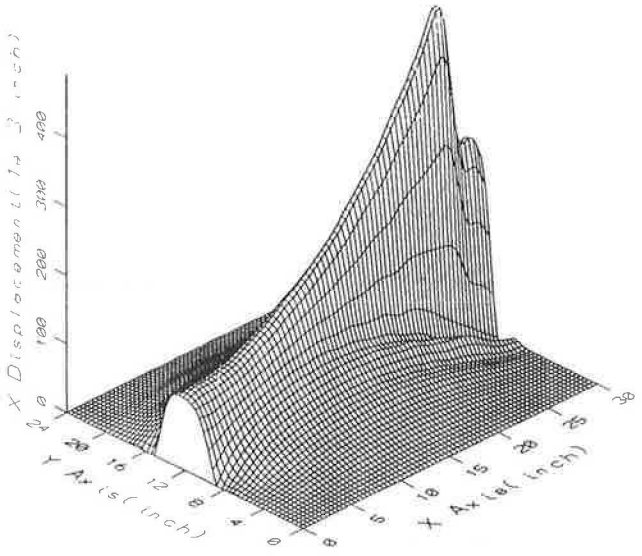

FIGURE 11 Three-dimensional display of x-displacement at maximum pullout load (10^{-3} in.).

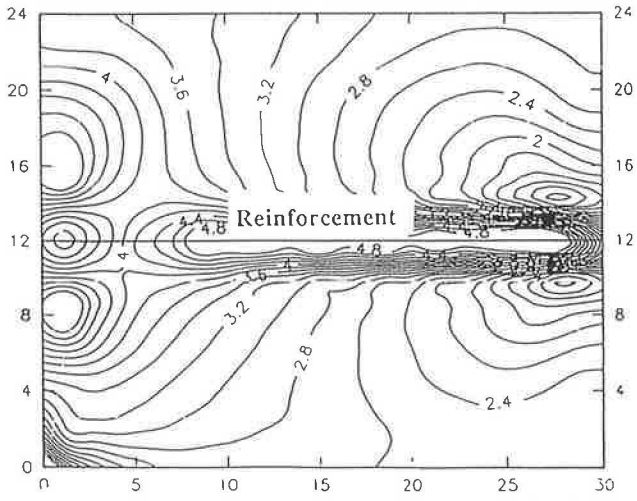

FIGURE 12 Contours of principal stress ratio at maximum pullout load.

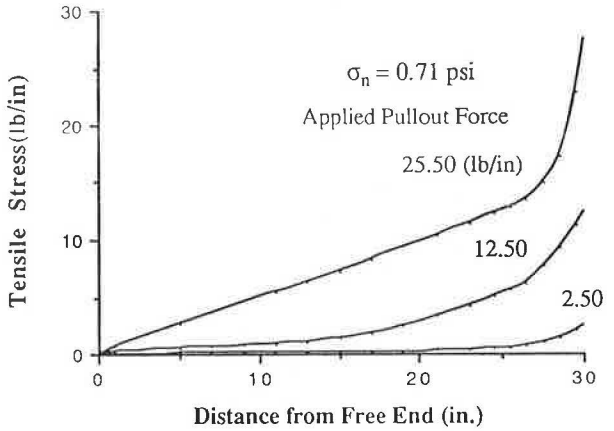

FIGURE 13 Predicted tensile stress distribution along Geolon 200.

OBTAINING INTERFACE PROPERTIES FROM PULLOUT TESTS

The interface properties of sheetlike reinforcements such as Geolon 200 can be obtained from the direct shear tests without difficulty. However, it is difficult to perform direct shear tests to obtain the interface properties for certain types of reinforcements, such as geogrids and wire meshes. For those types of reinforcements, the pullout testing method is more appropriate. The problem associated with the pullout test is how to obtain interface parameters from the pullout results and at the same time consider the nonuniform distribution of interface shear stresses and factors affecting the pullout results. This can be done by matching the measured pullout response numerically. The procedure for obtaining interface parameters from the pullout tests is as follows:

- Determine properties of soil and reinforcement and assign some reasonable values to interface parameters a and b;
- Use the interaction parameters as input and perform the numerical simulation by using GEOT2D or a similar numerical code;
- Compare the numerical pullout response with the measured response; and
- Change interface parameters until the measured pullout response is matched.

Interface Properties

This procedure was used to obtain nonlinear interface parameters a and b between Tensar SR2 geogrid and concrete sand from pullout test results. The stress-strain parameters α and β, obtained from a tensile test, are 0.00023 in./lb and 0.0024 in./lb, respectively. The soil is the same sand used in the study described earlier. Figure 14 presents a reasonably good match of the predicted and the measured pullout response of Tensar SR2 geogrid in the sand. The back-calculated a and b values at different overburden pressures σ_n obtained by the procedure are given in Table 3. By correlating a and b with σ_n, these two parameters can be expressed as functions of σ_n, which are also given in Table 3.

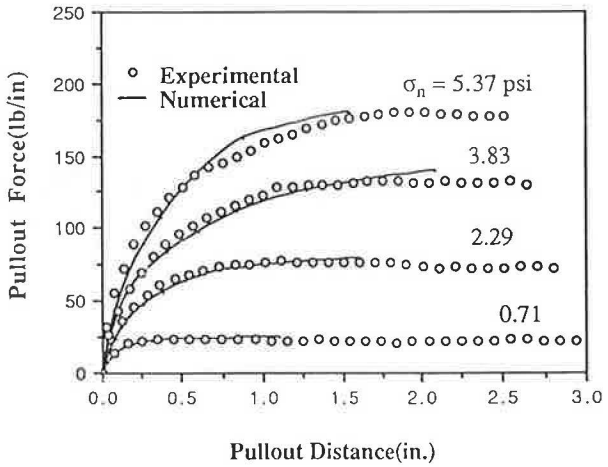

FIGURE 14 Comparison of experimental and numerical results of SR2 in sand.

TABLE 3 VARIATION OF a AND b FOR SAND-SR2 INTERFACE

σ_n (psi)	0.71	2.29	3.83	5.37
$a(10^{-3}$ in/lb)	3.92	1.61	1.18	0.98
$b(10^{-3}$ in^2/lb)	3.00	1.20	0.72	0.50

$a = 0.0030\ \sigma_n^{-0.7}$

$b = 2.67\ \sigma_n^{-1.0}$

Factors Influencing the Pullout Response

Extensibility

To investigate the effects of reinforcement extensibility or stiffness on pullout responses, a series of pullout tests was simulated by fixing interface parameters a and b and by varying reinforcement stiffness k_a. The reinforcement was assumed to be linearly elastic to simplify this investigation. Figure 15 shows predicted pullout responses with different k_a. From Figure 15 a higher k_a will result in a larger pullout resistance for a given pullout displacement.

Gap Size of the Pullout Box

The gap effect was investigated by simulating pullout tests of SR2 in concrete sand in the pullout box with different gap sizes. The results, given in Figure 16, indicate that the pullout resistance will increase as the gap size is made smaller. This is because the soil arches around the opening and thus provides more shear support to the reinforcement near the face of the front wall. The results indicate that this factor should be taken into account when a pullout box is designed. However, if the numerical approach presented here is followed, then the actual gap size can be simulated and, hence, be included in determining the pullout response.

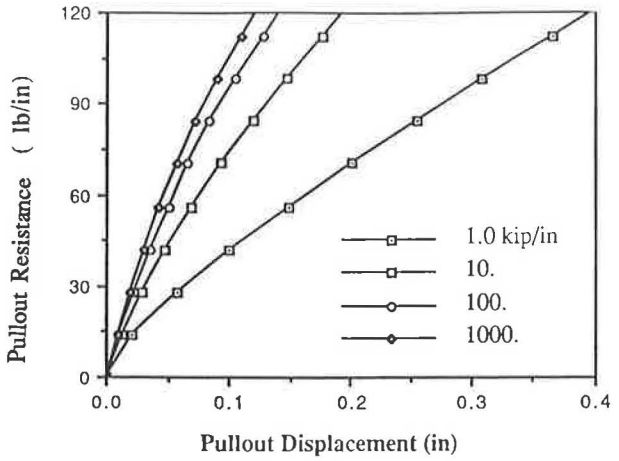

FIGURE 15 Predicted effect of reinforcement stiffness on pullout resistance.

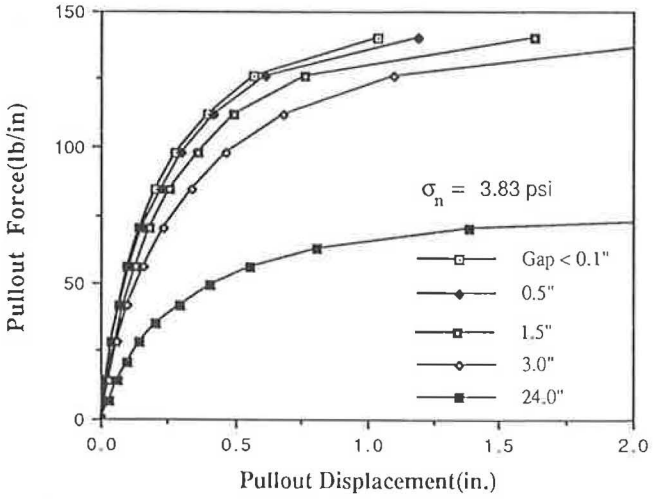

FIGURE 16 Predicted effect of gap size on pullout resistance.

CONCLUSIONS

Soil-reinforcement interface behavior can be obtained from the pullout test by using the test results in conjunction with the GEOT2D finite-element program. The pullout test is more versatile than the direct shear test and can be used to study wire meshes, strips, geogrids, geotextiles, and other types of reinforcements in different soils. The computer program GEOT2D can accurately predict pullout responses in pullout tests by using the nonlinear interface properties obtained from direct shear tests, which indicate that interaction parameters from the two testing methods are basically the same for sheetlike reinforcements.

The following conclusions were made regarding pullout resistance measured in the laboratory:

1. Pullout resistance measured directly from pullout tests should be used with caution because the response is a total response that depends on the configuration of the pullout box or the specimen dimension.
2. In pullout tests, soil-reinforcement interface shear stresses are not uniformly distributed along reinforcements. Average shear stresses and thus apparent interface parameters are functions of the specimen dimension.
3. The direct shear testing method can be easily used to evaluate interaction properties between soil and sheetlike reinforcements, such as Geolon 200, but is not appropriate for gridlike reinforcements, such as Tensar SR2.
4. A stiffer reinforcement will result in a larger pullout resistance for a given pullout displacement.
5. The pullout resistance appears to increase with a small gap size. It is suggested that the gap effect should be considered when comparing results of different test apparatus.

Finally, it should be realized that average or apparent soil-reinforcement interaction properties obtained from the direct and the pullout testing methods are different. This is mainly because of different methods of interpretation rather than by testing methods. However, the procedure presented here will take into account the different test configurations, soils, and

reinforcements to determine soil-reinforcement interface characteristic.

ACKNOWLEDGMENT

The authors are grateful to the Material Bureau of the New Mexico State Highway and Transportation Department for sponsoring this study.

REFERENCES

1. J. B. Carney and Z. Yuan. *Pullout Resistance of Tensar SR2 in Clay and Geofabrics in Sand*. Final Report C00893. Department of Civil Engineering, University of New Mexico, Sept. 1987.
2. *Guidelines for the Design of Tensar Geogrid Reinforced Soil Retaining Walls*. Technical Note, Tensar Corporation, TTN, RW1, Aug. 1986.
3. *Reinforced Earth Retaining Wall Systems*. Reinforced Earth Company, 1988.
4. K. M. Romstad, L. R. Herrmann, and C-K. Shen. Integrated Study of Reinforced Earth, I, Theoretical Formulation. *Journal of Geotechnical Engineering Division*, ASCE, Vol. 102, No. GT5, May 1976.
5. T. H. Wu. Behavior of Soil-Geotextile Composites and Its Application to Finite Element Analysis. *Proc., Geosynthetic '89 Conference*, San Diego, Calif., Feb 21–23, 1989, pp. 365–372.
6. J. M. Duncan. Hyperbolic Stress-Strain Relationships. *Proc., Work on Limit Equilibrium, Plasticity and Generalized Stress-Strain in Geotechnical Engineering*, McGill University, Montreal, Canada, May 1980, pp. 443–460.
7. C. W. Clough and J. M. Duncan. Finite Element Analysis of Retaining Wall Behavior. *Journal of Soil Mechanics and Foundation Engineering*, ASCE, Vol. 97, No. SM12, 1971, pp. 1657–1673.
8. I. Juran, G. Knochenmus, Y. B. Acar, and A. Arman. *Pull-out Response of Geotextiles and Geogrids (Synthesis of Available Experimental Data)*. Geotechnical Special Publication 18, ASCE, 1988, pp. 92–111.
9. R. S. Johnson. *Pull-Out Testing of Tensar Geogrids*. MS thesis, University of California, Davis, 1985.
10. D. E. Hornbeck. Laboratory Modeling of Reinforced Earth. Ph.D. thesis. Georgia Tech University, Atlanta, Georgia, 1982.
11. T. S. Ingold. Some Observation on the Laboratory Measurement of Soil-Geotextile Bond. *Geotechnical Testing Journal*, Vol. 5, No. 3/4, Sept./Dec. 1982, pp. 57–67.
12. T. S. Ingold. Laboratory Pull-Out Testing of Grid Reinforcements in Sand. *Geotechnical Testing Journal*, Vol. 6, No. 3, Sept. 1983, pp. 101–111.
13. J. B. Carney. *A Test Chamber for the Determination of the Pullout Resistance of Soil Reinforcing Members*. Report Ce-76(86)NMSHD-000757. Department of Civil Engineering, University of Mexico, March 1986.
14. Z. Yuan and K. M. Chua. A New Joint Element Stiffness Matrix for the Axisymmetric Interface. Presented at 11th U.S. National Congress of Applied Mechanics, April 1990.
15. R. E. Goodman, R. L. Taylor, and T. L. Brekke. A Model for the Mechanics of Jointed Rock. *Journal of Soil Mechanics and Foundation Division*, ASCE Vol. 94, No. SM3, May 1968.

Publication of this paper sponsored by Committee on Soil and Rock Properties.

Field Experience with the Back-Pressured K_o Stepped Blade

RICHARD L. HANDY, CHRIS MINGS, DAVID RETZ, AND DONALD EICHNER

The K_o stepped blade measures lateral pressures in situ in clay, silt, and sand soils. Pressures are measured after penetration of the soil by progressively thicker steps of a thin blade, and data points identified as representing consolidating behavior of the soil are extrapolated to obtain a hypothetical pressure on a zero-thickness blade. Pressures are measured with Teflon-covered pneumatic pressure cells designed to give 1–1 calibrations and ease of field repair. A new back-pressured readout system gives data reproducible to the nearest gauge dial increment, 1 psi (7 kPa). Most applications involve defining the soil stress history by measuring and plotting lateral stress versus depth. In nonexpansive soils the amount of prior surcharge may be estimated and the consolidation state established. Lateral stresses were used to delineate influences from compaction, expansive clays, adjacent shallow foundation loading, and interactions with pile and with retaining walls. For example, the lateral pressure on an existing wall was measured to test for pressures from expansive clay, relevant to the existing factor of safety. Passive pressures may indicate expansive clays or may warn of imminent bearing capacity failure per a cited example. Tests cannot be performed in stony soils, owing to difficulty in pushing the blade and the risk of damaging the pressure cells, nor can lateral stresses be measured in very soft clays where pressures from insertion of the blade exceed the limit pressure, which is probably attributable to the development of excess pore water pressure.

PRINCIPLE

The K_o stepped blade was developed to measure lateral soil pressures in situ. The blade is rectangular, sharpened at the lower end, and becomes progressively thicker up the shank in a series of flat rectangular steps (Figure 1). Each step has its own pressure cell to measure the lateral soil pressure exerted on that step after the blade has been pushed into the soil. Tests are performed by drilling to above the test depth and then alternately pushing one step length and reading all embedded pressure cells. Thus, a series of pressure readings is obtained at each subdepth. By plotting the several step pressures measured at each subdepth as a function of the step thickness, an extrapolation may be made (as indicated in Figure 1) to give hypothetical pressures on a zero thickness blade as an indication of the lateral total stress existing in the soil before blade insertion. Effective stresses are estimated by subtracting static pore pressures calculated from depth below a water table or measured with piezometers.

R. L. Handy and D. Eichner, Department of Civil and Construction Engineering, Iowa State University, Ames, Iowa, 50011. C. Mings, Geo-Hydro Engineers, Inc., 100 E. Callahan St., Rome, Ga., 30161. D. Retz, Burns & McDonald Engineering, 4600 E. 63d St., Kansas City, Mo. 64141.

HISTORY

The stepped blade was developed for the U.S. Federal Highway Administration to provide a rapid and accurate alternative for measuring lateral in situ stress in soil. The goal was a method that would be accurate to within 1 lb/in.^{2} (7 kPa) and be more rapidly and more readily performed than self-boring pressuremeter tests. The approach described here was borrowed from analytical chemistry; that is, to recognize that some disturbance to the soil is inevitable if a hole is bored or an instrument inserted into the soil so that instead of attempting to prevent disturbance the disturbance is allowed to happen and its effects removed by extrapolation.

The initial development of the stepped blade was made by Soil Systems, Inc., Marietta, Georgia, with Iowa State University as subcontractor from 1976 to 1981 under FHWA sponsorship. Tests and developments were continued at Iowa State from 1982 to 1987, with Eichner Engineering Co. as subcontractor for developmental work and J.-L. Briaud's group at Texas A&M University doing the comparative pressuremeter and finite-element studies. During this time the blade went through five major redesigns, the latest incorporating a back-pressure readout system and a back rib to stiffen and strengthen the blade without appreciably affecting pressure readings.

The blade development was preceded and was partly inspired by the pioneering work of Marchetti with the dilatometer. The main differences between the stepped blade and the dilatometer follow: The blade has several steps, each with its own pressure cell, and is several times thinner than the dilatometer. The blade cells are pneumatic and nonexpansive, and the dilatometer is electropneumatic and expansive. The dilatometer is shorter and more rugged and can be pushed continuously, and the blade requires predrilling to each test depth where it then is pushed. The soil responses differ, as do the methods for data interpretation. The dilatometer interpretations depend more on established empirical correlations.

DEVICE

Ratio of Width to Thickness

Most in situ soil testing devices are cylindrical in shape, with the lower end sharpened to a cone or hollow cone. An obvious difference between pushing a thin, flat blade and pushing or driving a cone is the reduction of the amount of soil displaced and disturbed. Further, the thinner the blade, the less soil should be disturbed.

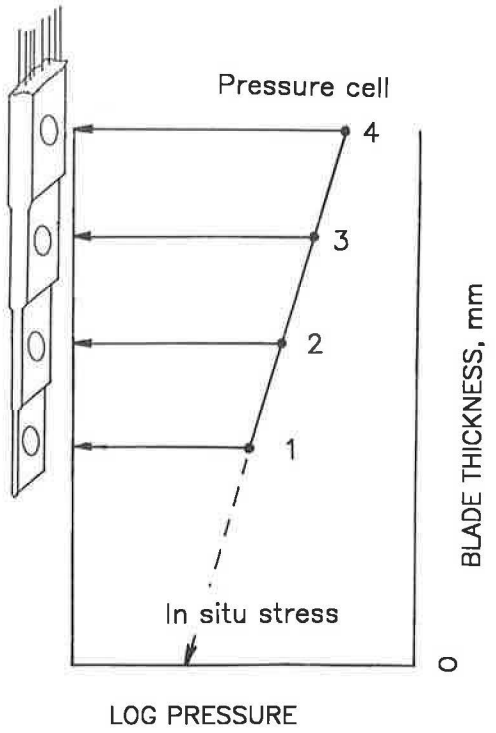

FIGURE 1 Principle of the K_o stepped blade test.

Laboratory tests with layered modeling clay showed a linear relationship between the thickness of the disturbed zone and the thickness of the blades, the blade width being constant (*1*). The ratio of width to thickness can be used as a dimensionless measure of relative blade thinness: the higher the ratio, the thinner the blade. In the case of solid cylindrical or conical test devices, the ratio is 1.0. Ratios for those and other devices including the current stepped blade are listed in Table 1 and presented in Figure 2. In the case of the two samplers listed, the (w) is taken as the inside circumference of the sampler and the thickness (t) is twice the wall thickness, since soil is displaced only toward the outside.

Back-Pressured Pneumatic Pressure Cells

A late development in blade research, and a key factor for improving the reliability and precision of the pressure readings, was the invention of a back-pressured system for operating and reading the pneumatic pressure cells (*2*). Most pneumatic cells, including those of earlier model blades, operate by applying inside gas pressure against a diaphragm exposed to the pressure to be measured. Then, when the pressures are equalized, the diaphragm lifts sufficiently to allow gas to flow through the cell and be detected with a flowmeter. Those are referred to as normally closed or venting type cells (*3*). In early versions of the blade, pressure was applied to area A in Figure 3, and area B was monitored for flow. After flow had been achieved, gas pressures may have been reduced to obtain a pressure reading for the initiation of a no-flow condition. This was not done in early blade testing because of the undesired effect of pushing the soil away and then allowing the soil to come back before taking a pressure reading. Difficulties were experienced when the diaphragms either leaked or stuck when monitoring for changes in gas flow through long pressure lines. In some instances, individual blade cells had calibration factors that not only were different for each cell but tended to change (*4*). A strain-gauge cell that directly measures effective stress also was developed (*5*) but was not sufficiently reliable for field use, so emphasis continued to be placed on the pneumatic cell.

TABLE 1 WIDTH-THICKNESS RATIOS FOR SOME SOIL PENETRATION TEST AND SAMPLING DEVICES

Device	t, mm	w, mm	w/t
Standard cone	35.7	35.7	1.0
SPT	15.9	110	6.9*
3-in. Shelby tube	3.3	229	69.4*
NX vane	3.2	25.4	8.0
Dilatometer	14	95	6.8
Glotzl cell	5	100	20.0
SBT step 1	3	63.5	21.2
step 2	4.5	63.5	14.1
step 3	6	63.5	10.6
step 4	7.5	63.5	8.5

* t is 2X the wall thickness and w is the inside circumference since the soil is presumed to be displaced only to the outside.

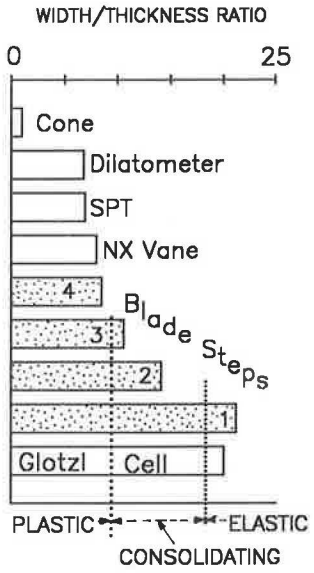

FIGURE 2 Width/thickness ratios for some soil-penetrating devices and dominating behavior as inferred from stepped blade tests.

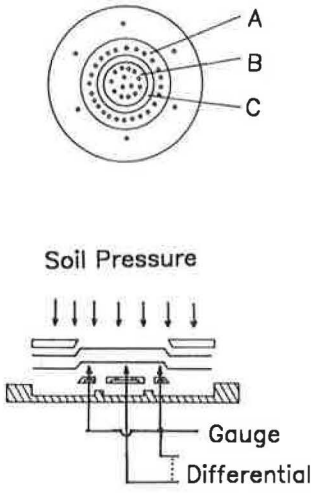

FIGURE 3 Components of the pneumatic pressure cell (not to scale).

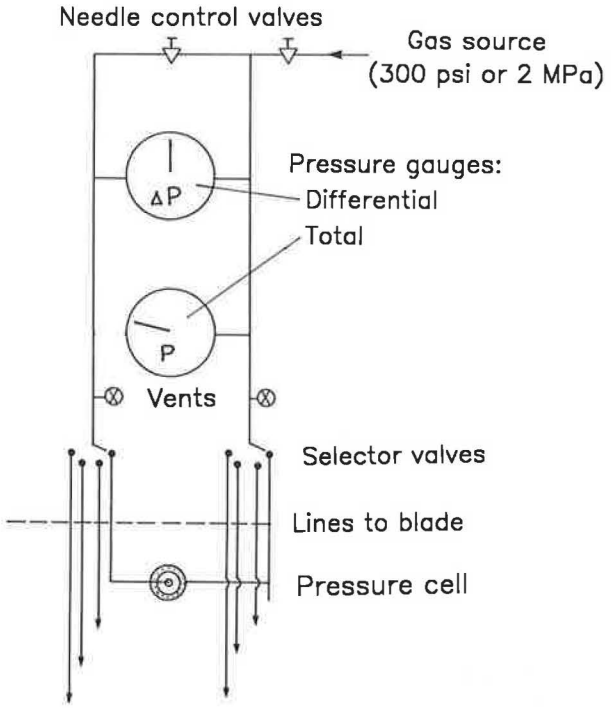

FIGURE 4 Schematic diagram of the back-pressured blade console.

Laboratory tests indicated that sticking of diaphragms was more likely to occur at high pressures and be quite sensitive to minor changes in the height of the threshold C in Figure 3. Because only part of the back side of the diaphragm was pressurized, which seemed a rather inefficient and possibly error-prone way to balance the soil pressure, a scheme was devised to pressurize both areas A and B simultaneously while maintaining a small differential pressure between the two areas. When the higher of the two pressures reached the soil pressure as the two pressures were raised, the membrane lifted sufficiently to allow a small amount of gas flow within the cell, thereby reducing the differential pressure to near zero and usually causing a perceptible pause in the rate of increase of the main gauge pressure. The loss of differential pressure told the technician when to read the pressure gauge, and the serendipitous pause in climb of the main gauge needle made it easier to read.

The method used for simultaneous pressurization is quite simple and is presented schematically in Figure 4. A needle valve T1 controls the rate of pressure increase and ordinarily is set for a rate of increase of about 1 psi/s (7 kPa/s). Nitrogen, compressed air, or carbon dioxide regulated to a maximum pressure of 300 psi (2000 kPa) is used as a gas source. The second needle valve T2 is left closed until both gauges approach 8 to 10 psi (60 to 80 kPa), and then the needle valve is opened slightly and adjusted to give a differential pressure that will tend to remain constant without further adjustment. Some leakage and reduction of differential pressure may occur as the soil pressure is approached, particularly if the soil pressure is unevenly distributed around the cell threshold C in Figure 3. In this case, T2 may be partially shut to sustain ΔP until a sharp drop occurs. It will be seen that if the diaphragm is lifted, then ΔP must go to near zero regardless of the position of T2.

SOIL RESPONSES

Consolidation Response

It was anticipated and then shown by laboratory experiments that the thicker the blade step the higher the pressure induced by insertion of that step into the soil (*1*). An empirical relationship was defined between thickness and log pressure, as indicated in Figure 5a. Regression of the data typically will give r^2 values in the range 0.97–1.0. The semilogarithmic response corresponds to a linear relation of void ratio to log pressure and on this basis is assumed to be indicative of consolidating behavior of the soil next to the blade. Consolidation may be aided by the relative thinness of the blade when compared with other devices and by a zone of reduced stress and low or negative pore pressures extending out from both edges of the blade after insertion. Because consolidation may be far from complete when blade cell pressures are read, approximately the same amount of time should lapse between insertion and reading of each pressure cell. Variable times from a few minutes to 2 weeks have been used without affecting the extrapolated soil pressures.

Elastic Response

Field use of the stepped blade indicated that the soil response might not always be so simple as was initially envisioned. The pressure sometimes is higher on the first and thinnest blade step than on the subsequent thicker steps. This behavior, presented in Figure 5b is followed by the more conventional behavior.

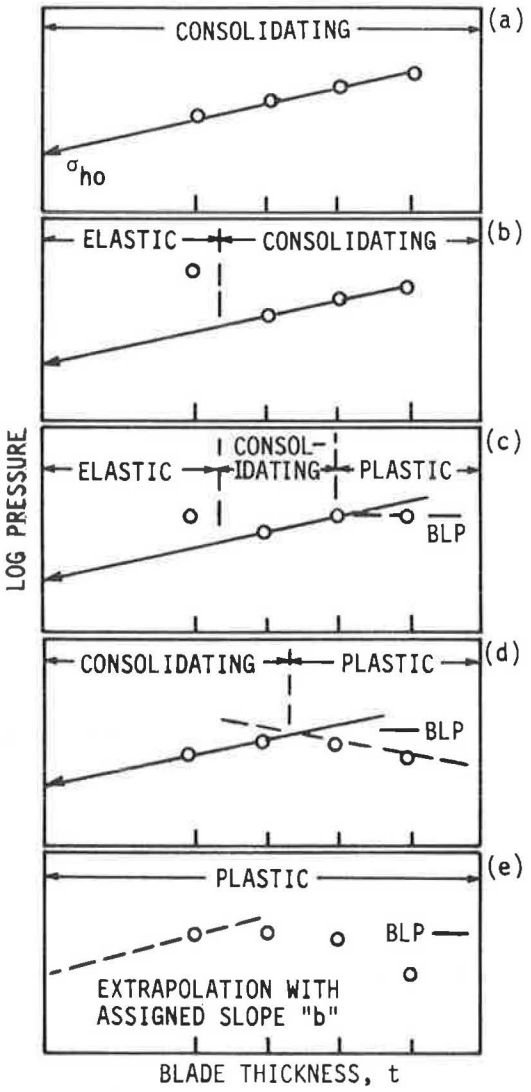

FIGURE 5 Selected data plots of log blade pressure as a function of blade thickness *t* and inferred soil response. BLP, blade limit pressure.

This anomaly did not occur in the laboratory developmental tests performed on remolded samples (*1*) and was most commonly observed in stiff clay loam soils such as glacial till and in lightly cemented silts and sands. Circumstantial evidence thus pointed to influences from a relict soil structure that may be left intact by penetration of the thinnest blade step only. The structure may cause the soil to behave elastically until broken down by penetration by the next thicker step.

The blade imposes constant deflection instead of constant stress conditions, as in a conventional laboratory consolidation test. Thus, as illustrated in Figure 6, a stress relief from B on the elastic response curve to C and D on the virgin compression curve should be possible if the soil structure were to break down. An analogous reduction does not occur in constant-stress consolidation tests because the path goes from C downward to E. When it occurs, this apparent discontinuity in soil behavior indicates that data should be separated into two stress regimes.

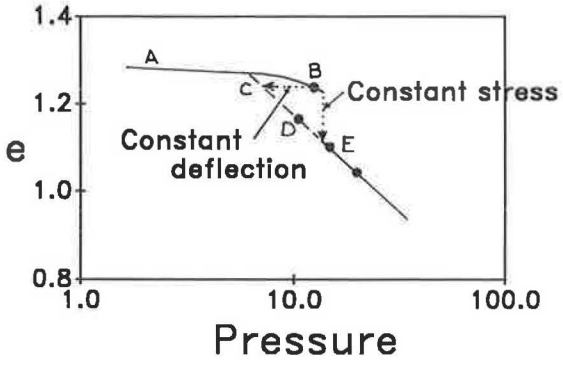

FIGURE 6 Hypothetical *e*-log *p* diagram of a slightly cemented soil to show how a high first point may develop in stepped blade tests. Collapse of the soil structure relieves the stress from B to C and D on the virgin compression curve.

If this interpretation is correct, then the pressure on the first step should be essentially an elastic response that may be used to compute a lateral subgrade modulus. In support of this, correlations between first-step pressures and the pressuremeter moduli were substantially better than were obtained by subtracting consecutive step pressures (*6*).

In no case was the elastic response observed on other than the first blade step, indicating that a width/thickness (*w/t*) ratio that is less than 14 must break down the soil structure. A value of 18 was arbitrarily selected to define an approximate elastic range indicated in Figure 2.

Plastic Failure

A second, more common, departure from a semilogarithmic relationship between soil pressure and blade thickness was previously described and attributed to a limit pressure; that is, relief of the consolidating pressure by plastic failure where the dominating behavior is pushed aside rather than being compressed (*1*). This behavior is noticed when there is a constant or decreasing blade pressure with increasing step thickness, as indicated on the right in Figures 5c, 5d, and 5e. The phenomenon is most common in soft, saturated clay soils where it probably reflects the development of excess pore pressure. What supports this interpretation is that the blade limit pressure has been shown to correlate with the pressuremeter limit pressure (*6*), and soil pressures measured in soft clays with the relatively thick dilatometer have been shown to be mainly excess pore water pressures (Lutenegger, unpublished data). A pore pressure port has been incorporated into the thickest step of the blade but has not yet been subjected to field tests. Pore pressure studies to illustrate consolidating behavior with the thinner blade steps are reported by Tse and Handy (*7*). The limit pressure response usually occurs by the fourth step and in soft soils may also occur when inserting thinner steps and, in some instances (as indicated in Figure 5e), preventing a meaningful extrapolation in obtaining a lateral in situ stress.

Because plastic failure often occurs with insertion of the fourth blade step, the consolidating response mechanism appears normally to be limited to *w/t* ratios that are less than

8.5, which is the value indicated in Figure 2. However, plastic failure is not inevitable with the fourth step, and the limiting *w/t* ratios will vary with the individual soil and moisture condition.

Implications

Although at first considered a nuisance, the different modes of soil behavior suggested in this analysis can give additional information relative to the tested soil and also may give important insights into other in situ test methods. For example, it would appear from Figure 2 that the pushing of cones—whether Dutch, piezo, expandable, or ice cream—can be expected to cause plastic failure sufficient to modify previously existing lateral stresses and to bring those stresses to a limit pressure. On the basis of their *w/t* ratios, the same interpretation may be applied to the stepped blade and dilatometer. This can be advantageous by removing the influence of variable K_o and by allowing a focus on other material properties. Where the stepped blade and dilatometer have been used in the same soil, P_0 pressures measured with the dilatometer are approximately the same as pressures measured by the thickest section of the stepped blade, both having about the same *w/t* ratios and appearing to induce limit-pressure responses. This also means that sleeve friction on a cylindrical probe probably is not a valid measure of both lateral stress and K_o, which existed before insertion of the test device, but be more a function of the limit pressure. The elastic modulus obtained with the dilatometer derives from the pressure to bulge out its central diaphragm, which probably does not reinitiate plastic failure. However, this also implies that the modulus measured by the dilatometer is buffered by an intermediate zone that has undergone plastic failure, supporting the need for empirical correlations.

Also, Figure 2 indicates that the only devices that appear to be thin enough to be pushed into soil without inevitably collapsing its structure are the Glotzl cell and the first step of the stepped blade. A correlation was discovered by Lutenegger (unpublished data) between the maximum elastic response pressure that can be measured by the blade and the lateral preconsolidation pressure as influenced by, for example, cementation or aging stress history. This is reasonable because pressures in excess of this amount should break down the soil structure and cause the soil to enter a consolidating stage.

The blade appears unique among in situ test instruments in showing an identifiable consolidating behavior. For example, the pressuremeter expanding in a prebored hole may be interpreted as causing elastic response with direct transition into plastic shear and perhaps be related to the relatively poor drainage in this test.

It is important in the interpretation of blade data to recognize possible changes in response mechanisms to avoid error from collective consideration of dissimilar data (i.e., the "apples and oranges" effect). For example, data points that are low because of the attainment of a limit pressure will tilt the slope of the graph and give too high an extrapolated in situ stress.

A flow path designed to remove subjectivity in assigning and interpreting blade data is presented next.

Flow chart for interpreting stepped blade pressure readings:

1. First data point higher than second? Then, elastic response; do not include in extrapolation.
2. Last data points equal or lower than previous points, or plot low on the graph? Then, limit pressure; do not include in extrapolation.
3. $r^2 < 0.97$ (where applicable). Then, reexamine data for influence from possible limit pressure.
4. Line slope < 0.05 mm^{-1}, possibly negative? Then, all data probably exceed limit pressure; extrapolation not reliable.
5. Three or four points with $r^2 > 0.98$ and with line slope > 0.05 mm^{-1}? Then, good test.

Representative Data

Representative data plots from tests in a hydraulic fill sand near San Francisco and a loessial silt in western Nebraska are presented in Figure 7. Test data from a soft alluvial clay in Nebraska, a medium stiff clay in Houston, and a very stiff clay near College Station, Texas, are presented in Figure 8. To reduce subjectivity in selecting the data to be shown, all are for tests at approximately the same depth, which was arbitrarily selected to be 15 ft (5 m). Only the uppermost,

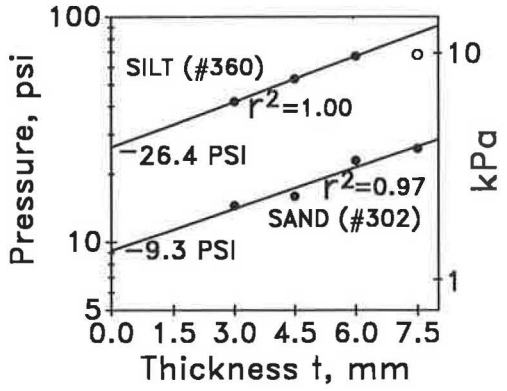

FIGURE 7 Representative test data for an unsaturated loessial silt and for a saturated sand. Open point was not included in the regression. Test numbers refer to Handy et al. (6).

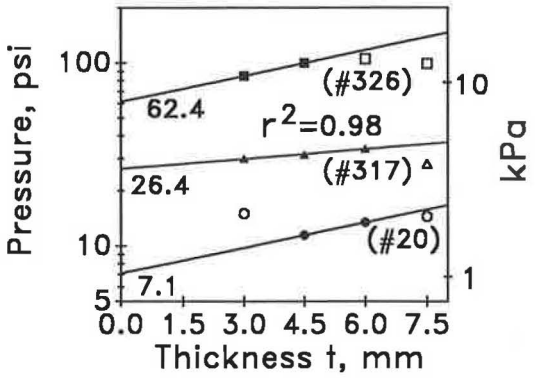

FIGURE 8 Representative test data for some clays. Open points were not included in the regressions, representing either initial elastic response or limit pressure.

four-point data sets are shown. (Additionally a three-point, a two-point, and a one-point set is obtained at each testing subdepth and is subjected to the same methods for data interpretation. Because of rapid variations in lateral stress with depth, probably as a result of localized influences and stratification, the data usually are not pooled or averaged but are reported separately.)

In Figure 7, the data plot for the silt indicates no elastic response and a high r^2, which supports the thesis that consolidation occurs and is the main factor that affects the measured pressures. A limit pressure was reached on the fourth blade step. The soil was not saturated, and K_o was calculated to be about 1.5, indicative of overconsolidation. Because the loess at this site has no known history of preloading but does contain montmorillonite, one interpretation is that the higher lateral stresses are attributable to aeolian deposition and drying followed by clay expansion on burial and wetting.

Also in Figure 7, the data for the sand show no clear indication of an elastic response or of a limit pressure and give an acceptably high r^2. The calculated value for K_o is about 0.8. As will be shown later, a graph of lateral stress versus depth in this sand indicates a small and measurable amount of overconsolidation.

In Figure 8, the very stiff clay is a Vertisol, meaning that field evidence indicates it has expanded to the point of lateral pressure relief through shearing (i.e., the passive earth pressure condition). Stepped blade measurements indicate that the lateral stress is quite high, giving K_o at the test depth of about 4. The limit pressure also is high, several times higher than the unconfined compressive strength, as would be expected for a lateral-bearing capacity-type failure.

The medium clay in Figure 8 also is a Vertisol, and blade tests at shallow depths at this site exactly duplicated lateral stresses obtained at the same site 6 years earlier with an older model blade (*1*)(*6*). At this depth, K_o is about 1.6. As is in the case of the very stiff clay, the limit pressure is several times higher than the undrained shear strength reported by Mahar and O'Neill (*8*).

The soft clay test in Figure 8 shows a breakdown of structure after penetration by the first step, suggesting that the pressure on that step may be used for calculation of a lateral subgrade modulus. The lateral stress is low for a soft clay, giving a K_o of about 0.5, which is possibly indicative of underconsolidation. This interpretation is consistent with the origin of this clay by recent sedimentation in an oxbow lake. The limit pressure approximates the calculated maximum for passive failure, which will be discussed later.

Those examples are included to show representative test data and soil responses. For full interpretations of stress history of a soil, it is necessary to determine the relationships between lateral stress and depth, which is the subject of the remainder of this paper.

ILLUSTRATIONS OF USES OF THE K_o STEPPED BLADE

Determination of the Consolidation State

Overconsolidation

The stiff clays of Figure 8 are determined to be overconsolidated, indicated by $K_o > 1$, and be attributable to their expansive nature. The shaded area in Figure 9 labeled "before pile driving" encloses a relatively narrow range of lateral stresses measured in this 50-year-old hydraulic fill sand. (The solid dot is the pressure extrapolated from sand data in Figure 7.) A trend line through the data intersects the ground surface at a lateral pressure of about 3 psi (21 kPa). The corresponding vertical surcharge load may be obtained by extending the trend line upward to intersect the y axis, which occurs at an above-ground height of 10.9 ft (3.3 m), indicating prior existence of that amount of surcharge or its weight equivalent. The prior surcharge thus obtained is 0.66 Tsf, indicative of a moderate degree of overconsolidation not unreasonable for a heavy-equipment storage yard. The slope of the trend line also allows an estimation of the friction angle from the Jaky equation. But, because this estimate is based on lateral stresses developed as a consequence of consolidation, it probably contains no dilatant component. The angle is 20 degrees, which is considerably lower than the total-strength friction angle estimated at this site from cone and stepped blade tests (*6*). The sand is micaceous, which also will contribute to low sliding friction.

Normal and Underconsolidation

Figure 10 presents SBT data from the site of Jackson Lake Dam, Jackson Hole, Wyoming, after the dam had been removed because of a potential risk of liquefaction in this active earthquake area. The short-dashed line shows lateral stresses, calculated assuming $K_o = 0.5$, without the dam in place. Below

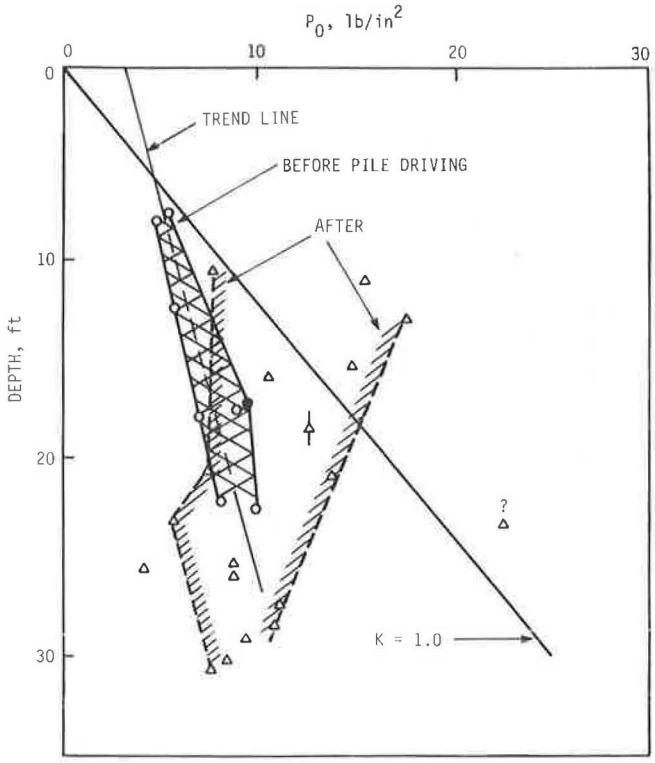

FIGURE 9 Lateral stresses measured in a sand at Hunter's Point Naval Base, San Francisco. Note that *K* lines are calculated based on effective stress and then are converted to total stress as measured by the blade.

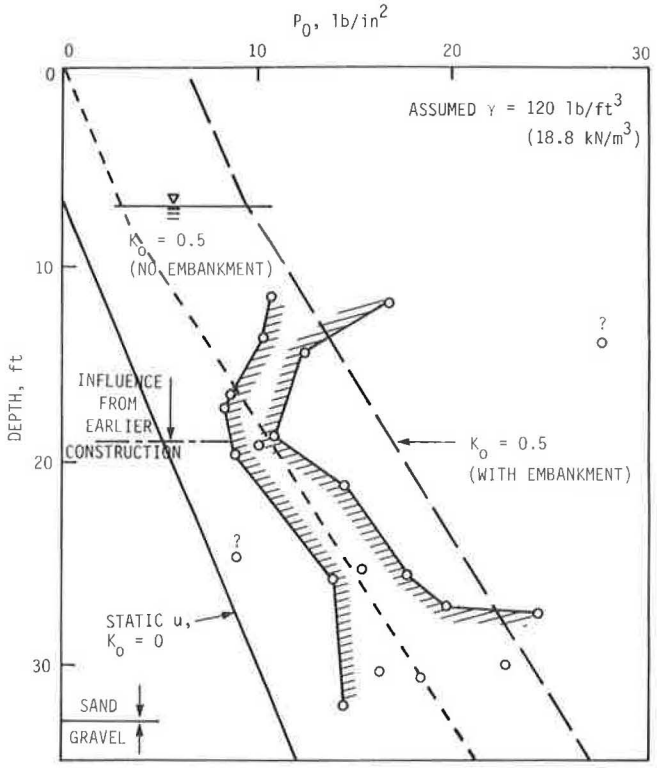

FIGURE 10 Lateral stresses in sands and silts at Jackson Lake Dam, Wyoming, after removal of the dam and before dynamic compaction.

a depth of about 19 ft (6 m) the line approximately bisects the data, which indicates that the soil there is normally consolidated if no consideration is given to the weight of the dam. With the dam in place, soil below this depth will be underconsolidated, which supports the thesis that the dam indeed is threatened by potential liquefaction of foundation soils, at least in the depth zone from 19 to 33 ft. At shallower depths the lateral stress data trend upward, approaching the K_o = 0.5 line. It, therefore, may be concluded that at the shallower depths the soil is normally consolidated under the weight of the dam, probably caused by the greater concentration of surcharge load at those depths. Many other devices, including the Menard pressuremeter, self-boring pressuremeter, and dilatometer, also were used at this site, with the dilatometer giving the most closely comparable lateral stress results (*12*).

Those examples illustrate the use of lateral stress data to diagnose the soil consolidation state without the necessity for sampling and laboratory determination of a preconsolidation pressure, which is very sensitive to sample disturbance and is all but impossible to determine from laboratory tests of a sand. Such information can be vital. For example, tests recently were performed for a metro tunneling project underneath an interstate highway, and the tests gave an unexpected result: the silt soil, presumed to be residual and hence under high lateral stress from weathering expansion, actually was normally consolidated, thus signaling that any additional load would cause appreciable settlement. On the other hand, in overconsolidated nonexpansive soils, the inferred prior load should indicate how much load can be added without exceeding the preconsolidation pressure and causing appreciable settlement.

Detection of Artificial Compaction

Figure 11 presents lateral stresses measured at the Jackson Dam site after dynamic compaction. Because the data are so erratic, an interpretation technique was used that involved determining average slopes "b" from the data plots and then applying that slope to individual points (*1*). While this did not reduce the data scatter—in fact it increased it—the additional points allow a range of lateral stresses to be sufficiently well defined to suggest that the average K_o after compaction is about 1.0, which indicate liquefaction during compaction and represent a substantial increase over the previous value of 0.5. The lateral stresses also are in the proper range for normal consolidation with the dam replaced, indicating that the soil now may be safe from liquefaction.

Figure 12 presents data obtained in back-fill soil behind a bridge abutment. Most of the lateral stresses are far below the line for K_o = 1, indicating that the soil had not been compacted. However, scattered high points, up to about 8 psi (60 kPa), occur scattered throughout the height of the embankment. Those random high stresses have the correct magnitude to have been caused from wheel contact pressures from earth-moving equipment during construction of the embankment.

Detection of Grouting

While rather incidental to the studies at hand, one of the abutments in Figure 12 give some perplexingly high lateral stresses in the upper 11 ft (3.4 m) of soil, as high as 24 psi (165 kPa), plotting far off of the graph to the right. It later was discovered that this soil had been pressure grouted to

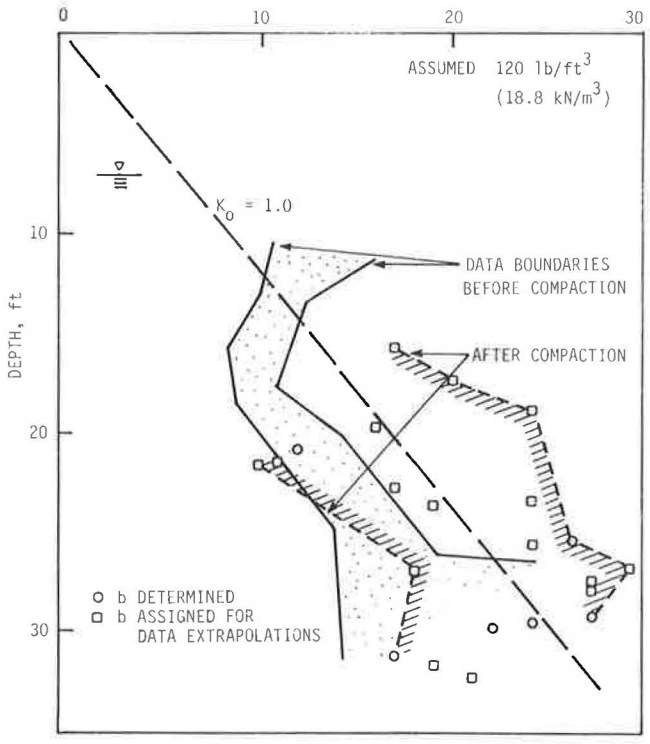

FIGURE 11 Test results from the Jackson Lake site of Figure 10 after deep dynamic compaction.

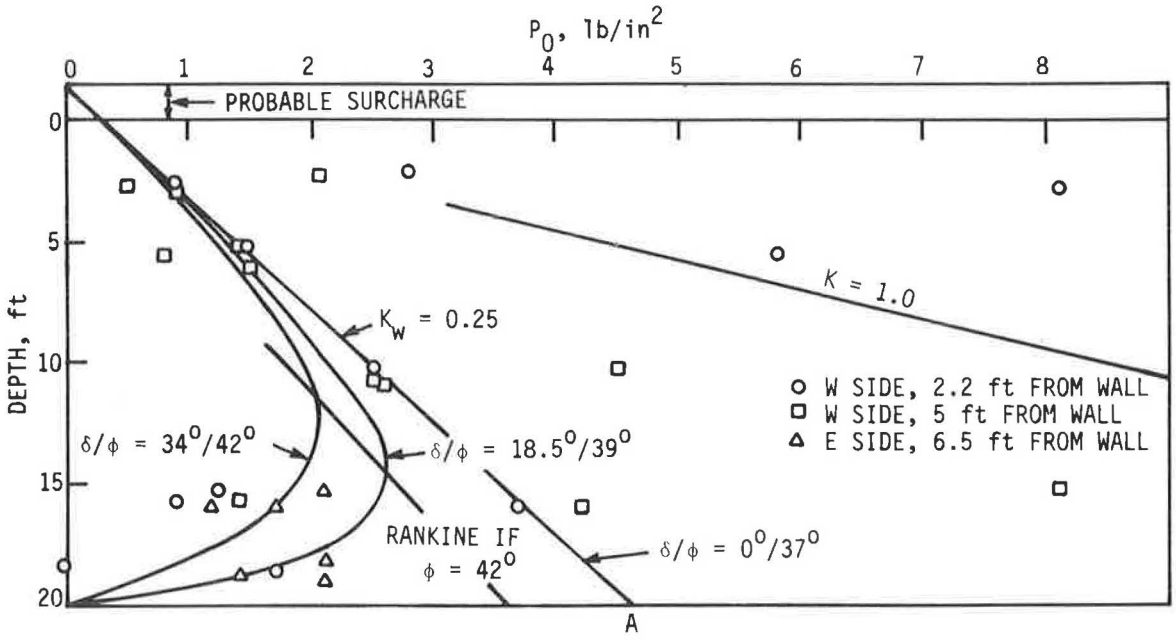

FIGURE 12 Pressures against bridge abutments compared with predictions from Rankine and from a recent arching theory (*10*). Data courtesy of Clyde Anderson, CTL/Thompson, Inc., Kellogg Engineering, Inc., and the City of Lakewood, Colo.

raise the approach slab. The average K_o in this zone is about 3, so pressures should have been high enough to do the job.

Passive Pressures

Bearing Capacity Failure

Figure 13 presents the distribution of lateral stress with depth in a soft oxbow lake clay immediately adjacent to a highway embankment then under construction. The tests were conducted before construction began and later when settlements became excessive and slope indicators showed lateral bulging outward of the foundation soil (*13*). Lateral stresses are approximately twice what had been measured prior to the construction and exceed the theoretical maximum dictated by K_p calculated from borehole shear test data. Those data were obtained before construction and do not reflect a probable increase in strength from the partial consolidation. The excessive settlement of the embankment, lateral bulging of the foundation soil, large increase in lateral pressures, and their proximity to K_p pressures suggest that it would be judicious to adjust the construction schedule to allow further dissipation of excess pore pressures through previously installed wick drains. This was done. The embankment was completed the following construction season without incident.

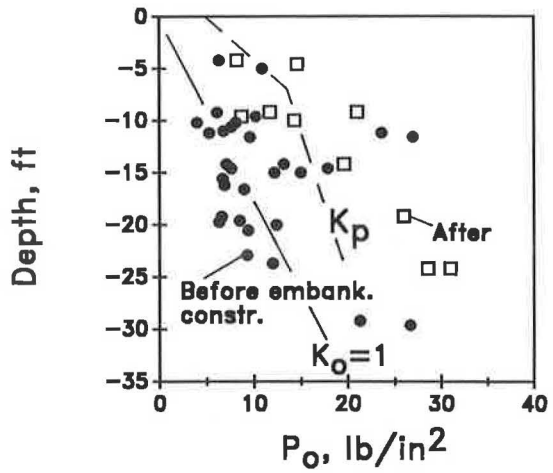

FIGURE 13 Lateral stresses in a soft lake bed clay adjacent to a highway embankment, Storz Expressway, Omaha, Nebr. Solid points are before embankment construction and open squares after, when there was concern for an impending bearing capacity failure. K_p line was drawn based on preconstruction shear tests.

Expansive clay

Tests presented in Figure 12 were performed in soil that was known to be expansive to determine if it was exerting undue pressure on adjacent bridge abutments. As can be seen from the data, this turned out not to be the case, because generally $K_o << 1$. The bridge was removed without difficulty.

Figure 14 presents lateral pressures versus depth in the very stiff expansive clay, including the data point from Figure 8. The shaded zone includes three-fourths of the data points in a relatively narrow band. Because $K_o >> 1$ and because this is a known Vertisol, passive conditions are suspected. To test this premise, two points were selected on the linear trend line for substitution of lateral and vertical stresses into the passive pressure equation. Then it was solved simultaneously to give drained shear strength parameters. The equation is

$$\sigma_h = \gamma z \tan^2[45 + (\phi/2)] + c \tan[45 + (\phi/2)] \quad (1)$$

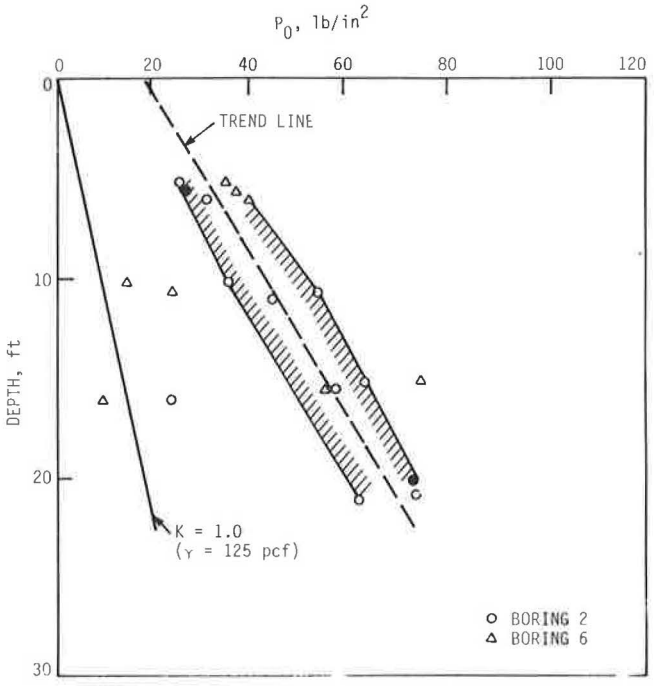

FIGURE 14 Lateral stress data from a very stiff expansive clay. Data from Texas A&M University, College Station, Texas.

By using this procedure with the data from Figure 14, one obtains $\phi = 28$ degrees and $c = 11.3$ psi (78 kPa). The equivalent unconfined compressive strength calculated from those values is 19 psi or 1.4 Tsf (131 kPa), which compares favorably with measured values that ranged from 0.8 to 1.6 Tsf, averaging about 1.2 Tsf (*6*) (*9*). This would appear to confirm that lateral stresses in this soil are being limited by passive failure and also demonstrates how lateral stress data versus depth multiplied by soil unit weight can be used to approximate drained c and for ϕ if the soil is in the passive state.

Slope Stability

Unfortunately, the potential for the blade test to measure passive pressures at the base of slopes and thus detect the potential for slope failure before movement occurs has not yet been realized owing to the difficulty of getting drilling machines into landslide toeslope areas. This application would appear to be useful for preventative maintenance of cut and fill slopes, because it should be cheaper and more effective to repair a slope before failure occurs than after the soil has moved and become permanently weakened through remolding and from dilatant shear creating suction and increasing water contents in the shear zone. Figure 15 indicates where pressures might appropriately be measured on the basis of finite-element analyses (*11*). As simulated excavation proceeds, progressive failure and the potential development of passive pressures should initiate in soil in the toe zone even though the overall factor of safety still exceeds 1.8. The detection of high lateral stresses in a toeslope thus would flag when preventative measures should be undertaken or when stability

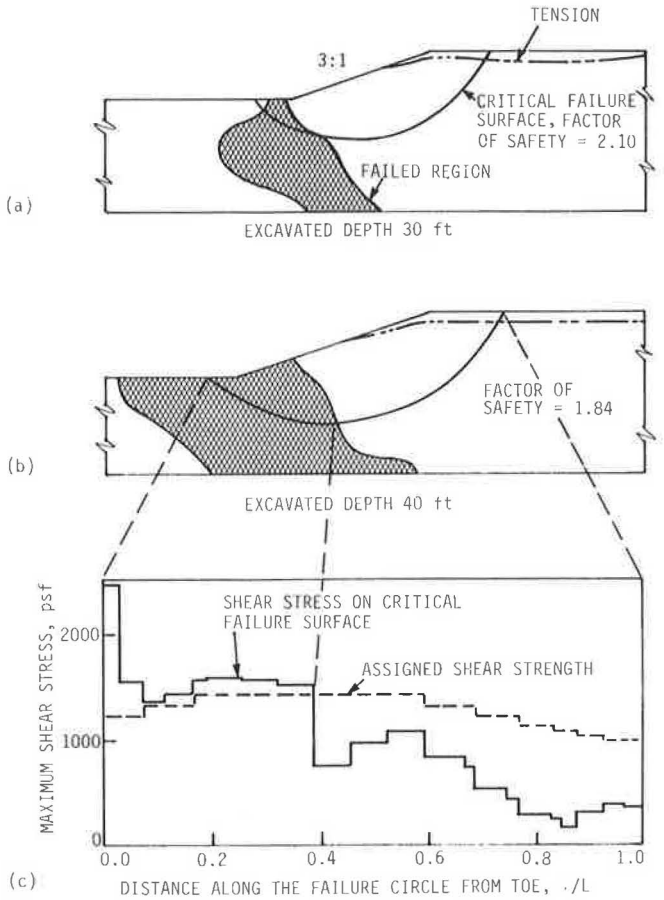

FIGURE 15 Hypothetical failure zones from finite-element analyses of a 3–1 slope excavated in overconsolidated clay. Data from Dunlop and Duncan (*10*).

of the slope should be reevaluated by a method of slices with soil strengths reduced for toe slices by a factor equal to the soil sensitivity.

Low lateral in situ stresses have been measured in soil above an active landslide in the zone frequently marked by the development of tension cracks.

Pressures Adjacent to Existing Structures and Driven Pile

Figure 12 presents lateral pressures measured in soil close to an existing wall, as has already been discussed. Figure 9 presents the increase in shallow lateral soil stresses as the result of driving pile and the erratic disposition of lateral soil pressures near the pile tip. The latter may help explain why test loading indicated that the pile group action factor at this site is about 1.

Subgrade Modulus and Limit Pressure

An estimate for a lateral subgrade modulus k_b is obtained by dividing the pressure measured on the first blade step by one-half the blade thickness, or 1.5 mm. The value of the modulus

depends in part on the size of the area being loaded, and experience with those k values is very limited and is not in the scope of this paper. Application of elastic theory to a blade area considered as a surface load gives the following relationship between k and the elastic modulus E:

$$E = 2.8\,k \tag{2}$$

Application of this equation to the Houston clay data gives E values comparable to those obtained from UU triaxial tests and lower by an order of magnitude than those obtained from cross-hole seismic studies (*8*). The modulus thus obtained from blade tests in a sand appeared to give an accurate prediction of settlement of a bridge abutment (*6*).

CONCLUSIONS

1. Elastic, consolidating, and limit pressure modes of soil behavior are suggested by different lateral pressure responses to penetration by different thickness steps of the K_o stepped blade. The consolidating mode is used for extrapolation to obtain hypothetical in situ pressure on a zero thickness blade.
2. The pattern of lateral in situ stresses with depth in sand, silt, and clay soils can be used to define the soil consolidation state and, in nonexpansive soils, to indicate the amount of prior surcharge or overburden. Lateral stresses usually are higher than from normal consolidation and are attributable to geological or man-induced unloading, clay expansion cycling, and, in residual soils, expansion of minerals on hydration weathering.
3. Lateral in situ stresses show influences from mechanical compaction and grouting and help define the depth and effectiveness of dynamic compaction.
4. Lateral stresses consistent with passive failure conditions were found in slicken-sided expansive clays and in a soft lake clay adjacent to a failing highway embankment. In the latter, construction was halted to prevent general bearing capacity failure. Measurement of passive stresses in toeslopes may help predict slope failures and lead to a timely application of remedial measures before slipping occurs.
5. The K_o stepped blade was used to measure lateral soil stress adjacent to existing structures including retaining walls and driven pile, thus helping to determine their stability.
6. The back-pressure system for reading pneumatic pressure cells of the stepped blade significantly improves its accuracy and ease of use.

ACKNOWLEDGMENTS

These studies were sponsored by the Federal Highway Administration with C. Ealy the persevering contract manager. Data in Figure 9 are used with the permission of Geo-Resource Consultants, Inc., San Francisco, courtesy of Eric Ng. Data in Figures 10 and 11 are used with permission of Woodward-Clyde Consultants, Inc., Denver, courtesy of Dick Davidson. Data in Figure 12 are used with permission of CTL-Thompson, Inc., Denver, and the tests were performed by C. Anderson. Data in Figure 13 are used with permission of Woodward-Clyde Consultants, Inc., Omaha, courtesy of Steve Saye. Data in Figure 14 are used courtesy of J.-L. Briaud and Texas A&M University. Many other companies and individuals also participated in these investigations, for which the authors extend their sincere thanks.

REFERENCES

1. R. L. Handy, B. Remmes, S. Moldt, and A. J. Lutenegger. In Situ Stress Determination by Iowa Stepped Blade. *Journal of the Geotechnical Engineering Division*, ASCE, Vol. 108, No. GT11, 1982, pp. 1405–1422.
2. R. L. Handy and D. Eichner. *Back-Pressured Pneumatic Pressure Cell*. U.S. Pat. 4,662,213, 1987.
3. J. Dunnicliff. *Geotechnical Instrumentation for Monitoring Field Performance*, John Wiley & Sons, New York, 1988.
4. A. J. Lutenegger and D. A. Timian. *In Situ Tests With K_o Stepped Blade*. ASCE Special Technical Publication 6, 1986, pp. 730–751.
5. M. Pabst and R. L. Handy. *Soil Effective Stress Sensor and Method for Using Same*. U.S. Pat. 4,524,626, 1985.
6. R. L. Handy, J.-L. Briaud, K. C. Gan, C. L. Mings, D. W. Retz, and J.-F. Yang. *Use of the K_o Stepped Blade in Foundation Design*. Vol. 1, Final Report D-87/102. FHWA, U.S. Department of Transportation, June 1987.
7. E. W. K. Tse and R. L. Handy. A New Development of the K_o Stepped Blade. *Proc., 10th SE Asian Geotechnical Conference*, 1990, pp. 479–484.
8. L. J. Mahar and M. W. O'Neill. *Field Study of Pile Group Action*. Report RD-81/005. FHWA, U.S. Department of Transportation, 1980.
9. K. C. Gan. *Evaluation of the Stepped Blade Using the Pressuremeter*. Ph.D. dissertation, Texas A&M University, College Station, Texas, 1987.
10. R. L. Handy. The Arch in Soil Arching. *Journal of the Geotechnical Engineering Division*, ASCE, Vol. 111, No. 3, 1985, pp. 302–308.
11. P. Dunlop and J. M. Duncan. Development of Failure Around Excavated Slopes. *Journal of the Soil Mechanics and Foundations Division*, ASCE, Vol. 96, 1970, pp. 471–493.
12. *Assessment of In Situ Stress Changes, Jackson Lake Dam, Minidoka Project, Jackson, Wyoming*. Woodward-Clyde Consultants, Denver, Colo.; Bureau of Reclamation Embankment Dams Branch, Denver, Colo., Sept. 1987.
13. *Analysis of Instrumentation Data, Arthur C. Storz Expressway, Omaha, Nebraska*, Woodward-Clyde Consultants, Aug. 1989.

Publication of this paper sponsored by Committee on Soil and Rock Properties.

Determination of Horizontal Stress in Normally Consolidated Sands by Using the Dilatometer Test: A Calibration Chamber Study

ROBERT S. LAWTER, JR., AND ROY H. BORDEN

The results of dilatometer tests (DMTs) performed in a calibration chamber on normally consolidated Cape Fear sand are presented and are interpreted with respect to both relative density and state parameter and are compared with those from calibration chamber tests on normally consolidated Hokksund and Ticino sands. The relationship between the amplification factor K_D/K_o and state parameter data for the Cape Fear sand tested and the combined data from the three sands discussed resulted in best-fit equations of the form $K_D/K_o = a \cdot e^{m\psi}$. In an effort to improve the ability of a single function to describe the amplification factor-state parameter relationship for the entire data base, normalization of the state parameter by the difference between the maximum and minimum void ratio and by the steady state void ratio at 10 kPa was investigated. However, neither of those normalizing factors produced a higher correlation coefficient for the best-fit relationship. The addition of the Cape Fear sand to the existing trend lines for the K_o^{DMT}/K_o relative density relationship developed from data on Hokksund and Ticino sands suggests a limiting value of K_o^{DMT}/K_o between 0.5 and 1.0 at low relative densities. At higher relative densities, a significant difference exists between the current data and that data obtained previously on the Hokksund and Ticino sands. Further study is needed to evaluate the potential influence of calibration chamber diameter on the measured results.

Penetration testing was developed as a method to obtain soil characteristic information from soils where undisturbed sampling was difficult or impossible. The flat dilatometer developed in the 1970s (*1*) is a penetration device that has been shown to provide reliable soil characteristic information. As with all penetration tests, the determination of the change in the in situ stress state created by the insertion of the dilatometer is a complicated boundary value problem. Therefore, the index parameters obtained from the dilatometer test have been empirically correlated to the actual soil properties. Recent development of large calibration chambers where penetration testing can be conducted has lead to improved correlations because of the capability of strictly controlling the stress state of the soil.

This paper presents the results of a study of existing correlations of horizontal stress index parameters obtained from the dilatometer with the actual horizontal stress applied in calibration chamber tests conducted in normally consolidated Cape Fear sand in the North Carolina State University (NCSU) calibration chamber. The results are interpreted in terms of relative density and the state parameter, introduced by Been and Jefferies (*2*), which incorporates both the void ratio and the stress level. Additional data incorporated into this study were obtained from similar calibration chamber tests performed on Hokksund and Ticino sands (*3*) (M. Jamiolkowski, personal communication).

Center for Transportation Engineering Studies, Department of Civil Engineering, Box 7908, North Carolina State University, Raleigh, N. C. 27695-7908.

MARCHETTI DILATOMETER

The flat dilatometer developed by Marchetti (*1*) is essentially a penetration device capable of obtaining an estimate of lateral pressure and soil stiffness. The body of the dilatometer has an approximate width of 95 mm (3.7 in.) and a thickness of 14 mm (0.6 in.). The external surface of the approximately 60-mm (2.4-in.) diameter membrane when at rest is flush with the surrounding flat surface of the blade. The blade is usually pushed into the ground at conventional penetration test rates (2 to 4 mm/sec). When the desired test depth is reached, the membrane is inflated through a small control unit at the ground surface with pressurized gas. Readings are taken of the pressure required to initiate movement of the membrane (related to the horizontal stress existing in the ground) and the pressure required to move its center an additional approximate 1 mm (0.04 in.) into the soil (related to the soil stiffness). Both of those pressure readings are corrected for the effect of membrane stiffness. The first of those corrected pressures is called the p_0 pressure. An index parameter similar to the at-rest earth pressure coefficient K_o, termed the horizontal stress index K_D, was developed by using the p_0 pressure. The horizontal stress index is determined by the following equation:

$$K_D = \frac{(p_0 - u_0)}{\sigma'_v} \tag{1}$$

where u_0 is the hydrostatic pore water pressure and σ'_v is the in situ vertical effective stress. On the basis of field tests results in uncemented clays Marchetti (*4*) proposed the following correlation for the relationship between the horizontal stress index K_D and the in situ at-rest earth pressure coefficient K_o.

$$K_o^{DMT} = \left(\frac{K_D}{1.5}\right)^{0.47} - 0.6 \tag{2}$$

Jamiolkowski et al. (5) have suggested, on the basis of calibration chamber tests conducted on Hokksund and Ticino sands and field experience, that this empirical formula overestimates K_o in dense to very dense sands and underestimates K_o in loose sands.

STATE PARAMETER

The state parameter φ, which is embodied in critical state soil mechanics, was introduced by Been and Jefferies (2) as a rational approach to combine the effects of void ratio and stress level into a single parameter that enables the behavior of a sand to be predicted. The state parameter is defined as the difference in the initial void ratio e_A and the void ratio at "steady state" e_{ssA} at the initial stress level, as is illustrated in Figure 1. The steady state for any mass of particles has been defined as that state where the mass is continuously deforming at constant volume, constant effective stress, constant shear stress, and constant velocity (6). The steady-state void ratio e_{ss} corresponding to a mean normal effective stress of 10 kPa has been suggested as an index for comparing various sands.

The sand used in the NCSU calibration chamber was a subangular to angular sand obtained from the Cape Fear River in North Carolina. A summary of its properties and a photograph of the sand appear in Table 1 and Figure 2, respectively. To determine the steady-state line (SSL) for Cape Fear sand, a series of strain-controlled isotropically consolidated undrained triaxial tests were performed. The test specimens were prepared by compacting six 1-in. layers to the desired density. The specimens were flushed with carbon dioxide and were saturated by using desired water. A minimum B-value of 0.97 was obtained before proceeding with compression testing. The initial and steady-state points for each test are presented in Figure 3 along with the best-fit SSL determined by regression analysis. The SSL for Cape Fear sand is compared in Figure 4 with those for the Hokksund and Ticino sands as well as the Kogyuk sand with 0 percent silt used by

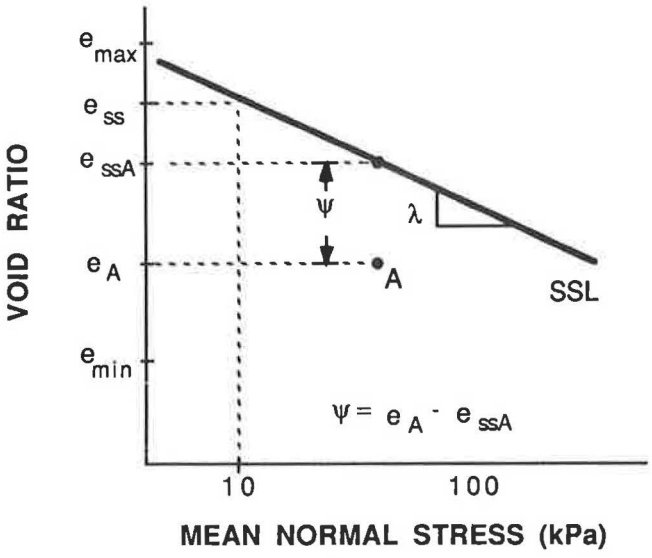

FIGURE 1 Definition of the state parameter.

TABLE 1 INDEX PROPERTIES OF SANDS USED IN VARIOUS CALIBRATION CHAMBERS

	CC TEST SANDS		
PROPERTY	CAPE FEAR SAND	HOKKSUND SAND	TICINO SAND
d_{50} (mm)	0.69	0.39	0.53
d_{10} (mm)	0.29	0.21	0.36
C_U	2.76	2.10	1.60
G_s	2.67	2.70	2.69
e_{max}	0.802	0.894	0.931
e_{min}	0.527	0.549	0.579
e_{ss}	0.858	0.934	0.986
λ_{ss}	0.074	0.054	0.056

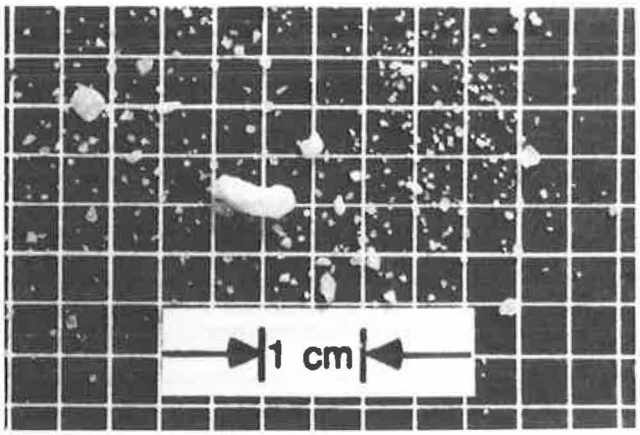

FIGURE 2 Photograph of Cape Fear River sand grains.

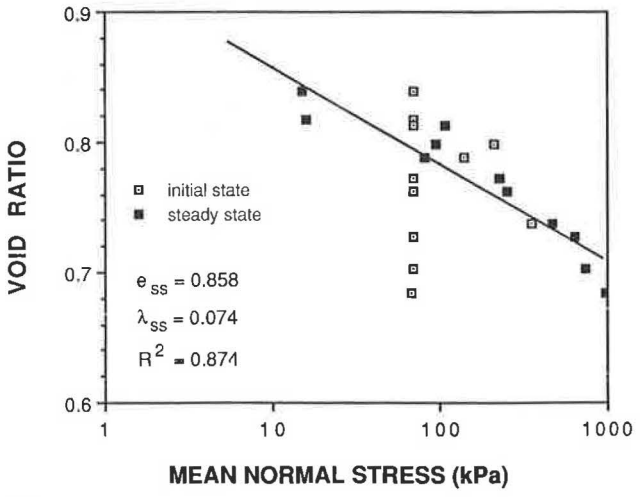

FIGURE 3 State diagram for Cape Fear sand.

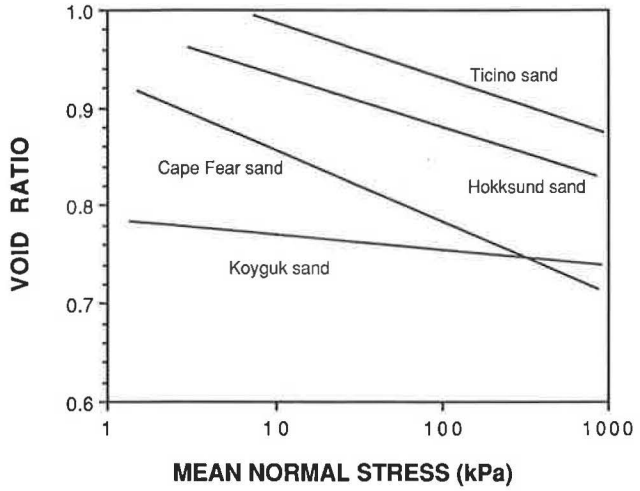

FIGURE 4 Steady state lines for calibration chambers sands.

Been and Jefferies (*2*) in their development of the state parameter. Table 1 also contains a summary of soil properties for the Hokksund and Ticino sands.

NCSU CALIBRATION CHAMBER

A diagram of the NCSU calibration chamber is presented in Figure 5. The NCSU calibration chamber is capable of accommodating a sand specimen 0.94 m (37 in.) in diameter and 0.94 m (37 in.) in height. The test specimens were prepared by pluviation in air. The specimens were then subjected to one-dimensional consolidation, from which the K_o of the sand was determined. Then, the dilatometer tests were conducted while constant vertical and horizontal stresses were maintained through a computer-controlled pneumatic pressure system. Table 2 summarizes the results of the NCSU calibration chamber tests. A detailed description of the NCSU calibration chamber, including test procedures and results, has been reported by Borden et al (*7*).

INTERPRETATION

Correlation of the K_D/K_o ratio, called the amplification factor, to the state parameter has been suggested by Jamiolkowski et al. (*5*) as a rational approach for interpreting the calibration chamber data. Jamiolkowski et al. have presented results of 57 calibration chamber tests on normally and overconsolidated Hokksund and Ticino sands (see Figure 6) and suggest fitting the two parameters with an equation of the following form:

$$K_D/K_o = a \cdot e^{m\Psi} \tag{3}$$

where a and m are empirical coefficients. For the combined data from the Hokksund and Ticino sands, a and m were determined to be 1.35 and -8.08, respectively.

A similar correlation was investigated for normally consolidated Cape Fear sand. Although other functions were investigated, none provided a significantly better fit. The relationship between the state parameter and the amplification factor for those tests and for the a and m coefficients determined by regression analysis are presented in Figure 7. Sig-

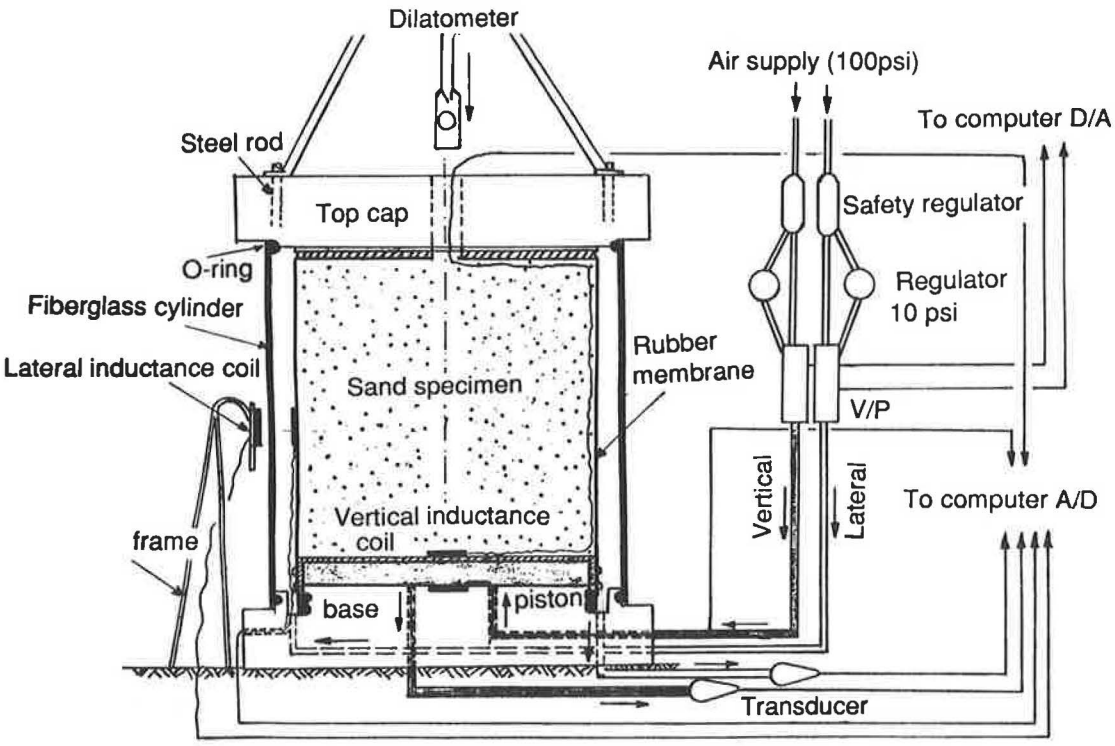

FIGURE 5 NCSU calibration chamber system.

TABLE 2 SUMMARY OF CALIBRATION CHAMBER TESTS PERFORMED ON CAPE FEAR RIVER SAND

TEST no.	σ'_v (kpa)	σ'_h (kpa)	D_R (%)	OCR	K_o	p_0 (kpa)	p_1 (kpa)	K_D	Ψ
2	62.06	27.58	73.3	1.00	0.44	151.07	823.88	2.43	-0.214
4	36.54	20.00	91.5	1.00	0.55	141.07	667.31	3.86	-0.280
9	20.69	27.58	76.7	1.00	1.33	87.04	845.39	4.21	-0.238
10	20.46	13.79	58.9	1.00	0.67	47.02	542.25	2.30	-0.202
11	34.32	6.90	87.1	1.00	0.20	35.02	512.24	1.02	-0.283
12	61.14	20.69	78.8	1.00	0.34	83.04	855.40	1.36	-0.234
16	61.37	28.96	6.0	1.00	0.47	78.04	592.27	1.27	-0.021
17	61.14	39.30	15.6	1.00	0.64	85.04	868.40	1.39	-0.044
18	34.32	25.17	23.5	1.00	0.73	90.04	471.22	2.62	-0.083
19	47.73	34.96	33.3	1.00	0.73	102.05	609.28	2.14	-0.100
20	61.14	39.30	-5.3	1.00	0.64	123.06	587.27	2.01	0.016
22	34.32	22.06	-0.8	1.00	0.64	85.04	435.20	2.48	-0.016

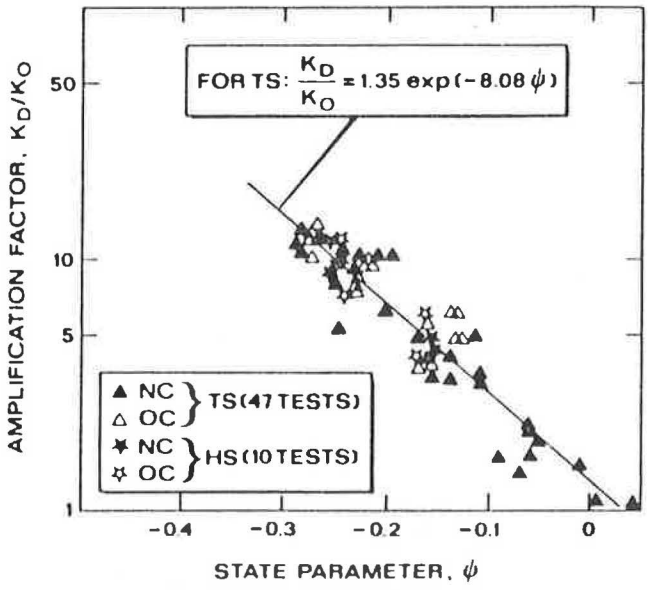

FIGURE 6 Dilatometer amplification factor for Hokksund and Ticino sands (*5*).

nificant scatter exists, and the resulting R^2 value is 0.58. Data for tests on the normally consolidated Hokksund and Ticino sands are presented in Figures 8 and 9, respectively. The corresponding R^2 values for those relationships are 0.77 and 0.76. Figure 10 illustrates a composite of the data from the three sands with the best-fit line determined according to Equation (3) (R^2 = 0.66). A comparison of those figures indicates that the slope of the state parameter verses amplification factor relationship for the Hokksund and Ticino sands appears to be steeper than that of the Cape Fear sand. This may suggest the influence of particle mineralogy, grain shape, and grain-size distribution of the individual sands on the state parameter.

It has been suggested (*8–10*) that the state parameter be normalized, with respect to the difference between the maximum and minimum void ratio, to account for this influence. This normalization procedure, and normalizing with respect to the steady state void ratio at 10 kPa, was investigated and was found not to influence the relationship of the trend lines for individual sands. The addition of the Cape Fear sand to the existing trend lines for the K_o^{DMT}/K_o relative density relationship presented by Jamiolkowski et al. (*5*) suggests that

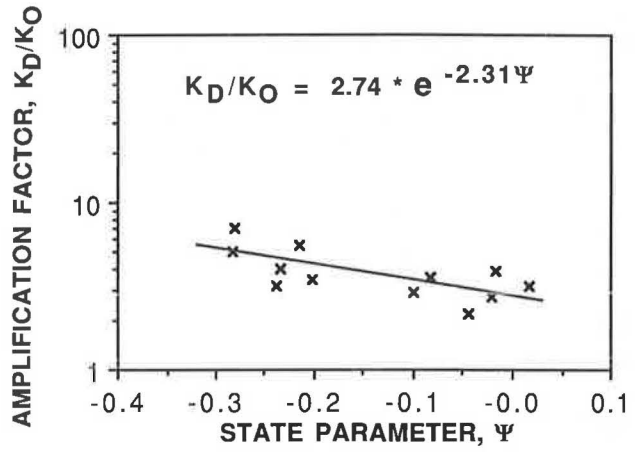

FIGURE 7 Dilatometer amplification factor for normally consolidated Cape Fear sand.

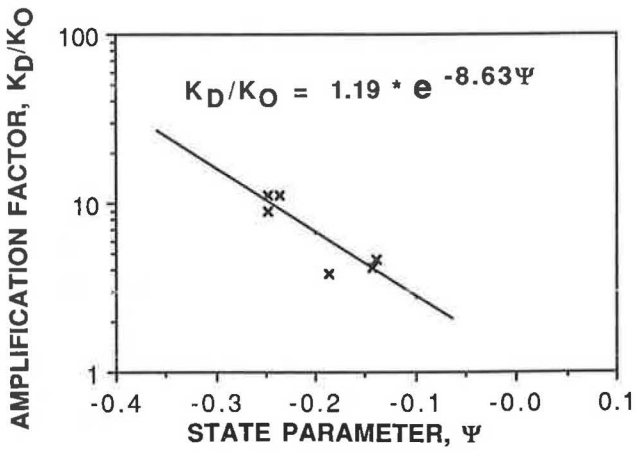

FIGURE 8 Dilatometer amplification factor for normally consolidated Hokksund sand.

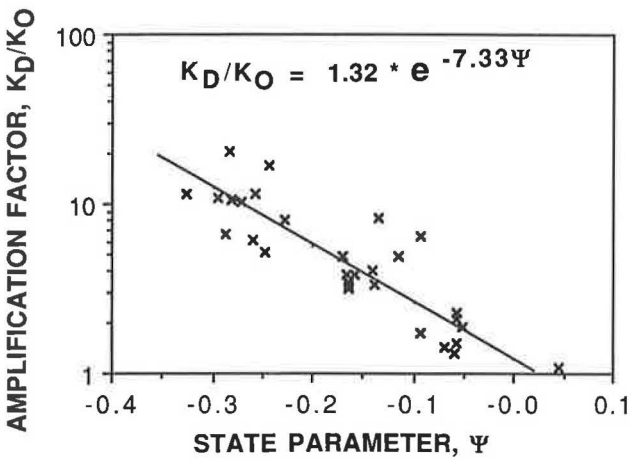

FIGURE 9 Dilatometer amplification factor for normally consolidated Ticino sand.

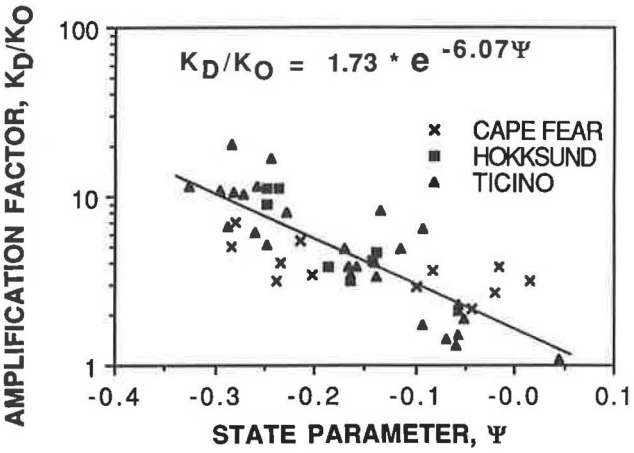

FIGURE 10 Dilatometer amplification factor for normally consolidated calibration chamber sands.

the trend line approaches a limiting value of K_o^{DMT}/K_o between 0.5 and 1.0 at low relative densities.

At the higher relative densities, corresponding to lower state parameter values, the K_o^{DMT}/K_o values are significantly lower for the Cape Fear sand than for either the Hokksund or Ticino sands. The latter tests were performed in a 1.5-m (59 in.) diameter chamber while the NCSU chamber is 0.97 m (37 in.) in diameter. It is possible that the difference in results in the more dilatant soils is related to the development of a plastic zone during penetration into the smaller chamber that extends to the boundary. In the more contractive materials, it would be expected that the plastic zone would be considerably smaller and thus would minimize the influence of chamber diameter. This concept would support the good agreement observed between the data obtained on medium density samples for all three soils.

As was stated previously, Jamiolkowski et al. have suggested that the empirical formula for K_o^{DMT} overestimates K_o in dense to very dense sands and underestimates it in loose sands. The results of the calibration chamber tests on Hokksund and Ticino sands presented in Figure 11 indicate this trend. Examination of the results from the tests on Cape Fear sand

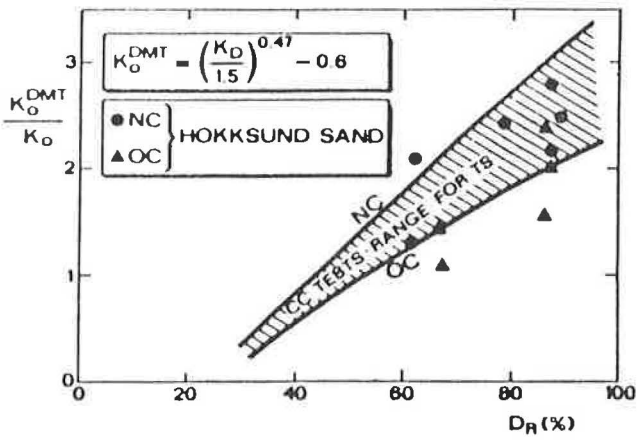

FIGURE 11 K_o^{DMT}/K_o for Hokksund and Ticino sands, using the original Marchetti correlation (5).

(Figure 12) suggest that at lower relative densities the trend is toward a K_o^{DMT}/K_o ratio of 0.5 to 1.0. As was previously suggested, Marchetti's correlation tends to overestimate K_o for dense sands and underestimates it for loose sands but to a smaller degree than for the Hokksund and Ticino sands.

When the K_o^{DMT}/K_o ratio is interpreted in terms of the state parameter, which includes the influence of the stress level, it appears that there is no significant reduction in the scatter of data. Similar data for the Hokksund and Ticino sands are presented in Figures 13 and 14, respectively. As with the K_D/K_o analysis, the slopes of the K_o^{DMT}/K_o verses D_R and Ψ relationships for the Hokksund and Ticino sands are again similar and again steeper than those for the Cape Fear sand. The trend lines for combined data from the three sands are presented in Figure 15. The data from several of the tests on Cape Fear sand at low relative densities suggest that the K_o^{DMT}/K_o ratio approaches a limiting positive value in the range of 0.5 to 1.0.

SUMMARY AND CONCLUSIONS

The relationship between DMT horizontal stress index parameter and existing horizontal stress was evaluated on the basis

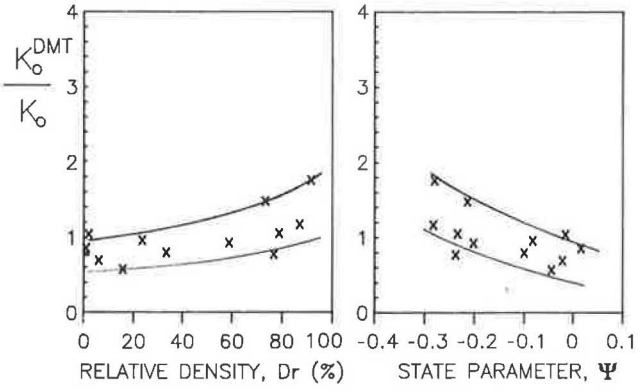

FIGURE 12 K_o^{DMT}/K_o for normally consolidated Cape Fear sand, using the original Marchetti correlation.

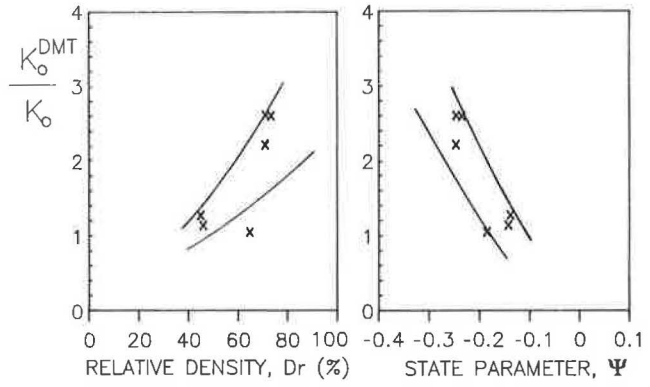

FIGURE 13 K_o^{DMT}/K_o for normally consolidated Hokksund sand, using the original Marchetti correlation.

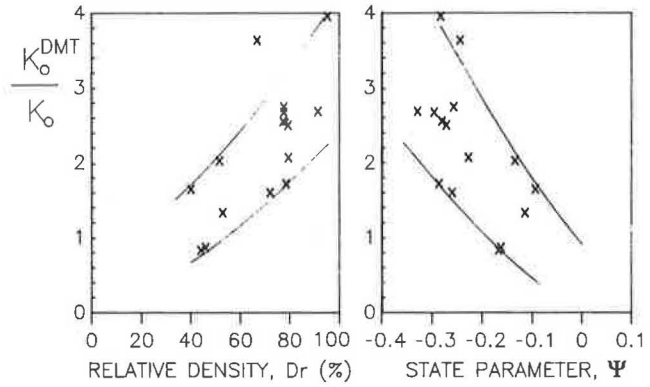

FIGURE 14 K_o^{DMT}/K_o for normally consolidated Ticino sand, using the original Marchetti correlation.

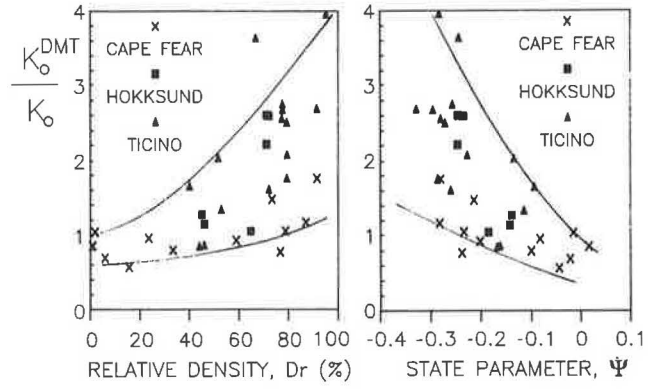

FIGURE 15 K_o^{DMT}/K_o for normally consolidated calibration chamber sands, using the original Marchetti correlation.

of dilatometer tests performed in calibration chambers on normally consolidated sands. The results are interpreted in terms of the existing lateral stress index parameter K_D and the original Marchetti correlation of K_D and K_o with respect to both relative density and state parameter.

Interpretation of the amplification factor-state parameter data for the Cape Fear sand tested in this study and the combined data from the three sands discussed resulted in best-fit equations of the form

$$K_D/K_o = a \cdot e^{m\Psi}$$

The addition of the Cape Fear sand to the existing trend lines for the K_o^{DMT}/K_o relative density relationship presented by Jamiolkowski et al. (*5*) suggests that the trend line approaches a limiting value of K_o^{DMT}/K_o between 0.5 and 1.0 at low relative densities.

Normalization of the state parameter by the difference between maximum and minimum void ratio did not result in better agreement between those functions for the three sands. It is possible that the difference in results between the Cape Fear sand and the Hokksund and Ticino sands at higher relative densities could be related to calibration chamber size. Further research is needed to evaluate the required chamber diameter as a function of relative density for dilatometer penetration such that the plastic zone does not extend to the boundary.

ACKNOWLEDGMENTS

The financial support of the first author on a North Carolina Research and Teaching Assistantship and the Ralph E. Fadum Graduate Fellowship is gratefully acknowledged. The calibration chamber tests were conducted under a research grant provided by the North Carolina Department of Transportation.

REFERENCES

1. S. Marchetti. A New In Situ Test for the Measurement of Horizontal Soil Deformability. *Proc., Conference on In Situ Soil Properties*, Vol. 2, ASCE Specialty Conference, Raleigh, June 1975, pp. 255–259.
2. K. Been and M. G. Jefferies. A State Parameter for Sands. *Geotechnique*, Vol. 35, No. 2, June 1985, pp. 99–112.
3. G. Baldi, R. Bellotti, V. Ghionna, M. Jamiolkowski, S. Marchetti, and E. Pasqualini. Flat Dilatometer Tests in Calibration Chambers. *Proc., Specialty Conference*, Geotechnical Engineering Division, ASCE, 1986, pp. 431–446.
4. S. Marchetti. In Situ Tests by Flat Dilatometer. *Journal of Geotechnical Engineering Division*, ASCE, Vol. 106, No. GT3, March 1980, pp. 299–321.
5. M. Jamiolkowski, V. N. Ghionna, R. Lancellotta, and E. Pasqualini. New Correlations of Penetration Tests for Design Practice. *Penetration Testing 1988*, ISOPT-1, Vol. 1, 1988, pp. 263–296.
6. S. J. Poulos, The Steady State of Deformation. *Journal of Geotechnical Engineering Division*, ASCE, Vol. 107, No. GT5, May 1981, pp. 553–562.
7. R. H. Borden, M. A. Gabr, C. Hsu, and W. Lien. *Evaluation of Lateral Coefficient of Subgrade Reaction Using the Dilatometer Test*. Research Report FHWA/NC-87-001. Center for Transportation Engineering Studies, North Carolina State University, Raleigh, 1987.
8. C. C. Hird and F. Hassana. Discussion of "A State Parameter for Sands." *Geotechnique*, Vol. 36, No. 1, 1986, pp. 124–127.
9. K. Been and M. G. Jefferies. Authors' reply, "A State Parameter for Sands." *Geotechnique*, Vol. 36, No. 1, 1986, pp. 127–132.
10. J. M. Konrad. Interpretation of Flat Plate Dilatometer Tests in Sands in Terms of the State Parameter. *Geotechnique*, Vol. 38, No. 2, 1988, pp. 263–277.

Publication of this paper sponsored by Committee on Soil and Rock Properties.

Direct and Indirect Determinations of In Situ K_o in Clays

PAUL W. MAYNE AND FRED H. KULHAWY

For natural clays encountered in the field, the in situ effective horizontal stress ($\overline{\sigma}_{ho}$) may be evaluated from the interpretation of direct measurements by using the self-boring pressuremeter test (SBPMT) or total stress cells (TSC) or may be evaluated indirectly from other tests such as the dilatometer test (DMT) and piezocone penetration test (CPTU). A review of K_o data summarized from 56 different sites tested by the SBPMT demonstrates that stress history (OCR) is a predominant factor affecting the magnitude of the in situ geostatic state of stress. For clay deposits that have developed their K_o profile primarily from stress history effects (i.e., mechanical overconsolidation), a simplified cavity expansion theory is used to express K_o in terms of the cone tip resistance (q_c) and penetration pore water stress (Δu) obtained during CPTU soundings and the DMT contact stress (p_o). Data derived from 17 sites tested by the SBPMT and CPTU and 12 sites tested by the SBPMT and DMT are used to verify the approach.

The geostatic state of stress in the ground can develop as a combination of a number of factors and processes that have occurred during the geologic history of the deposit (*1–3*). Variables potentially affecting the development of horizontal stress ($\overline{\sigma}_{ho}$) in situ may include, for example, stress history, geologic origin, mineralogy, cementation, aging, desiccation, pore water fluid, passive failure, strain history, temperature, wet-dry cycles, wave loading, degree of saturation, or weathering. For a given soil it is unlikely that a completely accurate scenario of all of the relevant factors and their chronology can be developed with a high level of confidence. Furthermore, the significance and effect of each variable may not be fully understood. However, dominant variables such as stress history usually can be estimated reasonably well. Alternatively, one can bypass evaluating those variables and attempt to measure σ_{ho} in situ when possible.

Laboratory triaxial and oedometer data on clays, silts, and sands indicate a rather strong relationship between the horizontal stress coefficient ($K_o = \overline{\sigma}_{ho}/\overline{\sigma}_{vo}$) and overconsolidation ratio (OCR $= \overline{\sigma}_p/\overline{\sigma}_{vo}$) (*4*). However, a recent study (*5*) has suggested that the in situ geostatic state of stress at one site in the Beaufort Sea may be independent of stress history. This opinion is contrary to K_o test data obtained on natural and remolded soils in laboratory triaxial cells and instrumented oedometers. For soils that experience virgin loading and simple rebound, the following expression appears appropriate:

$$K_o = (1 - \sin \overline{\phi})\ \mathrm{OCR}^{\sin \overline{\phi}} \quad (1)$$

where $\overline{\phi}$ is the effective stress friction angle of the material.

School of Civil and Environmental Engineering, Hollister Hall, Cornell University, Ithaca, N. Y. 14853-3501.

Therefore, it is of interest to examine whether direct field measurements of in situ K_o by self-boring pressuremeter test (SBPMT) are consistent with K_o-OCR trends observed in the laboratory.

SBPMT is one of the few devices capable of obtaining a direct measurement of horizontal stress in situ. Recent advances with the flat dilatometer, the stepped blade, and special cone penetrometers outfitted with horizontal stress sensors appear to be promising, but they are dependent on extrapolation procedures or empirical correlations for their estimation of σ_{ho}. Since the advent of the SBPMT, almost 2 decades of experience have been acquired, allowing for an overall assessment of the device for characterizing soil properties. In this paper, a brief review of the trend of K_o with OCR is examined, both from laboratory studies and from available field data acquired with the SBPMT.

As an alternative to the SBPMT, a direct measurement of σ_{ho} may be obtained by using total stress cells (TSC) or hydraulic fracturing (HF). Experience with the TSC has shown reasonable success in profiling horizontal stresses, although a considerable waiting time (i.e., several days or more) often is required for the dissipation of excess pore water stresses caused by insertion of the blade. Conversely, the hydraulic fracturing technique appears to be hampered by several difficulties, and the method may actually be restricted to measuring σ_{ho} in soils with K_o less than 1 (*6*).

Of additional interest is the notion that all in situ tests reflect, to some degree, the ambient geostatic state of stress in the ground. Traditionally, the cone tip resistance (q_c) has been used to provide an index of the undrained shear strength (s_u) of clay deposits. Because it has been well established that a relationship exists between s_u and OCR, logically it may be assumed that K_o also is reflected in the measured value of q_c. In this paper, approximate cavity expansion relationships are presented for determining K_o from piezocone measurement and dilatometer readings.

SBPMT DATA BASE

A data base of soil properties measured by SBPMT has been compiled from 56 separate clay sites that have been described in the geotechnical literature. A listing of the sites, sources of data, index properties, and identifying symbols is given in Table 1. Thirty-seven of the sites were tested using Cambridge-type probes (Camkometer) and are denoted by solid and partially darkened symbols. Eighteen sites were tested using the French-type probe (PAFSOR) and are shown by open symbols. Two sites (Boston Blue clay and Porto Tolle)

were tested by both the Camkometer and the PAFSOR probes. In addition, three of the open symbols are used to denote sites (Tokyo, Oyo, and Hachinohe) that were tested by using the Japanese Oyo monocell probe.

The data base includes sites from worldwide sources. Index properties summarized in Table 1 represent mean values or typical values for the deposits. Plasticity indices ranged from 10 to 73 percent for those clays, and sensitivities varied from 2 to 500. Stress states were reported to vary from normally consolidated (OCR = 1) to heavily overconsolidated (OCR $\approx$ 80). One site from the Beaufort Sea was not included in the data base because of an apparent controversy over the interpreted profile of stress history (*7*).

Values of the soil parameters for each site were digitized at the specific test depths at which the SBPMT were conducted. Usually, the companion series of oedometer tests were not performed on samples taken at the same depths, thereby requiring interpolation of OCR values. Also, some errors likely may have been incurred in the scaling of data and measurements from the original sources.

To provide as consistent a comparison as possible, values of σ_{ho} from the SBPMT generally were defined by the lift-off method (*8*), although not all sources of data actually specified the method of interpretation used. The conventional Casagrande technique of defining $\overline{\sigma}_p$ was used most often in interpreting the results of the consolidation data. Obviously, those methods of defining $\overline{\sigma}_{ho}$ and $\overline{\sigma}_p$ are subject to errors in judgment, scaling, and bias by the various researchers who presented the data.

The observed relationship between the in situ K_o from the SBPMT and OCR is presented in Figure 1, indicating a strong trend between K_o and stress history of the deposit. Adopting

TABLE 1 LIST OF CLAY SITES TESTED BY SELF-BORING PRESSUREMETER

TYPE PROBE	SITE SYMBOL	SITE	SUMMARY OF INDEX PROPERTIES w_n	w_L	PI	CF	S_t	REMARKS	REFERENCE
Camkometer		ADGO FIELD	30	35	12	5	na	stiff OC	Kack, et al., 1986
		BACKEBOL	95	90	60	na	28	soft NC	Massarsch & Broms, 1976
		BELL COMMON	25	63	39	45	na	fissured HOC	Tedd, et al., 1984
		BOSTON BLUE	43	41	22	44	7	OC to NC	Ladd, et al. 1980
		BOTANIC PARK	na	na	na	na	na	stiff OC	Arnold, 1981 (30)
		BURNT FEN	na	na	na	na	na	soft NC	Wroth, 1980 (33)
		CANVEY ISLAND	80	75	45	na	na	soft NC	Windle & Wroth, 1977a
		CHINA BASIN	95	na	na	na	na	soft LOC	Clough & Denby, 1980
		COWDEN	17	38	20	35	na	OC till	Powell & Uglow, 1985
		DRAMMEN	54	54	28	47	7	aged NC	Lacasse, et al., 1981
		DUNTON GREEN	33	85	58	na	na	fissured HOC	Clarke & Wroth, 1984; Samuels, 1975
		ESSEX	27	61	38	45	na	fissured HOC	Tedd & Charles, 1981
		FREDERICTON	27	30	10	50	na	sensitive	Landva, et al., 1988 (22)
		GLOUCESTER	80	55	28	80	60	sensitive aged NC	Konrad & Law, 1987
		GOTHENBERG	85	83	30	na	20	aged NC	Wroth & Hughes, 1974
		GRANGEMOUTH	65	75	40	35	na	soft NC	Clarke et al., 1979 (23)
		HAGA	35	40	15	45	6	sensitive OC	Aas, et al., 1986
		HAMILTON AFB	92	90	50	na	7	aged NC	Benoit & Clough, 1986
		HENDON	28	70	42	52	na	fissured HOC	Windle & Wroth, 1977b
		KINGS LYNN	65	95	57	na	3.5	organic LOC	Wroth & Hughes, 1973 (24)
		LA SPEZIA	52	75	55	50	5.5	soft NC	Ghionna, et al., 1982
		MADINGLEY	26	72	47	92	na	fissured HOC	Windle & Wroth, 1977b
		MASSENA	60	50	25	60	10	sensitive aged NC	Huang & Haefele, 1988 (25)
		MATAGAMI	70	80	47	na	na	sensitive NC	Eden & Law, 1980
		MELBOURNE	na	na	na	na	na	soft LOC	Ervin, 1983 (26)
		MERCER ISLAND	28	53	24	41	na	stiff OC	Denby, et al., 1981 (27)
		NRCC	80	60	35	70	200	aged NC	Law & Eden, 1980; Konrad & Law, 1987
		ONSOY	62	65	28	60	7.5	aged NC	Lacasse, et al., 1981
		OTTAWA	70	55	30	66	500	sensitive aged NC	Konrad & Law, 1987
		OXFORD	na	72	40	na	na	fissured HOC	Clarke & Wroth, 1988 (28)
		PADDLE RIVER	17	36	25	na	na	clay core	Ramage et al., 1986 (29)
		PANIGAGLIA	60	72	47	na	5	soft NC	Ghionna, et al., 1981, 1985
		PORT AUGUSTA	na	na	na	na	na	stiff OC	Arnold, 1981 (30)
		PORTO TOLLE	36	52	30	34	3	soft NC	Ghionna, et al., 1981, 1985
		SEA ISLAND	36	35	10	20	5	soft NC	Konrad, et al., 1985
		TARANTO	23	60	27	na	na	cemented HOC	Ghionna, et al., 1981, 1985
		UPPER LIAS	na	62	32	na	na	fissured HOC	Clarke & Wroth, 1988 (28)
Oyo		HACHINOHE	45	85	67	na	na	OC	Moroto & Muramatsu, 1987
		OYO	na	na	na	na	na	soft NC	Ohya, 1980
		TOKYO	52	38	28	35	na	aged NC	Mori, 1981

(*continued on next page*)

TABLE 1 (*continued*)

TYPE PROBE	SITE SYMBOL	SITE	SUMMARY OF INDEX PROPERTIES w_n	w_L	PI	CF	S_t	REMARKS	REFERENCE
PAFSOR		BANDAR ABBAS	28	44	22	27	2.5	LOC	Ghionna, et al., 1981
		BEAUMONT	30	65	40	na	na	desiccated OC	Mahar & O'Neill, 1983
		BOSTON BLUE	43	41	21	44	7	OC - NC	Ladd, et al. 1980
		CRAN	80	95	55	na	na	aged NC	Juran, et al. 1983
		CUBZAC LES PONTS	85	95	54	55	na	organic NC	Blondeau et al., 1977 (31)
		FLANDERS	na	na	na	na	na	soft silt	Baguelin et al., 1978 (32)
		GUASTICCE	68	88	63	52	na	NC	Ghionna, et al., 1981
		LANESTER	120	120	73	na	na	aged organic NC	Baguelin, et al., 1974
		MARE ISLAND	80	92	52	na	2	soft NC	John, 1980
		MONTALTO	26	52	34	38	na	intact OC	Ghionna, et al., 1981
		NEW ORLEANS	64	78	51	na	na	soft NC	Canou & Tumay, 1986
		PLANCOET	40	40	20	na	na	soft NC silt	Baguelin et al., 1978 (32)
		PORTO TOLLE	36	52	30	34	3	soft NC	Battaglio, et al., 1981
		RIO VISTA	200	180	30	na	3.5	soft NC	John, 1980
		SACRAMENTO	40	45	13	na	2	soft NC	John, 1980
		ST. ALBAN	75	45	22	38	15	sensitive aged NC	Roy & Chi Thien, 1987
		ST.ANDRE CUBZAC	100	70	35	na	na	soft NC	Baguelin, et al., 1972
		TRIESTE	50	71	47	46	na	soft NC	Battaglio, et al., 1981

Notes: NC = normally consolidated; LOC = lightly overconsolidated; OC = overconsolidated; HOC = heavily overconsolidated; na = not available; w_n = natural water content (%); w_L = liquid limit (%); PI = plasticity index (%); CF = clay fraction (% < 2μ); S_t = sensitivity by field vane

References not followed by reference number may be found in an earlier paper by Mayne and Kulhawy (7).

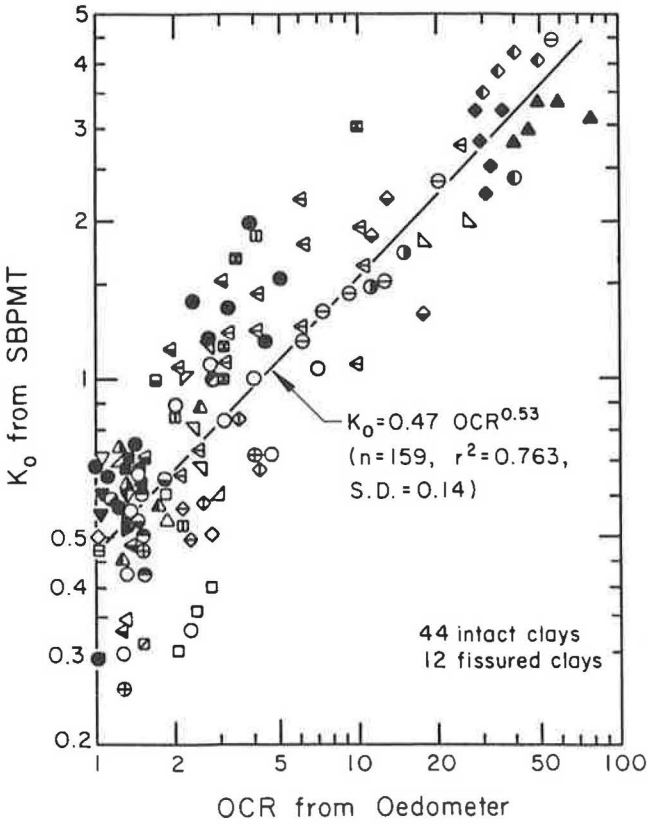

FIGURE 1 Observed trend between in situ K_o from SBPMT and overconsolidation ratio.

a format in terms of a power function, regression analyses for the SBPMT data give a best fit line (n = 159, r^2 = 0.763, S.D. = 0.14 for logarithmic scale):

$$K_o = 0.52\ \mathrm{OCR}^{0.51} \tag{2a}$$

where n is the number of data points, r^2 is the coefficient of determination, and S.D. is the standard deviation of the independent variable. For comparison, a least-squares regression assuming arithmetic relationships between K_o and OCR indicated an r^2 of only 0.562, and, therefore, the choice of the assumed power function relationship in Figure 1 appears more statistically significant. In addition, the power function has been adopted by many researchers (*6,9,10*) as a convenient and simple means of relating K_o to stress history.

The observed range of values about the statistical best-fit line in Figure 1 is likely caused by a number of factors not considered in this review. For one, by visual inspection, it can be seen that at low values of OCR the PAFSOR device consistently gives lower values of K_o than does the Camkometer. This result may be caused by differences in the length to diameter (L/d) ratios of the probes (L/d = 2 and 4 for the PAFSOR, 6 for the Camkometer, and L/d = 5 for the Oyo type). In concept, the SBPMT minimizes disturbances to the ground during installation. In reality, however, some disturbance is inevitable, and this may influence the interpreted value of K_o. In addition, the various environmental and geologic factors previously mentioned may have had some influence on the overall development of $\overline{\sigma}_{ho}$.

For comparison, it is of interest to summarize the apparent connection between K_o and OCR from laboratory studies. In

laboratory test series, the K_o condition is defined strictly by one-dimensional consolidation with zero lateral strain. In the field, the true imposed boundary conditions are not known, and the term K_o is used to infer the geostatic state of stress. In the laboratory series, specimens were subjected to vertical stresses sufficient enough to reach an OCR = 1 and then were unloaded to known values of OCR. A statistical analysis of laboratory K_o test data on 48 different clays unloaded in simple rebound has been summarized by Kulhawy and Mayne (*11*) and is presented in Figure 2. The average trend from regression analyses of the laboratory K_o data indicates

$$K_o = 0.54\ \text{OCR}^{0.44} \tag{2b}$$

where $n = 174$, $r^2 = 0.88$, and S.D. = 0.17. Figure 2 also indicates the specific trends for the K_o-OCR relationships by accounting for the influence of $\bar{\phi}$ as given by Equation 1. Whereas this effect of $\bar{\phi}$ has been justified for laboratory K_o relationships (*4*), it may also be taken as significant for field values of K_o, although values of $\bar{\phi}$ were mostly unavailable for the SBPMT data base. For soils reloaded after rebound, it is important to note that the relationship between K_o and OCR is different.

CAVITY EXPANSION THEORY FOR K_o

Although the SBPMT appears to be capable of providing direct measurements of the in situ K_o, the device has not gained sufficient popularity in practice because of its high cost and low productivity. In addition, the sophisticated nature of the device requires a high level of technical expertise in the field so that proper results are obtained. Moreover, the presence of dense sands, old fills, and gravelly layers often causes difficulties in the installation of the SBPMT for routine testing. Consequently, considerable interest exists in estimating K_o from more conventional and robust tests such as the CPT and DMT, even though those represent indirect approaches to the problem.

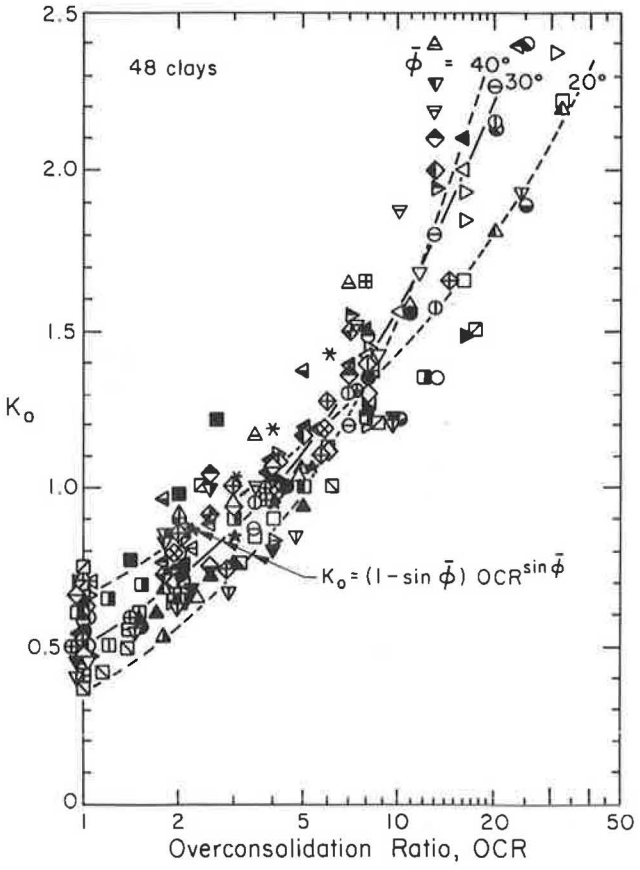

FIGURE 2 Observed and predicted relationships between K_o and OCR from laboratory test data [data compiled from work by Mayne and Kulhawy (*4*)].

Commonly, the cone tip resistance (q_c) measured during the CPT is used to determine the undrained shear strength (s_u) of clay deposits. Technically, a corrected cone tip resistance (q_T) should be used because pore water stresses act on unequal areas of the cone (*6*). Therefore, piezocone penetration tests (CPTU) are the preferred means of testing. The value of s_u is calculated from q_T according to

$$s_u = (q_T - \sigma_{vo})/N_k \tag{3}$$

where σ_{vo} is total overburden stress and N_k is the cone tip bearing factor.

The variation of normalized undrained strength ($s_u/\bar{\sigma}_{vo}$) with OCR is well documented and assumes a power law form

$$(s_u/\bar{\sigma}_{vo})_{OC} = (s_u/\bar{\sigma}_{vo})_{NC}\ \text{OCR}^{\Lambda} \tag{4}$$

where OC is overconsolidated, NC is normally consolidated, and Λ is plastic volumetric strain potential (*12*). For most natural clays, $\Lambda \approx 0.8$ for triaxial and direct simple shear modes of failure. If the strength corresponding to direct simple shear is assumed to be relevant, then the expression for the NC normalized strength is simply (*12*)

$$(s_u/\bar{\sigma}_{vo})_{NC} = \sin\bar{\phi}/2 \tag{5}$$

By combining Equations 1 and 3, Kulhawy et al. (*3*) were able to effectively remove the OCR term, resulting in

$$K_o = (1 - \sin\bar{\phi}) \left[\frac{(s_u/\bar{\sigma}_{vo})_{OC}}{(s_u/\bar{\sigma}_{vo})_{NC}}\right]^{\sin\bar{\phi}/\Lambda} \tag{6}$$

Adopting the cavity expansion theory of Vesić (*13*), the cone-bearing factor for tip resistance is

$$N_k = (4/3)\ [\ln I_r + 1] + \pi/2 + 1 \tag{7}$$

where $I_r = G/s_u$ is the rigidity index of the clay and G is the shear modulus. Keaveny and Mitchell (*14*) have substantiated the relevance of this cavity expansion expression for N_k for CPT results in clay. The apparent difficulty with the cavity expansion approach is its reliance on I_r. Because the stress-strain behavior of clay is known to be nonlinear, the relevant value of G (and I_r) depends on strain level and stress history and is not known a priori. Fortunately, however, the expression for N_k is in terms of the natural logarithm of I_r, and therefore only a first-order assessment of I_r is needed.

Generally, I_r decreases with OCR and increases with plasticity index of the soil (*9,14*). Alternatively, the modified Cam clay model can be used to provide an estimate of the undrained rigidity index ($I_r = G/s_u$). By using conventional soil param-

eters, the original Cam clay model may be utilized to evaluate I_r for normally consolidated clays (*15*):

$$(G/s_u)_{NC} = \frac{2\,M\,(1 + e_o)\,\ln 10}{3\,C_c\,\Lambda\,(1 - \Lambda)\,\exp(-\Lambda)} \tag{8}$$

where $M = 6 \sin \bar{\phi}/(3 - \sin \bar{\phi}) \approx \bar{\phi}/25.4$ degrees, e_o is the void ratio, and C_c is the virgin compression index. Wroth and Houlsby (*10*) further showed that the effect of OCR on I_r may be represented by using the following equation:

$$\frac{(G/s_u)_{OC}}{(G/s_u)_{NC}} = [1 + C \ln \text{OCR}]\ \text{OCR}^{-\Lambda} \tag{9}$$

where C is an experimentally determined constant between 0 and 2. A value of $C = 1$ appears to typify the trends observed from laboratory test data. By combining Equations 8 and 9 and adopting a typical value of $\Lambda = 0.8$, Kulhawy and Mayne (*11*) developed a simple approximation for I_r in terms of conventional soil parameters:

$$I_r = \frac{5\,\bar{\phi}}{6}\,\frac{(1 + e_o)}{C_c}\,\frac{(\ln \text{OCR} + 1)}{\text{OCR}^{0.8}} \tag{10}$$

Figure 3 presents the parametric effect of OCR, $\bar{\phi}$, and C_c on the calculated value of I_r for an assumed constant value of $e_o = 1$.

By combining Equations 3, 5, 6, and 7, K_o can be expressed as

$$K_o = (1 - \sin \bar{\phi}) \left[\frac{(q_T - \sigma_{vo})/\bar{\sigma}_{vo}}{(2/3) \sin \bar{\phi}(\ln I_r + 2.925)}\right]^{1.25 \sin \bar{\phi}} \tag{11}$$

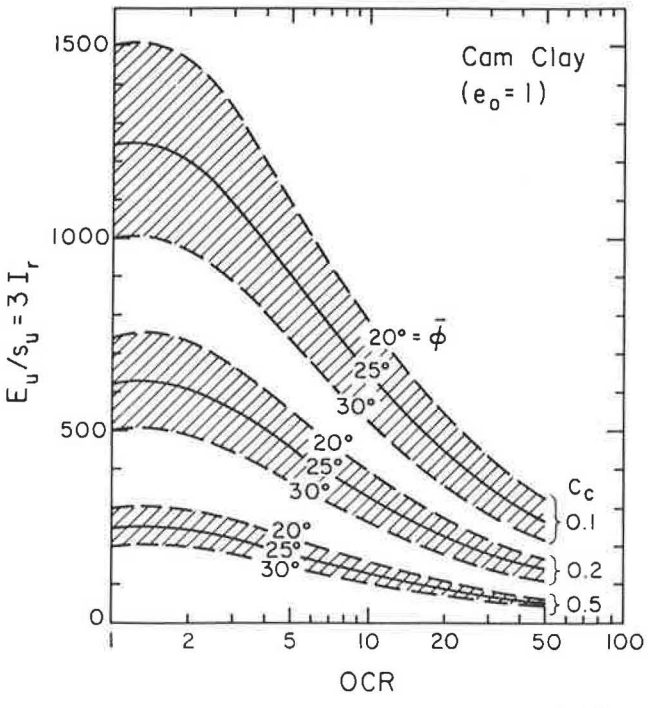

FIGURE 3 Parametric effects of effective friction angle ($\bar{\phi}$), compression index (C_c), and overconsolidation ratio (OCR) on calculated rigidity index ($I_r = G/s_u$).

which demonstrates that K_o is related to the normalized cone tip resistance, $(q_T - \sigma_{vo})/\bar{\sigma}_{vo}$, in terms of basic soil parameters ($\bar{\phi}$, C_c, and e_o). By using Equations 10 and 11, the parametric effect of compression index (C_c) on the theoretical relationship between K_o and normalized cone tip resistance is illustrated in Figure 4.

Cavity expansion theory also provides an evaluation of the excess pore water stresses (Δu) induced by a penetrating cone. For piezocones with porous elements located on the cone tip, Δu is caused primarily by changes in octahedral stresses, such that (*16*)

$$\Delta u = (4/3)\, s_u \ln I_r \tag{12}$$

which applies to spherical cavities. In accordance with Equations 4 and 10, Δu for piezocones with porous elements on the cone tip is always positive. By a similar combination of previous results, the derived expression for K_o in terms of the normalized excess pore water stress ($\Delta u/\bar{\sigma}_{vo}$) from piezocones with tip measurements becomes

$$K_o = (1 - \sin \bar{\phi}) \left[\frac{(\Delta u/\bar{\sigma}_{vo})}{(2/3) \sin \bar{\phi} \ln I_r}\right]^{1.25 \sin \bar{\phi}} \tag{13}$$

Figure 5 illustrates the parametric influence of $\bar{\phi}$ on the theoretical relationship between K_o and $\Delta u/\bar{\sigma}_{vo}$.

An approximate methodology for the DMT also can be formulated. The increase in total horizontal stress caused by a penetrating probe in cohesive ground may be estimated by using cylindrical cavity expansion theory (*16*):

$$\Delta\sigma_h = s_u\,[1 + \ln I_r] \tag{14}$$

Again, the previously mentioned approach yields

$$K_o = (1 - \sin \bar{\phi}) \left[\frac{(\Delta\sigma_h/\bar{\sigma}_{vo})}{(1/2) \sin \bar{\phi}\,(\ln I_r + 1)}\right]^{1.25 \sin \bar{\phi}} \tag{15}$$

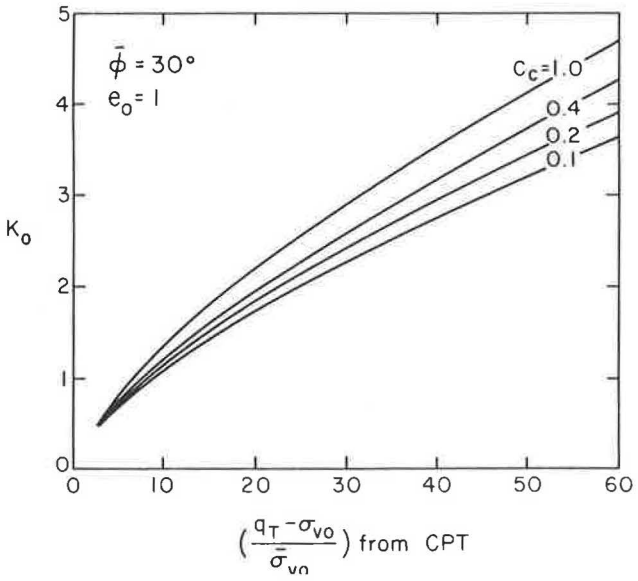

FIGURE 4 Theoretical relation for K_o in terms of normalized cone tip resistance.

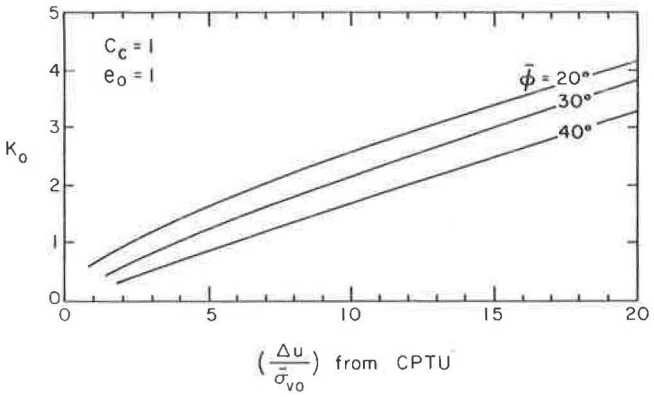

FIGURE 5 Theoretical relation for K_o in terms of normalized penetration pore water stress.

The dilatometer provides measurements of total horizontal stress after penetration by a flat blade. For purposes of correlating DMT results with estimated profiles of K_o, Marchetti (*17*) defined the horizontal stress index (K_D) as a dimensionless parameter

$$K_D = (p_o - u_o)/\bar{\sigma}_{vo} \tag{16}$$

where p_o is the initial total contact stress and u_o is the hydrostatic pore water stress. No specific cavity expansion theory exists for a penetrating flat blade having the same geometry as the dilatometer and using the precise definition of K_D. However, as a first approximation, the index K_D may be taken as the change in total horizontal stress, represented by the normalized term $(\Delta\sigma_h/\bar{\sigma}_{vo})$ in Equation 15. Figure 6 presents the effect of the normalized total horizontal stress change on the calculated value of K_o. The empirical relationship for K_o in terms of K_D given by Marchetti is also shown in Figure 6. Apparently, the empirical approach matches the theoretical curves for a soil with $\bar{\phi} \approx 30$ degrees, $C_c \approx 0.4$, and $e_o \approx 1$.

A preliminary assessment of OCR is required to calculate I_r from Equation 10. Because I_r depends roughly as a function of the natural logarithm of OCR, only a preliminary estimate of OCR is required for calculating I_r from Equation 10. This preliminary estimate of stress history may be made by using empirical correlations between the effective preconsolidation

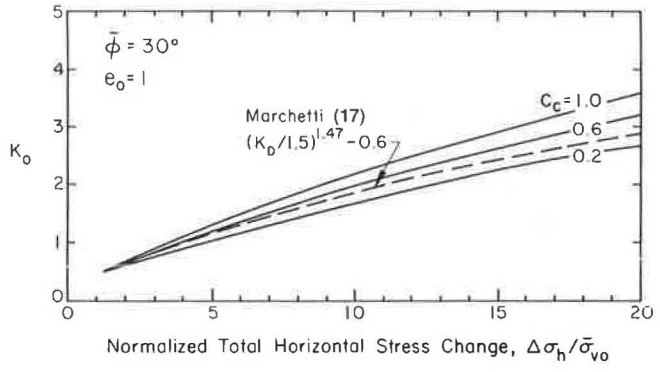

FIGURE 6 Theoretical relation for K_o in terms of normalized total horizontal stress change. Empirical correlation for DMT by Marchetti (*17*) also shown.

stress ($\bar{\sigma}_p$) and in situ test results from the cone penetration test, piezocone, and dilatometer (*18,19*) given by the following expressions:

CPT

$$\bar{\sigma}_p = 0.4\ (q_T - \sigma_{vo}) \tag{17a}$$

CPTU

$$\bar{\sigma}_p = 0.5\ \Delta u \tag{17b}$$

DMT

$$\bar{\sigma}_p = 0.5\ (p_o - u_o) \tag{17c}$$

For heavily overconsolidated fissured clays, these correlative trends provide conservative estimates (*19*).

DATA BASE TRENDS FOR K_o

The compiled SBPMT data base permits the development of direct correlations between K_o and normalized in situ test parameters. A total of 17 of the SBPMT sites cited in Table 1 also were tested by CPTU, allowing for a direct trend between K_o and the normalized cone-tip resistance $(q_T - \sigma_{vo})/\bar{\sigma}_{vo}$, as in Figure 7. The observed trend from the field data is consistent with the theoretical relation indicated previously in Figure 4. As was expected, the highest values of K_o and $(q_T - \sigma_{vo})/\bar{\sigma}_{vo}$ are associated with heavily overconsolidated and fissured clays [London, Gault, and Cowden (*20*)], as well as with the upper fissured crust of Haga clay (*21*). Very high values of K_o also are associated with Taranto clay, which is reported to be cemented and microfissured (*8*).

Because fissured clays have likely undergone passive failure, they do not behave as a true continuum. Consequently,

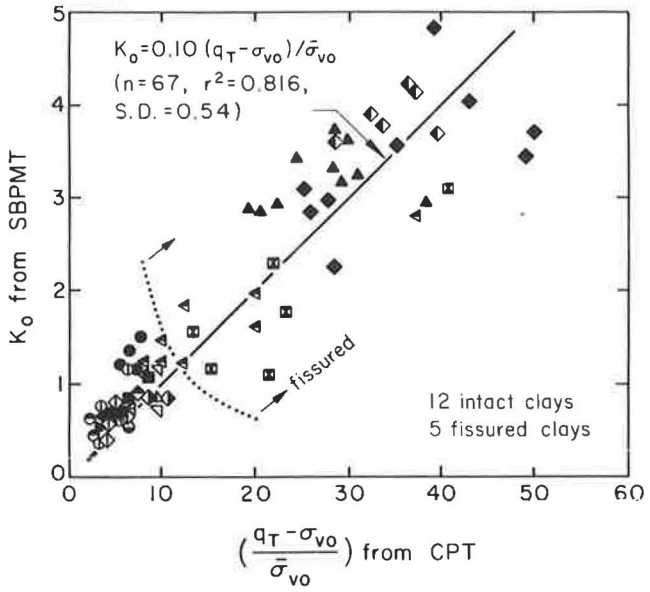

FIGURE 7 Observed trend between K_o from SBPMT and q_T from cone penetration tests.

measurements from in situ probes such as the cone penetrometer also reflect the effects of the secondary structure; that is, q_T reflects both the nature of the intact blocks of heavily preconsolidated clay and the degree, extent, and spacing of fissures. The result is that in heavily overconsolidated fissured clays measured values of q_T are high because of the stress history effects, but they are not as high as theoretical considerations because fissures allow for stress relief during cone penetration.

A similar trend is observed between the SBPMT value of K_o and the normalized excess pore water stress ($\Delta u/\bar{\sigma}_{vo}$) taken from piezocone soundings (Figure 8). Measurements of Δu are primarily from piezocones with tip or face elements. Again, observed trends for K_o are in line with theoretical curves shown in Figure 5. However, fissuring evidently affects the piezocone measurements of Δu in a manner described previously for q_T readings. For piezocones with porous elements located just behind the tip, the observed relationship does not hold in general, because at this location pore water stresses occur as a combination of shear- and octahedral-induced stress changes. Consequently, Δu for heavily overconsolidated and fissured clays tends to be zero or negative for those types of piezocones.

The direct correlation between the SBPMT value of K_o and the DMT index K_D is presented in Figure 9. The original correlation between K_o and K_D presented by Marchetti (*17*)

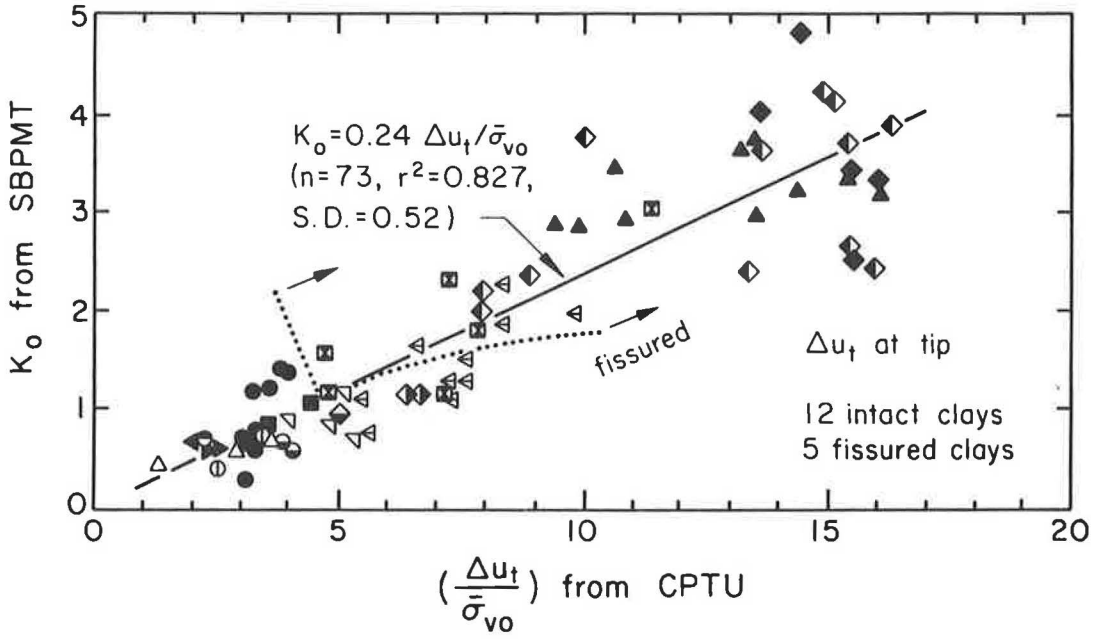

FIGURE 8 Observed trend between K_o from SBPMT and Δu from piezocone soundings with tip elements.

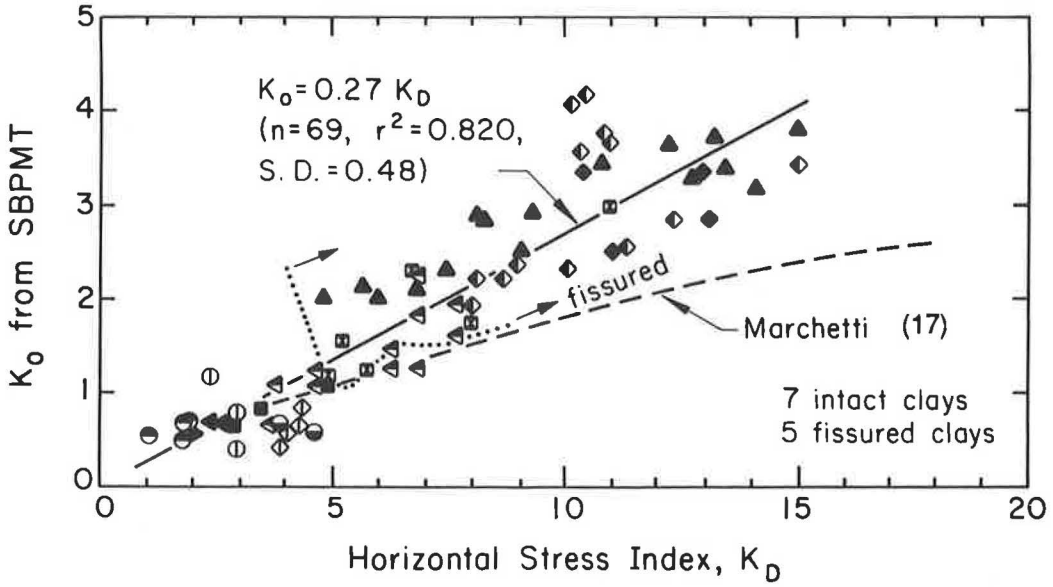

FIGURE 9 Observed trend between K_o from SBPMT and K_D from dilatometer soundings.

was, in fact, based largely on estimated values of K_o for the sites considered. In contrast, data presented in Figure 9 use values of K_o measured in situ by using the SBPMT. By comparing Figures 6 and 9 it is apparent that fissuring also affects the DMT lift-off pressures.

From a practical standpoint, only a first-order estimate of the in situ K_o may be required for geotechnical analysis. Often, the necessary values of $\bar{\phi}$, C_c, e_o, Λ, and OCR for the theoretical approach will be unavailable. Because the methodology is indirect and only approximate in nature, simplified statistical trends may be adopted that relate K_o directly to the normalized in situ test measurements. The best-fit lines from regression analyses indicate

CPT

$$K_o = 0.10\ (q_T - \sigma_{vo})/\bar{\sigma}_{vo} \tag{18a}$$

CPTU

$$K_o = 0.24\ (\Delta u/\bar{\sigma}_{vo}) \tag{18b}$$

DMT

$$K_o = 0.27\ K_D \tag{18c}$$

Summaries of the statistical results and best-fit lines forced through the origin are presented in Figures 7–9 for the CPT, CPTU, and DMT data.

CONCLUSIONS

A systematic approach to the study of K_o in situ leads to the following conclusions:

1. Direct measurements of in situ horizontal stress obtained from 56 clay sites tested by self-boring pressuremeter indicate a K_o-OCR relationship consistent and congruous with previous trends derived from laboratory data.
2. For clay deposits that have been subjected to relatively simple load-unload stress history, indirect assessments of K_o by cone penetration, piezocone, and dilatometer tests appear feasible. A simplified theoretical framework is formulated for this purpose in terms of basic soil parameters ($\bar{\phi}$, C_c, and e_o) by using cavity expansion theory.
3. Observed trends between SBPMT values of K_o and the normalized cone tip resistance ($q_T - \sigma_{vo}/\bar{\sigma}_{vo}$), excess pore water stress at the tip ($\Delta u/\bar{\sigma}_{vo}$), and DMT horizontal stress index (K_D) are consistent with theoretical relationships.
4. In situ penetration tests in heavily overconsolidated fissured clays also are influenced by secondary structure effects.

ACKNOWLEDGMENTS

This study was supported by the Electric Power Research Institute; V. J. Longo was the project manager. Appreciation is expressed to A. Avcisoy for drafting the figures.

REFERENCES

1. F. H. Kulhawy and J. F. Beech. Groundwater Influence on Foundation Side Resistance. *Proc., 9th European Conference on Soil Mechanics and Foundation Engineering*, Dublin, 1987, pp. 707–710.
2. F. H. Kulhawy, J. F. Beech, and C. H. Trautmann. Influence of Geologic Development on Horizontal Stress in Soil. In *Foundation Engineering: Current Principles and Practices*, (F. H. Kulhawy, ed.) ASCE, New York, 1989, pp. 43–57.
3. F. H. Kulhawy, C. S. Jackson, and P. W. Mayne. First Order Estimation of K_0 in Sands and Clays. In *Foundation Engineering: Current Principles and Practices*, (F. H. Kulhawy, ed.) ASCE, New York, 1989, pp. 121–134.
4. P. W. Mayne and F. H. Kulhawy. K_0-OCR Relationships in Soil. *Journal of the Geotechnical Engineering Division*, ASCE, Vol. 108, 1982, pp. 851–872.
5. M. G. Jefferies, J. Crooks, D. Becker, and P. Hill. Independence of Geostatic Stress From Overconsolidation in Some Beaufort Sea Clays. *Canadian Geotechnical Journal*, Vol. 24, 1987, pp. 342–356.
6. M. Jamiolkowski, C. C. Ladd, J. T. Germaine, and R. Lancellotta. New Developments in Field and Lab Testing of Soil. *Proc., 11th International Conference on Soil Mechanics and Foundation Engineering*, San Francisco, Calif., 1985, pp. 57–154.
7. P. W. Mayne and F. H. Kulhawy. Discussion: Independence of Geostatic Stress From Overconsolidation in Some Beaufort Sea Clays. *Canadian Geotechnical Journal*, Vol. 25, 1988, pp. 617–621.
8. V. Ghionna, M. Jamiolkowski, R. Lancellotta, M. Tordella, and C. C. Ladd. *Performance of SBPMT in Cohesive Deposits*. Report RD-81/173, FHWA, U.S. Department of Transportation, 1981.
9. C. C. Ladd, R. Foott, K. Ishihara, F. Schlosser, and H. G. Poulos. Stress-Deformation and Strength Characteristics. *Proc., 9th International Conference on Soil Mechanics and Foundation Engineering*, Tokyo, 1977, pp. 421–494.
10. C. P. Wroth and G. Houlsby. Soil Mechanics: Property Characterization and Analysis Procedures. *Proc., 11th International Conference on Soil Mechanics and Foundation Engineering*, San Francisco, Calif., 1985, pp. 1–56.
11. F. H. Kulhawy and P. W. Mayne. *Manual on Estimating Soil Properties for Foundation Design*. Report EL-6800, Electric Power Research Institute, Palo Alto, Calif., 1990.
12. C. P. Wroth. Interpretation of In-Situ Soil Tests. *Geotechnique*, Vol. 34, 1984, pp. 449–489.
13. A. S. Vesić. Design of Pile Foundations. *Synthesis of Highway Practice 42*, TRB, National Research Council, Washington, D.C., 1977.
14. J. M. Keaveny and J. K. Mitchell. Strength of Fine-Grained Soils Using the Piezocone. In *Use of In-Situ Tests in Geotechnical Engineering*, (S. P. Clemence, ed.) ASCE, New York, 1986, pp. 668–685.
15. P. W. Mayne. Discussion: Undrained Settlement of Plastic and Organic Clays. *Journal of the Geotechnical Engineering Division*, ASCE, Vol. 108, 1982, pp. 1354–1357.
16. A. S. Vesić. Expansion of Cavities in Infinite Soil Mass. *Journal of the Soil Mechanics and Foundations Division*, ASCE, Vol. 98, 1972, pp. 265–290.
17. S. Marchetti. In-Situ Tests by Flat Dilatometer. *Journal of the Geotechnical Engineering Division*, ASCE, Vol. 106, 1980, pp. 299–324.
18. P. W. Mayne and R. D. Holtz. Profiling Stress History from Piezocone Soundings. *Soils and Foundations*, Vol. 28, 1988, pp. 16–28.
19. P. W. Mayne and R. C. Bachus. Penetration Pore Pressures in Clay by CPTU, DMT, and SBP. *Proc., 12th International Conference on Soil Mechanics and Foundation Engineering*, Rio de Janeiro, 1989.
20. J. J. M. Powell and I. Uglow. Dilatometer Testing in Stiff Overconsolidated Clays. *Proc., 39th Canadian Geotechnical Conference*, Ottawa, 1986, pp. 317–326.
21. G. Aas, S. Lacasse, T. Lunne, and K. Hoeg. Use of In-Situ Tests for Foundation Design on Clay. In *Use of In-Situ Tests in Geo-*

technical Engineering (S. P. Clemence ed.), ASCE, New York, 1986, pp. 1–30.
22. A. O. Landva, A. Valsangkar, J. Alkins, and P. Charalambous. Performance of a Raft Foundation Supporting a Multistorey Structure. *Canadian Geotechnical Journal*, Vol. 25, 1988, pp. 138–149.
23. B. G. Clarke, J. P. Carter, and C. P. Wroth. In-Situ Determination of the Consolidation Characteristics of Saturated Clays. *Proc., 8th European Conference on Soil Mechanics and Foundation Engineering*, Brighton, 1979, pp. 207–211.
24. C. P. Wroth and J. M. O. Hughes. An Instrument for the In-Situ Measurement of the Properties of Soft Clays. *Proc., 8th International Conference on Soil Mechanics and Foundation Engineering*, Moscow, 1973, pp. 487–494.
25. A. B. Huang and K. C. Haefele. A Push-In Pressuremeter Sampler. *Proc., 1st International Symposium on Penetration Testing*, Orlando, 1988, pp. 533–538.
26. M. C. Ervin. The Pressuremeter in Geotechnical Investigations. In *In-Situ Testing for Geotechnical Investigations*, Balkema, Rotterdam, 1983, pp. 49–64.
27. G. M. Denby, C. A. Costa, and G. W. Clough. Laboratory and PMT on a Stiff Clay. *Proc., 10th International Conference on Soil Mechanics and Foundation Engineering*, Stockholm, 1981, pp. 577–580.
28. B. G. Clarke and C. P. Wroth. Comparison Between Results From Flat DMT and SBPMT. In *Penetration Testing in the U.K.*, Thomas Telford, London, 1988, pp. 141–144.
29. R. G. Ramage, M. C. Harris and J. Campbell. Predictions and Measurements of Lateral Stresses in a Zoned Earth Embankment. *Proc., 39th Canadian Geotechnical Conference*, Ottawa, 1986, pp. 263–269.
30. M. Arnold. An Empirical Evaluation of PMT Data. *Canadian Geotechnical Journal*, Vol. 18, No. 3, 1981, pp. 455–459.
31. F. Blondeau. Instrumentation du Remblai Experimental a de Cubzac-les-Ponts. *Proc., International Symposium on Soft Clay*, Bangkok, 1977, pp. 419–435.
32. F. Baguelin, J. Jezequel, and D. Shields. *The Pressuremeter and Foundation Engineering*, Trans. Tech. Publications, Clausthal, Germany, 1978.
33. C. P. Wroth. Cambridge In-Situ Probe. *Proc., Symposium on Site Exploration in Soft Ground Using In-Situ Techniques*, Report TS-80-202, FHWA, U.S. Department of Transportation, 1980, pp. 97–135.

Publication of this paper sponsored by Committee on Soil and Rock Properties.

Dilatometer Lateral Stress Measurements in Soft Sensitive Clays

JEAN BENOIT, LOUIS A. NEJAME, MICHAEL J. ATWOOD, AND R. CRAIG FINDLAY

Results from self-boring pressuremeter (SBPM) and dilatometer (DMT) tests at sites in Portsmouth, New Hampshire, and at Hamilton Air Force Base, California, are compared in terms of total lateral stresses. Site-specific correlations for soft sensitive clays between the dilatometer initial lift-off pressures and the range of self-boring pressuremeter horizontal stresses are observed, and it appears that the SBPM can be successfully used to calibrate the DMT. Results from lateral stresses measured at the end of DMT total stress dissipation tests are in close agreement with upper bound results from the SBPM.

Measurement of lateral stresses in the ground is best accomplished in situ by using the self-boring pressuremeter (SBPM). However, the high potential of the SBPM is somewhat overshadowed by its relatively low production testing and the complexity of its drilling and testing operations. In response to some of those difficulties, the dilatometer (DMT) was introduced in the mid-1970s (*1*) as a fast and simple tool having the capability to yield an empirically derived in situ lateral stress. The lateral stress from the DMT is based on the pressure necessary to initially move the flexible circular steel membrane from the face of the instrument into the soil. However, empirical correlations are only as good as the reference tests used for their development. To this end, extensive programs of self-boring pressuremeter and dilatometer testing have been carried out at two soft sensitive clay sites in an attempt to correlate the results from those in situ devices. The test sites are the Portsmouth I-95 Interchange in New Hampshire and Hamilton Air Force Base in California. Those sites were chosen because of the wealth of documentation available concerning the engineering properties of the soil deposits and because of ongoing research programs that use a unique nine-arm self-boring pressuremeter and the flat plate dilatometer.

This paper summarizes the lateral stress results obtained from the SBPM and the DMT at both sites. Comparisons are made between the measured horizontal stress from the SBPM, the initial lift-off pressure reading p_0 from the DMT, and the pressure at the end of DMT total stress dissipation tests. Assessment of the potential of the DMT as a primary tool to evaluate lateral stresses in the ground by using the SBPM for calibration is discussed.

SITE CHARACTERISTICS

The New Hampshire test site is located in Portsmouth and is adjacent to the test embankment investigated by Ladd (*2*) during the construction of the surrounding I-95 highway embankments. The site, situated on the premises of the Pease Air Force Base (PAFB), is a shallow swamp with the water table varying from the ground surface to more than 2 ft above ground. Beneath a surficial organic layer lies the silty clay deposit. Underlying 5 to 8 ft of stiff mottled silty clay is a layer of very soft and highly sensitive marine gray silty clay. Within this clay layer of thickness up to 19 ft are occasional silt and sand lenses. Glacial till underlies the deposit.

The California site is located in Novato at Hamilton Air Force Base (HAFB). Soil conditions at the site consist of 15 to 20 ft of gray stiff silty clay underlaid by a soft to medium gray clay known as Young Bay Mud. Occasional shells and silt lenses may be found within this medium sensitive clay, which extends to a depth of approximately 50 ft. The water table fluctuates from the ground surface to as low as 12 ft below ground.

Table 1 summarizes some of the basic engineering soil properties at the PAFB and HAFB test sites. Both soft clay deposits are slightly overconsolidated below the dessicated crust. The highly sensitive clay at PAFB is of low plasticity, with a liquidity index that suggests very viscous liquid behavior during shearing. The soft clay at HAFB is highly plastic and not nearly as sensitive as the PAFB clay. Natural water contents of the Young Bay Mud are approximately twice those of the Portsmouth clay. The normalized strengths range from 0.13 to 0.30 for the PAFB clay, and it is significantly higher for Young Bay Mud at 0.29 to 0.38.

TESTING PROGRAM

Flat Plate Dilatometer

The dilatometer tests at PAFB and HAFB were conducted in accordance with the suggested ASTM standard D18.02.10. The blade was generally pushed at a rate of 2 cm/sec. Figures 1 and 2 present typical profiles of DMT indices versus depth for both sites. For the PAFB profile in Figure 1, the material index I_d varies between 0.15 and 0.3 for the very soft portion of the deposit. The presence of silt and fine sand lenses observed in undisturbed tube samples obtained from an adjacent borehole is clearly shown by increases of the index. The lateral stress index K_d indicates a decreasing trend with depth and is higher than usually observed for soft, nearly normally consolidated clays. A similar trend is noticed in the preconsolidation pressures obtained from oedometer tests, which also indicate a decrease with depth relative to the assumed effec-

Department of Civil Engineering, University of New Hampshire, Durham, N.H. 03824.

TABLE 1 TYPICAL SOIL PROPERTIES AT PEASE AIR FORCE BASE HAMILTON AIR FORCE BASE SITES

Test Location	Soil Description	Water Content (%)	Plastic Limit (%)	Liquid Limit (%)	Plasticity Index (%)	Liquidity Index (%)	Normalized Strength* (s_u/σ'_{vo})	Sensitivity	References
Portsmouth I-95 New Hampshire (Pease Air Force Base)	Soft marine grey silty clay with occasional silt and sand lenses	35–50	20–25	25–40	10–15	1.3–2.3	0.13–0.30	10–15	2,3
Hamilton Air Force Base California	Soft grey clay with some shells and silt lenses	86–90	38–40	85–88	45–50	1.0–1.1	0.29–0.38	6–8	4,5

*The normalized strengths are shown as a range from various laboratory tests using different stress paths

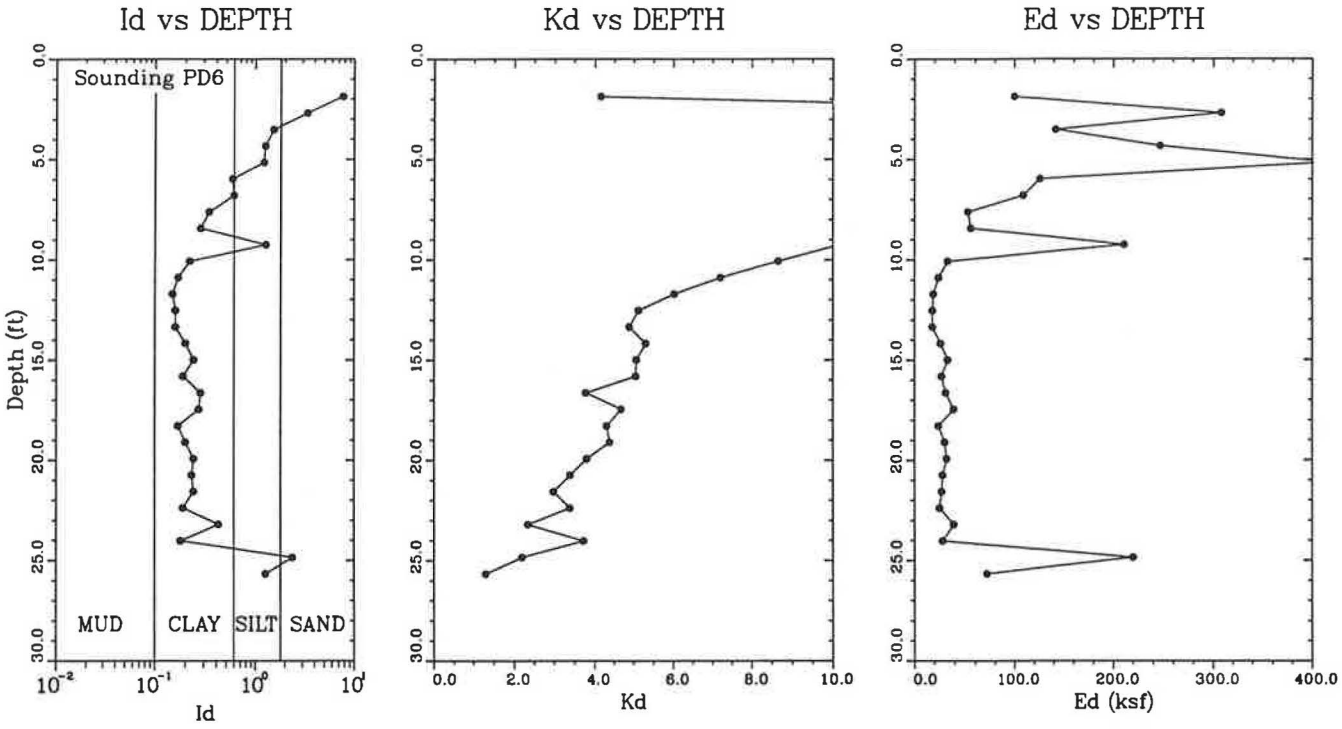

FIGURE 1 Typical profile of dilatometer indices at Pease Air Force Base, New Hampshire.

tive vertical stress. Although the water pressures at the site were measured as hydrostatic, the vertical stress may be more complex than simply geostatic because of the shape of the underlying bedrock. The dilatometer modulus E_d is nearly constant at 30 ksf for the soft material.

The HAFB index profiles are less variable with depth than those from PAFB. The material index varies from approximately 0.1 to 0.15 throughout the normally consolidated clay. The lateral stress index is approximately constant at 2.3, typical of normally consolidated clays. The dilatometer modulus increases slightly with depth from about 10 ksf at 20 ft to 30 ksf at 50 ft.

The indices determined from the DMT tests at each of the two sites are strikingly different. The material index is generally lower for the less-sensitive HAFB deposit. Although this contradicts expected soil behavior, it is consistent with test results in the Onsøy and Drammen clay deposits by Lacasse and Lunne (*6*). There, they observed a lower I_d for the less sensitive Drammen clay. Lutenegger (*7*) also suggests that I_d may be a function of sensitivity. From this testing program and that of Lacasse and Lunne, I_d may be related to both sensitivity and strength. The trends for lateral stress index show the same type of variability observed in results of lateral stress from SBPM tests, which will be discussed later. The

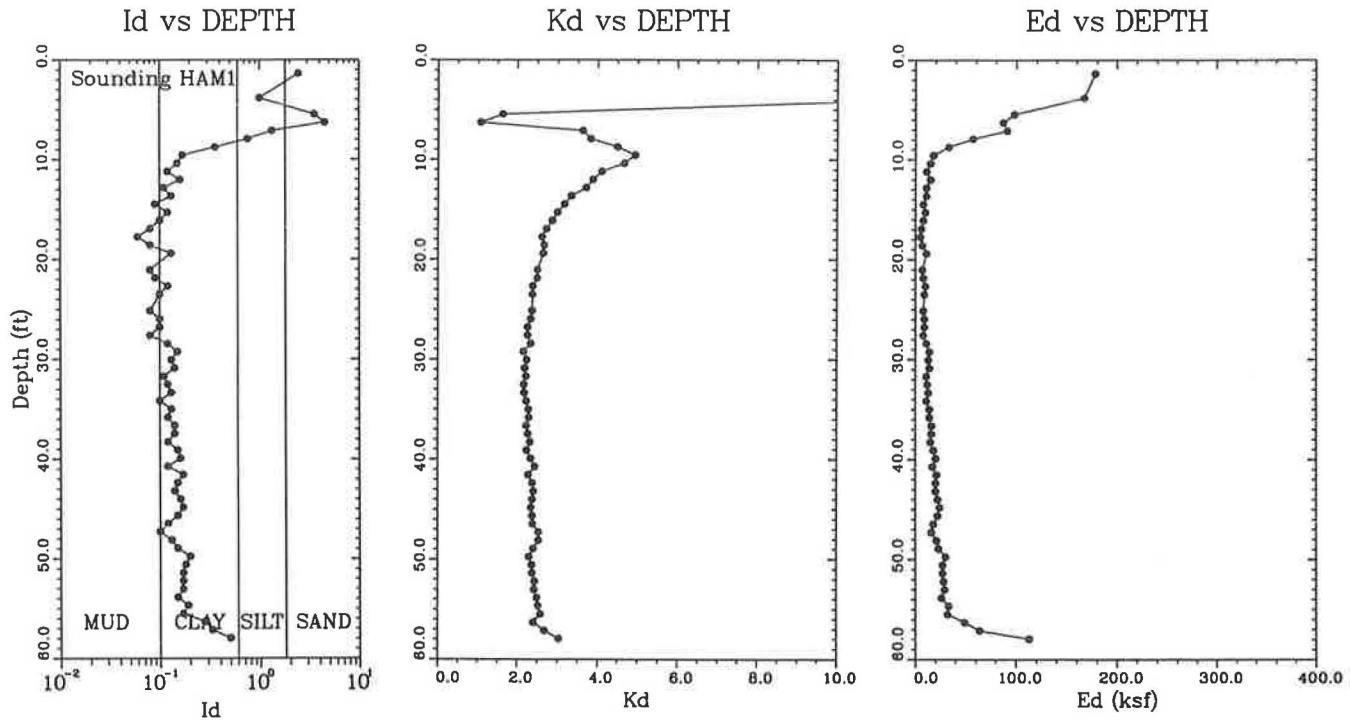

FIGURE 2 Typical profile of dilatometer indices at Hamilton Air Force Base, California.

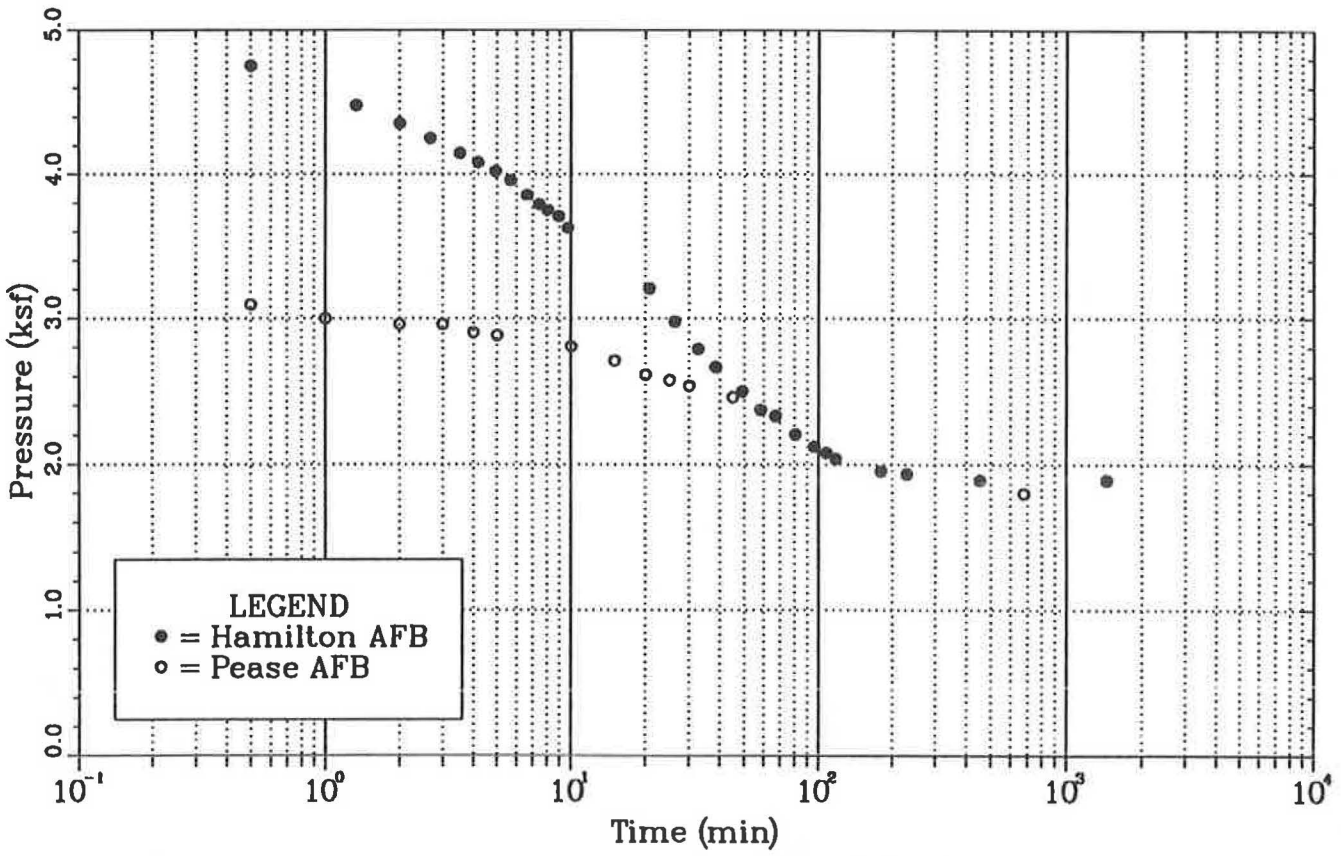

FIGURE 3 Typical dilatometer total stress dissipation tests at Hamilton and Pease Air Force Base sites.

DMT modulus is lower for the more plastic HAFB deposit. As was stated by Lacasse and Lunne (*6*), the sensitivity of the DMT for soft clays may be insufficient for shallow deposits, because the membrane corrections account for a major portion of the field pressure readings. For those testing programs, a very soft membrane was used, and several calibrations were carefully conducted prior to and after each sounding.

Special dilatometer tests designed to evaluate the coefficient of consolidation were performed at both sites. Typical total stress-type dissipation tests (DMTA) are presented in Figure 3 for both sites. The test involves taking initial pressure readings with time without ever deflecting the membrane beyond the plane of the blade. The pressure at the end of dissipation is taken as a total stress without the effects of excess pore pressures, yet it still includes remolding effects.

Self-Boring Pressuremeter

Different self-boring pressuremeters were used for the PAFB and the HAFB investigations, although both probes were fabricated by the firm Cambridge Insitu, England. The SBPM used at HAFB is of the conventional type and is equipped with three strain feeler arms at the midsection of the probe set 120 degrees apart to monitor cavity expansion. The probe used at PAFB was designed by the principal author and differs from the HAFB device in that it is specially equipped with three levels of strain arms. The three levels are located at the top fourth, midsection, and bottom fourth of the inflatable section of the probe. Each level has three arms also set 120 degrees apart. The increased number of strain arms tracking the expandable membrane allows for the entire cavity expansion to be monitored more accurately. The SBPM results presented in this paper are from tests where the conventional cutting method of insertion was used [following the procedure described in Benoit and Clough (*5*)]. Determination of lateral stresses was made in all of the SBPM tests conducted at both sites by using an enhanced visual inspection method. This method, described in Benoit and Clough (*8*), consists of magnifying the portion of the pressuremeter expansion curve associated with the "lift-off" pressure, and this allows a more accurate assessment of the in situ lateral stress. Appropriate corrections were made for the stiffness of the flexible membrane. The SBPM tests at PAFB also were corrected for excess pore pressures generated during insertion and which had not completely dissipated at the time of initial lift-off. Pore pressures were continuously monitored by using two pressure transducers located near midprobe, 180 degrees apart. Figures 4 and 5 present typical profiles of the lateral stress with depth for both sites and for each of the strain-monitoring arms. All nine measurements of lateral stress per test are shown in Figure 4. The PAFB stresses for each of the three levels of arms seem to indicate an inherent horizontal stress anisotropy that is more pronounced than that previously observed at HAFB (*8*).

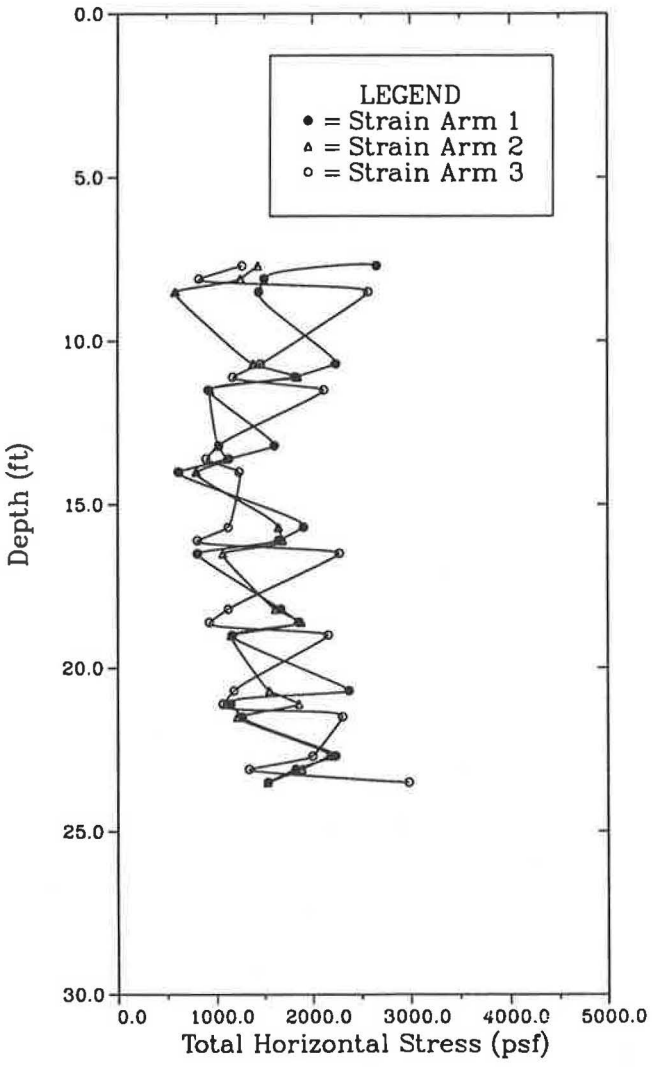

FIGURE 4 Total horizontal stresses from self-boring pressuremeter tests at Pease Air Force Base.

COMPARISON OF SBPM AND DMT LATERAL STRESS MEASUREMENTS

Lateral stresses from SBPM, DMT, and DMTA tests at PAFB and HAFB are presented in Figures 6 and 7. The SBPM horizontal stresses presented are the lower and upper bounds of the values presented in Figures 4 and 5. The DMT results are plotted in terms of initial lift-off pressures p_0 and in terms of total stress at the end of the DMTA dissipation tests, as was previously indicated in Figure 3.

The results seem to indicate that at PAFB and DMT p_0 pressures follow a trend similar to the range embraced by the minimum and maximum lateral pressures measured by the SBPM. The total stress at the end of the DMTA dissipation tests is midway between the minimum and maximum SBPM values in the overconsolidated clay but is in very close agreement with the maximum SBPM stresses in the normally consolidated clay. Similar trends are observed for the HAFB horizontal stresses. The DMT p_0 readings also follow the trend of the range of SBPM lateral stresses in both the overconsolidated and the normally consolidated clay. The total stress at the end of the DMTA dissipation tests are, as with PAFB, in excellent agreement with the maximum values of lateral stress measured by the SBPM. Owing to field time constraints, only the test presented in Figure 3 at 18.9 ft was conducted

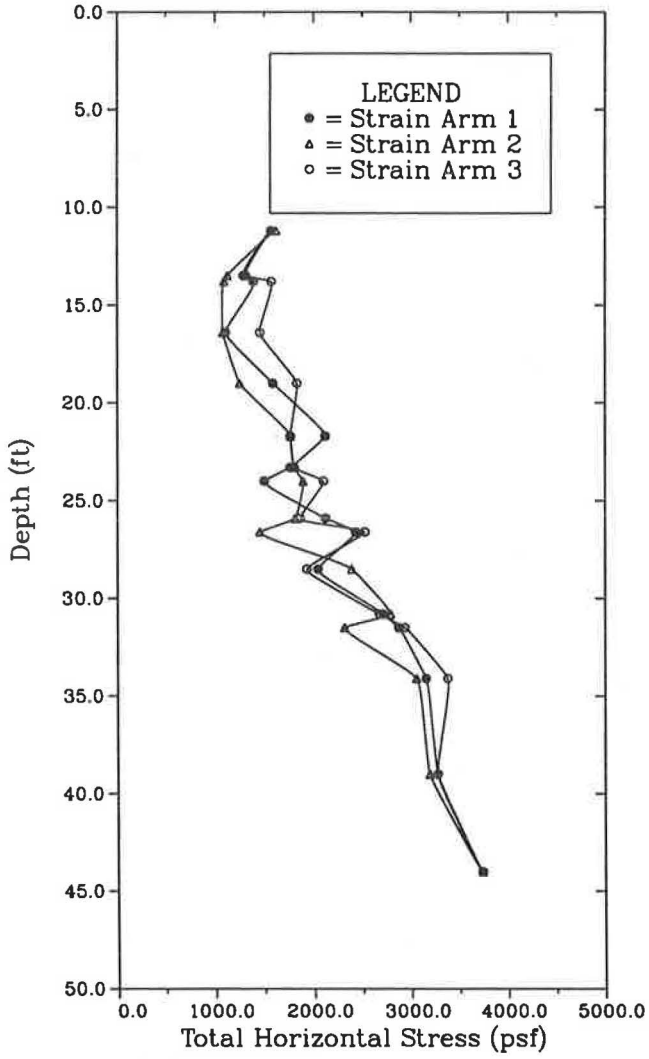

FIGURE 5 Total horizontal stresses from self-boring pressuremeter tests at Hamilton Air Force Base.

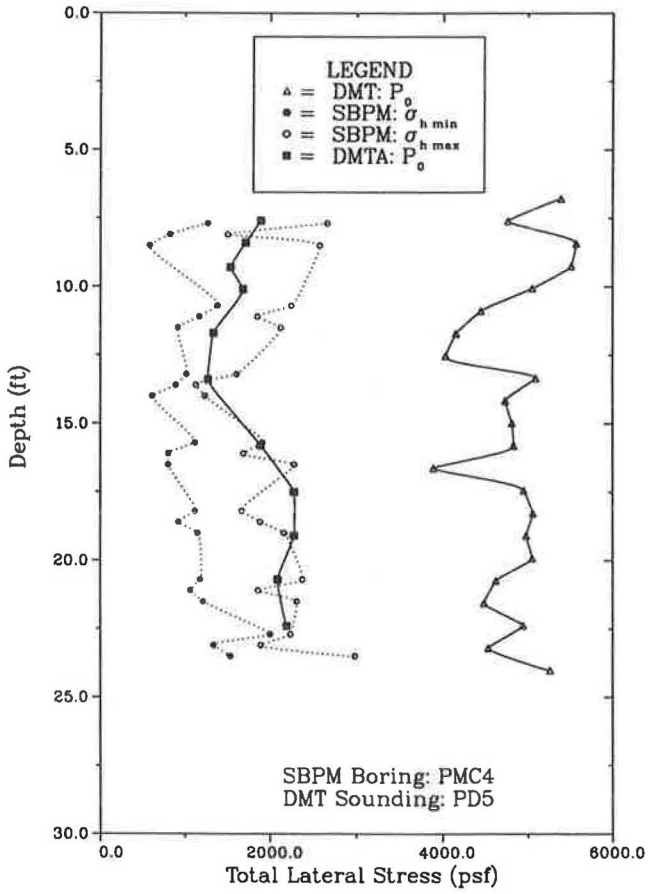

FIGURE 6 Comparison of dilatometer and self-boring pressuremeter total lateral stress test results at Pease Air Force Base.

overnight until dissipation had fully occurred. The other two DMTA tests were monitored for 2 hours, which is beyond the time for 50 percent consolidation, t_{50}. The pressure at 100 percent dissipation was estimated for those two tests based on the time for 50 percent consolidation of the fully dissipated test. It should be noted that t_{50} for the fully dissipated test is in very close agreement with the SBPM holding tests previously performed at this site (*9*).

Clarke and Wroth (*10*) compared results from DMT and SBPM tests at eight different sites in the United Kingdom. An attempt was made to correlate the change in pressure from lift-off to the 1-mm expansion for the DMT test ($p_0 - p_1$) with the difference between the pressuremeter limit pressure and the measured horizontal stress ($p_L - \sigma_h$). Their correlation seems to show a linear relationship over a wide range of stresses. This relationship was examined by using the results from the PAFB and HAFB sites, as is shown in Figure 8. For clarity, only the average strain channel for the HAFB tests and the three middle arms for the PAFB tests are plotted.

Also shown are SBPM results from tests at HAFB that showed disturbance caused by the oversizing of the cutting shoe or probe clogging. A relationship similar to that suggested by Clarke and Wroth appears to exist for the results from those two sites. However, the gradient of the relationship greatly differs for those low pressures, and, furthermore, disturbance does not seem to affect the correlation that suggests that limit pressure is a dominating factor.

SUMMARY AND CONCLUSIONS

Lateral stress results from self-boring pressuremeter and dilatometer tests are compared for two sensitive soft clay sites: Pease Air Force Base and Hamilton Air Force Base. The results seem to indicate that the p_0 readings from the DMT may be calibrated by using the SBPM because they follow very similar trends. Results of DMT p_0 readings at Pease Air Force Base are approximately 5 times greater than those from the minimum SBPM lateral stress values. At Hamilton Air Force Base, the DMT results are approximately 2.5 times greater than those from the SBPM tests. Clearly, DMT and SBPM lateral stress measurements can be correlated but should remain site specific at this time. Once calibrated, the more

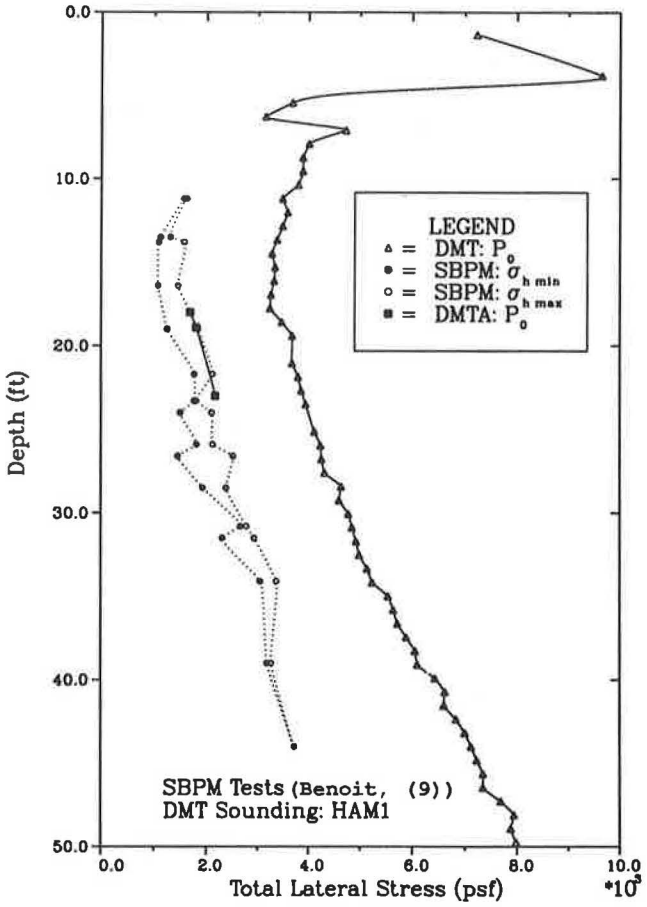

FIGURE 7 Comparison of dilatometer and self-boring pressuremeter total lateral stress test results at Hamilton Air Force Base.

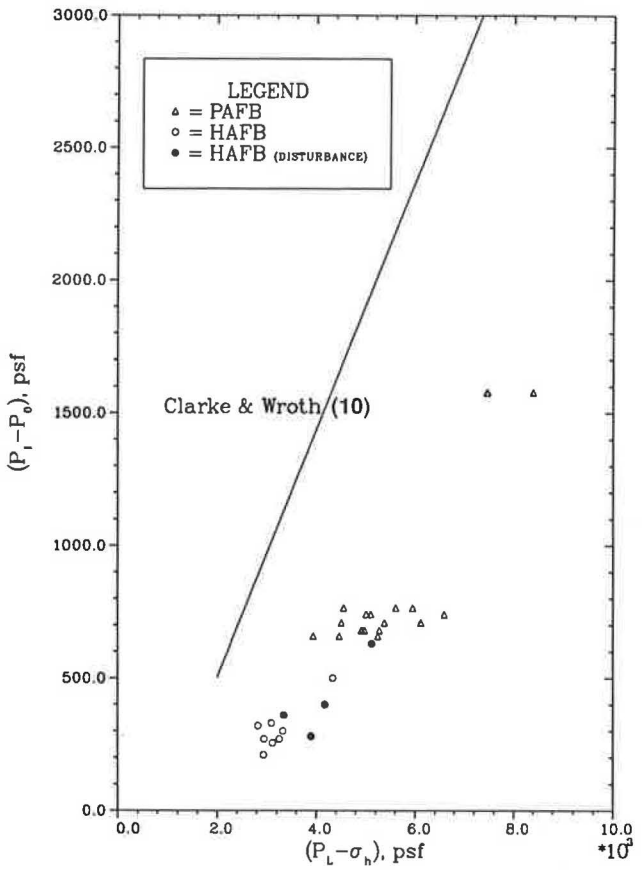

FIGURE 8 Comparison between DMT ($p_1 - p_0$) and SBPM ($p_1 - \sigma_h$) for Pease and Hamilton Air Force Base test results.

cost-effective dilatometer may be used to investigate spatial variability. Lateral stresses from DMTA dissipation tests are in very close agreement to the maximum values of horizontal stress measured with the SBPM and may be used to estimate the upper bound of in situ lateral stresses.

ACKNOWLEDGMENT

Funding for this work was partially provided by the National Science Foundation.

REFERENCES

1. S. Marchetti. A New In Situ Test for the Measurement of Horizontal Soil Deformability. *In Situ Measurement of Soil Properties*, ASCE, Vol. 2, 1975, pp. 225–259.
2. C. C. Ladd. Test Embankment on Sensitive Clay. ASCE, Presented at SMFD Specialty Conference on Performance of Earth and Earth-Supported Structures, Purdue University, June 1972.
3. M. J. Atwood. *Investigation of Jetting Insertion Procedures for Rapidly Deploying a Self-Boring Pressuremeter in Soft Clays*. Masters thesis, University of New Hampshire, Durham, 1989.
4. G. W. Clough and G. M. Denby. Self-Boring Pressuremeter Study of San Francisco Bay Mud. *Journal of the Geotechnical Engineering Division*, ASCE, Vol. 106, No. GT1, Jan. 1980, pp. 45–63.
5. J. Benoit and G. W. Clough. Self-Boring Pressuremeter Tests in Soft Clay. *Journal of the Geotechnical Engineering Division*, ASCE, Vol. 112, No. 1, Jan. 1986, pp. 60–78 (Errata Vol. 113, No. 1, 1987).
6. S. Lacasse and T. Lunne. Dilatometer Tests in Two Soft Marine Clays. Presented at Engineering Foundation Conference on Updating Subsurface Sampling of Soils and Rocks and Their In-Situ Testing, Santa Barbara, Calif., Jan. 1982.
7. A. J. Lutenegger. Current Status of the Marchetti Dilatometer Test. *Proc., First International Symposium on Penetration Testing*, ISOPT-1, Orlando, Fla., 1988, pp. 137–155.
8. J. Benoit and G. W. Clough. Principal Stresses Derived from Self-Boring Pressuremeter Tests in Soft Clay. In *The Pressuremeter and its Marine Applications: Second International Symposium*, ASTM STP 950 (J.-L. Briaud and J.M.E. Audibert, eds.), American Society for Testing and Materials, Philadelphia, Pa., 1986, pp. 137–149.
9. J. Benoit. *Analysis of Self-Boring Pressuremeter Tests in Soft Clay*. Ph.D. thesis, Stanford University, Calif., 1983.
10. B. G. Clarke and C. P. Wroth. Comparison Between Results from Flat Dilatometer and Self-Boring Pressuremeter Tests. *Proc., Geotechnology Conference on Penetration Testing in the U.K.*, University of Birmingham, July 1988.

Publication of this paper sponsored by Committee on Soil and Rock Properties.

Lateral Earth Pressure Measurements in a Marine Clay

AN-BIN HUANG AND KERRY C. HAEFELE

A series of self-boring pressuremeter (SBPM), self-boring lateral stress cell (SBLC), and flat dilatometer (DMT) tests have been performed at a marine clay test site in Massena, New York. Three strain arm readings from the SBPM tests were recorded individually. The SBLC has two stress cells 180 degrees apart. By rotating the SBLC it was possible to measure the lateral stresses in different directions. The DMT tests were performed by pointing the blade in five directions, each 45 degrees apart. The tests performed are described, and the performance of the individual methods are evaluated in light of the test results.

Measuring the field lateral earth pressure σ_{ho} is one of the most intriguing challenges for geotechnical engineers. Such measurements have included the use of hydraulic fracturing, different types of pressuremeters, and lateral stress probes (*1*,*2*) as well as a variety of flat-plate penetrometers (*3*–*5*). Among all the available methods, the self-boring probes (e.g., the camkometer) may be the most sophisticated and elaborate ones. Representing the other end is the flat dilatometer (*3*), which is simple and efficient. Little information is available as to the relative performance of those two different approaches (i.e., simplicity versus accuracy).

The at-rest lateral earth pressure coefficient K_o is often used in lieu of σ_{ho}. Here, the term K_o will be defined as

$$K_o = \frac{\sigma'_{ho}}{\sigma'_{vo}} \tag{1}$$

where σ'_{ho} is the effective lateral earth pressure, and σ'_{vo} is the effective overburden stress.

Apparently, because of its relatively low disturbance, the self-boring pressuremeter (SBPM), such as the Camkometer, has been accepted as one of the more reliable tools for measuring the in situ lateral earth pressure. Three strain arms are located at the mid height of the camkometer probe. In theory, as the probe pressure exceeds the surrounding lateral earth pressure it starts to expand. This "lift-off" pressure during the SBPM probe expansion has been linked directly to the lateral earth pressure. However, the lift-off pressures according to the individual strain arms do not always agree with one another. This can be attributed to the anisotropic nature of the lateral earth pressure or nonuniform disturbance of the soil. Despite the studies conducted (*2*), there has been no general conclusion as to which of the two is the more prominent factor (*6*).

A-B. Huang, Department of Civil and Environmental Engineering, Clarkson University, Potsdam, N.Y. 13676. K. C. Haefele, H & A of New York, 189 S. Water St., Rochester, N.Y. 14604.

The flat dilatometer (DMT) is a relatively new addition to the in situ testing devices. Many empirical methods have been proposed to relate K_o to the DMT horizontal stress index K_D [e.g., those of Marchetti (*3*) and Powell and Uglow (*7*)], which is defined as

$$K_D = \frac{P_0 - u_o}{\sigma'_{vo}} \tag{2}$$

where P_0 is DMT lift-off pressure, and u_o is hydrostatic pore water pressure before DMT insertion.

Reports of such applications have been encouraging (*7*–*9*). The DMT is generally considered a rugged, simple, and practical testing device. The SBPM, on the other hand, is viewed as being complicated and mainly a research tool. In an effort to evaluate the relative performance of such drastically different approaches, a series of SBPM, self-boring lateral stress cell (SBLC), and DMT tests were carried out at a test site. This paper presents the tests performed and discusses the efficacy of those methods in measuring lateral earth pressures.

FIELD EXPERIMENTS

Site Conditions

The test site is located east of the town of Massena, New York. Figure 1 presents the layout of the test site and the testing location. Highway 37 runs east to west immediately to the north of the test site. A creek located to the west of the test site had eroded the soil and created an approximately 4-m deep cut. The soil consists of approximately 12 m of a marine clay deposit underlain by glacial till. Below the 1.5-m thick highly weathered and fissured crust and a layer of overconsolidated clay (from 1.5 to 3.5 m), the marine clay is soft and lightly overconsolidated (OCR = 1.5–3). Figure 2 presents profiles of the available laboratory, field vane shear (FVT), and piezocone penetration (CPTU) test results at the site.

SBPM Tests

A total of 13 SBPM tests were performed by using a Camkometer. The use of the Camkometer has been widely reported. Readers are referred to Wroth and Hughes (*10*) for details of the Camkometer design and its operation. Depths of SBPM tests ranged from 3.5 to 6.7 m. The orientations of the three strain sensing arms were recorded before the probe insertion.

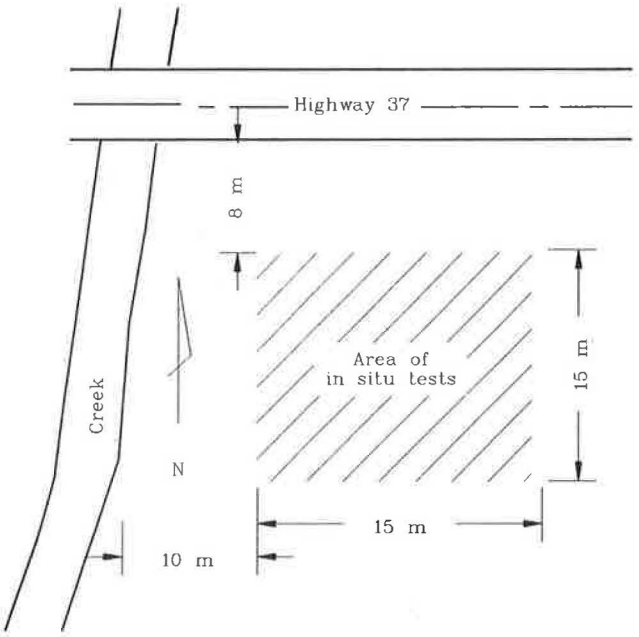

FIGURE 1 Layout of the test site.

Insertion of the SBPM was carried out at a rate of 80 mm/min. The cutter was set at 20 mm from the leading edge of the SBPM probe. Initial trials showed that cutter settings less than 20 mm could result in an apparent unloading to the surrounding soil, as was indicated by the negative pore pressure readings during and immediately after the probe insertion. The probe expansion started after the pore pressure had stabilized. Nine of the SBPM expansion tests were strain controlled. The strain rate of 1 percent/min was used in the probe expansions. The rest of the SBPM tests were stress controlled. Initial stress increment of 14 kPa was used until 1 percent strain was reached to facilitate P_0 readings. Beyond the 1 percent strain, a 28-kPa stress increment was used. A 1-min duration was used for each of the stress increments. An unload reload loop was applied at 2.5 percent radial strain for all the SBPM tests. The data were recorded at a rate of 2 per second, using a computer data logging system. Figure 3 shows the beginning part of the SBPM expansion curve recorded for the individual strain arms.

SBLC Tests

The SBLC (Figure 4) used in this study was manufactured by Cambridge Insitu. It has the same diameter as the Camko-

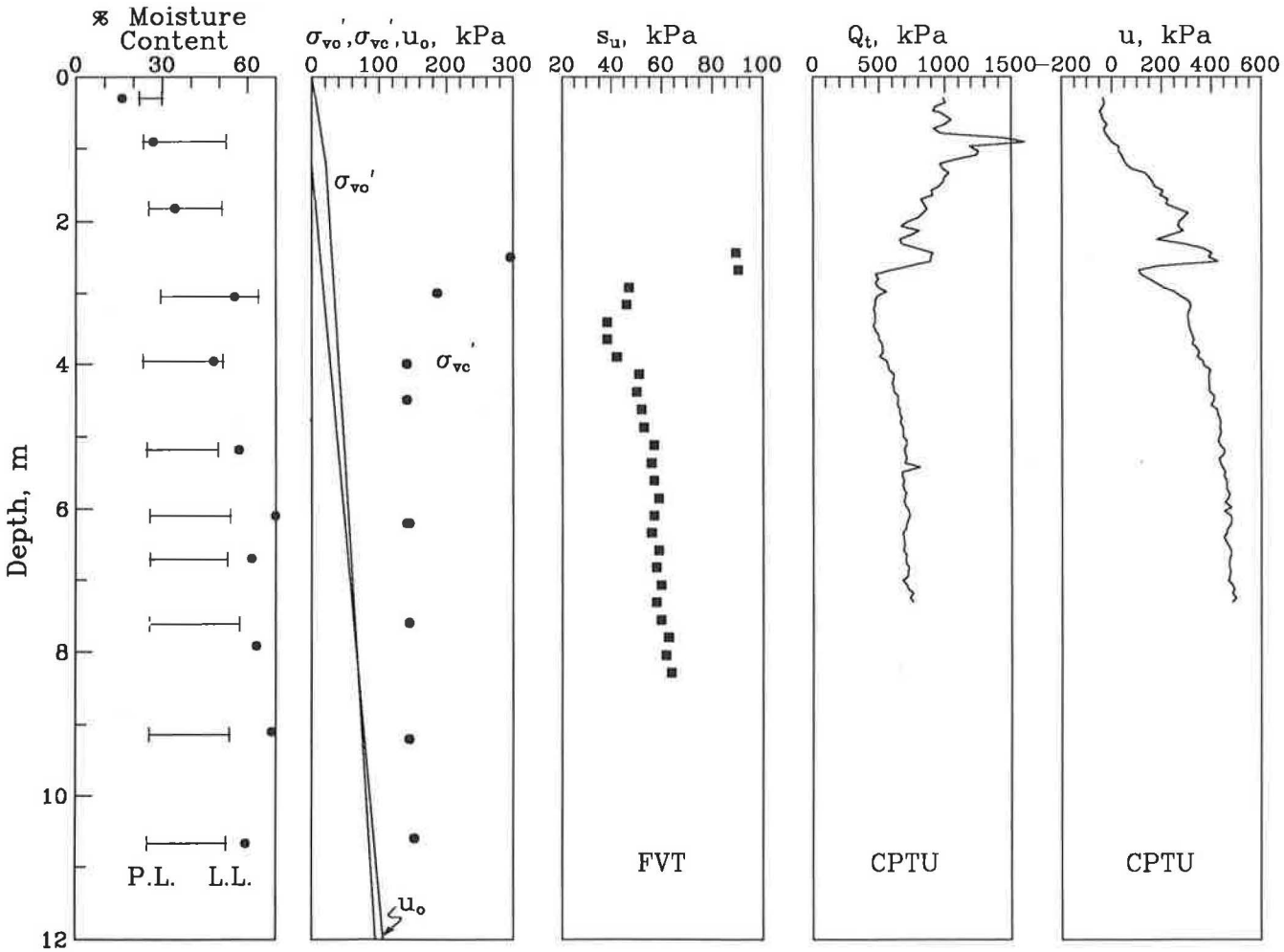

FIGURE 2 Soil profile at the test site.

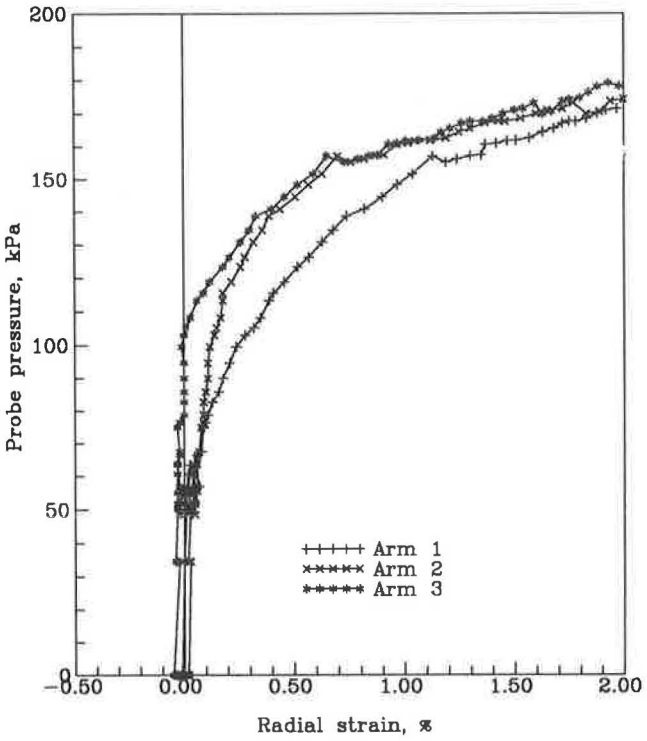

FIGURE 3 Typical SBPM expansion curves.

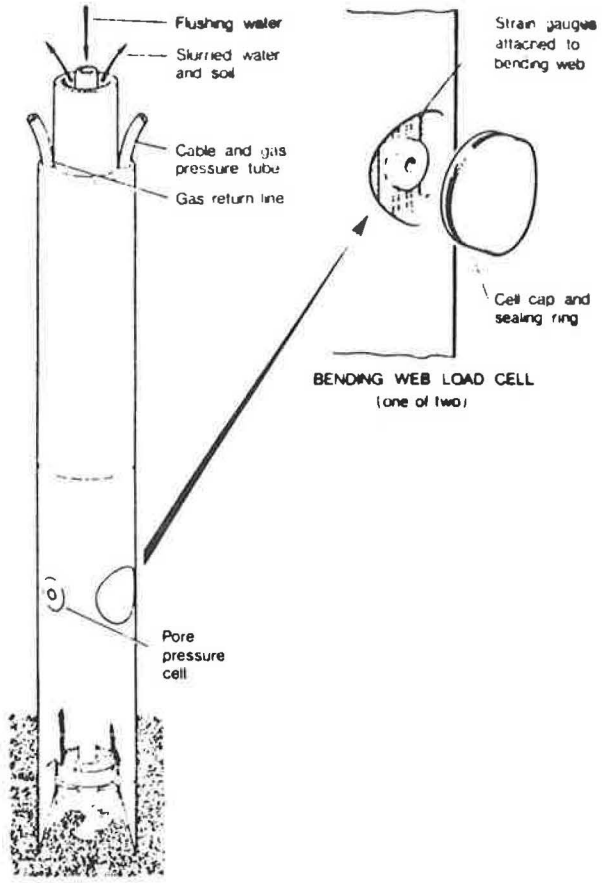

FIGURE 4 The Cambridge self-boring lateral stress cell [from Dalton and Hawkins (*2*)].

meter (80.4 mm). Experience on the use of SBLC has rarely been reported. The probe performs very limited expansion. The outside surface is fitted with two bending web load cells (cells C and D) located on the opposite sides near the midpoint of the instrument. The load cells are 44.4 mm in diameter. A pair of pore water pressure transducers are located between the two load cells at the same level. Any difference between the external stress on the load cells from the soil and the applied internal gas pressure would cause the load cells to deflect. The electrical output (in bits using a computer data logging system) is proportional to the load cell deflection. At the maximum allowable pressure difference of 280 kPa, the load cell deflection is 19 microns according to Dalton and Hawkins (*2*). The control unit was calibrated so that at zero pressure difference the output was zero bits. No inside pressure was applied during the SBLC insertion, and the soil pressure pushed the load cells inward. The "expansion" test is performed by increasing the internal pressure while monitoring the outward deflection of the load cell. The internal pressure at which the load cell reaches its neutral position (zero bits) is an indication of the lateral earth pressure. The SBLC can be thought of as a "passive" measuring device because it allows an inward movement of the soil/load cell to occur. The at-rest lateral earth pressure is reinstated upon expanding the load cells to their neutral position.

Insertion of the SBLC follows the same procedure as insertion of the SBPM. Two profiles of the SBLC tests were performed from depths of 3.5–7.5 m. The expansion started after the excess pore pressure dissipated, as was indicated by the pore pressure transducers. Figure 5 presents the typical results of SBLC expansion tests and the technique for deducing the lateral earth pressure. The probe was rotated 60 degrees clockwise upon deflation, and the test was repeated after stabilization of the pore pressure. By rotating the probe twice, a total of six lateral earth pressure readings can be taken to encompass 360 degrees. Experience indicated that rotating the SBLC probe did cause some variations of the lateral stress measurements. However, the variations were random and within the accuracy of the measurements. An additional evidence for this is that the data from SBLC and SBPM showed similar lateral earth pressure anisotrophy and its relationship with depth, as to be presented later.

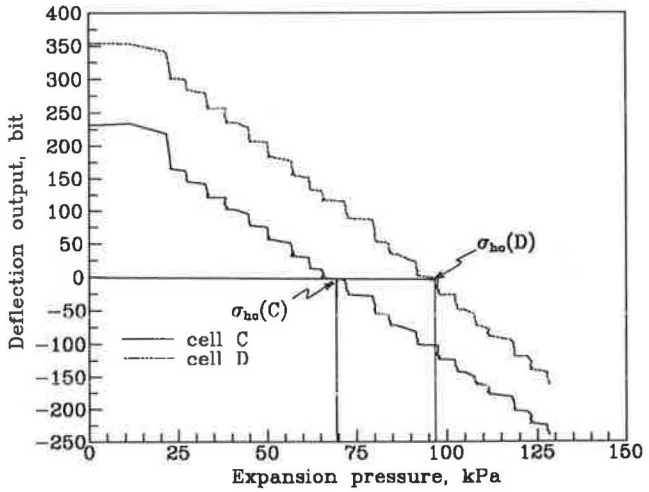

FIGURE 5 Typical SBLC expansion curves.

DMT Tests

A total of five profiles of the Marchetti (*3*) flat DMT tests were performed from 1 to 10 m at the test site. In each profile, the DMT blade was oriented to a different direction so that the five tests would cover directions from due north to due south at 45 degree rotations counterclockwise. The tests were performed at 0.3-m intervals. Figure 6 presents the profiles of the corrected lift-off pressure, P_0 and 1 mm expansion pressure, and P_1 from all the DMT tests.

TEST RESULTS AND INTERPRETATION

There are at least eight published methods for deducing σ_{ho} (*11*) from pressuremeter tests. All methods involve some subjective judgement, and none of them should be considered as measurements of σ_{ho}. Most of those methods are not applicable to SBLC tests because of the lack of significant probe expansion. To maintain consistency, the SBPM lift-off pressure is used to deduce σ_{ho}, because this method is similar to that used for SBLC tests. However, the design differences between the SBPM and SBLC can have significant effects on the deduction of σ_{ho}. Jefferies et al. (*12*) indicated that in stiff clays the lift-off pressure from SBPM tests could correspond to the soil lateral yield stress σ_{hy}, where the probe pressure starts to induce large, plastic deformation in the surrounding soil. The strain sensing arms movement at σ_{hy}, which is significantly higher than σ_{ho}, could be very small and difficult to detect. The same is not likely to occur for SBLC tests because it has a "passive" sensing system, as was described previously, and it does not involve any lift-off pressure.

Figure 7 presents the deduced σ_{ho} values from SBPM and SBLC tests. The SBLC readings came from tests (cell C facing north and cell D facing south) in the same bore hole. Table 1 summarizes the limit pressures P_1, undrained shear strengths s_u, initial shear moduli G_i, shear moduli from unload reload loops H_σ, and σ_{ho} values from all the SBPM tests. The simplex method developed by Huang et al. (*13*) was used in the interpretations of SBPM tests. The σ_{ho} values from SBPM tests are based on the average of the three strain arm readings. The results substantiate the argument by Jefferies et al. in that the σ_{ho} from SBPM are consistently higher than those from the SBLC tests within the stiff clay layer (see Figure 2) at depths from 3 to 4 m. From below that level and within the soft clay deposit, σ_{ho} values from both tests agree fairly well. Within the soft clay layer, the σ_{ho} from SBPM and SBLC correspond to K_o values on the border of 0.5 to 0.65, which is consistent with the oedometer test results (Figure 2).

The σ_{ho} values from load cells (i.e., C and D) located on the opposite sides of the same SBLC probe were different (Figure 7) by as much as 40 percent. There was significant and different levels of soil disturbance around the load cells. The same should also occur for the SBPM tests, as was indicated by Huang and Haefele (*14*).

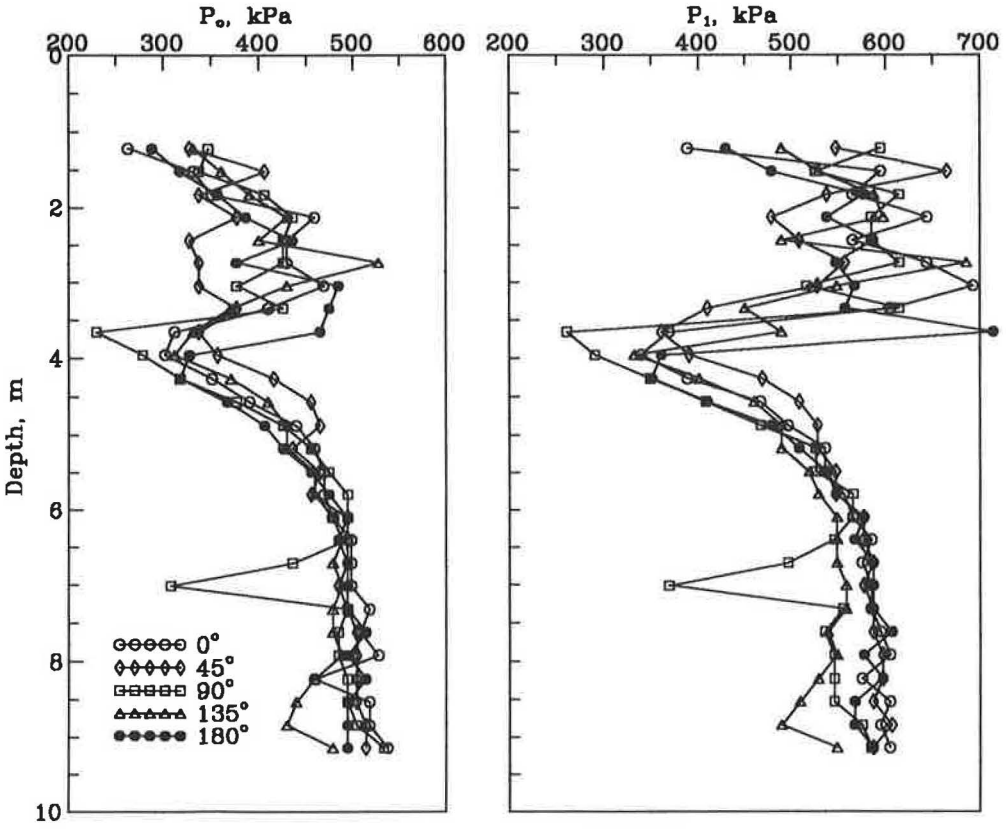

FIGURE 6 The DMT test results.

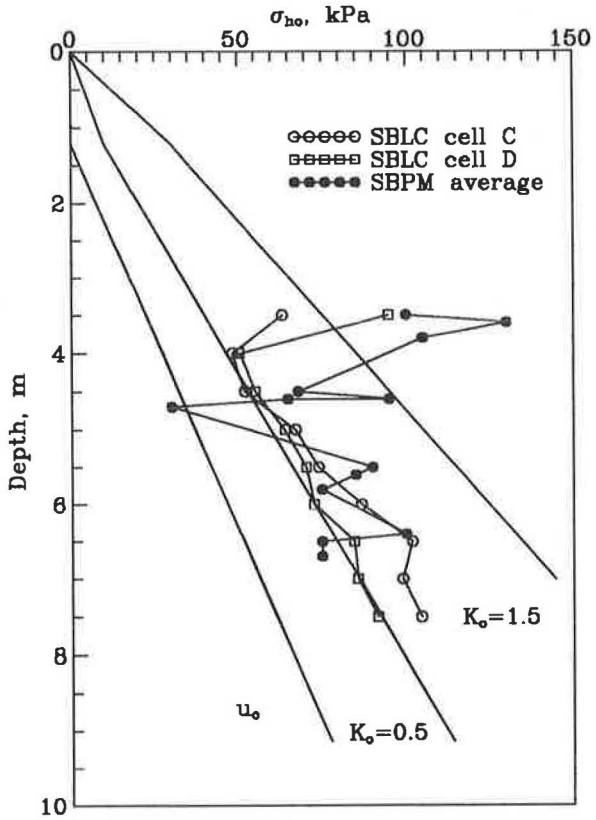

FIGURE 7 Deduced σ_{ho} from SBPM and SBLC tests.

TABLE 1 SUMMARY OF THE SBPM TEST RESULTS

Test	Depth	P_o	P_l	s_u	G_i	G_r
	m	kPa			MPa	
Strain Controlled Tests						
SBPM4	3.5	100	450	71	56.5	–
SBPM8	3.8	105	400	49	59.7	14.4
SBPM5	4.5	68	240	28	53.9	7.3
SBPM9	4.6	95	350	46	57.7	11.7
SBPM1	4.7	30	410	93	31.4	10.1
SBPM10	5.5	90	425	61	52.4	11.9
SBPM2	5.8	75	250	35	24.3	5.4
SBPM11	6.4	100	440	60	79.5	14.6
SBPM3	6.7	75	360	50	73.9	11.8
Stress Controlled Tests						
SBPM12	3.6	130	480	65	64.4	8.3
SBPM13	4.6	65	310	48	50.6	8.0
SBPM14	5.6	85	360	47	56.1	11.8
SBPM15	6.5	75	365	59	64.5	13.3

A direction index D_i is used to provide a quantitative indication of the lateral stress variations.

$$D_i = \frac{\sum_{d=1}^{nd} \left[\frac{(\sigma_{ho})_d}{(\sigma_{ho})_{avg}} \right]}{nd} \quad (3)$$

and

$$(\sigma_{ho})_{avg} = \sum_{i=1}^{6} \frac{(\sigma_{ho})_i}{6} \quad (4)$$

where nd is the number of depths where σ_{ho} was measured (nd = 4 for SBLC, nd = 8 for SBPM).

A higher D_i value, therefore, indicates greater σ_{ho} measurement in that direction. According to the D_i values, σ_{ho} in different directions for both SBPM and SBLC tests (Figures 8 and 9) seem to indicate a consistent axis of major lateral stress despite the existence of disturbance. The direction of the major lateral stress is approximately parallel to the creek adjacent to the test site (see Figure 1). There was no geological reason for an anisotropic stress field at the test site other than the erosion created by the creek. If indeed this was the case, then the test results are consistent with the direction of the creek. In any case, the results are not very convincing because the differences in lateral earth pressures are generally within the accuracy of the measurements.

Most of the available empirical methods assume an exponential relationship between K_o and K_D in analyzing the DMT data. For example, on the basis of his statistical analyses, Marchetti (*3*) suggested that

$$K_o = (K_D/1.5)^{0.47} - 0.6 \quad (5)$$

appears to be a reasonable approximation of such a relationship. P_0 represents the average normal stress on the expandable diaphragm at the end of DMT penetration. The normal stress, as inferred from strain path analysis (*15*), undergoes a monotonic loading followed by a slight unloading before the soil element reaches the DMT diaphragm (Figure 10). If Equation (5) is rearranged as

$$\sigma'_{ho} = \sigma'_{vo} [(K_D/1.5)^{0.47} - 0.6] \quad (6)$$

then this implies that for given σ'_{vo} and u_o there is an exponential relationship between $(P_0 - u_o)$ and σ'_{ho}, regardless of the state of stress, stress history prior to the DMT insertion, and the soil stress strain relationship. The authors are not aware of any studies in soil mechanics that would substantiate such a premise.

The deduced lateral earth pressure, using Equation (6), showed for the DMT data at the test site that the corresponding K_o values (Figure 11) are mostly higher than 1.5, even within the soft clay layer (between 4 and 7 m). They correspond to OCRs of 10 and higher according to Mayne and Kulhawy (*16*), which are much higher than those from oedometer tests (see Figure 2).

Figure 12 presents a plot of σ_{ho} normalized with respect to the average of all the σ_{ho} values in five directions and at the same depth. Except for a few rogue data points, there does not appear to be any noticeable anisotropy of lateral stresses. The results from the five DMT bore holes are extremely repeatable (see Figures 6 and 11). The repeatability is partly due to the large strains induced during the DMT insertion and compatible with the experience in pressuremeter tests where repeatable limit pressures (i.e., pressure readings at large strains) can be obtained regardless of the level of bore hole disturbance. The large strains might also have masked

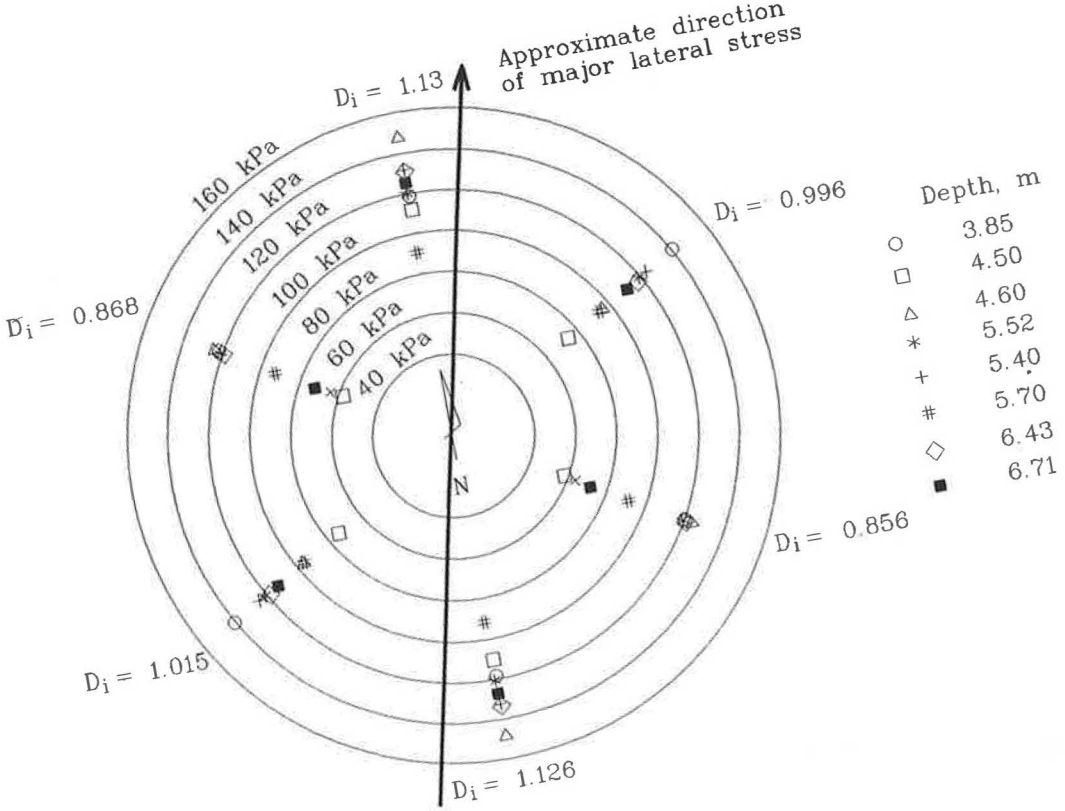

FIGURE 8 Results from SBPM tests.

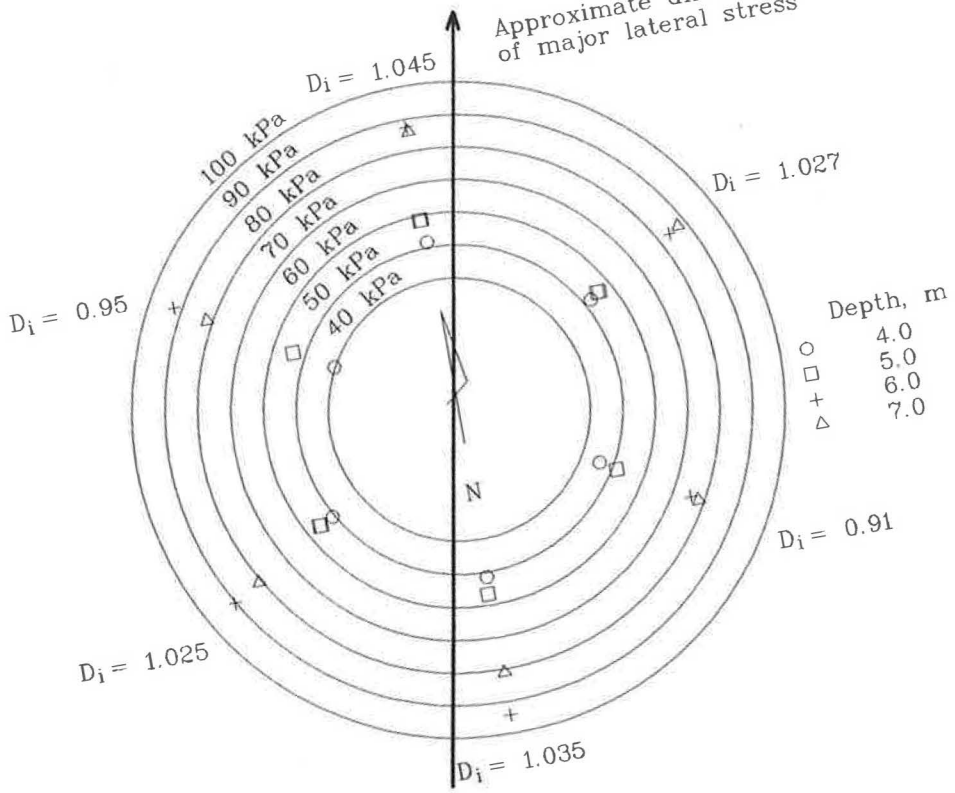

FIGURE 9 Results from SBLC tests.

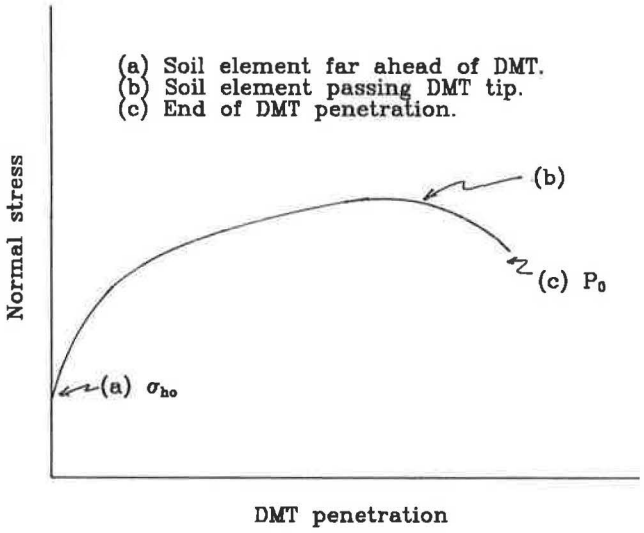

FIGURE 10 Inferred stress path during DMT penetration.

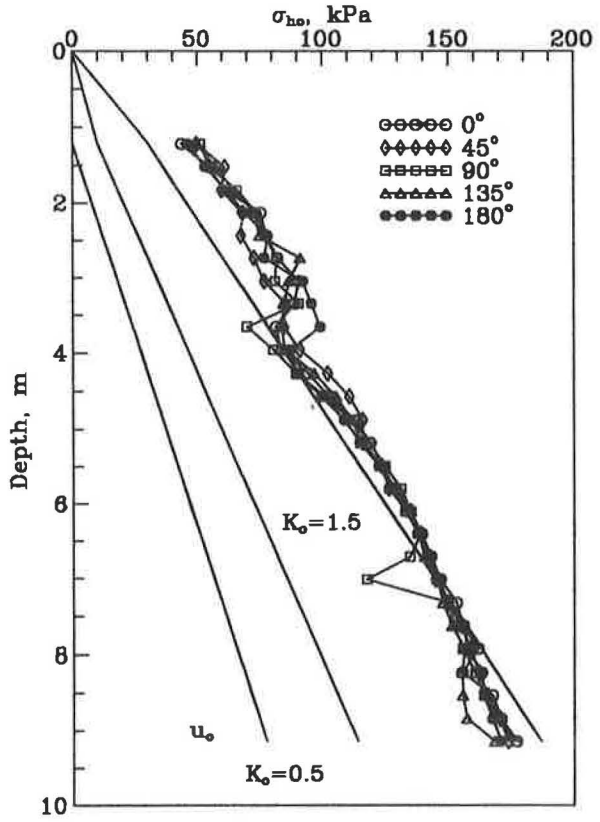

FIGURE 11 Deduced σ_{ho} from DMT tests.

the anisotropy in lateral earth pressures, if this indeed were the case.

CONCLUDING REMARKS

In the context of the study presented here, the following conclusions are drawn:

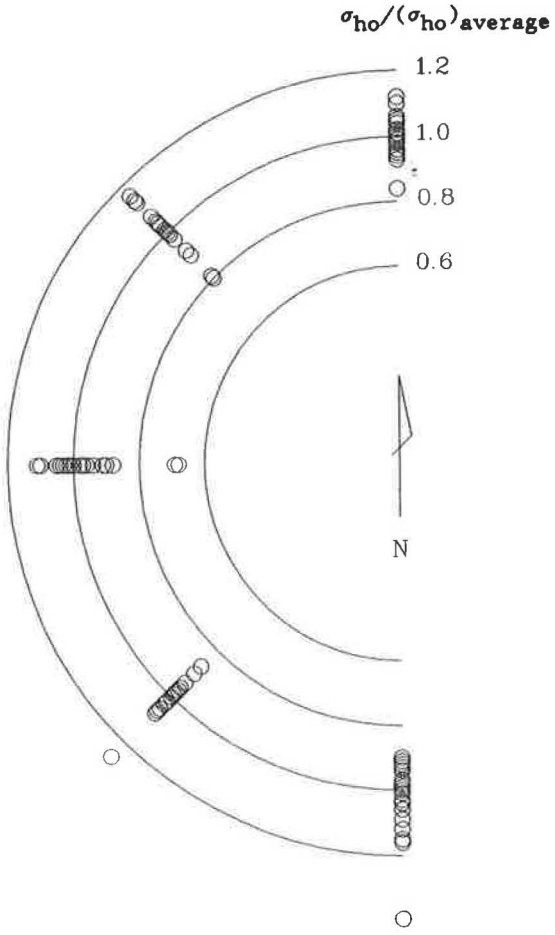

FIGURE 12 Normalized σ_{ho} from DMT tests.

1. In a stiff soil deposit where σ_{hy} is significantly larger than σ_{ho}, a passive measuring device such as the SBLC is likely to provide more reliable measurements of σ_{ho} than the SBPM.
2. Disturbance does occur even when self-boring probes (e.g., SBPM and SBLC) are used for lateral earth pressure measurements. However, the results should still be reasonable, provided the tests are properly performed.
3. Despite the soil disturbance, a limited number of SBPM and SBLC tests showed consistent directions of the major lateral stress. However, more studies are required to substantiate this finding.
4. The soil element is likely to experience a complicated strain path before reaching the DMT diaphragm where P_0 and P_1 readings are taken. By using DMT to estimate σ_{ho} based on an exponential relationship between K_D and K_o may therefore be premature.

ACKNOWLEDGMENTS

The data shown in Figure 2 were based on tests performed by A. J. Lutenegger. The research was sponsored in part by the National Science Foundation and in part by the U.S. Air Force Office of Scientific Research.

REFERENCES

1. K. R. Massarsch, R. D. Holtz, B. G. Holm, and A. Fredriksson. In Measurement of Horizontal In Situ Stresses. *Proc., ASCE Specialty Conference on In Situ Measurement of Soil Properties*, Vol. 1, Raleigh, N.C., 1975, pp. 266–286.
2. J. C. P. Dalton and P. G. Hawkins. Field of Stress. Some Measurements of the In-Situ Stress in a Meadow in the Cambridgeshire Countryside. *Ground Engineering*, No. 5, 1982.
3. S. Marchetti. In Situ Tests by Flat Dilatometer. *Journal of the Geotechnical Engineering Division*, ASCE, Vol. 106, 1980, pp. 299–321.
4. R. L. Handy, B. Remmes, S. Moldt, A. J. Lutenegger, and G. Trott. In Situ Stress Determination by Iowa Stepped Blade. *Journal of Geotechnical Engineering Division*, ASCE, Vol. 108, 1982, pp. 1405–1422.
5. P. Tedd and J. A. Charles. Evaluation of Push-In Pressure Cell Results in Stiff Clay. *Geotechnique*, Vol. 31, 1983, pp. 554–558.
6. M. Jamiolkowski, C. C. Ladd, J. T. Germaine, and R. Lancellotta. New Developments in Field and Laboratory Testing of Soils. Presented at 11th International Conference on Soil Mechanics and Foundation Engineering, San Francisco, Calif., 1985.
7. J. J. M. Powell and I. M. Uglow. Marchetti Dilatometer Testing in UK Soils. *Proc., Penetration Testing*, ISOPT-I, 1988, pp. 555–562.
8. G. W. Clough and P. M. Goeke. In Situ Testing for Lock and Dam 26 Cellular Cofferdam. *Proc., In Situ '86, Use of In Situ Tests in Geotechnical Engineering*, 1986, pp. 131–145.
9. S. R. Saye and A. J. Lutenegger. Site Assessment and Settlement Evaluation of Firm Alluvial Silts and Clays with the Marchetti Dilatometer. *Proc., Penetration Testing*, ISOPT-I, 1988, pp. 589–596.
10. C. P. Wroth and J. M. Hughes. An Instrument for the In Situ Measurement of the Properties of Soft Clays. *Proc., 8th ICSMFE*, Moscow, Vol. 1.2, 1973, pp. 487–494.
11. S. Lacasse and T. Lunne. In Situ Horizontal Stress from Pressuremeter Tests. *Proc., Symposium on Pressuremeter and Marine Application*, Paris, 1982, pp. 187–208.
12. M. G. Jefferies, J. H. A. Crooks, D. E. Becker, and P. R. Hill. Independence of Geostatic Stress from Overconsolidation in Some Beaufort Sea Clays. *Canadian Geotechnical Journal*, Vol. 24, 1987, pp. 342–356.
13. A. B. Huang, R. D. Holtz, and J. L. Chameau. Interpretation of Pressuremeter Data in Cohesive Soils by Simplex Algorithm. *Geotechnique*, Vol. 36, 1986, pp. 599–604.
14. A. B. Huang and K. C. Haefele. Effects of Penetration on Pressuremeter tests in Clays. *Proc., 3rd International Symposium on Pressuremeters*, Oxford, England, 1990.
15. A. B. Huang. Strain Path Analysis for Arbitrary Three-Dimensional Penetrometers. *International Journal for Numerical and Analytical Methods in Geomechanics*, Vol. 13, 1989, pp. 551–564.
16. P. W. Mayne and F. H. Kulhawy. K_o-OCR Relationships in Soil. *Journal of the Geotechnical Engineering Division*, ASCE, Vol. 108, 1982, pp. 851–872.

Publication of this paper sponsored by Committee on Soil and Rock Properties.

Measurement of Lateral Stress in Cohesive Soils by Full-Displacement In Situ Test Methods

J. P. SULLY AND R. G. CAMPANELLA

Estimation of lateral stress in cohesive soils from in situ tests by using full displacement probes is considered. The stress and pore pressure changes around a penetrating probe are briefly discussed before comparisons between data obtained from four different test methods are made. The application of cavity expansion models to the evaluation of lateral stress cone data in clays is evaluated with favorable results. A normalized pore pressure parameter is also introduced as an indicator of K_o conditions.

Increased understanding of soil behavior has emphasized the importance of the contribution of in situ stress state. Numerical and analytical methods almost routinely incorporate stress-dependent behavior in some form. Recent developments in the interpretation of in situ test data suggest that horizontal stress is one of the major factors controlling soil response.

Specific data related to in situ lateral stress conditions at a site may be obtained from either laboratory or field tests. A review of existing methods is given by Schmertmann (*1*), Jamiolkowski et al. (*2*), and Tavenas and Leroueil (*3*).

The evaluation of K_o can be classified into four main groups according to type of measurement made:

1. Direct methods such as the self-boring pressuremeter and self-boring load cell: Direct methods suffer from the significant effects of even small degrees of disturbance, the consequences of which become more important as the soil stiffness increases.
2. Semidirect or back-extrapolation methods: Developments in this area include the stepped blade and wedge blade, both of which require additional calibration or correlations at specific sites prior to general use.
3. Indirect methods used where a lateral stress value is measured during or after the installation of a full-displacement probe: In some cases, the dissipation of stress and pore pressure induced during insertion can be monitored with time so that an equilibrium value for the inserted probe can be obtained. Each of the full-displacement methods causes significant but repeatable disturbance to the soil.
4. Empirical methods as an important source of information for evaluating the stress history of soil deposits: Existing correlations are generally derived from laboratory or calibration chamber data and modified to incorporate field parameters.

University of British Columbia, Vancouver, B.C., Canada.

The measurement of horizontal stress, using the self-boring pressuremeter, is generally considered to be the best available technique for evaluating in situ stress state and is often taken as the reference value for any comparative study. The results of disturbance during installation of the probe and quantifying its effect on the measured data are, however, problematical. Full-displacement probes were developed to produce conditions of repeatable degrees of disturbance. The problem is then one of relating the measured lateral stress to the pre-penetration value as opposed to one that evaluates whether or not the soil has been disturbed during probe installation. The idea of predicting small strain behavior from large strain parameters has been validated, at least in sands, by results of calibration chamber tests (*4*).

In the ideal case for undrained penetration, the initial lateral stress σ_* measured by a full-displacement probe results from two components:

$$\sigma_* = \sigma_{ho} + \Delta\sigma \tag{1}$$

where σ_{ho} is in situ total horizontal stress and $\Delta\sigma$ is the total stress increment caused by insertion.

In any particular soil, the magnitude of the total stress increment is made up of both stress and pore pressure components and can be expected to be related to the relative displacement caused during penetration of a probe. The idealized change in the lateral stress coefficient (defined in terms of an effective stress ratio) for various in situ testing probes is shown schematically in Figure 1. Although this simplified representation is instructive, it is, however, complicated by the fact that for each test method the stress/strain paths are very different and that for even under undrained conditions no single curve exists. The relative positions of the tests are also very subjective and dependent on individual probe characteristics.

A series of in situ tests has been performed to compare and evaluate lateral stresses measured by full-displacement probes as part of a research program being carried out at the University of British Columbia (UBC). The results of tests performed at two research sites are presented here to illustrate the effects of equipment and soil characteristics on measured lateral stresses in cohesive soils. In addition, several empirical correlations that provide a rational basis for correlation between large strain and small strain behavior are presented for evaluating K_o.

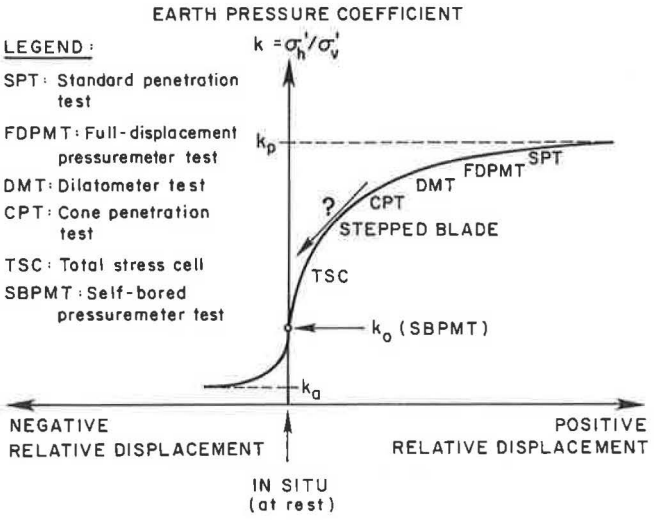

FIGURE 1 Idealized change of lateral stress coefficient, *K*, caused by full displacement probes.

DESCRIPTION OF TEST SITES

The data presented here were obtained from two sites in the Lower Mainland of British Columbia, where fine-grained soils predominate. The soils are very similar in terms of geotechnical parameters (Table 1) but have undergone differing mechanisms of overconsolidation.

Strong Pit is the site of an abandoned gravel pit. The well-graded surface sand and gravel in the area is fluvioglacial in origin and overlies marine and glaciomarine clayey silt. The stony clayey silt is of varying thickness with numerous discontinuous lenses of dense fine sand. The present-day profile consists of 1 m of gravel underlain by up to 9 m of stony clayey silt. Approximately 15 m of gravel overburden have been removed at the location of the test site.

The equilibrium pore pressure in the clay varies between 0 and 10 kPa. Those conditions result from a perched water table at the base of the surface gravel layer and underdrainage at the base of the clay. The overconsolidation of soil can be explained solely on the basis of unloading owing to overburden removal (*5*).

The second site is known as Lower 232 St. and is located in Langley, British Columbia. The Quaternary sequence consists of marine silt to clay deposited during the glacial regression, which is occasionally interbedded with minor sand layers. The slightly organic silts and clays are underlain by dense glaciomarine sands and gravels. The fine-grained soils have been subjected to leaching subsequent to deposition. The soils are overconsolidated at the surface primarily because of dessication and minor unloading and become normally consolidated at depth.

TABLE 1 AVERAGE GEOTECHNICAL PARAMETERS FOR TEST SITES

Index/Parameter	Strong Pit	Lower 232 St.
Water content (%)	19	45
<60 μm (%)	85	100
<2 μm (%)	45	48
LL	27	40
PI	13	21
Unit weight (kN/m³)	21	16
S_t (FVT)	2-5	5-25
OCR	2-10	1-6
$(S_u/\sigma'_v)_{nc}$	0.35*	0.26

* Calculated using $S_u(FVT)/\sigma'_{vm}$ where σ'_{vm} is the maximum past pressure obtained from incremental oedometer tests.

EVALUATION OF LATERAL STRESS CONDITIONS AT TEST SITES

For comparative purposes, the measurements of lateral stress with depth at each site, using the total stress cells, were taken as reference values. The total stress cells are 6 mm thick and are installed in a full displacement mode. Consequently, the lateral stress measured may be altered by this process, and some correction is required. Tedd and Charles (*6*) evaluated field data from several sites and suggested that the over-read of lateral stress approximates to one half the undrained shear strength at the depth of measurement for firm-to-stiff soils. On the basis of field data, they established an undrained shear strength limit of about 30 kPa below which no correction was recommended.

The adjustment of measured stress to account for disturbance caused during the insertion of the spade cell is approximate and does not necessarily guarantee the correct result. Nevertheless, on the basis of 10 years' experience, Tedd et al. (*7*) suggest that the method approximates to the average over-read conditions in firm-to-stiff soils.

FIELD TESTING PROGRAM

The following equipment is available at UBC for measurement of horizontal stresses with full-displacement probes:

- Push-in spade-shaped total stress cells (TSC),
- Flat dilatometer (DMT),
- Lateral stress piezocone (LSC), and
- Seismic cone pressuremeter (SCPM).

Push-In Total Stress Cells

In situ lateral stresses have been measured at both sites with push-in spade cells (*8,9*). The TSC that were used measure both the total pressure in the cell and the piezometric pressure and were supplied by Solinst Canada Ltd. Minor modifications were made to the pressure cells by using the UBC Geotechnical Research Vehicle to facilitate insertion. In addition, platinum RTD temperature sensors were installed in several of the cells to allow temperature correction of field data. All the total stress cells were calibrated, before installation, in the laboratory for the effects of temperature and external applied pressure. Identical calibrations were performed again after the stress cells were recovered from the ground.

All temperature corrections applied to the blade pressures were made with respect to the equilibrium temperature in the ground, as measured by the sensors placed on several of the

stress cells. At other depths, where blades were not instrumented for temperature, the ground temperature was estimated by interpolation from the other temperature measurements. The complete calibration results, description of installation, and interpretation of data obtained at Strong Pit are detailed by Sully and Campanella (*5*).

The total stress cell is a spade-shaped oil-filled chamber approximately 100 mm wide, 200 mm long, and 6 mm thick. The oil-filled chamber is formed by two welded plates and pressurized to maintain plate separation. The chamber is connected to a pneumatic transducer. The pore pressure filter is connected hydraulically to a second pneumatic transducer, which is also located in the cell housing. Total stress and pore pressure measurements were taken by using a portable pneumatic readout box incorporating a Druck electronic transducer with a 0- to 2000-kPa range. Accuracy of the transducer is ±0.05 percent FS (i.e., ±1 kPa). The corrected lateral stress measurements obtained by using the spade cells were taken as the reference values for comparison with data from other in situ methods.

For comparison with other measurements, the penetration lateral stress and pore pressure measured with the spade cells were taken as the values recorded immediately after the cell had been pushed to the required depth.

Flat Dilatometer

The flat DMT was first introduced by Marchetti (*10,11*) and since has become increasingly popular as an in situ testing tool. Interpretation of the test data is based on empirical correlations, using the measured parameters (thrust, P_0, P_1, P_2). Details of test procedures and interpretation methods are given by Marchetti (*11*) and Lutenegger (*12*). The penetration lateral stress is taken to be equal to the DMT lift-off pressure (P_0), and the P_2 reading is taken as the penetration pore pressure.

Lateral Stress Piezocone

The LSC developed at UBC consists of a standard UBC 15 cm² piezocone unit followed by a lateral stress module. The lateral stress module is located 0.69 m behind the cone tip and consists of a friction sleeve instrumented to measure hoop stresses in an under-reamed section of the sleeve. Pore pressure measurements are also performed at the LS sleeve location. Lateral stress measurements are made both during cone penetration and during the dissipation phase when penetration is halted. The total lateral stress and the pore pressure measured during penetration are considered here. Further details of the LSC and its calibration are given by Campanella et al. in another paper in this Record.

Seismic Cone Pressuremeter

The concept of the UBC SCPM has been described by Campanella and Robertson (*13*). Details of the test procedures and interpretation methods are given by Hers (*14*) and Howie (*15*). During penetration, the SCPM allows simultaneous measurement of cone resistance, sleeve friction, pore pressure at two locations, slope, and temperature. During pauses in the penetration, the shear wave velocity can be evaluated by using the downhole technique and a pressuremeter expansion curve obtained. The PM lift-off pressure is used for comparison with stresses measured by the other in situ probes. Pore pressure measurement near the PM section is not possible with the UBC SCPM.

STRESS AND PORE PRESSURE AROUND FULL DISPLACEMENT PROBES

Disturbance as a result of the installation of full-displacement probes causes significant changes in the in situ stress state of the soil. Those changes occur for both flat plate and cylindrical probes, although the relative magnitude for each type depends on many factors.

Stress Measurements

Results obtained by Azzouz and Morrison (*16*) for lightly overconsolidated Boston Blue Clay indicate that the total stress on a probe immediately after halting penetration is dominated by the pore pressure generated during full displacement installation. Thereafter, the effective stress reduces during an initial relaxation period before finally climbing to approach a K_o condition as the excess pore pressure dissipates. For tests performed by the same authors in Lower Empire Clay, the final effective stress after complete dissipation of the generated excess pore pressure was considerably larger than the initial condition prior to insertion of the probe. Boston Blue Clay (OCR = 1.2) is a sensitive clay (S_t = 7), whereas Lower Empire Clay (OCR ~ 1.5) is insensitive. This confirms the importance of soil characteristics on the stress induced during probe insertion because the same probe was used for the data presented.

Stress measurements around flat total stress cells in soft-to-stiff clays give similar results to those presented by Azzouz and Morrison (*16*) for a cylindrical piezo-lateral stress cell.

Pore Pressure Measurements

Most of the pore pressure comparisons have been performed with data from piezocone (CPTU) testing. It has been demonstrated that in a particular deposit the measured pore pressure is dependent on the location and geometry of the pore pressure sensor (*17*). Evaluation of pore pressure during cone penetration suggests that the measured pore pressure is maximum on the cone face. A large gradient of pore pressure (and stress) exists at the cone shoulder. Behind the tip, the dynamic pore pressure during penetration may be either positive or negative, depending on the soil characteristics. At some distance behind the tip and along the shaft, the pore pressure attains a reasonably constant value. Those changes can be related qualitatively to changes in normal and shear stresses as the soil moves around the cone (*18*). Numerical analyses, using simplified soil models, confirm the results obtained from field tests (*19,20*).

In conclusion, stress and pore pressure changes around a penetrating probe are very complex. Furthermore, the distribution and dissipation of excess pressures will also be a function of probe geometry and soil characteristics during pauses in penetration.

COMPARISON OF PENETRATION PRESSURES

This paper only evaluates the initial stresses and pore pressures measured during penetration at those sites. No consideration is given to the dissipation phase and associated stress and pore pressure changes.

The stresses recorded by the four methods described previously (TSC, DMT, SCPM, LS-CPTU) for the Lower 232 St. site are presented on Figure 2, where the relative magnitude of lateral stress (LS) obtained is

$$LS_{DMT} > LS_{LS\text{-}CPTU} > LS_{SCPM} \approx LS_{TSC} \quad (2)$$

The dominance of the generated excess pore pressure in the essentially normally consolidated clay is illustrated by comparison with Figure 3. Only pore pressures for the DMT, TSC, and LS-CPTU are shown. The SCPM does not measure pore pressure at the location of the pressuremeter module. In the near-surface overconsolidated soils, the pore-pressure response is relatively small and the initial effective stress level may rapidly decrease to an expected K_o condition. This may result in part because of partial saturation above or close to the water table. The difference between the total stresses and pore pressures gives very low initial K values in the normally consolidated horizon. This is generally true of all the full-displacement probes installed.

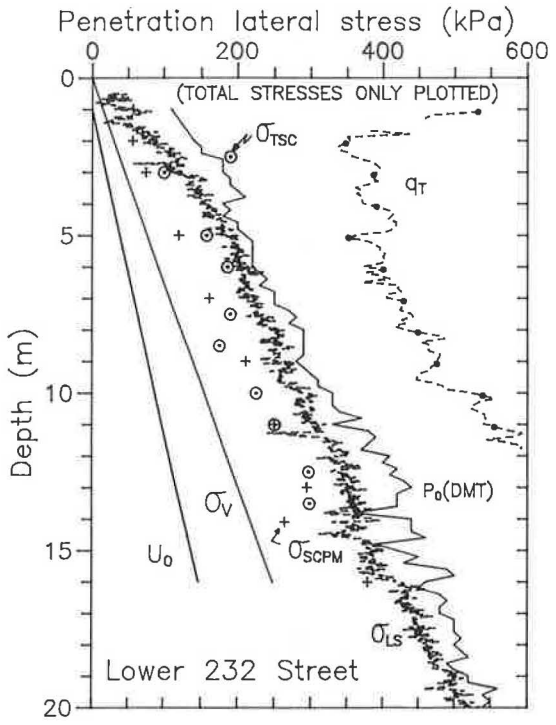

FIGURE 2 Comparison of stress measurements at Lower 232 St.

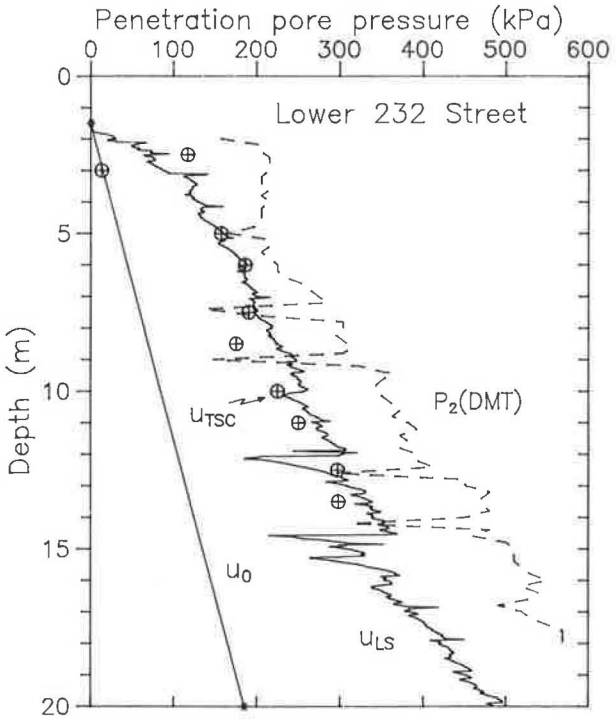

FIGURE 3 Comparison of pore pressure measurements at Lower 232 St.

The data presented in Figures 4 and 5 for the overconsolidated silty clay at Strong Pit give total stress measurements approximately 50 percent higher than the generated pore pressure, even though the hierarchy given in Equation 2 is maintained (no SCPM data exist for this site at present). On the basis of a comparison of the stress and pore pressure response at those two sites of differing overconsolidation states, it would appear that the ratio between total stresses and pore pressures

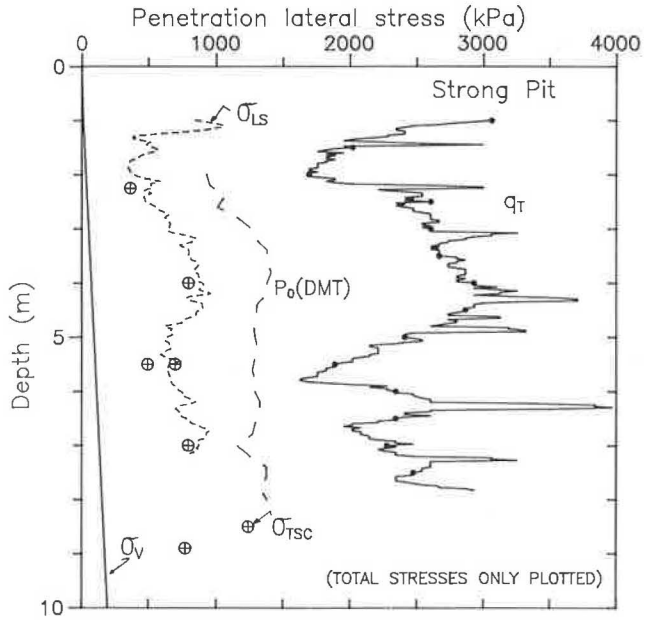

FIGURE 4 Comparison of stress management at Strong Pit.

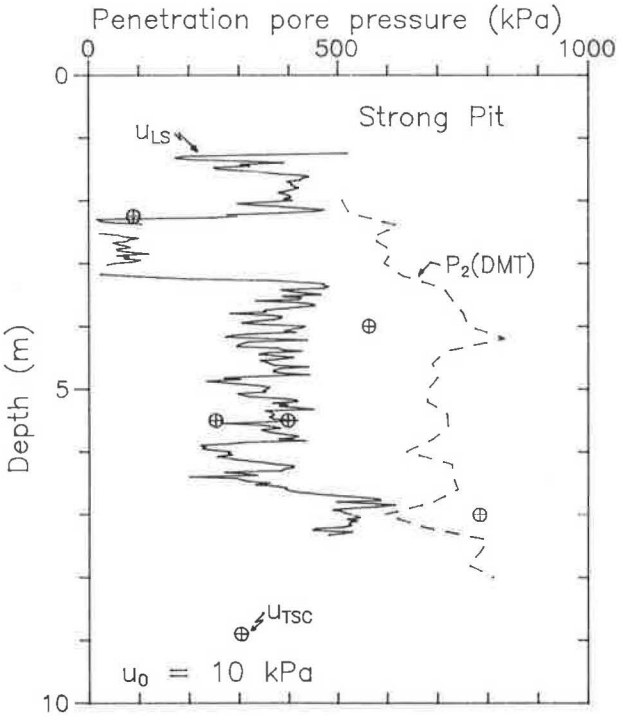

FIGURE 5 Comparison of pore pressure measurements at Strong Pit.

measured by full-displacement probes may be indicative of the stress history of the deposit.

Also presented on Figures 2 and 4 are the cone resistance profiles. Although q_t is more a limit rather than lift-off pressure, its dependence on horizontal effective stress has been demonstrated (in granular soils) and, as such, can be considered as a good indicator of horizontal stress changes.

The initial decrease and subsequent increase in q_t at Lower 232 St. suggests the presence of an overconsolidated surficial crust (with higher K_o), which becomes normally consolidated at about 5 m depth (Figure 2). Below 5 m, q_t increases linearly with depth. With the possible exception of the TSC data, none of the direct lateral stress measurements show the same pronounced near-surface changes as does q_t. The data from the LS-CPTU give rise to increased lateral effective stresses near the surface, because the pore pressures are proportionally lower than the total stress. This may be a consequence of partial saturation of the soils above the water table. The ratio of the two becomes reasonably constant at about 5 m. Finally, the disturbance caused by the SCPM and DMT appears to mask the near-surface feature, even though at depth the SCPM and TSC pressures are in remarkable agreement.

This latter effect, with respect to the cone pressuremeter, may result from the unloading caused by the slightly undersized pressuremeter section (*15*) or it may indicate that similar pore pressure trends to those measured with the LS-CPTU are in existence during SCPM penetration.

It should be possible to estimate a pore pressure value corresponding to the location of the pressuremeter module considering the pore pressure distribution around a penetrating cone and the absence of large gradients along the shaft away from the tip. However, the pore pressure measured at the lateral stress module (0.69 m behind tip) is larger than the total stresses at the PM location (1.31 m behind tip). Thus, it would appear that the true pore pressure that would be measured at the PM location, if a sensor were present, would also be reduced owing to the unloading effect. This emphasizes the importance of pore-pressure measurement in the vicinity of the pressuremeter section if rational interpretation of measured total stresses is to be attempted. The fact that the PM section is slightly undersized does not preclude at least an empirical interpretation of the measured stresses, that is, provided that the corresponding pore pressures are also known.

The cone bearing is reasonably uniform at Strong Pit with depth suggesting a similar trend in horizontal stress (Figure 4). The trends in both initial stress and pore pressure measured by the four methods also give data similar to that from the CPTU.

EVALUATED K_o CONDITIONS FROM FULL-DISPLACEMENT PROBES

The variation of the lateral stress coefficient is defined by

$$K = \sigma_h'/\sigma_v' \tag{3}$$

where

$K = K_{DMT}$, using the Marchetti (*11*) DMT correction,
$K = K_{TSC}$, using corrected TSC pressures (*6*), and
$K = K_{LS}$, using LS-CPTU data interpreted by using a cylindrical cavity expansion solution.

The variation has been evaluated from full-displacement probe measurements.

The variation of those coefficients is presented in Figure 6 for Lower 232 St. Also presented is the variation of K_{lab},

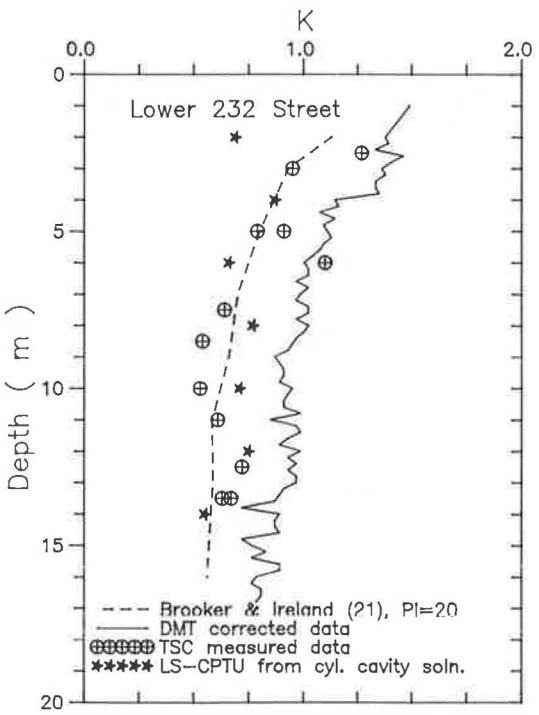

FIGURE 6 Evaluated K condition from full displacement probes: Lower 232 St.

obtained by using the correlation of Brooker and Ireland (*21*), which is based on an empirical relationship between PI and $(K_o)_{nc}$ from laboratory tests and adjusted for the effects of OCR (*22*). The TSC data presented have not been corrected for over-read owing to the low undrained shear strength of the soil. A good degree of similarity exists between the K_{TSC}, K_{lab}, and K_{LS} values. Assuming the K_{TSC} value provides the best estimate of the in situ lateral stress coefficient, the K_{DMT} value overestimates the true K_o at this site.

The LS-CPTU data have been interpreted by assuming that the stress measured by the LS cone corresponds to the cylindrical cavity limit pressure. The total horizontal stress σ_{ho} in an elastic perfectly plastic soil for the infinite expansion of a cavity is given by Gibson and Anderson (*23*):

$$\sigma_{ho} = P_L - \left[S_u * (1 + \ln I_r) \right] \tag{4}$$

where

P_L = assumed to be equivalent to σ_{LS} measured by LS module,
S_u = the undrained shear strength obtained by using the field vane,
I_r = the rigidity index of the soil ($I_r = G/S_u$), and
G = shear modulus obtained in this case from pressuremeter data.

Initially, attempts were made to use I_r defined in terms of G_{max} (from seismic cone penetration test), but this gave rise to excessive stress increments in Equation 4. I_r obtained from the Houlsby and Withers (*24*) unloading analysis gave data better suited to this type of analysis (*14*) and was subsequently used to obtain the K_o data in Figure 6.

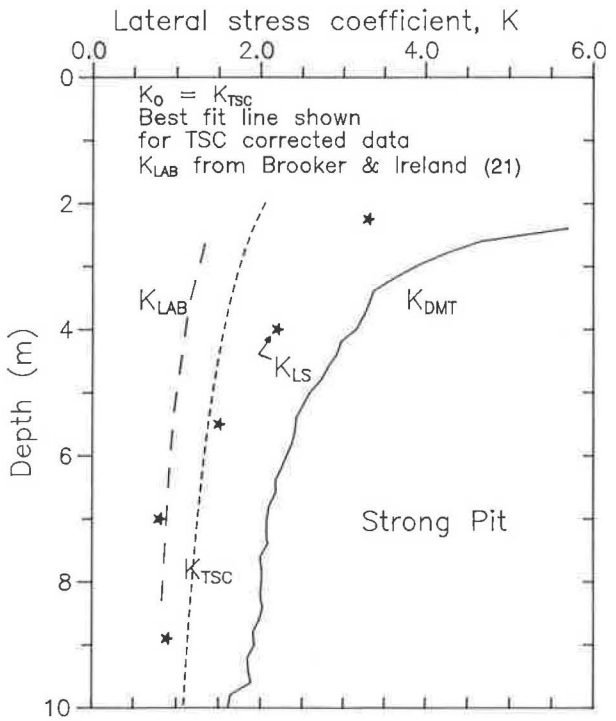

FIGURE 7 Evaluated *K* condition from full displacement probes: Strong Pit.

Data obtained at Strong Pit is presented in Figure 7. The DMT profile again overestimates the K_o value if K_{TSC} is taken as the reference value.

To date, no SCPM data have been obtained at this site, so it was not possible to evaluate the rigidity index $(G/S_u)_{HW}$ from the Houlsby and Withers method. However, evaluation of the Lower 232 St. data suggests that

$$\frac{(G_{max}/S_u)\text{SCPM}}{(G/S_u)_{HW}} \approx 9\text{–}10 \tag{5}$$

where $(G_{max}/S_u)_{SCPM}$ is the rigidity index calculated by using G_{max} from seismic cone penetration test data.

To interpret the LS-CPTU data as before, this relationship has been employed to evaluate I_r for use in Equation 4. The results are also indicated on Figure 7. The agreement between K_{LS} and K_{TSC} is remarkably good. Those data would suggest that interpretation of stresses measured by full displacement probes may be possible by using (cylindrical) cavity expansion theory. Theoretical studies performed by Teh (*20*) lead to the same conclusion and indicate that the solution improves for locations away from the shoulder area of the cone.

Calculated K_{LAB} values are also presented in Figure 7 and would appear to provide a lower bound to the range of measured lateral stress coefficients.

EMPIRICAL CORRELATIONS TO OBTAIN K_o

Various empirical correlations exist for evaluating K_o coefficients in cohesive soils. Probably the most widely used are those suggested by Brooker and Ireland (*21*) and Mayne and Kulhawy (*22*). Those methods estimate the overconsolidated K_o value from a relationship between PI, $(K_o)_{nc}$, and OCR, usually based on laboratory-derived correlations (K_{lab} in Figures 6 and 7). Reasonable estimates of $(K_o)_{nc}$ can be obtained by using index properties of the soil. Stress history is the main factor to be evaluated. Recently, various methods have been proposed for evaluating stress history from CPTU (*25,18*). Undrained shear strength data can also provide good estimates of OCR (*26,27*). Once the stress history (OCR) and $(K_o)_{nc}$ have been ascertained,the empirical relationship described can be employed to evaluate $(K_o)_{oc}$.

The method proposed by Sully et al. (*18*) relates the OCR of the soil to a pore pressure difference parameter (PPD) defined as

$$\text{PPD} = \frac{u_1 - u_2}{u_o} \tag{6}$$

where

u_1 = the penetration pore pressure measured on the face of the cone,
u_2 = the pore pressure measured behind the cone tip, and
u_o = the equilibrium in situ pore pressure.

measured pore pressures are a function of both soil (PI, G, S_u, K_o, OCR, S_t) and cone characteristics.

The pore pressure gradient around the cone tip is related to $u_1 - u_2$ and, thus, also to q_t; that is,

$$u_1 = f_1(q_t) \tag{7}$$

$$u_2 = f_2(q_t) \tag{8}$$

Because the cone resistance is a function of the in situ horizontal effective stress, as was discussed earlier, it follows that

$$u_1 - u_2 = f_4(q_t) = f_5(\sigma'_h) \tag{9}$$

Therefore, the normalized pore pressure parameter (PPSV) can be defined as

$$\text{PPSV} = \frac{u_1 - u_2}{\sigma'_{vo}} = f_6(K_o) \tag{10}$$

The PPSV-K_o data for Strong Pit is presented in Figure 8. The PPSV parameter appears to map directly onto the best fit variation of K_o.

The same data for Lower 232 St. are presented in Figure 9. For this site the correlation is not 1–1 (PPSV = 2 K_o), but similar depth trends are shown. Data from other clays are being evaluated to determine other factors that affect the PPSV-K_o correlation (Figure 10).

CONCLUSIONS

The evaluation of stresses and pore pressures induced during full displacement penetration has shown that measurements at any particular site are dependent on soil and probe characteristics. For flat plate penetrometers, the excess pressures appear to correlate well with the degree of displacement. However, location of the stress or pore-pressure sensor and its geometry appear to have an important influence. This is confirmed by results obtained with the stepped blade. For successive increases in blade thickness the zone of unloading around the step shoulder extends farther back because of the progressively higher stress levels involved. This causes discrepancies between the measured step stresses and consequently problems in the extrapolation of σ_{ho} arise. The problem may possibly be resolved by maintaining a constant ratio between blade thickness and distance of the sensor behind the shoulder.

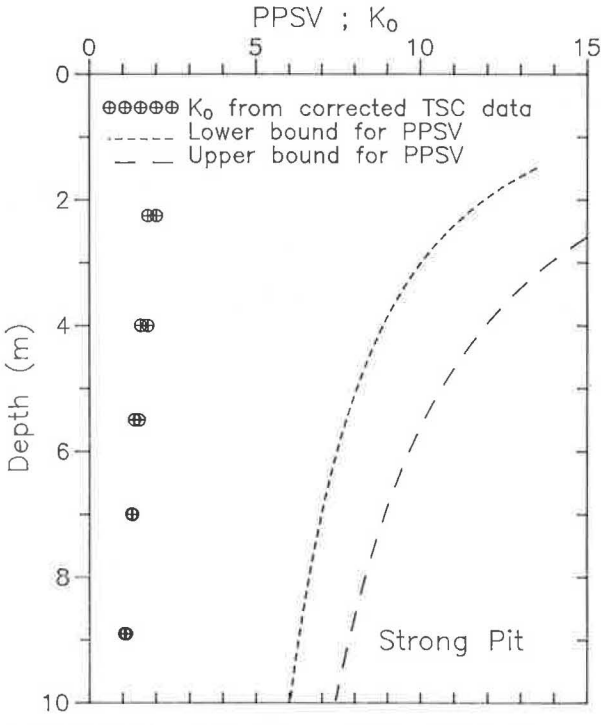

FIGURE 8 Correlation between PPSV and K_o for Strong Pit.

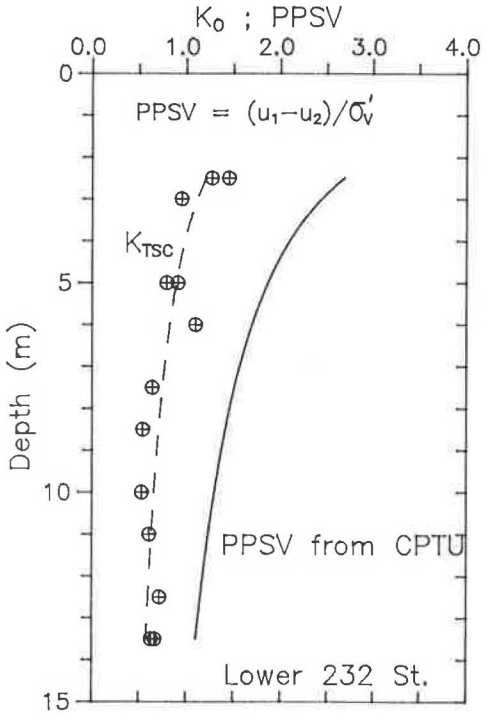

FIGURE 9 Correlation between PPSV and K_o for Lower 232 St.

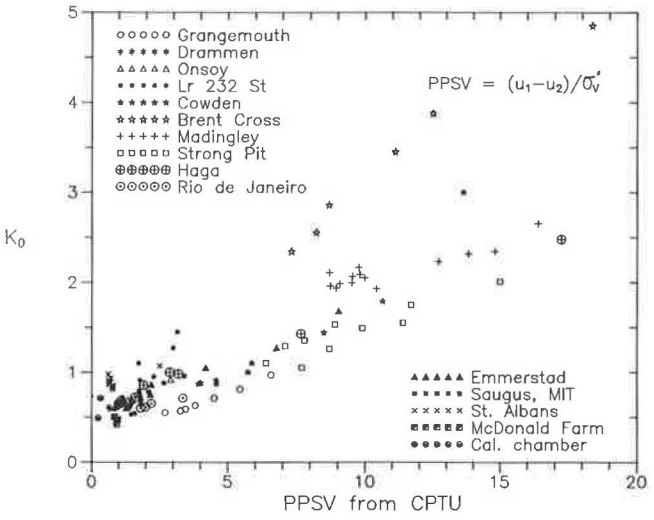

FIGURE 10 PPSV-K_D correlation for clays.

Where cylindrical probes are used, it appears that, provided the lateral stress and pore pressure sensors are at least 12D behind the cone shoulder (*13*), stress and pore pressure measurements are comparable provided no local unloading/reloading occurs owing to changes in section geometry near the sensors. The application of cylindrical cavity expansion theory to interpret stresses measured at remote locations on the shaft may provide rational estimates of the in situ pre- and postpenetration stress conditions. Further studies are being conducted to verify this finding.

On a more general note, as was discussed by previous researchers, the definition of K_o is problematical especially for near-surface data, where small errors in either σ'_h or σ'_v can cause large changes in K_o. Similar problems were encountered when defining pore pressure parameters from CPTU (*5*). In that case, a pore pressure difference parameter was found to be more convenient. To correlate the results of numerical analyses for differing stress ratios, Houlsby and Teh (*28*) define a horizontal stress factor in clay, Δ, based on a normalized stress difference:

$$\Delta = \frac{(\sigma_v - \sigma_h)}{2\,S_u} \tag{11}$$

The adoption of a similar expression for in situ data may provide more consistent parameter correlations for soils with near-surface overconsolidated crusts.

ACKNOWLEDGMENTS

An SERC (UK) NATO Scholarship awarded to the first author for the period of study and additional assistance from the Natural Science and Engineering Research Council of Canada are gratefully acknowledged. The assistance of the technical staff in Civil Engineering at UBC, who made and maintain the penetration probes used in this research, is also appreciated. The authors are grateful to P. K. Robertson, University of Alberta, for his discussion on some of the ideas presented here.

REFERENCES

1. J. H. Schmertmann. *Measure and Use of the In Situ Lateral Stress*. Osterberg Volume, Department of Civil Engineering, Northwestern University, Evanston, Ill., 1985.
2. M. Jamiolkowski, C. Ladd, J. Germaine, and R. Lancellotta. New Developments in Field and Laboratory Testing of Soils. *Proc., 11th ICSMFE*, Vol. 1, San Francisco, Calif., 1985, pp. 57–153.
3. F. Tavenas and S. Leroueil. S-O-A on Laboratory and In Situ Stress-Strain-Time Behavior of Soft Clays. *Proc., International Symposium of Geotechnical Engineering of Soft Soils*, Mexico City, Aug. 13–14, 1987.
4. G. Baldi, R. Bellotti, N. Ghionna, and M. Jamiolkowski. *Stiffness of Sands from CPT, SPT and DMT: A Critical Review*. Penetration Testing in the UK, CPT-88. Institute of Civil Engineers, London, July 1988, pp. 145–151.
5. J. P. Sully and R. G. Campanella. Lateral Stress Measurements in a Glaciomarine Silty Clay. Presented at 25th Annual Conference, Geology Society of London, Sept. 1989.
6. P. Tedd and J. A. Charles. Evaluation of Push-In Pressure Cell Results in Stiff Clay. *Proc., International Symposium of Soil and Rock Investigation*, Vol. 2, Paris, 1983, pp. 579–584.
7. P. Tedd, J. J. Powell, J. A. Charles, and I. M. Uglow. In Situ Measurements of Earth Pressures Using Spade-Shaped Pressure Cells: Ten Years' Experience. In *Instrumentation in Geotechnical Engineering*, Thomas Telford, London, 1989.
8. K. R. Massarsch. New Method of Measurement of Lateral Earth Pressure in Cohesive Soils. *Canadian Geotechnical Journal*, Vol. 12, 1975, pp. 142–146.
9. P. Tedd and J. A. Charles. In Situ Measurement of Horizontal Stress in Overconsolidated Clay Using Push-In Spade-Shaped Pressure Cells. *Geotechnique*, Vol. 31, 1981, pp. 554–558.
10. S. Marchetti. A New In Situ Test for the Measurement of Horizontal Soil Deformation. *Proc., ASCE Special Conference, In Situ Measurement of Soil Properties*, Vol. 2, 1975, pp. 255–259.
11. S. Marchetti. In Situ Tests by Flat Dilatometer. *Journal of the Geotechnical Engineering Division*, Vol. 106, No. GT3, 1980, pp. 299–321.
12. A. J. Lutenegger. Current Status of the Marchetti Dilatometer Test. *Proc., ISOPT-1*, Orlando, Fla., Vol. 1, 1988, pp. 137–155.
13. R. G. Campanella and P. K. Robertson. Research and Development of the UBC Cone Pressuremeter. Presented at 3rd Canadian Conference Marine Geotechnical Engineering, Mem. University, St. Johns, Newfoundland, June 1986.
14. G. I. Hers. *The Interpretation and Analysis of the Cone Pressuremeter in Cohesive Soils*. MASc thesis, Department of Civil Engineering, University of British Columbia, Vancouver, 1989.
15. J. A. Howie. Ph.D. thesis. University of British Columbia, Vancouver, 1989.
16. A. Azzouz and M. J. Morrison. Field Measurements and Model Pile in Two Clay Deposits. *Journal of the Geotechnical Engineering Division*, ASCE, Vol. 114, 1988.
17. P. K. Robertson, R. G. Campanella, D. Gillespie, and J. Greig. Use of Piezometer Cone Data. *Proc., In Situ Testing in Geotechnical Engineering*, Institute '86, ASCE Special Conference, June 1986, pp. 1263–1280.
18. J. P. Sully, R. G. Campanella, and P. K. Robertson. Interpretation of Penetration Pore Pressures to Evaluate Stress History in Clays. *Proc., ISOPT-1*, Vol. 2, Orlando, Fla., 1988, pp. 998–1000.
19. J. Levadoux and M. Baligh. *Pore Pressures During Cone Penetration*. Sea Grant Report 8012, MIT, Cambridge, Mass., 1985.
20. C. I. Teh. An Analytical Study of the Cone Penetration Test. DPhil. thesis, Oxford University, U.K., 1987.
21. E. W. Brooker and H. O. Ireland. Earth Pressures at Rest Related to Stress History. *Canadian Geotechnical Journal*, Vol. 11, 1965.
22. P. W. Mayne and F. Kulhawy. K_o-OCR Relationships in Soil. *Journal of the Geotechnical Engineering Division, ASCE*, Vol. 108, No. GT6, 1982, pp. 851–872.
23. R. E. Gibson and W. F. Anderson. In Situ Measurement of Soil Properties with the Pressuremeter. *Civil Engineering and Public Works Review*, Vol. 56, 1961, pp. 615–618.
24. G. T. Houlsby and N. J. Withers. Analysis of Cone Pressuremeter Test in Clay. *Geotechnique*, Vol. 38, 1988, pp. 575–587.
25. J. M. Konrad and K. T. Law. Preconsolidation Pressure From Piezocone Tests in Marine Clay. *Geotechnique*, Vol. 37, 1987, pp. 177—190.
26. C. C. Ladd, R. Foott, K. Ishihara, F. Schlosser, and H. G. Poulos. Stress-Deformation and Strength Characteristics. SOA Report, *Proc. 9th ICSMFE*, Tokyo, 1977.
27. P. W. Mayne and J. K. Mitchell. Profiling of Overconsolidation Ratio in Clays by Field Vane. *Canadian Geotechnical Journal*, Vol. 25, 1988, pp. 150–157.
28. G. T. Houlsby and C. I. Teh. Analysis of the Piezocone in Clay. *Proc., ISOPT-1*, Vol. 1, Orlando, Fla., 1988, pp. 777–783.

Publication of this paper sponsored by Committee on Soil and Rock Properties.

Measuring and Predicting Lateral Earth Pressures in Slopes in Soft Clays in Sweden

KARIN RANKKA

Results of a study of the lateral stress distribution in slopes in soft clays is reported. Many slopes in soft clays in the southwestern part of Sweden have a very low factor of safety against failure. Valuable information has been collected over the past years about those slopes, but, as yet, very little is known about the lateral stress distribution and the development of failures. The lateral stress distribution in a slope varies from top to toe of the slope. A better understanding of the behavior of slopes can be obtained with a better knowledge of those stresses and how they change with time and the factor of safety. When a slope is close to failure, the resulting deformations yield higher lateral stresses in the passive zone and lower in the active zone. To take this fully into account in slope modeling, full-scale field tests are imperative. In a research project at the Chalmers University of Technology, measurement of lateral stresses with Glötzl cells in natural clay slopes was started at four sites and will continue over a period of at least 2 years. The results obtained will be compared with the results obtained by analytical and numerical methods to find out whether or not those methods can serve as a reliable means for the prediction of the lateral stress distribution in the slope studied. Up to now, only Janbu's generalized procedure has been utilized. For the slopes investigated, this method has been found to give lateral stresses quite close to those measured.

At Chalmers University of Technology, Göteborg, Sweden, a project named "Slope Stability Analysis Accounting for Stresses, Deformations, and Statistical Variability in Geotechnical Parameters" was started in spring 1988, and it continues. The project is financed by the Swedish Board of Building Research (BFR). So far, the project has focused mainly on lateral stresses in clay slopes in the area around Göteborg.

Many areas in the western part of Sweden consist of soft marine clays. On top of the glacial clays were deposited the more finely grained postglacial clays. The soft clays along valley sides often contain layers of sand and silt.

The water content is generally high and often higher than the liquid limit. The clays have a low hydraulic conductivity owing to the high clay content and also to a low preconsolidation pressure, which implies low undrained shear strength. An undrained shear strength just below the dry crust as low as 10 to 15 kPa is common, and there is usually an increase of shear strength with depth of 1 to 2 kPa/m. Clays with extremely high sensitivity (>400) exist, but, typically, the sensitivity ranges from 10 to 20.

Landslides occur in those soft clays every year. The Göta River valley and its side valleys have been subjected to many slides in modern times (e.g., Göteborg harbor in 1916, Surte in 1950, Göta in 1957, and Tuve in 1977).

Very few measurements of lateral stresses in natural clay slopes have been carried out through the years. The intention of this project is to measure lateral stresses in at least five slopes in different conditions and to compare the measurements with results obtained from theoretical analyses. So far, measurements have been carried out (and are still going on) in slopes with the following conditions:

- A steep slope in a stiff glacial clay;
- A slope in mostly postglacial clay with a very low factor of safety, which has been stabilized by soil filling in the passive zone (measurements have taken place both before and after stabilization);
- A slope in postglacial clay with a low factor of safety that is to be stabilized by removing masses from the active zone; and
- A slope in postglacial clay in an area where many small slides have taken place.

The ratio of the effective horizontal and effective vertical stress, σ'_h/σ'_v has been determined for all sites. For in situ conditions with no lateral strain (horizontal ground surface) the ratio is usually called K_o. For those slopes with a low factor of safety the ratio σ'_h/σ'_v is designated K.

Theoretical analysis of predicted lateral stress distribution for the slopes has been done by using Janbu's generalized method and will be done by using a finite-difference method later in this paper.

When comparing predicted and measured horizontal stresses, the following classification has been used: A difference of less than 10 percent is classified as very good, 10 to 20 percent as good, 20 to 30 percent as fair, and, if the difference is greater than 30 percent, it is classified as poor (unacceptable).

TYPE OF EARTH PRESSURE CELLS

A pneumatic system was chosen to measure stress cell response in this project (Figure 1). A spade-shaped thin Glötzl cell was used. The cell, 100 mm × 200 mm × 5 mm, consists of two parallel thin steel sheets welded together and is filled with oil. The oil is in contact with a sensitive membrane that shuts a counter-pressure lead. By slowly increasing the air pressure in the counter-pressure lead, the membrane will open at a

Department of Geotechnical Engineering, Chalmers University of Technology, S-412 96 Göteborg, Sweden.

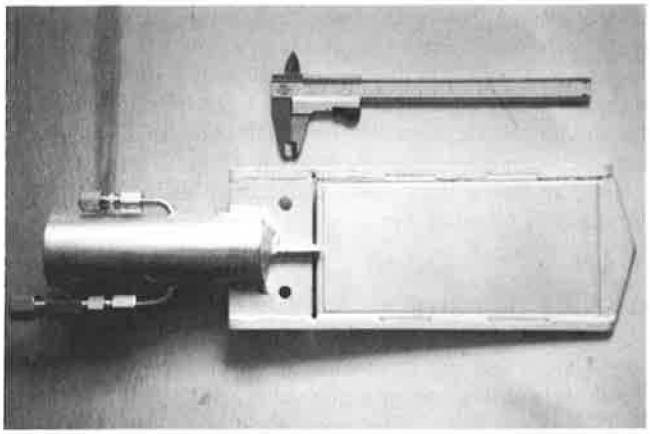

FIGURE 1 Glötzl earth pressure cell.

pressure that slightly exceeds the oil pressure in the cell. This opening pressure can be read on a manometer.

The Glötzl cells have shown to give reasonable lateral stresses in other projects, both at Chalmers and at the Royal Institute of Technology in Stockholm. Larsson (*1*) carried out a comprehensive series of tests both in the field and in the laboratory to determine the lateral stresses in Bäckebol clay. The tests showed good agreement between different kinds of field test methods; that is, Glötzl earth pressure cells, the Ménard pressuremeter, and a self-boring pressuremeter (Cambridge type). Schmidt's empirical relation, $K_{nc}^{o} = 1 - 1.2 \sin \phi'$, was used to calculate the in situ horizontal stresses. The calculated stresses were close to those measured (Figure 2).

A method by which in situ lateral load tests in soft clay can be carried out was developed by Olsson (*2*). The system was used to test earth pressure cells in the field (Glötzl type). Two large, soft flat jacks were pushed down into the soil and inflated by air to the desired pressure. Glötzl earth pressure cells were installed to measure the imposed pressure. The tests showed that the cells give very good measurements of the lateral stresses in the soil and that about 5 days are required after the installation of the cells before the excess pressures have dissipated. The tests also showed that the cells respond very quickly to changes in lateral stresses.

Standard dilatometer (DMT) tests have also been carried out in some of the areas studied. The DMT test is an in situ method used to determine strength and deformation properties by empirical correlations. The coefficient of lateral earth pressure can also be determined (*3*).

INSTALLATION TECHNIQUE

A good working technique for pushing cells into the ground was developed at the Royal Institute of Technology, Stockholm, in the mid 1970s (*4*). The technique has been modified to work even better and to protect the cells during installation. The cell is protected during installation by a steel cylinder (h = 500 mm, ϕ = 120 mm) connected to piston sampler rods (Figure 3). About 50 cm above the intended measuring level, the cell is pushed out of the protection cylinder by sounding rods inside the piston sampler rods. The cylinder

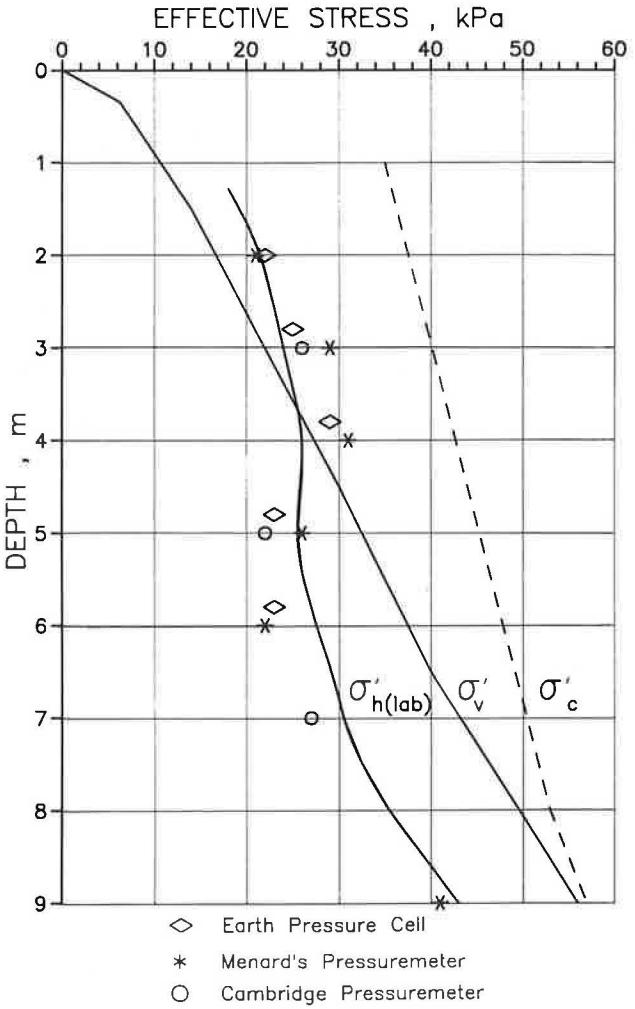

FIGURE 2 Comparison of measured lateral in situ stresses with lateral stresses according to Schmidt's relation [after Larsson (*1*)].

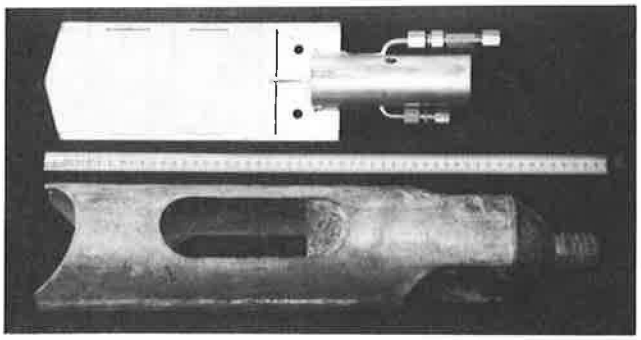

FIGURE 3 Glötzl earth pressure cell and instrumentation tool.

and the rods are then withdrawn. Wires are connected to the cells to make it possible to recover the cells after the measurement period.

By using this method, earth pressure cells can be pushed to great depth with little risk of damage. The dry crust has to be predrilled before pushing the cells into the ground.

JANBU'S GENERALIZED PROCEDURE OF SLICES FOR PREDICTION OF HORIZONTAL STRESS DISTRIBUTION

There are many ways of solving slope stability problems for shear surfaces of any shape. The differences are to be found in the assumptions regarding interslice forces.

Forces acting on the boundaries of a single slice in Janbu's generalized procedure of slices (*5*) are assumed as indicated in Figure 4. By assuming the position of the line of thrust for the total slice force E for the selected shear surface, the average factor of safety and the four unknowns for each slice, E, T, σ, and τ, can be determined by an iterative procedure. All the slopes in this project have been investigated under undrained conditions, and the line of thrust has been placed somewhat below the lower third point in the active zone and somewhat above it in the passive zone.

A computer program, originally made by Grande (*6*), has been used for determination of the interslice stress distribution with Janbu's method for all four test sites.

BÄCKEBOL TEST AREA

The Bäckebol test area, 10 km north of Göteborg, is an almost horizontal field next to the Göta River. The clay is known to be exceptionally homogenous and has been subjected to several investigations. The soil profile comprises a 1-m thick dry crust underlain by a slightly organic gray clay. The undrained shear strength is around 15 kPa.

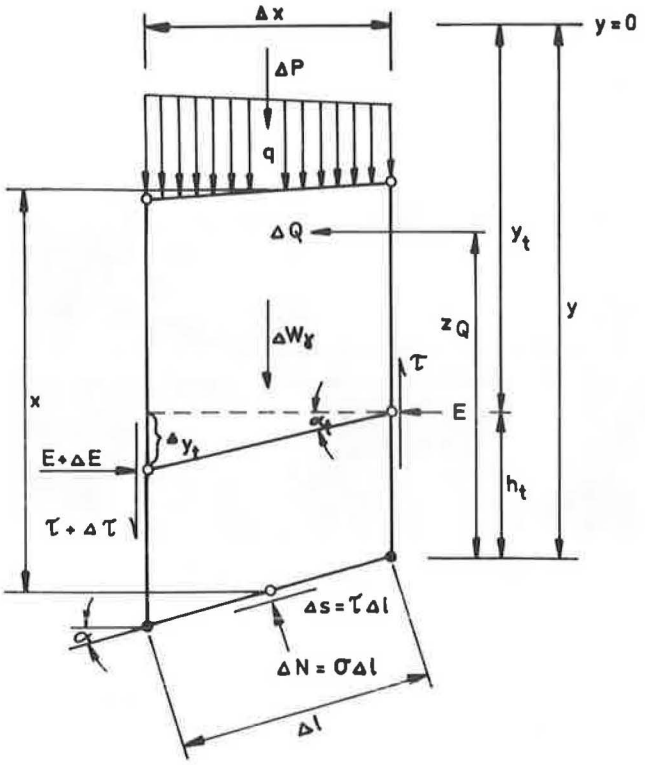

FIGURE 4 Forces acting on the boundaries of a single slice in Janbu's generalized procedure of slices [after Janbu (*5*)].

Measurements of in situ lateral earth pressure have been made with Glötzl earth pressure cells (*1*). DMT tests have been carried out (*7*) in the area. The K_o values are presented in Figure 5. The values decrease with depth from 0.8 close to the ground surface down to 0.6 at 10 m of depth. The agreement between earth pressure cells and DMT is very good at 5 and 7 m below the ground surface, but an unacceptable difference is found at 3 m of depth.

ALAFORS TEST SITE

The Alafors test site is situated about 25 km northeast of Göteborg and is a part of a side valley, the Sköld valley, to the Göta River valley. The investigated area of the valley is narrow, just about 130 m wide, and the difference in altitude between the slope crest and the Sköld stream is 12 m. A slide occurred just 30 m to the east of the test site in 1901.

The soil in the area consists of soft clay, which is about 25 m thick in the center of the valley. The undrained shear strength is 10 to 15 kPa just below the dry crust and then increases with depth (1 kPa/m). The dry crust is 1 to 2 m thick. Thin silt layers (not continuous ones) and quick clay are found in some places. Noncohesive soil of different thickness underlies the clay (Figures 6 and 8).

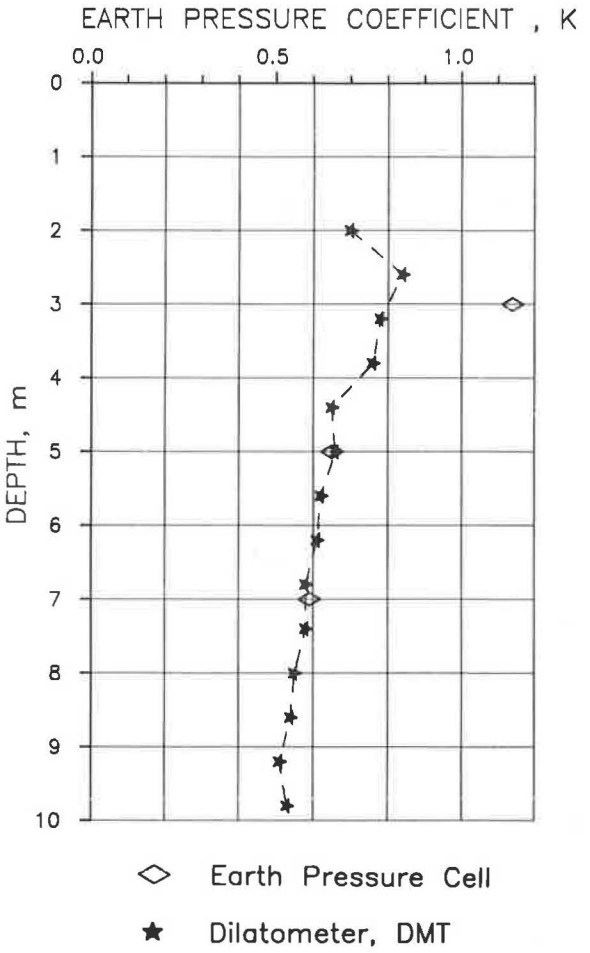

FIGURE 5 *K* values determined by earth pressure cells and DMT at the Bäckebol test site.

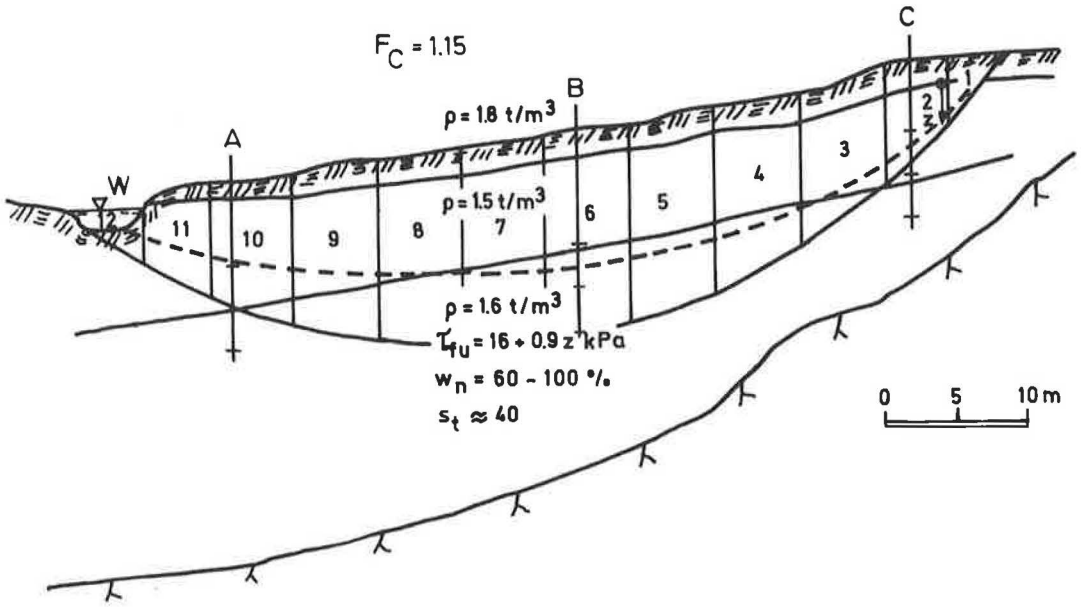

FIGURE 6 Profile with geotechnical parameters, shear surface, and line of thrust used for the Alafors test site before stabilization.

Stability calculations in the late 1970s indicated that the factor of safety of the slope was very low, F_c = 1.07. The slope was stabilized through a 2-m thick clay fill in the passive zone, and the stream was relocated in a culvert (Figure 7).

Predicted Lateral Earth Pressures

Predictions of lateral earth pressures at the Alafors test site have been done by assuming undrained conditions both before and after the stabilization. The same, noncircular, 16-m-deep shear surfaces were used in both analyses. The shear surfaces and lines of thrust are presented in Figures 6 and 7. The calculations gave reasonable values of the lateral earth pressures and K values. In the passive zone the lateral earth pressures were higher in the stabilized slope than in the original slope (Tables 1 and 2).

The lateral pressures in the active zone at the shear surface were also higher in the stabilized than in the original, which was not expected. Accordingly, the K_o values were calculated to be higher throughout the slope after the stabilization (Tables 7 and 8).

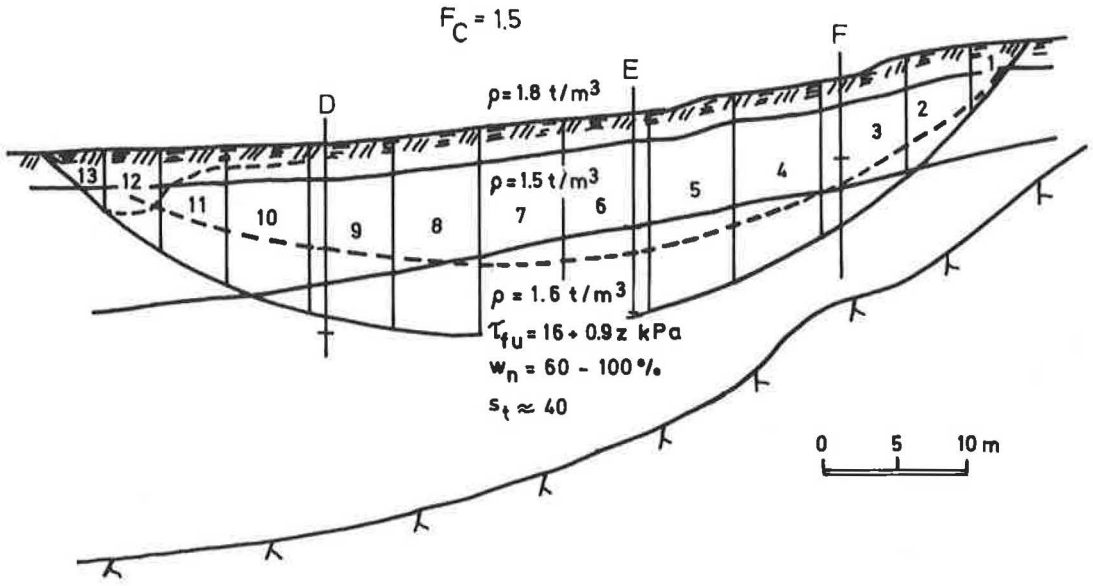

FIGURE 7 Profile with geotechnical parameters, shear surface, and line of thrust used for the Alafors test site after stabilization.

TABLE 1 PREDICTED LATERAL EARTH PRESSURES AND *K* VALUES AT THE ALAFORS TEST SITE BEFORE STABILIZATION

Slice inter-section	Lateral pressure at the ground level σ_{hg} (kPa)	Lateral pressure at the shear surface σ_{hs} (k a)	K -values at the shear surface
1-2	-10.9	33.3	0.11
2-3	-26.5	97.7	0.40
3-4	-30.9	171.2	0.96
4-5	-16.2	194.7	0.78
5-6	-0.2	206.9	0.81
6-7	-0.2	216.7	0.89
7-8	23.7	185.8	0.68
8-9	25.2	176.2	0.75
9-10	27.3	148.6	0.83
10-11	16.0	111.6	0.78
11-12	41.7	55.8	0.77

TABLE 2 PREDICTED LATERAL EARTH PRESSURES AND *K* VALUES AT THE ALAFORS TEST SITE AFTER STABILIZATION

Slice inter-section	Lateral pressure at the ground level σ_{hg} (kPa)	Lateral pressure at the shear surface σ_{hs} (kPa)	K -values at the shear surface
1-2	-13.4	49.0	0.28
2-3	-30.9	114.0	0.67
3-4	-35.4	194.2	1.26
4-5	-18.4	220.2	1.06
5-6	0	242.4	1.19
6-7	6.4	241.2	1.10
7-8	21.4	219.6	0.87
8-9	39.3	210.1	1.01
9-10	36.0	179.6	0.91
10-11	34.3	148.3	0.95
11-12	23.8	118.8	1.07
12-13	37.4	65.2	0.80

Comparison Between Predicted and Measured Lateral Earth Pressures

Measurements with earth pressure cells have been carried out both before and 10 years after the stabilization. Before the stabilization, cells were installed in section A at 6, 9, and 12 m depth; in section B at 8, 11, and 14 m; and in section C at 5, 8, and 11 m depth (see Figure 6). After the stabilization, cells were installed in section D at 7.4 and 13.4 m depth, in section E at 8 and 14 m, and in section F at 5.5 m depth (see Figure 7). The measurements indicated the same results as the prediction with increasing pressures and *K* values from the crest to the toe of the slope. However, the difference between the pressures in the passive zone before and after the stabilization was not as high as was predicted (Tables 3 and 4).

The agreement between the measured and predicted pressures and *K* values was good in the case of the original slope but not as good (some unacceptable values) in the case of the stabilized slope (Tables 3 and 4).

TABLE 3 COMPARISON BETWEEN MEASURED AND PREDICTED LATERAL EARTH PRESSURES AND *K* VALUES AT THE ALAFORS TEST SITE BEFORE STABILIZATION

Section	Depth z(m)	Total lateral earth pressure			K -values		
		Measured (kPa)	Predicted (kPa)	Δσ (%)	Measured	Predicted	ΔK (%)
A	6	91	89	2	0.95	0.89	6
	9	124	124	0	0.73	0.73	6
	12	175	160	9	0.86	0.63	27
B	8	104	119	14	0.61	0.88	44
	11	139	162	16	0.55	0.87	58
	14	175	205	17	0.51	0.84	65
C	5	56	46	18	0.50	0.30	40
	8	70	89	14	0.18	0.45	150
	11	-	132	-	-	0.55	-

TABLE 4 COMPARISON BETWEEN MEASURED AND PREDICTED LATERAL EARTH PRESSURES AND *K* VALUES AT THE ALAFORS TEST

Section	Depth z(m)	Total lateral earth pressure			K -values		
		Measured (kPa)	Predicted (kPa)	Δσ (%)	Measured	Predicted	ΔK (%)
D	7.4	103	124	20	0.70	1.04	49
	13.4	181	198	9	0.65	0.84	29
E	8.0	99	142	43	0.58	1.26	117
	14.0	171	246	44	0.50	1.24	148
F	5.5	74	79	7	0.67	0.79	18

LÄRJEÅN TEST SITE

The Lärjeån test site in the Lärje stream valley is situated 10 km northeast of Göteborg. The Lärje stream has cut its way down 15 m into the clay layers and has formed many steep slopes (some with an inclination as high as 1–2) and a meandering stream line. Many small slides occur in this area every year.

The investigated slope has an altitude between the slope crest and the slope toe of 14 m and an inclination of 30 to 35 degrees in its steepest part. A slide occurred in the slope early in 1988, and the investigations and measurements have been made only after the slide.

The soil consists of clay overlying noncohesive soil on the rock. The rock surface is found 31 m below the ground level at the slope crest and is almost lateral. The undrained shear strength is 40 kPa right below the dry crust and increases with depth, 2.5 kPa/m. The dry crust is 5 m thick at the top of the slope and 2 m thick at the toe (Figure 8). The pore pressure is hydrostatic with a zero value at the lower part of the dry crust.

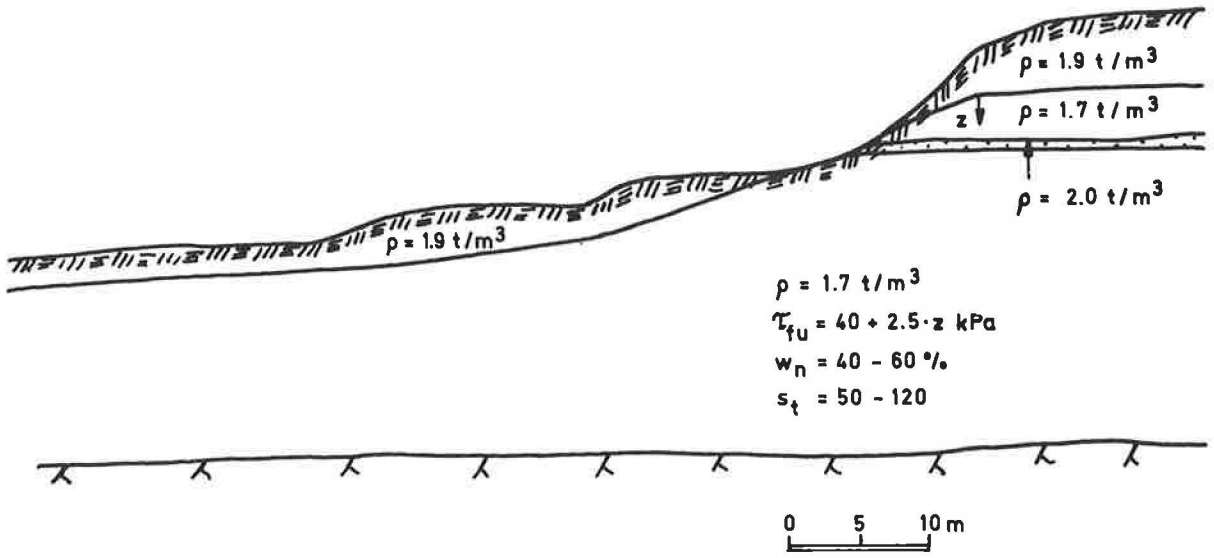

FIGURE 8 Profile with geotechnical parameters for the Lärjeån test site.

Predicted Lateral Earth Pressures

For the Lärjeån test site two different, noncircular, shear surfaces were assumed in an attempt to predict the stress distribution. A 14-m-deep shear surface in the upper part and a 10-m-deep shear surface in the lower part of the slope were applied. The two shear surfaces were chosen to obtain stresses at the places where pressure cells had been installed. The calculations indicate very high lateral pressures and K values in the passive zone. K values as high as 2.7 to 3.1 were found (Tables 5 and 6).

Comparison Between Predicted and Measured Lateral Earth Pressures

Measurements of lateral earth pressures have been performed with two earth pressure cells. The cell was installed at a depth of 7.25 m in section A and at a depth of 12 m in section B (Figures 9 and 10). The agreement between the measured and predicted earth pressures and K values was found to be very good (Table 7).

Two DMT soundings were done with the blade perpendicular to the slope in section D1 and D2 (Figures 9 and 10). Those tests also showed high K values but not as high as those obtained by the pressure cells. The results from the DMT

TABLE 5 PREDICTED LATERAL EARTH PRESSURES AND K VALUES AT THE LÄRJEÅN TEST SITE IN THE UPPER PART OF THE SLOPE SITE AFTER STABILIZATION

Slice intersection	Lateral pressure at the ground level σ_{hg} (kPa)	Lateral pressure at the shear surface σ_{hs} (kPa)	K -values at the shear surface
1-2	-3.8	13.4	0.51
2-3	-12.0	199.2	0.60
3-4	-29.4	250.6	0.76
4-5	-24.3	343.9	1.56
5-6	13.0	357.4	2.86
6-7	16.7	316.7	2.01
7-8	29.5	281.1	2.13
8-9	29.8	227.2	1.81
9-10	30.0	163.6	1.84

TABLE 6 PREDICTED LATERAL EARTH PRESSURE AND K VALUES AT THE LÄRJEÅN TEST SITE IN THE LOWER PART OF THE SLOPE

Slice intersection	Lateral pressure at the ground level σ_{hg} (kPa)	Lateral pressure at the shear surface σ_{hs} (kPa)	K -values at the shear surface
1-2	-5.9	33.8	0.68
2-3	-19.8	99.0	0.84
3-4	-16.8	184.4	2.05
4-5	-27.5	260.3	3.02
5-6	-28.9	262.3	2.13
6-7	-18.1	288.9	2.47
7-8	-0.2	240.4	1.60
8-9	42.9	213.9	2.41
9-10	38.3	183.1	1.98
10-11	40.8	139.0	2.19

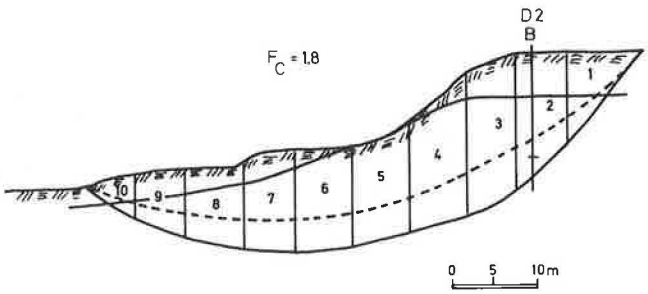

FIGURE 9 Shear surface and line of thrust used for the Lärjeån test site in the upper part of the slope.

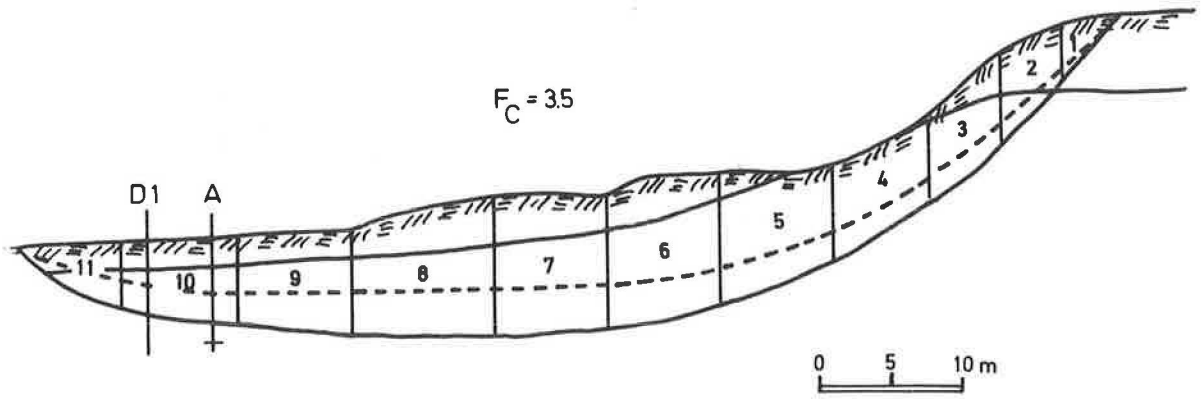

FIGURE 10 Shear surface and line of thrust used for the Lärjeån test site in the lower part of the slope.

TABLE 7 COMPARISON BETWEEN MEASURED AND PREDICTED LATERAL EARTH PRESSURE AND *K* VALUES AT THE LÄRJEÅN TEST SITE, MEASUREMENTS WITH EARTH PRESSURE CELLS

Section	Depth z(m)	Total lateral earth pressure			K -values		
		Measured (kPa)	Predicted (kPa)	Δσ (%)	Measured	Predicted	ΔK (%)
A	7.25	214	202	5	2.78	3.01	8
B	12.0	140	146	4	0.56	0.64	14

TABLE 8 COMPARISON BETWEEN *K* VALUES MEASURED WITH DMT AND EARTH PRESSURE CELLS AT THE LÄRJEÅN TEST SITE

Section	Depth z(m)	K -values		
		Dilatometer	Earth pressure cell	ΔK (%)
D1, A	7.25	1.5	2.78	85
D2	12.0	0.8	0.56	30

soundings are shown in Table 8. The difference between the DMT results and those obtained by the earth pressure cells was unacceptable.

KVIBERG TEST SITE

The Kviberg test site (see Figure 11) is situated in the eastern part of Göteborg. The area consists of a ravine where the Utby stream meanders its way down in a north-south direction. The slope inclination within the area varies between 1–5 and 1–10 except next to the stream where it can be higher. The soil consists of 2 to 3 m of dry crust and soft clay underlain by a silty clay with silt and sand layers. The depth to rock was not investigated but is greater than 20 m at the crest and more than 15 m at the toe of the slope. The undrained shear strength varies between 20 and 30 kPa and increases somewhat with depth. The groundwater level is 1.5 to 2.0 m below the ground level in the upper part of the slope. At the toe of the slope the groundwater is artesian. The sensitivity is rather low (20 to 30). The water level in the Utby stream varies a great deal and causes erosion and many small slides.

Predicted Lateral Earth Pressures

Prediction of the lateral earth pressure distribution at the Kviberg test site was based on the assumption of a noncircular 12-m-deep shear surface (Figure 11). The calculations showed increasing lateral earth pressures and *K* values from the crest

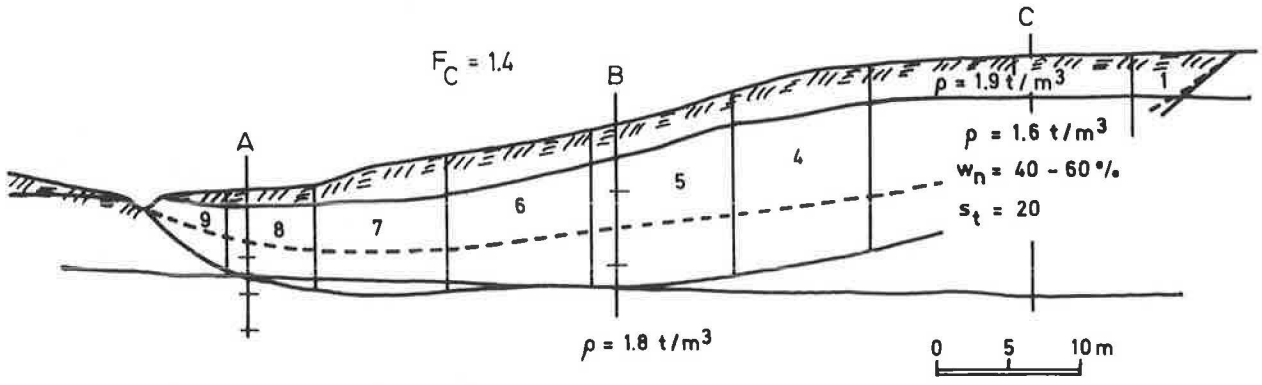

FIGURE 11 Profile with geotechnical parameters, shear surface, and line of thrust used for the Kviberg test site.

to the toe of the slope (Table 9). The differences in K values between the active and passive zone were of the same order as at the Alafors test site.

Comparison Between Predicted and Measured Lateral Earth Pressures

Seven earth pressure cells were installed at three sections of the slope: at the toe, at the crest, and in the middle (Figure 11). The cells were installed at depths of 5, 7.5, and 10 m in sections A and C and at depths of 5 and 10 m in section B. The results show increasing K values from the top to the toe of the slope but the values were not as high in the passive zone as those found at the Alafors and Lärjeån test sites (Table 10). The agreement between the measured and the predicted values was good (Table 10).

TABLE 10 COMPARISON BETWEEN MEASURED AND PREDICTED LATERAL EARTH PRESSURES AND K VALUES AT THE KVIBERG TEST SITE

Section	Depth z(m)	Total lateral earth pressure			K -values		
		Measured (kPa)	Predicted (kPa)	Δσ (%)	Measured	Predicted	ΔK (%)
A	5	79	99	25	0.83	1.47	77
	7.5	136	136	0	1.26	1.26	0
	10	194	173	11	1.38	1.02	26
B	5	83	87	5	0.92	0.99	48
	10	148	171	16	0.73	1.05	44
C	5	74	51	31	0.73	0.40	45
	7.5	95	79	17	0.50	0.28	44
	10	109	109	0	0.30	0.30	0

UGGLUM TEST SITE

The Ugglum test site is in an area with postglacial clay in the eastern part of Göteborg. The Säve stream, which is an affluent to the Göta River, passes through the site. Rather flat slopes with a height of about 6 m have been formed by the stream. Quick clay can be found in some areas next to the stream and have caused many slides through the years.

The soil consists of soft, homogenous clay capped by a dry crust 1 to 2 m thick overlying noncohesive soil rock. The undrained shear strength is about 10 to 15 kPa right under the dry crust and increases with depth, 1 kPa/m (Figure 12). The groundwater is hydrostatic from the ground level.

In September 1989 a new railway bridge was built in the area. Since the factor of safety is low, $F_{c\phi} \approx 1.2$ to 1.3, the investigated slope had been stabilized by removing masses from the active zone. Measurements of lateral earth pressures with cells are still going on and continued during and after the stabilization.

TABLE 9 PREDICTED LATERAL EARTH PRESSURES AND K VALUES AT THE KVIBERG TEST SITE

Slice intersection	Lateral pressure at the ground level σ_{hg} (kPa)	Lateral pressure at the shear surface σ_{hs} (kPa)	K -values at the shear surface
1-2	-8.5	59.9	0.18
2-3	-8.0	113.2	0.24
3-4	-12.0	153.6	0.35
4-5	-13.2	174.0	0.60
5-6	3.6	181.4	1.02
6-7	11.1	185.1	1.75
7-8	28.6	142.8	1.51
8-9	27.6	102.8	1.36

Predicted Lateral Earth Pressures

A noncircular 9-m-deep shear surface was used to predict the stress distribution at the Ugglum test site (Figure 12). From the results of the calculations it can be seen that the earth pressures and K values constantly increase from the crest to the toe of the slope (Table 11). The K values were in the same range as the values at the Alafors test site.

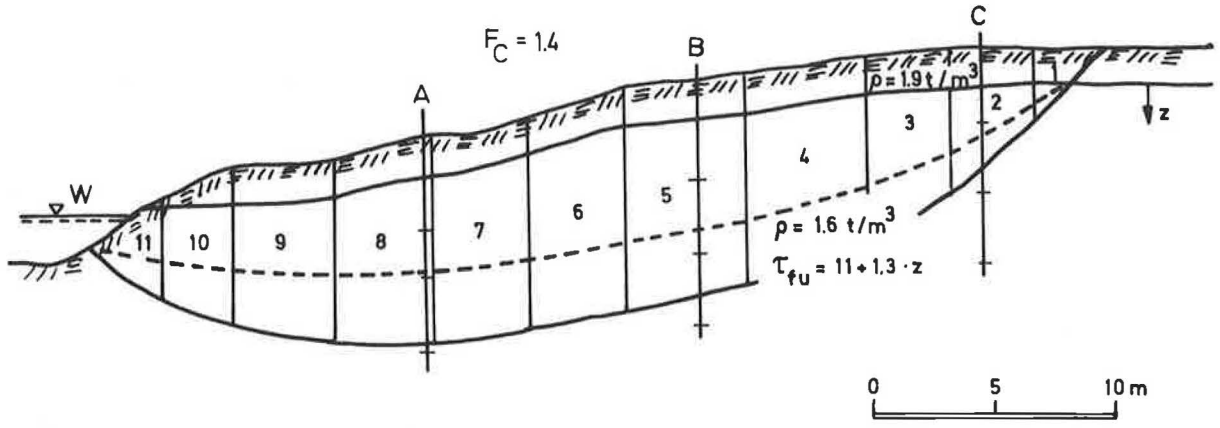

FIGURE 12 Profile with geotechnical parameters, shear surface, and line of thrust used for the Ugglum test site.

TABLE 11 PREDICTED LATERAL EARTH PRESSURES AND K VALUES AT THE UGGLUM TEST SITE

Slice inter-section	Lateral pressure at the ground level σ (kPa)	Lateral pressure at the shear surface σ (kPa)	K -values at the shear surface
1-2	-8.4	36.2	0.28
3-2	-8.1	75.1	0.44
3-4	-14.5	104.9	0.60
4-5	-8.1	124.5	0.71
5-6	-9.1	128.3	0.59
6-7	-2.9	134.7	0.83
7-8	4.7	129.7	0.82
8-9	12.3	117.1	0.88
9-10	9.9	94.3	0.71
10-11	19.4	71.0	1.11

Comparison Between Predicted and Measured Lateral Earth Pressures

Nine earth pressure cells were installed in three sections of the slope: close to the Säve stream, in the middle, and at the crest.

In section A, cells were installed at depths of 4, 6, and 9 m; in section B at 4.35, 7.35, and 10.35 m; and in section C at 3, 6, and 9 m. The measurements showed increasing K values from 0.60 in the active zone to 0.98 in the passive zone (Table 12). A very good agreement between measured and predicted lateral earth pressures was noted (Table 12). The earth pressure cell at 4.35 m of depth in section B gave a very low earth pressure value, which probably was not correct.

DMT soundings with the blade perpendicular to the slope have been carried out in all three sections. The results are shown in Figures 13–15. The agreement between measured K values with DMT and earth pressure cells was very good in sections B and C and good in section A.

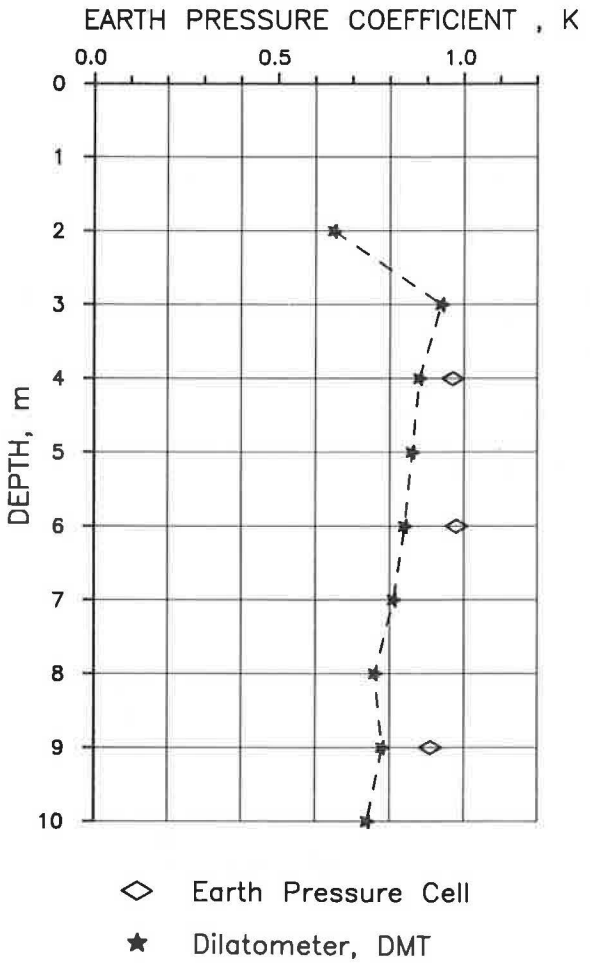

FIGURE 13 Earth pressure coefficient K determined by earth pressure cells and DMT at the Ugglum test site in section A.

DISCUSSION OF RESULTS

The investigation showed that the lateral earth pressures and K values increased from the crest to the toe of a slopes. This was found both through direct observations and by Janbu's generalized procedure of slices. The K values were about 0.4 to 0.7 in the active zones and about 0.8 to 1.4 in the passive zones. In one very steep slope with a low factor of safety, K in the passive zone reached values close to the passive earth pressure coefficient K_p ($K \approx 3$).

TABLE 12 COMPARISON BETWEEN MEASURED AND PREDICTED LATERAL EARTH PRESSURES AND K VALUES AT THE UGGLUM TEST SITE

Section	Depth z(m)	Total lateral earth pressure			K -values		
		Mea-sured (kPa)	Pre-dicted (kPa)	$\Delta\sigma$ (%)	Mea-sured	Pre-dicted	ΔK (%)
A	4.0	65	63	3	0.97	0.91	6
	6.0	97	93	4	0.98	0.90	8
	9.0	140	137	2	0.91	0.86	5
B	4.35	38	54	42	(0.30)	0.64	113
	7.35	97	98	1	0.63	0.64	2
	10.35	143	143	0	0.68	0.67	1
C	3.0	35	35	0	0.60	0.60	0
	6.0	75	76	1	0.58	0.60	3
	9.0	110	95	14	0.46	0.23	50

A good or very good agreement between measured and calculated total earth pressures was found. The differences were less than 20 percent except for the Alafors test site after stabilization. At the Alafors site the differences were about 20 to 50 percent. The explanation to those results may be that the Janbu's generalized procedure only works for natural slopes and not for stabilized ones. This hypothesis will be further investigated when masses from the active zone at the Ugglum test site have been removed.

The K values obtained by DMT soundings and the pressure cells were in good agreement at two sites but were unacceptably different at one site.

The calculations with Janbu's generalized procedure have only been done for undrained conditions, though. Lateral stresses obtained from calculations in drained conditions will be studied in the near future.

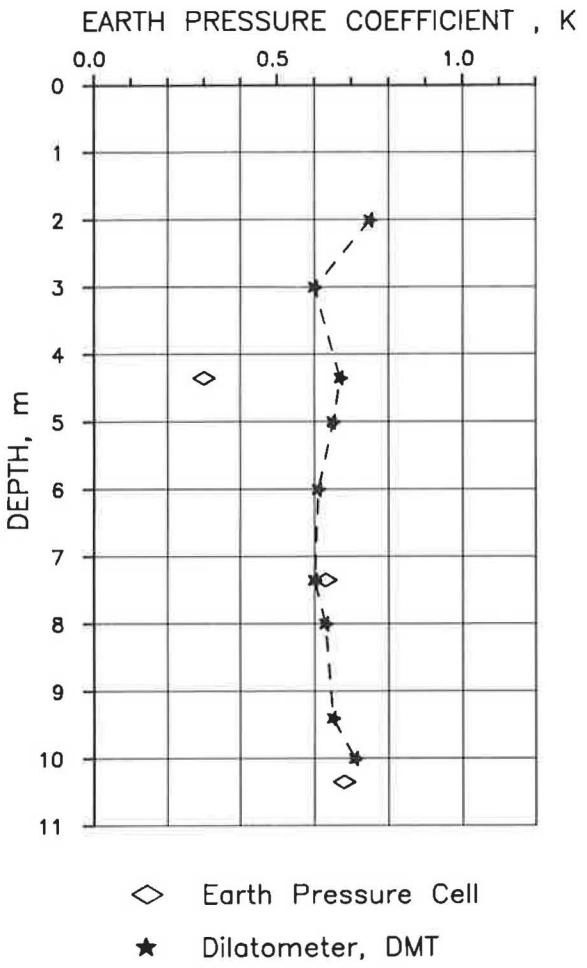

FIGURE 14 Earth pressure coefficient K determined by earth pressure cells and DMT at the Ugglum test site in section B.

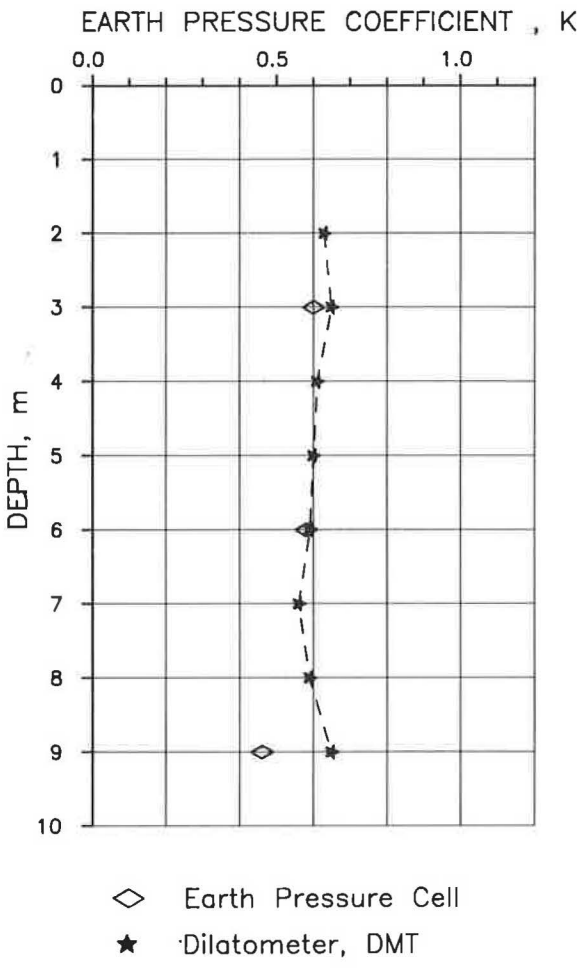

FIGURE 15 Earth pressure coefficient K determined by earth pressure cells and DMT at the Ugglum test site in section C.

The effect of the position of the line of thrust on the predicted earth pressures will be investigated more thoroughly in the second phase of this project. The effect on the lateral stresses at a given point of shear surfaces reaching different depths will also be investigated.

The measurements at the Alafors test site did not show any large differences in lateral earth pressures before and after the stabilization. The differences in the stabilized zone were around 10 kPa but were not noticeable in the other parts of the slope.

Predictions of lateral earth pressures will also be made by using numerical methods. An investigation with the finite-element method will start during autumn 1989.

CONCLUSIONS

The following conclusions can be drawn from the investigation:

1. Lateral earth pressures and K values increase from the crest to the toe of slopes.
2. K values can be extremely high ($K > 3$) in the passive zone of the steep slopes with a low factor of safety.
3. Janbu's generalized method of slices gives acceptable values of the existing lateral earth pressures in natural slopes.
4. Glötzl earth pressure cells have been found to be very reliable in soft clays.

ACKNOWLEDGMENT

The author wishes to thank the Swedish Building Research Board for their financial support of this project.

REFERENCES

1. R. Larsson. *Measurement and Calculation of Lateral Stresses in Clay and Their Importance for Strength and Deformation Parameters*. Department of Geotechnical Engineering, Chalmers University of Technology, Göteborg Sweden, 1975.
2. L. Olsson. Lateral Load Tests in Clay Using Inflatable Air Jacks. *Canadian Geotechnical Journal*, Vol. 18, 1981, pp. 316–321.
3. S. Marchetti. In Situ Tests by Flat Dilatometer. *Journal of the Geotechnical and Engineering Division*, ASCE, Vol. GT3, 1980.

4. K. R. Massarch. New Method for Measurement of Lateral Earth Pressure in Cohesive Soil. *Canadian Geotechnical Journal*, Vol. 12, 1975, pp. 142–146.
5. N. Janbu. Slope Stability Computations. In *The Embankement Dam Engineering*. John Wiley, New York, 1973, pp. 47–86.
6. L. Grande. *The Lammet Computer Programme: Slope Stability Analysis by Janbu's Generalized Procedure of Slices*. Norwegian University of Technology, Trondheim, 1975.
7. M. G. Smith. *Dilatometer Tests in Soft Swedish Clays*. MSc. dissertation. Chalmers University of Technology, Göteborg, Sweden, 1989.
8. J. Ekström, A. Samuelsson, and G. Sällfors. *Analysis of the Stability of Slopes*. (In Swedish). Department of Geotechnical Engineering, Chalmers University of Technology, Göteborg, Sweden, 1982.

Publication of this paper sponsored by Committee on Soil and Rock Properties.

Correlation of Dilatometer Readings with Lateral Stress in Clays

T. LUNNE, J. J. M. POWELL, E. A. HAUGE, K. H. MOKKELBOST, AND I. M. UGLOW

Published methods of predicting in situ lateral stress from the dilatometer test are reviewed. A data base containing high-quality information from clay test bed sites mainly in Norway and the United Kingdom has been established. Reference K_o values have been evaluated from a number of methods including self-boring pressuremeter, hydraulic fracture, total stress cells, laboratory measurements, and empirical correlations. A new correlation between the dilatometer parameter K_D and K_o is proposed for young clays.

The in situ horizontal stress σ_h (or the lateral stress ratio K_o) is an important parameter that needs to be assessed for many geotechnical problems:

- Input in engineering analyses (e.g., skin friction of piles, pressures on walls, fracturing of dams);
- Selection of consolidation stresses for laboratory tests (e.g., triaxial test consolidated to in situ stresses);
- Evaluating borehole stability, designing mud program; and
- Input for interpretation of in situ tests [e.g., K_o required in several methods for computing strength from cone penetration tests (CPTs)].

Schmertmann (*1*) discussed those points in more detail and, in addition, these items: natural causes for K_o variation in the ground, how K_o can be measured in the laboratory and in the field, and sources of error when attempting to measure K_o.

After the standard penetration test (SPT), the CPT is probably the most widely used in situ test. Interpretation of the CPT in several cases requires that the in situ horizontal stress σ_h is known. Even though methods of finding σ_h from CPT results have been presented in the literature, including the incorporation of a lateral stress sensor in the friction sleeve, the ability at present to estimate reliable values of σ_h is still far from satisfactory (*2*).

One of the reasons that the authors advocate the use of the dilatometer test (DMT) is the potential of the test to yield a more reliable measurement of σ_h. The DMT is, therefore, an extremely valuable supplement to the CPT. However, the original Marchetti (*3*) correlation can, in some cases, be greatly in error and, therefore, need to be updated (*4–6*).

As part of a collaborative research program between the Norwegian Geotechnical Institute (NGI) and the Building Research Establishment (BRE) in Great Britain, a data base of high-quality information on in situ stresses, soil parameters, and in situ test results has been established. One of the main purposes of this work is to arrive at better methods for interpreting various in situ tests (*7*). This paper concentrates on the results of work to improve the correlations between the DMT test results and in situ horizontal stresses.

The DMT testing equipment and procedures are not described here, but reference is made to Marchetti (*3*) and Lutenegger (*8*).

T. Lunne, E. A. Hauge, and K. H. Mokkelbost, Norwegian Geotechnical Institute, Postbox 40, Taasen, Oslo 8, Norway. J. J. M. Powell and I. M. Uglow, Building Research Establishment, Garston, Watford WD2 7JR, England.

PREVIOUS CORRELATIONS

The original correlation between the DMT horizontal stress index K_D and the coefficient of earth pressure at rest K_o was given by Marchetti (*3*) (see Figure 1). The correlation

$$K_o = \left(\frac{K_D}{1.5}\right)^{0.47} - 0.6$$

was based mainly on tests in Italian clays and is meant to be valid for uncemented clays with a $K_D > 0.3$.

This correlation appeared to work in some cases for soft and medium-to-stiff uncemented clays (*9*). In medium to heavily OC clays, the Marchetti (*3*) correlation can significantly overpredict and underpredict K_o, depending on soil type (*5,6*).

Lacasse and Lunne (*9*), on the basis of data in a wide range of clays, proposed a new correlation of the form

$$K_o = 0.34\ K_D^m$$

with m between 0.44 and 0.64 (Figure 2). A value of $m = 0.44$ is associated with highly plastic clays, and a value of $m = 0.64$ corresponds to low plasticity clays. Lacasse and Lunne stated that in soils with $K_D > 4$, more evaluated experience is needed but that the correlations given by Marchetti (*3*) and Lacasse and Lunne (*9*) could be used to obtain a range of K_o values.

Following a similar approach, Powell and Uglow (*6*) suggested that for "young" U.K. clays (i.e., less than 70,000 years old) the following correlation could be used:

$$K_o = 0.34\ K_D^{0.55}$$

For old U.K. clays (i.e., more than 60 million years) the experimental data fell considerably above the Marchetti correlations (see Figure 3) and tended to be more site specific.

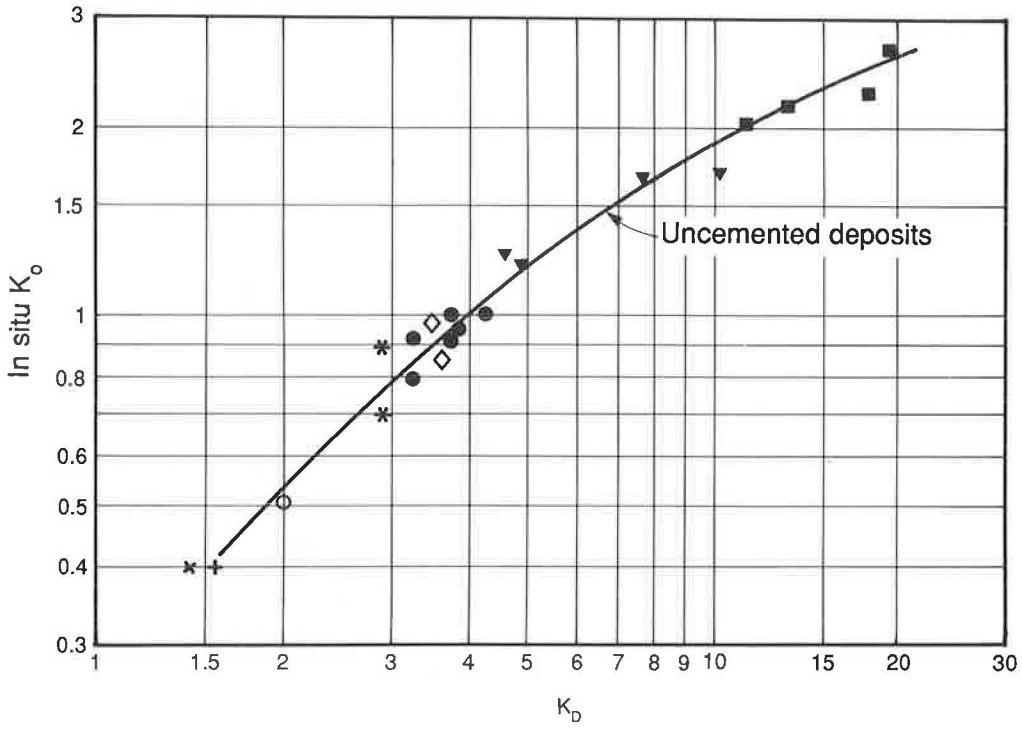

FIGURE 1 K_D versus K_o after Marchetti (*3*).

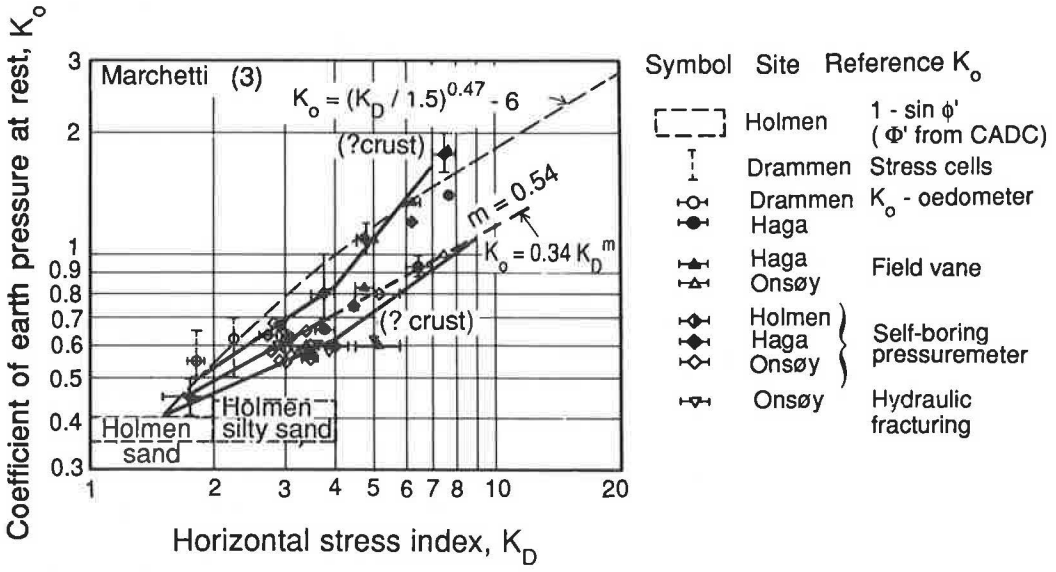

FIGURE 2 K_D versus K_o after Lacasse and Lunne (*4*).

Roque et al. (*10*) suggested the use of the "total horizontal effective stress" after DMT insertion to obtain a parameter, K_N:

$$K_N = \frac{(\sigma'_{h0} + \Delta\sigma'_h) + a}{\sigma'_{v0} + a}$$

where a is attraction as defined by Janbu and Senneset (*11*). The classical term cohesion (c) is related to the attraction by the expression $c = a \cdot \tan \phi'$. To obtain $\bar{\sigma}'_{h0} + \bar{\Delta}\sigma'_h$, it is necessary to take DMT readings with time until full dissipation of pore pressure has occurred. The in situ K_o value is then found by dividing K_N by an empirical factor. An example from the Glava clay in Norway is presented in Figure 4. Tests at other clay sites in the Trondheim area indicate that this empirical value may vary considerably from clay to clay (*10*). The necessity to wait for full dissipation, which can take several hours or days and thus becomes a costly operation par-

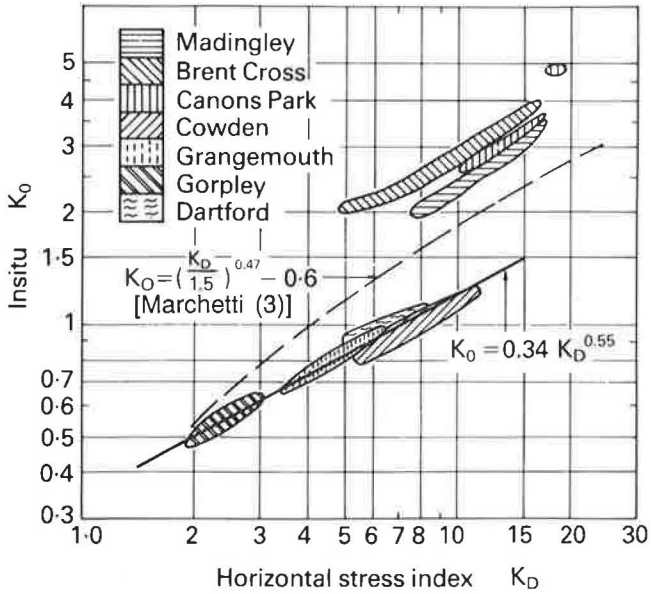

FIGURE 3 K_D **versus** K_o **after Powell and Uglow (*5,6*).**

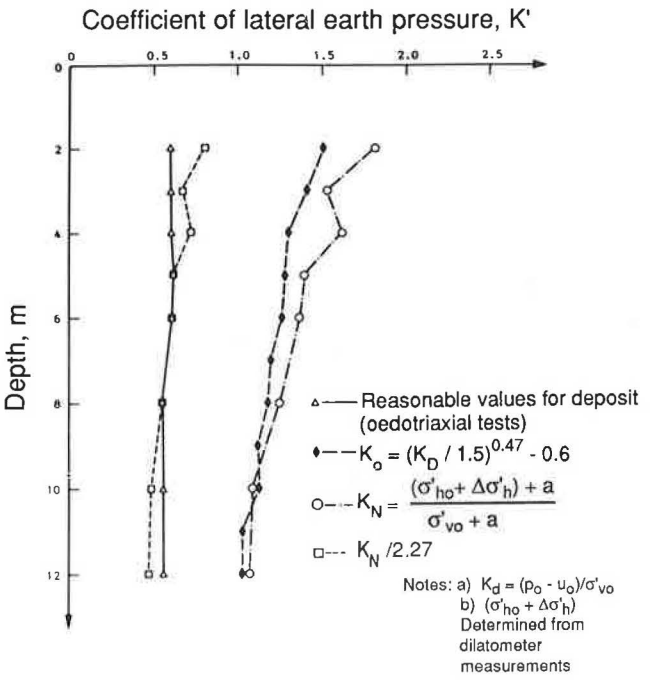

FIGURE 4 K **values from dilatometer and laboratory tests for Glava clay [after Roque et al. (*10*)].**

ticularly in offshore testing, is a further limitation of this approach.

Clarke and Wroth (*12*) compared results of high-quality self-boring pressuremeter tests (SBP) with DMT results and indicated that "A relationship between $(p_1\text{-}p_0)$ and $(p_1\text{-}\sigma_h)$ exists and appears to be independent of the soil type and stress level" (see Figure 5). Here, σ_h is the horizontal stress found from the SBP. This correlation may seem promising as a way of finding σ_h (and, hence, K_o) from DMT tests. However, Houlsby (*13*) rightly points out a problem with this

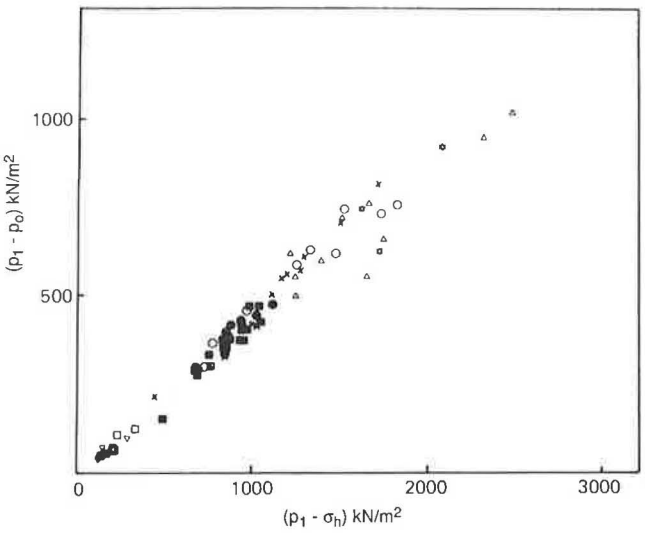

FIGURE 5 Relationship between $(p_1 - p_0)$ **and** $(p_1 - \sigma_h)$ **[after Clarke and Wroth (*12*)].**

correlation in that σ_h is a small quantity that has to be found as the difference between two large quantities.

ESTABLISHED DATA BASE

While the complete data base contains information from many sites, only four of NGI's test sites in Norway and five of BRE's United Kingdom test sites and the test bed site of University of California, Berkeley (Hamilton Air Force Base), are considered here.

The DMT tests were carried out with both the Marchetti standard DMT and NGI's offshore dilatometer (ODMT), which is somewhat smaller (see Figure 6) than the Marchetti because it was designed to pass inside an API drillstring (*14*). Extensive testing has indicated that the two DMTs give results that for most practical purposes are similar, as will be discussed later.

In what follows, only detailed results for one Norwegian soft clay site and one U.K. very stiff overconsolidated clay site will be shown. The method of selection of the parameters for the data base will then be discussed. For the other sites considered here, only reference data and the sources of more detailed information have been supplied.

NGI's Reference Clays in Norway

NGI's four sites presented here are Drammen, Onsøy, Haga, and Lierstranda. The Drammen and Onsøy test bed sites are among some of the most thoroughly investigated clays in the world and have been used as reference sites by NGI for 20 to 30 years.

All the four clay deposits were sedimented under marine conditions. The Haga clay is overconsolidated owing to excavation of soil, and the other three clays are only slightly overconsolidated, most likely caused by secondary compression. Plasticity indices of the clays mostly range from 15 to 40

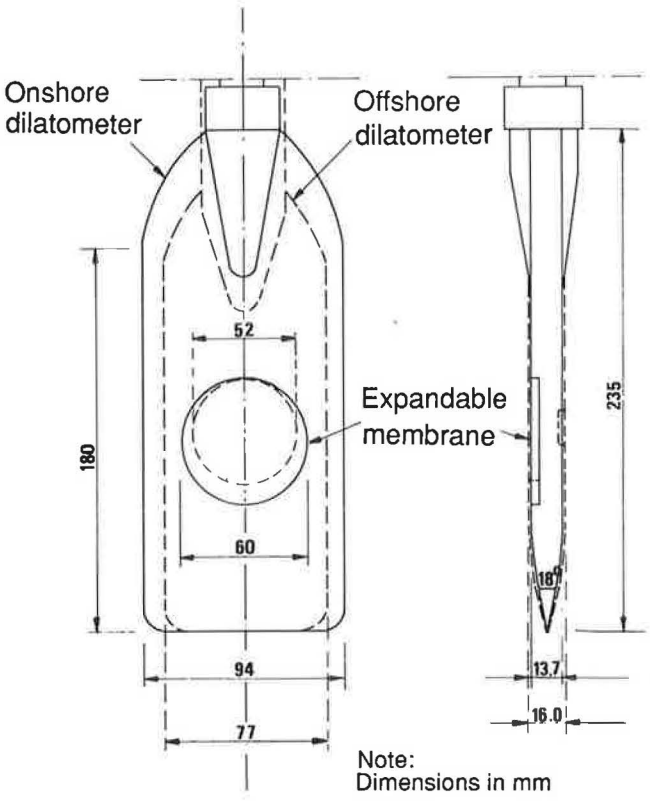

FIGURE 6 Comparison of Marchetti dilatometer and NGI's offshore dilatometer.

percent. [More information about these sites can be found elsewhere (*4,9,15*).]

As an example, Figure 7 presents the soil profile at Onsøy. The reference K_o values have been based on self-boring pressuremeter and hydraulic fracture tests (HFTs). Also presented in Figure 7 are K_o values derived from field vane test (FVT) results combined with CAU triaxial tests by using the method outlined by Aas et al. (*16*), and also laboratory correlations between OCR (from oedometer tests), plasticity index, and K_o [using Brooker and Ireland (*17*)]. Figure 8 gives dilatometer test results from both Marchetti and NGI's offshore DMTs. Here, p_0 and p_1 readings from the two devices are somewhat different at shallow depths, resulting in different Id values but that the DMT parameters K_D and E_D remain essentially similar.

Results from total stress cells and laboratory K_o oedometer tests were used for the Drammen site in addition to the SPB, HFT, and FVT to arrive at a best-estimate K_o profile. FVT, SBP, and laboratory correlations where used at the Haga site to establish the K_o profile. Results of FVT and laboratory correlations were used at Lierstranda.

BRE's Reference Clays in the United Kingdom

BRE's five sites presented here are Brent Cross, Canons Park, Madingley, Cowden, and Bothkennar. London clay, found at two of BRE's sites (Brent Cross and Canons Park), has been thoroughly investigated by BRE and others over the last 30 to 40 years. Cowden is a glacial till site and has been used by BRE for 15 years.

The Madingley site (Gault clay) has been used by Cambridge University for 15 years for several of their research programs on overconsolidated clay. BRE has had access to the site for 12 years and has carried out various in situ testing programs.

The Bothkennar clay in Grangemouth has recently been established in the United Kingdom as a national reference site on soft clay. BRE plays a central role in testing this site and has carried out in situ and laboratory programs.

The London clays (Brent Cross and Canons Park) and the Gault clay (Madingley) are very old clays (>60 million years) and are heavily overconsolidated.

The Cowden clay is a "young" (<70,000 years) consolidated glacial till, and the Bothkennar clay is a young lightly overconsolidated soft clay.

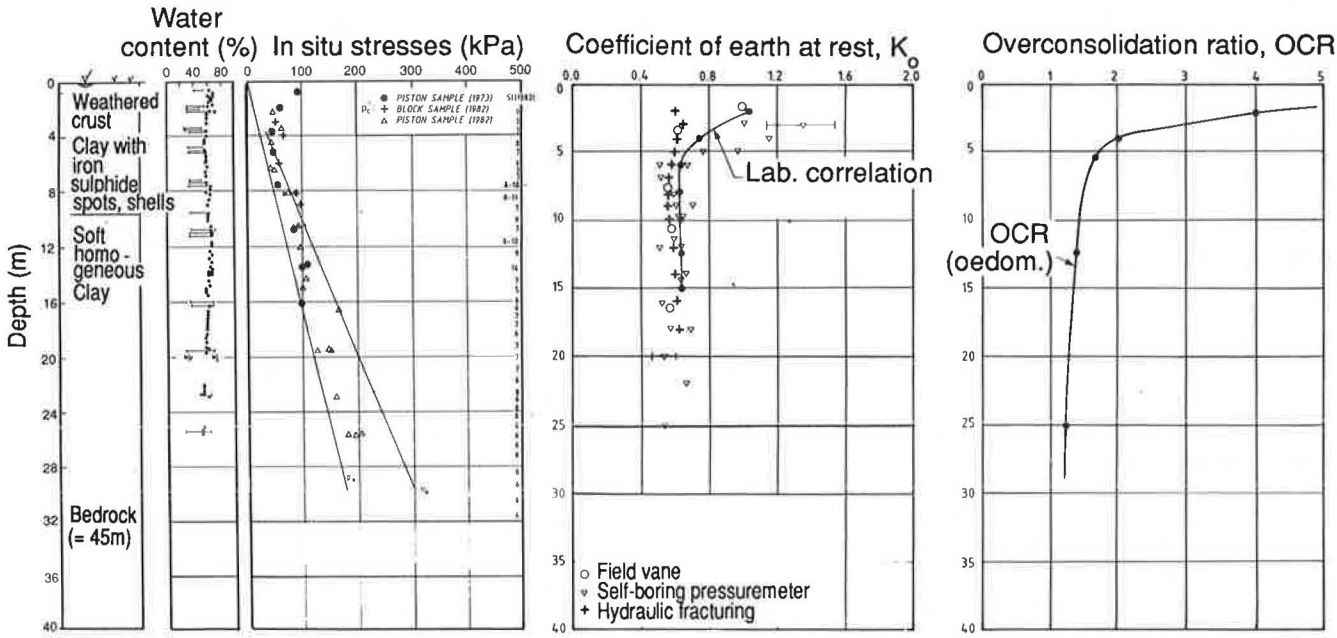

FIGURE 7 Onsøy soil profile.

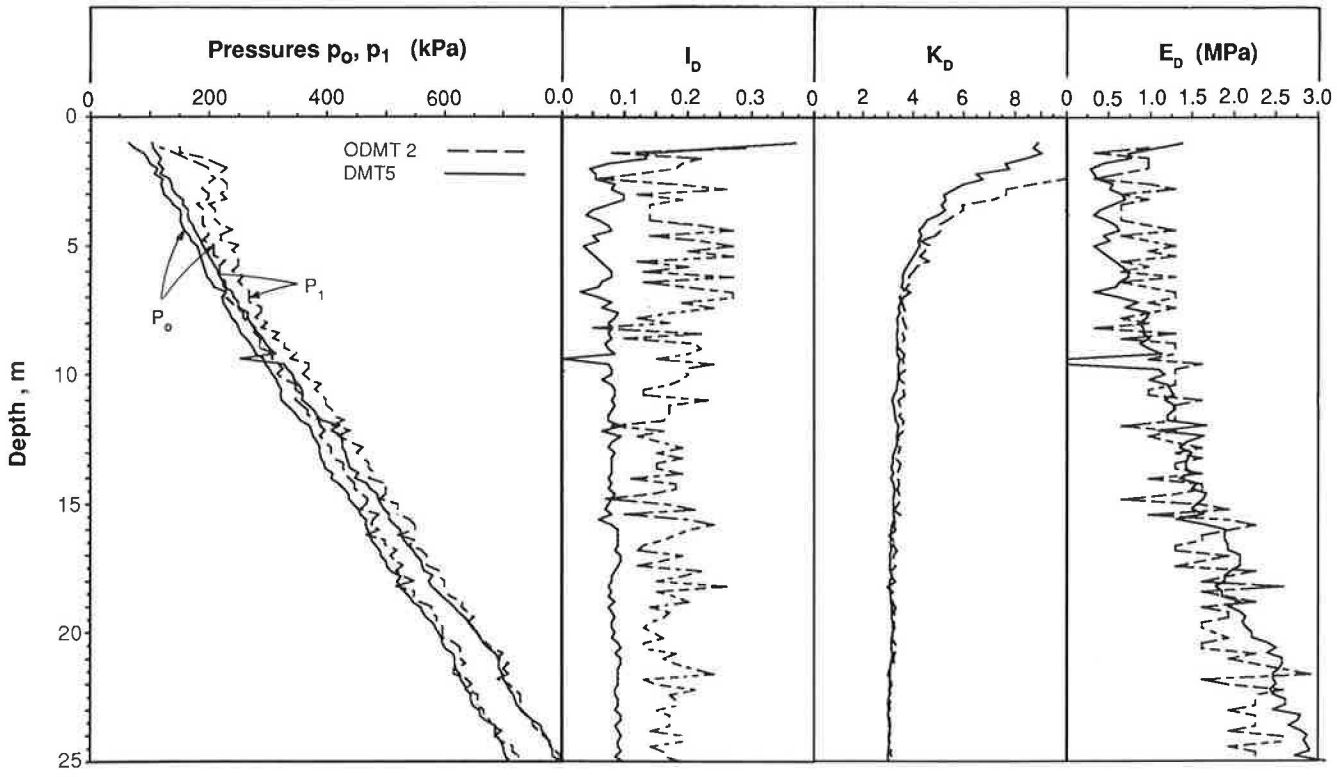

FIGURE 8 Dilatometer test results and Onsøy.

The plasticity index of those clays lies in the range 20 to 50 percent. [More information about these clays can be found elsewhere (*5,6–7*).]

As an example, Figure 9 gives the soil profile for Madingley. The K_o profile at Madingley is based on results of total stress cells and self-boring pressuremeter tests and oedometer tests by using empirical correlations (*17*). Figure 10 gives results from both Marchetti and NGI offshore dilatometers at this site. Excellent agreement between the results from the two devices can be seen.

At Cowden the K_o profiles were based on total stress cell measurements, laboratory suction tests, and laboratory correlations. At the other UK sites, pressuremeter tests, total stress cells, and laboratory correlations were used to establish K_o.

San Francisco Bay Mud

As part of a joint research program between the University of California, Berkeley (UCB) and NGI, a series of dilatometer tests were run at UCB's research site, Hamilton Air Force Base (*18*), near San Francisco.

The San Francisco Bay Mud is a marine-deposited soft clay with a plasticity index in the range 45 to 55 percent and is lightly overconsolidated. K_o values where based on self-boring pressuremeter tests, total stress cells, and laboratory correlations.

Criteria for Selecting Values for the Data Base

The soil profiles were divided into layers, and only uniform clay layers were included in the data base. Each layer was represented by one (or two, if a thick layer) point(s) normally in the middle of the layer (or equally spaced if two). The depths of those points are presented as reference depths in Table 1. The laboratory and in situ test results for each layer were then found at each reference depth.

The original data base also included a number of offshore sites. Those are not included here because of doubt as to the reliability of the values of σ_h.

All relevant data were put into a spread sheet system. Table 1 gives part of the data base. Generally, the data from the offshore dilatometer have been used. However, when results from this device were not available, the Marchetti DMT information was substituted. As was discussed, the parameters K_D and E_D, as determined from the two DMTs, are very similar.

ANALYSIS OF DATA AND NEW CORRELATIONS

In Figures 11–13, the data from the spread sheet have been plotted as K_o versus K_D on a double logarithmic scale that was originally used by Marchetti. In Figure 11, values of plasticity index I_p have been noted beside each point. Similarly, Figures 12 and 13 indicate values of DMT material index I_D and normalized shear strength s_u/σ'_{v0}, respectively, beside each point in the plots. For the U.K. clays, undrained shear strength (s_u) from UU tests have been used; and for the other sites, s_u has been determined by consolidated undrained triaxial tests (CIU or CAU). Marchetti's original correlation is also included in the figures.

The following observations can be made:

1. Marchetti's correlation appears to overpredict K_o for young clays and underpredict K_o for the very old U.K. clays (Brent

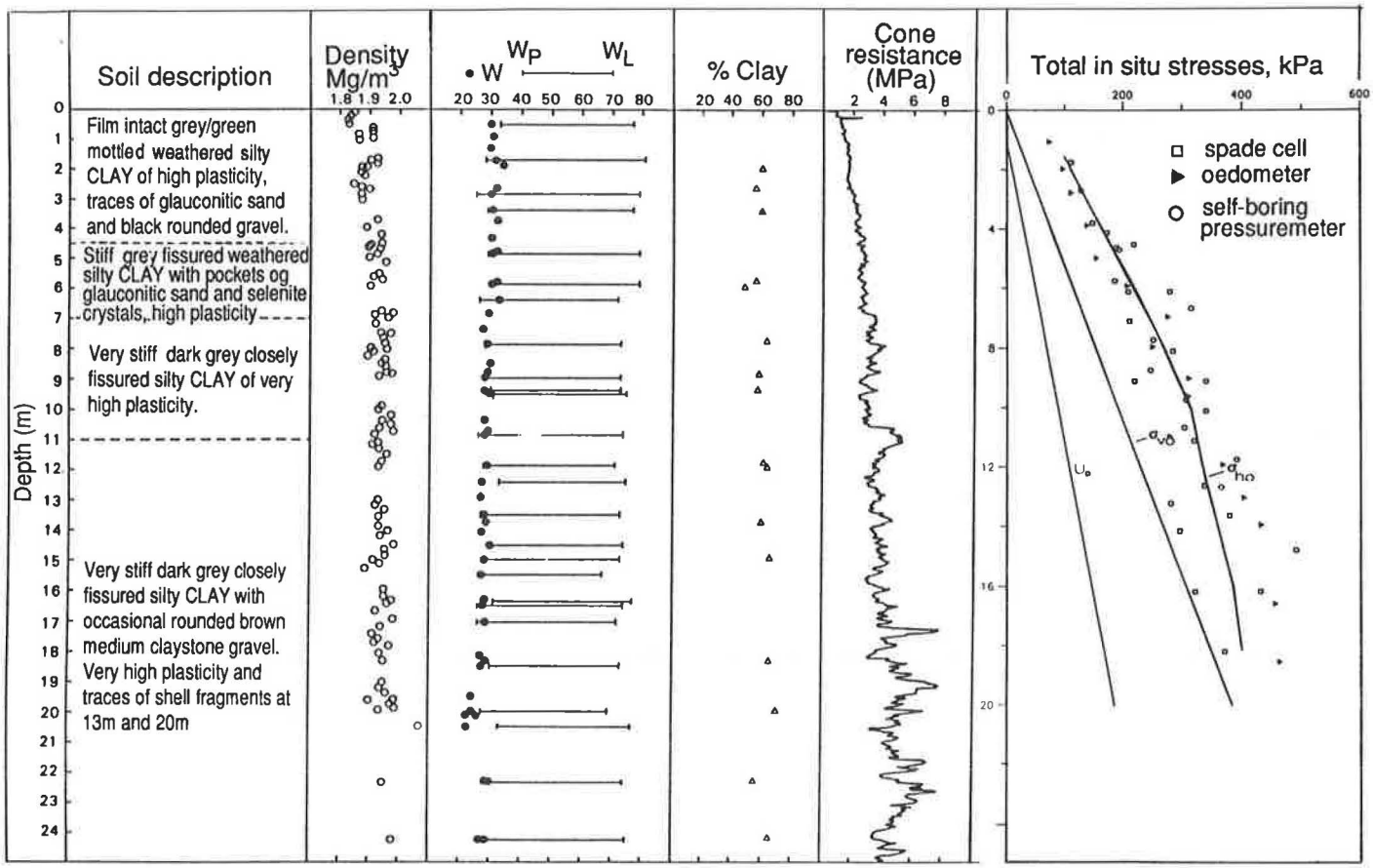

FIGURE 9 Madingley soil profile.

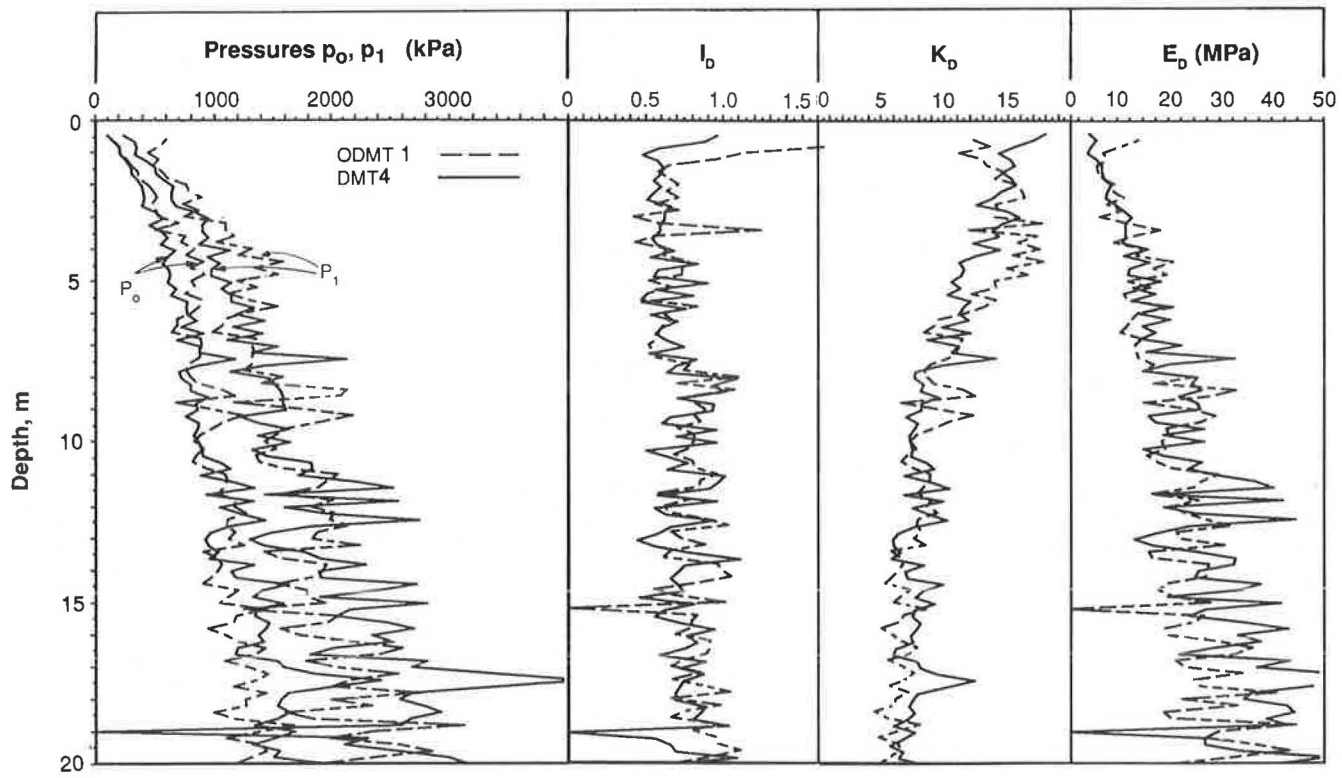

FIGURE 10 Dilatometer test results at Madingley.

TABLE 1 SUMMARY OF TEST SITES AND DILATOMETER TEST RESULTS

GENERAL				INDEX DATA					IN SITU STRESSES							DILATOMETER RESULTS						
TEST SITE	DEPTH INTERV. m	DEPTH REF. m	SOIL DESCRIPTION	wp %	Ip %	w %	Clay cont. %	Gamma kN/m³	U_o kPa	Sigma vert.eff. kPa	Sigma hor.eff. kPa	K_o	OCR	Su CAU kPa	St vane	Dilato-meter type	PO kPa	P1 kPa	ID	KD	ED MPa	REFER-ENCES
ONSOEY	4-5	5.0	CLAY, plastic clay	27	66	39	50	16.5	51	34	22	0.65	1.7	17.5	10	Offshore	201	223	0.15	4.41	0.68	4, 9
ONSOEY	5-15	7.0	CLAY, plastic clay	29	46	75	59	16.5	72	46	30	0.65	1.5	21.0	9	Offshore	228	255	0.17	3.39	0.83	
ONSOEY	15-20	16.0	Homogeneous, plastic clay	28	45	73	69	16.5	168	98	64	0.65	1.4	33.0	5	Offshore	476	525	0.16	3.14	1.51	
ONSOEY	20-40	24.0	Homogeneous, plastic clay	24	40	74	51	16.5	263	152	99	0.65	1.2	48.0	5	Offshore	667	740	0.18	2.66	2.26	
DRAMMEN	5-8	7.0	Plastic Drammen Clay	30	28	55	48	17.1	57	65	42	0.65	1.5	26.0	8	Offshore	255	275	0.10	3.05	0.62	4, 9
DRAMMEN	8-12	9.0	Plastic Drammen Clay	29	25	51	48	17.1	77	80	49	0.61	1.5	32.0	7	Offshore	305	329	0.11	2.85	0.74	
DRAMMEN	12.5-14	13.0	Lean Drammen Clay	23	17	34		19.1	116	113	62	0.55	1.2	38.4	5	Offshore	372	384	0.05	2.27	0.37	
DRAMMEN	14-16	15.0	Lean Drammen Clay	23	10	30		19.1	135	131	72	0.55	1.2	44.5	3.5	Offshore	411	421	0.04	2.11	0.31	
HAGA	1-2	1.5	Lean O.C. Clay	25	13	36	45	18.2	0	30	47	1.55	12.0	59.5	5	Onshore	241	333	0.38	8.03	2.84	15
HAGA	2-4	3.5	Lean O.C. Clay	27	16	40	50	18.0	0	70	69	0.98	4.5	63.0	4.5	Onshore	419	507	0.21	5.99	2.72	
HAGA	4-5	4.5	Plastic O.C. Clay	29	35	49	68	17.5	0	88	89	1.01	4.0	65.0	7	Onshore	547	699	0.28	6.22	4.70	
HAGA	5-6.5	6.0	Plastic O.C. Clay	25	17	36	45	18.4	0	118	85	0.72	2.2	65.5	4.5	Onshore	507	578	0.14	4.30	2.19	
HAGA	6.5-7.5	7.0	Plastic O.C. Clay	21	12	31	42	19.0	0	135	90	0.67	2.0	66.0	4	Onshore	520	584	0.12	3.85	1.98	
LIERSTR.	6-10	8.0	Plastic Drammen Clay	25	25	41	34	18.0	85	65	49	0.75	2.5	32.0	5.5	Offshore	345	383	0.15	4.00	1.17	Unpub-lished
LIERSTR.	10-15	12.5	Plastic Drammen Clay	24	25	42	34	18.1	140	93	60	0.65	1.8	35.0	4.5	Offshore	490	535	0.13	3.76	1.39	
LIERSTR.	15-25	20.0	Lean Drammen Clay	21	16	34	29	19.1	230	142	71	0.50	1.0	57.0	3.5	Offshore	648	672	0.06	2.94	0.74	
LIERSTR.	25-35	30.0	Lean Drammen Clay	20	12	27	20	19.1	341	220	99	0.45	1.0	85.0	3.5	Offshore	820	910	0.06	2.44	0.93	
BAY MUD	3-6	4.4	Soft, silty Clay	40	50	90	46	14.6	30	34	19	0.55	2.5	16.0	4	Offshore	131	177	0.46	2.97	1.42	18
BAY MUD	6-11	8.6	Soft, silty Clay	38	48	92	46	14.5	72	54	30	0.55	2.5	22.0	8	Offshore	198	240	0.33	2.33	1.30	
BAY MUD	11-16	13.4	Soft, silty Clay	39	48	94	46	14.4	119	77	54	0.70	1.2	32.0	6	Offshore	315	360	0.23	2.55	1.39	
BRENT	0-6	4.0	London weathered clay	26	54	30	54	19.1	26	50	182	3.64	> 60	66 [1]		Onshore	700	980	0.42	13.48	9.7	5, 6, 7
CROSS	6-9	8.0	London weathered clay	27	54	29	58	19.0	60	93	280	3.01	50	92 [1]		Onshore	930	1310	0.44	9.35	13.1	
	9-16	13.0	London unweathered clay	28	50	28	57	19.5	106	144	349	2.42	30	118 [1]		Onshore	1000	1640	0.72	6.21	22.1	
		16.0		28	45	27	60	19.5	133	175	393	2.25	25	136 [1]		Onshore	1250	1950	0.63	6.38	24.2	
COWDEN	0-5	3.0	Weathered Glacial till	21	20	18	30	21.4	20	44	130	2.95	11.5	141 [1]		Offshore	1138	3850	0.64	25.41	22.0	5, 6, 7
	5-10	7.0	Weathered Glacial till						30	55	80	1.45	6.5			Offshore	787	1110	0.44	7.30	10.0	
	10-12	11.0	Unweathered Glacial till	18	17	17	32	21.8	50	101	95	0.94	5	85 [1]		Offshore						
BOTHKENNAR	0-3	3.0	Soft black silty clay	27	35	58	36	16.0	25	23	20	0.87	1.6	17 [1]		Onshore	148	196	0.39	5.35	1.7	5, 6
	3-6	6.0		29	39	64	32	15.5	50	45	25	0.56	1.3	25 [1]		Onshore	222	274	0.30	3.82	1.8	
	6-9	9.0	Soft dark grey micaceous	31	44	68	26	15.2	80	60	35	0.58	1.3	34 [1]		Onshore	296	363	0.31	3.60	2.3	
	9-12	12.0	clay with thin silt	32	38	64	20	15.7	110	77	50	0.65	1.2			Onshore	385	474	0.32	3.57	3.1	
	12-15	15.0	laminations, more silty with depth	32	41	54	28	16.2	140	96	60	0.63	1.2	53 [1]		Onshore	460	570	0.34	3.33	3.8	
MADINGLEY	0-4	3.0	Firm intact silty clay	30	50	30	60	18.5	20	35	108	3.09	> 50	105 [1]		Offshore	550	900	0.66	15.14	10.8	5, 6, 7
	4-7	5.0	Stiff grey fissured clay	29	49	31	59	18.8	37	56	135	2.41	40	152 [1]		Offshore	780	1200	0.57	13.27	13.0	
	7-11	9.0	Very stiff fissured clay	29	44	30	61	19.0	72	96	188	1.96	25	130 [1]		Offshore	900	1500	0.72	8.63	18.5	
	11-20	15.0	Very stiff fissured silty	29	43	29	62	19.0	124	139	276	1.99	18	208 [1]		Offshore	1000	1700	0.80	6.30	21.6	
		20.0	clay. Very high plasticity.	28	43	28	65	19.1	168	191				220 [1]		Offshore	1600	2600	0.70	7.50	30.9	
CANONS	0-2	1.0	Gravel in a clay matrix					19.2		19												
PARK	2-4	3.0	Firm silty fissured clay	30	46	27	43	19.4	20	38	163	4.29		72 [1]		Offshore	500	723	0.67	12.63	10.0	5, 6
	4-7	6.0	Stiff silty fissured clay	28	40	28	42	19.6	43	73	287	3.93		115 [1]		Offshore	1234	1575	0.56	16.32	20.6	
	7-10	9.0	Blue London clay	28	44	29		19.6	66	109	274	2.51		120 [1]		Offshore	1128	1617	0.68	9.74	22.3	

[1] UU tests

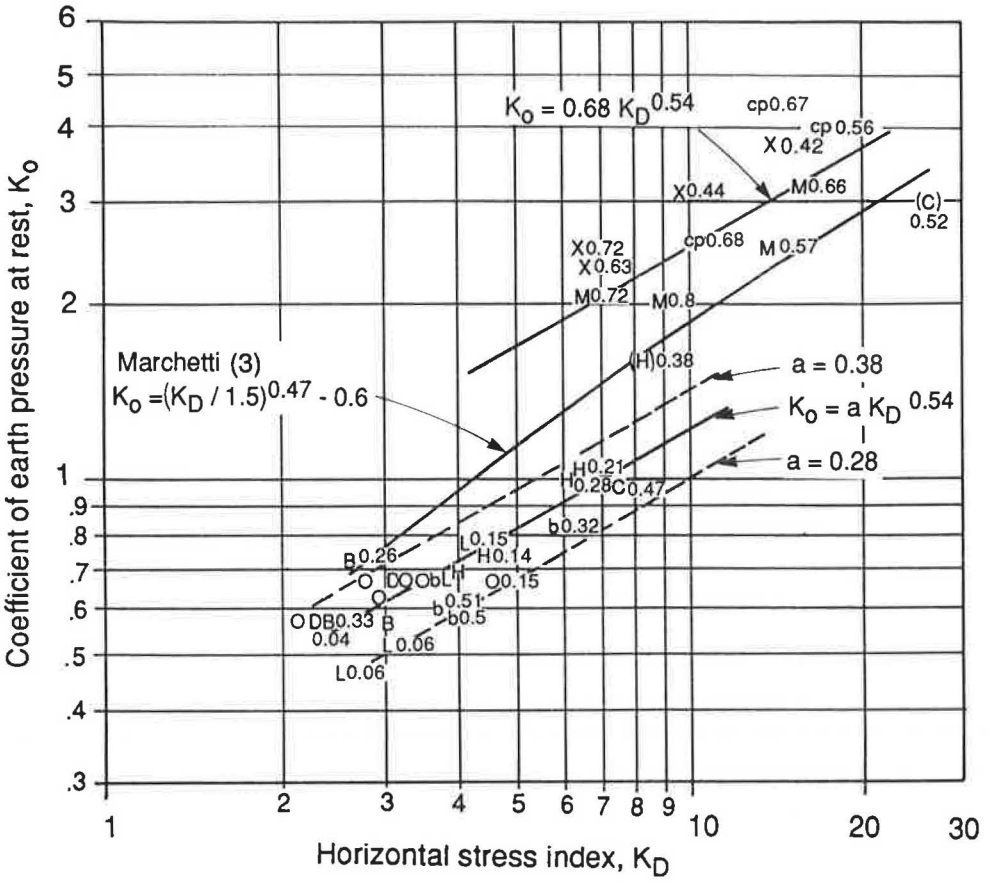

LEGEND:

Brent Cross:	X
Cowden:	C
Bothkennar:	b
Madingly:	M
Canons Park:	cp
Onsoey:	O
Drammen:	D
Haga:	H
Lierstranda:	L
Bay Mud:	B

FIGURE 11 K_D versus K_o with values of I_p.

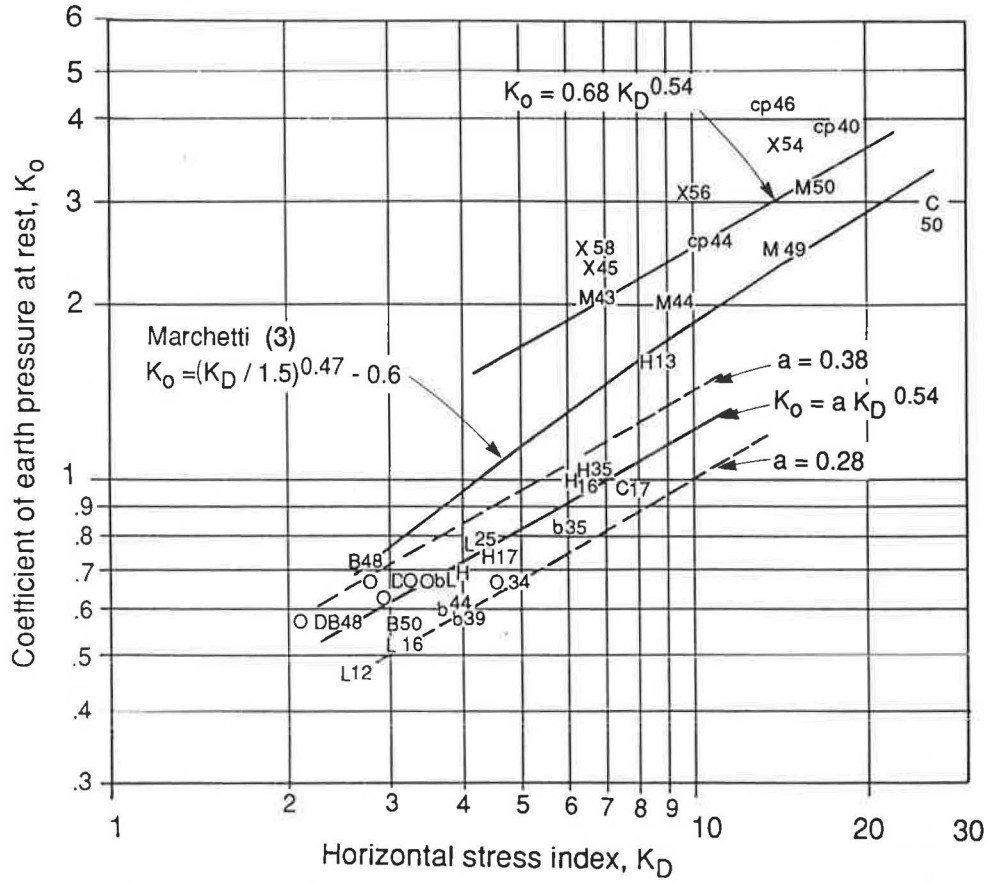

LEGEND:

Brent Cross:	X
Cowden:	C
Bothkennar:	b
Madingly:	M
Canons Park:	cp
Onsoey:	O
Drammen:	D
Haga:	H
Lierstranda:	L
Bay Mud:	B

FIGURE 12 K_D versus K_o with values of I_D.

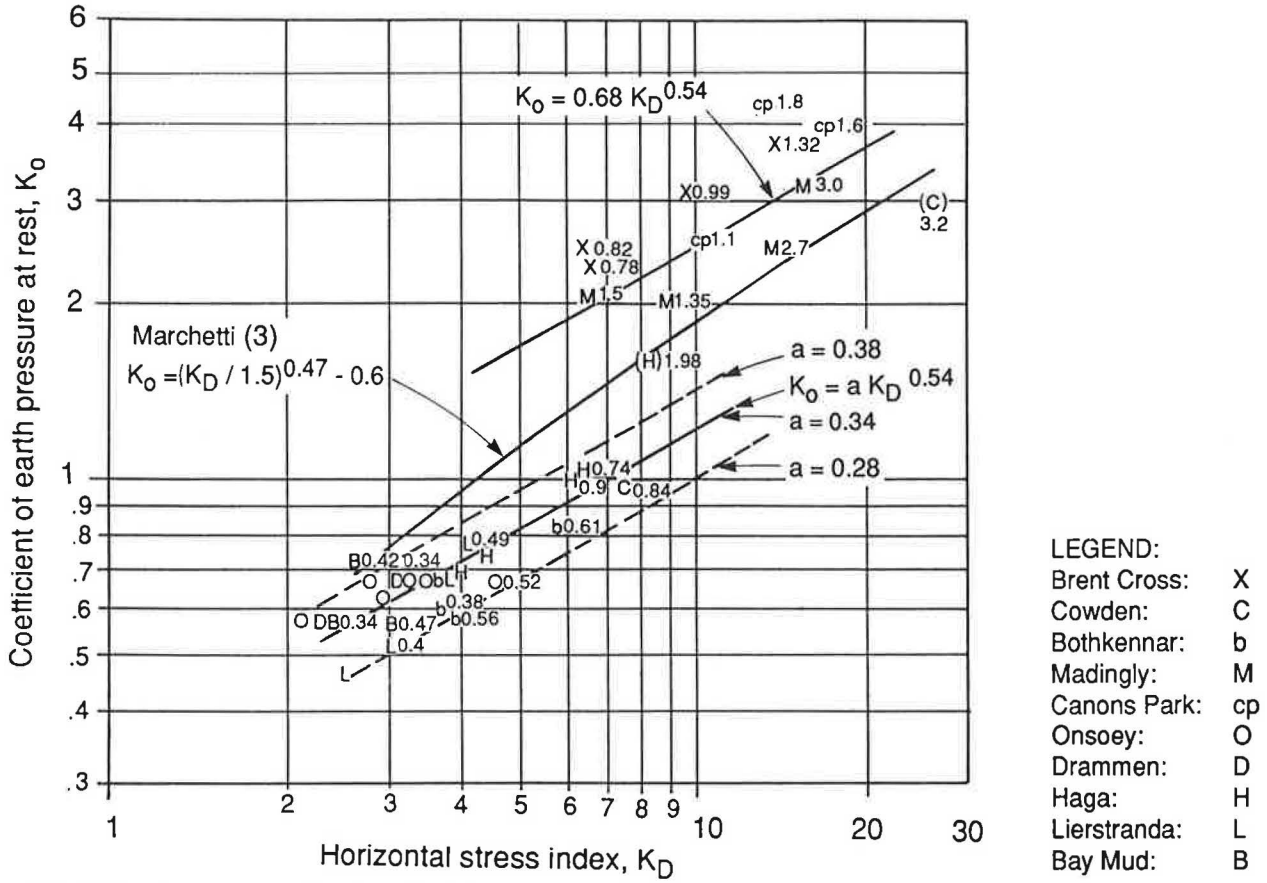

FIGURE 13 K_D versus K_o with values of s_u/σ'_{v0}.

Cross, Madingley, and Canons Park). This confirms the finding of Powell and Uglow (*6*).

2. Young clays fall within a relatively narrow band, which can be expressed as

$$K_o = a \cdot K_D^{0.54}$$

where a on the average is 0.34, but it varies between 0.38 and 0.28.

3. Referring to Figures 11 and 12 and the band for the "young" clays, there does not appear to be any systematic trend with I_p or I_D, and neither is it possible to differentiate between the "old" and the "young" clays on the basis of those two parameters.

4. Although not completely conclusive, Figure 13 indicates that s_u/σ'_{v0} may be used to separate the old from the young clays. Here, the way of measuring s_u is very important (test method and sample size, particularly in the older fissured clays).

5. Referring to Figure 13, on average, K_o for the "old" clays is related to K_D as $K_o = 0.68 \cdot K_D^{0.54}$ with a wide scatter band. However, for any one site and clay layer a site-specific correlation would appear to exist.

Figure 14 plots p_1-p_0 versus p_1-σ_h as proposed by Clarke and Wroth (*12*). The figure also includes the correlation found by Clarke and Wroth. Especially for low values of p_1-p_0, there is too much scatter for this approach to be useful, and, furthermore, it falls away from the original correlation line (*12*).

On the basis of this, what follows is recommended:

1. Use s_u/σ'_{v0} or general geological evidence to group the clay as "old" or "young." Young clays generally have $s_u/\sigma'_{v0} < 0.7$ and old clays generally > 0.7.

2. If the clay is young, then use the correlation $K_o = 0.34 \cdot K_D^{0.54}$. The uncertainty associated with this correlation is unlikely to exceed ± 20 percent.

3. For old clays, either use has to be made of existing experience on that soil type to establish a correlation or, if some information on K_o and OCR is known for the site (1 or 2 values), then those should be plotted against K_D on Figure 13 and a new correlation drawn through them parallel to the $K_D = 0.68 \cdot K_D^{0.54}$ line.

Most clays are "young" clays.

Obviously, the new correlations do not fit with Marchetti's data. One likely explanation is that Marchetti (*3*) determined K_o based on OCR from laboratory oedometer tests and then used the empirical correlation of Brooker and Ireland (*17*). Thus, the K_o values may not be representative of the in situ condition.

The new data, for a wide range of clays from different parts of the world, are all based on direct in situ measurements by using self-boring pressuremeter, hydraulic fracture, total stress cells, and other relevant tests. There are also uncertainties

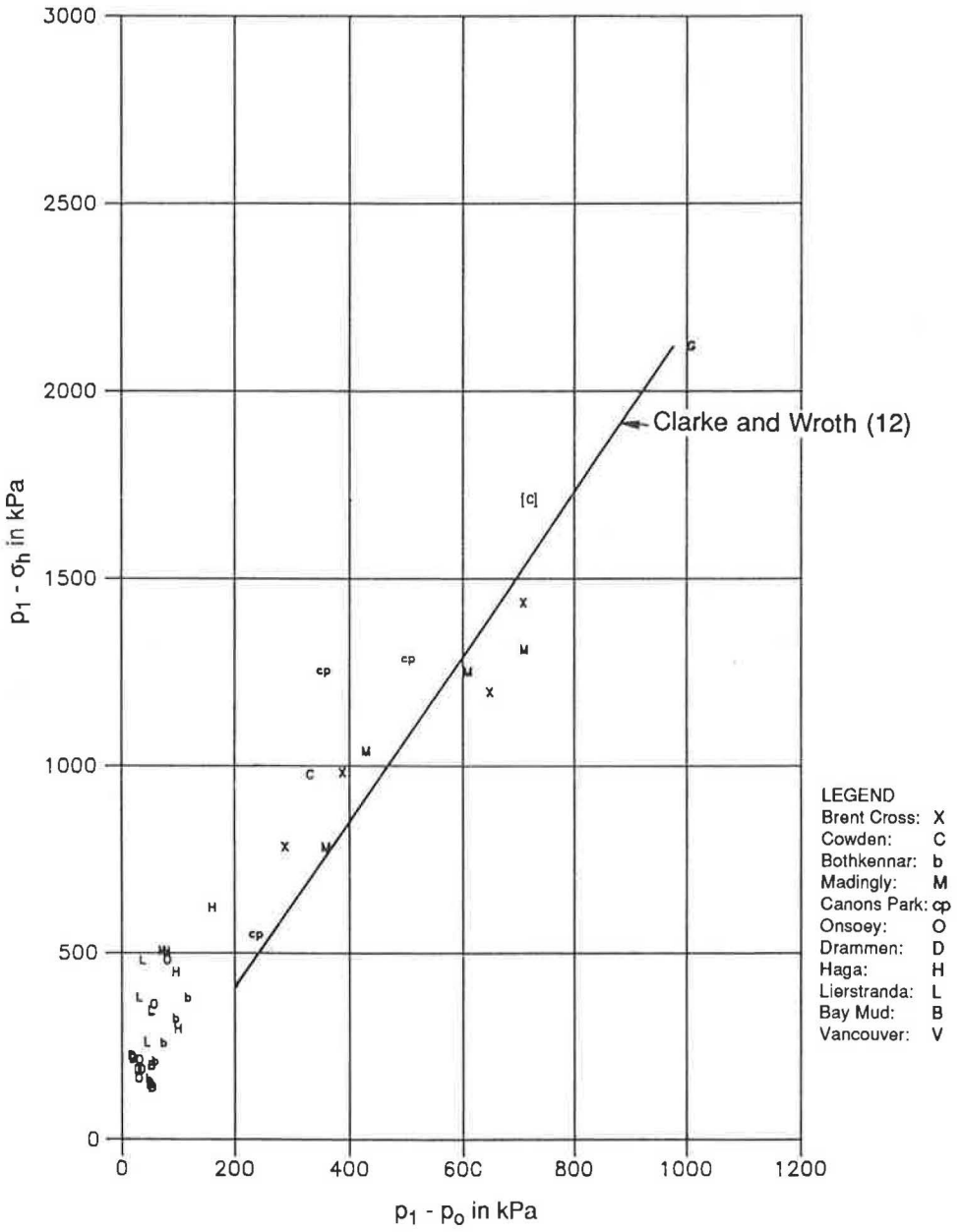

FIGURE 14 $p_1 - p_0$ versus $p_1 - \sigma_{h0}$.

associated with those values but much less so than those determined from empirical correlations.

ACKNOWLEDGMENTS

The contribution of BRE to this project forms part of the research program of the Building Research Establishment and is published with the permission of the director. The authors would like to acknowledge the support to the project of the following companies: Norsk Hydro A.S., Saga Petroleum A.S., and BP Petroleum Development (Norway) Ltd.

REFERENCES

1. J. H. Schmertmann. *Measure and Use of the In Situ Lateral Stress.* Osterberg Volume, Northwestern University, Evanston, Ill., 1986, pp. 189–213.
2. T. Lunne, S. Lacasse, N. S. Rad, and L. Decourt. SPT, CPT, Pressuremeter Testing and Recent Developments on In Situ Testing. Presented at 12th International Conference on Soil Mechanics and Foundation Engineering, Rio de Janeiro, 1989.
3. S. Marchetti. In Situ Tests by Flat Dilatometer. *Journal of the Geotechnical Engineering Division*, ASCE, Vol. 106, No. GT3, 1980, pp. 299–321.
4. S. Lacasse and T. Lunne. Calibration of Dilatometer Correlations. *Proc., International Symposium on Penetration Testing ISOPT-1*, Orlando, Fla. Vol. 1, 1988, pp. 539–548.

5. J. J. M. Powell and I. M. Uglow. Marchetti Dilatometer Testing in UK Soils. *Proc., International Symposium on Penetration Testing ISOPT-1*, Orlando, Fla., Vol. 1, 1988, pp. 555–562.
6. J. J. M. Powell and I. M. Uglow. The Interpretation of the Marchetti Dilatometer Test and UK Clays. *Proc., Conference on Penetration Testing in the UK*, Birmingham, 1988, pp. 269–273.
7. J. J. M. Powell, R. S. T. Quarterman, and T. Lunne. Interpretation and use of Piezocones in UK Clays. *Proc., Conference on Penetration Testing in the UK*, Birmingham, 1988, pp. 151–156.
8. A. J. Lutenegger. Current Status of the Marchetti Dilatometer Test. *Proc., International Symposium on Penetration Testing ISOPT-1*, Orlando, Fla., Vol. 1, 1988, pp. 137–156.
9. S. Lacasse and T. Lunne. Dilatometer Tests in Two Soft Marine Clays. Presented at Conference on Updating Subsurface Sampling of Soils and Rocks and Their In Situ Testing, Santa Barbara, Calif., Jan. 1982.
10. R. Roque, N. Janbu, and K. Senneset. Basic Interpretation Procedures of Flat Dilatometer Tests. *Proc., International Symposium on Penetration Testing ISOPT-1*, Orlando, Fla., Vol. 1, 1988, pp. 577–588.
11. N. Janbu and K. Senneset. Effective Stress Interpretation of In Situ Static Penetration Tests. *Proc., European Symposium on Penetration Testing ESOPT 1*, Stockholm, Vol. 2.2, 1974, pp. 181–193.
12. B. Clarke and P. Wroth. Comparison Between Results From Flat Dilatometer and Self-Boring Pressuremeter Test. *Proc., Conference on Penetration Testing in the UK*. Birmingham, 1988, pp. 295–298.
13. G. Houlsby. Discussion of Paper 41. *Proc., Conference on Penetration Testing in the UK*, Birmingham, 1988, p. 319.
14. T. Lunne, R. Jonsrud, T. Eidsmoen, and S. Lacasse. The Offshore Dilatometer. Presented at 6th International Symposium on Offshore Engineering: Brasil Offshore '87, Rio de Janeiro, Aug. 1987.
15. K. Karlsrud and T. Haugen. Axial Static Capacity of Steel Model Piles in Overconsolidated Clay. *Proc., ICSMFE 11*. San Francisco, Calif., Vol. 3, 1985, pp. 1401–1406.
16. G. Aas, S. Lacasse, T. Lunne, and K. Høeg. Use of In Situ Tests for Foundation Design on Clay. *Proc., ASCE Special Conference, In Situ '86: Use of In Situ Tests in Geotechnical Engineering*, Blacksburg, Va., 1986, pp. 1–30.
17. E. W. Brooker and H. O. Ireland. Earth Pressure at Rest Related to Stress History. *Canadian Geotechnical Journal*, Vol. 2, No. 1, 1965, pp. 1–15.
18. T. Masood, J. K. Mitchell, T. Lunne, and E. A. Hauge. In Situ Testing at Hamilton Air Force Base and Bay Farm Island, California. Department of Civil Engineering, University of California, Berkeley, 1988.

Publication of this paper sponsored by Committee on Soil and Rock Properties.

Determination of In Situ Lateral Stresses in a Dense Glacial Till

ALAN J. LUTENEGGER

A comparison of different techniques for determining in situ lateral stresses in a dense glacial till is presented. The site is located north of Des Moines, Iowa, in the late Wisconsinan drift plain. The till is generally composed of a cohesive matrix (P.I. = 12; L.I. = 0) and extends to a depth of 19 m. In situ tests conducted at the site included flat dilatometer (DMT), full-displacement pressuremeter (FDPMT), hydraulic fracture (HFT), and prebored pressuremeter (PMT) tests. Push-in earth pressure cells were installed at various depths and were allowed to come to equilibrium to provide an upper-bound value of the in situ lateral stress conditions. Those data are also compared with DMT dissipation tests, which give an equilibrium value of σ_H. A comparison of the effective horizontal stresses obtained with the in situ tests is presented and is based on field pore pressure measurements obtained from electric and pneumatic piezometers. Estimates of the at-rest coefficient of earth pressure, K_o, were made and are based on laboratory tests, using empirical relationships between K_o and OCR. OCRs were obtained from incremental loading laboratory oedometer tests. The work energy method was also used to predict in situ effective horizontal stresses, using results of oedometer tests on horizontally trimmed samples. Results indicate that full displacement tests, such as the DMT, HFT, and FDPMT, tend to overestimate the in situ stresses while the nondisplacement PMT provided results very close to the spade cell and laboratory data. A discussion of the test results is presented concerning the accuracy of each of the tests in predicting in situ stresses in dense cohesive soils.

The prediction of at-rest horizontal stresses in natural soils often represents one of the more difficult tasks in geotechnical engineering and yet has a wide application in practice. Currently, there are a number of well-known field methods to estimate in situ lateral stresses in cohesive soils and a number of techniques that use results of laboratory tests on undisturbed samples. Generally, the prediction of K_o in softer and normally consolidated clays does not present a particularly difficult task, because theoretical and empirical methods for estimating K_o provide reasonably accurate values for most design situations. Conversely, stiff or highly overconsolidated cohesive deposits present somewhat of a formidable problem: there are limited data in the literature from field investigations and what constitutes a reasonable estimate of K_o is not clearly defined.

In the midcontinental United States, abundant cohesive glacial till deposits are present and provide the base for both deep and shallow foundations. Deep excavations in many areas are also conducted in those materials, and, therefore, the in situ state of horizontal stresses is of some practical significance for design. The tills are matrix dominated in most areas (i.e., composed of sand, silt, and clay and generally behave as cohesive soils). The tills are often very dense and stiff because of the mechanics of glacial deposition, and there is a tendency to think that the soils are highly overconsolidated. This can lead to the belief that the in situ lateral stresses are high, although this has never been directly substantiated.

To study the magnitude of lateral stresses that exists in those deposits, a site consisting of Late Wisconsinan glacial deposits near Ames, Iowa, was selected for laboratory and field investigation. In situ lateral stresses were estimated on the basis of field measurements by using several in situ test methods and were predicted on the basis of the results of laboratory tests on undisturbed samples. The purpose of this paper is to present the results of tests conducted and to provide a comparison of the results.

SITE GEOLOGY AND SOIL CONDITIONS

The site investigated is located near Ames, Iowa, in a physiographic region known as the Late Wisconsinan Drift Plain. The surficial geologic sediments are glacial deposits, representing the advance and retreat of the Late Wisconsinan glacier into the area about 12,000 years ago. The glacial sediments in this area generally fall into two broad genetic classifications: (a) subglacial till (representing materials transported and deposited beneath or near the base of the ice mass) and (b) supraglacial diamicton (representing materials transported and deposited on or in the ice mass). Those two materials have widely different geotechnical characteristics that result from the transport and depositional modes.

The subglacial till (often referred to as "basal" till) is generally dense to very dense and is very uniform in composition. By contrast, the supraglacial diamictons (often referred to as "ablation" till) are much more heterogeneous and can range from poorly sorted to well sorted and are often highly stratified depending on the degree to which water has dominated the transport or deposition. Those materials tend to be less dense and often are loose when compared with the subjacent subglacial till. Detailed studies of differences in geotechnical characteristics of those deposits in the study area have been previously described (*1*).

Subsurface conditions at the investigated test site are generally representative of a wide geographical area in the state and, on the basis of other regional site investigations, are typical of the glacial deposits. Beneath the soil solum, the sediments are oxidized and mottled down to a depth of about 4 m. Immediately below this the soil color changes from brown to gray, indicative of unoxidized conditions. The water level in numerous boreholes at the time of field investigations was

Department of Civil Engineering, University of Massachusetts, Amherst, Mass. 01003.

measured at about 1.5 m; however, the soil colors indicate that past water levels have been as low as the boundary between the oxidized and unoxidized materials (i.e., at a depth of about 4 m). Pneumatic and vibrating wire piezometers installed at the site indicate that in situ pore water pressures are hydrostatic in the till. The unoxidized zone represents a condition of permanent saturation and negligible oxygen activity, which accounts for the gray colors. Investigations were performed to a depth of 18.3 m and ended near the base of the unoxidized till, which is at about 22 m.

Geotechnical characteristics of the site are illustrated in Figure 1. While the grain-size distribution and plasticity data shown indicate that the site is very uniform, in actuality the upper 2 m was quite stratified on the basis of visual classification of a CME continuous core. Water content and plasticity data all show that the natural water content is very close to or less than the plastic limit, which gives a liquidity index near zero. Thus, the soils may be highly overconsolidated.

Grain-size distributions obtained by hydrometer analysis indicate that the tills are matrix dominated (i.e., clay-silt-sand) and cohesive. Matrix carbonates constitute almost 20 percent of the composition and are dominated by dolomite. Previous studies of the clay mineralogy of this till indicate that the dominant mineral is montmorillonite (*2*).

SITE INVESTIGATION

Drilling and sampling at the site were performed by using hollow stem augers and 76-mm-diameter Shelby tubes at 1.5 m intervals. A standard penetration test profile was conducted in an adjacent borehole through the center of the hollow stems. Shelby tube samples were used to conduct oedometer tests and laboratory shear strength tests. Oedometer specimens were trimmed in both vertical and horizontal directions. Tests were performed on 63-mm-diameter samples in fixed-ring lever-arm consolidometers by using a load duration of 24 h and a load increment ratio of 1. Determination of the oedometric yield stress (preconsolidation stress) was made by the Casagrande construction. A summary of geotechnical properties is presented in Figure 2.

Results of oedometer tests interpreted in the conventional sense show that the soils are generally normally consolidated below a depth of about 8.4 m. SPT blow counts and undrained shear strength determined from unconfined compression and CIUC triaxial tests show stiff to very stiff materials.

In situ tests were conducted at various depths throughout the profile to provide an estimate of in situ lateral stresses. Those included Marchetti dilatometer (DMT), prebored (Menard) pressuremeter (PMT), full-displacement pressure-

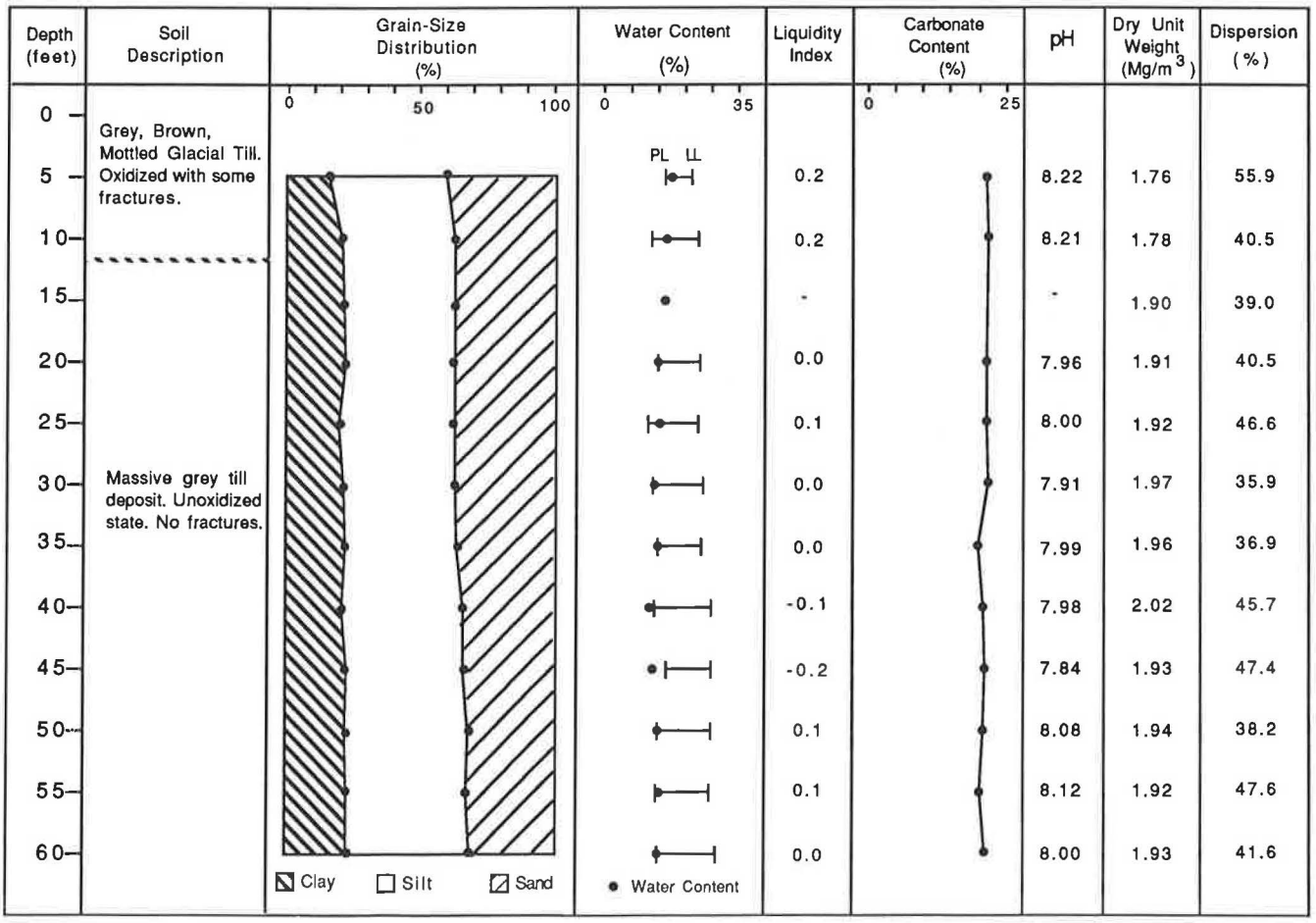

FIGURE 1 Subsurface site characteristics.

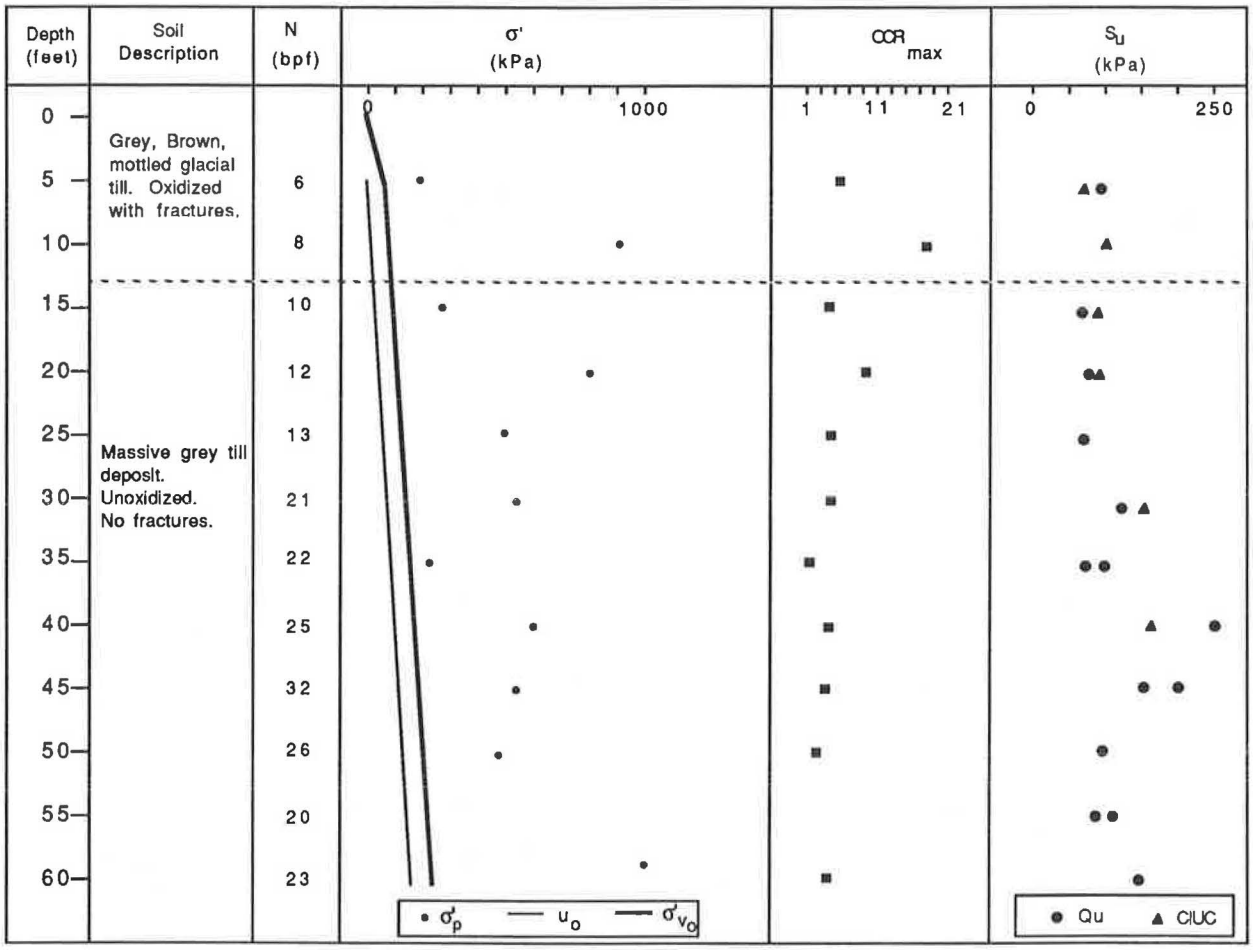

FIGURE 2 Site geotechnical characteristics.

meter (FDPMT), and hydraulic fracture (HFT) tests. DMT, FDPMT, and HFT represent a "full-displacement" method of installation (i.e., soil is forced away to install the measurement device). PMT represents a nondisplacement method of insertion and is actually installed after soil unloading. Clearly, the method of installation will affect the measured soil response. A brief description of the test procedures used for each test follows.

Dilatometer Tests

DMT tests were conducted by using a modification of the procedure suggested by ASTM subcommittee D18.02 (*3*). In addition to obtaining the lift-off (P_0) and 1 mm (P_1) expansion pressures, the recontact pressure obtained by controlled deflation (P_2) was also recorded. In soft saturated and normally consolidated clays, this last pressure reading has been shown to closely match the penetration pore pressures created by advancing the DMT blade (*4,5*). Beginning at the ground surface, tests were performed at 0.3-m intervals throughout the entire 18-m profile.

Tests were also performed by using the DMT as a total stress spade cell. After installation, repeated measurements of the lift-off (P_0) pressure were made without obtaining the P_1 reading. In this way the change in total stress on the face of the blade as a function of time after installation was obtained. Measurements were made at each test depth until a stable value of P_0 was obtained.

Prebored Pressuremeter Tests

Because the till is stiff and contains occasional gravel particles, self-boring pressuremeter tests would not be feasible. Instead, tests were performed by using prebored probe. Tests were conducted in 76-mm-diameter Shelby tube cavities, using an NX-size PMT probe. A monocell probe (sans guard cells) with a nominal height/diameter ratio of 6 was used. The probe is designed with twin sets of instrumented strain arms located at 120 degree increments around the diameter of the probe such that the strain response in three directions would be obtained. Nitrogen is used as the expansion medium. Therefore, the problems with deairing a liquid-filled probe are eliminated.

Tests were performed by using a metallic-sheathed rubber membrane. Testing was performed through the hollow stem augers immediately after opening the borehole cavity. Sufficient data points were obtained to define the in situ stress condition accurately by using graphical interpretation. Total testing time for each test was approximately 40 min.

Full Displacement Pressuremeter Tests

The FDPMT is a total stress expansion test that measures the soil response to insertion and expansion of an assumed cylindrical cavity. FDPMTs were conducted by using a Pencel pressuremeter, which was pushed into the ground at a rate of 200 mm/sec by using the quasi-static thrust of the drilling rig.

The probe has a diameter of 28 mm and is designed with a nominal cavity length to diameter ratio of 7. A 60 degree apex cone is attached to the front of the probe at about 6 diameters from the center of the probe. Because fluid is used in the cavity, the probe acts like a pressure cell during installation and the cavity total stress immediately after installation may be obtained.

Tests were performed by using two techniques: (a) immediately after installation the probe was expanded to give the cavity pressure/radial strain response and (b) after installation the total stress acting on the probe was allowed to come to equilibrium prior to conducting the cavity expansion. In both cases, a simple electrical screw pump was used to expand the probe.

Hydraulic Fracture Tests

HFTs were performed by using a push-in Casagrande-type piezometer. The probe consists of a bronze filter element 92 mm in length with an external diameter of 32 mm, giving a length-to-diameter ratio of 2.9. The tip of the probe was located 5 diameters in front of the leading edge of the filter and was constructed with a 60-degree apex.

Test procedures for hydraulic fracture have been described by Bjerrum and Andersen (*6*) and essentially involve pushing the piezometer to the test depth, forcing water through the piezometer, and then monitoring the change in water pressure with the increased volume of pushed fluid. Fluid volume was injected at a constant rate by using an electrical screw pump, and water pressure was measured by using a simple pressure gauge control console. Tests were conducted in three stages, referred to as first fracture, close up, and reopen.

First fracture refers to the first hydraulic fracture generated after the probe was pushed to the test depth. The point where this occurred was indicated by a sudden drop or a leveling off in pressure during pumping. After this occurred, the fracture was allowed to close by stopping the screw pump and then recording the drop in pressure with time. When the fracture closed, there was a sharp break in the rate of water flow into the soil. Following this, water was again forced into the fracture by using the same first-fracture procedure to reopen the fracture.

Spade Cells

To provide a basis for comparison of the in situ and laboratory test results, four push-in spade cells were installed at the site and were allowed to come to equilibrium. Earth pressure cells, manufactured by Soilinst, Inc., with dimensions of 200 mm $\times$ 100 mm and a thickness of 5 mm, were statically pushed at the bottom of drilled holes at depths of 3.0, 4.5, 7.6, and 13.7 m. Spade cells have been in place for over 5 months and are being monitored at the present time (December 1989). The use of similar spade cells for estimating in situ lateral stresses in cohesive soils has been described by a number of researchers (*7–9*).

INTERPRETING IN SITU LATERAL STRESSES FROM IN SITU TESTS

Dilatometer Tests

Marchetti had presented an empirical correlation between the DMT parameter K_D and K_o with K_D defined as

$$K_D = \frac{P_0 - u_0}{\sigma_{v0} - u_0} \tag{1}$$

in which P_0 is DMT "lift-off" pressure, u_0 is in situ pore water pressure, and σ_{v0} is in situ vertical total stress. The value of K_o in this correlation was primarily based on interpretation of laboratory oedometer tests by using the Brooker and Ireland (*10*) correlations between OCR and PI and K_o. Therefore, the accuracy of the prediction of K_o is directly related to the accuracy of the prediction of OCR.

The results of DMT tests are presented in Figure 3, in which the DMT pressure readings, P_0, P_1, and P_2 are presented along with the parameter K_D and interpreted K_o values at each 0.3 m depth. There is a rapid increase in P_0 down to a depth of about 3 m, after which the increase with depth is more gradual. K_o values interpreted from the DMT are all above a value of 1 and show a gradual decrease with increasing depth.

In clays it has been shown (*4*) that the value of P_2 represents a close approximation of the pore water pressures acting on the face of the blade as a result of penetration. Therefore, the difference $P_0 - P_2$ should closely approximate the effective horizontal stress acting on the face of the blade shortly after penetration. Those values are presented in Figure 4 in comparison with the predicted values of σ'_{H0} from the DMT K_o values. The values of $P_0 - P_2$ are about 2–3 times higher than the predicted σ'_{H0}, which may suggest that significant initial overstressing occurs in those materials as a result of the blade penetration, assuming, that is, that the DMT values are reasonably close to the correct values. This behavior is opposite of what occurs in softer clays where the initial horizontal effective stresses are very low and in fact are much lower than at-rest stresses [e.g., as measured with the piezolateral stress cell (*11*)]. This behavior is also consistent with results of spade cells (*8*), which show significant overstressing effects in stiff clays. In soft clays, spade cells generally return to K_o horizontal stress conditions.

The DMT was also used as a "spade cell" in the upper 13.7 m by conducting only the first pressure expansion or "lift-off" inflation until a constant stress reading was obtained. An example of a typical response is presented in Figure 5. Generally, equilibrium was reached in a short period, usually less than 4 hr. Those measurements represent the total horizontal stress acting on the face of the blade following dissipation of pore water pressure and relaxation of total stress generated during penetration. Those are not at-rest horizontal stresses but are in situ horizontal stresses created as a result of the

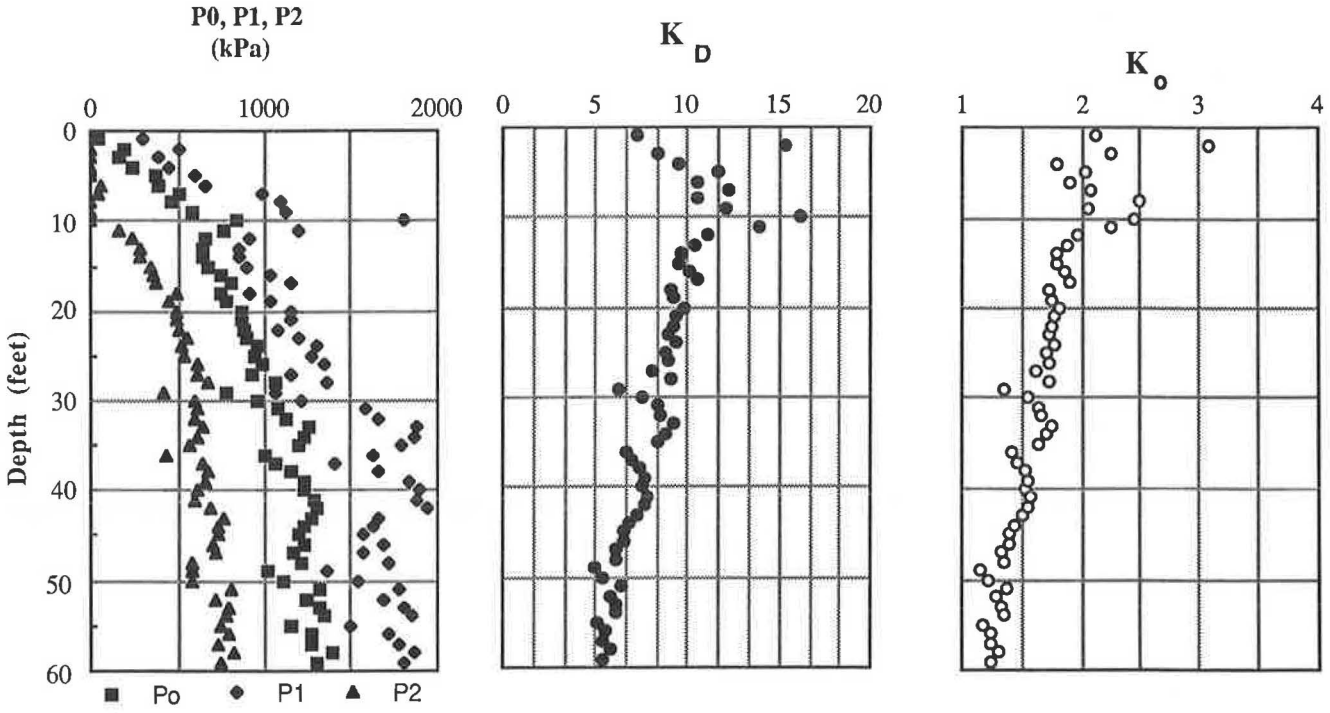

FIGURE 3 DMT results and prediction of K_o.

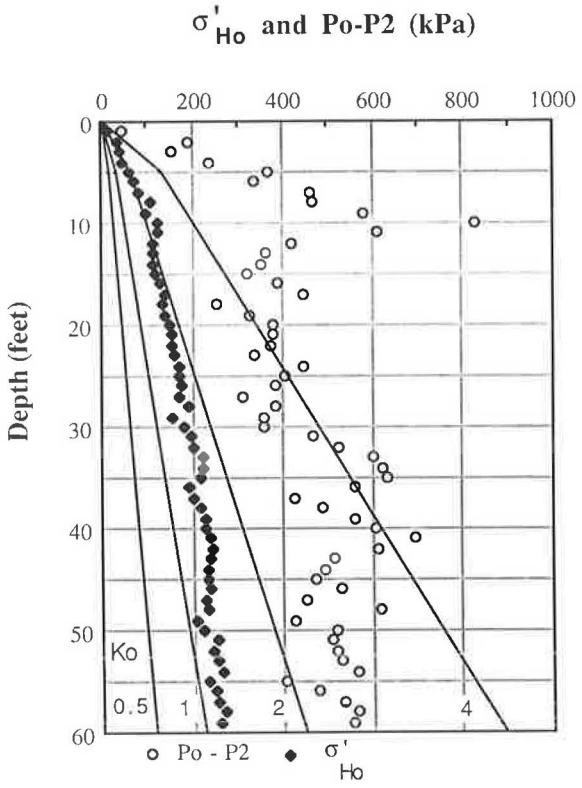

FIGURE 4 Comparison of DMT-predicted σ_{H0} and $P_0 - P_2$.

blade penetration. They may be thought of as representing an absolute upper-bound value of horizontal stress (i.e., the actual at-rest stresses must lie below those values). Thus, they provide a boundary below which all other estimates of in situ lateral stresses must lie. The profile of those values, corrected for in situ pore water pressure, are presented in Figure 6 along with lines of effective horizontal stress for various K_o values.

The trend in Figure 6 indicates increasing effective stress with depth, which would be expected in a material with a

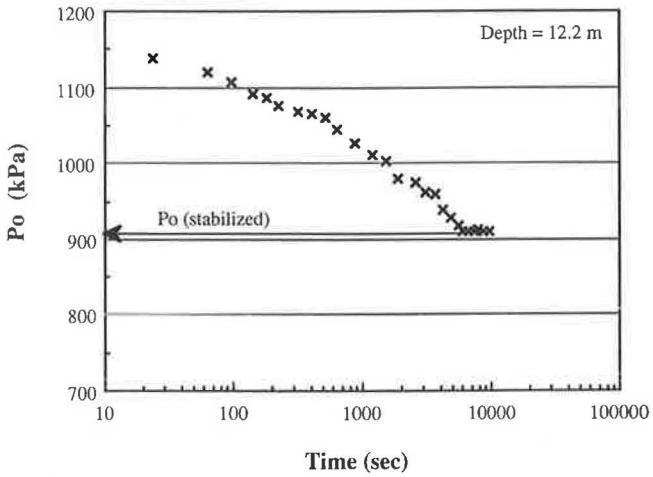

FIGURE 5 Typical results of DMT P_0 dissipation test.

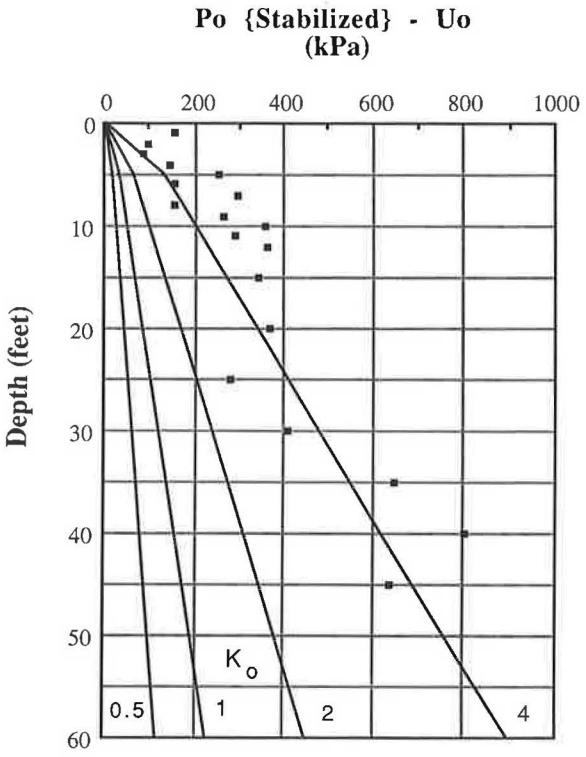

FIGURE 6 DMT P_0 dissipation results.

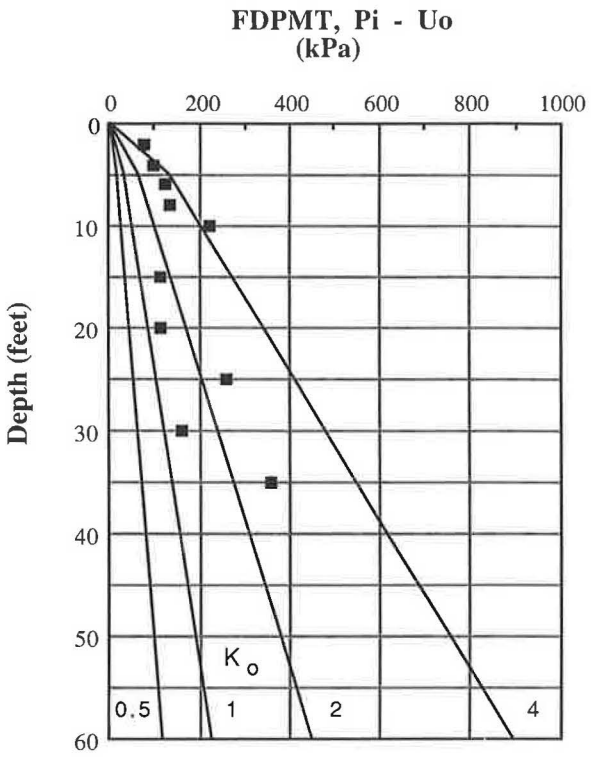

FIGURE 7 Results of full-displacement pressuremeter stabilization tests.

constant K. The values, however, indicate stress conditions generally well above a K_o value of 4 in the upper 6 m, which may seem unrealistic.

Full-Displacement Pressuremeter Tests

The insertion of the cylindrical probe of the FDPMT is much like the installation of a fluid-filled stress cell. In this study, the probe was installed by quasi-static penetration in the same way that the DMT was installed. After insertion, the stress was allowed to come to equilibrium in the same way that the DMT P_0 dissipation tests were conducted (i.e., sufficient time was allowed for the stress to reach a constant value).

The results of those stabilization tests are presented in Figure 7. Those results are generally lower than those measured with the DMT P_0 dissipation tests.

Hydraulic Fracture Tests

HFTs were interpreted by using the reopen curve following initial fracture and close up. In this way it is postulated that any tensile strength in the soil is eliminated from the stress measurement. A typical fracture curve is presented in Figure 8. The abrupt drop in pressure on first fracture represents a brittle response and was typical for most of the tests conducted in this stiff till. This is unlike fracture tests conducted in softer clays or silts by using the same probe (*12*) in which the first fracture and reopen stresses are nearly the same.

The majority of the literature concerning HFT in clays has suggested that it is not possible to measure horizontal stresses higher than vertical stresses, despite the fact that K_o values greater than 1 have been reported in a number of cases (*13,14*). The estimate of horizontal stresses in soils, using hydraulic fracture, is predicated on the fact that a vertical fracture must develop. In the past (*6,13,15*), HFT, using push-in piezometers, used a probe with a short filter located on or just above the conical tip. Lefebvre et al. (*16*) have shown that an increase in the length of the filter element increases the likelihood that a vertical fracture will develop. In the present study, the probe had a long ($L/D \approx 3$) filter located 5 diameters behind the tip. This increases the likelihood of developing vertical fractures in the soil and thus the measurement of horizontal stresses. This is also consistent with cylindrical cavity expansion theory (*17*).

The results of HFTs conducted at the site are presented in Figure 9. Two of the tests did not show brittle behavior and gave low stresses. The probe may have been in sand lenses at those two depths. The magnitude of stresses indicated in Figure 9 are close to DMT P_0 dissipation stresses previously illustrated in Figure 6 but higher than the FDPMT results in Figure 7.

Spade Cells

Tedd and Charles (*8*) suggested that a correction should be applied to the stresses measured with spade cells to account for the over stress created by insertion. The tentative correction is based on undrained shear strength, in this case obtained from unconfined compression and CIUC triaxial tests. The results of spade cell readings, both uncorrected and corrected, are presented in Figure 10. The spade installed at a depth of

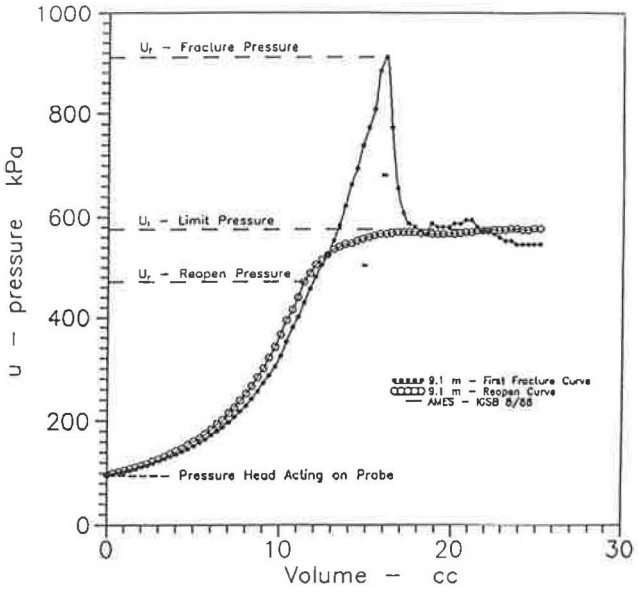

FIGURE 8 Typical hydraulic fracture test results.

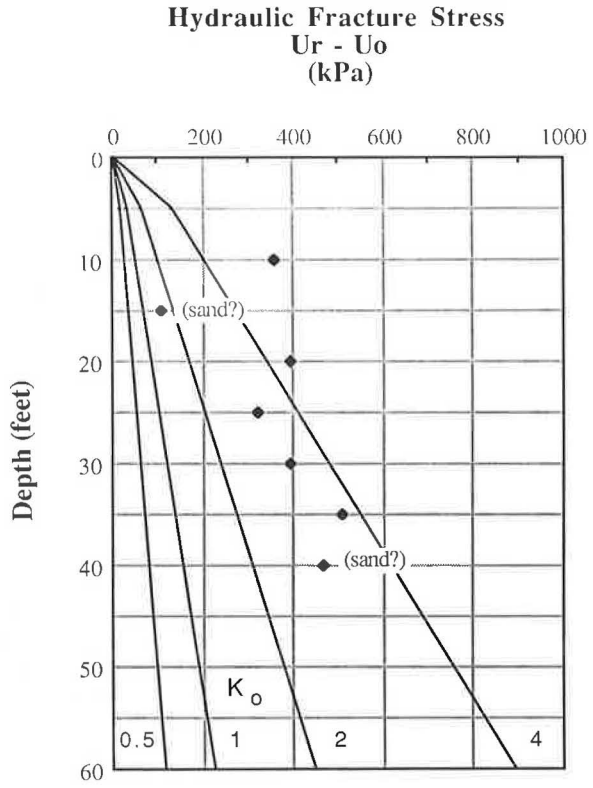

FIGURE 9 Summary of hydraulic fracture tests.

7.6 m may have been damaged during installation because the measured stress is very low.

The uncorrected values illustrated in Figure 10 are considerably less than stresses obtained from DMT P_0 dissipation tests. This suggests that in this material there is a dependency of the stabilized σ_H on geometry of the flat plate. This is the basis behind the K_o-stepped blade. Because the spade cell

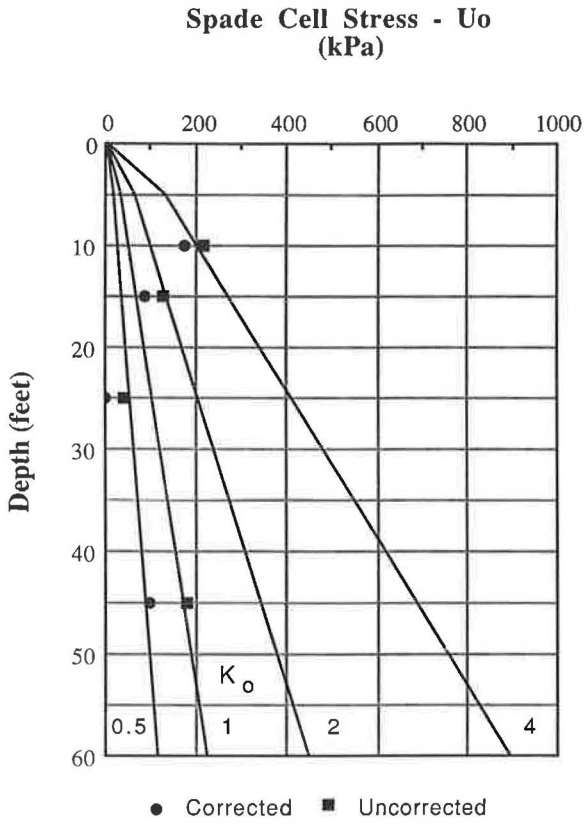

FIGURE 10 Spade cell results.

may represent a condition of less disruption in the stress field in a very stiff clay when compared with the DMT, the uncorrected values illustrated in Figure 10 may now be considered to represent upper-bound values of in situ stresses.

Prebored Pressuremeter Tests

Results of individual PMTs were analyzed graphically to provide a measure of in situ stresses. The probe alignment was fixed during testing such that the strain arms were located at the same orientation for each test depth. The results from each set of strain arms were analyzed individually to give an independent measure of horizontal stress. The results indicated very little difference and no trend with depth. Therefore, it appeared that the stresses were equal in all directions. The value of horizontal stress for each depth was taken as the average of the three directional values.

The results of interpreted horizontal effective stresses are presented in Figure 11. In the upper 5 m, values of K_o on the order of 3–5 are indicated. However, below a depth of 6 m, it appears that K_o approaches a much lower value of about 0.6. The interpreted horizontal stresses from the PMTs were taken as the tangent stress to the linear portion of the pressure expansion curve. Therefore, those values represent the maximum possible value of stress that could be interpreted from the curve. Even so, the results of Figure 11 indicate that in the lower till K_o values are all less than 1. The results of Figure 11 compare very well with corrected spade cell stresses.

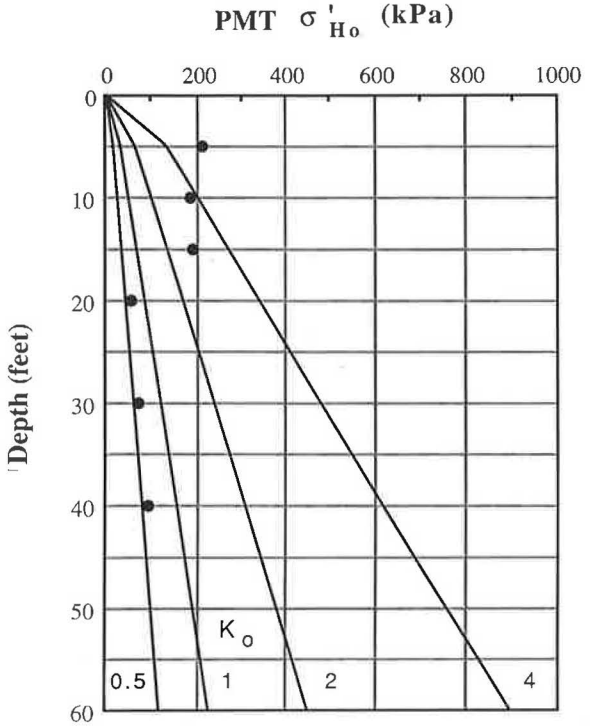

FIGURE 11 Results of pressuremeter tests.

ESTIMATING IN SITU LATERAL STRESSES FROM LABORATORY TESTS

The prediction of in situ lateral stresses based on laboratory tests in cohesive soils has generally relied on empirical relationships between stress history and K_o (most notable are those presented by Brooker and Ireland (*10*)]. Those generally make use of the oedometer OCR and plasticity. More recently, Mayne and Kulhawy (*18*) have presented suggestions for estimating lateral stresses based on stress history and effective friction angle. A distinctly different approach to estimating lateral stresses more directly was presented by Becker et al. (*19*), where the work energy method was used to estimate the in situ stress state. In this method an oedometer test on a horizontally oriented sample is needed to estimate the horizontal stress.

An accurate measure of the preconsolidation stress is needed to make use of the laboratory oedometer tests and OCR. For the tills tested in the current study, some difficulty was experienced in accurately predicting σ'_c because of the gentle curvature in the e log p curves. For this reason, and to provide an upper-bound laboratory estimate of K_o, the maximum possible value of σ'_c was taken from the oedometer curves. Therefore, OCR_{max} was used to predict K_o for the first two methods.

Brooker and Ireland

Perhaps one of the most oft-quoted methods for estimating the at-rest coefficient of lateral stress is that presented by Brooker and Ireland (*10*). A series of laboratory tests were conducted in their study, using an instrumented oedometer, by consolidating artificially remolded soil mixtures and then unloading to give a desired OCR. Thus, the results do not simulate other than young soils without a developed structure under simple mechanical unloading. The resulting curves relate K_o to OCR and P.I., although in no case is K_o greater than 3. K_o values estimated for the site investigated by using the Brooker and Ireland's data and results of oedometer tests are presented in Table 1. Those data show a decrease in K_o below a depth of 3 m as OCR decreases with K_o values all less than 1. Obviously, the prediction of K_o is solely a function of how well the oedometer yield stress may be evaluated.

Mayne and Kulhawy

Mayne and Kulhawy (*18*) conducted a comprehensive review of the literature and presented several relationships between OCR and K_o on the basis of laboratory test results. An approximate upper limit of $K_o = 3$ is again noted in cohesive

TABLE 1 PREDICTED K_o VALUES FROM LABORATORY TESTS

Depth (m)	Brooker & Ireland (10)	Mayne & Kulhawy (18)	Becker, et al. (19)
1.5	1.1	1.1	1.1
3.0	2.0	2.2	2.0
4.6	1.0	0.9	0.9
6.1	1.2	1.5	0.7
7.6	0.9	0.9	0.6
9.1	0.9	0.9	0.3
10.7	0.8	0.8	0.3
12.2	0.8	0.8	0.3
13.7	0.8	0.8	0.4
15.2	0.7	0.6	0.3
18.3	0.9	0.9	0.3

$$K_a = \frac{1 - \sin\phi'}{1 + \sin\phi'} = 0.2 \qquad K_p = \frac{1 + \sin\phi'}{1 - \sin\phi'} = 4.9$$

soils. Mayne and Kulhawy suggest that K_o during loading-unloading may be related to the effective friction angle of the soil, ϕ', and OCR by

$$K_o = (1 - \sin \phi)' \ OCR^{\sin \phi'} \quad (2)$$

A series of consolidated-drained direct shear tests conducted on the unoxidized till from the test site gave $\phi' = 41$ degrees. Resulting values of K_o predicted from Equation (2) are given in Table 1. Interestingly, those values are very close to the K_o values predicted from the Brooker and Ireland method. It is reasonable to expect that the soils at this site have undergone simple unloading as a result of removal of the ice overburden during deglaciation. No evidence of groundwater fluctuations are present in the unoxidized zone.

Work Energy Method

The two previous techniques described yield values of K_o and, therefore, give indirect estimates of at-rest lateral stress. The work energy method presented by Becker et al. (*19*) gives a more direct estimate of σ'_{H0} making use of laboratory oedometer data.

This method is essentially a graphical technique to enhance data presentation from oedometer tests to provide estimates of yield stress. Data are presented in terms of work-per-unit-volume and are plotted on arithmetic scales. By trimming a sample to apply loading in the horizontal direction, an estimate of the in situ horizontal effective stress is obtained. See the paper by Becker et al. (*19*) for more complete details.

Results of interpretations of horizontal loading oedometer tests by using this procedure are given in Table 1. K_o values calculated by using this method range from 2.0 at a depth of 3 m to 0.3 below a depth of 9.1 m. Except for the tests at 1.5 and 3.0 m, this method appears to give estimates of K_o that are lower than other estimates and, thus, may be unrealistic. Active and passive earth pressure coefficients calculated by using a simple Rankine analysis and direct shear test results are also shown in Table 1.

COMPARISON OF RESULTS

The comparison of different methods to predict at-rest horizontal ground stresses or alternatively K_o presents a dilemma: what is considered correct and what is expected? None of the methods presented have any particular preference over the others in stiff cohesive materials; that is, all of the in situ tests were performed with about the same degree of difficulty. On the basis of simple classification and property tests (i.e., liquidity index and unit weight), the soil might be expected to behave as highly overconsolidated. On the basis of geologic history (i.e., prior loading by a continental ice sheet), the soil might be expected to behave as highly overconsolidated. By themselves, those conditions may lead to a belief that the in situ state of horizontal stress is high.

Results of laboratory oedometer tests tend to indicate that although the soils are very dense they are only lightly to moderately overconsolidated below a depth of about 9 m. On the basis of various laboratory predictions, K_o would have a value of between 0.6 and 0.9 in this zone. Those values are reasonably close to the prebored PMT and the spade cell located at 13.7 m, which suggests a K_o value close to 0.5. The full-displacement tests (DMT, FDPMT, and HFT) give much higher stress values and suggest K_o values between 2 and 4, still below the theoretical predicted passive failure ratio of 4.9. Those high values should generally be expected and suggest that significant overstressing occurs in this stiff till as a result of the full-displacement mode of installation.

The overstressing should be related to the geometry and volume displacement of the probe, which may indicate that the stepped blade or tapered blade may be applicable in those stiff materials. However, to provide a more appropriate interpretation, it may be better to allow the tests to reach a stabilized value prior to extrapolating for the in situ value of effective stress.

Investigations of in situ stresses in glacial clay tills and other stiff clays by using in situ and laboratory tests have suggested that the K_o values presented from the laboratory tests in this study are reasonable. Powell et al. (*9*) presented results of oedometer, spade cell, suction tests, and Menard pressuremeter tests at Cowden in the United Kingdom. The tills have nearly the same P.I., liquidity index, texture, and unit weight as the Ames test site described here. K_o values in the upper 4 m ranged from 6 to 1.2. Below this depth, $K_o = 1$. At another site in the United Kingdom, Al-Shaikh-Ali et al. (*20*) presented K_o values ranging from 1.0 to 0.7 for a "lodgement till" with similar classification properties. The values were based on in situ packer (nondisplacement) hydraulic fracture tests, laboratory fracture tests, and oedometer tests. The material investigated was a low-plasticity low-water content-saturated till, which had a liquidity index near zero. Carder and Symons (*21*) also reported very good agreement between push-in spade cells, self-boring pressuremeter, and dilatometer tests in stiff London clay.

Because of the grain-size distribution and glacial deposition, the till investigated in the present study has a high unit weight. The cohesive nature of the material apparently has led to the development of substantial tensile strength in the soil, as was evidenced by a sudden drop in pressure during hydraulic fracture tests. This tensile strength contributes to the general conception that the till should behave as overconsolidated and exhibit high in situ stresses throughout the full depth, although this does not appear to be the case.

CONCLUSIONS

Results of a laboratory and field investigation to predict in situ horizontal effective stresses at rest in a dense, stiff glacial till have been presented. In the upper 3 m of the deposit, K_o values as high as 4 may be realistic. However, in what appear to be moderately overconsolidated soils, K_o values on the order of 0.7 to 0.9 appear more realistic below a depth of about 7 m.

The full-displacement in situ tests used only serve to provide an upper bound on the actual at-rest horizontal stresses, while the prebored strain-arm pressuremeter gave results more in line with conventional laboratory interpretation and push-in spade cells. In this soil, the empirical correlation offered by the dilatometer gave reasonably good estimates of K_o. How-

ever, this should be expected, considering the source of the correlation. In a strain-hardening soil that requires significant strain to reach peak strength such as investigated in this study, field techniques such as the stepped blade or tapered blade, used in a full dissipation mode, may provide meaningful results.

ACKNOWLEDGMENTS

The work presented in this paper was sponsored by the Iowa Geological Survey Bureau, Department of Natural Resources. Their financial support is greatfully acknowledged. Hydraulic fracture tests were conducted by J. Blanchard. Other field assistance was provided by R. Bruner, IGSB.

REFERENCES

1. A. J. Lutenegger, T. J. Kemmis, and G. R. Hallberg. Origin and Properties of Glacial Tills and Diamictons. *Geological Environment and Soil Properties*, ASCE, 1983, pp. 310–331.
2. T. J. Kemmis, G. R. Hallberg, and A. J. Lutenegger. *Depositional Environments of Glacial Sediments and Landforms on the Des Moines Lobe, Iowa.* Guidebook Series No. 6, Iowa Geological Survey, 1981.
3. J. H. Schmertmann. Suggested Method for Performing the Flat Dilatometer Test. *Geotechnical Testing Journal*, ASTM, Vol. 9, 1986, pp. 93–101.
4. A. J. Lutenegger and M. G. Kabir. Dilatometer C-Reading to Help Determine Stratigraphy. *Proc., Ist International Symposium on Penetration Testing*, Vol. 1, 1988, pp. 549–554.
5. P. K. Robertson, R. G. Campanella, and D. Gillespie. Excess Pore Pressures and the Flat Dilatometer Test. *Proc., Ist International Symposium on Penetration Testing*, Vol. 1, 1988, pp. 567–576.
6. L. Bjerrum and K. H. Andersen. In Situ Measurement of Lateral Pressures in Clay. *Proc., 5th European Conference on Soil Mechanics and Foundation Engineering*, Vol. 1, 1972, pp. 11–20.
7. R. Massarch. New Method for Measurement of Lateral Earth Pressure in Cohesive Soils. *Canadian Geotechnical Journal*, Vol. 12, 1975, pp. 142–146.
8. P. Tedd and J. A. Charles. Evaluation of Push-in Pressure Cell Results in Stiff Clay. *Proc., International Symposium on Soil and Rock Investigations by In Situ Testing*, Vol. 2, 1983, pp. 579–584.
9. J. J. M. Powell, A. Marsland, and A. N. Al-Khafagi. Pressuremeter Testing of Glacial Clay Tills. *Proc., International Symposium on Soil and Rock Investigations by In Situ Testing*, Vol. 2, 1983, pp. 373–378.
10. E. Brooker and H. Ireland. Earth Pressure at Rest Related to Stress History. *Canadian Geotechnical Journal*, Vol. 1, 1965, pp. 1–15.
11. A. Assouz and M. Morrison. Field Measurements on Model Piles in Two Clay Deposits, *Journal of Geotechnical Engineering*, ASCE, Vol. 114, 1988, pp. 104–121.
12. J. Blanchard. *Interpretation of Hydraulic Fracture Tests in Clay Using a Push-In Type Piezometer.* Report IGS 89-363P, Department of Civil Engineering, University of Massachusetts, 1989.
13. M. Bozozuk. Minor Principal Stress Measurements in Marine Clay with Hydraulic Fracturing Tests. *Proc., ASCE Specialty Conference: Subsurface Exploration for Underground Excavation and Heavy Construction*, 1974, pp. 333–349.
14. K. Massarch and B. Broms. Lateral Earth Pressure at Rest in Soft Clay. *Journal of the Geotechnical Engineering Division*, ASCE, Vol. 102, 1976, pp. 1041–1047.
15. F. Tavenas, G. Blanchette, S. Lerougil, M. Ray, and P. LaRochelle. Difficulties in the In Situ Determination of K_o in Soft Sensitive Clay. *Proc., In Situ Measurement of Soil Properties*, ASCE, Vol. 1, 1975, pp. 450–476.
16. G. LeFebvre, A. Philibert, M. Bozozuk, and J. J. Pare. Fissuring from Hydraulic Fracture of Clay Soil. *Proc., 10th International Conference on Soil Mechanics and Foundation Engineering*, Vol. 2, 1981, pp. 513–518.
17. K. Massarch. New Aspects of Soil Fracturing in Clay. *Journal of the Geotechnical Engineering Division*, ASCE, Vol. 104, 1978, pp. 1109–1123.
18. P. W. Mayne and F. H. Kulhawy. K_o-OCR Relationships in Soil. *Journal of the Geotechnical Engineering Division*, ASCE, Vol. 108, 1982, pp. 851–872.
19. D. Becker, J. H. A. Crooks, K. Been, and M. G. Jefferies. Work as a Criterion for Determining In Situ and Yield Stresses in Clays. *Canadian Geotechnical Journal*, Vol. 24, 1987, pp. 549–564.
20. M. M. H. Al-Shaikh-Ali, A. G. Davis, and M. J. Lloyd. In Situ Measurement of K_o in a Stiff Fissured Glacial Till by Hydraulic Fracturing. *Ground Engineering*, Vol. 14, 1981, pp. 19–25.
21. D. R. Carder and I. F. Symons. Long-term Performance of an Embedded Cantilever Retaining Wall in Stiff Clay. *Geotechnique*, Vol. 39, 1989, pp. 55–75.

Publication of this paper sponsored by Committee on Soil and Rock Properties.

Laboratory Measurement of Lateral Stress Induced by a Cavity Expansion in a Hollow Cylinder Cell

I. JURAN AND B. MAHMOODZADEGAN

The use of a specially designed hollow cylinder cell in the measurement, under laboratory controlled conditions, of the lateral stress and the excess pore water pressure induced by a cavity expansion in both claycy and granular soils is discussed. The hollow cylinder cell permits the performance of a cavity expansion test in an annular soil specimen under three independent stresses (i.e., axial stress, radial cavity pressure, and lateral confining stress) with measurement of cavity volume change and excess pore water pressures at several locations in the soil specimen. Effective stress analysis of the soil response to the cavity expansion illustrates that the effective lateral stress is independent of the specimen geometry, and intrinsic effective stress-strain relationships can be derived from the experimental expansion curve. However, the specimen geometry does affect the excess pore water pressure generated under undrained conditions, and, therefore, the total stress analysis conventionally used for interpretation of pressuremeter test results is not appropriate for analysis of hollow cylinder cavity expansion test.

Today, pressuremeter and dilatometer tests are being used increasingly to measure the soil response to cavity expansion and to obtain engineering soil properties for design purposes. For fine-grained saturated soils, a total stress interpretation procedure to derive the shear curve (i.e., modulus and undrained cohesion) from the pressuremeter expansion curve was proposed by Baguelin et al. (*1*).

More recently, electric piezo-cells have been incorporated in the pressuremeter probe, as was reported by Baguelin et al. (*2*), Canou and Tumay (*3*), and Juran and Beech (*4*). Measurement of the excess pore water pressure generated by the expanding cylindrical cavity can be used to develop effective stress interpretation procedures capable of providing the in situ effective shear strength characteristics, compressibility, and dilatancy properties of the soil (*4*).

This study has been conducted to investigate the effective lateral stress response to a cavity expansion in both granular and saturated clayey soils. A hollow cylinder cell (HCC) was designed to perform cylindrical cavity expansion tests in annular soil specimens under three independent stresses (i.e., axial stress, radial cavity pressure, and lateral confining stress). The instrumentation of the HCC allows the measurement of the cavity volume change and the excess pore water pressures at three locations within the specimen.

The HCC equipment and its instrumentations have been described by Juran and BenSaid (*5*), who indicated that the procedure proposed by Baguelin et al. (*1*) to derive the intrinsic shear curve of the soil from expansion curves obtained from pressuremeter tests cannot be used for the interpretation of hollow cylinder cavity expansion tests in annual soil specimens of finite dimensions. Juran and BenSaid proposed a total stress analysis procedure that takes into account the effect of sample geometry on the soil response and yields the shear modulus and undrained cohesion of the soil.

This paper focuses on the effective stress analysis of the soil response to cylindrical cavity expansion in the HCC. Interpretation procedures, based on effective stress analysis, are proposed that permit simulation of cavity expansion in both granular and saturated clayey soils. The proposed interpretation procedures are evaluated through the analysis of hollow cylinder cell cavity expansion tests (CETs) in both Fontainbleau sand and silty clay specimens. It is illustrated that the effective lateral stress generated by the cavity expansion is independent of the specimen geometry and that intrinsic effective stress-strain relationships can be derived from the cavity expansion curve. However, the specimen geometry does affect the excess pore water pressure generated under undrained conditions and, therefore, the total stress soil response.

CAVITY EXPANSION TESTS IN A SATURATED CLAYEY SOIL

Laboratory cavity expansion tests, under controlled drainage conditions, yield measurement of the total lateral stress and the excess pore water pressure generated during cavity expansion. Those results can be used for two main purposes: (a) to derive the effective stress-strain relationships of the soil or (b) to evaluate analytical/numerical models developed to predict the lateral stress response of the soil to cavity expansion.

Theoretical Considerations and Interpretation Procedure

The first part of this study focuses on development and evaluation of an effective stress analysis procedure to predict the effective lateral stress generated by the cavity expansion in saturated annular (HCC) specimens of a silty clay. The proposed interpretation procedure is based on the assumptions that follow.

Department of Civil and Environmental Engineering, Polytechnic University, 333 Jay Street, Brooklyn, N.Y. 11201.

Soil Model

A soil model, proposed by Juran and Beech (*4*), is considered, assuming the soil to be an isotropic, elastoplastic, strain-hardening material with a nonassociated flow rule. The strain hardening is assumed to be isotropic, with the hardening parameter being the shear strain defined as

$$\gamma = \frac{1}{\sqrt{2}}[(\varepsilon_1 - \varepsilon_2)^2 + (\varepsilon_2 - \varepsilon_3)^2 + (\varepsilon_3 - \varepsilon_1)^2]^{1/2} \quad (1)$$

where ε_1, ε_2, and ε_3 are the principal strains, with $\varepsilon_1 > \varepsilon_2 > \varepsilon_3$. For a plane strain cylindrical cavity expansion, $\varepsilon_1 = \varepsilon_r$, $\varepsilon_2 = \varepsilon_z$, and $\varepsilon_3 = \varepsilon_\theta$, where ε_r, ε_z, and ε_θ are the radial, vertical, and tangential strains, respectively.

Yield Function

A Mohr-Coulomb-type yield criterion is considered to define the yield surface with an open elastic domain. The assumed yield function can be written as

$$F(\boldsymbol{\sigma},\gamma) = \frac{q - q_0(\gamma)}{p'} - h(\gamma) = 0 \quad (2)$$

where

$\boldsymbol{\sigma}$ = stress tensor,
q = $(\sigma_1' - \sigma_3')/2$ (deviatoric stress),
p' = $(\sigma_1' + \sigma_3')/2$ (average effective stress),
$h(\gamma)$ = strain-hardening function,
$q_0(\gamma)$ = deviatoric stress at $p' = 0$, and
σ_1', σ_3' = major and minor principal stresses, respectively (for cylindrical cavity expansion, $\sigma_1' = \sigma_r'$ and $\sigma_3' = \sigma_\theta'$, where σ_r' and σ_θ' are the effective radial and tangential stresses).

For a contracting (normally consolidated) cohesive soil, the hardening function $h(\gamma)$ is assumed to be of hyperbolic form:

$$h(\gamma) = \frac{\gamma}{a + b\gamma} \quad (2a)$$

with

$$a = \sigma_0'/G \qquad b = 1/\sin\phi_{cv}$$

where

σ_0' = initial consolidation pressure,
G = shear modulus, and
ϕ_{cv} = effective critical state friction angle.

As was indicated by Juran and Beech (*4*), the soil reaches the critical state (i.e., plastic flow at constant volume) at a finite shear strain γ_f, and, therefore, the assumption of a hyperbolic strain-hardening function results in an underestimation of the stress ratio q/p' at large shear strains. Considering this experimental observation, the yield function was modified to take into account the perfectly plastic soil behavior at large strains (i.e., $\gamma > \gamma_f$), assuming that the failure shear strain γ_f is independent of the stress path and a "modified" strain-hardening function is considered.

$$h^*(\gamma) = \frac{\gamma}{a + b^*\gamma} \quad (2b)$$

where

$$a = \sigma_0'/G \qquad b^* = 1/\sin\phi_{cv} - \sigma_0'/G \cdot \gamma_f$$

The hyperbolic and "modified" $h(\gamma)$ functions are illustrated in Figure 1a.

Plastic Flow Function

A stress ratio-dilatancy function of the form proposed by Nova and Wood (*6*) is assumed:

$$\eta = \frac{d\varepsilon_v}{d\gamma^p} = \eta(q/p') \quad (3)$$

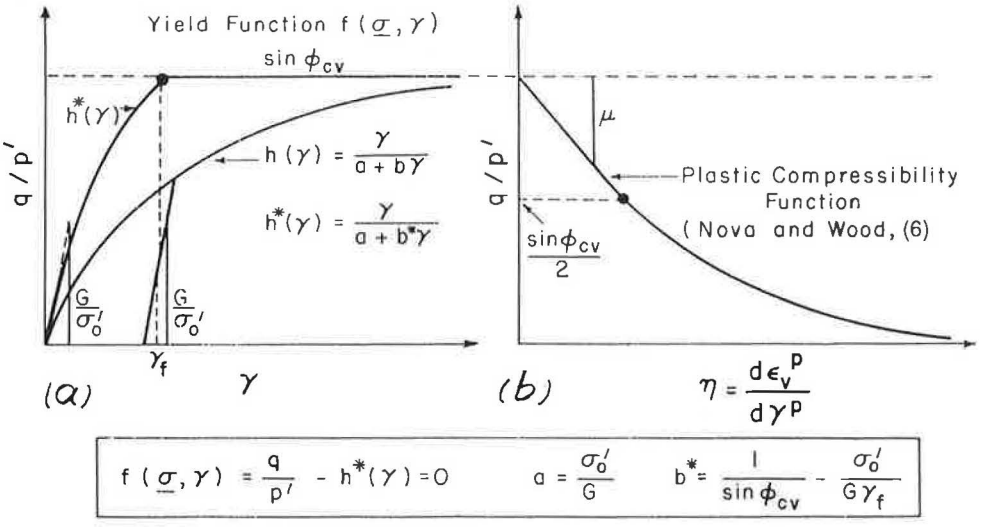

FIGURE 1 Definitions of (a) yield function and (b) stress ratio-dilatancy function.

where $d\varepsilon_v^p$ and $d\gamma^p$ are the plastic volumetric and deviatoric strain increments, respectively. The assumed hyperbolic function $\eta(q/p')$, with an initial linear portion characterized by a contractancy modulus (μ), is schematically illustrated in Figure 1b. As the soil reaches the critical state ($\gamma \geq \gamma_f$), η is equal to zero, indicating no plastic volume change. Having defined $\eta(q/p')$, a nonassociated plastic flow function $Q(q/p')$ can be derived, assuming the coincidence of the axes of principal stresses with those of the corresponding plastic strain increments.

The proposed model defined by Equations 2b and 3 (Figure 1) requires an experimental determination of five soil characteristic parameters: G/σ_0', ν (Poisson's ratio), ϕ_{cv}, γ_f, and μ. If the soil shear strength parameters include a cohesion intercept, then the function $q_0(\gamma)$ must also be determined. Those parameters can be obtained from either triaxial tests (CD test with measurement of the volume change or CU test with measurement of the pore water pressure) or hollow cylinder cell tests with measurement of the pore water pressure generated at the expanding cavity facing.

Effective Stress Analysis Procedure

To simulate numerically an undrained cavity expansion test in a saturated fine-grained soil specimen, the proposed soil model is incorporated in an effective stress analysis procedure. This procedure, an extension of the analytical method proposed by Juran and Beech (*4*) for interpretation of pressuremeter tests in a clayey soil, takes into account the boundary conditions corresponding to the HCC and involves the following steps:

1. A boundary displacement increment Δx_0 is applied at the cavity facing. The induced total strain increments ($d\varepsilon_r$, $d\varepsilon_\theta$) are calculated from the compatibility relationship considering the specific test conditions of vertical plane strain ($d\varepsilon_z = 0$) and undrained expansion ($d\varepsilon_v = 0$). The shear strain increment $d\gamma$ at a radial coordinate r is given by

$$d\gamma(r) = \sqrt{3}\, d\varepsilon_\theta = \sqrt{3}\,\frac{\Delta x_0 r_0}{r^2} \tag{4a}$$

at the cavity facing ($r = r_0$)

$$d\gamma(r_0) = \sqrt{3}\,\frac{\Delta x_0}{r_0} \tag{4b}$$

2. The test conditions (i.e., $d\varepsilon_z = 0$, $d\varepsilon_v = 0$) yield the following expression for the $\left(\frac{q}{p'}\right)$ function:

$$\eta = \frac{d\varepsilon_v^p}{d\gamma^p} = \frac{d\varepsilon_v - d\varepsilon_v^e}{d\gamma \quad d\gamma^e} = \frac{\left(\frac{1-2\nu'}{G}\right)\cdot\left(\frac{dp'}{d\gamma}\right)}{1-\left(\frac{1}{2G}\right)\cdot\left(\frac{d\tau_{oct}}{d\gamma}\right)} \tag{5a}$$

or

$$d\gamma = -\left(\frac{1-2\nu'}{G\eta}\right) dp' + \left(\frac{1}{2G}\right) d\tau_{oct} \tag{5b}$$

where

$d\varepsilon_v$, $d\varepsilon_v^e$ = total and elastic volumetric strain increments, respectively,
$d\gamma$, $d\gamma^e$ = total and elastic shear strain increments, respectively, and
$\tau_{oct} = 1/\sqrt{2}\,[(\sigma_r - \sigma_\theta)^2 + (\sigma_\theta + \sigma_z)^2 + (\sigma_z - \sigma_r)^2]^{1/2}$ (octahedral shear stress).

The vertical plane strain condition implies $\sigma_\theta = \nu'(\sigma_r + \sigma_z)$, and, therefore,

$$\tau_{oct} = p'[3h^*(\gamma) + (1 - 2\nu')^2]^{1/2} \tag{6}$$

3. The constitutive equations (i.e., Equations 2b and 3) derived from triaxial test results, coupled with Equations 5b and 6 provide a solution for the effective stress increments at the cavity facing, $d\sigma_r'(r_0)$ and $\sigma_\theta'(r_0)$, as a function of the shear strain.

As will be indicated, the solution for the effective stresses at the cavity facing is independent of the sample geometry and the boundary conditions applied at the external facing of the specimen. Therefore, the HCC can be adequately used to evaluate numerical models and analytical procedures developed to predict the effective stress soil response. However, the sample geometry and the boundary lateral stress do affect the excess pore water pressures generated by the cavity expansion and, thus, the total stress response.

4. The shear strain variation $\gamma(r)$ throughout the sample can be determined from Equation 4a. The solution derived for the effective stresses at the cavity facing can then be used to establish the variation of effective stresses [$q = q(r)$, $p' = p'(r)$] as a function of the spatial coordinate r.

5. The total stress increment $d\sigma_r$ can be calculated from the radial equilibrium condition

$$\frac{d\sigma_r}{d\rho} + \frac{2q}{\rho} = 0 \tag{7}$$

(where ρ is the actual radius) considering the boundary conditions $d\sigma_r(R) = 0$, where R is the external radius of the specimen.

The excess pore water pressure is given by

$$u(\rho) = \sigma_r(\rho) - \sigma_r'(\rho) \tag{8}$$

recalling that

$$\sigma_r'(\rho) = q(\rho) + p'(\rho) \tag{9}$$

Experimental Study

The soil used in this part of the study was a low plasticity silty clay with liquid and plastic limits of 35 percent and 21 percent, respectively. The grain size distribution of this soil contains 95 percent < 80 μm, 50 percent < 2 μm, and 26 percent < 0.2 μm.

Soil Properties

Triaxial undrained (CU) and drained (CD) tests were performed to obtain the material properties for the proposed soil model (i.e., Equations 2b and 3). Figure 2 presents the typical results of CU tests on two lightly overconsolidated specimens of the soil used in this study. In the q-p' plane, the effective stress paths followed by the soil in different tests are geometrically similar, and the "iso-γ" curves can be approximated by straight lines (Equation 2). For normally consolidated specimens, $q_0(\gamma) = 0$. Figure 2 also illustrates that the stress paths actually reach the failure envelope at a finite shear strain γ_f of about 8 percent, contrary to the assumption of the hyperbolic model that implies $\gamma_f = \infty$.

Figure 3 illustrates the strain-hardening function $h^*(\gamma)$ and the stress ratio-dilatancy relationship $\eta(q/p')$ derived from the results of the triaxial CU and CD tests. CU and CD tests yield nearly an identical $h^*(\gamma)$ function. However, a significant difference exists in the $\eta(q/p')$ functions obtained from the results of those two tests. The contractancy modulus (μ) values obtained from the CU test results were found to be significantly greater (i.e., 2.5 to 2.9) than those obtained from the CD tests (i.e., 1.0 to 1.2). This substantial difference in the experimentally determined μ values indicates that in a normally consolidated clay the $\eta(q/p')$ function appears to be stress-path dependent.

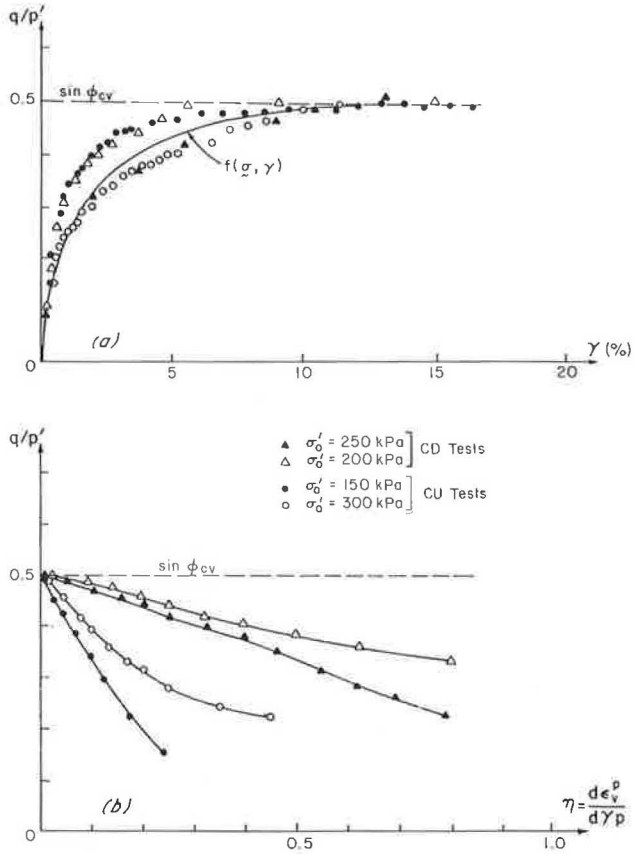

FIGURE 3 (a) Strain-hardening and (b) stress ratio-dilatancy functions derived from triaxial CU tests results.

Cavity Expansion Tests

To investigate the validity of the proposed effective stress analysis procedure, cavity expansion tests (CETs) were performed in a specially designed HCC. Figure 4 presents a schematic view of the HCC and its instrumentation (*5*).

In this cell, an annular soil specimen (internal and external radii of 1 and 5 cm, respectively) is subjected to three independent stresses: the axial stress, σ_z; the radial cavity pressure, σ_c; and the lateral confining stress, σ_R. The cell is equipped with three pore water pressure transducers located at the bottom of the cell at distances of 16, 30, and 44 mm from the cavity center. The volume changes of both the soil and the internal cavity are recorded during the expansion test. A cavity expansion curve relating the applied cavity pressure σ_c to the cavity volume change Δv_c is obtained, which is similar to typical results of in situ self-boring pressuremeter tests (*1*).

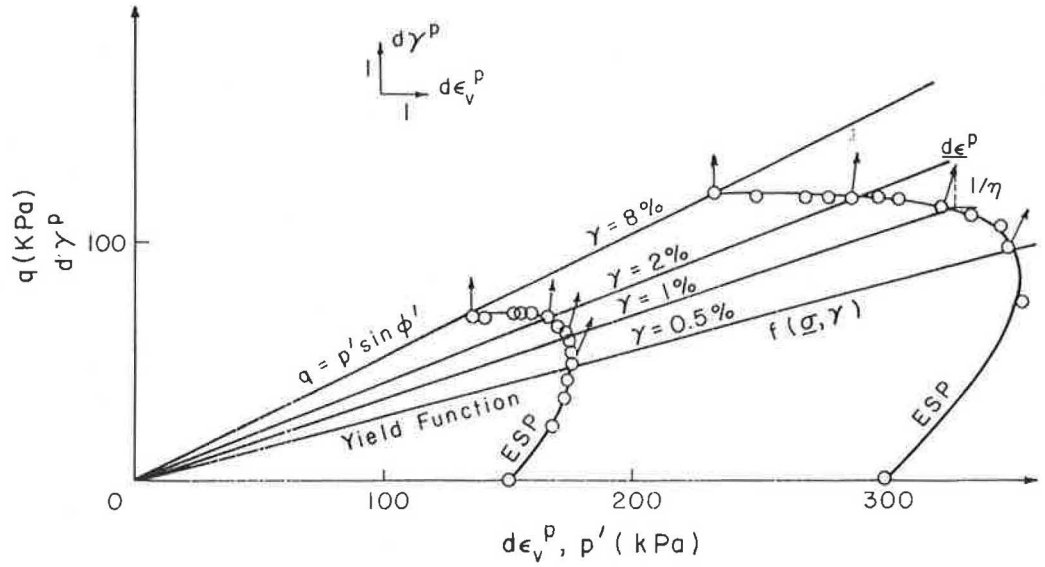

FIGURE 2 Effective stress paths obtained from triaxial CU tests on specimens of a silty clay.

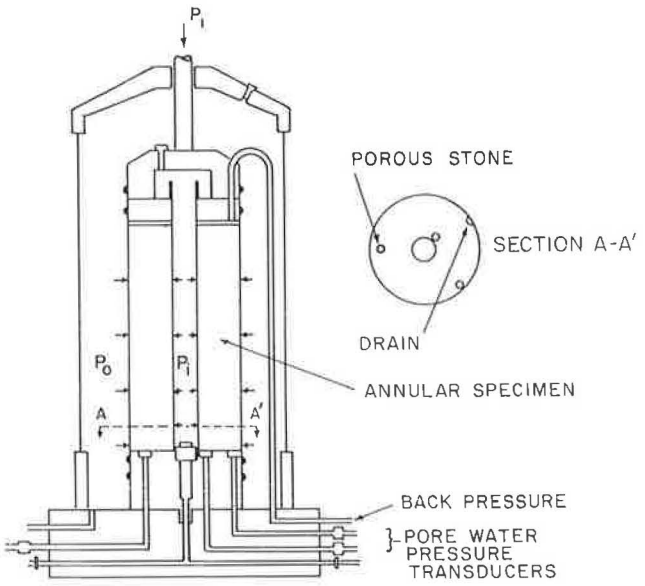

FIGURE 4 Cross-sectional scheme of the hollow cylinder cell [after Juran and BenSaid (5)].

Figure 5 presents typical results of an undrained CET with initial consolidation pressure of $P_0' = 250$ kPa. In addition to the expansion curve and the measured excess pore water pressures, the measured vertical strain is presented in this figure. As observed, the maximum vertical strain measured during this test was less than 1 percent, which is an indication of the validity of the plane strain assumption for the test conditions of the HCC.

Figures 6 and 7 present the cavity expansion curves and the excess pore pressures at the cavity facing measured during two additional CET tests with initial consolidation pressures of 150 and 200 kPa, respectively.

Analysis of the CET Results

The proposed effective stress analysis procedure permits simulation of the effective radial stress response to a cavity expansion in the annular HCC specimen and requires an appropriate determination of the soil constitutive equations (2b and 3) from the results of triaxial CU and CD tests. However, analysis of the triaxial test results (Figure 3) illustrate that for the normally consolidated clay specimens, while a rather unique $h^*(\gamma)$ function can be obtained, the derived stress ratio-dilatancy relationship $\eta(q/p')$ appears to be stress path dependent. Therefore, in evaluating the proposed procedure, rather than arbitrarily selecting a $\eta(q/p')$ function to predict the effective lateral and tangential stress (i.e., σ_r', σ_θ') response, an attempt is made to compare the $\eta(q/p')$ function obtained directly from the CET results with those derived from the triaxial CU and CD tests.

To determine the stress ratio-dilatancy function directly from the cavity expansion test results, Equations 5a and 6 were used simultaneously, along with the $h^*(\gamma)$ function determined from the triaxial CU and CD test results. Figure 8a illustrates that the stress ratio-dilatancy function $\eta(q/p')$ determined from the CET results ($1.5 < \mu < 2.0$) lies within

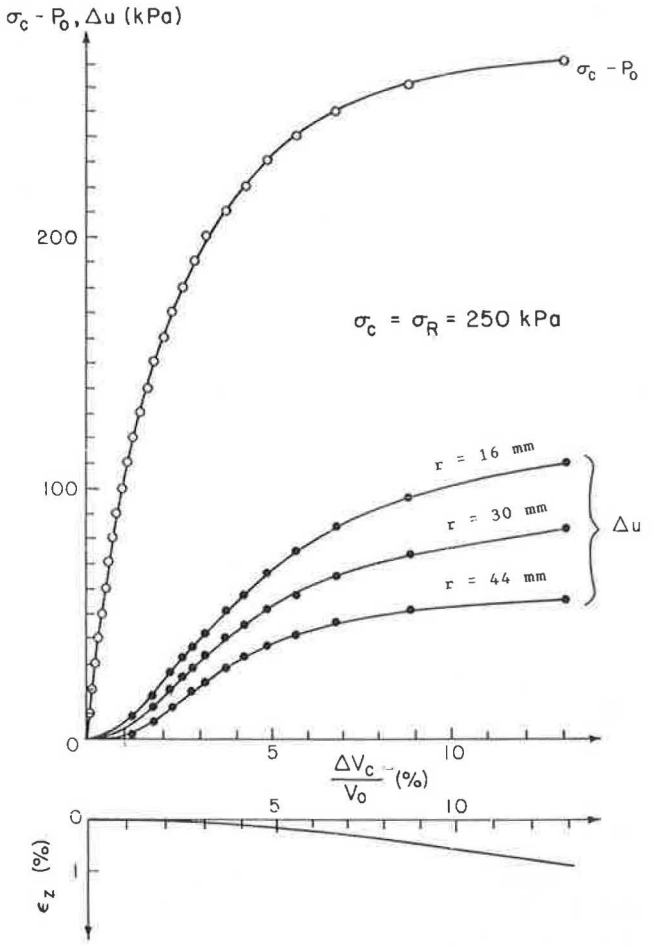

FIGURE 5 Typical results of an undrained cavity expansion test.

a range bounded by those obtained from triaxial CU ($2.5 < \mu < 2.9$) and CD ($1.0 < \mu < 1.2$) tests. Those results are consistent with the effective stress paths, obtained for those three types of tests, as is indicated in Figure 8a for $P_0' = 250$ kPa.

The proposed effective stress analysis was used, considering the obtained $\eta(q/p')$ function and taking μ values of 1 and 2, to simulate the cavity expansion tests conducted with $p_0' = 150$ and 200 kPa. Figures 9 and 10 present the comparison between the predicted and measured total lateral stress response and the generated excess pore water pressures for the two tests. Those comparisons illustrate that with the derived μ value ($1.5 < \mu < 2.0$), the proposed model will predict fairly well the range of the excess pore water pressures generated by the cavity expansion. However, the lateral stress soil response is underestimated. For a value of contractancy modulus (μ) of 2, the difference between the predicted and experimental lateral stress response curves (Figure 9a) attains a maximum of about 15 percent. This difference is partially due to sample preparation effects that result in local heterogeneities within the specimen. Such heterogeneities were evidenced by irregularities in the cavity shape at the completion of the test. End effects were minimized, using a double membrane system lubricated with grease. However, the difference between the predicted and experimental results also can be attributed to

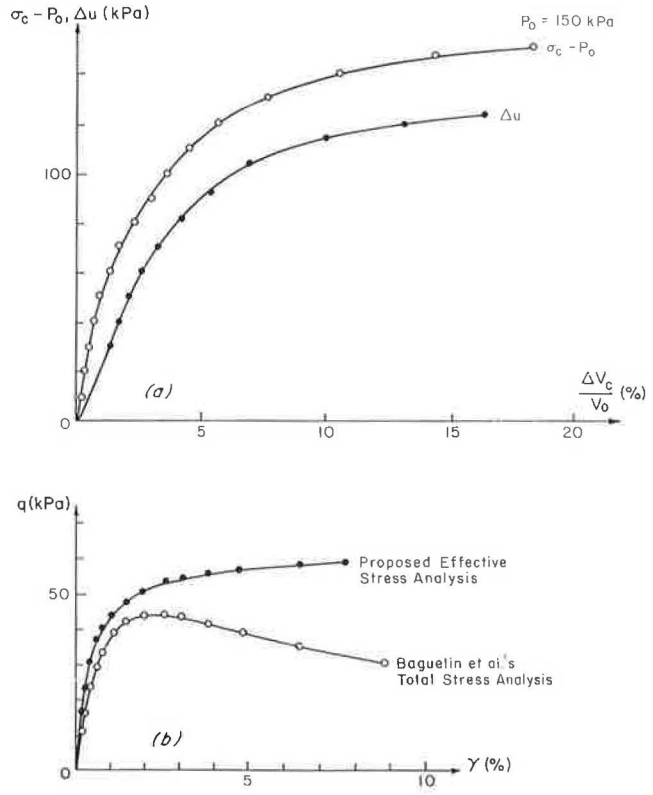

FIGURE 6 (a) Cavity expansion test results under $P_0' = 150$ kPa and (b) comparison of the derived shear curves by using effective and total stress analyses.

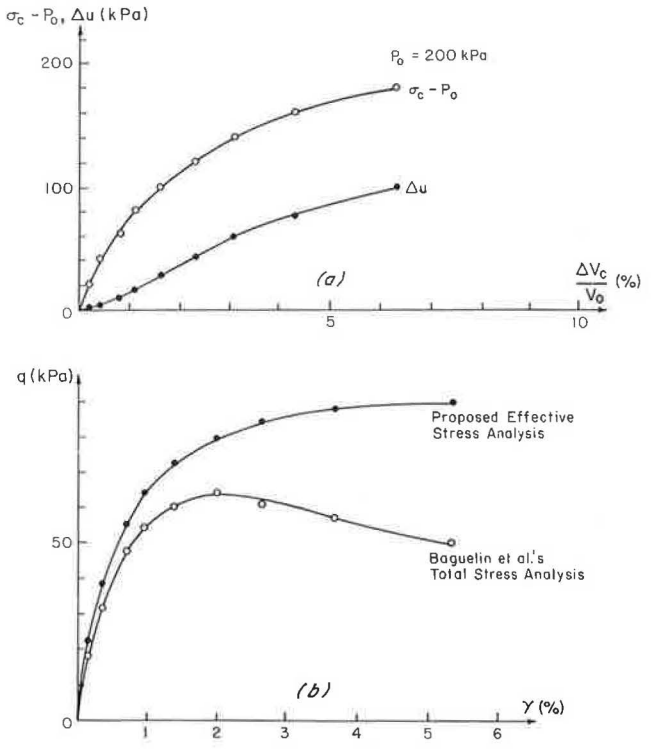

FIGURE 7 (a) Cavity expansion test results under $P_0' = 200$ kPa and (b) comparison of the derived shear curves by using effective and total stress analyses.

the limitations of the proposed soil model and particularly to the high sensitivity of the predicted results to small variations in μ values.

Evaluation of the Specimen Geometry Effect on the Derived Shear Curve

Interpretation of cavity expansion curves produced by pressuremeter in saturated clayey soils is conventionally based on the total stress analysis procedure proposed by Baguelin et al. (*1*). This analysis procedure is derived by using the radial equilibrium and compatibility equations, assuming that a unique shear curve $q = g(\varepsilon_\theta)$ can be obtained for the saturated incompressible semi-infinite soil medium, which would be independent of the spatial coordinate r. This shear curve can be expressed as

$$q = \frac{d(\sigma_c - p_0)}{dg_0} g_0(1 + 2g_0) \tag{10}$$

where

$$g_0 \cong \varepsilon_\theta = \frac{\sqrt{3}}{3}\gamma \tag{11}$$

Because the HCC specimen does not represent a semi-infinite medium, the shear curve derived from this total stress analysis is not unique. In particular, at the external facing of the specimen ($r = R$), the boundary conditions imply $d\sigma_R = 0$ while $d\varepsilon_\theta = dx_R/R$ (dx_R and $d\sigma_R$ are the radial displacement and the lateral stress increments at $r = R$, respectively). Therefore, this total stress analysis does not permit an appropriate consideration of the effect of specimen geometry and the boundary conditions on the soil response to cavity expansion.

To evaluate the effect of specimen geometry, the shear curves derived from the HCC test results, using Baguelin's procedure, are compared with reference shear curves. Those reference curves were established by coupling the soil strain-hardening function, obtained from triaxial tests, with the effective lateral stress measured at the cavity facing. The equation used to determine the reference shear curves is independent of the boundary conditions and can be written as

$$q = p' \cdot h^*(\gamma) = \frac{h^*(\gamma)}{1 + h^*(\gamma)}[\sigma_c - \Delta u] \tag{12}$$

Figures 6b and 7b illustrate the comparisons between the shear curves obtained by using Equations (10) and (12) for the cavity expansion tests conducted under $p_0' = 150$ and 200 kPa. Those comparisons illustrate the substantial effect of the analysis procedure on the derived shear curve, indicating that the specimen geometry significantly affects the total stress soil response to cavity expansion.

To investigate the specimen geometry effect further, the test conducted under $p_0' = 150$ kPa was numerically simulated for increasing values of the external to internal specimen radius ratios (R/r_0). The results of those simulations (Figure 11) indicate that a unique lateral effective stress curve is obtained

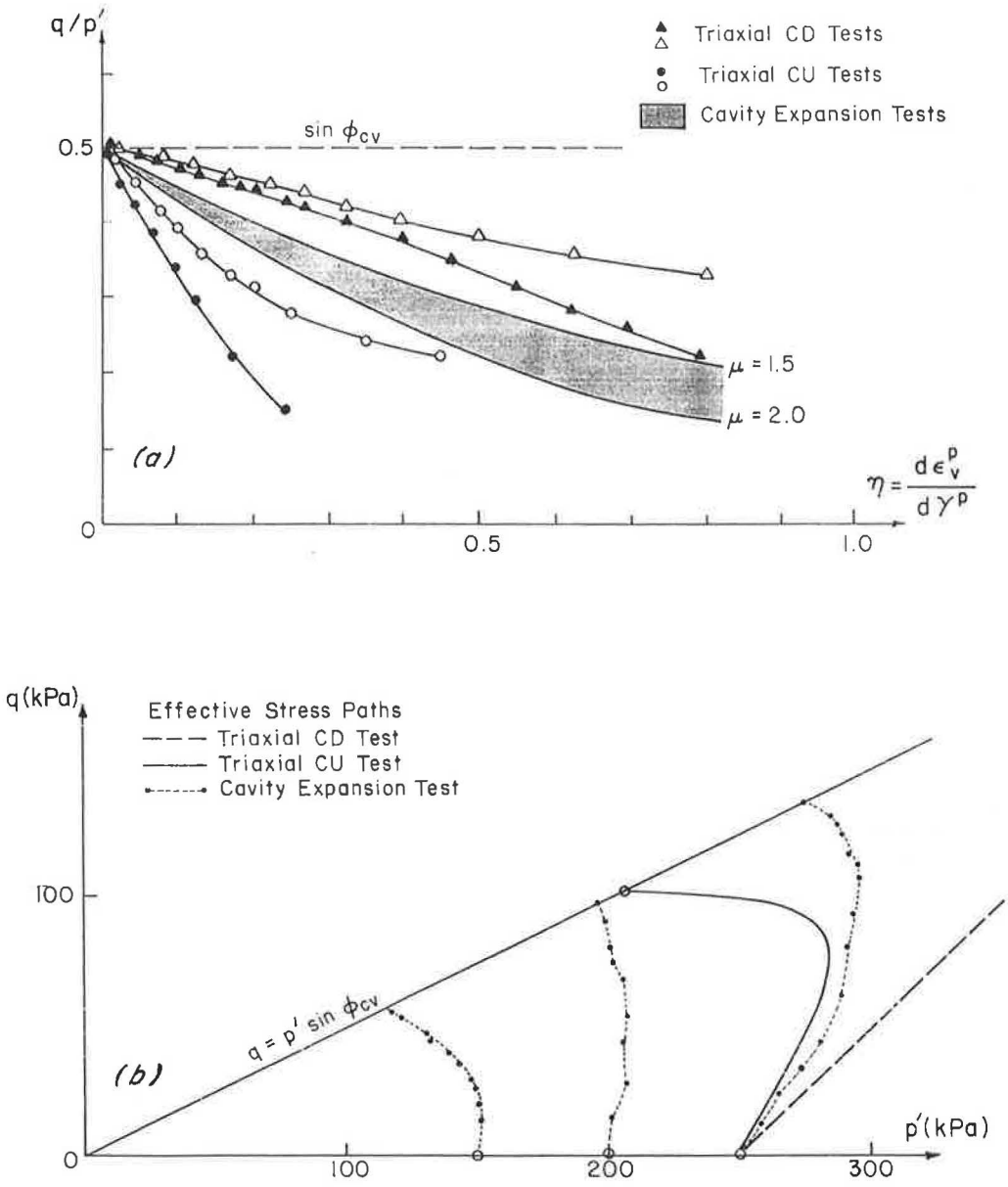

FIGURE 8 Comparisons of (a) the derived stress ratio-dilatancy functions and (b) the effective stress paths from triaxial CU, CD, and cavity expansion tests.

and the total stress and excess pore water pressure depend on the specimen geometry. An increase in the R/r_0 ratio of 5 to 50 results in an increase of only 10 percent in the total lateral stress and an equal decrease of the excess pore water pressure.

Figure 12 presents the shear curves derived from the theoretical expansion curves in Figure 11, using Baguelin et al.'s total stress analysis. Those results indicate, that as the R/r_0 increases the shear curves approach the reference shear curve.

The results presented in Figures 11 and 12 indicate that the specimen geometry has no effect on the effective lateral stress response of soils to cavity expansion but can significantly affect the total lateral stress response and the generated excess pore water pressure.

CAVITY EXPANSION TESTS IN SANDS

Theoretical Considerations and Interpretation Procedure

The soil model described earlier was extended by Juran and Mahmoodzadegan (*7*) for analysis of cavity expansion tests in sands. This soil model, which takes into account the dilating and contracting sand behavior or both, was incorporated in an analysis procedure for interpretation of pressuremeter tests in sands. This analysis procedure, derived from the compatibility and the radial equilibrium conditions for cylindrical cavity expansion, yields an expression for the shear curve,

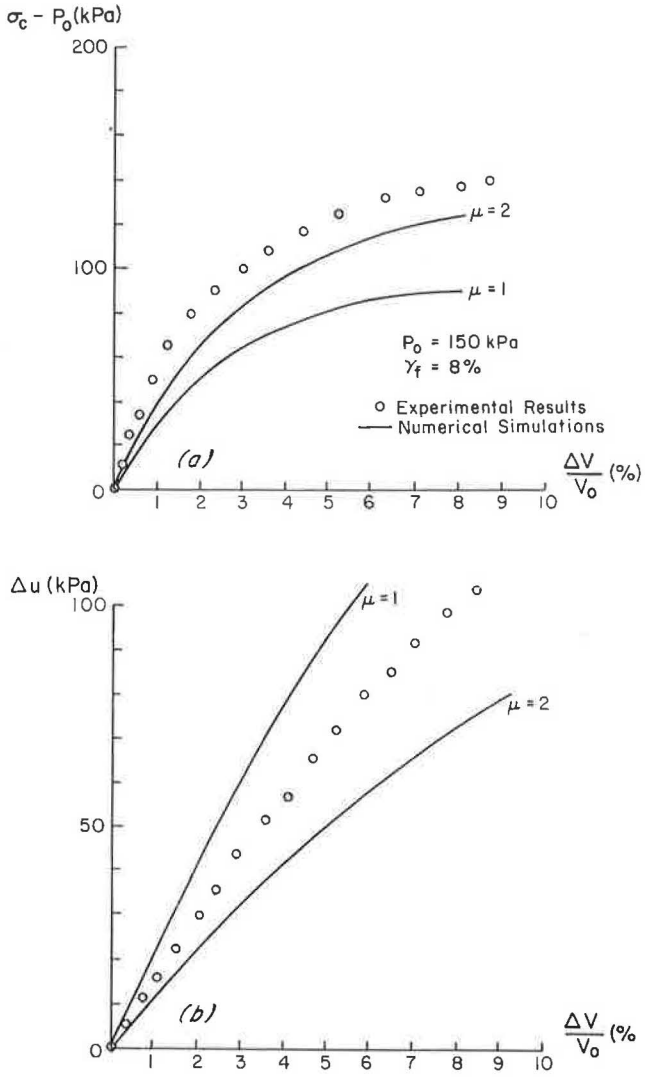

FIGURE 9 Comparisons of (a) the experimental and predicted expansion curves and (b) experimental and predicted excess pore water pressure curves under $P_0' = 150$ kPa.

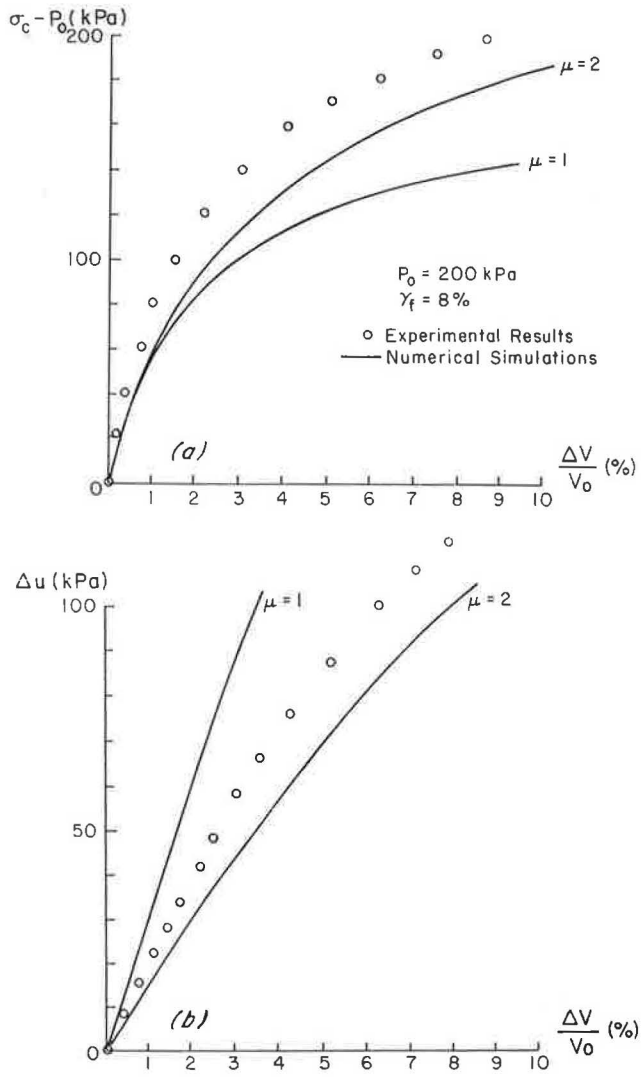

FIGURE 10 Comparisons of (a) the experimental and predicted expansion curves and (b) experimental and predicted excess pore water pressure curves under $P_0' = 200$ kPa.

which can be incrementally derived as

$$q = \frac{\partial(\sigma_c - P_0)}{\partial \varepsilon_\theta} \cdot \frac{\varepsilon_\theta}{1 - \sin \xi} \cdot \frac{1 + \varepsilon_\theta}{1 - \varepsilon_\theta} \tag{13}$$

where

$$\sin \xi = \sin \psi - \gamma \cdot \frac{\partial(\sin \xi)}{\partial \gamma} \tag{14a}$$

and ψ is the dilation angle of the sand that can be obtained from the following relationship:

$$\sin \psi = 1 + 2 \frac{d\varepsilon_\theta}{d\gamma} \tag{14b}$$

Equation 13 is obtained independently of any assumption regarding the constitutive equation of the soil.

At the cavity facing, the radial stress σ_r is equal to the applied cavity pressure σ_c. The average effective stress at this location is, therefore, given by

$$p' = (p_0 + \Delta\sigma_c) - q - \Delta u \tag{15}$$

where Δu is the excess pore water pressure generated at the cavity facing, $\Delta\sigma_c$ is the applied cavity pressure increment, and p_0 is the initial cavity pressure.

Coupling Equations 12, 13, and 15 with the constitutive equations of the soil yields the following incremental relationship for the effective lateral stress in the soil:

$$\frac{\Delta(\sigma_c - p_0)}{\Delta \varepsilon_\theta} = \frac{1 - \sin \xi}{1 + h^*(\gamma)} \cdot \frac{h^*(\gamma)}{\varepsilon_\theta} \cdot \frac{1 - \varepsilon_\theta}{1 + \varepsilon_\theta} [\sigma_c - \Delta u] \tag{16}$$

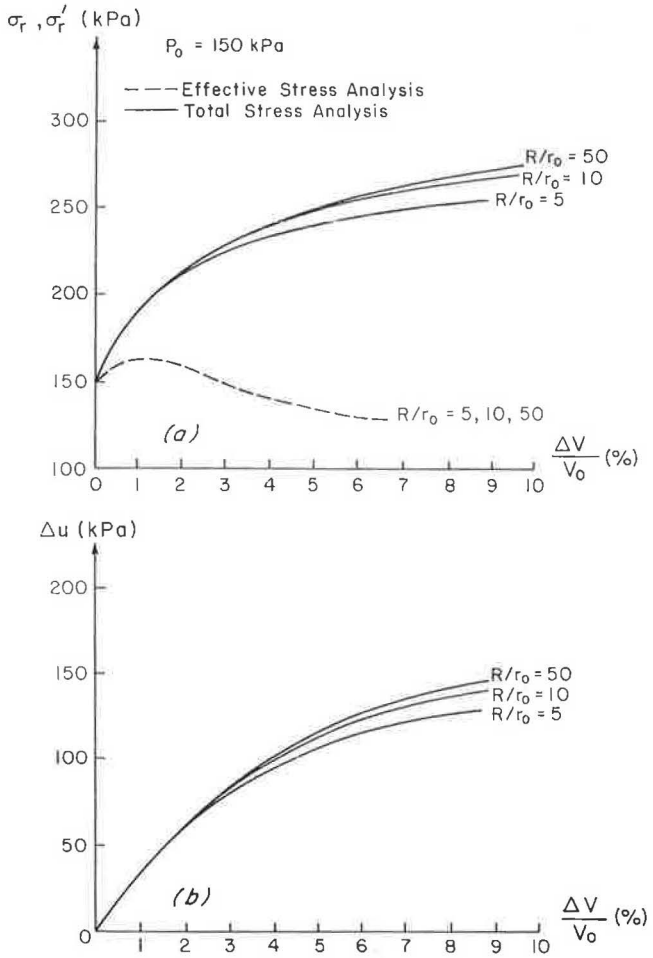

FIGURE 11 Effect of specimen geometry on (a) the lateral stress and (b) the excess pore water pressures.

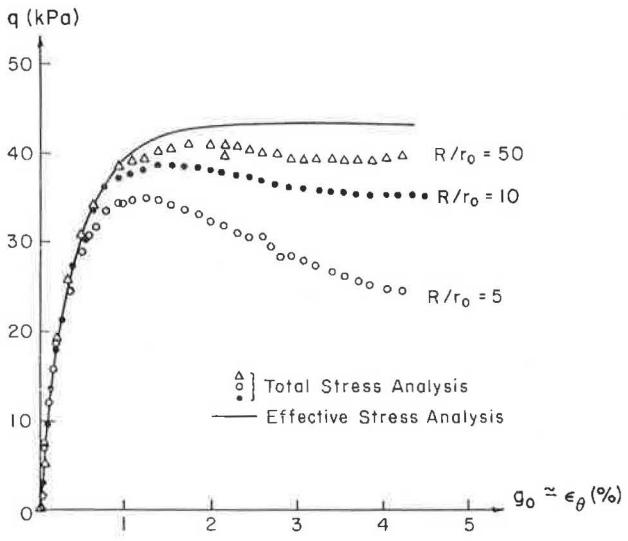

FIGURE 12 Comparison of the shear curves determined by using total and effective stress analysis procedures.

Equations 13 and 15 allow determination of the soil properties (i.e., shear strength characteristics, dilation properties, and shear modulus) through an analysis of CET results. Equation 16 permits simulation of the CET in an annular specimen of a soil with given constitutive equations (i.e., strain-hardening function and stress ratio-dilatancy relationship).

Analysis of CET Results

To evaluate the proposed interpretation procedure, laboratory cavity expansion tests were performed on Fontainbleau sand specimens in an HCC (*8*).

The soil used in this study was a fine Fontainbleau sand (average grain diameter of 0.10 mm) of which the mechanical properties were obtained from the analysis of consolidated drained triaxial test results reported by Habib and Luong (*9*). Figures 13a and 13c present the stress ratio-shear strain curves [$q/p' = h(\gamma)$] and the volumetric strain-deviatoric strain curves [$\varepsilon_v = f(\gamma)$] obtained under confining pressures of σ_0' = 100, 300, and 600 kPa. The figures illustrate the effect of confining pressure on the peak shear strength characteristics and volume change properties of this sand. Figure 13b indicates that in spite of significant differences in volume changes measured in those three tests the confining pressure has a rather minor effect on the stress ratio-dilatancy relationship $\eta(q/p')$, which can be approximately represented by a bilinear curve with a contractancy modulus μ_1 and a dilatancy modulus μ_2. The experimental curves are compared with numerical simulations by using the proposed soil model with the following mechanical properties:

1. For σ_0' = 300 kPa: G/σ_0' = 60, ϕ = 39.5 degrees, ϕ_{cv} = 32.5 degrees, μ_1 = 2, μ_2 = 0.85 and
2. For σ_0' = 600 kPa: G/σ_0' = 60, ϕ = 37 degrees, ϕ_{cv} = 32.5 degrees, μ_1 = 1.7, μ_2 = 1.0.

As is indicated in Figure 13, the model predictions agree fairly well with the experimental results. For the sake of analysis, the following average soil properties are considered: G/σ_0' = 60, ϕ = 38.5 degrees, ϕ_{cv} = 32.5 degrees μ_1 = 1.8, and μ_2 = 0.9.

The hollow cylinder cells with internal to external radius ratios, τ_0/R, of 1.5 and 1.10 were used in those tests to evaluate the effect of the boundary conditions on the effective stress response of the sand.

Figure 14 presents typical results of an undrained expansion test, including an expansion curve and measured excess pore water pressures. The measured excess pore pressures illustrate that in this highly permeable sand the gradient of the generated excess pore pressures dissipate instantaneously and the pore pressures become uniform throughout the specimen. Therefore, the measured excess pore water pressures are indicative only of the global tendency of the sand specimen to dilate during expansion, while locally the sand can be contracting or dilating depending on the actual shear strain level at the specific point (r) under consideration. The vertical displacement measured during the tests were found to be very small, illustrating a plane strain expansion.

Figure 15 illustrates the comparison of the experimental and predicted cavity expansion curves obtained by using the

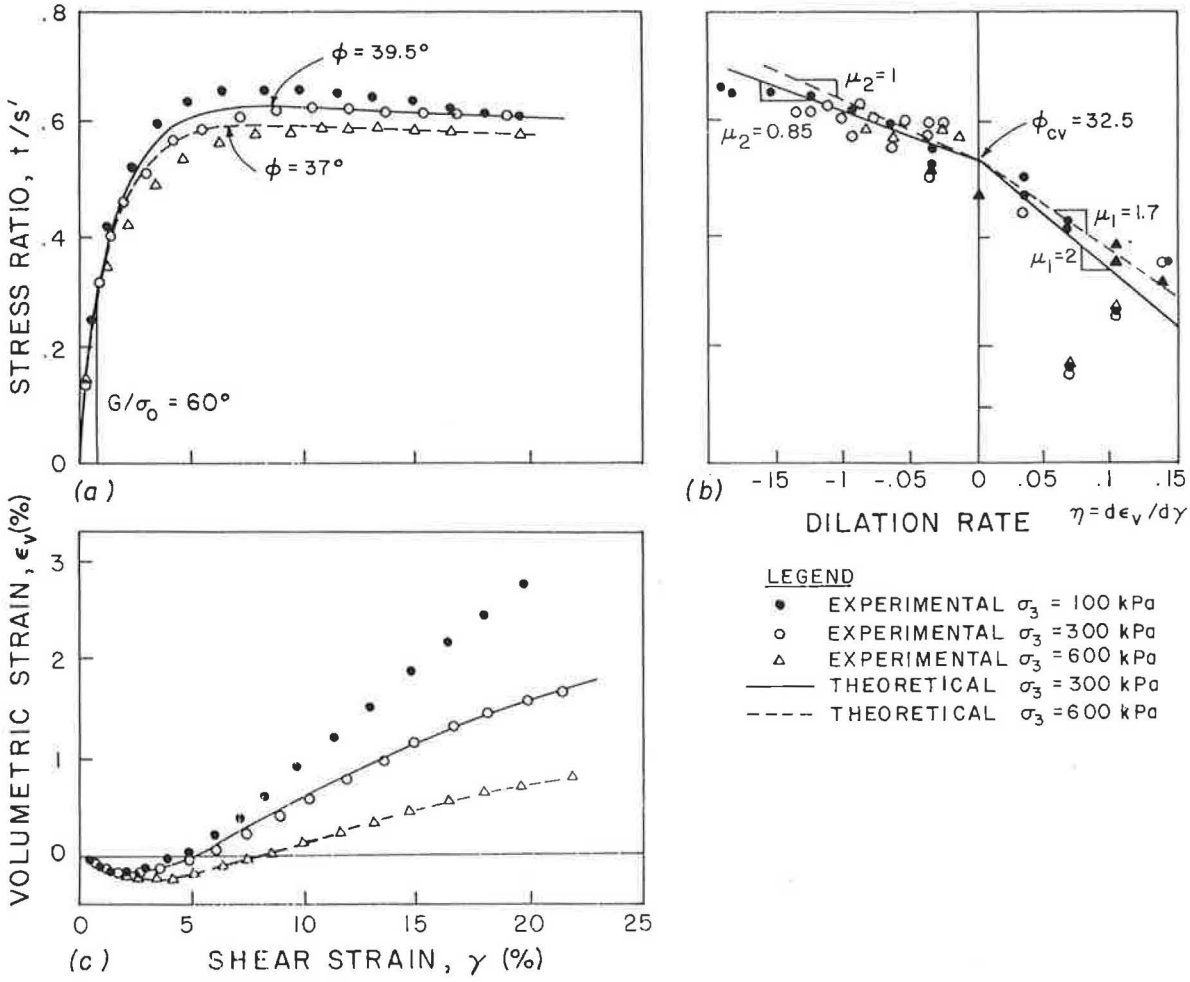

FIGURE 13 Prediction of the response of the Fontainbleau sand during triaxial compression tests.

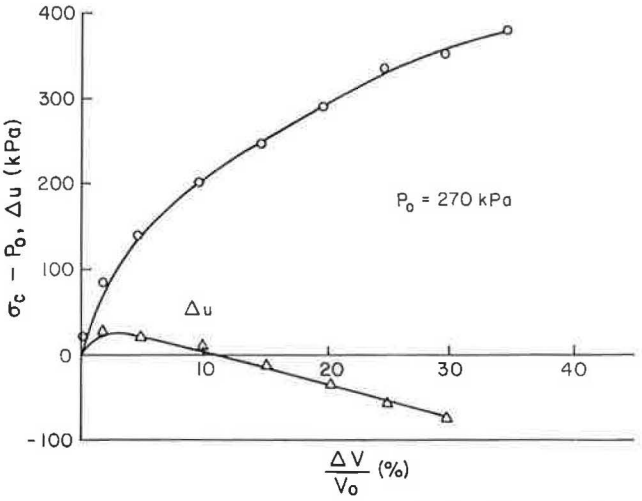

FIGURE 14 Typical results of an undrained cavity expansion test on a Fontainbleau sand specimen.

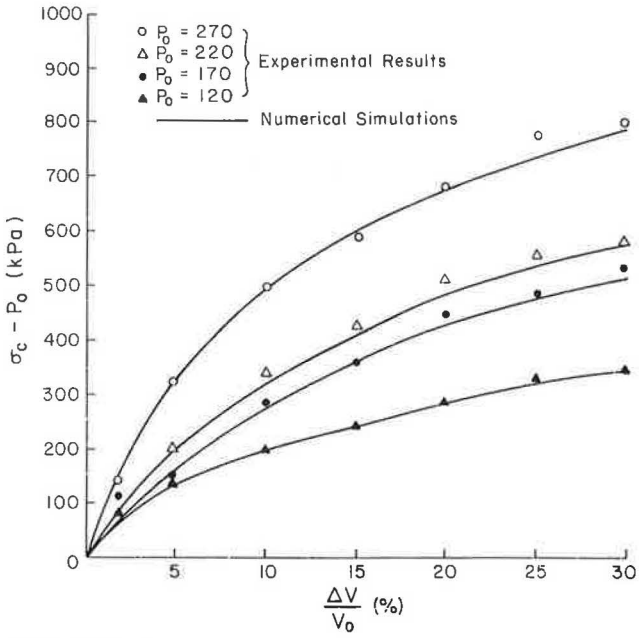

FIGURE 15 Comparison of the experimental expansion curves with numerical predictions by using the proposed procedures.

proposed interpretation procedure with the soil properties indicated before that in spite of the substantial differences in the effective stress paths followed during the triaxial CD and the cavity expansion tests (7) the proposed interpretation procedure predicts fairly well the experimental results. Those results indicate that for dense dilating sands the assumed constitutive equations (i.e., strain-hardening function and stress ratio-dilatancy relation) are rather stress-path independent. This analysis also illustrates that the specimen geometry has practically no effect on the stress response of the sand. Therefore, in spite of basic differences in boundary conditions between the laboratory specimen and the in situ semi-infinite soil medium, the proposed procedure is anticipated to be relevant for interpretation of pressuremeter tests in sandy soils.

SUMMARY AND CONCLUSIONS

The HCC equipment developed for the purpose of this study permits laboratory simulation of the soil response to cavity expansion and provides an appropriate means for evaluating analytical/numerical models that have been developed to predict the total and effective lateral stress soil response of both saturated clayey and sandy soils.

An interpretation procedure for cavity expansion test in the HCC has been developed and allows evaluation of the effect of the boundary conditions and specimen geometry on the effective and total lateral stresses and on the excess pore water pressures generated in the soil.

A laboratory study has been conducted to evaluate the proposed interpretation procedure. The analysis of the test results has demonstrated that the lateral effective stress response in saturated clayey soils (or the total/effective lateral stress response in sandy soils) is independent of specimen geometry and boundary conditions. Therefore, it is anticipated that (a) the proposed effective stress analysis procedure would be relevant for interpretation of (in situ) pressuremeter tests results and that (b) the effective stress-shear strain relationships derived from the laboratory cavity expansion tests could be extrapolated to field conditions.

Analysis of the test results has also shown that in saturated clayey soils specimen geometry and boundary conditions may significantly affect the total stress and excess pore water pressure generated during cavity expansion. Therefore, the total stress analysis conventionally used in interpretation of pressuremeter tests is not appropriate for the analysis of a laboratory cavity expansion test in the HCC.

The proposed interpretation procedure incorporates a relatively simple elastoplastic soil model with a nonassociated flow rule. Analysis of triaxial CU, CD, and undrained cavity expansion tests in the HCC has demonstrated that in normally consolidated clayey soils the assumed stress ratio-dilatancy function appears to be stress path dependent and the predicted cavity expansion curves are highly sensitive to the value of the contractancy modulus. In dilating sands, however, the assumed $\eta(q, p')$ function appears to be stress-path independent, and the proposed model predicts the experimental results fairly well.

Finally, in light of differences between the laboratory reconstituted specimens and the in situ soil (e.g., depositional history, fabric, in situ stress state), field testing is required for further evaluation of the proposed procedure to predict the in situ lateral stress soil response.

REFERENCES

1. F. Baguelin, J. F. Jezequel, and D. H. Shields. *The Pressuremeter and Foundation Engineering*. Trans Tech Publications SA, Clausthal, Germany, 1978.
2. F. Baguelin, J. F. Jezequel, and Le Mehaute. Etude des Pressions Interstitielles Developées lors de l'Essai Pressiometrique. *Proc., 8th ICSMFE*, Moscow, 1973.
3. J. Canou and M. T. Tumay. Field Evaluation of French Self-boring Pressuremeter PAF-76 in a Soft Deltaic Louisiana Clay. *Proc., 2nd ISPMT*, Texas A&M University, 1986, pp. 97–118.
4. I. Juran and J. F. Beech. Effective Stress Analysis of Soil Response in a Pressuremeter Test. *Proc., Pressuremeter and Its Marine Applications, Second International Symposium*, ASTM STP 950, 1986, pp. 150–168.
5. I. Juran and M. A. BenSaid. Cavity Expansion Tests in a Hollow Cylinder Cell. *Geotechnical Testing Journal*, Vol. 10, No. 4, 1987, pp. 203–212.
6. R. Nova and D. M. Wood. A Constitutive Model for Sand in Triaxial Compression. *Int. J. Num. Anal. Meth. Geomech.*, Vol. 3, 1979.
7. I. Juran and B. Mahmoodzadegan. Interpretation Procedure for Pressuremeter Tests in Sand. *Journal of the Geotechnical Engineering Division*, ASCE, Vol. 115, No. 11, 1989, pp. 1617–1632.
8. M. A. BenSaid. Mesures In Situ des Pressions Interstitielles: Application a' la Reconnaissance des Sols. Ph.D. dissertation. CERMES, ENPC, Paris, 1986.
9. P. Habib and M. P. Luong. Sols Pulverulents sous Chargements Cycliques. Presented at Seminaire Materiaux et Structures Sous Chargement Cycliques, Ecole Polytechnique, France, 1979.

Publication of this paper sponsored by Committee on Soil and Rock Properties.

Research and Development of a Lateral Stress Piezocone

R. G. CAMPANELLA, J. P. SULLY, J. W. GREIG, AND G. JOLLY

The possibility of evaluating in situ horizontal stress during cone penetration has been suggested by recent laboratory calibration chamber research (*1–6*). This has been confirmed by field trials with lateral stress sensing cones. A lateral stress piezocone developed at the University of British Columbia is described. Detail is given of the laboratory calibration procedures and corrections for cross talk and temperature effects. Field data from two Lower Mainland sites are presented to evaluate the amplification of lateral stress that occurs in sands during penetration of full-displacement probes. The results suggest that lateral stresses measured in granular soils with the LS cone are dependent on, *inter alia*, the existing horizontal stress, in situ state of the sand, and its grain characteristics.

Recent research into the behavior of granular soils during cone penetration has highlighted the importance of the existing in situ horizontal effective stress (σ'_h) on the parameters being measured. Laboratory measurements made by using calibration chambers (CC) have demonstrated the effects of in situ stress state on both cone resistance and sleeve friction (*7*). Similar effects noted for other penetration parameters are consistent with those findings.

The development of cones capable of measuring lateral stress originated from the idea that the sleeve friction measured during penetration in sand should be related to the pre-penetration lateral stress. Robertson (*6*) evaluated the CC data for sand presented by Baldi et al. (*7*) and showed that the ratio of pre- and post-penetration horizontal stress, as was deduced from sleeve friction measurements, varied from 1 to 7 and was related to the maximum dilation angle of the soil. The data were obtained for the friction sleeve located directly behind the tip. The CC tests were performed under conditions of constant lateral stress (BC1).

Huntsman (*2*) reviewed similar CC data from Italy and related σ'_h and sleeve friction f_s by means of the relative density D_r of the sand. Two sets of data were presented corresponding to the boundary conditions of constant lateral stress (BC1) and zero lateral strain (BC3). The scatter in the results is appreciable. However, the data trends do illustrate the effect of boundary condition on the σ'_h-f_s correlation (Figure 1) and indicate that at low relative densities the measured sleeve friction is less sensitive to the applied boundary condition. The true correlation representing "in-ground" conditions probably lies somewhere between the two data sets in Figure 1 and can be estimated by applying the appropriate chamber corrections.

R. G. Campanella, J. P. Sully, and J. W. Greig, Department of Civil Engineering, University of British Columbia, Vancouver, B.C. V6T 1W5 Canada. G. Jolly, Adara Systems Ltd., 2443 Beta Avenue, Burnaby, British Columbia, V5C 5N1, Canada.

On the basis of those findings, several types of cone penetrometer have been produced that are capable of measuring the lateral stress that act on an under-reamed section of a friction sleeve: (a) lateral stress sensing cone penetrometer (*2*) and (b) horizontal stress cone (*4*). A similar type of instrument designed specifically for evaluation of pile capacity in cohesive soils—the piezo-lateral stress cell—has been built and tested at MIT (*8*).

This paper describes a lateral stress (LS) piezocone designed and built at the University of British Columbia (UBC) for use as part of a research project that will evaluate in situ lateral stress from full displacement probes.

DETAILS OF LATERAL STRESS PIEZOCONE

The LS piezocone designed and built at UBC comprises two separate measurement systems: a standard UBC piezocone unit followed by a LS module. The eight-channel cone has a tip area of 15 cm^2, a friction sleeve area of 225 cm^2, and allows the simultaneous measurement of the following parameters:

- Cone resistance, q_c (bar);
- Pore pressure on the face, u_1, or behind the tip, u_2 (m of water);
- Sleeve friction, f_s (bar);
- Pore pressure behind the friction sleeve, u_3 (m of water); and
- Temperature (°C).

Those channels operate over a 7.5-V range. The calibration factors for each channel are given in Table 1. The LS module, which essentially consists of an instrumented friction sleeve, is located 0.69 m behind the tip and permits the following values to be recorded:

- Sleeve friction, LS-FS (bar);
- Pore pressure, u_{LS} (m of water);
- Lateral stress, σ_{LS} (kPa); and
- Temperature (°C).

Even though two temperature sensors are located in the LS-CPTU, only the temperature at the lateral stress module position is recorded when the cone is being used in this format.

The transducer ranges are again 7.5 V for all the channels except the lateral stress channel, which operates on 1 V full scale. The choice of location for the lateral stress module requires some comment.

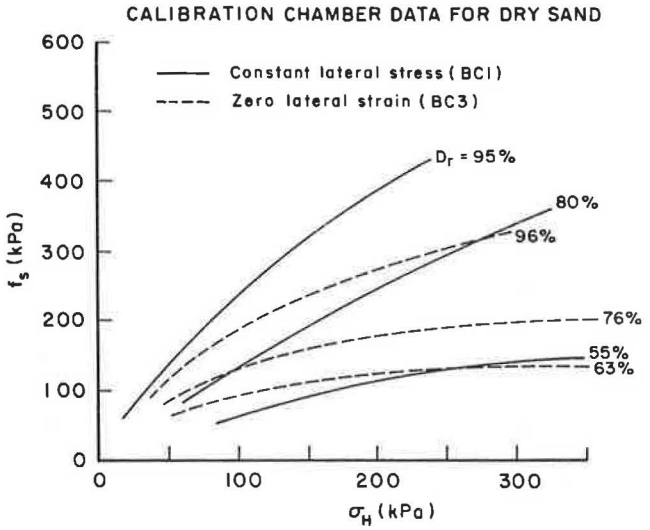

FIGURE 1 Influence of relative density on $f_s - \sigma'_h$ relationship from CC test data [after Huntsman (*2*)].

Design Considerations

Studies into soil behavior have demonstrated that large gradients of both stress and pore pressure exist around a penetrating cone and that those gradients are related primarily to the geometry of the equipment. In effect, the singularity at the base of the cone tip causes a large normal stress reduction to occur as the soil passes the shoulder. The extent of the reduction has been experimentally evaluated with respect to pore pressures (*9*), but little information exists with respect to lateral stress reduction and the relative importance of stress redistribution and creep. Indirect evidence for sands based on the variation of average sleeve friction, f_s, with distance (*10*) suggests that at approximately 12*D* (*D* = diameter of cone) behind the tip the lateral stress should be essentially constant for any particular D_r.

Location of the lateral stress sensor close to the tip would require measurement in an area of highly variable stress. Furthermore, at this location, dimensional tolerances may have unacceptable effects on the measured values (i.e., a slightly undersized friction sleeve may promote a larger stress reduction whereas an oversized sleeve may reduce the unloading effect). Strain rate changes near the tip and rotation of principal stresses may also be important. This aside, both Huntsman (*2*) and Jefferies et al. (*4*) present data where the lateral stress measured during cone penetration by a sensor located 1*D* behind the tip corresponds remarkably well to results of self-bored pressuremeter tests. This is surprising, considering the disturbance caused by insertion of the cone, and may well result from the loose nature of the soils tested. When penetration is stopped, however, the tests performed by Huntsman in the Beaufort Sea (*2*) indicated a slight increase in measured total lateral stress with time. That increase may result from redistribution and dissipation or both of excess pore pressures generated during penetration. However, no pore pressure measurements are available to confirm this.

The location of the sensor close to the tip is advantageous where reference tests are performed in calibration chambers. Calibration of an upper stress sleeve is not possible owing to the limited penetration distance that results from chamber size. CC data suggest that the measured lateral stress is always lower when measured close to the tip. Field data from the Beaufort Sea indicate that the difference between the stresses measured behind the tip (1*D*) and up the shaft (8*D*) decreases with depth, becoming equal at approximately 20 m (*2*). However, the relative magnitudes of σ_{LS} would depend on the location and spacing of the lateral stress sensors.

No CC facility exists at UBC, and, consequently, it was planned to calibrate the LS cone initially in the laboratory and then in the field at sites where the K_o condition was approximately known. As such, the geometry of the cone in terms of sensor location was not a restriction.

Finally, with a view to developing some kind of theoretical interpretation, it is reasonable to expect that data obtained away from the tip may more closely represent conditions of cylindrical cavity expansion. Stress changes near the tip may cause significant deviation from the cavity expansion condition.

Details of LS Module

For the UBC LS piezocone, the sensor is located 0.69 m (15.6*D*) behind the cone shoulder (Figure 2). The LS sleeve is 88 mm long and 44 mm in diameter (surface area of 121.6 cm^2) with a wall thickness of 3 mm. At the center of the sleeve, a 20-mm-long section has a reduced wall thickness of 1 mm. An arrangement of strain gauges is oriented at this location to measure the hoop stress in the section induced by the lateral stress acting on the sleeve. Several different gauge

TABLE 1 CALIBRATION DATA FOR LS PIEZOCONE

Channel No.	Parameter	Units	Calibration Factor
1	Cone resistance	bar	0.13 bar/mV
2	Sleeve friction	bar	0.013 bar/mV
3	Lower pore pressure	m of water	0.23 kPa/mV
4	Upper pore pressure	m of water	0.23 kPa/mV
5	Temperature	degree C	*
6	LS-FS	bar	0.013 bar/mV
7	LS-PP	m of water	0.23 kPa/mV
8	σ_{LS}	kPa	1.44 kPa/mV

* Temperature in degrees Celsius is obtained from $(V_T x4)-11$ where V_T is the voltage measured from a resistance temperature device (RTD).

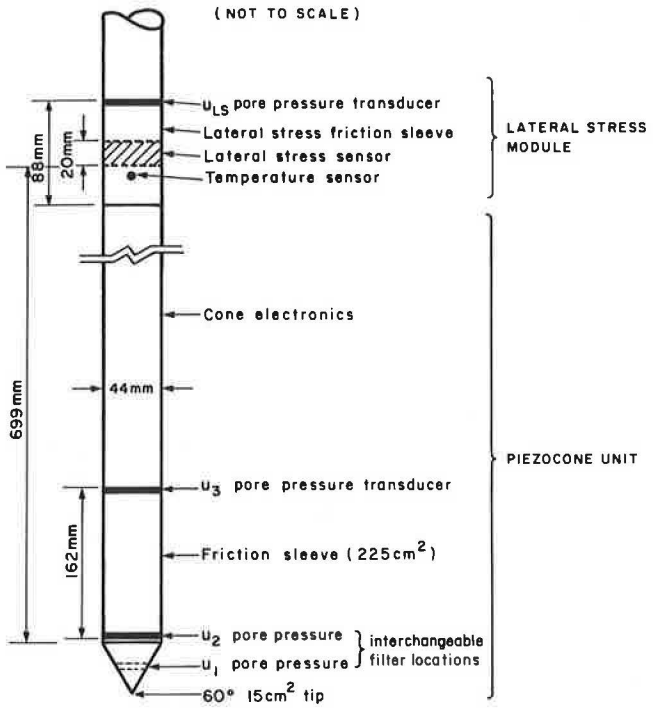

FIGURE 2 LS cone details.

arrangements were tested to optimize the lateral stress response and minimize both temperature and friction cross-talk effects.

A full bridge configuration is mounted on the sleeve. Each arm of the bridge consists of two 1,000 ohm strain gauges. The active arms are located on the thin-walled section of the sleeve, and the inactive arms are on the thicker section. The current design remains temperature sensitive to some degree, and, consequently, a platinum RTD sensor has been installed in the sleeve to allow for temperature compensation corrections to both the LS and the sleeve friction measurements.

The differential signals from the LS gauges are amplified in the cone to give a full-scale output of 1 V for an external hydrostatic pressure of approximately 1,500 kPa. The analog signals are converted at the surface to a 12-bit representation of the voltage, giving a sensitivity of 4.9 mV or 7.4 kPa of lateral stress. The IBM PC-based data acquisition system (UBC DAS) consists of an analog-to-digital (A/D) converter, depth controller board, counter timer board, and a battery backed-up power supply (*11*). A schematic layout of the UBC DAS is presented in Figure 3.

The data acquisition program interfaces the various components of the system to provide a means of collecting and storing the data. Data storage is either on floppy or hard disk. The program operates in two modes: cone penetration and dissipation. The change to dissipation mode is automatic when penetration is halted.

LABORATORY CALIBRATION OF LSC

Laboratory calibration of the load cells and pore pressure transducers for the piezocone unit were performed according to standard procedures adopted at UBC. Only the laboratory calibration of the lateral stress module is considered here.

Owing to the nature of the design of the module, it was necessary to calibrate the module for the following conditions:

- Hydrostatically applied confining pressure,
- LS cross talk on friction sleeve owing to axial loads,
- Temperature sensitivity, and
- Time-dependent stability of all channels.

During each of the calibrations performed, all eight cone channels were monitored to ensure the absence of channel interference.

Hydrostatic Calibration of LS Module

A special sleeve was fitted over the LS module and connected to a dead weight pressure tester to calibrate the bridge output for applied hydrostatic pressure. Pressure increments of 20 psi (~138 kPa) were used, up to a maximum of 250 psi (1724 kPa), and a constant temperature was maintained throughout. Hydrostatic loading and unloading sequences were performed for conditions of zero axial load. The results are presented in Figure 4 that give a calibration factor of 0.000695 V/kPa or 1440 kPa/V, with little or no hysteresis effects and no baseline drift over full-scale cycling. The factor was independent of temperature for the range of application (6° to 20°C).

FRICTION-LS CROSS TALK

Axial loading of the friction sleeve causes an output voltage on the LS channel because of the Poisson effect. Increasing sleeve friction on the LS sleeve for the strain gauge arrangement employed causes a negative offset on the LS channel.

The cone was set up in a frame so that the axially applied load was transferred by slip rings to the LS friction sleeve. Data from both the LS and the sleeve friction channels were recorded by an HP7090A measurement-plotting system. The load-unload was performed under zero confining pressure over a period of approximately 1 min, with readings taken every 0.1 sec. Linear regression of the data gave gradients of -0.2136 and -0.2150 for loading and unloading (Figure 5). A correction factor of 0.807 is applied to the slope in Figure 5, which takes into account the difference between the axial load distribution imposed for the laboratory calibration and actual field conditions.

An average value was used to correct the lateral stress data according to the equation

$$(V_{LS})_C = (V_{LS})_M + (0.2143 \times V_{fs}) \quad (1)$$

where

$(V_{LS})_C$ = corrected relative LS voltage,
$(V_{LS})_M$ = measured relative LS voltage, and
V_{fs} = relative sleeve friction voltage.

Calibration for Temperature Effects

To evaluate the temperature sensitivity of the LS module, the whole cone was immersed in a bath of ice water and was left

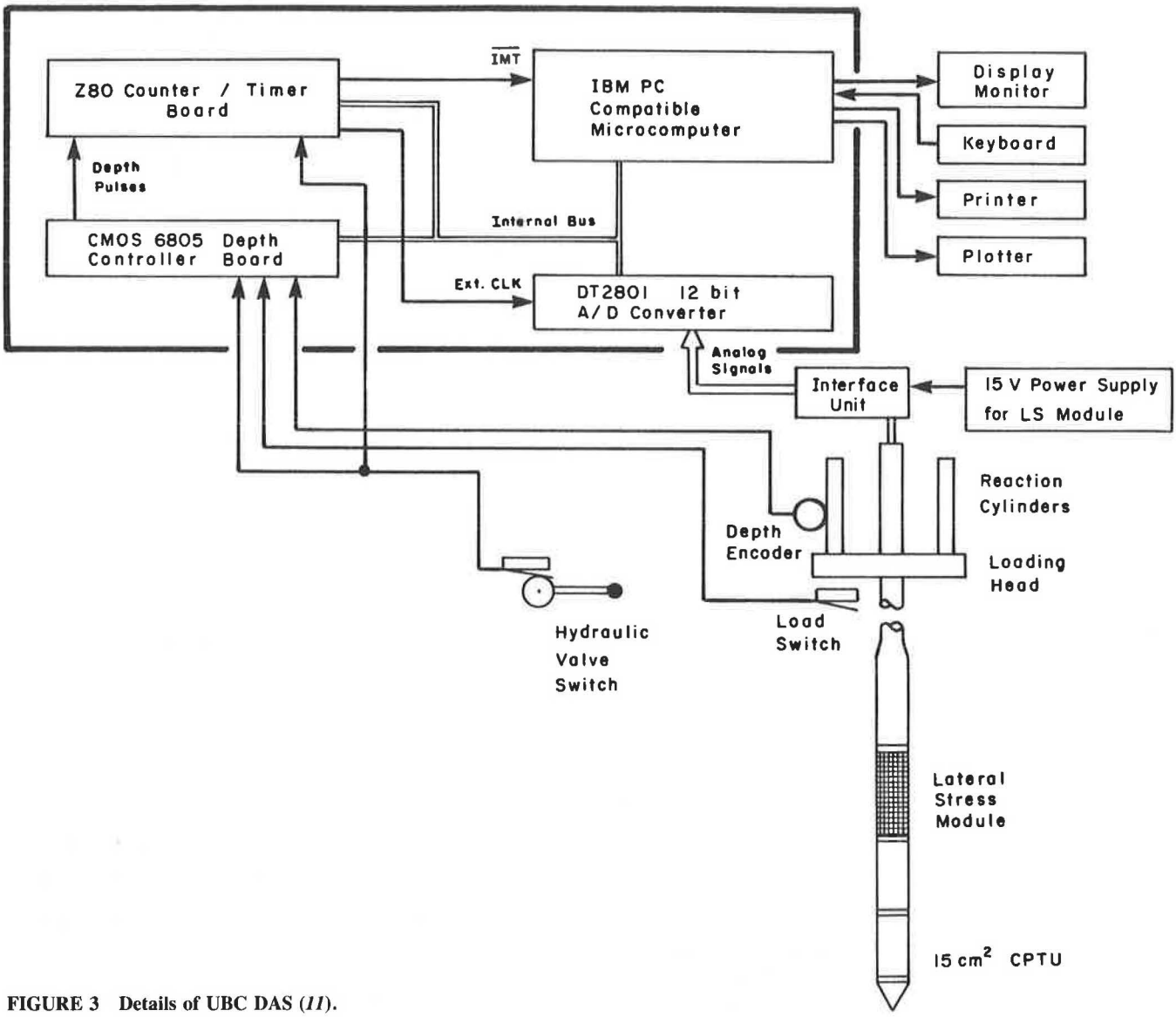

FIGURE 3 Details of UBC DAS (*11*).

to warm to room temperature over a 24-hr period, during which time readings on all channels were taken every minute. The results for the LS channel are presented in Figure 6. The temperature coefficient B_T for the LS channel was calculated to be +3.6 mV/°C on cooling. (Similarly, temperature coefficients were also evaluated for other channels.)

Evaluation of Baseline Drift

During the latter part of the temperature calibration, when the system was in equilibrium with the ambient temperature, continued monitoring allowed baseline drift on each channel to be evaluated. The time-dependent drift was found to be negligible for all eight channels.

The calibration factors obtained as just outlined have been incorporated into the data-acquisition program so that the output is given in corrected engineering units.

FIELD CALIBRATION OF LS PIEZOCONE

As was mentioned, field calibration of the LS cone equipment were performed at UBC test sites where information on LS conditions was available. For the purpose of this paper, only tests in granular soils are considered. Data obtained in cohesive soils are presented in a companion paper to this symposium (*12*).

The LS measured during cone penetration is generally larger than the pre-penetration in situ horizontal stress and results from the full-displacement mode of insertion where soil is displaced both laterally and vertically to permit penetration of the cone. Consequently, an overall stress increase around the penetrating cone usually occurs, and it is this value measured by the instrumented sleeve. The magnitude of the measured stress increase depends on the location of the sensor, geometry of the probe, and soil characteristics. For a partic-

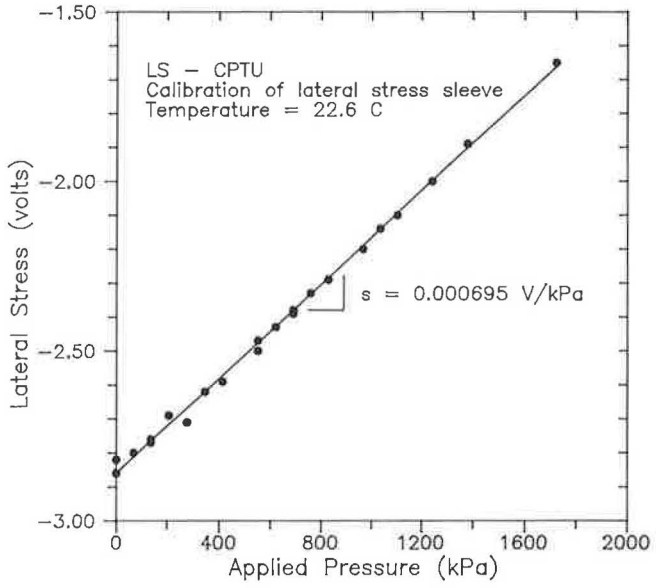

FIGURE 4 Pressure calibration of LS module.

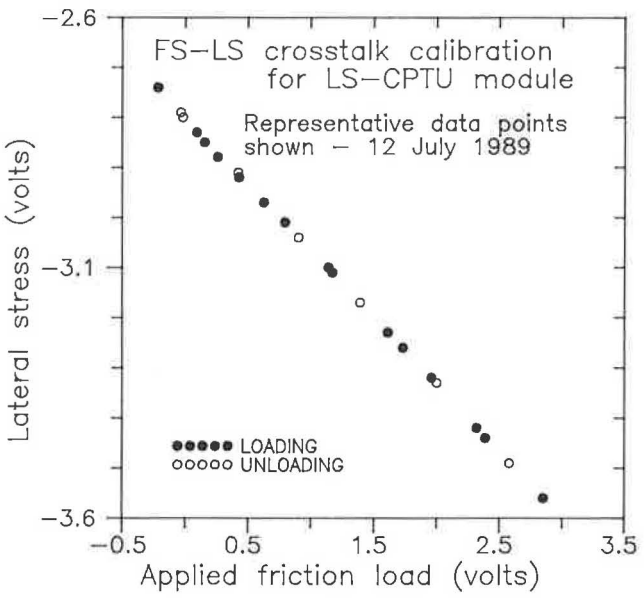

FIGURE 5 Evaluation of cross talk on LS channel owing to axial friction load.

ular probe the stress increase can thus be related to one or more soil parameters.

Studies have suggested that the stress increment caused by full-displacement penetration in granular soils is a function of one or more of the following points:

- Relative density of the soil, D_r (*2*);
- Peak friction angle, ϕ, or maximum angle of dilation, μ (*6*);
- Voids ratio, e (*4*); and
- State parameter, ψ (*2,4*).

The state parameter/voids ratio approach has been used primarily for evaluating CC data where sample characteristics can be controlled and measured with acceptable accuracy (*4*).

The application of the state parameter approach to in situ data appears promising but requires further confirmation. As was suggested by Sladen (*13*), the approach may necessitate additional specialized in situ tests to confirm the void ratios evaluated on the basis of CPT data (i.e., nuclear density/electrical resistivity voids ratio determinations) and also requires, a priori, knowledge of the in situ LS.

A considerable data base exists for estimating both relative density and peak friction angle from CPT data. The use of either one of those parameters would also concur with the philosophy of field calibration. Alternatively, correlation with the ratio q_c/σ'_v would appear logical as the dependence on a CC-derived relationship is removed.

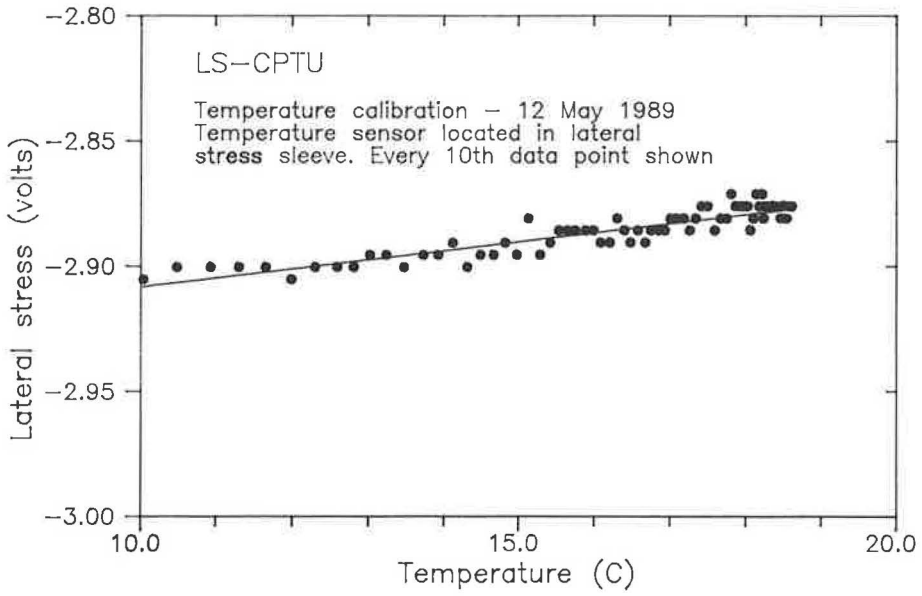

FIGURE 6 Temperature sensitivity of LS baseline.

Description of Test Sites

Data from two UBC test sites in the Lower Mainland of British Columbia are presented where consistent information on K_o conditions exists: Laing Bridge South (LBS) and McDonald Farm (MDF). The two sites are located on Sea Island at Vancouver International Airport, are about 1 km apart, and have very similar characteristics. The sediments are post-glacial Holocene deltaic deposits, which are essentially normally consolidated. The surficial soils (<4 m) are underlain by granular marine and tidal flat deposits (medium sands) to a depth of around 20 m. The granular layer is finer grained, more uniform, and deeper at LBS than at MDF. Underlying the sands are at least 40 m of soft-to-firm marine silts and clayey silts.

The variation of K_o for the LBS site is presented in Figure 7 and has been evaluated by three empirical correlations (*14*). The K_o value varies between 0.45 and 0.5. Preliminary results obtained by using the UBC self-boring pressuremeter confirm the K_o values in Figure 7.

Data presented by Hughes and Robertson (*15*) from self-bored pressuremeter tests suggest that the LBS trend of K_o is a good lower bound for the MDF site, where an average coefficient of 0.6 is taken as representative for the normally consolidated sands.

RESULTS OF IN SITU TESTS

A summary of the measured cone resistance and lateral stress profiles for MDF and LBS are presented in Figures 8 and 9.

Considering the proximity of the sites, the trends in q_c at the two sites are notably different. At MDF the q_c values are reasonably constant over specific depth intervals within the sand. The gradual increase in q_c with depth at LBS is a good indicator of the uniformity of the sand at this location. The effects of interbedded silt on the cone resistance at both sites can be seen throughout the profile. Pore pressures throughout the profile are close to hydrostatic for both the behind friction sleeve (u_3) and the lateral stress (u_{LS}) pore pressure sensor locations. A small excess pore pressure is measured behind the tip (u_2). At around 14 m, the anomalously high q_c results from the presence of an organically cemented sand layer, a remnant of an active beach deposit. At the base of the sand layer the q_c values drop rapidly to around 10 bar, and large excess pore pressures are recorded that indicate the presence of the soft normally consolidated clay silt.

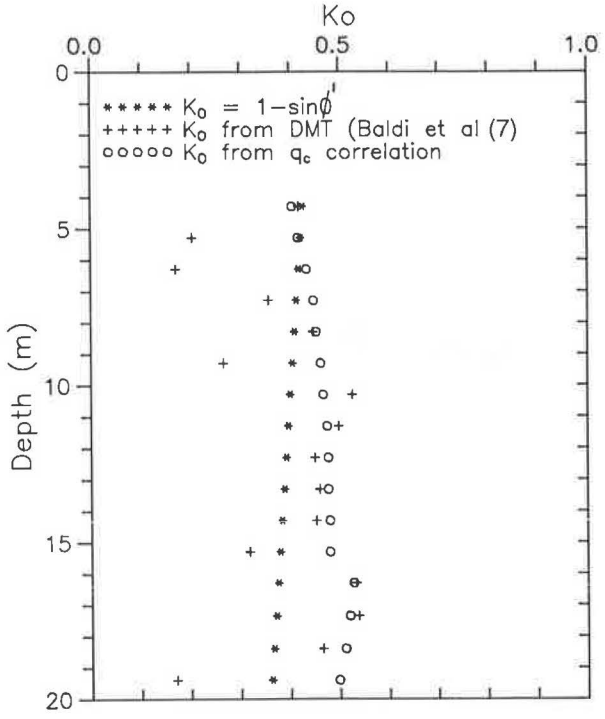

FIGURE 7 Evaluated K_o conditions for LBS.

The lateral stress profiles measured by the LS cone at the two sites are also presented in Figures 8 and 9. Contrary to the relative magnitudes of cone resistance, the measured total LS σ_{LS} in the sand layer at LBS is consistently larger than that at MDF. The σ_{LS} profiles are otherwise very similar. The variation in measured σ_{LS} at both sites is increased in the transition layer between the sand and clay silt.

A comparison of average friction stress measured at the two sleeve locations is presented in Figure 10 for LBS. Good agreement between the two measurements is evident and concurs with the distribution suggested earlier by Campanella and Robertson (*10*). This also suggests that the LS measurements at the 15.6*D* position might be similar to those at the 1*D* location previously investigated. However, this conclusion would depend on the stress gradient behind the tip and the exact location of the LS sensing section in relation to the stress distribution.

The penetration pore pressures measured at the three sensor locations, (i.e., behind tip, behind friction sleeve, and at LS sleeve), are presented in Figure 11 for the MDF LS-CPTU. The similarity of the pore pressures measured behind the friction sleeve (u_3) and at the LS section (u_{LS}) indicate the absence of large gradients once away from the tip-shoulder singularity. Also apparent when comparing Figures 8 and 11 is that the measured LS in fine-grained materials is dominated by the pore pressure response.

LS Coefficient from LS-CPTU

The LS coefficient obtained from LS-CPTU profiling K_{LS} is defined as

$$K_{LS} = \frac{\sigma_{LS} - u_{LS}}{\sigma'_v} \tag{2}$$

where

σ_{LS} = measured total LS,
u_{LS} = penetration pore pressure measured at LS section, and
σ'_v = calculated effective overburden pressure.

Statistical filtering of calculated K_{LS} values at 2.5-cm intervals was performed over a 25-cm window. All data outside 1 standard deviation of the median were removed and replaced by the mean value (*16*). The filtered profiles of K_{LS} for both sites are presented in Figure 12, where it can be seen that, in

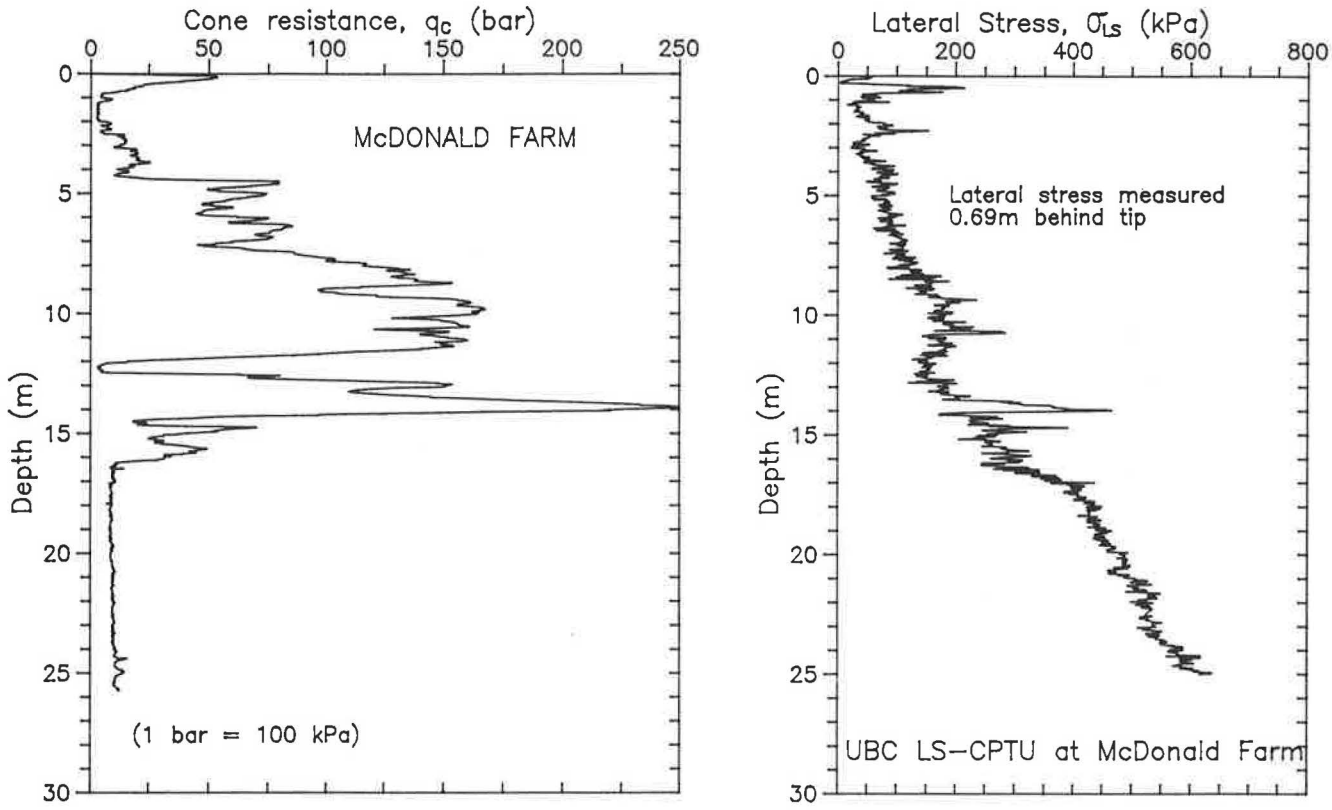

FIGURE 8 LS-CPTU results at MDF.

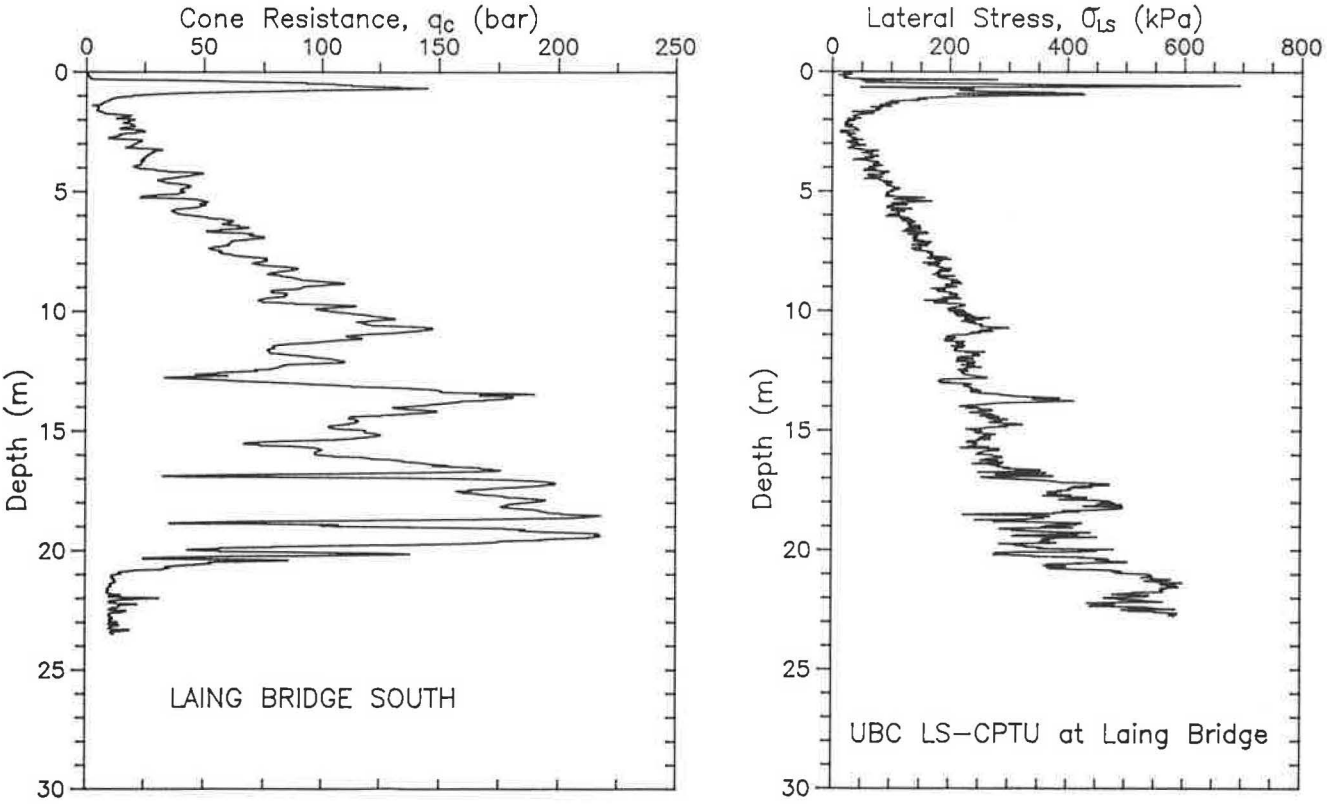

FIGURE 9 LS-CPTU results at LBS.

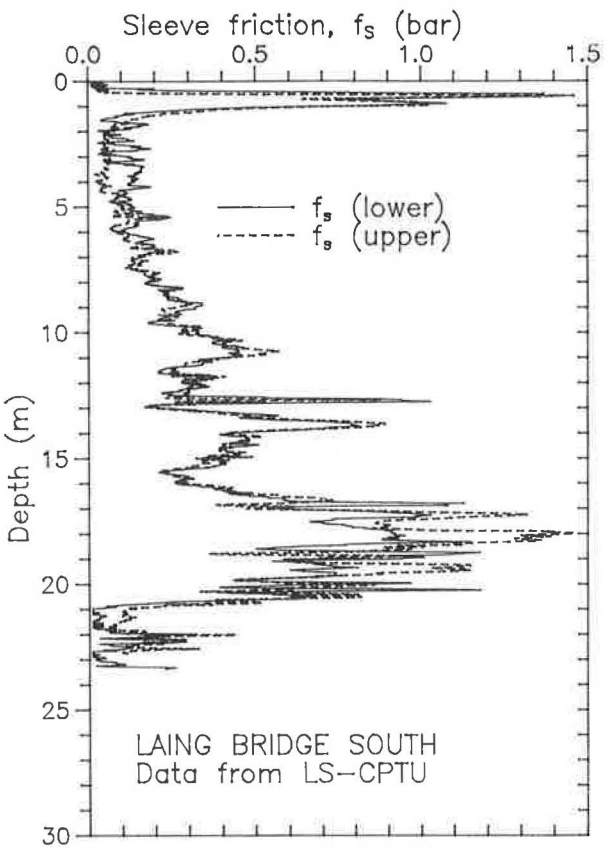

FIGURE 10 Comparison of average sleeve friction measured at two locations on LS cone.

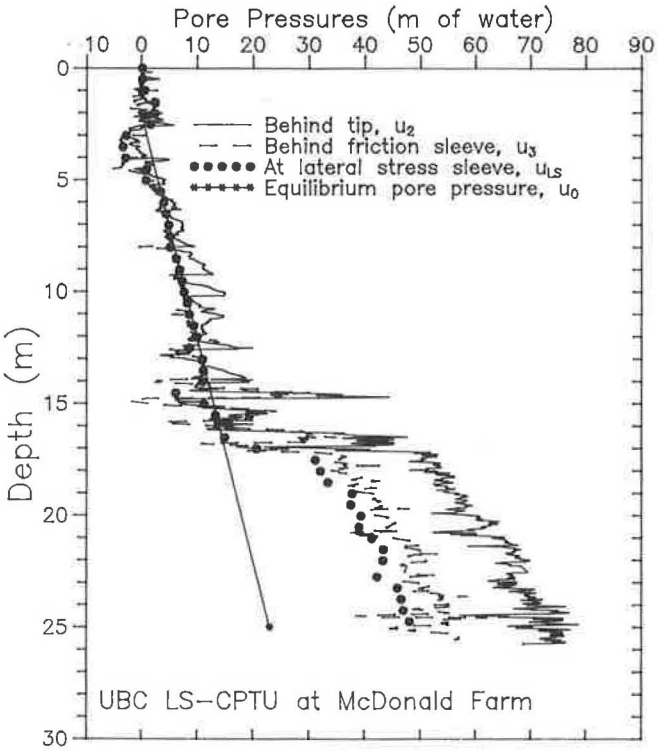

FIGURE 11 Pore pressures measured during LS-CPTU.

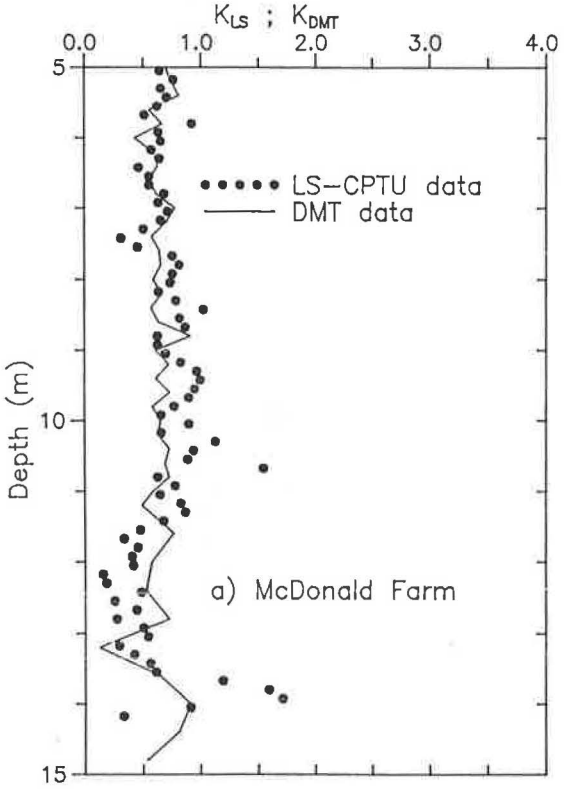

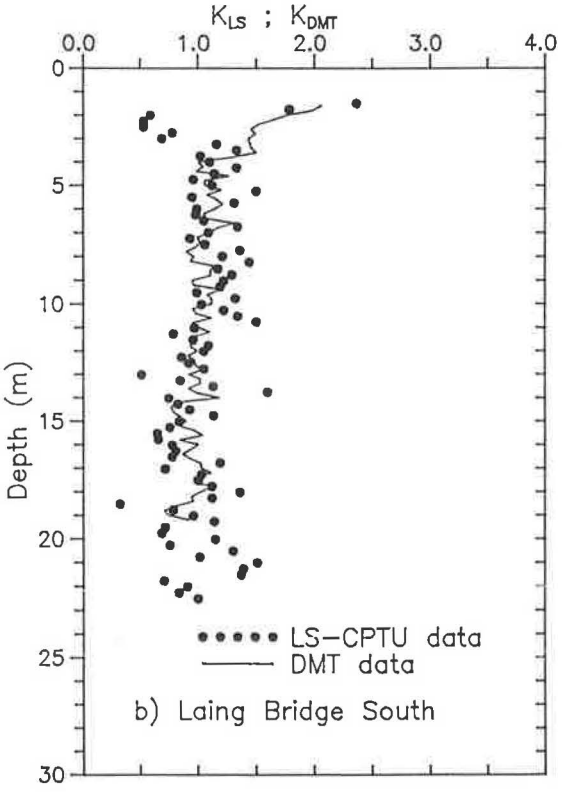

FIGURE 12 K_{LS} factors for test sites.

general, $K_{LS} > K_o$. To evaluate the amplification of LS caused by cone penetration, the effective LS in Figure 12 has been normalized with respect to the in situ σ'_h and replotted in Figure 13 against q_c/σ'_v. The amplification factor for the LS cone A_{LS} is defined as

$$A_{LS} = \frac{\sigma'_{LS}}{\sigma'_h} = \frac{\sigma_{LS} - u_{LS}}{\sigma_h - u_0} \tag{3}$$

where σ'_h is the prepenetration effective horizontal stress and u_0 is the equilibrium in situ pore pressure. By definition

$$K_o = \frac{K_{LS}}{A_{LS}} \tag{4}$$

The basis of obtaining σ'_h was discussed earlier. Use of q_c/σ'_v as an index parameter appears logical because it is related to the principal soil behavior characteristics thought to control the stress amplification effect (*2,4,6*). Furthermore, q_c is a parameter measured during the LS-CPTU and correlates directly with the σ_{LS} values measured (i.e., at the same location).

Two effects are apparent from the trends shown in Figure 13:

1. The amplification factor A_{LS} is very sensitive to small changes in q_c/σ'_v ratio.
2. The shape of the $A_{LS} - q_c/\sigma'_v$ relationship appears to be similar for the two sites studied. However, the curves are offset laterally owing to some secondary effect.

The position of a tentative curve for data obtained in silt/silty sand is also shown and further suggests that grain size characteristics (D_{50}, silt content, grain angularity) of the sand may be important factors when evaluating LS amplification factors in the manner used here.

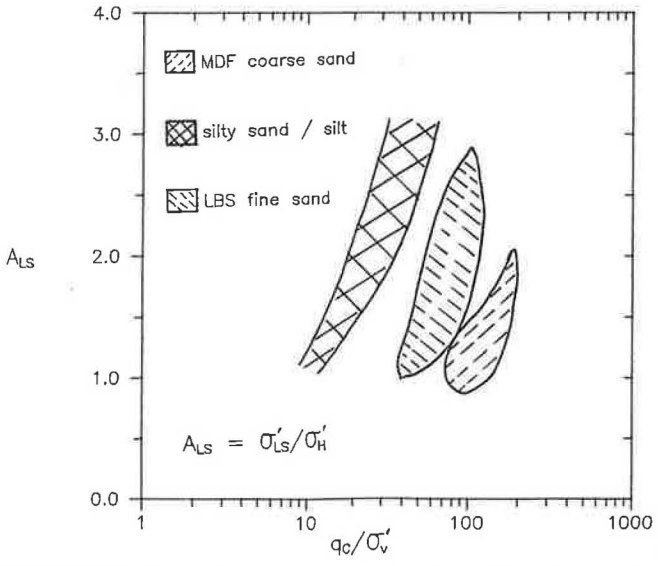

FIGURE 13 Lateral stress amplification factor for soils tested.

DISCUSSION

The results obtained in this study agree with other data trends obtained from calibration chamber tests and interpreted to evaluate LS from full-displacement tests (*1,3,5,6*). In clays, the LS cone response is dominated by pore pressure effects.

It is interesting to note that LS coefficients obtained from the DMTs performed at MDF and LBS, interpreted by using Schmertmann's method (*17*) to give an estimate of in situ K_o, give the same relative magnitudes as those obtained from direct measurements during LS-CPTU profiling (Figure 12). In general terms,

For MDF

$$K_{LS} \approx K_{DMT} = 1\text{–}1.2\ (K_o) \tag{5}$$

for LBS

$$K_{LS} \approx K_{DMT} = 1.5\text{–}2.5\ (K_o) \tag{6}$$

where K_{DMT} is the K_o value obtained from the interpreted DMT profile (*17*).

The DMT soil type index I_D also suggests that the LBS sand is finer than the MDF sand, as indicated in Figure 13.

Measurement of both friction and normal stress at the upper sleeve location permits an evaluation of the average mobilized soil to steel friction angle during penetration. Friction angles varying between 18 and 25 degrees were obtained for the sand layer at MDF. Lower values were measured for LBS. Tomlinson (*18*) suggests from his experience with steel piles in sand that a soil-steel friction angle of 20 degrees is appropriate. The data are also in agreement with results suggested by a literature review of measured soil-steel friction coefficients and with measurements in ring shear tests performed at UBC (*19*). This would suggest that the relative values of the parameters being measured during LS-CPTU profiling are realistic.

SUMMARY AND CONCLUSIONS

Data have been presented from laboratory and field measurement by using a LS piezocone. Laboratory calibrations have shown that the measured LS is sensitive to both axial loads on the friction sleeve and on temperature. However, those effects can be calibrated out by making corrections to the measured data. The corrections applied are stable and repeatable.

Field measurements suggest that the LS measured by the LS cone is greater than the in situ horizontal stress. The increase over and above the in situ condition in sand has been shown to be partly a function of the normalized cone resistance q_c/σ'_v. It would also appear that grain size, grain size distribution, and angularity may be important.

The measured LS undergoes some degree of dissipation during stops in the penetration of the cone. The reduction in LS appears to be controlled by the characteristics of the soil at the tip and at the sleeve location. Further work is being done to evaluate those effects. Additional studies are presently being performed to evaluate the application of LS cone

data to the interpretation of in situ horizontal stress. Refined signal processing will allow the present ±7 kPa resolution on the LS channel to be considerably improved. Variations in the mechanical design of the LS module are also underway.

ACKNOWLEDGMENTS

Financial assistance for the design and construction of the lateral stress module was provided by NSERC as part of a University-Industry Cooperative grant. The second author was supported by an SERK (U.K.) NATO scholarship during this study and which is gratefully acknowledged. The assistance of members of the Civil Engineering Department at UBC is gratefully appreciated. S. Jackson and H. Schrempp are thanked for their assistance in the development of the lateral stress cone.

REFERENCES

1. K. Been, J. H. A. Crooks, and L. Rothenburg. A Critical Appraisal of CPT Calibration Chamber Tests. *Proc., Penetration Testing 1988, ISOPT-1*, Florida, Vol. 2, 1988, pp. 651–660.
2. S. R. Huntsman. *Determination of In Situ Lateral Pressure of Cohesionless Soils by Static Cone Penetrometer.* Ph.D. thesis, University of California, Berkeley, 1985.
3. M. G. Jefferies. Verification of the q_c-ψ Function in Sand Strata. *Proc., Penetration Testing 1988, ISOPT-1*, Florida, Vol. 1, 1988, pp. 793–804.
4. M. G. Jefferies, L. Jönsson, and K. Been. Experience With Measurement of Horizontal Geostatic Stress in Sand During Cone Penetration Test Profiling. *Geotechnique*, Vol. 37, 1987, pp. 483–498.
5. S. Marchetti. On the Field Determination of K_o in Sand. Panel discussion to Session 4A. *Proc., 11th ICSMFE*, San Francisco, Calif., Vol. 4, 1985.
6. P. K. Robertson. *In Situ Testing of Soil With Emphasis on Its Application to Liquefaction Assessment.* Ph.D. thesis, University of British Columbia, Vancov
7. G. Baldi, R. Bellotti, V. (Pasqualini. Design Parameters for Sands From CPT. *Proc., ESOPT II*, Amsterdam, Vol. 2, 1982, pp. 425–438.
8. M. M. Baligh, R. T. Martin, A. S. Azzouz, and M. J. Morrison. The Piezo-Lateral Stress Cell. *Proc., 11th International Conference on Soil Mechanics and Foundation Engineering*, San Francisco, Calif., Aug. 1985, pp. 841–844.
9. D. G. Gillespie. *Evaluating Velocity and Pore Pressure Data From the Cone Penetration Test.* Ph.D. thesis, University of British Columbia, Vancouver, in preparation, 1990.
10. R. G. Campanella and P. K. Robertson. Applied Cone Research. Presented at Symposium on Cone Penetration Testing and Experience, Geotechnical Engineering Division, ASCE, Oct. 1981.
11. J. W. Greig, P. K. Robertson, and R. G. Campanella. Microcomputer Software to Collect, Plot, and Interpret Cone Penetration Test Data. *Proc., 1st Canadian Symposium on Microcomputer Applications to Geotechnics*, Oct. 1987, pp. 75–83.
12. J. P. Sully and R. G. Campanella. Measurement of Lateral Stress in Cohesive Soils by Full-Displacement In Situ Test Methods. *TRB*, this issue.
13. J. A. Sladen. Problems with Interpretation of Sand State From Cone Penetration Test. *Geotechnique*, Vol. 39, 1989, pp. 323–332.
14. J. P. Sully and R. G. Campanella. Correlation of Maximum Shear Modulus With DMT Test Results in Sand. *Proc., 12th ICSMFE*, Rio de Janeiro, Aug. 1989.
15. J. M. O. Hughes and P. K. Robertson. *Full Displacement Pressuremeter Testing in Sand.* Soil Mechanics Series 78. Department of Civil Engineering, University of British Columbia, Vancouver, April 1984.
16. D. S. Wickremesinghe. *Statistical Characterization of Soil Profiles Using In Situ Tests.* Ph.D. thesis, University of British Columbia, Vancouver, June 1989.
17. J. H. Schmertmann. Revised Procedure for Calculating K_o and OCR from DMTs With $I_D > 1.2$ and Which Incorporates the Penetration Force Measurement to Permit Calculating the Plane Strain Friction Angle. Presented at DMT Workshop, March 16–18, Gainesville, Fla., 1983.
18. M. J. Tomlinson. *Pile Design and Construction Practice.* Cement and Concrete Association, London, 1981.
19. N. F. Rinne. *Evaluation of Interface Friction Between Cohesionless Soil and Common Construction Materials.* M.A.Sc. thesis, University of British Columbia, Vancouver, 1989.

---

aper sponsored by Committee on Soil and Rock